Rock mass and rippability evaluation for a proposed open pit mine at Globe-Progress, near Reefton

---

A Thesis

submitted in partial fulfilment

of the requirements for the Degree

of

Master of Science in Engineering Geology

by

Philip B. Clark

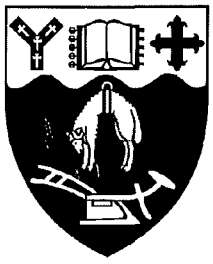

University of Canterbury

1996

Frontispiece

I like rain

by

JPS Experience

I like rain falling on my window
I like rain splashing on the roof
I like rain dancing on the pavement
I like rain when I'm inside
Falling down
Falling down
I like rain

(sentiments not felt by most ' Coasters)

Fog starting to settle on New Zealand's fog capital, Reefton.

Abstract

Rock mass classification schemes such as the Q System and Rock Mass Rating (RMR) System have been designed for prediction of tunnel support, but these systems can be modified from stability analyses to excavatability assessments. Five methods have been used to classify the rock mass at Globe-Progress with the objective of predicting the type of equipment that may be used to excavate the open pit:

- Seismic velocity determination
- Size-Strength Method
- RMR System
- Weaver's (1975) Rippability Rating System
- MacGregor *et al's* (1994) Productivity Prediction Method

Seismic velocity determination and the Size-Strength Method are both easily performed during the feasibility stages of a project. Seismic velocities are influenced by the degree of fracturing, compaction, porosity, density and weathering, and they can therefore be used to provide a preliminary characterisation of the rock mass. The Size-Strength Method uses the two most important properties of a rock mass for classification, the discontinuity spacing and the strength of the rock material. Both methods, therefore, provide quick and accurate assessments of the rock mass quality.

At the investigation or design stage of a project a complete rock mass characterisation method is used that involves a collection of geological and geotechnical parameters to fully characterise the rock mass. The method chosen for use at Globe-Progress was the RMR system, as this method is easily adapted from a stability prediction method to an excavatability prediction method. Most data required for calculation of the RMR Index is available from drillcore data logs.

Simple analyses of drillcore log data show that drillcore data has been correctly logged except for the strength parameter. This was revised for every logged rock mass unit (RMU) based on quantitative strength determinations and the lithology of each RMU, so that more accurate excavatability analyses could be made using the RMR System, a

modified version of Weaver's 1975 Rippability Rating Method, and MacGregor *et al's* 1994 Productivity Prediction Method.

The ratings for the three rock mass classification methods employed have been contoured on plans at 20 metre bench levels. The plans show that zones of poor rock, where digging to easy ripping should be expected, exist in the western pit wall, where the Chemist Shop Fault is located, and along the northern and eastern walls, following the Globe-Progress Shear Zone. Most of the overburden is classed as fair to poor rock, where easy to moderate ripping will be expected, and there is a zone of weaker rock in the axial fold of the Globe-Progress Shear Zone.

This study indicates that the proposed open pit is geotechnically feasible to rip. The preliminary assessments suggest that 90% of the pit area is rippable or marginal and 10% is expected to non-rippable. The final assessments suggest that ripping will be very easy (> 3500 m^3/hr) to difficult (250 - 750 m^3/hr) using a Komatsu D575A-2 Bulldozer. Some areas of overburden may require blasting to further fragment the rock mass and aid productivity. But there are other factors, such as the bulldozer operator's experience in ripping similar rock masses, wear and tear on ripper blades, bulldozer maintenance time and transportation costs, and other restrictions that influence overall productivity and costs associated with ripping, and which cannot be determined until ripping actually proceeds.

Contents

Chapter One

Introduction

Chapter Two

Rock Mass Classification Systems

Chapter Three

Principles and Methods of Rippability Assessment

Chapter Four

Geotechnical investigations

Chapter Five

Rippability evaluation of the proposed open pit mine at Globe-Progress

Chapter Six

Summary, conclusions and further work

Appendix A

Historical Overview

Appendix B

Terminology

Appendix C

Barrell's (1992) Structural mapping

Appendix D

Field and laboratory test results

Appendix E

Determination of parameters used in rock mass and rippability evaluation methods

Figures

Tables

Chapter One

Introduction

1.1 Background

> *"Should the efforts of the few prospectors still active in the district result even in a single instance in a successful mine, confidence would probably be restored to an extent such that capital would be forthcoming for the development of known lodes, and the reopening of old mines where ore was left which could profitably be worked by modern methods..... Lodes prospected in earlier years may repay investigation in view of the present high price of gold."*
>
> M Gage, 1948.

The above quote seems to be just as apt today as when it was written in a 1948 review of the Reefton Goldfield, and Globe-Progress, near Reefton, will hopefully be the site for Macraes Mining Company Limited's (Macraes) first successful mine within the goldfield. Macraes are also exploring other areas within the Reefton Goldfield that may be mined at a later date.

The Reefton Goldfield (Figure 1.1) is an area extensively mined between 1872 and 1951. Globe-Progress, which was the second largest mine in the area, was previously mined by underground methods between 1878 and 1920. Nearly 420 000 ounces (13 000 kg) of gold was extracted at an average grade of 12.2 g/t (Barry, 1993). In the early 1980s CRA Exploration Limited (CRAE) acquired exploration licences over most of the Reefton Goldfield and began a regional exploration programme that resulted in 39 holes being drilled on Globe Hill. The drilling defined an area of disseminated gold mineralisation adjacent to the quartz veins. In 1991 Macraes took over the licences for the area and are now proposing to develop an open pit mine at Globe-Progress based on a total resource of 10.68 Mt at 2.23 g/t gold, and with a cut off grade of 1.25 g/t (MMCL, 1996).

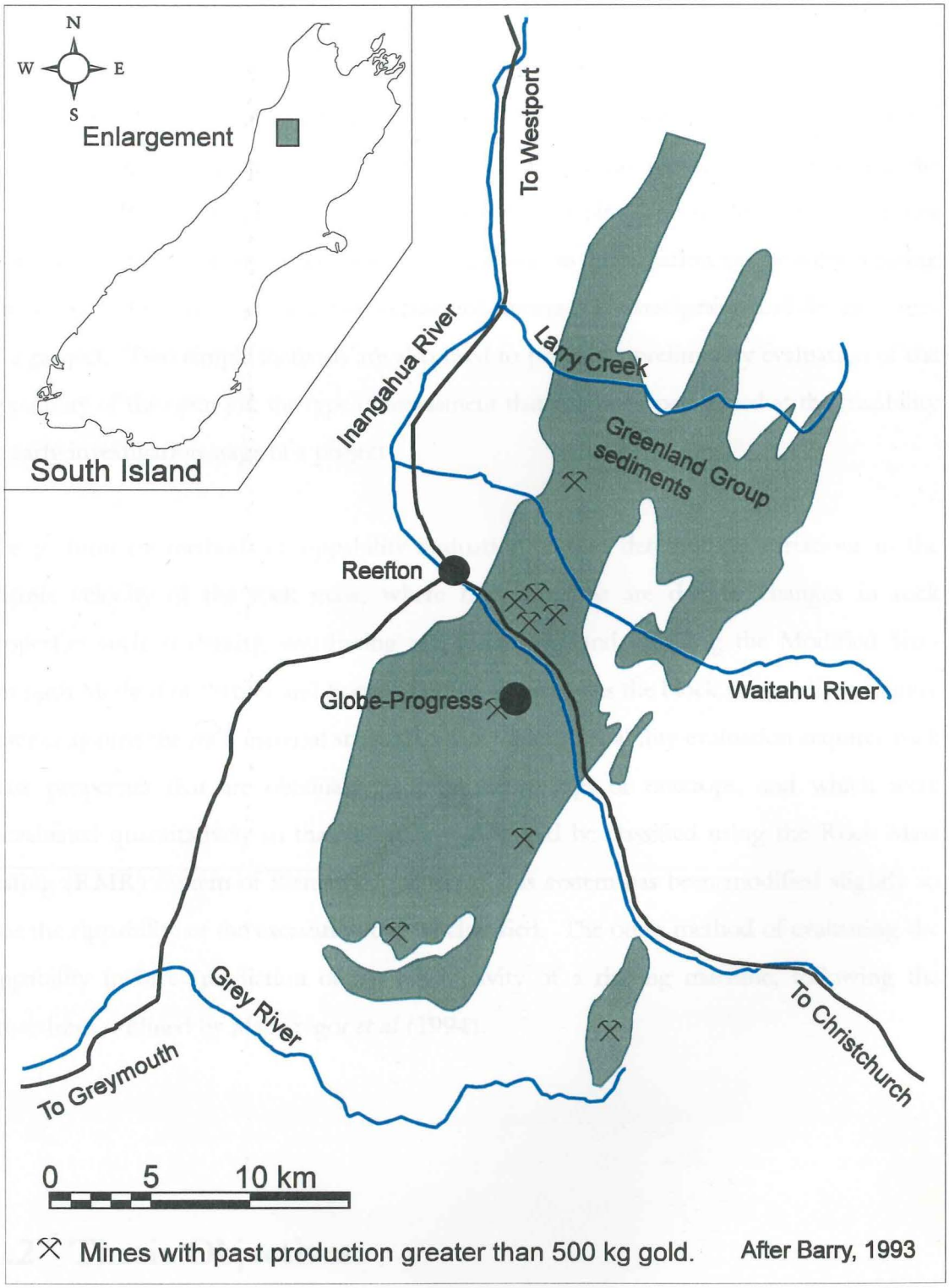

Figure 1.1: Location map of the Reefton Goldfield and Globe-Progress.

To excavate the pit either bulldozer ripping, drill and blast methods, or a combination of the two will be used. There are two different approaches to estimating the rippability of a site, one involving characterisation of the rock mass, and the other prediction of the productivity of a ripping machine. This thesis uses both methods in evaluating the rippability of the rock mass within the proposed open pit. The site evaluation requires rock mass and rock material characteristics, as well as information on possible ripping machinery to be used, and should be performed during the investigation and design stages of a project. Two simple methods are also used to provide a preliminary evaluation of the rippability of the open pit, the type of assessment that might be performed at the feasibility or early investigation stage of a project.

The preliminary methods of rippability evaluation involve determining variations in the seismic velocity of the rock mass, where the variations are due to changes in rock properties such as density, weathering and fracturing, and by using the Modified Size-Strength Method of Pettifer and Fookes (1994), which plots the block size or discontinuity spacing against the rock material strength. A complete rippability evaluation requires rock mass properties that are obtainable from drillcore logs or outcrops, and which were reevaluated quantitatively so that the rock mass could be classified using the Rock Mass Rating (RMR) System of Bieniawski (1989). This system has been modified slightly so that the rippability of the excavation can be classified. The other method of evaluating the rippability involves prediction of the productivity of a ripping machine, following the procedures outlined by MacGregor *et al* (1994).

1.2 Thesis Objectives

This thesis provides an evaluation of the rock mass and rippability of a proposed open pit gold mine. Ripping is not a method of excavation commonly used in New Zealand, so this study provides an excellent opportunity to evaluate methods of rippability evaluation and apply them to a large database of drillhole data, so that a three dimensional rock mass and rippability model of the open pit may be produced.

There are three specific objectives that are covered by this study:

- To review existing methods of rock mass and rippability classification methods to find the methods most suited for use at Globe-Progress.

- To carry out field and laboratory testing to provide necessary geotechnical parameters such as porosity and density; strength; relationship between stress and strain; and seismic and sonic velocities for rock mass characterisation.

- To analyse existing drillhole data and carry out additional surveys to develop a three-dimensional geotechnical model of the open pit that may assist pit development.

1.3 The study area

1.3.1 Regional Setting

The Reefton Goldfield lies in the western foothills of the Victoria Ranges and extends from Larry's Creek in the north to the Grey River in the south (Figure 1.1). The Inangahua River bisects the goldfield, and most creeks in the goldfield eventually drain into either the Inangahua River or Grey River.

The goldfield is located with the Buller Terrane, one of two tectonostratigraphic terranes in Northwest Nelson (Figure 1.2). Basement rocks in the Buller Terrane consist of Ordovician Greenland Group metasediments (Cooper, 1974; Adams *et al*, 1975), Early Devonian Reefton Group shallow marine sediments (Bradshaw and Hegan, 1983), and Late Palaeozoic granitoids from the Karamea Batholith (Cooper, 1989). Overlying the basement rocks are Cretaceous to Tertiary conglomerates, coal measures and mudstones; Pleistocene glacial and fluvioglacial deposits; and recent river gravels (Suggate, 1957). All units are discussed below.

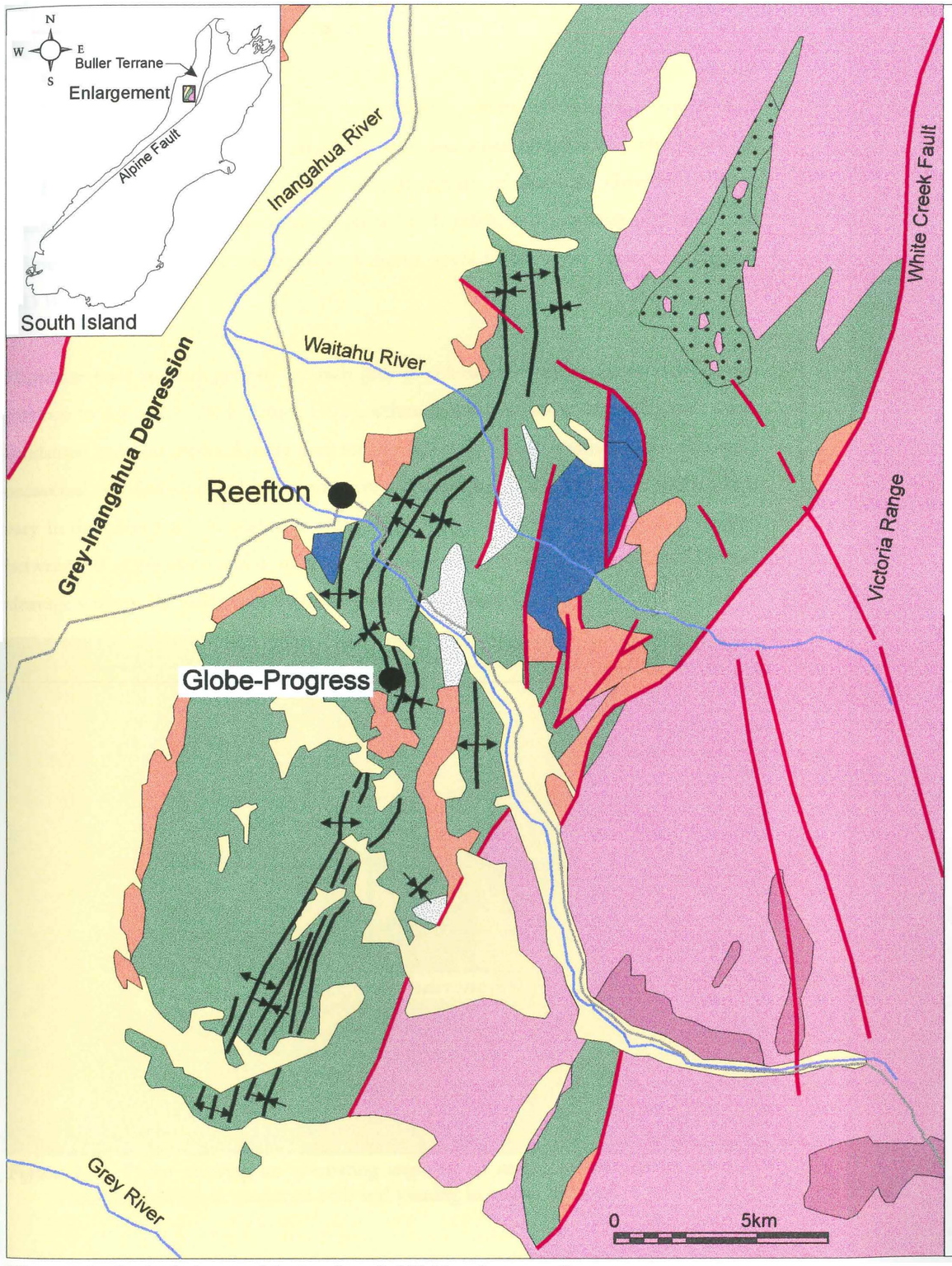

Geology of the Reefton Goldfield

Geological Legend	Formation	Age
Weathered greywacke and schist conglomerate, glacial and fluvioglacial deposits, recent river gravels.		Quaternary
Conglomerate, sandstone, siltstone and coal. Marine siltstone. Quartzose sandstone, carbonaceous mudstone and coal.	Rotokohu Coal Measures Kaiata Formation Brunner Coal Measures	Tertiary
Conglomerate and Breccia Volcanogenic sandstone, mudstone and coal.	Hawks Crag Breccia Topfer Formation	Cretaceous Triassic
Quartzite, fossiliferous mudstone and muddy limestone	Reefton Formation	Devonian
Undifferentiated Karamea Batholith granitoids	Karamea Batholith	Devonian, Carboniferous and Cretaceous
Weakly metamorphosed quartzose sandstone and argillite (thermal metamorphism indicated by dots).	Greenland Group	Ordovician
Metasedimentary gneiss and migmatite.	Victoria Paragneiss	Ordovician
Fold Fault		

Modified from Barry, 1993

Figure 1.2: Geological map of the Reefton Goldfield and surrounding area.

1.3.1.1 The Greenland Group

Greenland Group metasediments outcrop discontinuously from Milford Sound in the south to Karamea in the north. The metasediments consist of alternating sequences of Ordovician indurated mudstones (argillites) and sandstones (greywackes) interpreted by Laird (1972) to be turbidite successions. Northeast of Reefton, Greenland Group sediments have been thermally metamorphosed to hornfels, and southeast of Reefton the sediments have been metamorphosed to a higher grade to form the Victoria Paragneiss (SD Weaver, *pers com*).

Mudstone beds are dark grey to greenish grey in colour and vary in thickness from thin partings to 4.5 metres thick (Laird, 1972), although most are about 20 millimetres thick. Sandstone beds are predominantly grey to greenish grey, fine to medium grain size, with occasional very fine sand and coarse and very coarse grains (Laird, 1972). Sandstone beds vary in thickness from 40 millimetres to greater than 9 metres, with most beds ranging between 30 centimetres and 1 metre. The mudstones have a well developed fracture cleavage whereas the sandstones have well developed jointing (Figure 1.3).

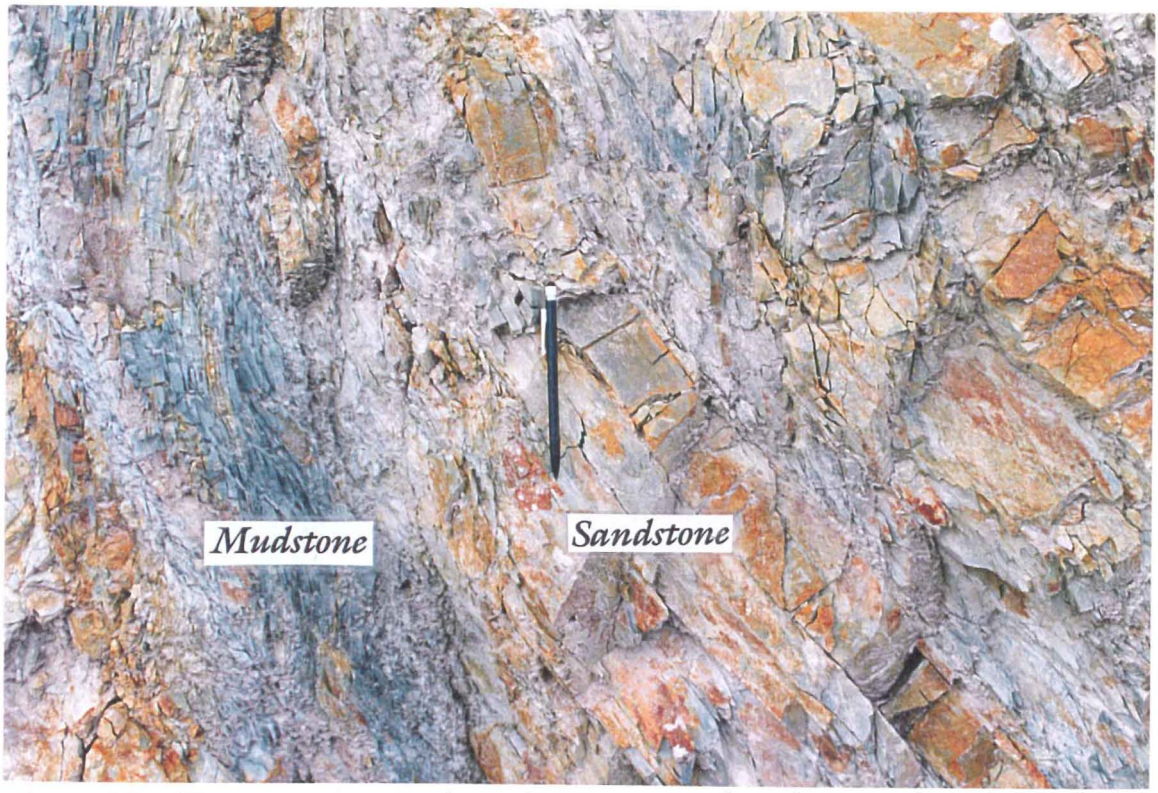

Figure 1.3: Photo showing an alternating sequence of mudstone and sandstone beds. Note the cleavage in mudstone beds and jointing in sandstone beds.

Petrographic studies by Laird (1972), Laird and Shelley (1974), Nathan (1976) and Cooper and Craw (1992) show that the Greenland Group has undergone low grade metamorphism, with the clay matrix being recrystallised to sericitic muscovite. The predominance of angular quartz clasts, occasional feldspar clasts and detrital clasts of tourmaline, zircon, apatite and muscovite indicates that the provenance was an acidic granitic source (Laird, 1972; Cooper and Craw, 1992); and the inclusion of lithic clasts of chert and mica rich pelites suggests the source rock was most likely to be a quartzose metasediment that originated from a granitic source (Nathan, 1976; Cooper and Craw, 1992).

1.3.1.2 The Karamea Batholith

The granitoids in the Karamea Batholith form the Victoria Ranges east of Reefton and part of the Paparoa Range west of Reefton. The batholith is divided into two suites, the Karamea Suite (Carboniferous and Devonian) and the Rahu Suite (Early to Mid Cretaceous). The Karamea Suite Granitoids contain both I and S type intrusives of biotite and muscovite granites, granodiorites and tonalites, whereas the Rahu Suite Granitoids are mainly I-S intermediate type intrusives of biotite granodiorites and muscovite granite (Muir *et al*, in press). Karamea Suite Granitoids form most of the Karamea Batholith and intrude into the Greenland Group. The Rahu Suite Granitoids intrude as high level plutons and stocks adjacent to and within the batholith.

1.3.1.3 The Reefton Group

The Reefton Group is found west and southwest of Reefton and contains Lower Devonian fossiliferous mudstone, flaggy limestone and quartzite in fault bounded outliers (Bradshaw and Hegan, 1983). A thick sandstone unit (Murray Creek Formation) is overlain by an alternating sequence of limestone (Forgotten Limestone, Lankey Limestone, Yorkey Limestone and Pepperbush Limestone) and mudstone (Bolitho Mudstone, Adam Mudstone, Ranft Mudstone and Alexander Mudstone) formations, which are in turn overlain by a thin quartzite unit (Kelly Sandstone). The outliers lie unconformably on Greenland Group rocks and are not penetrated by the mineralised quartz lodes found in the Greenland Group.

1.3.1.4 The Hawks Crag Breccia and Topfer Formation

The Hawks Crag Breccia and Topfer formation were originally mapped as units belonging to the Cretaceous Pororari Group (Bowen, 1964), but Raine (1980) found Mid and Late Triassic flora in the Topfer Formation to the east of Reefton. The Topfer Formation consists of volcanogenic sandstone and mudstone and minor coal seams and occurs in faulted outliers. The Late Cretaceous Hawks Crag Breccia outcrops south and east of Reefton in normal fault bounded grabens. It is composed largely of granitic clasts with minor amounts of hornfelsic Greenland Group clasts and is assigned to the Pororari Group (Raine, 1984).

1.3.1.5 Tertiary Deposits

Tertiary sediments in the Reefton Goldfield are divided into Mid Eocene Brunner Coal Measures, Mid to Late Eocene Kaiata Formation and Pliocene Rotokohu Coal Measures (Barry, 1993). The Brunner Coal Measures occur on the east side of the Inangahua Depression and south of Reefton as sequences of basal conglomerate, quartzose sandstone, sandstone, carbonaceous mudstone and coal (Suggate, 1957). The Kaiata Formation conformably overlies the Brunner Coal Measures, ranging between glauconitic siltstone with sandstone and conglomerate to conglomeratic sandstone and siltstone, and represents a change from a freshwater environment to a marine environment (Suggate, 1957). The Kaiata Formation is unconformably overlain by the Rotokohu Coal Measures northeast of Reefton and contains non-marine conglomerate, sandstone, siltstone and lignite. South of Reefton, the Rotokohu Coal Measures lie directly on Greenland Group (Suggate, 1957).

1.3.1.6 Quaternary Deposits

Overlying the Rotokohu Coal Measures, and possibly infilling the Grey-Inangahua Depression, are Early Pleistocene freshwater conglomerates and sandstones, known as Old Man Gravels (Suggate, 1957). In the Late Pleistocene piedmont glaciation and valley glaciation formed moraines and terraces within the Reefton Goldfield (Suggate, 1957). Postglacial river gravels have covered the Grey-Inangahua Depression and floodplains of other rivers in the Reefton Goldfield, and together with the glacial deposits are the source of placer gold deposits in the region.

1.3.2 Mine site setting and geology

1.3.2.1 Introduction

Globe-Progress is located on Globe Hill (see Figure 4.1 located in the map and table box), at the northern end of what Henderson (1917) called the Reefton Plateau. The proposed open pit is bound to the north by Oriental Creek and to the south by Union Creek South. Both these creeks are deeply incised and drain into Devils Creek. Tailings will be stored in Devils Creek behind a waste rock stack that will dam Devils Creek and Fossickers Creek, and a freshwater reservoir will be located in the Fossickers Creek catchment.

The mine site is located almost entirely within Greenland Group sediments. The only area not underlain by Greenland Group sediments is part of Fossickers Creek, a section of which is underlain by Tertiary Brunner Coal Measures. There is also widespread colluvium ranging in thickness from less than one metre to in excess of fifty metres on most slopes within the mine site. Descriptions of Greenland Group and Brunner Coal Measures have been given in Section 1.3.1, therefore, this section discusses structural geology, mineralisation and geotechnical studies at Globe-Progress.

1.3.2.2 Structural geology

Greenland Group sediments at Globe-Progress are dominated by medium-thick (100 to 1000 mm) bedded sandstone and mudstone, with lesser thick beds (> 1000 mm) and thin beds (30 to 100 mm; Rattenbury, 1994). Sedimentary structures such as crossbedding, grading and scouring are apparent in some places, but cleavage and shearing have overprinted and destroyed most of the earlier sedimentary structures. Cleavage is weakly developed in mudstone and very weak in sandstone (Rattenbury, 1994).

Folds at Globe-Progress are well constrained by the identification of changes in symmetry of bedding-cleavage relationships. Folds are generally close tight structures steeply inclined to the west, and the position of their axial trace is well constrained and truncated by the Globe-Progress Shear Zone. Numerous faults are identifiable in outcrops, most of which are west dipping reverse faults with a small displacement. Large faults often contain zones of pug and breccia, and may have sulphide mineralisation associated with them

(Rattenbury, 1994). They generally occur in gullies and rarely outcrop (Rattenbury, 1994) as pug and breccia erode more easily than competent Greenland Group rock.

The Globe-Progress Shear Zone is situated in a structurally complex zone near the axis of the Globe Hill Anticline and is discordant with the regional structure (Hughes, 1992; Rattenbury, 1994). The shear zone trends WNW and links the NNE trending General Gordon and Empress shear zones in the south with the Auld Creek and Bonanza shear zones north of Globe-Progress, as shown by the trend of the fold axes on Figure 1.2.

The Globe-Progress Shear Zone contains three auriferous lodes: the Oriental, Globe and Progress. The lodes are interpreted to be en echelon structures stacked above each other (Hughes, 1992). They curve concavely to the SSW with a 70° dip at the surface, flattening out with depth and terminating against the Chemist Shop Fault. The shear curves around the northern and eastern slopes of Globe Hill and is discordant to the north trending folds in the hangingwall and footwall of the shear (Figure 1.4). The sense of movement and displacement is unknown, but Rattenbury (1994) suggests displacement is greater than 500 m based on displacement of fold axes.

The Chemist Shop Fault trends NNW and dips at a high angle to the east, although the sense of movement is not known. It separates distinctly different sedimentary facies; to the east are thin to thick bedded sandstone and mudstone; and to the west are very thin to thin bedded sandstone layers (Rattenbury, 1994; Figure 1.5). Despite considerable exploration during mining and later in the 1930s, the continuation of the shear zone west of the Chemist Shop Fault has not been discovered.

1.3.2.3 Structural domains

Barrell (1992), based on geotechnical line mapping of outcrops at Globe-Progress, divided the open pit area into eight structural domains based on differences in bedding and fold axes orientation, (Appendix C). Barrell inferred the position of nine faults and eleven fold axes on the surface, noting that there may be more that were not exposed at the time of mapping.

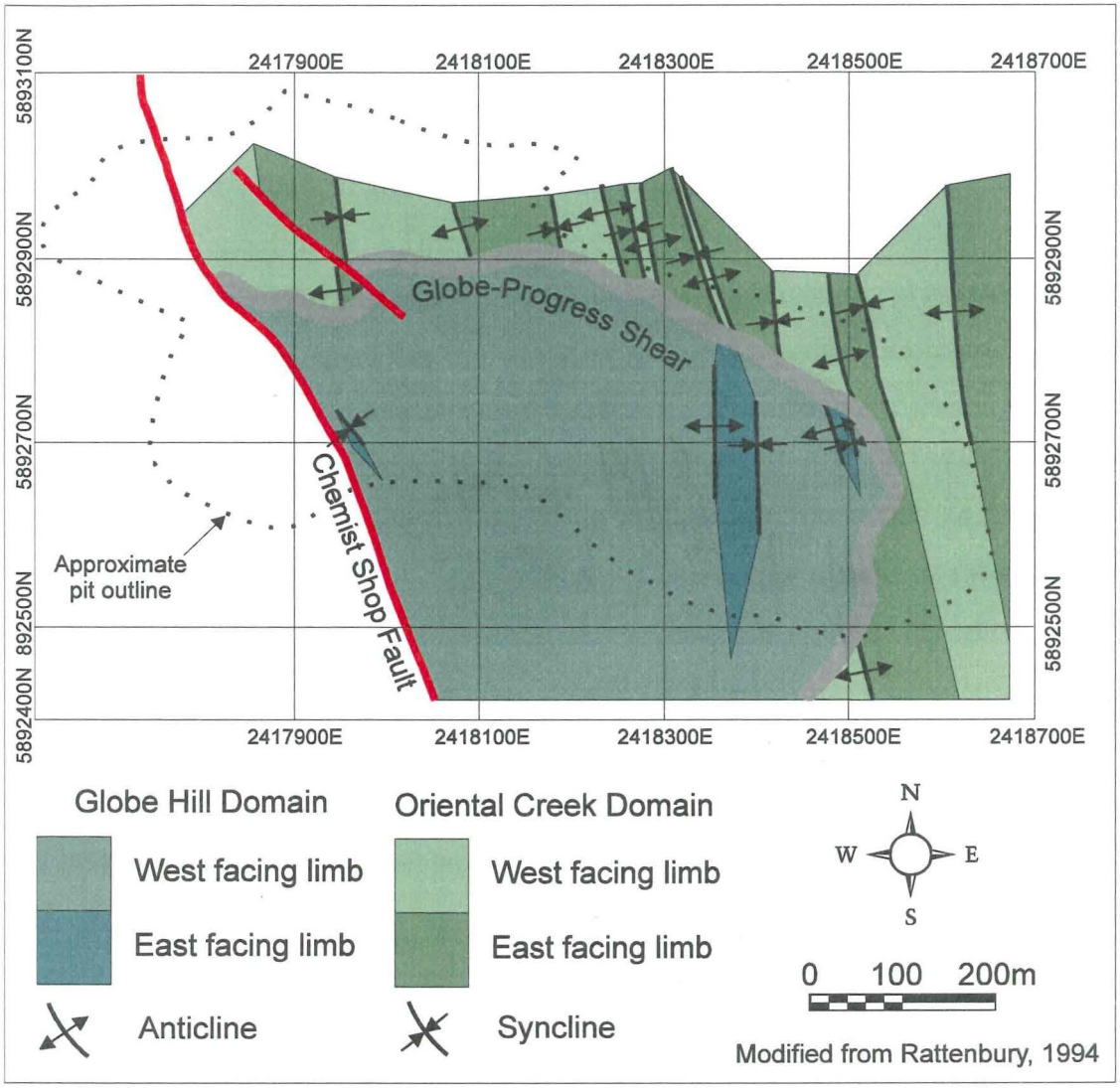

Figure 1.4: Rattenbury's (1994) structural domain plan. The coordinates follow the New Zealand Map Grid (NZMG).

Rattenbury (1994) simplified the open pit site into two structural domains separated by the Globe-Progress Shear Zone. The Globe Hill Domain is the hangingwall block of the Globe-Progress Shear and the Oriental Creek Domain is the footwall block. Both domains have been further subdivided into west and east facing fold limbs (Figure 1.4).

1.3.2.4 Mineralisation at Globe-Progress

Mineralisation at Globe-Progress occurs in the form of a gold-antimony-arsenic (Au-Sb-As) deposit (Hughes, 1992). There are four types of ore: sulphide bearing quartz veins (largely extracted by previous mining); quartz breccia; pug breccia; and host rock breccia (Barry, 1994). CRAE found that mineralisation occurred in a disseminated sulphide halo that shows evidence of post mineralisation brecciation, deformation and shearing (Hughes, 1992) resulting in mineralisation within sulphide rich pug zones, as disseminations in sulphide bearing sediments, and in quartz veins (Figure 1.6). The main sulphide bearing minerals are arsenopyrite, pyrite and stibnite. Gold occurs mainly as submicroscopic inclusions in fine pyrite and arsenopyrite crystals, and rarely as free gold (Hughes, 1992).

The mineralisation is thought to have formed during the Greenland Tectonic event (Late Ordovician to Silurian), when the Greenland Group rocks were subjected to greenschist facies metamorphism, which initiated the flow of metamorphic fluids that resulted in gold and arsenic mineralisation. The stibnite (antimony) mineralisation occurred at a later stage, but before the Late Devonian (Hughes, 1992). The Reefton Goldfield is similar to goldfields in the Lachlan Fold Belt in Central Victoria, Australia, where identical mineralisation styles occur (Hughes, 1992).

1.3.2.5 Mine site geotechnical investigations

Two major geotechnical studies have been performed on the mine site, one by Coffey and Partners (1989) on behalf of CRAE and the other by Dight and Cadman (1992) for Macraes. Information in these reports have been largely superseded in subsequent work by Rattenbury (1994; structural mapping), Beetham and Coote (1994; geotechnical relogging and systematic point load strength testing of selected drillcore) and Beetham and Richards (1995; assessment of open pit geometry), and so is not discussed.

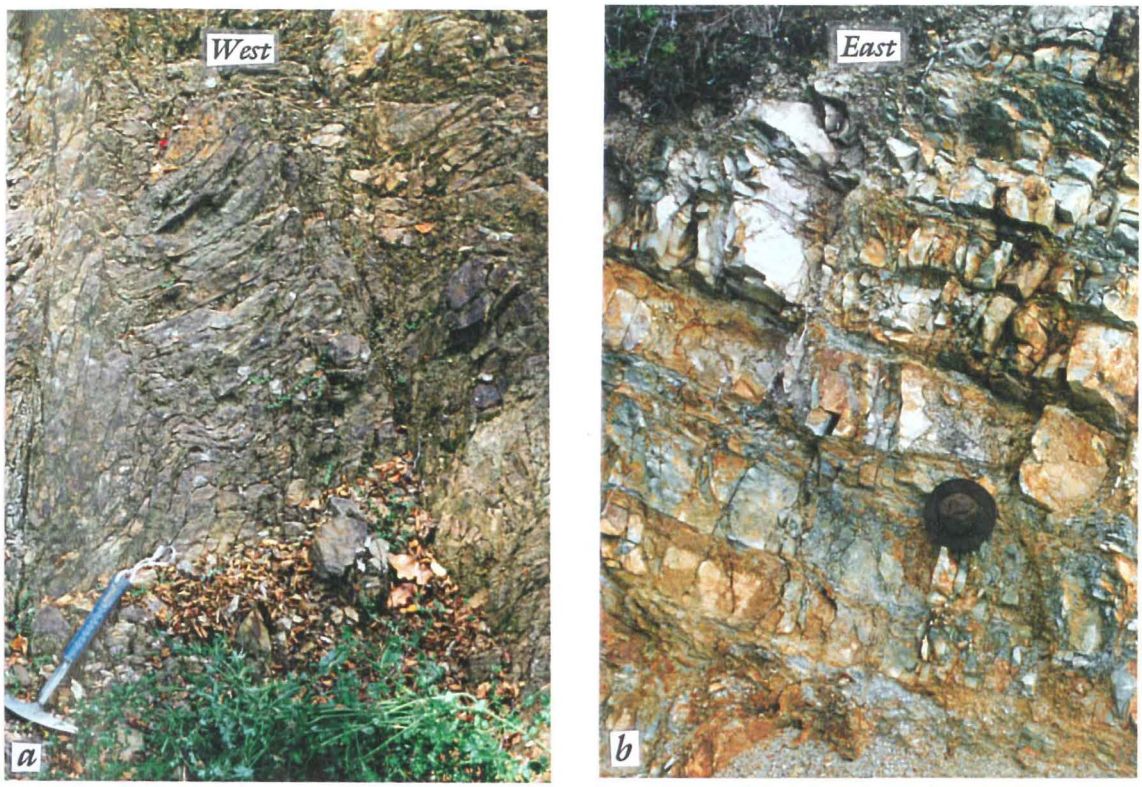

Figure 1.5: Contrasting sedimentary facies on either side of the Chemist Shop Fault. West (*a*) of the Chemist Shop Fault are very thin to thin bedded sandstone layers, intensely folded, whereas east of the Chemist Shop Fault (*b*) are thin to thick bedded sandstone and mudstone layers.

Figure 1.6: Typical view of Globe-Progress Shear Zone with a geological hammer for scale. Mineralisation at this location is composed of host rock breccia and pug breccia.

Rattenbury (1994) concluded that:

- Bedding surfaces are the most dominant penetrative discontinuity, and that they mostly dip at a shallow to moderate angle to the west in Globe Hill Domain (hanging wall domain).
- The Oriental Creek Domain (footwall domain) is more complexly folded and contains more steeper dipping folds and shear zones than the Globe Hill Domain.
- Shear zones are either steeply dipping or subparallel to bedding and fold axial planes are typically sheared, especially synclines.
- Rock structures in the western wall are not well known due to a lack of outcrop and drillcore data but the structural change across the Chemist Shop Fault is significant, with the western side containing thinly bedded sandstone facies and the eastern side containing medium bedded sandstone facies.

Beetham and Coote (1994) found:

- Rock masses in the western wall are highly sheared because of the presence of the Chemist Shop Fault.
- The Globe-Progress Shear is a zone of very poor rock mass quality 15 to 58 metres wide.
- The footwall rock mass appears to be of better quality than the hanging wall rock.
- Rock material strengths are greater than previously thought, with $I_{s\ (50)}$ = 4.9 MPa for sandstone and 2.9 MPa for mudstone.
- Much of the core has a distinctive drilling-induced breakage that are often logged as natural fractures, thereby giving the core lower than expected discontinuity spacing and RQD values.
- Effects of weathering on rock material occur to a depth of approximately 30 metres and weathering along discontinuities extend to greater depths.

Beetham and Richards (1995) concluded:

- The pit can be divided into three general sectors based on rock mass quality: the footwall or northern sector; the hangingwall or southern sector; and the western end or Chemist Shop Fault sector.

- Stability analyses on the pit slopes using the Modified Hoek-Brown failure criterion (Hoek and Brown, 1980) and a bench angle of 47° give factors of safety greater than 1 for all walls except the western wall, where the bench angles should be reduced to approximately 35°.
- The assessment of pit slope angles in Greenland Group rocks is supported by natural slopes in the Reefton area that have shown very few signs of slope failure, even under strong seismic loading (MM VIII-IX) and, seismic shaking greater than MM IX has a low probability of occurring during the expected mine life.

1.3.3 Seismic hazard assessment of the goldfield

The Reefton Goldfield is located in a region of moderately high seismicity, approximately 35 km west of the Alpine Fault. Within the region are numerous active faults trending approximately north-south (Figure 1.2), and two faults in the region have had major earthquakes on them this century. The Glasgow and Rotokohu Faults moved during the M_s7.4 1968 Inangahua earthquake, and the White Creek Fault moved during the M_s7.8 1929 Murchison earthquake.

Both of these earthquakes caused strong shaking of MM VIII-IX in the Reefton region, but there were no major slope failures in the Globe-Progress area (Beetham and Richards, 1995), although some buildings in Reefton suffered structural damage. A hazard assessment study by Hancox and Beanland (1994) found active faults and structures in the Reefton area that could cause intense shaking if they were to move, but no active faults or structures were found on the mine site. Smith and Berryman's 1983 earthquake hazard map of New Zealand suggests that MM VII shaking on the mine site would occur once every 20-50 years, MM VIII shaking would occur once every 100 years and MM IX shaking would occur once every 500 years. Therefore it is unlikely that shaking similar to that experienced in 1929 and 1968 will occur during the expected mine life.

1.3.4 Region and mine site climate and vegetation

Reefton is located on the edge of the Grey-Inangahua Depression, bordered to the west by the Paparoa Ranges, and to the east by the Victoria Range (Figure 1.2). The depression experiences warm to hot temperatures in summer and cold temperatures in winter. The Paparoa Ranges act as a wind and rain shelter against the prevailing southwest wind, although the predominant rain-bearing wind comes from the northwest. Rainfall and rainfall intensity at Globe-Progress is higher than at Reefton because of Globe-Progress' higher elevation and position further inland (Table 1.1; Woodward Clyde, 1994). Snow rarely falls at Reefton, but is more common at Globe-Progress. Severe frosts and thick fog are common at both Reefton and Globe-Progress.

Table 1.1: Summary of climate data from weather stations at Globe-Progress (560 m), Reefton (240 m) and Westport (4 m). The seasonal means have been calculated from seasons with complete data. The Globe-Progress annual mean was based on 1991 and 1992 data (the only years with complete data). Data has been summarised from Woodward-Clyde (1994).

Climate Station	Data period	Mean annual rainfall (mm)	Seasonal distribution (mm)			
			Summer	Autumn	Winter	Spring
Globe-Progress	1989-1993	2194	534	372	716	475
Reefton	1960-1993	1982	427	467	538	551
Westport	1944-1980	2192	508	565	552	567

The mine site is located within Victoria Forest Park on Department of Conservation estate. The area to be affected by the mine site is mainly covered in regenerating beech forest, but podocarp (mainly rimu) forest occur along ridge lines and should not be affected by the mine (Parry, 1993). On some of the lowlands, areas of pakihi (swampy, depleted growth) are common.

1.3.5 Historical Overview of the goldfield

A historical overview of the Reefton Goldfield is beyond the scope of this thesis, but a brief review of previous geological investigations, history of mining and the archaeological significance of the area, placing particular emphasis on Globe-Progress, are included as Appendix A.

1.4 Investigation methodology

1.4.1 Rock mass characterisation

A search through the literature was undertaken to find the most appropriate rock mass classification and rippability evaluation methods for use on the proposed open pit. It was decided to perform two simple tests (seismic velocity determination and size-strength determination) that may be performed at the feasibility or early site investigation stage of a project and to compare these results with Bieniawski's 1989 RMR System; Weaver's 1975 Rippability Rating System and a modified version of this system; and MacGregor *et al's*, 1994 Productivity Prediction Method that could be performed during the investigation or design stages of a project.

1.4.2 Geotechnical investigations

A combination of field tests and laboratory tests were performed to characterise the rock mass and rock material in order to provide additional data for rock mass and rippability classifications. Field investigations involved performing seismic velocity tests at Globe-Progress and General Gordon, collecting samples for strength and slake durability tests, and inspections of most outcrops and drillcore. Laboratory tests involved determining unweathered rock material properties such as porosity, density, sonic velocity, point load strength and uniaxial compressive strength on core, and strength and slake durability tests on slightly and moderately weathered irregular samples.

The primary field investigation method involved performing seismic velocity tests on the rock mass at Globe-Progress and General Gordon (proposed site of the waste rock stack, but also containing significant quantities of ore that may be extracted). Fifteen seismic refraction traverse lines were performed at Globe-Progress and five seismic refraction lines were carried out at General Gordon. The seismic refraction surveys were performed so that a preliminary rippability assessment could be estimated, and so that seismic velocities could be used in more detailed rippability assessments and compared to sonic velocities determined from drillcore samples.

Core samples were tested for the following geotechnical parameters: porosity, density, sonic velocity, strength and strain. Both uniaxial compressive strength and point load strength tests were performed on core to find a correlation between the two and to compare the correlation constant with published values. Where possible both diametric and axial tests were performed to find any anisotropy in the core. The sonic velocity can be compared to the seismic velocity found on the rock mass and strength test data can be compared with logged strength values to check the accuracy and consistency of drillcore logs. Porosity and density values correlate with sonic velocities and strength values, so have been determined as a check on the sonic velocity and strength data to find any highly anomalous samples. The point load test and slake-durability tests were also performed on irregular samples collected from outcrops and logged as slightly weathered, moderately weathered and highly weathered to find the effect of weathering on the strength and durability of the rock material.

1.4.3 Outcrop and drillcore analysis

Outcrops from roads, drill tracks and drill pads at Globe-Progress and General Gordon had previously been logged on a Husky data logger by Barrell (1992) using line traverse mapping, where all rock material and discontinuity data crossing a line on the outcrop surface is recorded. Graphical relogging, whereby outcrops were drawn at a scale of 1:250, by Jowett *et al* (1996) has also been also performed. Therefore, only visual inspection and photography of outcrops were required and comparisons were made with the actual logs to check for consistency in logging. Seismic refraction velocity profiles

were also compared with photo logs and graphic logs of Jowett *et al* (1996) to assist with seismic refraction interpretation.

A total of 106 diamond drillholes, totalling in excess of 17000 m in length have been drilled at Globe-Progress by CRAE and Macraes. Drillcore logs exist in graphical form and as ASCII computer files. The computer files were reanalysed using a spreadsheet so that the RMR and rippability assessments could be made. The total length of diamond drillcore from which rock mass and rippability assessments were determined was 10360 m. Only data recorded as rock mass units (RMU) were analysed, as other units lacked the data required to evaluate the rock mass. Some drillcore was inspected and compared with the drillcore logs to check for consistency in logging.

1.5 Thesis organisation

This thesis consists of six chapters and associated appendices. The first chapter lists the aims of the research and provides an introduction to the study area and methods of research. The second chapter introduces the concepts of rock mass characterisation and discusses six common rock mass classification methods, detailing the RMR System as this is the most suitable method for use on the open pit. Chapter Three introduces the concepts of rippability and discusses various factors that influence rippability. Six different methods of rippability estimation are described and their advantages and disadvantages are discussed. The fourth chapter describes the various geotechnical investigations used and summarises and discusses the results of each investigation. An analysis of the drillcore data used in the rock mass and rippability classifications is also discussed in Chapter Four. Chapter Five details the rock mass characterisation and rippability assessment performed at Globe-Progress. It first provides a preliminary rippability assessment using two methods that could be performed during the feasibility or early investigation stages of a project, then the computation of the RMR System from drillhole data, then provides a final rippability assessment using two different approaches, one involving characterising the rock mass and the other estimating the productivity of three sizes of bulldozers that might be used to rip the pit. The final chapter summarises all the results and conclusions and discusses further research and work that could be performed.

Appendix A provides a historical overview of the Reefton Goldfield, detailing previous geological and geotechnical investigations in the area, the history of mining in the Reefton Goldfield and an archeological review of Globe-Progress. Appendix B provides description sheets used by Macraes to log drillcore and outcrops; ISRM (1981) discontinuity and rock material descriptions and MacGregor's *et al* (1994) variable descriptions. Appendix C provides a map of Barrell's (1992) structural domains. Results of all tests are included as Appendix D and Appendix E discusses all the generalisations and assumptions made in calculating the RMR, rippability ratings and expected productivity of the rock mass.

Chapter 2

Rock Mass Classification Systems

2.1 Introduction

2.1.1 Background

Classification systems in general have been defined as the ordering or arrangement of objects into groups or sets on the basis of their relationships, which can be based on observable or inferred properties (Sokal, 1974). Rock mass classification systems are no different and in the last twenty years have become an essential part of the investigation and design stages of engineering projects. They are an empirical approach to design based on previous projects and case studies. Most classification systems in use today include characteristics of both rock material and discontinuities, but other classification systems only use a simple description of the rock mass, for example the Rock Load Classification System. Others may only be used for one form of excavation, for example underground excavations (RSR System or the Q System), slope stability (Slope Mass Rating System), or rippability (Weaver's 1975 Rippability Rating). Most classification systems have been designed with the prediction of tunnel support in mind, but others, such as the RMR System, are easily modified so that they may be applied to excavations, slope stability or mining projects.

In general, rock mass classification systems categorise rock masses into classes with similar geotechnical properties. To categorise the rock mass, a number of geotechnical properties are selected and quantified. These properties can normally be found from drillcore or line traverses and include rock type, grain size, weathering, fracturing, condition of discontinuities and groundwater flow. The properties are assigned ratings, depending on how much they are thought to influence the behaviour of the rock mass. The ratings may be added or multiplied according to the system used. Rock masses with similar total

ratings are expected to behave in the same way and may be used to predict the stand-up time of tunnels, slope stability parameters, rock mass deformability, type of excavation technique and so on.

Rock masses are normally classified by geologists or engineers, therefore the classification system should be designed so that anyone using a particular system will get the same result. Einstein *et al* (1983) independently classified rock masses using classification systems outlined in Section 2.2 and 2.3 and found that the classification systems were not affected by the subjectivity of the user. This study was very important as rock mass classification systems need to be reliable and reproducible.

When characterising a rock mass the observations and tests that need to be performed should be simple, rapid and relevant (Bieniawski, 1973). Most of the data should be available from drillcore logs, but other data, such as discontinuity persistence, may need to be estimated based on observations from outcrops or closely spaced drillholes (ISRM, 1981). Other factors, such as rock strength, that have been determined using one form of identification may need to be correlated with another form of testing. For example, drillcore strength values qualitatively determined by hardness methods, such as pocketknife scratch tests or relative hammer hardness (see Appendix B2 for strength definitions), need to be correlated with their uniaxial compressive strength values by quantifying the logged data with strength values determined from uniaxial compressive strength or point load strength.

Brief discussions on the main rock mass classification systems are included as Section 2.2, explaining their advantages and disadvantages and noting reasons why they were not chosen for use in classifying the rock mass in the open pit. The Rock Mass Rating (RMR) System is explained in greater detail in Section 2.3 as this method was chosen to classify the rock mass in the open pit because of its adaptability, whereby it is easily modified to classify slope stability or rippability.

2.1.2 Aims of rock mass classifications

Sokal (1974) stated that the main purpose of a classification system is to describe the structure and relationship of the constituent objects to each other and to similar objects and to simplify these relationships in such a way that general statements can be made about classes of objects. For this reason rock mass classifications have been designed to standardise site investigations and also to be used as design aids in conjunction with analytical studies, field observations and engineering judgement.

Bieniawski (1993) stated the main aims of rock mass classifications as:

- To identify the most significant parameters influencing the behaviour of a rock mass.
- To divide a particular rock mass formation into a number of rock mass classes of varying quality.
- To provide a basis for understanding the characteristics of each rock mass class.
- To derive quantitative data for engineering design.
- To recommend support guidelines for engineering projects.
- To provide a common basis for communication between engineers and geologists.
- To relate the experience on rock conditions at one site to the conditions and experience encountered at others.

2.1.3 Advantages and disadvantages

Like most classification systems, rock mass classifications have their advantages and disadvantages. If the classification system is used correctly, it can aid an engineering project considerably, but if it is used for the wrong purpose, or incorrectly, it may be counterproductive.

Bieniawski (1993) listed the major advantages and disadvantages of rock mass classifications as:

Advantages of rock mass classifications

- Improving the quality of site investigations by calling for the minimum input data as classification parameters.
- Providing quantitative information for design purposes.
- Enabling better engineering judgement and more effective communication on a project.

Disadvantages of rock mass classifications

- Using rock mass classifications as the "ultimate empirical cookbook", that is, ignoring analytical and observational design methods.
- Using one rock mass classification system only, that is, without cross-checking the results with at least one other system.
- Using rock mass classifications without enough input data.
- Using rock mass classifications without full realisation of their conservative nature and their limits arising from the database on which they were developed.

2.2 Rock mass classification systems

2.2.1 Rock Load Classification

The Rock Load Classification Method was developed by Terzaghi (1946). It was one of the first systems that evaluated rock masses, however, the method can only be used for the design of steel sets in tunnel support, therefore its use as a classification system is very limited, especially considering rock bolts and shotcrete are more commonly used as support in modern tunnels.

Terzaghi defined the rock load as the height of the mass of rock that tends to drop out of the roof. The rock load occurs in a zone of arching (Figure 2.1), above which the rock mass remains unaffected by the tunnel excavation. Terzaghi's classification system is shown in Table 2.1 and predicts support requirements for the rock load. The original scheme was modified by Deere *et al* (1970), who correlated the classification system with RQD values (see Section 2.2.2), and Rose (1982), who modified some of the rock load formulae so that the results are reduced by about 50% (Table 2.2). These formulae were adjusted because Brekke (1968) found the strength of a rock load was not affected by groundwater.

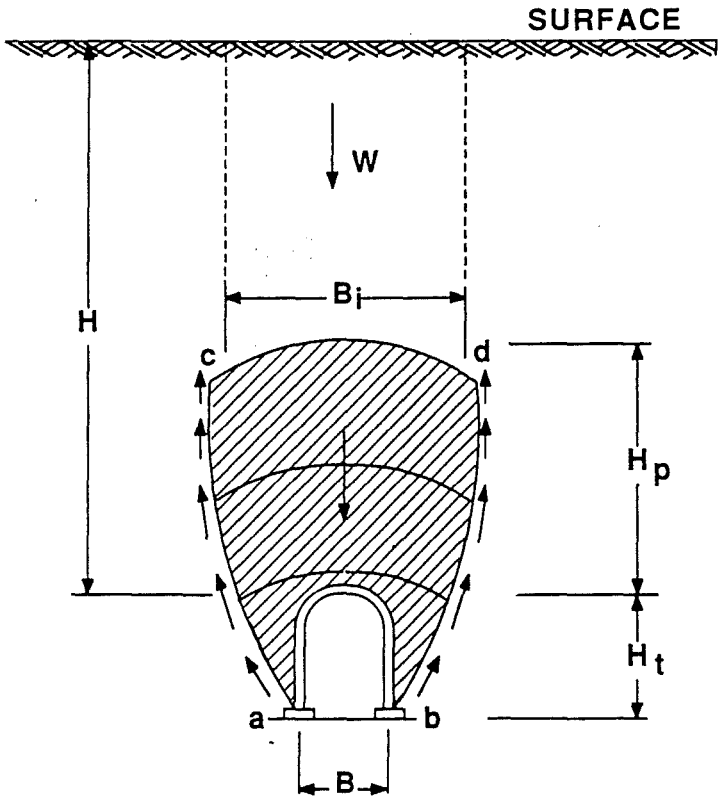

Figure 2.1: Terzaghi's rock load concept. The variables are used in formulae included in Tables 2.1 and 2.2 (from Bieniawski, 1989).

Table 2.1: Terzaghi's Rock Load Classification (after Terzaghi, 1946).

Rock condition[1]	Rock load H_p (feet)	Remarks
• Hard and intact	0	• Light lining required only if spalling or popping occurs
• Hard stratified or schistose	0 - 0.5 B	• Light support, mainly for protection against spalls. Load may change erratically from point to point
• Massive, moderately jointed	0 - 0.25 B	
• Moderately blocky and seamy	0.25B - 0.35 (B + H_t)	• No side pressure
• Very blocky	(0.35 -1.10) (B + H_t)	• Little or no side pressure
• Completely crushed	1.10 (B + H_t)	• Considerable side pressure. Softening effects of seepage toward bottom of tunnel require either continuous support for lower ends of ribs or circular ribs
• Squeezing rock, moderate depth	(1.10 - 2.10) (B + H_t)	• Heavy side pressure, invert struts required. Circular ribs are recommended
• Squeezing rock, great depth	(2.10 - 4.50) (B + H_t)	
• Swelling Rock	up to 250 feet irrespective of the value of (B + H_t)	• Circular ribs are required. In extreme cases, use yielding support.

[1]*Definitions:*

Intact rock contains neither joints nor hair cracks. Hence, if it breaks, it breaks across sound rock. On account of the injury to the rock due to blasting, spalls may drop off the roof several hours or days after blasting. This is known as a spalling condition. Hard, intact rock may also be encountered in the popping condition involving the spontaneous and violent detachment of rock slabs from the sides or roof.

Stratified rock consists of individual strata with little or no resistance against separation along the boundaries between strata. The strata may or may not be weakened by transverse joints. In such rock, the spalling condition is quite common.

Moderately jointed rock contains joints and hair cracks, but the blocks between joints are locally grown together or so intimately interlocked that vertical walls do not require lateral support. In rocks of this type, both spalling and popping conditions may be encountered.

Blocky and seamy rock consists of chemically intact or almost intact rock fragments that are entirely separated from each other and imperfectly interlocked. In such rock, vertical walls may require lateral support.

Crushed but chemically intact rock has the character of a crusher run. If most or all of the fragments are as small as fine sand grains and no recementation has taken place, crushed rock below the water table exhibits the properties of a water-bearing sand.

Squeezing rock slowly advances into the tunnel without perceptible volume increase. A prerequisite for squeeze is a high percentage of microscopic and submicroscopic particles of micaceous minerals or of clay minerals with a low swelling capacity.

Swelling rock advances into the tunnel chiefly on account of expansion. The capacity to swell seems to be limited to those rocks that contain clay minerals such as montmorillonite, with a high swelling capacity.

Table 2.2: Modified Rock Load Classification (from Bieniawski, 1989).

Rock condition	RQD	Rock load H_p (feet)	Remarks
• Hard and intact	95 - 100	0	• Same as Terzaghi (1946)
• Hard stratified or schistose	90 - 99	0 - 0.5 B	• Same as Terzaghi (1946)
• Massive, moderately jointed	85 - 95	0 - 0.25 B	• Same as Terzaghi (1946)
• Moderately blocky and seamy	75 - 85	0.25B - 0.20 (B + H_t)	• Formulae and support required is reduced by about 50% from the values of Terzaghi because the water table has little effect on rock load (Brekke, 1968)
• Very blocky and seamy	30 - 75	(0.20 -0.60) (B + H_t)	
• Completely crushed but chemically intact	3 - 30	(0.60 - 1.10) (B + H_t)	
• Sand and gravel	0 - 3	(1.10 - 1.40) (B + H_t)	
• Squeezing rock, moderate depth	NA	(1.10 - 2.10) (B + H_t)	• Same as Terzaghi (1946)
• Squeezing rock, great depth	NA	(2.10 - 4.50) (B + H_t)	• Same as Terzaghi (1946)
• Swelling Rock	NA	up to 250 feet irrespective of the value of (B + H_t)	• Same as Terzaghi (1946)

2.2.2 Rock Quality Designation Index

The Rock Quality Designation (RQD) Index was proposed by Deere (1967) to provide an indication of rock mass quality from drill core. The RQD is defined as the length of sound core recovered with pieces greater than 100 mm, expressed as a percentage of the total length drilled. It is a modification of the core recovery percentage, which is the total length of core recovered as a percentage of the total length drilled. Figure 2.2 illustrates how the RQD index is calculated.

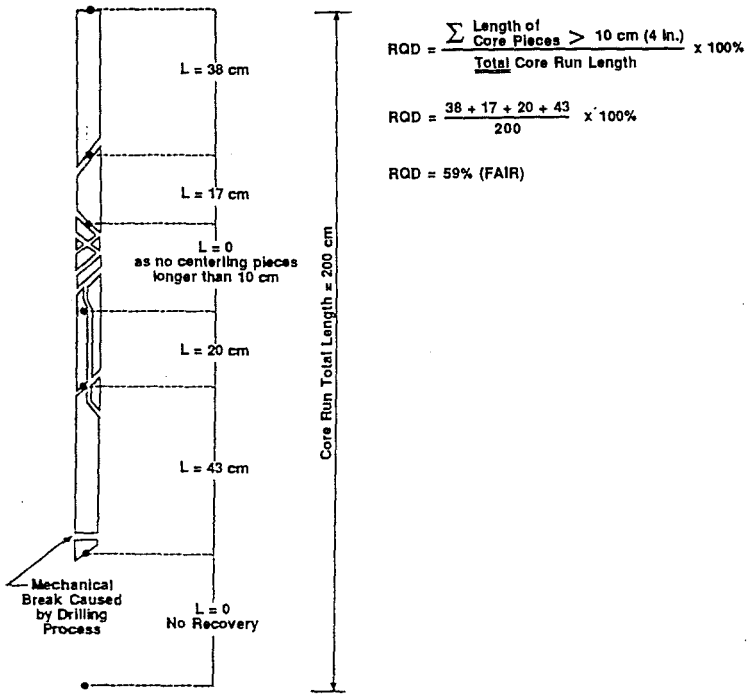

Figure 2.2: Calculation of the RQD Index. Note that measurement of the core is along the centreline according to ISRM standards (1981).

Only sound (or hard) core with lengths greater than 100 mm is used, and only natural fractures are recognised as breaks in the core. If the core is highly weathered, brecciated or fault gouge, then the RQD should be 0 (Bieniawski, 1989). Core diameters should be at least NX (54.7 mm) size so that good core recovery is possible. RQD should be calculated from drill core but if drill core is not present, or if line traverse mapping is performed, then the RQD may be estimated from Barton *et al's* (1974) empirical expression:

$$RQD = 115 - 3.3J_v$$

where J_v is the number of joints per cubic metre or, if the discontinuities are randomly distributed through a rock mass, then the RQD can calculated from the discontinuity spacing using Priest and Hudson's (1976) theoretical equation:

$$RQD_{Theoretical} = 100e^{-0.1I_f}(0.1I_f + 1) \quad (\%)$$

where e is the natural log and I_f is the discontinuity spacing index measured in metres. Deere (1968) found RQD to be a more sensitive and consistent indicator of general rock quality than the core recovery percentage, and so proposed a general relationship between the RQD Index and rock mass quality:

RQD (%)	Rock Quality
< 25	Very Poor
25 - 50	Poor
50 - 75	Fair
75 - 90	Good
90 - 100	Excellent

The RQD index is simple to calculate but it is only a measure of the fracture frequency, and so does not fully describe a rock mass as it ignores the influence of discontinuity orientation, persistence and infilling. For this reason, it is used as a standard parameter in drill core logging and also as a parameter in two major rock mass classification systems, the Q System (discussed in Section 2.2.4) and the RMR System (discussed in Section 2.3).

2.2.3 Rock Structure Rating System

The Rock Structure Rating (RSR) System was developed in 1972 and modified in 1974 by Wickham *et al* (1972, 1974). The RSR System was unique at the time of development because it is quantitative (rather than qualitative like Terzaghi's Rock Load Classification) and incorporated a suite of geotechnical parameters (unlike the RQD Index, which is limited to core quality). The system also empirically selects an appropriate form of ground support.

The RSR System requires both geological and geotechnical parameters, which are simplified into three parameters (Table 2.4). Parameter A is a rock structure rating, Parameter B considers the effects of discontinuities and Parameter C considers the effect of groundwater flow. The three parameters are totalled to give an RSR value out of 100.

Table 2.4: Rock Structure Rating System (after Wickham, 1974).

Parameter A: General area geology

	Basic Rock Type			
	Hard	Medium	Soft	Decomposed
Igneous	1	2	3	4
Metamorphic	1	2	3	4
Sedimentary	2	3	4	4

	Geological structure			
	Massive	Slightly faulted or folded	Moderately faulted or folded	Intensely faulted or folded
Rock Type 1	30	22	15	9
Rock Type 2	27	20	13	8
Rock Type 3	24	18	12	7
Rock Type 4	19	15	10	6

Parameter B: Joint pattern and direction of drive

Average joint spacing	Strike perpendicular to axis Direction of drive With dip			Direction of drive Against dip		Strike parallel to axis Direction of drive With dip		
	Dip of Prominent joints[1]			Dip of Prominent joints[1]		Dip of Prominent joints[1]		
	Flat	Dipping	Vertical	Dipping	Vertical	Flat	Dipping	Vertical
Very closely jointed (< 2 in)	9	11	13	10	12	9	9	7
Closely jointed (2 - 6 in)	13	16	19	15	17	14	14	11
Moderately jointed (6 - 12 in)	23	24	28	19	22	23	23	19
Moderate to blocky (1 - 2 ft)	30	32	36	25	28	30	28	24
Blocky to massive (2 - 4 ft)	36	38	40	33	35	36	34	28
Massive	40	43	45	37	40	40	38	34

[1]Dip: flat = 0 - 20°; dipping = 20 - 50°; vertical = 50 - 90°

Parameter C: Groundwater and joint condition

Anticipated water inflow (gpm/1000 feet)[1]	Sum of parameters A + B					
	13 - 44			45 - 75		
	Joint condition[2]					
	Good	Fair	Poor	Good	Fair	Poor
None	22	18	12	25	22	18
Slight (< 200 gpm)	19	15	9	23	19	14
Moderate (200-1000 gpm)	15	11	7	21	16	12
Heavy (> 1000 gpm)	10	8	6	18	14	10

[1]gpm = gallons per minute

[2]Joint condition: Good = tight or cemented; fair = slightly weathered or altered; poor = severely weathered, altered or open.

The system estimates the type of support required assuming the excavation technique will be blasting. If tunnel boring machines (TBMs) are used for excavation rather than drill and blast methods, then less support would be required and the RSR may be adjusted by a factor related to the tunnel diameter (Wickham, 1974). The RSR is correlated to support requirements by the rib ratio (RR), which is a factor related to the theoretical support required. Structures with RSR values less than 19 will require heavy support and structures with RSR values greater than 80 should stand unsupported.

Like the Rock Load Classification, RSR prediction is developed primarily for tunnels requiring steel rib support and therefore the system should not be used for any other type of prediction. Wickham *et al* (1972, 1974) did not clearly define parameters A, B and C, therefore this may lead to considerable confusion in defining a rock mass. Sinha (1988) showed that to calculate the rib ratio, Terzaghi's rock load and steel rib spacing are required, and therefore the RSR System may be considered an improvement on Terzaghi's Rock Load Classification rather than an independent system.

2.2.4 The Q System

The Q system, also known as the Norwegian Geotechnical Institute (NGI) Classification, was developed by Barton *et al* (1974). The system is based on 212 case studies from Scandinavia, and, like the RSR and RMR systems, it is a quantitative classification system. The Q System uses six parameters that are multiplied by each other to give the rock quality variable Q:

$$Q = \left(\frac{RQD}{J_n}\right)\left(\frac{J_r}{J_a}\right)\left(\frac{J_w}{SRF}\right)$$

where RQD is the rock quality designation, J_n is the joint set number, J_r is the joint roughness value, J_a is the joint alteration value, J_w is the joint water reduction number and SRF is the stress reduction factor. The first two variables (RQD/J_n) represent the overall structure of the rock mass and gives a measure of the block size; J_r/J_a estimates the condition and shear strength of a joint; and J_w/SRF describes the stress conditions of the rock mass. Q ranges from 0.001 through to 1000 on a logarithmic scale and classification parameters and ratings are shown in Table 2.5.

Barton *et al* (1974) noted that the six parameters make tunnel stability prediction simple, but if the rock mass prediction was for drillability, ease of excavation or slope stability, then the first four parameters (RQD, J_n, J_r, J_a) could form the basis of a rock mass classification, although the ratings may need adjusting and other parameters, such as joint orientation, may need to be added. This was done by Kirsten (1982) who modified the Q system for use in surficial excavations, and Kirsten's Excavatability Index is discussed in Section 3.5.4.

Table 2.5: Descriptions and ratings used to calculate Q (after Barton, *et al*, 1974).

A: Descriptions and ratings for RQD and J_n

1	Rock Quality designation (RQD)[1]	Rating
A	Very poor	0 - 25[2]
B	Poor	25 - 50
C	Fair	50 - 75
D	Good	75 - 90
E	Excellent	90 - 100

2	Joint set number (J_n)[3]	Rating
A	Massive, no or few joints	0.5 - 1.0
B	One joint set	2
C	One joint set plus random joints	3
D	Two joint sets	4
E	Two joint sets plus random joints	6
F	Three joint sets	9
G	Three joint sets plus random joints	12
H	Four of more joint sets, random, heavily jointed	15
I	Crushed rock, earthlike	20

[1]RQD intervals of 5, that is, 90, 95, 100 and so on, are sufficiently accurate.
[2]Where RQD is reported as <10, a nominal value of 10 is used in evaluating Q.
[3]For intersections, use 3.0(J_n); for portals, use 2.0(J_n).

B: Descriptions and ratings for J_r and J_a

3	Joint roughness number (J_r)[1]	Rating
	Rock wall contact and rock wall contact before 10 cm shear	
A	Discontinuous joints	4
B	Rough or irregular, undulating	3
C	Smooth, undulating	2
D	Slickensided, undulating	1.5
E	Rough or irregular, planar	1.5
F	Smooth, planar	1.0
G	Slickensided, planar[2]	0.5
	No rock wall contact when sheared	
H	Zone containing clay minerals thick enough to prevent rock wall contact	1.0 (nominal)
I	Sandy, gravelly or crushed zone thick enough to prevent rock wall contact	1.0 (nominal)

4	Joint alteration number (J_a)	Rating	ϕ_r (approx.)
	Rock wall contact		
A	Tightly healed, hard, non-softening, impermeable filling such as quartz or epidote	0.75	-
B	Unaltered joint walls, surface staining only	1.0	25 - 35°
C	Slightly altered joint walls. Non-softening mineral coatings, sandy particles, clay free disintegrated rock.	2	25 - 30°
D	silty or sandy clay coatings, small clay fraction (non-softening)	3	20 - 25°
E	Softening or low friction clay mineral coatings such as kaolinite or mica. Also chlorite, talc, gypsum and graphite and so on, and small quantities of swelling clays (discontinous coatings < 2 mm in thickness).	4	8 - 16°
	Rock wall contact before 10 cm shear		
F	Sandy particles, clay free disintegrated rock and so on	4	25 - 30°
G	Strongly overconsolidated, non-softening clay mineral fillings (continuous coatings < 5 mm in thickness).	6	16 - 24°
H	Medium or low overconsolidation, softening, clay minerals fillings (continuous, < 5 mm in thickness)	8	12 - 16°
I	Swelling clay fillings such as montmorillonite (continuous, < 5 mm in thickness). Value of J_a depends on the percentage of swelling clay size particles and access to water and so on.	8 - 12	6 - 12°
	No rock wall contact when sheared		
J K L	Zones or bands of disintegrated or crushed rock and clay (see G, H, I for description of clay condition).	6 8 8 - 12	6 - 24°
M	Zones or bands of silty or sandy clay, small clay fraction (non-softening).	5	6 - 24°
N O P	Thick, continuous zones or band of clay (see G, H, I for description of clay condition).	10 13 13 - 20	6 - 24°

[1]Add 1.0 if the mean spacing of the relevant joint set is greater than 3.0 m.
[2]J_r = 0.5 can also be used for planar slickensided joints having lineations, provided the lineations are favourably orientated.
[3]Values of ϕ_r are intended as an approximate guide to the mineralogical properties of the alteration products, if present.

Table 2.5(continued): Descriptions and ratings used in the Q System.

C: Description and ratings for J_w and SRF

5	Joint water reduction factor (J_w)[1]	Rating	Approximate water pressure (kg/cm²)
A	Dry excavations or minor inflow such as < 5 l / min.	1.0	< 1
B	Medium inflow or pressure occasional outwash of joint fillings	0.66	1.0 - 2.5
C	Large inflow of high pressure in competent rock with unfilled joints[2]	0.5	2.5 - 10.0
D	Large inflow or high pressure considerable outwash of joint fillings	0.33	2.5 - 10.0
E	Exceptionally high inflow or water pressure at blasting, decaying with time	0.1 - 0.2	> 10
F	Exceptionally high inflow or water pressure continuing without noticeable decay[2]	0.05 - 0.1	> 10

6	Stress reduction factor (SFR)	Rating
	Weakness zones intersecting excavation, which may cause loosening of rock mass when tunnel is excavated[3]	
A	Multiple occurrences of weakness zones containing clay or chemically disintegrated rock, very loose surrounding rock (any depth)	10
B	Single weakness zones containing clay, or chemically disintegrated rock (depth of excavation < 50m)	5.0
C	Single weakness zones containing clay, or chemically disintegrated rock (depth of excavation > 50m)	2.5
D	Multiple shear zones in competent rock (clay free), loose surrounding rock (any depth)	7.5
E	Single shear zones in competent rock (clay free; depth of excavation < 50m)	5.0
F	Single shear zones in competent rock (clay free; depth of excavation > 50m)	2.5
G	Loose open joints, heavily jointed (any depth)	5.0
	Competent rock, rock stress problems	
H	Low stress, near surface; $\sigma_c/\sigma_1 > 200$; $\sigma_t/\sigma_1 > 13$	2.5[5]
I	Medium stress; $\sigma_c/\sigma_1 = 10 - 200$; $\sigma_t/\sigma_1 = 0.66 - 13$	1.0
J	High stress, very tight structure (usually favourable to stability, may be unfavourable to wall stability); $\sigma_c/\sigma_1 = 5 - 10$; $\sigma_t/\sigma_1 = 0.33 - 0.66$	0.5 - 2.0
K	Mild rock burst (massive rock); $\sigma_c/\sigma_1 = 2.5 - 5.0$; $\sigma_t/\sigma_1 = 0.16 - 0.33$	5 - 10
L	Heavy rock burst (massive rock); $\sigma_c/\sigma_1 < 2.5$; $\sigma_t/\sigma_1 < 0.16$	10 - 20
	Squeezing rock, plastic flow of incompetent rock under the influence of high rock pressures	
M	Mild squeezing rock pressure	5 - 10
N	Heavy squeezing rock pressure	10 - 20
	Swelling rock, chemical swelling activity depending on presence of water	
O	Mild swelling rock pressure	5 - 10
P	Heavy swelling rock pressure	10 - 15

[1]Special problems caused by ice formation are not considered.

[2]Factors C and F are crude estimates. Increase J_w if drainage measures are installed.

[3]Reduce these values of SRF by 25 - 50% if the relevant shear zones only influence but do not intersect the excavation.

[4]For strongly anisotropic stress field (if measured): when $5 \leq \sigma_1/\sigma_3 \leq 10$, reduce σ_c and σ_t to $0.8\sigma_c$ and $0.8\sigma_t$; when $\sigma_1/\sigma_3 > 10$, reduce σ_c and σ_t to $0.6\sigma_c$ and $0.6\sigma_t$, where σ_c = unconfined compressive strength, σ_t = tensile strength from point load test and σ_1 and σ_3 = major and minor principal stresses.

[5]There are few case studies available where the depth of crown below the surface is less than the span width. Suggest SRF increase from 2.5 to 5 for such cases.

Table 2.5 (continued): Descriptions and ratings used in the Q System.

Notes on the use of Tables A, B and C

When making estimates of the rock mass quality (Q) the following guidelines should be followed, in addition to the notes listed in Tables A, B and C:

- When drill core is unavailable, RQD can be estimated for the number of joints per unit volume, in which the number of joints per metre for each joint set are added. A simple relation can be used to convert this number to RQD for the case of clay free rock masses:

  $$RQD = 115 - 3.3J_v$$

  where J_v is the total number of joints per cubic metre. If $J_v < 4.5$, then RQD = 100.

- The parameter J_n representing the number of joint sets will often be affected by foliation, schistocity, slaty cleavage or bedding. If strongly developed these parallel discontinuities should obviously be counted as a complete joint set. However, if there are few of these discontinuities visible, or only occasional breaks in drill core due to these features, then it will be more appropriate to count them as random joints when evaluating J_n.

- The parameters J_r and J_a (representing shear strength) should be relevant to the weakest significant joint set or clay filled discontinuity in a given zone. However, if the joint set or discontinuity with the minimum value of (J_r/J_a) is favourably orientated for stability, then a second, less favourably orientated joint set or discontinuity may sometimes be of more significance, and its higher value of (J_r/J_a) should be used when evaluating Q.

- When a rock mass contains clay, the factor SRF appropriate to loosening loads should be evaluated (Table C, 6A). In such cases, the strength of the intact rock is of little interest. However, when jointing is minimal and clay is completely absent, the strength of the intact rock may become the weakest link and the stability will then depend on the ratio of rock stress to rock strength (Table C, 6B). A strongly anisotropic stress field is unfavourable to stability and is roughly accounted for in Table C, note 4.

- In general, the compressive and tensile strengths (σ_c and σ_t) of the intact rock should be evaluated in the direction that is unfavourable for stability. This is especially important in the case of strongly anisotropic rocks. In addition, the test samples should be saturated if this condition is appropriate to present or future in situ conditions. A very conservative estimate of strength should be made for those rocks that deteriorate when exposed to moist or saturated conditions.

2.2.5 ISRM geotechnical description of rock masses

The International Society of Rock Mechanics (ISRM) developed a method of describing a rock mass and its associated discontinuities (ISRM, 1981). The rock mass is not rated like the other described methods, but geotechnical parameters of the rock mass are defined and standardised. The following ten parameters are used to describe rock masses and discontinuities:

- ***Discontinuity orientation:*** the strike (or dip direction) and dip of a discontinuity.
- ***Discontinuity spacing:*** the perpendicular distance between adjacent discontinuities and is normally expressed as the mean of a set of discontinuities.
- ***Discontinuity persistence:*** the length of discontinuity exposed in an outcrop.
- ***Discontinuity roughness:*** the surface roughness and waviness both contribute to a discontinuity's shear strength.
- ***Wall strength:*** The compressive strength of rock adjacent to a discontinuity. It is normally lower than rock material strength because of weathering and alteration of the wall.
- ***Aperture:*** The perpendicular distance between adjacent discontinuity walls.
- ***Filling:*** Material that infills between adjacent discontinuity walls. It may include air, water, rock fragments, sand, gouge, quartz, calcite and so on.
- ***Seepage:*** Water flow in the rock mass or from discontinuities.
- ***Number of discontinuity sets:*** The number of types of discontinuities in the rock mass with differing orientations.
- ***Block size:*** The size of rock material between intersecting discontinuity sets.

Descriptions and classes of each parameter are fully described in Appendix B2. The parameters form the basis of core logging descriptions, for example, compare Macraes core logging descriptions with ISRM classifications in Appendix B1 and B2, and some parameters used in rock mass classification systems, such as the RMR system to characterise the rock mass.

2.3 The RMR System

The Rock Mass Rating (RMR) system, also known as the Geomechanics Classification, was initially developed by Bieniawski (1973) and has been modified over time to conform to international standards and as more case studies become available. Bieniawski's most recent version (1989) is explained in detail in Section 2.3.2.

2.3.1 The 1973 version

Bieniawski (1973) stated that parameters in a classification system should be found during a conventional site investigation, and he therefore devised a classification system that incorporated:

- RQD
- Weathering of rock material
- Unconfined compressive strength (UCS) of rock material
- Spacing of discontinuities
- Discontinuity orientation
- Discontinuity separation
- Discontinuity continuity
- Groundwater flow

Bieniawski divided each parameter into five classes and assigned weighted ratings to each parameter (Table 2.6). The ratings used were based on those originally used by Wickham *et al* (1972) in the RSR System, but Bieniawski considers his system to be much simpler and more concise.

As more case studies and projects used the RMR System to classify rock masses, modifications were made to further refine the system (Bieniawski 1976, 1979, 1989). These changes may be viewed as either an advantage or a disadvantage of the system. It would be advantageous to use the most accurate rock mass classification, which should be the most refined system, but if a system is altered too often, site investigators and designers may not be able to keep up with the changes and a rock mass assigned to a certain rock class in an earlier system may be assigned to a different rock mass class in a later system.

Use of the wrong system may help decide whether or not an engineering project proceeds past the investigation and design stages.

Table 2.6: Bieniawski's 1973 RMR System.

Classification system

	Parameter	Class Number and its description				
		1 Very good	2 Good	3 Fair	4 Poor	5 Very poor
1	RQD (%) Rating	90 - 100 16	75 - 90 14	50 - 75 12	25 - 50 7	< 25 3
2	Weathering Rating	Unweathered 9	Slightly Weathered 7	Moderately weathered 5	Highly weathered 3	Completely weathered 1
3	Rock Strength (MPa) Rating	> 200 10	100 - 200 5	50 - 100 2	25 - 50 1	< 25 0
4	Discontinuity spacing Rating	> 3 m 30	1 - 3 m 25	0.3 - 1.0 m 20	50 - 300 mm 10	< 50 mm 5
5	Discontinuity separation Rating	< 0.1 mm 5	< 0.1 mm 5	0.1 - 1.0 mm 4	1 - 5 mm 3	> 5 mm 1
6	Discontinuity continuity Rating	Not continuous 5	Not continuous 5	Continuous No gouge 3	Continuous With gouge 0	Continuous With gouge 0
7	Groundwater inflow Rating	None 10	None 10	Slight 8	Moderate 5	Heavy 2
8	Discontinuity orientation Rating Tunnels Foundations	Very favourable 15 15	Favourable 13 13	Fair 10 10	Unfavourable 5 0	Very unfavourable 3 -10

Total ratings for rock mass classes

Class number	1	2	3	4	5
Description of class	Very good rock	Good rock	Fair rock	Poor rock	Very poor rock
Total rating	90 - 100	70 - 90	50 - 70	25 - 500	< 25

2.3.2 The 1989 version

2.3.2.1 Classification Procedure

Bieniawski's 1989 RMR System uses six major parameters to classify the rock mass:

- Strength of the rock material (either uniaxial compressive or point load strength)
- RQD
- Spacing of discontinuities
- Condition of discontinuities
- Groundwater conditions
- Orientation of discontinuities

The first step in applying the revised RMR System (Table 2.7) is to divide the rock mass into structurally similar domains. The next step is to assign ratings to the parameters. Part A of Table 2.7 groups five parameters into five classes. The various parameters are not equally important in influencing the rock mass, therefore weighted ratings are assigned to the different parameters and classes. For example, the discontinuity condition parameter is given a maximum rating of 30 whereas the groundwater condition parameter is given a maximum rating of 15. The condition of the discontinuities is thought to be twice as important as the effect of groundwater on the rock mass.

Ratings for rock material strength, RQD and discontinuity spacing classes may be determined exactly from Figures 2.3 to 2.5 rather than using the averaged ratings in Table 2.7. If either RQD or discontinuity spacing data are lacking, then Figure 2.6 can be used to estimate the missing parameter. The condition of discontinuities may be further defined using part B in Table 2.7, which uses five parameters recommended by ISRM (1981) to describe discontinuity conditions.

The sum of the five parameters returns a basic RMR value that must be adjusted for the orientation of discontinuities. The discontinuity orientation rating reduces the basic RMR to give the adjusted RMR (Table 2.7C). Definitions of the discontinuity orientation classes applicable to tunnelling, mining and rippability applications are shown in Table 2.8, along with the ratings adjustment. Note that for rippability applications the ratings are reversed, that is, a favourable discontinuity rating in a rippability application will be unfavourable in a tunnelling and mining application. For characterisation of slopes, the Slope Mass Rating (SMR) System proposed by Romana (1985) should be used. Part D of Table 2.7 groups the RMR value into one of five rock mass classes, which are in groups of 20% each. Part E of Table 2.7 shows that the RMR can be correlated to approximate values of rock mass cohesion, rock mass friction angle and average stand up time of underground excavations.

Table 2.7: The Rock Mass Rating System (Geomechanics Classification of Rock Masses). After Bieniawski (1979).

A: Classification Parameters and their ratings

Parameter			Ranges of Values						
1	Strength of intact rock material	Point load strength index ($I_{s(50)}$; MPa)	> 10	4 - 10	2 - 4	1 - 2	For this low range, the uniaxial compressive test is preferred		
		Uniaxial compressive strength (UCS; MPa)	> 250	100 - 250	50 - 100	25 - 50	5 - 25	1 - 5	< 1
	Rating		15	12	7	4	2	1	0
2	Drill core quality (RQD; %)		90 - 100	75 - 90	50 - 75	25 - 50	< 25		
	Rating		20	17	13	8	3		
3	Spacing of discontinuities		> 2 m	0.6 - 2 m	200 - 600 mm	60 - 200 mm	< 60 mm		
	Rating		20	15	10	8	5		
4	Condition of discontinuities		Very rough s urfaces No Separation Unweathered wall rock Not continuous	Slightly rough surfaces Separation < 1 mm Slightly weathered walls	Slightly rough surfaces Separation < 1 mm Highly weathered walls	Slickensided surfaces or Gouge < 5 mm thick or Separation 1 - 5 mm Continuous	Soft gouge > 5 mm thick or Separation > 5 mm Continuous		
	Rating		30	25	20	10	0		
5	Groundwater	Inflow per 10 m tunnel length (l/min)	None	< 10	10 - 25	25 - 125	> 125		
		Ratio of joint water pressure to the major principal stress	0	< 0.1	0.1 - 0.2	0.2 - 0.5	> 0.5		
		General conditions	Completely dry	Damp	Wet	Dripping	Flowing		
	Rating		15	10	7	4	0		

B: Rating classification for discontinuity conditions

Parameter	Ranges of values				
Length (persistence/continuity)	< 1 m	1 - 3 m	3 - 10 m	10 - 20 m	> 20 m
Rating	6	4	3	1	0
Separation (aperture)	None	< 0.1 mm	0.1 - 1.0 mm	1 - 5 mm	> 5 mm
Rating	6	5	4	1	0
Roughness	Very rough	Rough	Slightly rough	Smooth	Slickensided
Rating	6	5	3	1	0
Infilling (gouge)		Hard filling		Soft filling	
	None	< 5 mm	> 5 mm	< 5 mm	> 5 mm
Rating	6	4	2	2	0
Weathering	Unweathered	Slightly weathered	Moderately weathered	Highly weathered	Extremely weathered
Rating	6	5	3	1	0

C: Rating adjustment for discontinuity orientations

	Strike and Dip Orientations of discontinuities		Very Favourable	Favourable	Fair	Unfavourable	Very unfavourable
6	Ratings	Tunnels and mines	0	-2	-5	-10	-12
		Foundations	0	-2	-7	-15	-25
		Slopes	0	-5	-25	-50	-60

D: Rock mass classes determined from total ratings

Rating	81 - 100	61 - 80	41 - 60	21 - 40	< 20
Class Number	I	II	III	IV	V
Description	Very good rock	Good rock	Fair rock	Poor rock	Very poor rock

E: Meaning of the rock mass classes

Class Number	I	II	III	IV	V
Average stand-up time	20 yr for a 15m span	1 year for a 10m span	1 week for a 5m span	10hr for a 2.5m span	30 minutes for a 1m span
Cohesion of the rock mass (kPa)	> 400	300 - 400	200 - 300	100 - 200	< 100
Friction angle of the rock mass (°)	> 45	35 - 45	25 - 35	15 - 25	< 15

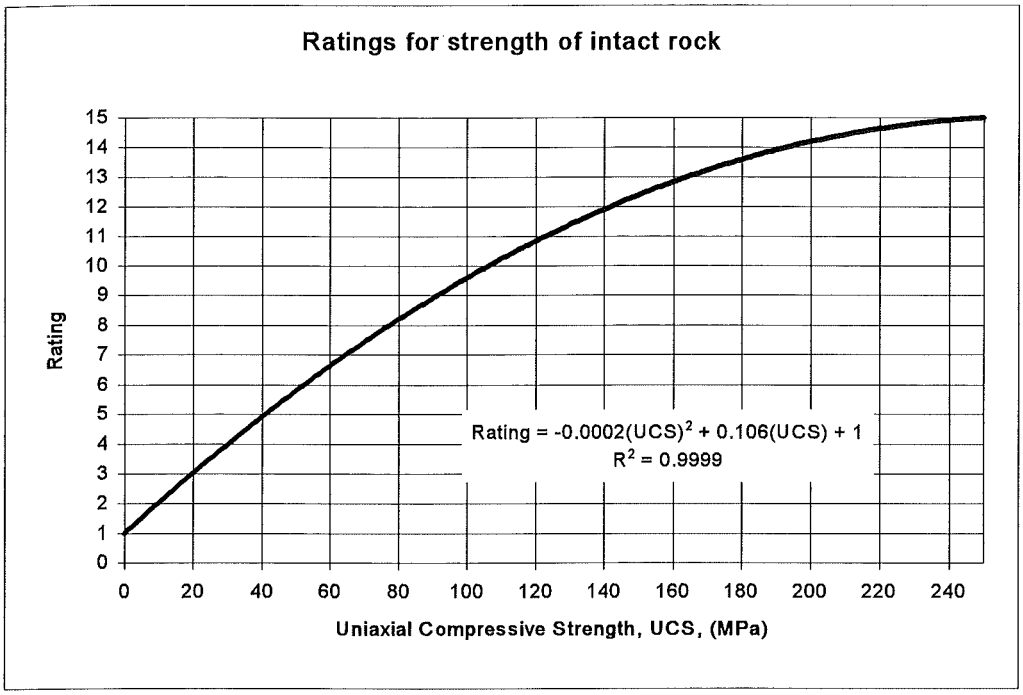

Figure 2.3: Ratings for strength of rock material (after Bieniawski, 1989). The formula may be used to calculate the strength from the rating. The formula was not provided in Bieniawski (1989), but the correlation between the curve and the formulae (R^2 = 0.9999) is excellent, and therefore can be used as a reliable estimate.

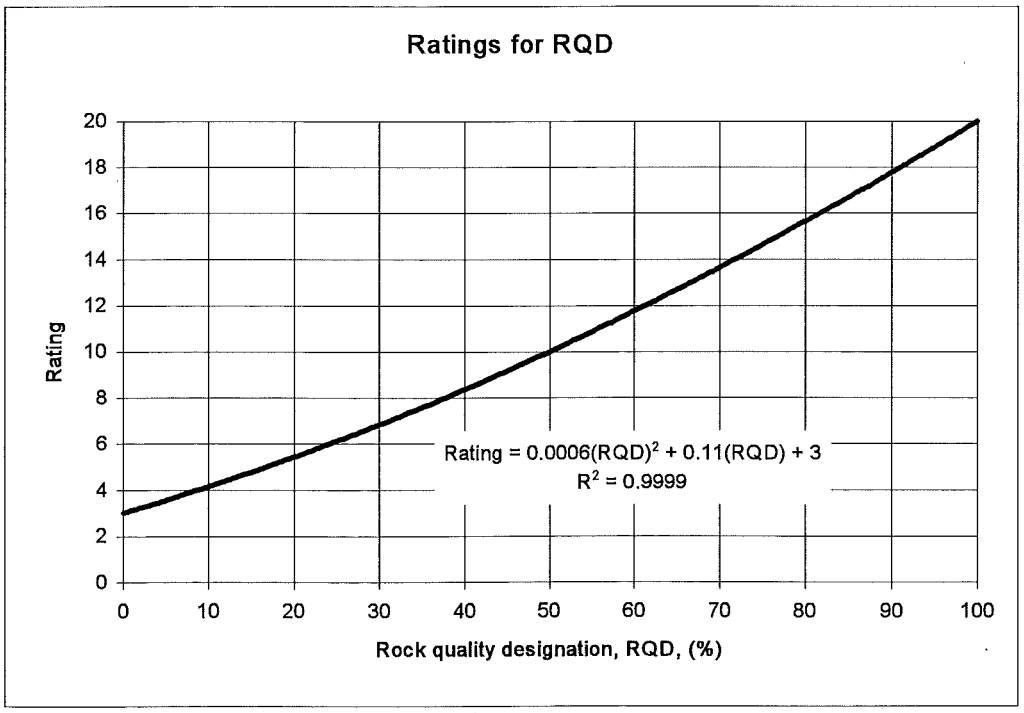

Figure 2.4: Ratings for RQD (after Bieniawski, 1989). The formula may be used to calculate the exact rating from the RQD value. The formula was not provided in Bieniawski (1989), but the correlation between the curve and the formulae (R^2 = 0.9999) is excellent, and therefore can be used as a reliable estimate.

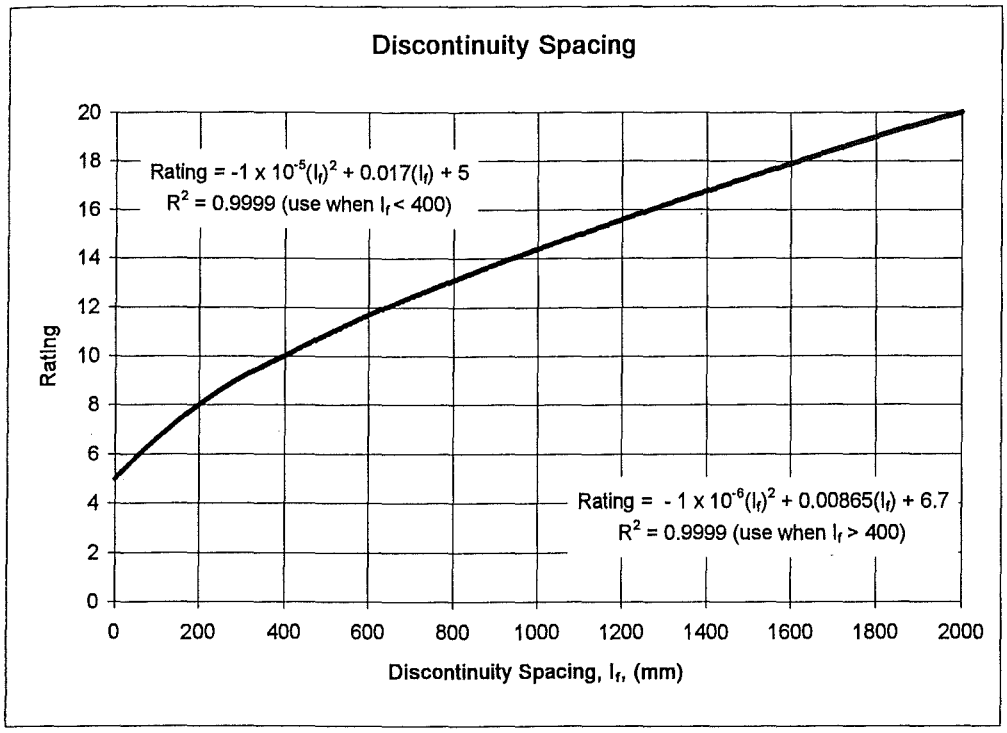

Figure 2.5: Ratings for discontinuity spacing (after Bieniawski, 1989). The formulae may be used to calculate the rating instead of using the graph. The formula was not provided in Bieniawski (1989), but the correlation between the curve and the formulae ($R^2 = 0.9999$) is excellent, and therefore can be used as a reliable estimate.

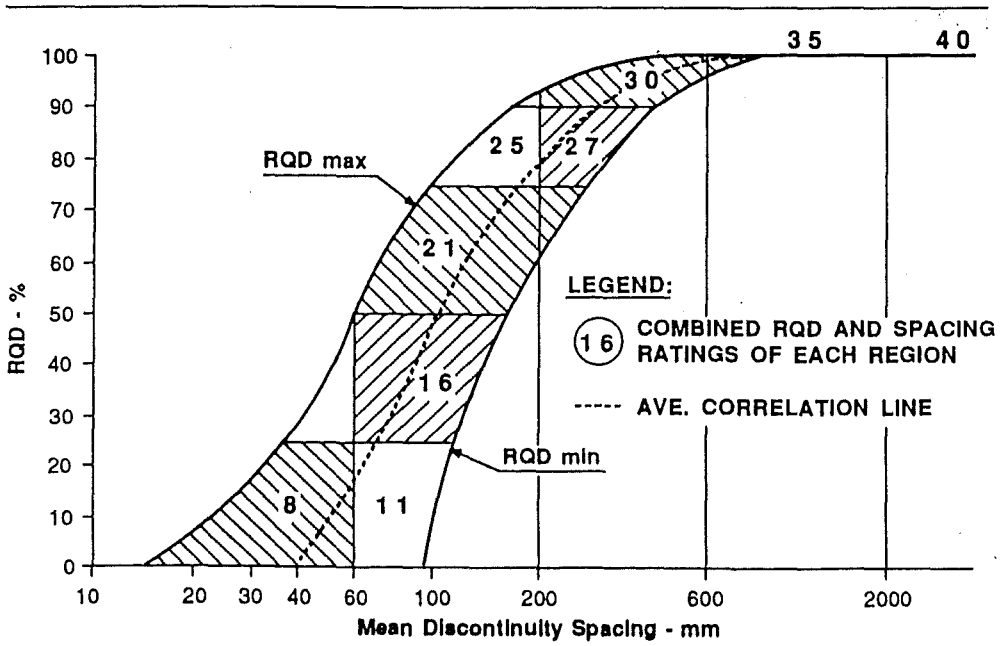

Figure 2.6: Chart correlating RQD and discontinuity spacing (after Bieniawski, 1989).

Table 2.8: Assessment of discontinuity orientation for use in tunnelling, mining and rippability applications. The ratings for each class may be found in Table 2.7c (after Bieniawski, 1989 and Minty and Kearns, 1983).

Tunnelling and mining applications			
Orientation of strike	Dip < 20°	Dip 20 - 45°	Dip 45 - 90°
Perpendicular to tunnel axis: drive with dip	Fair	Favourable	Very favourable
Rating	-5	-2	0
Perpendicular to tunnel axis: drive against dip	Fair	Unfavourable	Fair
Rating	-5	-10	-5
Parallel to tunnel axis	Fair	Fair	Very unfavourable
Rating	-5	-5	-12

Rippability applications			
Orientation of strike	Dip < 20°	Dip 20 - 45°	Dip 45 - 90°
Perpendicular to ripping direction, with dip	Unfavourable	Favourable	Very favourable
Rating	-2	-10	-12
Perpendicular to ripping direction, against dip	Unfavourable	Unfavourable	Fair
Rating	-2	-2	-5
Parallel to ripping direction	Unfavourable	Fair	Very unfavourable
Rating	-2	-5	0

2.3.2.2 Applications

The RMR System has been applied to a variety of engineering projects all over the world. Most applications have been in the field of tunnel design and other underground excavations (Bieniawski, 1984) but others have been in slope stability, foundation design and mining applications.

Use of the RMR System in mining applications mainly involves underground mining. Applications are by Laubscher, 1977 (asbestos mining in Africa); Ghose and Raju, 1981, Abad, *et al*, 1983 and Venkateswarlu, 1986 (coal mining in India); Unal, 1983 (coal mining in USA); and Kendorski *et al*, 1983 (hard rock mining in USA). Romana (1985) and Orr (1992) have applied the RMR System to slope stability and Bieniawski and Orr (1986) have applied the RMR System to foundation design. Other applications have been in estimating rippability (Weaver, 1975; discussed in detail in Section 3.4.3); weathering and durability of rock (Olivier, 1979); boreability (Sandbak, 1985); and dredgeability (Smith, 1987).

The RMR System has been correlated empirically with other rating systems, such as the Q System (Bieniawski, 1976; Abad *et al*, 1983) and the RSR System (Rutledge and Preston, 1978), as well as with rock mass parameters not used in the rating system, such as modulus of deformability (Bieniawski, 1978; Serafim and Pereira, 1983) and rock mass strength (Hoek and Brown, 1980). However, Farmer (1983) states that using these extra rock mass properties as a description of a rock mass may lead to confusion and overdesign, rather than improvements in design.

2.3.2.3 Advantages and disadvantages of the RMR System

The classification system is simple to use and understand. The data required may be easily found from drillhole data or tunnel drives. The system was originally designed for use in tunnels, but has subsequently been applied to many other applications and used in empirical relationships with other rating systems and various rock mass parameters. The ratings have been altered with further development of the system, but they have not changed since 1979. The weightings of the ratings have been proven by Nakao *et al* (1983) who statistically reconsidered each parameter and rating of the RMR System for tunnel design in Japan. The results were found to virtually agree with each other.

The system uses properties of both rock material and discontinuities, whereas the other major system, the Q System, uses only discontinuity data and completely ignores rock material properties and the orientation of discontinuities. Rock material properties should be used in a classification system because if discontinuities were widely spaced, or the rock material was highly altered or weak, then the rock material properties will affect the behaviour of the rock mass (Bieniawski, 1973). Farmer (1983) went even further by stating that discontinuities are only important in rock engineering where they constitute a major failure plane or zone of weakness. He found short term rock behaviour, when excavated, to be controlled by the performance of rock material.

The RMR System is rated out of 100 giving a rock mass a sense of relative quality in terms of the maximum possible result. Open ended systems like the Q System do not give a sense of relative quality, thus, it may be harder to visualise the result. The Q System is classed using log scales, therefore errors in measurement of parameters become

insignificant, whereas with the RMR System errors are significant, although because all the parameters in the RMR System are quantifiable, there should be no errors or subjectivity.

The other advantage of the RMR System over the Q System is that the Q System has been found to be more conservative than the RMR System (Abdullatif and Cruden, 1983; Udd and Wang, 1985). From a safety aspect, such as the stability of slopes, tunnels or foundations, conservatism is beneficial but from an economic point of view, such as the excavatability of a mine or quarry, conservatism is undesirable (Udd and Wang, 1985).

The major problem with the system is that, like most rock classifications, the system was developed initially for tunnel design, therefore, the results are likely to be conservative. Data in Table 2.7e, used to correlate the RMR with tunnel support and slope stability parameters are underestimated, which results in the system's conservatism. Bell and Crampton (1986) found that the system severely underestimated the stand up time for tunnels, therefore support requirements will be overestimated. The system has also been found to underestimate cohesion and the friction angle of the rock mass (Romana, 1985; Tsiambaos and Tulli, 1992), thus overestimating the stability of a slope.

2.4 Rock mass classifications in rippability investigations

To evaluate the rippability of a site, a combination of geological and geotechnical properties of the rock mass are required (Weaver, 1975; Pettifer and Fookes, 1994). Some properties influence the rippability of a rock mass more than others and therefore, rock mass classification systems similar to those detailed in Section 2.2 and 2.3 are required to characterise the rock mass. The two most common rock mass classification systems, the RMR System and the Q System, have been modified from stability orientated classification systems to excavatability orientated classification systems, to form Weaver's (1975) Rippability Rating System (discussed in detail in Section 3.5.3) and Kirsten's (1982) Excavatability Index (discussed in detail in Section 3.5.4), for the purpose of determining the rippability of a site. The modification in Weaver's (1975) system was made by reversing the discontinuity orientation ratings, such that a favourable orientation is changed to an unfavourable orientation in an excavatability evaluation, and by replacing

RQD and groundwater parameters with a seismic velocity parameter. Kirsten's (1982) system was modified from the Q system by replacing the stress component with two other components, one related to the uniaxial compressive strength and the other related to the orientation of discontinuities with respect to the ripping direction. A detailed discussion of commonly used rippability classification methods is included as Section 3.5.

Rock mass classification systems should not be used as the only methods of determining the excavatability of a rock mass for design purposes. At least two different methods of rippability assessment should be used and compared. If both compare well, then they can be used as reliable guides during design and construction (or excavation) project stages, however, the actual rippability of a site cannot be determined exactly until excavation proceeds and ripping trials are performed as there are many other variables that influence rippability that can not be quantified until excavation takes place, such as wear and tear on ripper tips, maintenance times, operator experience and so on.

2.5 Use of rock mass classifications in open pit mining

There have been many applications of rock mass classifications in mining but most are applicable to underground mining, where stress is more of a problem than discontinuities. Open pits are generally near surface where the ground has undergone stress relief, therefore, rock mass classification systems such as the Q System, that require a stress parameter generally can not be used in characterising the rock mass in a open pit. The most appropriate rock mass classification system from those described in Section 2.2 and 2.3 to characterise the rock mass in an open pit is the RMR System because of its ease of use, standardisation and applicability to shallow ground excavations. The results may be easily modified for various mining applications. Pit slope stability may be investigated using Romana's (1985) RMR extension, likewise, rippability or the excavatability characteristics of the rock may be estimated using Weaver's (1975) approach.

A study performed by Abdullatif and Cruden (1983) determined the relationship between the ease of excavation and rock mass quality in English quarries. The rock masses were characterised using the RMR System and the Q System. Rocks were excavated by digging

ripping or blasting. They found a good correlation between the Q System and the RMR System. Rock masses with RMR values up to about 60 were found to be rippable, therefore rocks classed as good or better should be blasted. The Q System was not as accurate an estimator of the rock mass as the RMR System because of the inclusion of the active stress component, which showed little variation. They found Q to be a product of only four parameters, none of which considered the joint orientation, unlike the RMR System. They concluded that the RMR System gives a better assessment of the rock mass quality than the Q System in quarry excavations.

2.5 Synthesis

Classification systems such as the Rock Load Classification System and the RSR System are too specific for use as general rock mass classification systems but they do accurately predict the type of support that the methods are designed to predict. Other systems use many parameters to classify the rock mass. These classification systems become general and may not be optimal for any specific purpose, but may be useful for a variety of purposes. The Q System is an excellent method to use when estimating rock conditions in underground excavations as it considers the influence of the local stress field. The RMR System is useful for a variety of purposes. It was originally designed for use in tunnel excavations but has been adapted for use in classifying foundation conditions, slope stability, underground mining and rippability.

When designing a classification system, there is a difficulty in assigning rating values to the various parameters. Bieniawski, in his original 1973 RMR System, based his ratings on Wickham's (1972) RSR System. Bieniawski's system has subsequently been modified as more case studies fine tune the system. The ratings in the current system have been proven statistically to be accurate estimators of the rock mass (Nakao, 1983). Most rock mass classification systems are conservative in their estimation of support requirements or correlation with other rock mass properties. This means that if the classification system is followed exactly, tunnel support and slope stability costs will be higher than that necessary and the excavatability of the rock will be underestimated.

Chapter 3

Principles and Methods of Rippability Assessment

3.1 Introduction

Rippability is defined as a measure of the ease with which earth materials can be broken by mechanical ripping equipment to facilitate their removal by other equipment (Allaby and Allaby, 1991). Church (1981) defined ripping as the fragmentation of rock by bulldozers equipped with ripper shanks [or tines] and points [or tips]. Note that this differs from excavating, which is the cutting down of the natural ground surface (Church, 1981) by methods such as digging, ripping or blasting or a combination of the three.

The first recorded use of ripping as a means of fragmenting rock was by the Romans in 312 BC, when oxen pulled a wheel mounted plough (Church, 1981). In fact ripping techniques employed today are nothing more than large scale use of a farmer's plough that rips soils. Until about 1930, when ripping became commercially viable as an excavation technique, excavations were described as either common, which could be dug easily, or rock, which required blasting prior to digging (Church, 1981). Ripping allowed the introduction of a third, intermediate category.

Today, because of advances in technology and ripping techniques, more detailed classification systems are used to describe the rippability of a site, but there is no one system that is generally accepted. Rippability classification systems all vary substantially. One of the first systems was the Size-Strength Excavatability Graph by Franklin, Broch and Walton (1971). This has recently been modified by Pettifer and Fookes (1994), and is discussed in detail in Section 3.5.2. These graphs plot rock strength against discontinuity

assessment of the rippability of a site. Rippability equipment manufacturers have their own rippability classification systems, plotting rippability versus the seismic velocity of the rock mass. The first classification scheme using a complete array of geological parameters that affect rippability was proposed by Weaver (1975), based on the Rock Mass Rating System of Bieniawski (1973). Other systems have tried to predict the productivity of a bulldozer (Minty and Kearns, 1983; MacGregor, *et al*, 1994). The most common rippability estimation methods are reviewed in Section 3.4 with the aim of finding the most appropriate methods for use in characterising the rippability of the open pit.

Fowell (1993) listed many advantages of mechanical excavation over blasting, including:

- economically advantageous in suitable ground
- improved safety
- ease of automation
- accuracy of finished excavation dimensions
- excavation walls remain undamaged
- product size usually handled by conveyors
- suitable where there are limitations on the level of vibrations

If the ground is suitable and ripping machinery is well maintained then there are very few advantages of using blasting instead of ripping methods. One advantage of blasting over ripping in excavating a mine open pit would be the extra grade control information gathered from drilling blast holes, but by far, the advantages of mechanical excavations in suitable ground outweigh any disadvantages.

3.2 Types of rippers and ripping methods

To rip the ground bulldozers are used with the addition of a ripper mounted on the rear (Figure 3.1 and 3.2). The most commonly used bulldozers are manufactured by Caterpillar and Komatsu, both of which make bulldozers in a range of sizes (Table 3.1). It has been estimated that a bulldozer can put about 25% of its mass onto the ripper (Brewster, 1984), and Church (1981) states some can put up to 40% of their mass onto the ripper.

Table 3.1: Komatsu and Caterpillar Bulldozer models and masses. Caterpillar data from Pettifer and Fookes (1994) and Komatsu data from Motor Holdings Komatsu Limited (1996).

Komatsu's Bulldozers		Caterpillar's bulldozers	
Model	Mass (tonnes)	Model	Mass (tonnes)
D155AX-3	39.2	D7G	20.1
D275A-2	50.7	D8L	37.3
D375A-2	63.2	D9L	52.0
D475A-2	95.3	D10	79.6
D575A-2	134	D11N	95.8

There are three types of rippers: hinge, parallelogram and adjustable parallelogram. The most commonly used ripper is the adjustable parallelogram and is shown in Figure 3.1 and 3.3. The important parts of a ripper are the tip, the shank, the tool bar and the power assembly. The tip enters the rock mass at a critical angle depending on the discontinuity orientation. The critical angle may be varied by configuring the tip or by adjusting the shank. The shank holds the tip and is mounted into the tool bar, which is raised, lowered and inclined by the power assembly. Figure 3.4 shows the most efficient action of a ripper, illustrating the movement of the important parts. Rippers may also have single or multishanks (Figure 3.3 and 3.4). Multishanked rippers have the advantage of being able to cover more ground that a single shanked ripper, although they cannot apply as much pressure to each tip and therefore, are not as effective in ground difficult to rip.

Easier ripping may be achieved in two ways, either the ground could be preblasted or the ground could be kept saturated. Saturated ground makes ripping easier by lubricating the tips and shanks, therefore making them easier to penetrate the ground and resulting in less wear on them and leading to higher productivity and less maintenance. Water is also known to reduce the strength of a rock mass (as illustrated in Figure 5.11, which compares the frequency distribution of a dry, damp and saturated rock mass at Globe-Progress) Where a rock mass is rated too strong, or is not fractured enough to allow ripping, then the rock could be preblasted, however a complete cost analysis comparing preblasting and ripping with blasting should be evaluated first.

Figure 3.1: Komatsu's D575A bulldozer ripping a bauxite deposit at Jarrahdale Mine, Western Australia (Photo courtesy of Des McKenzie).

Figure 3.2: The same bulldozer as in Figure 3.1 with people for scale. Note the lift for gaining access to the bulldozer controls (Photo courtesy of Des McKenzie).

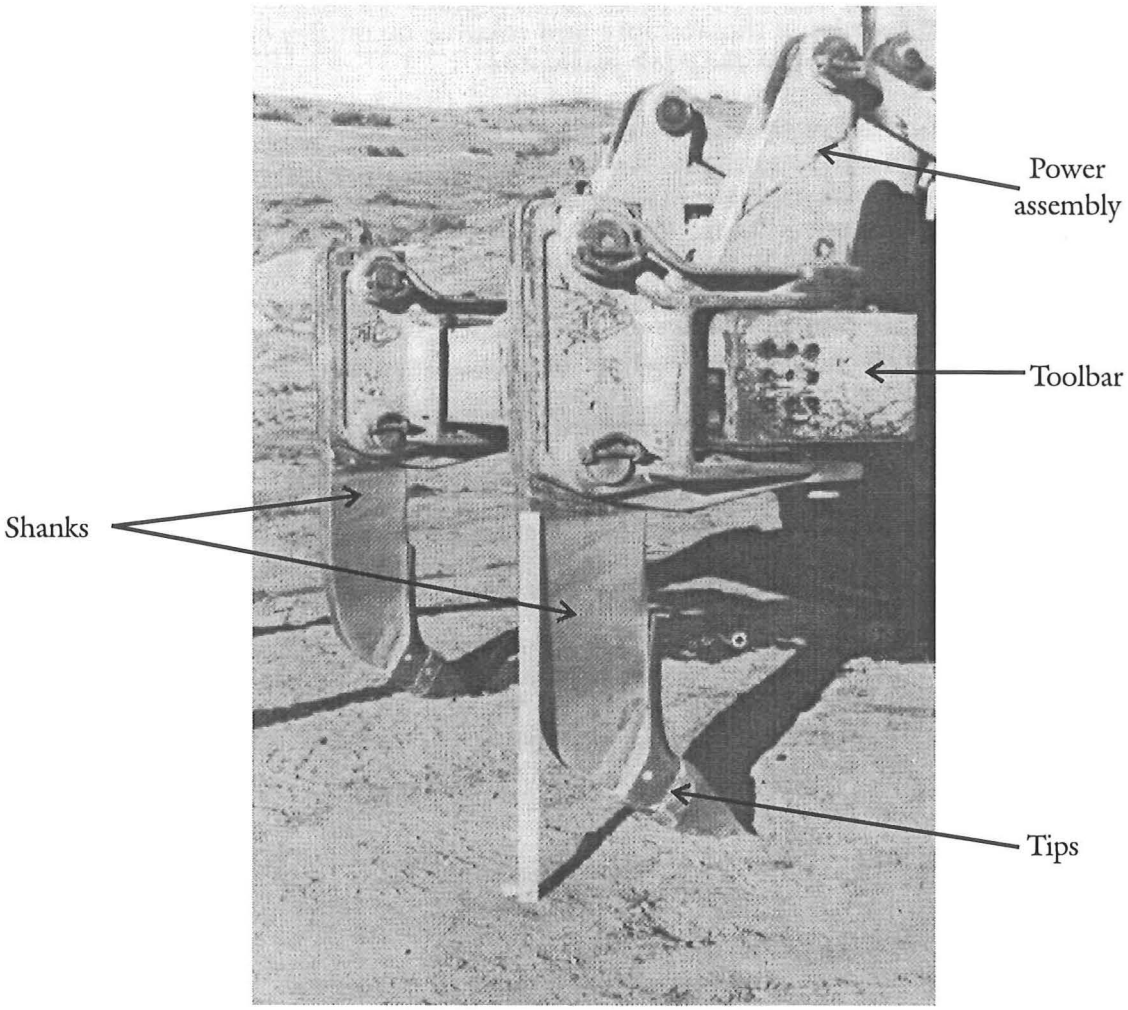

Figure 3.3: Close up of a multi-shanked ripper illustrating the important working parts. The ruler is one metre (Reproduced from Church, 1981).

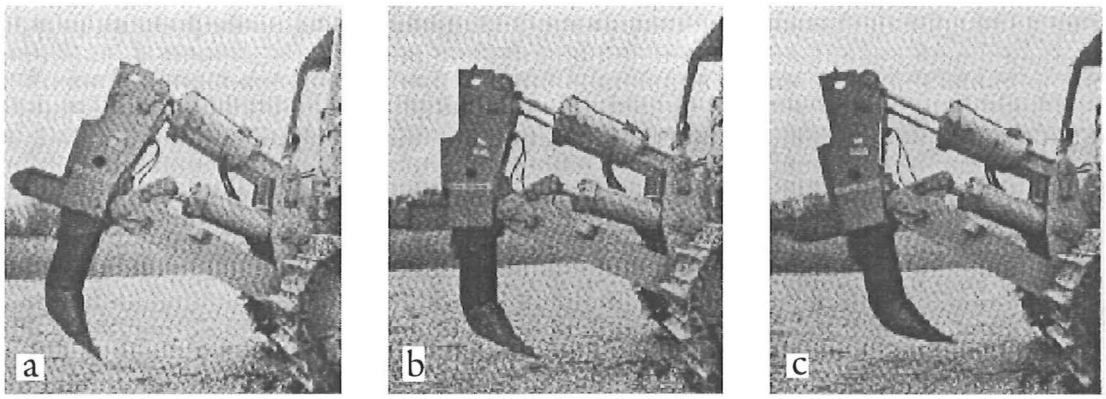

Figure 3.4: The most efficient ripping technique of a adjustable parallelogram ripper. (*a*) The tip is placed at the critical angle required for penetration of the rock mass. (*b*) The tip, having entered the rock mass and reached the desired depth for ripping the rock mass. The best ripping angle is found by adjusting the shank to the near vertical position. (*c*) The shank is adjusted forward to pry out difficult rock mass. Reproduced from Church (1981).

3.3 Geological factors affecting rippability

3.3.1 Introduction

Factors likely to be influential in a rippability assessment may be divided into geological factors and contractor and machinery factors, both of which are discussed in Section 3.4). The rippability assessment methods discussed in Section 3.5 are all methods that use a number of geological factors to predict the type of machinery that may be required. The methods assume that the machinery is operating correctly and that the operator is sufficiently skilled. If the prediction of rippability proves to be incorrect once excavation has commenced, then it may be because of an insufficient site investigation, an unskilled operator, or poorly chosen ripping machinery.

The following factors all influence the rippability of a rock mass to some degree:

- Rock type
- Rock hardness or rock strength
- Rock mass structure
- Rock material fabric
- General site conditions

Of the above factors, the most important are the rock hardness or rock strength and rock structure. Rock strength dictates the ability of a bulldozer to mechanically break the rock and the rock structure defines the ease at which a bulldozer can rip the rock mass. A highly fractured rock mass will be easy to rip, whereas a massive rock mass may be easy to very hard to rip, depending on its strength.

Seismic velocities provide a useful estimation of the above factors. Seismic waves travel through different rock types at different velocities. The velocity depends on the density, porosity and strength of rock material as well as the fractures in the rock mass. For example, a dense, strong rock with little or no fractures, will have a high seismic velocity relative to a highly fractured, dense, strong rock. Seismic velocities are normally determined from the Generalised Reciprocal Method of interpreting seismic refraction data (explained in Appendix D2). Seismic velocities are not indicative of the type of rock being ripped as velocities will vary between lithologies, rather, seismic velocities provide a measure of the influencing parameters listed above.

3.3.2 Rock type

Igneous, metamorphic and sedimentary rock types all vary in their ability to be ripped. Igneous rocks are the most difficult to rip as they generally lack bedding and cleavage planes that are essential to ripping hard rock and the strength of igneous rocks is normally very strong to extremely strong. Sedimentary rocks are often the easiest to rip as they generally contain bedding planes and other fractures that act as planes of weakness. Metamorphic rocks vary in their ability to be ripped. Often they have cleavage planes or laminations that act as planes of weakness, other metamorphic rocks may appear as more indurated sedimentary rocks and others may appear similar to igneous rocks. Metamorphic rocks are often anisotropic, implying that they may be easily ripped in one direction but not in another direction.

3.3.3 Rock hardness or strength

The hardness or strength of a rock type influences rippability by the ability of an excavator or bulldozer to be able to break the rock. Rock strength is described quantitatively if tested by point load or uniaxial compressive strength tests or qualitatively, where the strength or hardness is determined by scratch tests, for core logging purposes. For example, very soft rock can be gouged by a pocket knife (ISRM, 1981; see Appendix B2), therefore will be easy to rip, whereas very strong rock requires many blows of a geological hammer and cannot be scratched by a pocket knife (ISRM, 1981), therefore, will be extremely hard to rip, and may even require blasting.

3.3.4 Rock mass structure

A rock mass is defined as rock material plus associated discontinuities. Discontinuities refer to any structural feature that alters the homogeneity of a rock mass (Weaver, 1975) and includes structures such as faults, shear zones, joints, bedding planes, cleavage, foliation surfaces and so on. The effect of discontinuities is to reduce the overall strength

of a rock mass. A structural investigation of the site to be excavated needs to record all discontinuities and their characteristics such as discontinuity continuation or length; discontinuity separation and infilling; and discontinuity weathering and roughness, as well as the orientation of each discontinuity.

The spacing between discontinuities is the most important parameter in a rock mass (Fowell, 1993) as it governs the degree of reduction in the overall strength of a rock mass. The length, continuity or persistence of discontinuities influence the overall strength of a rock mass such that persistent discontinuities such as bedding planes and faults make ripping easier than non persistent discontinuities such as cleavage and veins. Infilled discontinuities may reduce the overall strength of a rock mass, depending on the type of infilling material. If the infilling is soft (such as gouge) and the aperture or separation sufficiently wide enough, ripping will be easier, whereas if the infilling is hard (such as limonite or calcite) and the aperture narrow, ripping becomes more difficult. Weathering and discontinuity roughness may either reduce or increase the shear strength of the discontinuity depending on whether the discontinuity is fresh or highly weathered, or rough or smooth.

Discontinuity orientation may be favourable or unfavourable for ripping. Unfavourable ripping conditions exist when the dominant discontinuity is subhorizontal or subvertical, where the run direction is parallel to bedded rocks or where bedding is massive and lacks discontinuities. Ripping is favourable when the run direction is down dip in inclined bedding, thinly bedded rock or rock with cleavage. The ideal situation is when the dominant discontinuity is at around 45°. The most favourable ripping conditions exist when the ripping direction is perpendicular to the strike of vertical discontinuities. Minty and Kearns (1983) define favourable and unfavourable ripping conditions in their Geological Factors Rating (Table 3.7).

Ripping should not be performed on rock masses that behave in a plastic manner but elastic or plastic-elastic rock masses can be ripped (Atkinson, 1970). Plastic material such as wet clay or pug is not conducive to ripping because the bulldozer is likely to get stuck in the clay, and because of the bulldozer's large mass, they may prove difficult to remove from wet clay.

3.3.5 Rock material fabric

Rock material fabric relates to arrangement of mineral grains in a rock. Grains may be of similar size, composition or orientation (NZGS, 1988). Generally, coarse grained rocks (greater than 5 mm) such as plutonic rocks or conglomerates are more easily ripped than fine grained rocks (less than 1 mm) such as volcanic rocks, sandstones and mudstones. Likewise, dense, compacted rock materials will be harder to rip than loose, unconsolidated rock materials. The hardness of the minerals also influences the rippability of the rock material. For example quartz has a Mohs hardness of 7 whereas calcite has a Mohs hardness of 3, therefore, rocks composed predominantly of quartz, such as quartzite, will be harder to rip than rocks composed predominantly of calcite, such as fossiliferous limestone. Rocks with minerals in a preferred orientation, such as regionally metamorphosed rocks may be easy or hard to rip depending on the favourability of the preferred orientation with respect to the ripping direction. The favourability of orientations is defined in Section 3.3.4.

3.3.6 Site conditions

Site conditions such as the location and level of the area to be ripped, the topography of the site, the thickness of loose rock or soil cover, the weather conditions and the presence of surface water are all important when trying to estimate rippability on a site. Local landscape features and weathering patterns can help determine characteristics of the rock mass likely to be encountered in the excavation. The shape of the excavation relative to the excavating equipment is also important. If an excavation is difficult to rip, then the excavator or bulldozer needs sufficient space in a ripping run to acquire enough pulling force to break the rock before turning around.

3.4 Excavating factors affecting rippability

3.4.1 Introduction

These factors deal with the abilities of the contractor and the type and condition of equipment used. The methods outlined in section 3.5 all assume that the contractor and bulldozer operator are sufficiently skilled and that the equipment used is in good working condition. If these assumptions are not correct then the productivity of the bulldozer will be less than expected and an area predicted to be easy to rip may prove difficult to rip.

These factors may be divided into three groups:

- Bulldozer productivity
- The contractor, and type and condition of equipment
- Method of ripping

3.4.2 Bulldozer productivity

The production rate of a bulldozer may vary substantially and is dependent upon whether the bulldozer is involved in activities other than ripping such as scraping and dozing loose material; whether the bulldozer operates at a reduced production rate because of site or production restrictions; whether there is a required size of ripped material; and the idle time due to machinery breakdown and maintenance. Bulldozers also spend time reversing and turning and this may result in a false impression of productivity.

These problems led MacGregor *et al* (1994) to define two types of productivity:

$$\text{Run productivity: } P = CLWD/T$$

$$\text{Area productivity: } P = \sum_{1}^{n} (LWD)/\Sigma T$$

where C is a correction factor for the shape of the area affected by a ripper, L (in metres) is the run length, W (in metres) is the width between successive runs, D (in metres) is the depth of penetration of the tip, T (in hours) is the time the tip is in the ground for a run and n is the number of runs in an area. Where productivity is referred to in subsequent

sections, it refers to the area productivity. Where bulldozers have to doze and scrape loose material the percentage of time the tine was in the ground was calculated by MacGregor, *et al* (1994) to be around 20%, therefore estimates of the productivity using the above formulae may be five times greater than the actual productivity but when the bulldozers only rip and turn to rip the next line, then the tine was in the ground approximately 50% of the time. MacGregor, *et al* (1994) also defined groups of productivity and these are tabulated in Table 3.2.

Table 3.2: Productivity grouping (from MacGregor, *et al*, 1994).

Productivity (m^2/hr)	Ease of ripping
0 - 250	Very difficult / blasting
250 - 750	Difficult
750 - 2000	Medium
2000 - 3500	Easy
>3500	Very easy

3.4.3 The contractor, type and condition of equipment used

The company contracted to rip the excavation should be experienced, and have experienced operators. Otherwise the productivity may be lower than expected. The bulldozer manufacturer and the model is also important. If they are not chosen correctly, then ripping may prove to be more difficult than expected. The size of the bulldozer needs to be carefully chosen. The larger a bulldozer, the more mass it can place on the ripper and the easier it becomes to rip rocks, however if the bulldozer rips the rock mass easily, then the bulldozer may not be operating at full efficiency. On the other hand, if ripping proves to be very difficult, and the productivity is low, then the bulldozer is under-powered and a larger bulldozer should be selected for greater efficiency. The bulldozer should be kept in excellent working order. Substandard equipment may slow down the productivity and may also result in more maintenance time than expected.

3.4.4 Method of ripping

Ripping runs should be performed perpendicular and down dip to the dominant discontinuity orientation. The material ripped may be required to be a certain shape and size, and may require additional crushing or closer spaced ripping runs. Factors such as overall area to be ripped, average depth of ripping, average width between ripping runs and length and time of each run may be planned during the design stages of a project and modified as ripping proceeds during the excavation stage of a project. Other factors such as the surface area affected by the tip during ripping, the penetration angle and depth of the tip, any loss of traction during the ripping run and the mechanisms of how the rock breaks can only be observed once ripping proceeds, and should be noted so that the bulldozer productivity can be further refined and a more accurate estimation of the rippability and productivity of a site may be determined as excavation proceeds.

3.5 Previous methods of rippability assessments

3.5.1 Bulldozer Manufacturer's seismic velocity charts

Probably the most widely performed rippability predictions are based on Caterpillar or Komatsu Ripper Performance Charts. Different charts are produced for each bulldozer and show the rippable, marginal and non-rippable seismic velocity zones for various rock types (for example, Figure 3.5). Other charts plot seismic velocity of a site versus the expected productivity for each bulldozer (for example, Figure 3.6).

Komatsu have also related rippability to rock strength and hardness. The uniaxial compressive strength, tensile strength and shore hardness ranges have been calculated for some of their bulldozers (Figure 3.7a) . The major problem with this prediction technique is that the strength and hardness measurements are based on rock materials rather than rock masses, thereby predicting a bulldozer more powerful than is actually required. MacGregor, *et al* (1994) plotted productivity versus uniaxial compressive strength where Komatsu bulldozers were used and found Komatsu's rippable, marginal and non-rippable limits to be over-estimated (Figure 3.7b).

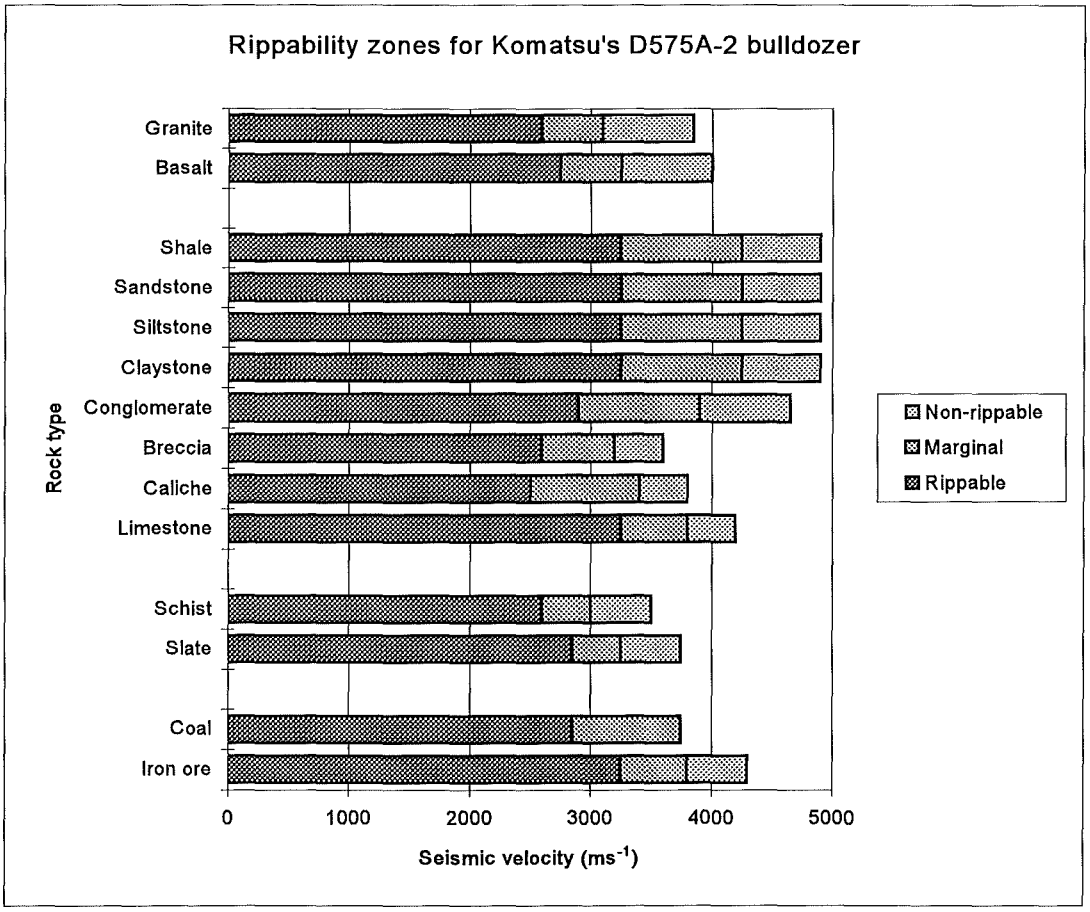

Figure 3.5: An example of the Komatsu Ripper Performance Chart for model 575A-2 (After John, 1994).

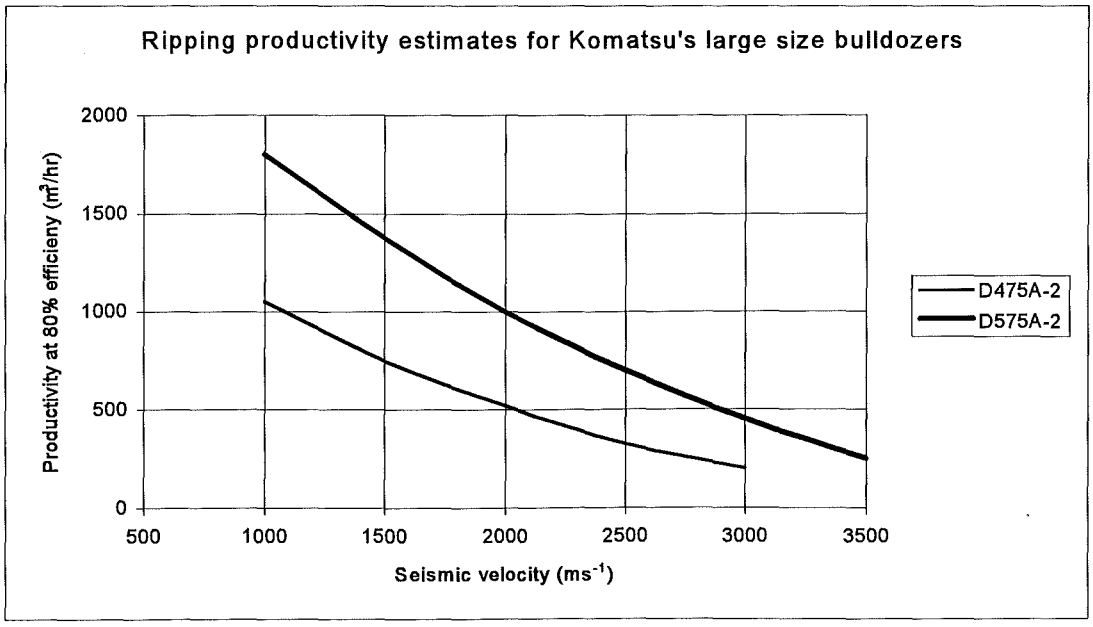

Figure 3.6: Plot of expected productivity versus seismic velocity for Komatsu's super bulldozers (After John, 1994).

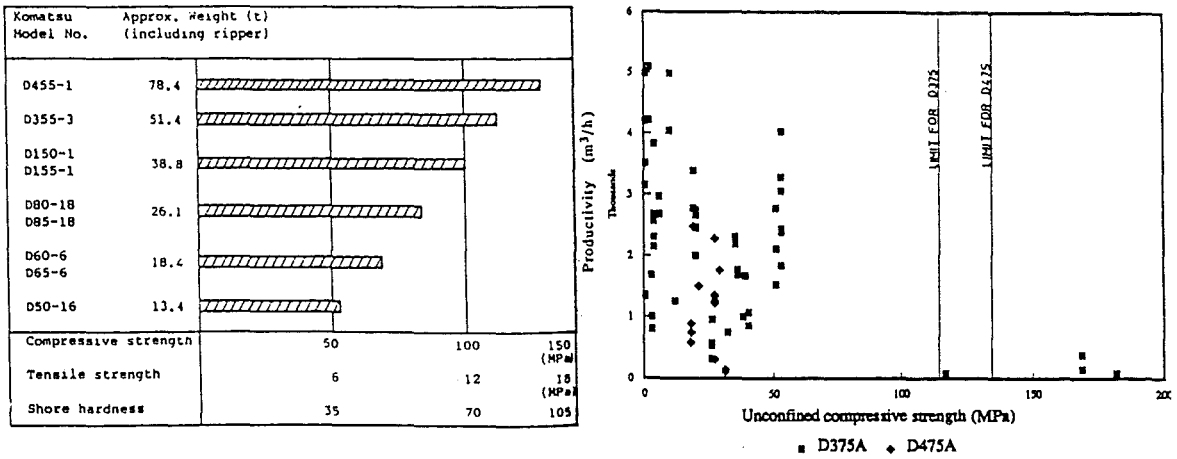

Figure 3.7: (*a*) Komatsu's rippable ranges for UCS, tensile strength and shore hardness (from Braybrooke, 1988) and (*b*) productivity versus unconfined compressive strength for Komatsu's D375A and 475A bulldozers (from MacGregor *et al*, 1994).

Minty and Kearns (1983), using 40 case studies, plotted productivity versus seismic velocity using Caterpillar's Charts and found the ideal, marginal and adverse ripping conditions to be too optimistic, so were reduced by a factor of five (a value considered from experience to make the results more realistic). They also found that productivity and seismic velocity were poorly correlated. Martin (1986), using data from 28 sites in sandstone, compared rippability with Caterpillar's charts and found that over a third of the case studies over-estimate productivity. MacGregor *et al* (1994) also found that the Caterpillar charts are over-optimistic, predicting that a rock mass should be ripped economically where in fact field tests showed that ripping was difficult, with lower than expected productivity. A possible explanation for the over-estimation is that Caterpillar includes the time reversing and turning in their productivity values. MacGregor *et al* (1994) found that the tine is in the ground on average 54% of the time, therefore a rough estimate of the true productivity would be to halve Caterpillar's productivity values. Koczanowski, *et al* (1991) suggested choosing a bulldozer one model above that recommended by the bulldozer manufacturer to overcome the optimism.

3.5.2 Size-Strength Graphs

Franklin, Broch and Walton (1971) published a graphical excavatability method relating discontinuity spacing and rock strength with an appropriate method of excavation (Figure 3.8). The graph is divided into zones of digging, ripping, blast to loosen and blast to fracture. More or less the same graph was published by Fookes, Dearman and Franklin (1971), who emphasised that the graph was in its development stage.

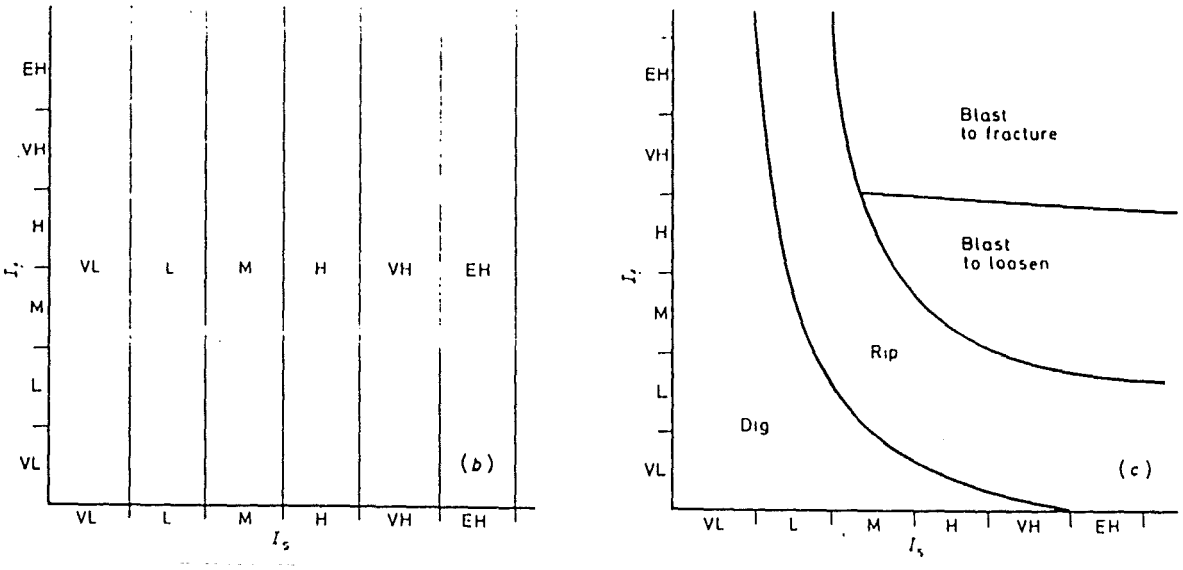

Figure 3.8: Size-Strength Graph (from Franklin, Broch and Walton, 1971).

The graph is now out of date because of advances in technology, therefore Pettifer and Fookes (1994) revised the graph based on new and published ripping data. The revised graph (Figure 3.9) is based on 120 case studies of ripping or blasting mainly sedimentary rock masses, and with a few igneous and metamorphic rocks. On one axis is the block size and discontinuity spacing, and on the other axis is the rock mass strength. The block size can be expressed as the average discontinuity spacing, but where possible, the block size should be used. The point load strength index is used for the rock strength and can be correlated with uniaxial compressive strength by UCS = 20 × $I_{s(50)}$ (Pettifer and Fookes, 1994), although $I_{s(50)}$ values less than 0.5 MPa, because of their unreliability, should be tested using UCS testing methods (Bieniawski, 1979; Hawkins, 1986; Pettifer and Fookes, 1994).

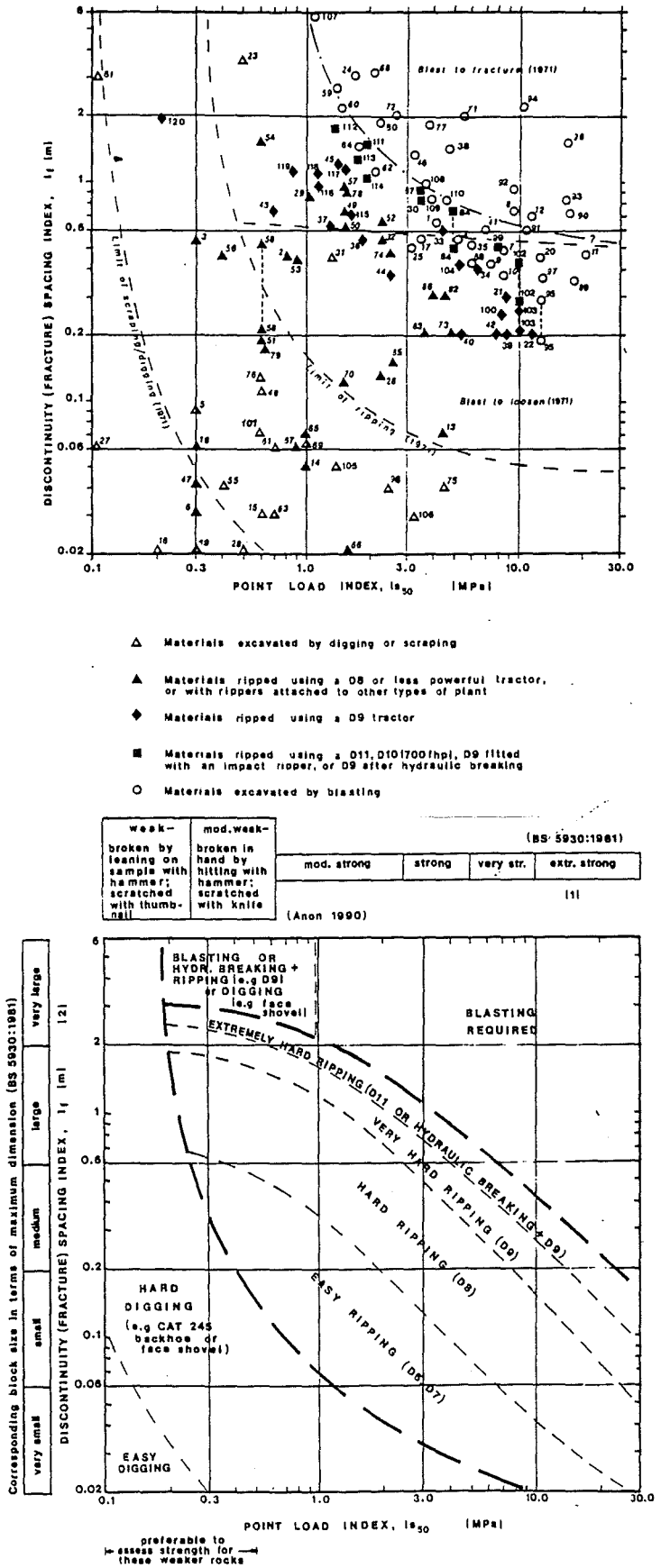

Figure 3.9: (*a*) the original Size-Strength Graph with Pettifer and Fookes' case studies superimposed and (*b*) Pettifer and Fookes' updated Size-Strength Graph (from Pettifer and Fookes, 1994)

No adjustment is needed for weathering as weathered rocks should have a corresponding reduction in strength and block size (Pettifer and Fookes, 1994). However the effect of the block shape and orientation relative to the ripping direction need to be considered. Where there are unfavourable ripping conditions outlined in Section 3.3.4, then Pettifer and Fookes (1994) suggest increasing the discontinuity spacing by 20 - 50%.

This graphical system allows for a rapid assessment of the excavatability of a site as both rock strength and discontinuity spacing may be determined quickly and at low cost. The system also uses strength and discontinuity spacing, arguably the two most important geotechnical properties that influence the excavatability of a site.

The major problem with the graph is that it does not recommend potential equipment or the expected productivity, therefore it should be used as a preliminary investigation method only. Pettifer and Fookes (1994) state that a comprehensive assessment should ideally consider a full range of information obtained from boreholes, seismic surveys and laboratory tests, so that assessments using different systems can be compared.

3.5.3 Weaver's Rippability Rating System

Weaver (1975) was the first person to use a suite of geological factors in a rippability classification system. Weaver's Rippability Rating System (Table 3.3) is based on Bieniawski's 1973 RMR System. Ratings are the same as for Bieniawski's classification system (Table 2.6), except that the RQD and groundwater components of Bieniawski's system have been replaced with a seismic velocity component, and the strike and dip orientations have been reversed such that a very favourable discontinuity orientation in Bieniawski's system is considered very unfavourable in a rippability evaluation. This is because a discontinuity orientation favourable in a classification system designed for stability evaluations will be unfavourable in an excavation classification system.

Table 3.3: Weaver's Rippability Rating Chart (from Weaver, 1975). Adapted from Bieniawski (1973).

Rock Class	I	II	III	IV	V
Description	Very good rock	Good rock	Fair rock	Poor rock	Very poor rock
Seismic velocity (ms^{-1})	> 2 150	2 150 - 1 850	1 850 - 1 500	1 500 - 1 200	1 200 - 450
Rating	26	24	20	12	5
Rock hardness	Extremely hard rock	Very hard rock	Hard rock	Soft rock	Very soft rock
Rating	10	5	2	1	0
Rock weathering	Unweathered	Slightly weathered	Weathered	Highly weathered	Completely weathered
Rating	9	7	5	3	1
Joint spacing (mm)	> 3 000	3 000 - 1 000	1 000 - 300	300 - 50	< 50
Rating	30	25	20	10	5
Joint continuity	Noncontinuous	Slightly continuous	Continuous No gouge	Continuous Some gouge	Continuous With gouge
Rating	5	5	3	0	0
Joint gouge	No separation	Slight separation	Separation <1 mm	Gouge < 5 mm	Gouge > 5 mm
Rating	5	5	4	3	1
Strike and dip orientation[1]	Very unfavourable	Unfavourable	Slightly unfavourable	Favourable	Very favourable
Rating	15	13	10	5	3
Total Rating	90 - 100	70 - 90[2]	50-70	25-50	< 25
Rippability assessment	Blasting	Extremely hard ripping and blasting	Very hard ripping	Hard ripping	Easy ripping
Tractor selection	-	D9G/DD9G	D8/D9	D7/D8	D7
Horsepower	-	385/770	270/385	180/270	180
Kilowatts	-	290/575	200/290	135/200	135

[1] The RMR discontinuity orientation now revised for rippability assessment.
[2] Ratings in excess of 75 should be regarded as unrippable without pre-blasting.

Weaver's method of rippability estimation is outdated as it is based on the largest bulldozer being Caterpillar's D9G (Caterpillar now produce a D11; see mass comparisons in Table 3.1), and the boundaries between ripping categories should be conservative, which has been confirmed in an analysis by MacGregor *et al.* (1994) comparing bulldozer productivity and rippability using Weaver's method (Figure 3.10a). However another study by Martin (1986) found Weaver's prediction boundary between ripping and blasting compared well with actual data based on data from 28 sandstone locations (Figure 3.10b). Therefore, because Weaver's method was based on Bieniawski's 1973 Rock Mass Classification, which has subsequently been modified as more case studies have been have been analysed, it is suggested that Weaver's method be modified to follow Bieniawski's 1989 Rock Mass Classification. This has been done and the modified ratings chart is shown in Table 3.4. The seismic velocity ranges have also been modified to be more representative of larger bulldozer's ripping capabilities. A comparison between Weaver's original system and the Modified Weaver Rippability Rating Chart, using drillhole data from Globe-Progress, is discussed in Section 5.5.2.1.

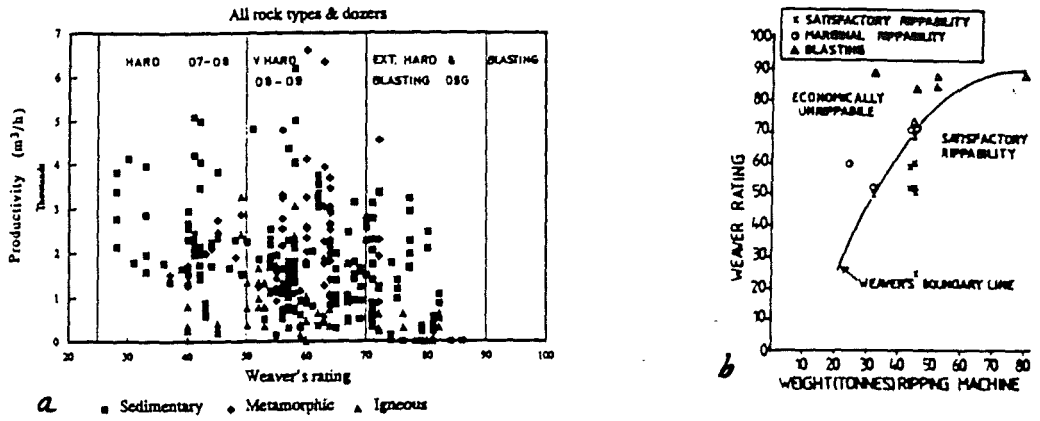

Figure 3.10: (*a*) Comparison between bulldozer productivity and Weaver's Rippability Rating by MacGregor, *et al* (1994) and (*b*) a similar comparison by Martin (1986).

Table 3.4: The Modified Weaver Rippability Rating Chart. Adapted from Bieniawski (1989).

A: Classification parameters and their ratings

	Parameter		Ranges of values					
1	Seismic velocity (ms^{-1})		> 2 500	2 100 - 2 500	1 800 - 2 100	1 500 - 1 800	< 1 500	
	Rating		35	27	20	12	3	
2	Strength of intact rock material	Point load strength index ($I_{s(50)}$, MPa)	> 10	4 - 10	2 - 4	1 - 2	For this low range, UCS is preferred	
		Uniaxial compressive strength (UCS, MPa)	> 250	100 - 250	50 - 100	25 - 50	5-25	1 - 5	<1
	Rating		15	12	7	4	2	1	0
3	Spacing of discontinuities (mm)		> 2 000	600 - 2 000	200 - 600	60 - 200	< 60		
	Rating		20	15	10	8	5		
4	Condition of discontinuities		See below for detailed description					
	Rating		30	25	20	10	5		

B: Rating classification for discontinuity conditions

Parameter	Ranges of values				
Length (persistence/continuity)	< 1 m	1 - 3 m	3 - 10 m	10 - 20 m	> 20 m
Rating	6	4	3	1	0
Separation	None	< 0.1 mm	0.1 - 1.0 mm	1 - 5 mm	> 5 mm
Rating	6	5	4	1	0
Roughness	Very rough	Rough	Slightly rough	Smooth	Slickensided
Rating	6	5	3	1	0
Infilling		Hard filling		Soft filling	
	None	< 5 mm	> 5 mm	< 5 mm	> 5 mm
Rating	6	4	2	2	0
Weathering	Unweathered	Slightly weathered	Moderately weathered	Highly weathered	Extremely weathered
Rating	6	5	3	1	0

C: Rating adjustment for discontinuity orientations

	Parameter	Ranges of values				
5	Strike and dip orientations of discontinuities	Very unfavourable	Unfavourable	Fair	Favourable	Very Favourable
	Rating	0	-2	-5	-10	-12

D: Rock mass classes and rippability assessment

Combined Rating	81 - 100	61 - 80	41 - 60	21 - 40	< 20
Class Number	I	II	III	IV	V
Description	Very good rock	Good rock	Fair rock	Poor rock	Very poor rock
Rippability assessment	Extremely hard ripping / blasting	Very hard ripping	Hard ripping	Moderately hard ripping	Easy ripping

3.5.4 Kirsten's Excavatability Index

Kirsten's (1982) excavatability classification scheme is similar to Barton *et al's* (1974) Q System discussed in Section 2.2.4, although it has been adapted to characterise excavations rather than tunnel supports. Kirsten uses four parameters, which are multiplied by each other to give the excavatability index (N). His four parameters are:

- **Mass strength number (M_s):** Represents the unconfined uniaxial compressive strength multiplied by the coefficient of relative density (Table 3.5a). Strength, density, weathering and seismic velocity are all thought to be dependant on the mass strength number (Kirsten, 1982).
- **Block size number (RQD/J_n):** RQD is the rock quality designation and J_n equals the number of different joint sets (Table 3.5b).
- **Relative ground structure number (J_s):** This is related to the dip direction and apparent angle of dip relative to the direction of ripping and represents the orientation of a block relative to the direction of ripping (Table 3.5c)
- **Joint strength number (J_r/J_a):** This is the strength of a joint and is related to the joint roughness, alteration, infilling and separation. (Table 3.5d)

The excavatability index (N) is expressed as:

$$N = M_s \times \frac{RQD}{J_n} \times J_s \times \frac{J_r}{J_a}$$

The mass strength number represents the ability to excavate a rock mass assuming it is homogeneous, unjointed and dry. The other three terms are all reducing effects that discontinuities have on a homogeneous rock mass.

The classification system has been fitted into eight logarithmic ranges, which equate to excavating categories ranging from excavation by hand spade to blasting (Table 3.6a). The system was classed this way because mass, flywheel power and maximum drawbar pull of Caterpillar bulldozers also approximate logarithmic ranges (Kirsten, 1982). The classification system has also been simplified into four classes representing major stages in excavating ability, that is, from hand pick and spade, to easy ripping, to hard ripping, through to extremely hard ripping and blasting (Table 3.6b).

Braybrooke (1988) reinterpreted Martin's (1986) data and found that the boundary between satisfactory ripping and uneconomic ripping was, like Weaver's boundary,

reasonably accurate (Figure 3.11a). However, MacGregor *et al*, (1994) found Kirsten's method to be very conservative, predicting, for example, extremely hard ripping where ripping was medium to hard (Figure 3.11b).

Table 3.5: Kirsten's excavatability characterisation ratings (after Kirsten, 1982).

A: Mass Strength number (M_s) for rocks

Hardness	Identification in profile	UCS (MPa)	Dry density (kg/m^3)	Coefficient of relative density	Mass strength number (M_s)
Very soft rock	Material crumbles under firm (moderate blows with the sharp end of a geological hammer and can be peeled off with a knife	< 1.7	2130	0.79	0.87
		1.7 - 3.3	2270	0.84	1.86
Soft rock	Can just be scraped and peeled with a knife; indentations 1mm to 3mm show in the specimen after firm (moderate) blows of a geological hammer	3.3 - 6.6	2400	0.89	3.95
		6.6 - 13.2	2570	0.95	8.39
Hard rock	Cannot be peeled or scraped with a knife; hand specimen can be broken with the hammer end of a geological hammer with a firm (moderate) blow.	13.2 - 26.4	2700	1.00	17.70
Very hard rock	Hand specimen can be broken with the hammer end of a geological hammer after more than one blow	26.4 - 53.0	2700	1.00	35
		53 - 106	2700	1.00	70
Extremely hard rock	Specimen requires many blows with a geological hammer to break through the intact material	106 - 212	2700	1.00	140
		> 212	2700	1.00	280

B: Joint count number (J_c) and Joint count number (J_n)

Number of joints per cubic metre (J_c)	Rock quality designation (RQD)	Number of joints per cubic metre (J_c)	Rock quality designation (RQD)
33	5	18	55
32	10	17	60
30	15	15	65
29	20	14	70
27	25	12	75
26	30	11	80
24	35	9	85
23	40	8	90
21	45	6	95
20	50	5	100

Number of joint sets	Joint set number (J_n)
• Intact, no or few joints	1.00
• One joint set	1.22
• One joint set plus random joints	1.50
• Two joint sets	1.83
• Two joint sets plus random joints	2.24
• Three joint sets	2.73
• Three joint sets plus random joints	3.34
• Four joint sets	4.09
• Multiple joint sets	5.00
• Intact granular material	5.00

Table 3.5 (continued): Kirsten's excavatability characterisation ratings (after Kirsten, 1982).

C: Relative ground structure number (J_s)

Dip direction[1] of the closest spaced joint sets (°)	Dip angle[2] of the closest spaced joint sets (°)	Ratio of joint spacing (r)[3]			
		1:1	1:2	1:4	1:8[4]
180/0	90	1.00	1.00	1.00	1.00
0	85	0.72	0.67	0.62	0.56
0	80	0.63	0.57	0.50	0.45
0	70	0.52	0.45	0.41	0.38
0	60	0.49	0.44	0.41	0.37
0	50	0.49	0.46	0.43	0.40
0	40	0.53	0.49	0.46	0.44
0	30	0.63	0.59	0.55	0.53
0	20	0.84	0.77	0.71	0.68
0	10	1.22	1.10	0.99	0.93
0	5	1.33	1.20	1.09	1.03
0/180	0	1.00	1.00	1.00	1.00
180	5	0.72	0.81	0.86	0.90
180	10	0.63	0.70	0.76	0.81
180	20	0.52	0.57	0.63	0.67
180	30	0.49	0.53	0.57	0.59
180	40	0.49	0.52	0.54	0.56
180	50	0.53	0.56	0.58	0.60
180	60	0.63	0.67	0.71	0.73
180	70	0.84	0.91	0.97	1.01
180	80	1.22	1.32	1.40	1.46
180	85	1.33	1.39	1.45	1.50
180/0	90	1.00	1.00	1.00	1.00

[1] Dip direction of the closest spaced joint sets relative to the direction of ripping.

[2] Apparent dip angle of the closest spaced joint sets in a vertical plane containing the direction of ripping.

[3] For intact material take J_s = 1.00.

[4] For values of r less than 1:8 (0.125), take J_s as for r = 1:8.

D: Joint roughness number (J_r) and joint alteration number (J_a)

Joint roughness Number (J_r)		
Joint separation	Condition of joint	Joint roughness number (J_r)
Joints tight or closing during excavation	• Discontinuous joints	4.0
	• Rough or irregular, undulating	3.0
	• Smooth undulating	2.0
	• Slickensided undulating	1.5
	• Rough or irregular, planar	1.5
	• Smooth planar	1.0
	• Slickensided planar	0.5
Joints open and remain open during excavation	• Joints either open or containing soft gouge of sufficient thickness to prevent joint wall contact upon excavation	1.0
	• Shattered or micro-shattered clays	1.0

Joint alteration number (J_a)			
Description of gouge	Joint alteration number (J_a) for joint separation (mm)		
	< 1.0[1]	1.0 - 5.0[2]	> 5.0[3]
• Tightly healed, hard, non-softening impermeable filling	0.75	-	-
• Unaltered joint walls, surface staining only	1.0	-	-
• Slightly altered, non-softening, non cohesive rock mineral or crushed rock filling	2.0	4.0	6.0
• Non-softening, slightly clayey, non-cohesive filling	3.0	6.0	10.0
• Non-softening, strongly over-consolidated clay mineral filling, with or without crushed rock	3.0	6.0	10.0
• Softening or low friction clay mineral coatings and small quantities of swelling clays	4.0	8.0	13.0
• Softening moderately over-consolidated clay mineral filling, with or without crushed rock	4.0	8.0	13.0
• Shattered or micro-shattered (swelling) clay gouge, with or with out crushed rock	5.0	10.0	18.0

[1] Joint walls are effectively in contact

[2] Joint walls come into contact after approximately 100 mm shearing

[3] Joint walls do not come into contact at all upon shearing

Table 3.6: Kirsten's excavatability classes (after Kirsten, 1982).

A: Eight class excavation classification system for soil, detritus and rock

Material type	Class	Ratings	Excavation technique	Bulldozer characteristics				
				Type	Mass (tonnes)	Flywheel power (kW)	Drawbar pull (kN)	
							Stalling speed	1.6 km/h
Soil / detritus	1	< 0.01	• Hand spade	D3	6	46	151	65
	2	0.01 - 0.09	• Hand pick and spade	D4E / D5B	9 / 12	56 / 78	165 / 202	77 / 110
	3	0.1 - 0.9	• Power tools	D6D	14	104	250	147
Rock	4	1.0 - 9.9	• Easy ripping	D7G	20	149	376	220
	5	10 - 99	• Hard ripping	D8K	32	224	500	323
	6	100 - 999	• Very hard ripping	D9H	43	306	667	445
	7	1000 - 9999	• Extremely hard ripping	D10	78	522	1230	778
	8	> 10000	• Blasting	-	-	-	-	-

B: Four class excavation classification system for soil, detritus and rock

Material type	Class	Ratings	Excavation technique	Bulldozer characteristics				
				Type	Mass (tonnes)	Flywheel power (kW)	Drawbar pull (kN)	
							Stalling speed	1.6 km/h
Soil / detritus	1	< 0. 1	Hand pick and spade	D3/ D4E/ D5B	6 - 12	46 - 78	151 - 202	65 - 110
Soft rock	2	0.1 - 9.9	Power tools / easy ripping	D6D / D7G	14 / 20	104 / 149	250 / 376	147 / 220
Average rock	3	10 - 999	Hard - very hard ripping	D8K / D9H	32 / 43	224 / 306	500 / 667	323 / 445
Hard rock	4	> 1000	Extremely hard ripping - blasting	D10	78	522	1230	778

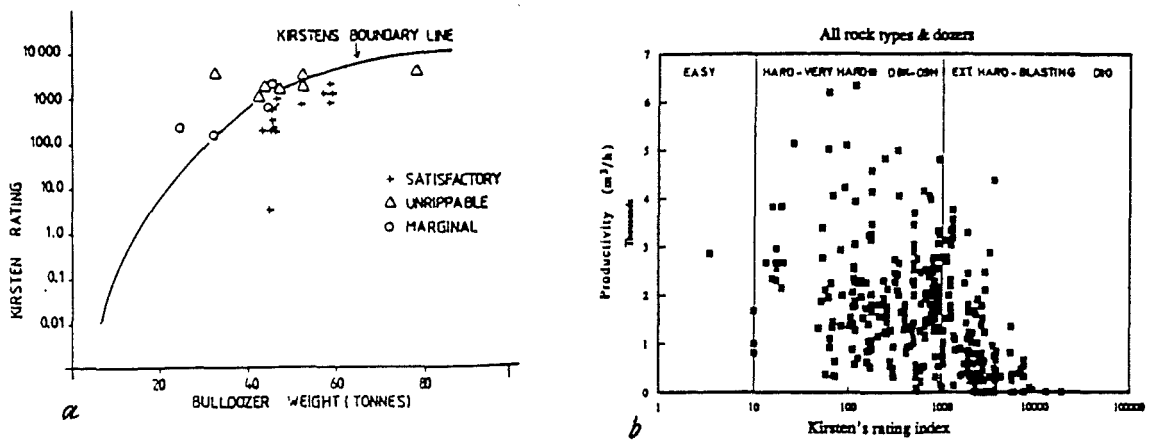

Figure 3.11: (*a*) Braybrooke's (1988) reinterpretation of Martin's (1986) data, showing Kirsten's boundary between satisfactory ripping and uneconomic ripping and (*b*) MacGregor's, *et al* (1994) analysis of ripping data using Kirsten's method.

3.5.5 Minty and Kearns' rippability rating system

Minty and Kearns (1983), like Weaver, combined geological data and the seismic velocity of a rock mass in producing their Rock Rippability Graph. This graph (Figure 3.12) plots the mass of a ripping machine against the product of a geological factors rating (GFR) and the seismic velocity. This graph was based on forty case studies involving ripping on road cuts and open pits.

The GFR is obtained from Table 3.7. The factors are similar to those used by Weaver, except groundwater conditions are added and the subdivisions and ratings are slightly different. The table is divided into two categories - rock substance (or rock material) factors and rock defect (or discontinuity) factors - which are combined to give a total rating for the rock mass.

Minty and Kearns (1983) originally tried plotting their case studies against the expected productivity of a ripping machine, however the correlation between rippability and productivity was poor, leading Minty and Kearns to conclude that it is unrealistic to use graphs with production as one axis. They also attempted plotting seismic velocity versus

the GFR for four machinery weight ranges, but there was insufficient data to delineate rippable, marginal and non-rippable zones. Therefore they plotted the machinery weight against the product of the GFR and seismic velocity, resulting in a boundary between satisfactory rippability and marginal rippability. It must be noted however, that their inferred boundary position does not delineate rippability zones, rather it delineates workability zones where workability is the ability of the rock mass to be broken into a product of a desired size for the purpose intended (Minty and Kearns, 1983). Sometimes ripping breaks up a rock mass into blocks too large and, therefore require further splitting. In these cases, the rock mass is rippable but not workable.

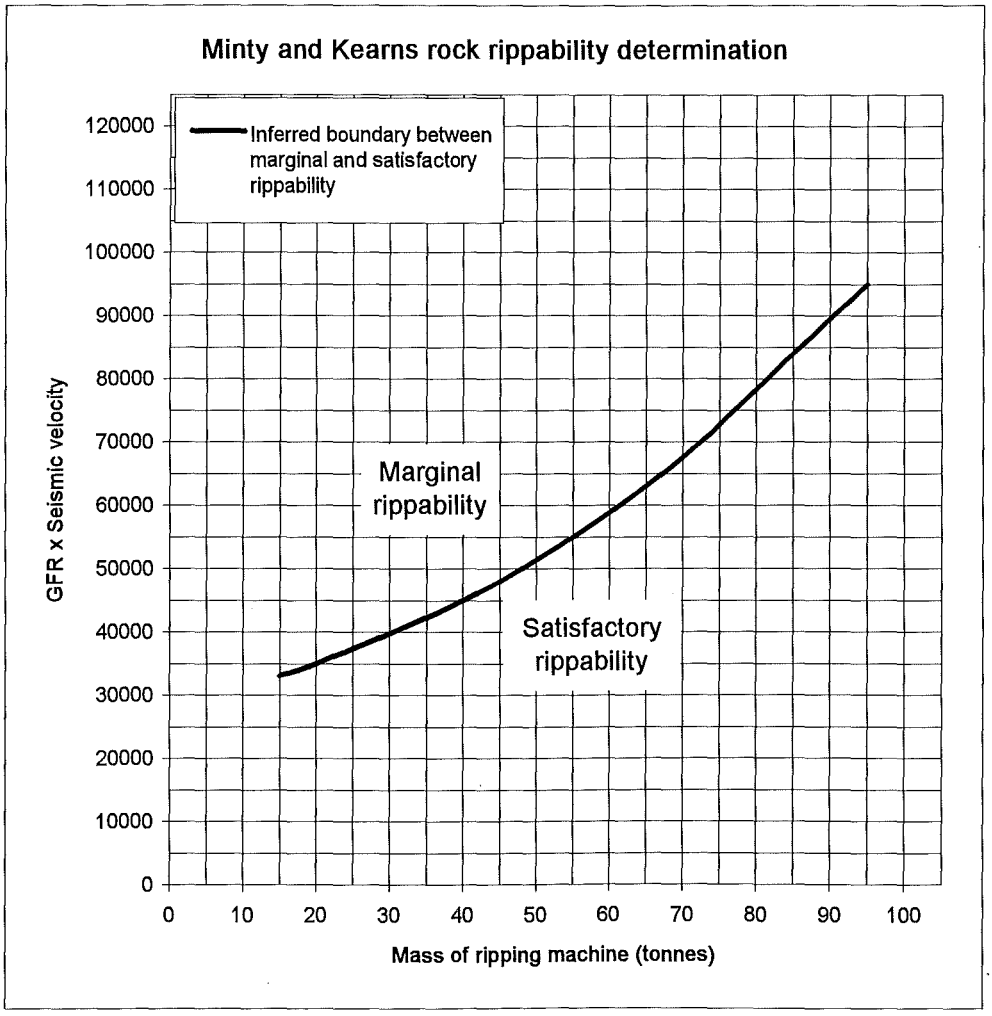

Figure 3.12: Minty and Kearns' Rock Rippability Determination Chart (after Minty and Kearns, 1983).

Table 3.7: Minty and Kearns' Geological factors rating scale (after Minty and Kearns, 1983).

Rock substance factors

Weathering	Residual soil	Extremely weathered	Highly weathered	Moderately weathered	Slightly weathered	Fresh	Silicified
Rating	-12	-10	-7	0	5	10	12
Rock strength	Extremely weak	Very weak	Weak	Medium strong	Strong	Very strong	Extremely strong
Rating	-12	-10	-7	0	5	10	12
Groundwater	Wet		Moist		Completely dry		
Rating	0		1		3		

Rock defect factors

Continuity	Continuous				Non-continuous		
Rating	0				5		
Roughness	Polished - Smooth		Rough		Very rough with small steps		
Rating	0		1		2		
Separation	Wide (>20 mm)		Narrow (2 - 20 mm)		close to tight (0 -2 mm)		Cemented
Rating	0		1		2		5
Spacing	Very narrow < 6 mm	Narrow 6 - 20 mm	Mod. narrow 20 - 60 mm	Mod. wide 60-200mm	Wide 200-600mm	Very wide 600mm-2m	Ext. wide > 2 m
Rating	0	5	10	15	20	25	30
Discontinuity Orientation	Dip 0 - 20° Unfavourable	Strike perpendicular to ripping direction With dip: Dip 20-45° Favourable	Strike perpendicular to ripping direction With dip: Dip 45 - 90° Very favourable	Strike perpendicular to ripping direction Against dip: Dip 20 - 45° Unfavourable	Strike perpendicular to ripping direction Against dip: Dip 45 - 90° Fair - favourable	Strike parallel to ripping direction: Dip 20 - 45° Fair	Strike parallel to ripping direction: Dip 45 - 90° Very unfavourable
Rating	13	5	3	13	6	10	15

Analysis of Minty and Kearns' rating system have shown that the boundary between satisfactory and marginal ripping is conservative (Pells, 1985; Braybrooke, 1988; MacGregor, *et al*, 1994). Braybrooke (1988), plotting Martin's (1986) data, showed that for half the case studies (of which half were unrippable rock), correlation was good, but for the other half, the correlation was poor, indicating that unrippable rock is easily predicted but the ease of rippability is not. MacGregor *et al* (1994) found that many case studies of medium to very easy ripping plotted in the marginal rippability zone. The rippability assessments are most likely to be conservative because of the rippability (workability) prediction line being drawn so as to avoid oversized material in the ripped rock (Pells, 1985). Koczanowski *et al* (1991) suggested downgrading the predicted bulldozer by one model to overcome the conservatism.

3.5.6 MacGregor *et al* productivity prediction method

MacGregor *et al* (1994) performed a very detailed investigation into the estimation of rock rippability. A total of 527 ripping data sets were collected. Data included geotechnical and structural information, machinery and contractor data, as well as site conditions. The study involved trying to correlate rippability with machine productivity. Every variable in the data set was correlated with productivity.

MacGregor *et al* (1994) found all correlations to be poor, but the best two correlations were with uniaxial compressive strength (UCS) and seismic velocity (Figure 3.13). For each UCS value there is a large range in productivity and the correlation coefficient, R^2, equalled 0.32, indicating that UCS by itself is not an adequate predictor of productivity. The correlation coefficient between seismic velocity and productivity was also 0.32. The data showed that there is a limiting value of about 2000 ms^{-1}, beyond which, ripping is difficult to very difficult and above 3000 ms^{-1} rock is not rippable with bulldozers of size D10 or less.

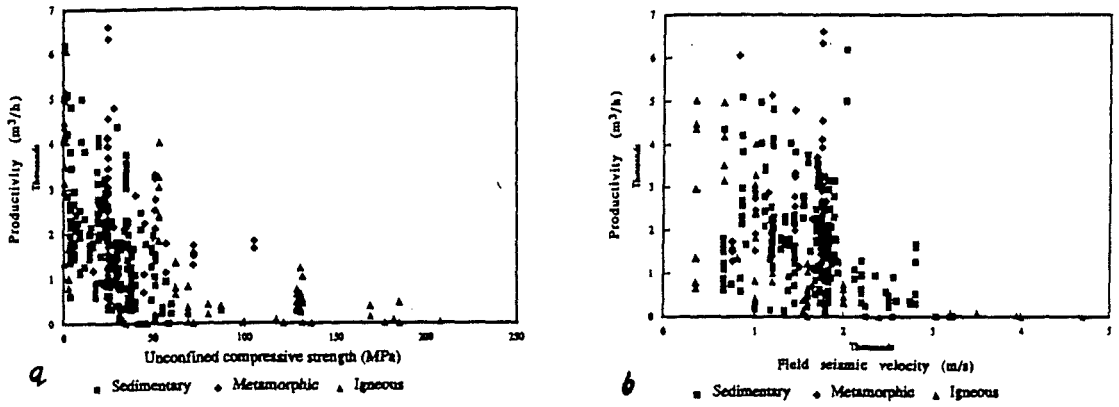

Figure 3.13: Plots of unconfined compressive strength (*a*) and seismic velocity (*b*) versus productivity for all rock types.

The study found that no one variable could accurately predict machine productivity, therefore a stepwise multiple regression analysis was performed. This involved correlating a total of 22 factors most likely to affect rippability using 351 data sets (all factors are described in Appendix B3). Factors such as weathering, strength, defect spacing and bulldozer track conditions were correlated with bulldozer productivity.

A preliminary analysis of the results revealed that some machinery factors such as the condition of bulldozer and restrictions on movement were very important but these factors cannot be predicted in a preliminary estimation of the rippability of a site, and therefore were removed from the regression analysis along with block volume and defect wall strength, which were also considered too hard to determine during a project's investigation stage. Despite these factors being removed from the regression, the final accuracy of the predictions were not significantly reduced (MacGregor *et al*, 1994).

A list of regression equations with the seven most dominant factors (weathering, grain size, seismic velocity, defect roughness, the number of defect sets, defect spacing, and a structural rating) are given in Table 3.8. The correlation coefficients, R^2, are poor but they are they best possible correlations from variables easily determined during the investigation and design stage of a project. The ratings and calculation of the parameters listed in Table 3.8 are shown in Table 3.9, and a full list of ratings as well as their definitions is reproduced in Appendix B3.

The dip angle of the dominant defect and the orientation of ripping relative to the strike of the main defect were not found to be significant in the stepwise regression, implying that the defect orientation does not affect productivity, although MacGregor *et al* (1994) do recognise that the relative orientation of a defect does have a significant effect on the rippability of a rock mass.

When productivity was estimated, MacGregor *et al* (1994) had to estimate the length of a ripping run, the depth of penetration of the tip and the width between ripping runs so that excavation was not hindered. MacGregor *et al* calculated that the largest possible error in a run productivity estimation would be 40%, but the area productivity should not have an error this large as the run productivity errors should average out.

Table 3.8: Regression equations for all rock types (after MacGregor *et al*, 1994)

Equation Number	1 PROD[2]	2 PROD/MASS	3 √ PROD	4 (√ PROD)/MASS
Constant	+1830	+14.5	+53.7	+0.469
UCS (MPa)	-14.5	-0.197	-0.203	-0.00321
Weathering Rating	+157	+2.20	+1.36	+0.0230
Grain size rating	-190	-1.73	-2.99	-0.0205
Seismic Velocity (ms^{-1})		-0.00453	-0.006	-0.00011
Seismic weight	-24.7			
Roughness rating	+109[1]	+2.99	1.09[1]	+0.0535
Number of defect sets	+164[1]	+3.35		+0.0524
Defect spacing (mm)	-0.105[1]		-0.00153[1]	
Structure rating		+0.464		+0.0114
R^2 [3]	0.41	0.46	0.50	0.58
s [4]	950	13.6	11.4	0.18

Equation Number	8 Sedimentary (√ PROD)/MASS	9[5] Metamorphic (√ PROD)/MASS	10 Igneous (√ PROD)/MASS	11 Igneous (√ PROD)/MASS
Constant	+0.866	+0.895	-0.138	+0.347
UCS (MPa)	-0.00736	-0.00516		-0.00118
Weathering Rating		+0.0368[1]	+0.112	
Grain size rating		-0.254	-0.0599	
Seismic Velocity (ms^{-1})	-0.000119		-0.000084	-0.00014
Roughness rating	+0.0496		+0.106	+0.108
Defect spacing (mm)	-0.00004		-0.000225	
Structure rating		+0.00132[1]		
R^2	0.52	0.44	0.85	0.67
s	0.17	0.19	0.10	0.15

Notes:
[1] These variables have a lower statistical significance
[2] PROD = productivity in m^3/hr; MASS = bulldozer mass in tonnes including the ripper
[3] R^2 = correlation coefficient of regression
[4] s = standard error of the estimate
[5] This equation is not statistically valid.

To estimate the productivity for a site the appropriate value or rating for each parameter is multiplied by the variable in Table 3.8. These numbers are totalled and relate back to the productivity according to the mass of the bulldozer used. Table 3.10 compares the expected productivity from using different equations on different rocks. It should be noted in Table 3.10 that equation 8 usually estimates lower productivity than equation 4, but MacGregor *et al* (1994) suggest, when estimating the rippability of sedimentary rocks that equation 8 should be used.

Table 3.9: Ratings for the variables used in Table 3.8 (after MacGregor, *et al*, 1994).

Unconfined compressive strength

The best estimate of the unconfined compressive strength of the rock mass in a ripped area is taken primarily from UCS tests on ripped material, but can also be taken from tests such as the point load test and other sources of information from an area. The UCS value (in MPa) used should be the in situ moisture condition rather than a saturated value.

Structural description

Rating	Rocks with bedding		Rocks without bedding		
	Bedding	Defects	Joint set 1	Joint set 2	Joint set 3
1	Massive	Very wide	Very wide	Very wide	Very wide
2	Massive	Wide-very wide			
3	Massive-thick	Wide-very wide	Wide	Very wide	Very wide
4	Thick	Wide-very wide	Wide	Wide	Very wide
6	Thick	Wide	Wide	Wide	Wide
7	Thick, but weakness parallel to bedding	Wide-very wide			
8	Medium-thick	Wide-very wide	Medium	Wide	Wide
9	Medium-thick	Medium-wide	Medium	Medium	Wide
11	Medium	Medium-wide	Medium	Medium	Medium
12	Medium A	Medium-wide			
13	Medium B	Medium-wide			
14	Medium C	Medium-wide	Close	Medium	Medium
15	Thin-Medium	Close-wide			
16	Thin	Close-wide	Close	Close	Medium
17	Laminated	Close-wide			
18	Thin	Close	Close	Close	Close
19	Soil		Soil		

Bedding		Joints	
Massive	> 2 m	Very wide	> 2 m
Thick	0.6 m - 2 m	Wide	0.6 m - 2 m
Medium	200 mm - 0.6 m	Medium	200 mm - 0.6 m
Medium A (interbedded sst and cong)	200 mm - 0.6 m	Close	60 mm - 200 mm
Medium B (interbedded sst and shale	200 mm - 0.6 m	Very close	< 60 mm
Medium C (interbedded sst)	200 mm - 0.6 m		
Thin	60 mm - 200 mm		
Laminated or very thin	< 60 mm		

Field seismic velocity

The seismic refraction velocity (in ms^{-1}) obtained before excavation at the site begins.

Number of defect sets

The number of defect sets including bedding.

Defect spacing

Spacing of the dominant defect set (in mm)

Defect roughness

Rating	Description	
1	Smooth	A/L = < 0.05
2	Medium	A/L = 0.05 - 0.10
3	Rough	A/L = 0.10 - 0.15
4	Very rough	A/L = > 0.15

Note: A/L is the ratio of amplitude to length.

Table 3.9 (continued): Ratings for the variables used in Table 3.8 (after MacGregor, *et al*, 1994).

Weathering rating

Rating	Description
1	Fresh
3	Fresh with stained joints
3	Slightly weathered to fresh
4	Slightly weathered
5	Moderate to/and slightly weathered
6	Moderately weathered
7	Highly to moderately weathered
8	Highly weathered
9	Highly to extremely weathered
10	Extremely weathered

Note: The rating applies to the rock substance not the joints or weathering adjacent to joints.

Grain size

Sedimentary rocks		
Description	**Grain diameter**	**Rating**
Boulders	200 - 600 mm	7
Cobbles	60 - 200 mm	7
Coarse gravel	20 - 60 mm	7
Medium gravel	6 - 20 mm	6
Fine gravel	2 - 6 mm	5
Coarse sand	0.6 - 2 mm	4
Medium sand	0.2 - 0.6 mm	3
Fine sand	0.06 - 0.2 mm	2
silt, clay	< 0.06 mm	1
Igneous rocks		
Very coarse	> 30 mm	7
Coarse	5 - 30 mm	5
Medium	1 - 5 mm	3
Fine	< 1 mm	1
Glassy	0 mm	1

Table 3.10: Application of productivity equations (From MacGregor, *et al*, 1994).

Rock Properties	Sandstone				Sandstone and siltstone					Igneous		
	A	B	C	D	E	F	G	H	I	J	K	L
UCS (MPa)	40	30	40	50	40	40	40	30	30	100	100	80
Weathering rating	3	3	3	3	3	3	3	6	6	4	4	4
Number of defects	2	2	2	2	3	3	3	3	3	3	3	3
Roughness rating	2	2	2	2	1	1	1	1	2	2	2	2
Structure rating	4	4	4	4	11	11	11	11	11	2	2	2
Seismic velocity	3000	2600	3000	3400	2500	2500	3000	2200	2200	2500	2000	2000
Grain size	3	3	3	3	2	2	2	2	2	5	5	5
Bulldozer size	D9L	D9L	D10	D9L	D9L	D10	D9L	D9L	D10	D9L	D9L	D9L
Productivity Estimates												
Equation 2	530	750	800	225	980	1475	850	1550	2350	30	170	400
Equation 4	270	430	600	140	650	1450	500	1100	2500	80	140	250
Equation 8	260	550	590	80	350	750	220	550	1250	-	-	-
Equation 10	-	-	-	-	-	-	-	-	-	200	270	270
Equation 11	-	-	-	-	-	-	-	-	-	90	160	200

Plots of residuals (difference between actual value and predicted value, where positive residuals underestimate productivity and negative residuals overestimate productivity) versus the number of ripping runs a bulldozer performs (Figure 3.14) showed an even scatter between positive and negative residual values, although the scatter is large, implying that MacGregor *et al's* (1994) method does not consistently under-estimate or over-estimate productivity and that productivity estimation may not be very accurate. Residual plots versus the operator of a bulldozer show that some operators consistently underproduced and some operators consistently overproduced, meaning that the experience of the bulldozer operator is relatively important.

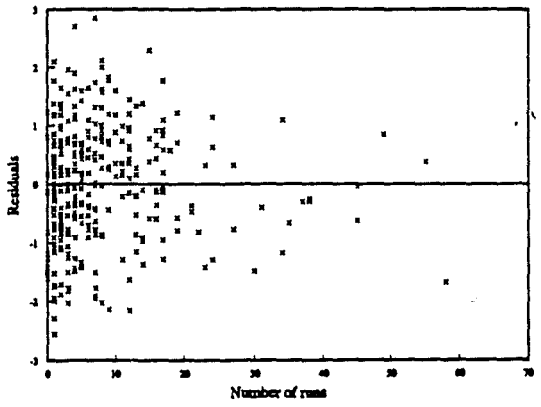

Figure 3.14: Plot of residuals versus the number of ripping runs a bulldozer performs (from MacGregor, *et al*, 1994).

Based on the fact that productivity is almost impossible to reliably estimate, MacGregor *et al's* (1994) recommendation for rippability prediction is to:

- Predict the run productivity using the appropriate equation for the rock type and comparing with equation 4 (for all rock types). The predicted productivity should be slightly conservative to compensate for data quality and any potential economic consequences of underestimation or overestimation of productivity.
- Identify areas or conditions that should be difficult to rip and may require blasting. If the estimated productivity is less than 750 m^3/hr, then difficult ripping conditions should exist. If the productivity is estimated to be less than 250 m^3/hr, then very difficult ripping should exist and blasting should be considered.

3.6 Ripping versus blasting

In suitable ground, there are many reasons why ripping is a more suitable form of excavation technique than blasting, but in ground classed as marginal to rip, bulldozer productivity may be lower than expected, maintenance time may be higher than expected and replacement parts may be required more often, making blasting a more cost-effective excavation method. In suitable ground, ripping is more cost effective, safer and more flexible (Atkinson, 1970).

When blasting is performed, labour and machines must be moved from the blast areas, thus reducing labour utilisation and machine availability, whereas ripping bulldozers can operate continuously. From a safety aspect, ripping is clearly less hazardous than blasting although good blasting procedures should eliminate most of the dangers associated with blasting (Atkinson, 1970). Ripping bulldozers can also be used for a variety of purposes aside from ripping, such as scraping, dozing, moving machinery and stockpiling, making the purchase of a bulldozer almost mandatory whether or not the site is to be ripped.

Ripping at a site results in significantly less ground and air vibrations than blasting (Atkinson, 1970). Blasting near urban areas may lead to bad public relations, or may not even be allowed, depending on local by-laws. Vibrations from blasting may trigger slope failures as most pit slopes are near equilibrium, resulting in wasted time clearing the debris.

Fragmentation of the rock mass is normally greater by ripping methods than blasting methods meaning less oversized material would need to be split before processing. Ripping machines have more accuracy and control over the excavation dimensions than blasting and pit slope walls will not be damaged by a ripping bulldozer, but they may be damaged by blasting (Fowell, 1993).

One of the greater advantages of ripping over blasting in an open pit is that ripping bulldozers excavate a thin slice at a time, which, if the orebody is modelled accurately enough, can result in improved blending of stockpiles (if ore is stockpiled). For example, the orebody may be modelled into mineable blocks that will be thinner if ripping is used instead of blasting, resulting in more accurate stockpile blending when ripping.

3.7 Synthesis

Rippability classification methods have been developed as a tool to predict the excavatability or rippability of a rock mass. Seismic velocity determination and size-strength determination are two methods discussed that are simple and quick and roughly determine the excavatability of a site. The other methods discussed all require a suite of geological and geotechnical data to provide a more accurate assessment of the rippability of a site. This type of assessment should be performed at the investigation or design stages of a project. However, no rippability classification system is completely accurate, only field trials can determine exactly the rippability of the rock mass on a excavation site. The best approach in evaluating the rippability of a site is to use a system involving all geotechnical parameters likely to affect the rippability. However, during the feasibility or preliminary investigation stage of a project, the graphical method of Pettifer and Fookes or seismic velocity determination may be considered reliable estimates that should be investigated in greater detail if required.

Where possible, data from drillholes, outcrops, seismic surveys and laboratory tests should be combined so that a complete rippability assessment, using a number of different methods, may be appraised.

Rippability site assessments should be performed independent of the likely contractor as contractors obviously have an interest in acquiring a contract to excavate the site, therefore are likely to make their rippability assessment optimistic. If no other assessment is possible, then bulldozer manufacturers assessments should be treated with caution and any productivity estimate should be roughly halved.

If the productivity is estimated to be difficult or very difficult ripping (less than 750 m^3/hr) then blasting should be considered. However the definition of whether ripping is economic or not is site-specific. The project may only allow limited blasting, excavation may need to proceed rapidly, thereby allowing more blasting, or excavation may need to proceed at a certain rate. The economics of ripping on a site, therefore, need to be carefully planned and may vary from site to site.

Chapter Four

Geotechnical investigations

4.1 Introduction

To apply the rock mass classification methods outlined in Section 2.2 and rippability classification methods outlined in Section 3.5, a combination of laboratory and field data from the mine site was required to characterise the rock mass and rock material. Rock material (also called rock substance or intact rock) is defined as intact rock or soil that is composed of mineral grains or crystals and the associated void or pore space, which may be air or water filled (Bell and Pettinga, 1983); whereas a rock mass is the rock material and its associated discontinuities (also called, fractures or defects). Rock materials are studied at the hand specimen scale and are commonly homogeneous. Rock masses are studied at the outcrop scale and are often inhomogeneous because of the presence of two or more different types of rock material and/or discontinuities such as bedding planes, cleavage, jointing and shears.

Irfan and Dearman (1978) listed the requirements of tests used for classification purposes as:

- Rapid and simple, involving a minimum of specimen preparation,
- Relevant to the rock properties and engineering problems,
- Capable of discriminating between grades of engineering significance.

All geotechnical tests performed in this study comply with these requirements.

The purpose of the geotechnical testing programme was to:

- Characterise the rock mass and rock material at Globe-Progress,
- Quantify for use in rock mass classifications, drillcore data that had been qualitatively logged,
- Provide extra data for rippability evaluations.

Field testing involved determining the seismic velocity of the rock mass using the seismic refraction method. No other field tests were required as all outcrops had been geotechnically logged by Barrell (1992) and Jowett *et al* (1996), and structurally mapped by Rattenbury (1994). A database of 106 diamond-cored drillhole logs of the rock mass at Globe Hill exists, and these have been logged by many workers over time, for example Hughes (1992) and Barry (1994). Because the outcrop and drillcore logs existed all that was required was consistency checks and comparisons between samples collected and their logged descriptions.

Laboratory testing involved evaluating physical and mechanical properties of the rock material, and using these properties to provide a rough prediction of the behaviour of the rock mass. Laboratory tests were also performed to check quantitative rock material data with qualitatively logged drillhole and outcrop data. The tests performed were:

- Porosity and density determination
- Sonic velocity determination
- Stress-strain relationship
- Uniaxial compressive strength (UCS) and point load strength determination
- Slake-durability determination

4.2 Field Investigations

4.2.1 Seismic refraction surveys

4.2.1.1 Introduction

The seismic velocity of a rock mass is seen as being related to many geological and physical properties such as density, compaction and fracturing of the rock mass (Weaver, 1975; Palmer, 1980; Braybrooke, 1988). For this reason, and because seismic velocity determination is an easy, inexpensive and non-destructive form of site investigation providing information on the quality and variability of a rock mass, twenty seismic refraction surveys were performed on Globe Hill. Sites were chosen to cover the open pit

in as much detail as possible, but the location of surveys lines was restricted by the steep and curving nature of many of the tracks. The seismic velocities found on Globe Hill were then used to provide a preliminary assessment of the rippability of the mine site and as an additional parameter in rippability classification systems (detailed in Section 3.5). The seismic velocities can also be compared to the sonic velocities found on rock material (Section 4.4).

The surveys were performed between March 1995 and March 1996 in weather conditions ranging from fine to drizzle to persistent rain. Fifteen of the line traverses are on Globe Hill and five of the line traverses are at General Gordon, proposed location of the rock waste stack. The location of each line traverse is shown on Figure 4.1 (in map and table box).

4.2.1.2. Methodology

The seismic refraction equipment used (Soiltest single channel signal enhancement seismograph, model MD-9A) requires a sledgehammer to be impacted against a metal plate, creating a small seismic wave that is detected by geophones at both ends of the line traverse. The energy source is moved along the line, while the geophones remain stationary (Figure 4.2). The elevation of each hammer point was surveyed using a Sokkisha automatic level, model B-2. Line traverses were between 20 m and 86 m in length, and most ranged between 30 m and 40 m. Seismic refraction lines 2.1-2.2 and 3.1-3.2 were resurveyed six months later to check for consistency and repeatability of results and this data is included in Appendix D2.3.

The travel time of the first P wave recorded by the seismograph from a hammer point to a forward and a reverse geophone were recorded for data analysis using the Generalised Reciprocal Method (GRM; see Appendix D2 for theory and data processing methodology). This method enables the seismic velocity (or changes in seismic velocity) of the refracting layer (normally bedrock) underlying the line traverses to be determined from travel time graphs. The method also allows the radial depth to the refracting layer to be determined so that seismic refraction profiles can be plotted, although these were not drawn as only seismic velocities were required for this study.

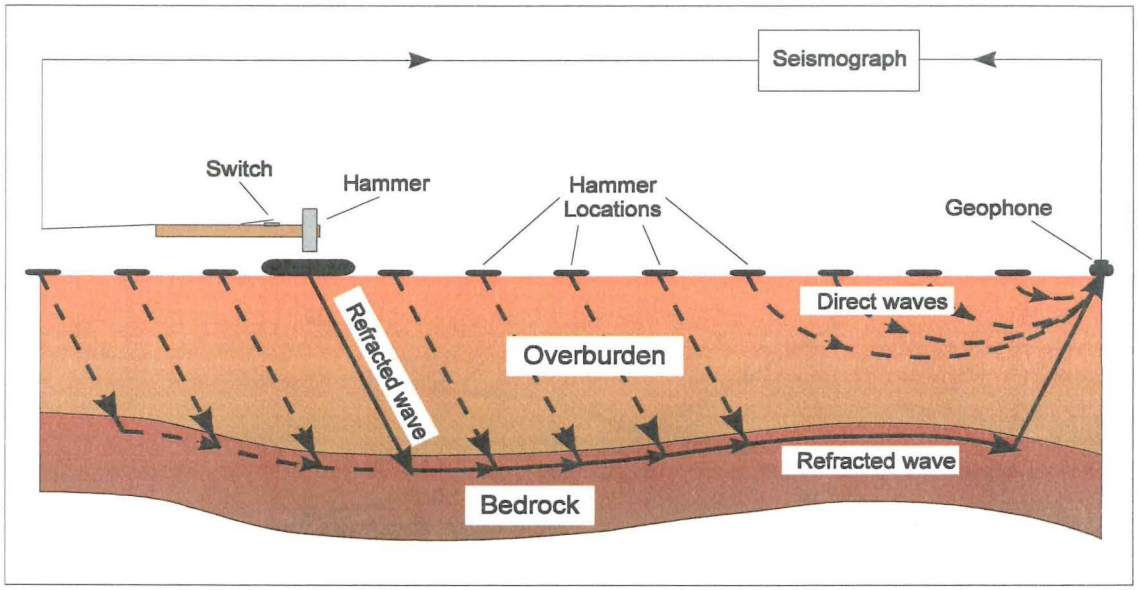

Figure 4.2: Summary diagram of the single channel seismic refraction method for a two layer model (after Bullock, 1978).

4.2.1.3 Results

The results of all seismic refraction line traverses are tabulated in Appendix D2.2 as Tables D2.1-D2.24. Uncorrected and corrected travel time graphs are also included in Appendix D2.2 as Figures D2.1-D2.24 and an example is shown as Figure 4.3. Seismic velocities are calculated from the corrected travel time graphs whereas only apparent seismic velocities may be determined from the uncorrected travel time graphs. A total of 959 m was surveyed and bedrock seismic velocities were determined from 765 m, of which 615 m were on Globe-Progress and 150 m at General Gordon (see Figure 4.1 for position of lines). Seismic velocities were grouped into zones of 500 ms^{-1} and plotted against the distance covered by velocities within each zone, and the data are tabulated in Tables 4.1 and 4.2. They are also plotted in Figures 4.4 and 4.5 for Globe-Progress and General Gordon, and the combined data is shown in Table 4.3 and Figure 4.6. Also included on Figures 4.3 to 4.6 is the cumulative frequency (solid line), which can be used to estimate the total percentage of velocities in each seismic velocity zone. The radial depths at each hammer point to the refracting layer are included Tables D2.1-D2.24 in case the thickness of road fill or colluvium is required at some future stage.

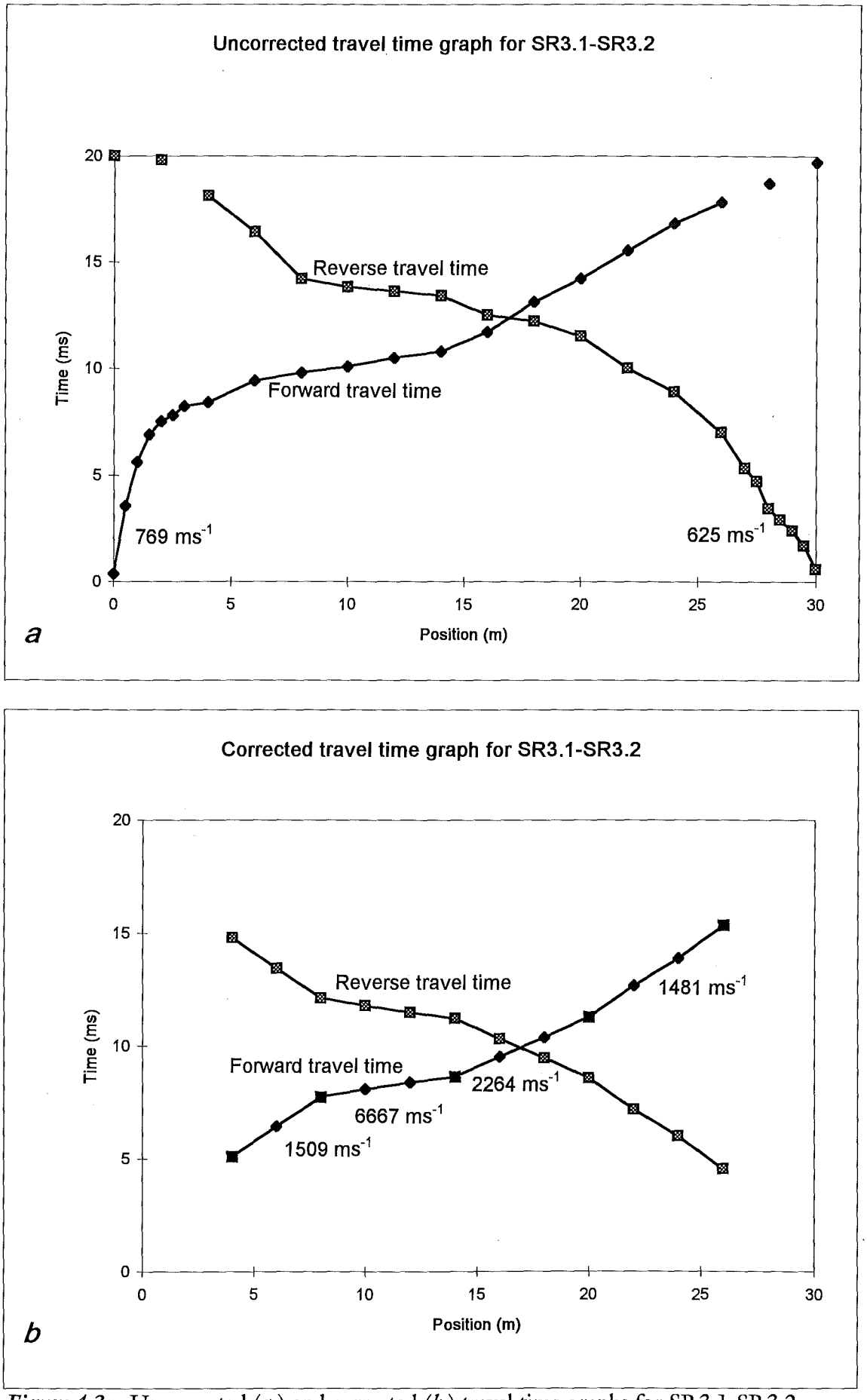

Figure 4.3: Uncorrected (*a*) and corrected (*b*) travel time graphs for SR3.1-SR3.2.

Table 4.1: Summary of seismic velocity data found at Globe-Progress

Velocity range (ms^{-1})	Distance over which velocities occur (m)	Cumulative frequency (%)
0-500	3	0
500-1000	120	20
1000-1500	124	40
1500-2000	84	54
2000-2500	141	77
2500-3000	33	82
3000-3500	30	87
3500-4000	18	90
4000-4500	8	91
4500-5000	8	93
5000-5500	10	94
5500-6000	16	97
6000-6500	12	99
6500-7000	8	100
Total	615	100

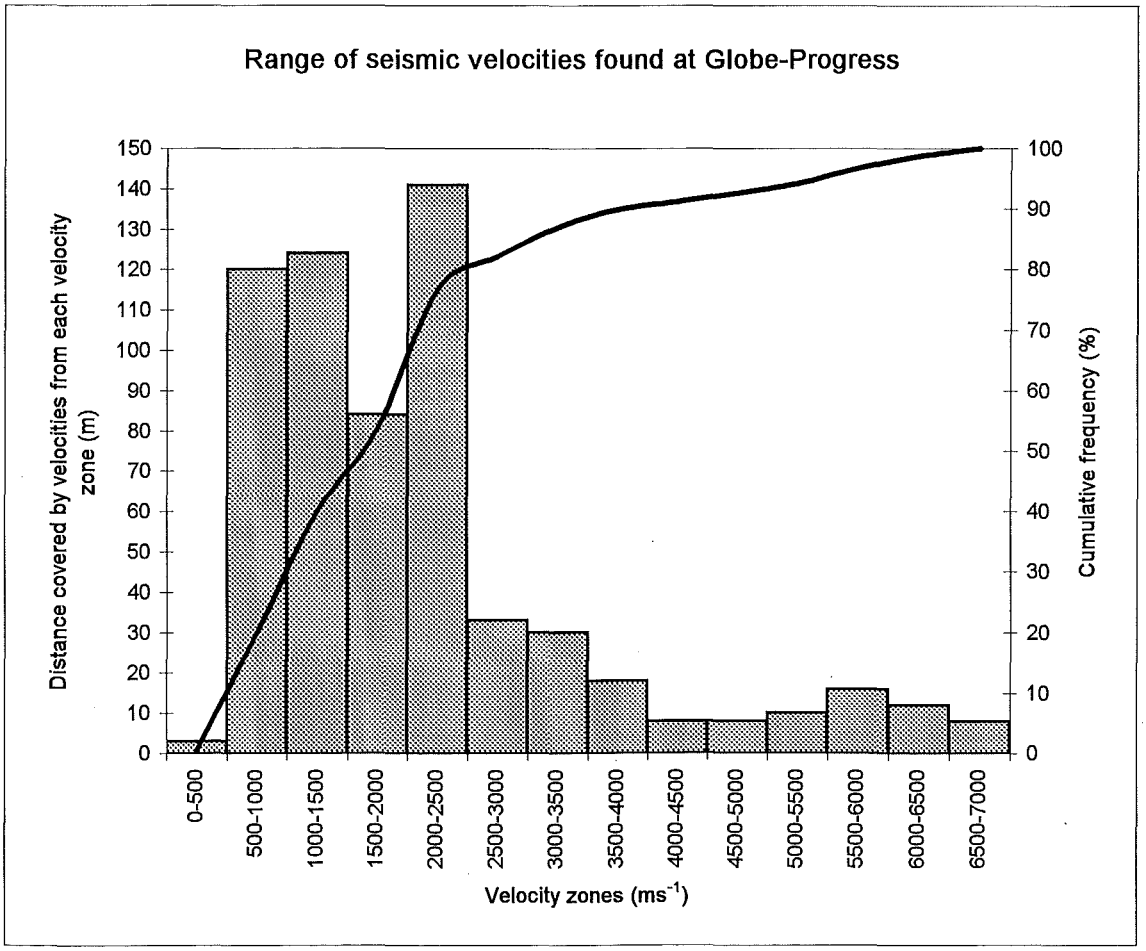

Figure 4.4: Histogram plotting the range and distance covered by velocities within each velocity zone, as well as the cumulative frequency of seismic velocities at Globe-Progress.

Table 4.2: Summary of seismic velocity data found at General Gordon.

Velocity range (ms^{-1})	Distance over which velocities occur (m)	Cumulative frequency (%)
0-500	0	0
500-1000	42	28
1000-1500	38	53
1500-2000	28	72
2000-2500	8	77
2500-3000	0	77
3000-3500	0	77
3500-4000	18	89
4000-4500	8	95
4500-5000	0	95
5000-5500	8	100
5500-6000	0	100
6000-6500	0	100
6500-7000	0	100
Total	150	100

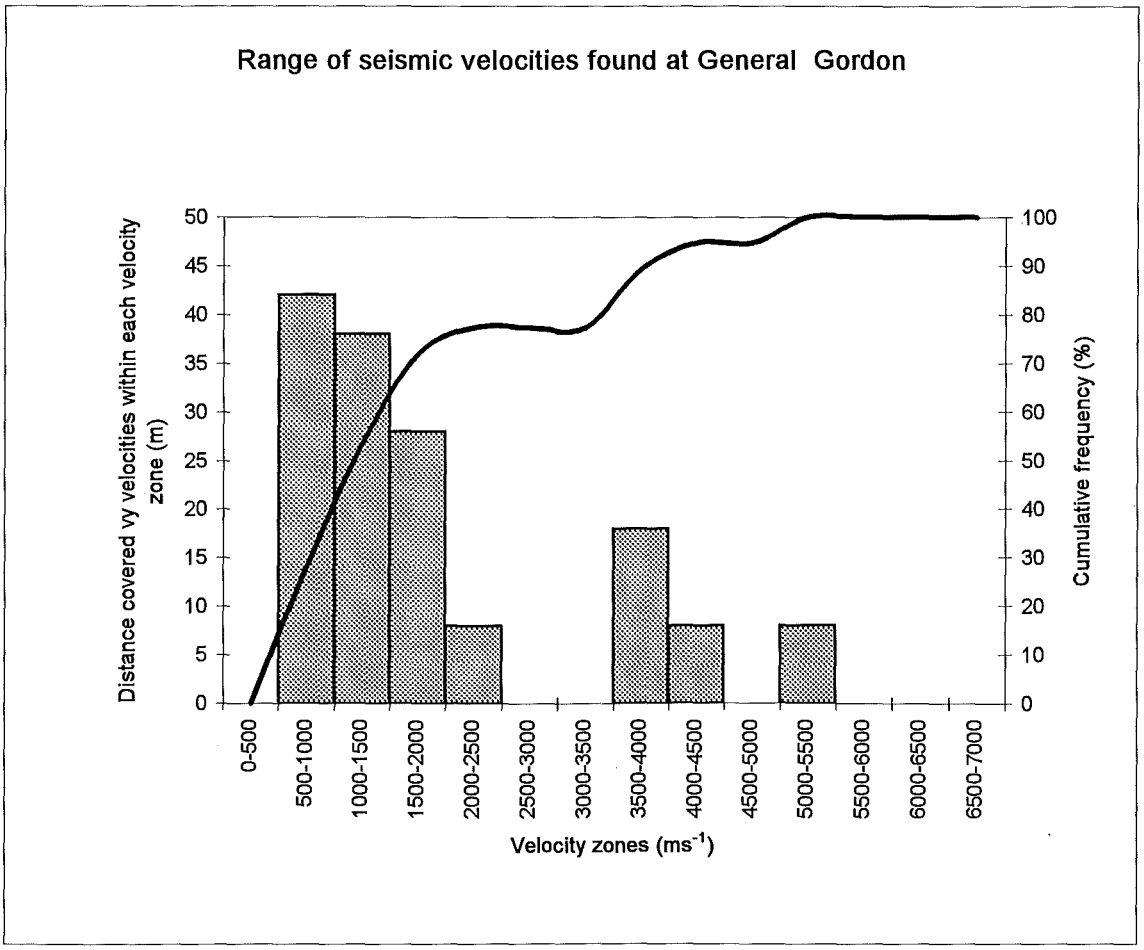

Figure 4.5: Histogram plotting the range and distance covered by velocities within each velocity zone, as well as the cumulative frequency of seismic velocities at General Gordon.

Table 4.3: Complete summary of seismic velocity data found on the mine site.

Velocity range (ms^{-1})	Distance over which velocities occur (m)	Cumulative frequency (%)
0-500	3	0
500-1000	162	22
1000-1500	162	43
1500-2000	112	57
2000-2500	149	77
2500-3000	33	81
3000-3500	30	85
3500-4000	36	90
4000-4500	16	92
4500-5000	8	93
5000-5500	18	95
5500-6000	16	97
6000-6500	12	99
6500-7000	8	100
Total	765	100

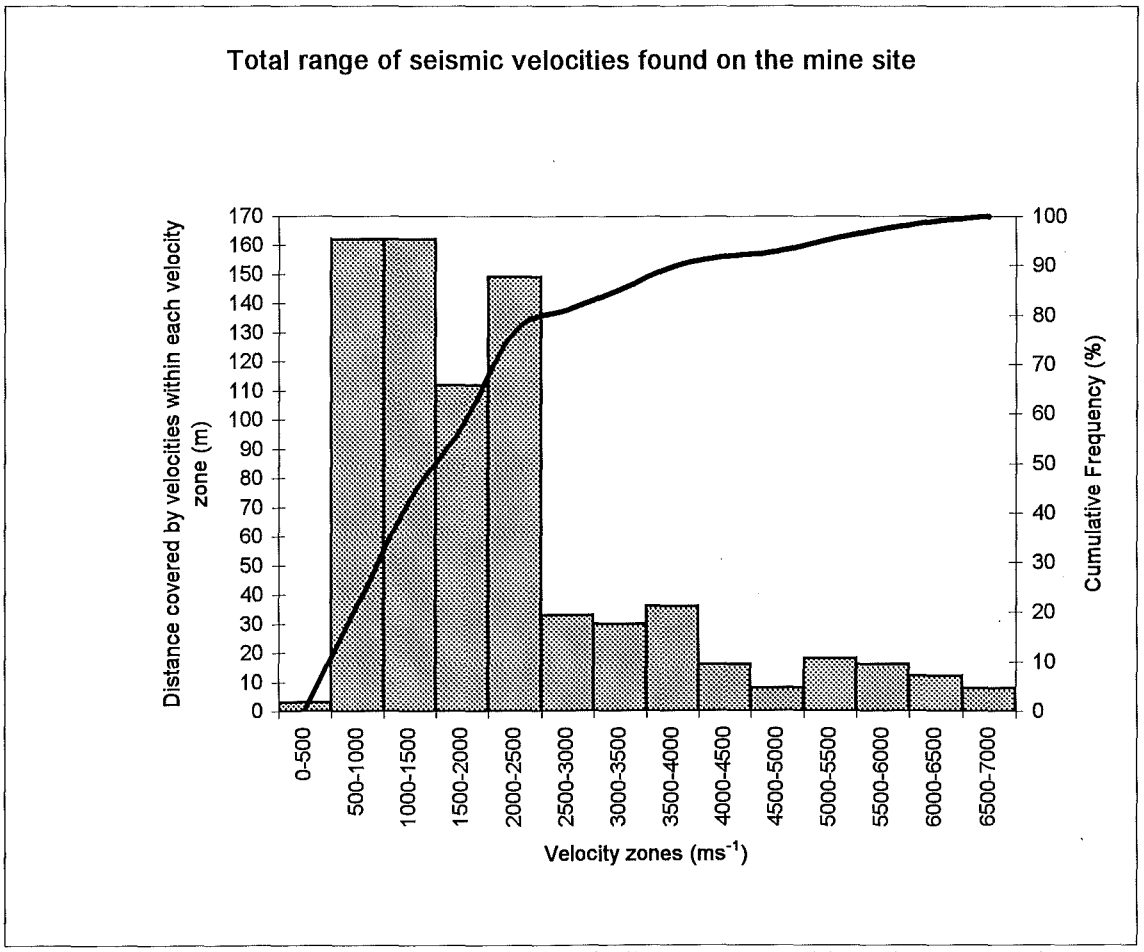

Figure 4.6: Histogram plotting the range and distance covered by velocities within each velocity zone, as well as the cumulative frequency of seismic velocities around Globe Hill.

4.2.1.4 Discussion

Seismic velocities found at Globe-Progress range between 620 ms^{-1} and 6667 ms^{-1}, with a mean of 2100 ms^{-1}. Figure 4.4 shows the spread of data for Globe-Progress, which is very finely skewed and indicates that most of velocities found are less than 2500 ms^{-1}. The same trend occurs at General Gordon (Figure 4.5), where the more limited data ranges between 508 ms^{-1} and 5000 ms^{-1}, with a mean of 1950 ms^{-1}. Figure 4.6 combines the data from Globe-Progress and General Gordon to give the range of seismic velocity data for the mine site.

Scattering of travel times occurs on some of the corrected travel time graphs (Figures D2.1-D2.24), and where it is minor the velocities have been averaged for the rock mass. Where scattering is major, the velocities have been calculated over 2 m intervals (the hammer spacing), for example SR6.1 - SR6.2, where there is an alternating sequence of high and low velocities representing an interbedded sequence of siltstone and sandstone (Figure 4.7).

Two seismic refraction survey lines, both of which contained a spread of seismic velocities, were repeated to check for consistency and repeatability of data (Appendix D2.3). This was done as a check on Kirsten's (1982) statement that the seismic velocity cannot be determined to an accuracy better than approximately 20%, and that there may be variances in the order of 1000 ms^{-1} in apparently identical materials. The results show that the repeated seismic surveys are more or less identical to the original surveys, and any scatter in the results may be accounted for by the degree of ground saturation, as the first surveys were performed in June when the ground was more saturated and the repeat surveys performed the following March after a significant dry spell. The repeatability of the seismic refraction data proves that seismic velocity determination is a viable method to use in estimating characteristics of the rock mass, but the seismic velocities should be compared with sonic velocities determined on rock material to note variations between rock mass properties and rock material properties.

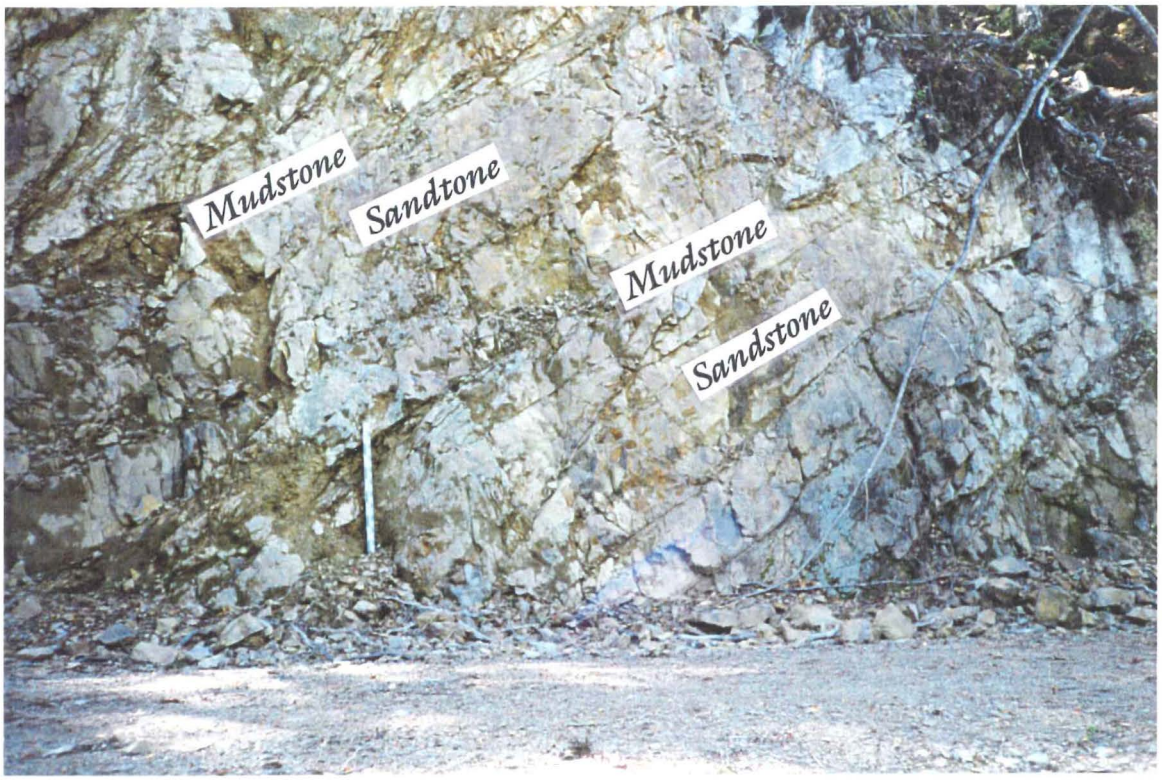

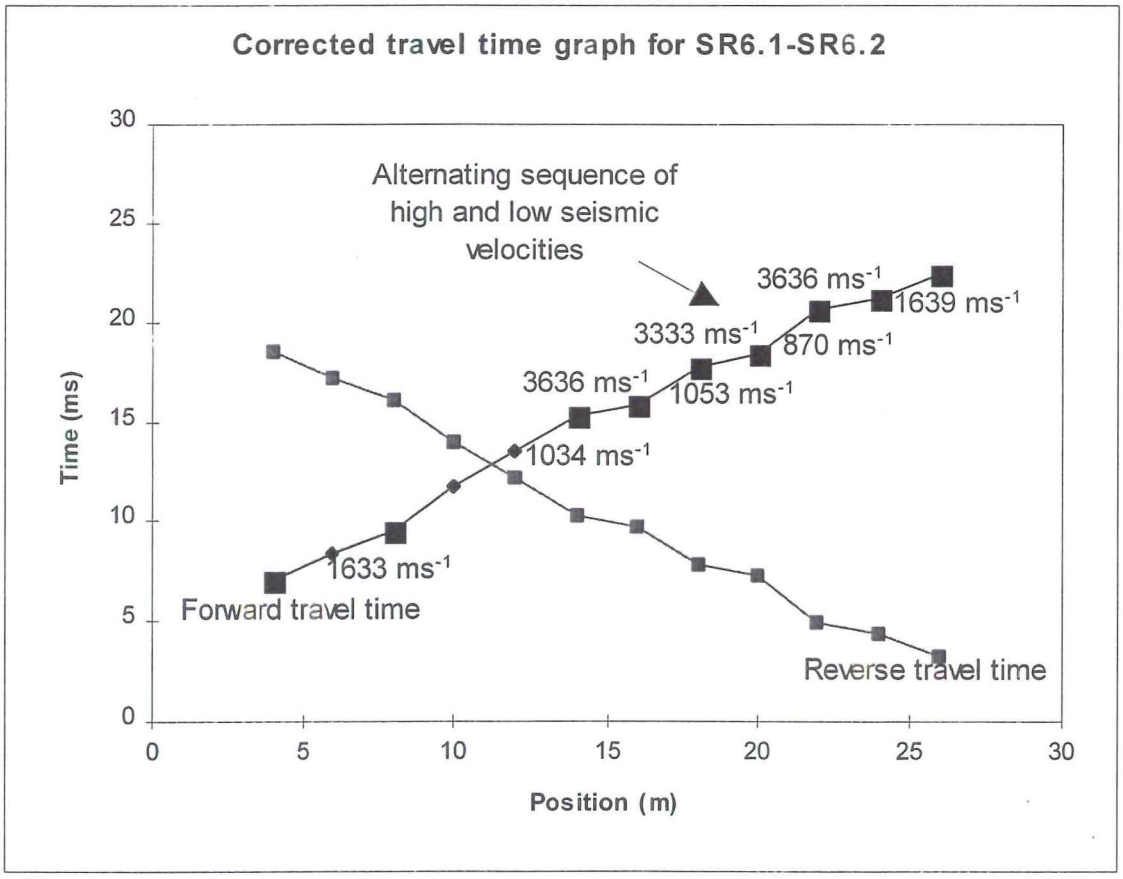

Figure 4.7: Scattering of corrected seismic refraction data relating to interbedded sequence of siltstones and sandstones. The photo is of position 15 to 30 metres and the stake is one metre high.

4.2.2 Observations made on outcrops

Outcrops within the open pit had been geotechnically logged by Barrell (1992) and Jowett *et al* (1996), and structurally mapped by Rattenbury (1994). Therefore only observations on outcrops were made to check for consistency in mapping and to aid in seismic refraction data interpretation. Geotechnical properties of discontinuities types were noted to assist in forming generalisations and assumptions made in calculating the rock mass and rippability classifications in Chapter 5, and which are listed in Appendix E.

4.3 Laboratory investigations

4.3.1 Introduction

Laboratory tests were performed to quantify data collected from drillhole logs and to provide additional data for use in rippability evaluations. Due to the high degree of core fracturing (both natural and drilling induced), and the need for core to be sampled for grade control, not many suitable samples were found for testing, but intact core samples 30 to 50 cm long of HQ (diameter = 61 mm) sized core were selected from six drillholes. Nineteen core samples were later recut to 15-18 cm in length so that porosity-density, sonic velocity and stress-strain laboratory tests could be performed, and the remaining core was cut so that point-load and slake durability tests could be performed on it. Irregular lumps of slightly weathered and moderately weathered rock material were also collected and used with unweathered core samples to the effects of weathering on slake-durability and point load strength.

4.3.2 Geotechnical sample descriptions

There were three types of core tested: very well indurated sandstone (greywacke); brecciated or highly fractured sandstone; and mudstone (argillite), where very well indurated sandstone form most of the overburden or waste rock in the open pit, brecciated and highly fractured sandstone is found close to the Globe-Progress Shear Zone and mudstones are part of interbedded and flysch sequences. The majority of samples collected

were very well indurated sandstone as this rock material is expected to be hardest to rip because of its high intact strength. Mudstones, and brecciated sandstones are all expected to be relatively easy to rip because of their many laminations and fractures. Only one mudstone sample was tested for its geotechnical properties as other samples were damaged during sample preparation. Tested core samples have been labelled according to the drillhole they originated from and the sample number from that hole; for example GB92.19 is the 19th sample tested from hole GB92. Samples were then described (Table 4.4) using hand specimen descriptions similar to that used in drillcore logs (see Appendix B2) so that comparisons could be made between core samples and drillcore logs.

4.3.3 Porosity-Density Determination

4.3.3.1 Introduction

ISRM (1981) state that porosity-density determination is one of the fundamental physical properties that should be determined for rock classification systems. Although the properties are not utilised in any of the classifications systems discussed in Chapter 2 and Chapter 3, the test was still performed because the mechanical performance of rock material is highly dependent upon porosity and density. This is because the presence of voids in the fabric of a rock material decreases its strength and increases its deformability (ISRM, 1981). Density is inversely proportional to porosity, so that rocks with a high density are expected to have low porosity.

4.3.3.2 Methodology

Samples were prepared and tested following the procedures suggested by ISRM (1981). The saturation and calliper testing procedure was followed. This method requires specimens that are geometrically uniform, such as core samples, to be used. All core samples tested had a small shaving of approximately one millimetre thickness and one centimetre width that was used for assaying. The shavings volume was estimated and subtracted from the total volume of each core sample to obtain more accurate values of porosity and density.

Table 4.4: Hand specimen description and position of core sample in drillhole for core samples used in geotechnical laboratory tests.

Sample Number	Position (m)	Description
Sample GB23.3	153.7 - 153.8	Unweathered, light olive grey, medium to fine grained, brecciated sandstone.
Sample GB65.3	44.4 - 44.6	Unweathered, light grey, medium to very fine grained, very well indurated sandstone.
Sample GB87.1	188.3 - 188.5	Unweathered, light olive grey, medium to fine grained, brecciated sandstone.
Sample GB87.4	175.3 - 175.5	Unweathered, light olive grey, medium to very fine grained, very well indurated sandstone.
Sample GB87.6	239.1 - 239.3	Unweathered, light olive grey, medium to fine grained, laminated sandstone.
Sample GB92.1	32.8 - 33.0	Unweathered, light olive grey, medium to very fine grained, very well indurated sandstone.
Sample GB92.4	41.7 - 41.9	Unweathered, greenish grey, medium to very fine grained, very well indurated sandstone.
Sample GB92.7	42.7 - 42.9	Unweathered, light olive grey, medium to very fine grained, very well indurated sandstone.
Sample GB92.9	43.1 - 43.3	Unweathered, dark greenish grey, medium to very fine grained, very well indurated sandstone.
Sample GB92.12	43.5 - 43.7	Unweathered, light olive grey, medium to very fine grained, very well indurated sandstone.
Sample GB92.14	48.2 - 48.4	Unweathered, greenish grey, medium to very fine grained, very well indurated sandstone.
Sample GB92.17	50.0 - 50.2	Unweathered, greenish grey, fine to very fine grained, very well indurated sandstone.
Sample GB92.19	53.4 - 53.6	Unweathered, dark greenish grey, laminated mudstone.
Sample GB92.21	113.1 - 113.3	Unweathered, light olive grey, medium to very fine grained, very well indurated sandstone.
Sample GB97.1	187.5 - 187.7	Unweathered, light olive grey, medium to fine grained, highly veined sandstone.
Sample GB97.3	217.6 - 217.8	Unweathered, light olive grey, medium to fine grained, highly veined sandstone.
Sample GB98.1	106.4 - 106.6	Unweathered, greenish grey, medium to fine grained, very well indurated sandstone.
Sample GB98.3	173.2 - 173.4	Unweathered, greenish grey, medium to very fine grained, very well indurated sandstone.
Sample 106.1	213.5 - 213.7	Unweathered, greenish grey, medium to very fine grained, very well indurated sandstone.

Core samples had been in storage for up to seven years and no information was available on the *in situ* moisture content, therefore samples were only weighed oven dried and at saturation. However, because all samples tested were from below the water table the *in situ* sample conditions may be assumed to be saturated, which may not be the case if groundwater is able to drain along discontinuities, adits or shafts. Samples were not saturated under vacuum as recommended by ISRM (1981) as they did not saturate completely within an hour. Instead, samples were saturated in a deep basin, under hydrostatic pressure, for 48 hours, until no airbubbles were observed on the surface. Samples were completely saturated by this method as proven by observations on core fractured during the strength tests.

Each sample's dry density (ρ_d) was calculated by dividing oven dried mass by its volume. Saturated density (ρ_{sat}) for each sample was determined by dividing the saturated mass by its volume. The porosity (n) is the ratio of the volume of voids (V_v) to the total volume (V) and is expressed as a percentage. Also determined was the Saturation Moisture Index (I_{sat}), which is the ratio of the mass of water at saturation to the dry mass of the sample. It is a measure of the quantity of water present in the sample upon saturation of the voids and is expressed as a percentage of the mass of grains in the sample.

4.3.3.3 Results

A summary of the results is given in Table 4.5 and a full list of results is included as Appendix D3.1. Samples of brecciated or highly fractured sandstone generally had higher porosity and saturation moisture content and lower density (mean values: n = 1.84%; I_{sat} = 0.68%; ρ_d = 2676 kgm^{-3}; and ρ_{sat} = 2694 kgm^{-3}) than very well indurated sandstone samples (mean values: n = 0.84 %; I_{sat} = 0.31 %; ρ_d = 2718 kgm^{-3}; and ρ_{sat} = 2726 kgm^{-3}). The mudstone sample (GB92.19) had both higher porosity and density (mean values: n = 2.02 %; I_{sat} = 0.72 %; ρ_d = 2785 kgm^{-3}; ρ_{sat} = 2806 kgm^{-3}). Porosity and the Saturation Moisture Index have also been plotted against the dry density to show the inverse relationships (Figure 4.8). The correlation coefficient (r) for sandstone samples has been calculated and is also shown in Figure 4.8 (r is determined rather than R^2 to show the direction of the relationships, that is, positive or negative). The plots show similar correlation values (r = ¯0.63 and ¯0.64) as they are interrelated variables.

Table 4.5: Porosity - density summary statistics for all core samples, brecciated and highly fractured samples, and very well indurated samples.

All samples

Summary statistic	L (mm)	D (mm)	V (mm^3)	M_{sat} (kg)	M_{dry} (kg)	V_v (mm^3)	ρ_{sat} (kgm^{-3})	ρ_{dry} (kgm^{-3})	n (%)	I_{sat} (%)
Mean	164.01	61.02	0.479	1.301	1.306	0.005	2724	2713	1.11	0.41
sd	17.25	0.19	0.052	0.141	0.140	0.002	31	32	0.52	0.19
Median	172.95	61.07	0.502	1.374	1.378	0.004	2715	2707	0.99	0.36
Range	59.65	0.63	0.181	0.496	0.493	0.008	134	130	1.62	0.60
Maximum	178.47	61.31	0.526	1.424	1.428	0.010	2806	2785	2.03	0.75
Minimum	118.82	60.68	0.345	0.928	0.935	0.002	2672	2656	0.40	0.15

Brecciated and highly fractured samples (4 samples)

Statistic method	L (mm)	D (mm)	V (mm^3)	M_{sat} (kg)	M_{dry} (kg)	V_v (mm^3)	ρ_{sat} (kgm^{-3})	ρ_{dry} (kgm^{-3})	n (%)	I_{sat} (%)
Mean	146.83	60.76	0.425	1.137	1.145	0.008	2694	2676	1.84	0.68
sd	23.05	0.08	0.066	0.171	0.172	0.000	18	16	0.19	0.07
Median	147.36	60.75	0.426	1.143	1.151	0.008	2699	2679	1.88	0.70
Range	54.95	0.18	0.157	0.406	0.407	0.001	37	34	0.44	0.15
Maximum	173.77	60.85	0.502	1.334	1.342	0.008	2709	2690	2.03	0.75
Minimum	118.82	60.68	0.345	0.928	0.935	0.007	2672	2656	1.59	0.60

Very well indurated samples (14 samples)

Statistic method	L (mm)	D (mm)	V (mm^3)	M_{sat} (kg)	M_{dry} (kg)	V_v (mm^3)	ρ_{sat} (kgm^{-3})	ρ_{dry} (kgm^{-3})	n (%)	I_{sat} (%)
Mean	168.60	61.09	0.494	1.342	1.346	0.004	2726	2718	0.84	0.31
sd	13.21	0.15	0.039	0.101	0.101	0.001	22	23	0.25	0.09
Median	174.63	61.15	0.510	1.382	1.388	0.004	2721	2715	0.78	0.29
Range	40.54	0.46	0.126	0.314	0.314	0.005	84	82	0.96	0.36
Maximum	178.47	61.31	0.526	1.424	1.428	0.007	2780	2770	1.37	0.50
Minimum	137.93	60.85	0.401	1.110	1.114	0.002	2697	2688	0.40	0.15

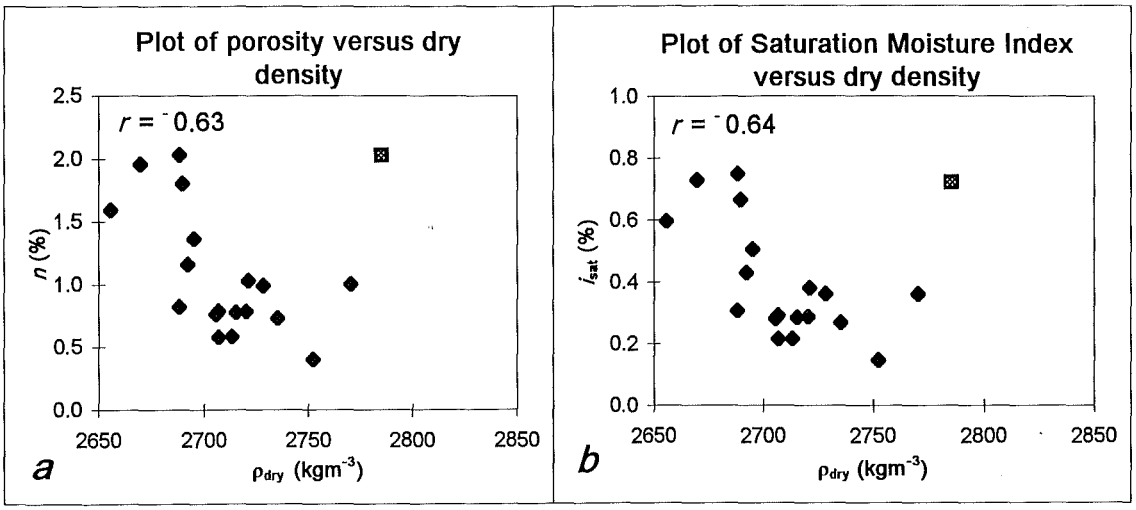

Figure 4.8: Correlation between porosity and dry density (*a*) and Saturation Moisture Index and dry density (*b*). The mudstone sample is denoted by the square symbol and the sandstone samples, by the diamond shape.

4.3.3.4 Discussion

In general, the porosity values are very low (mean = 1.06 %, range = 0.40 - 2.03 %) and the density values are very high (ρ_{sat} mean = 2719 kgm^3, range = 2672 - 2780 kgm^3; ρ_d mean = 2709 kgm^3, range = 2656 - 2770 kgm^3) for sandstones. This is an effect of the metamorphic alteration that Greenland Group sediments have undergone by compaction, void closure, and matrix recrystallisation to form sericitic muscovite (Cooper and Craw, 1992).

The brecciated and highly fractured sandstone samples all have higher porosity and lower density values than the very well indurated sandstones. This higher porosity is probably associated with secondary porosity, which is a direct result of fracturing and veining. The mudstone sample had both higher porosity and density values than the very well indurated sandstone samples, which may be explained by differences in grain lithologies, where sandstone samples are mainly quartz and lithic fragments (specific gravity: $\approx$ 2.6), and mudstone samples are mainly sericitic muscovite (specific gravity: $\approx$ 2.8; Cooper and Craw, 1992). In addition, the mudstone sample swelled slightly upon saturation, resulting in an increase in void volume and porosity.

The plots of porosity and Saturation Moisture Index with dry density (Figure 4.8) also include the correlation coefficient (r) for the sandstone samples. The scatter in the results may be partly accounted for by the estimation of the shaving volume sampled from each core sample, where if the exact volume is not used minor errors in the results will occur, but the main reason is the inhomogenity of rock material caused by small fractures and veins within samples. Fractures will normally be air or water filled (depending on the saturation condition of the sample), and therefore will affect density and porosity results. Veins may be calcite or quartz, both of a similar specific gravity to the rock material, but the veins' porosity will be almost zero, thus affecting the density and porosity results.

4.3.4 Sonic velocity determination

4.3.4.1 Introduction

This test was performed to determine the sonic velocities of the rock material, which can then be compared to the rock mass seismic velocity (Section 4.4) to find the Seismic Velocity Index. The sonic velocities may also be used to determine the dynamic modulii of elasticity, which are measures of the deformability of rock material. The same core samples used for porosity-density determination were also used to determine saturated and oven dry P and S wave sonic (or seismic) velocities ($v_{P\,(sat)}$; $v_{s\,(sat)}$; $v_{P\,(dry)}$; and $v_{s\,(dry)}$).

4.3.4.2 Methodology

The time taken for an elastic compressional wave (P wave) and an elastic shear wave (S wave) to propagate through each core sample was measured following the suggested methods of ISRM (1981) whereby platens able to generate P and S elastic waves are connected to a seismic analyser and an oscilloscope to identify the first arrival P and S waves. The sonic velocity may then be calculated by dividing the time taken for the first P or S wave to travel through the sample by the sample's length. A correction factor, accounting for the time taken for each wave to travel through the platens (platen delay constant) and zeroing of the seismic analyser, is also subtracted.

The seismic velocities also may be used to calculate the dynamic moduli of elasticity from the following formulae:

$$E_{dyn} = \rho v_s^2 \frac{\left(3v_p^2 - 4v_s^2\right)}{\left(v_p^2 - v_s^2\right)}$$

$$\nu_{dyn} = \frac{\left(v_p^2 - 2v_s^2\right)}{2\left(v_p^2 - v_s^2\right)}$$

where E_{dyn} is Young's Modulus (GPa), ν_{dyn} is Poisson's Ratio (dimensionless), ρ is density (kgm^{-3}), v_s is the shear wave velocity (ms^{-1}) and v_p is the compressional wave velocity (ms^{-1}). When calculating the sonic velocities and dynamic moduli of elasticity, the samples are assumed to be homogeneous, isotropic and purely elastic, which is rarely the case as samples may contain minor fractures and veins that affect the sample's homogeneity and isotropy. Samples normally do behave in an elastic fashion for the low stresses the platens

induce upon the samples, but if the sample is extremely weak, then the platen low stresses may alter the samples, affecting the results. It is assumed that no samples tested were affected by the low stresses as all behaved in an elastic manner at low stresses (see stress-strain relationships for each sample in Appendix D3.3).

4.3.4.3 Results

The results are summarised in Table 4.6 and the complete data are tabulated in Appendix D3.2. Brecciated and highly fractured core had lower sonic velocities and dynamic elasticity modulii than very well indurated core samples, and the mudstone sample had very low sonic velocities and dynamic elasticity modulii. Graphs correlating P wave velocities with S wave velocities, saturated density and porosity are shown in Figure 4.9, and Figure 4.10 contains graphs correlating dynamic Young's Modulus with dynamic Poisson's Ratio, density and porosity. The correlation coefficient (r) for sandstone samples was included on each plot in Figures 4.9 and 4.10 instead of R^2 to show whether or not data follows a positive or negative trend.

4.3.4.4 Discussion

Values of $v_{p\,(sat)}$ for all sandstone samples range between 3700 ms^{-1} and 4900 ms^{-1} and have a mean of 4357 ms^{-1}, whilst $v_{p\,(dry)}$ data ranges between 2700 ms^{-1} and 4500 ms^{-1} with a mean value of 3911 ms^{-1}. This data is comparable to the results found by Anon (1994), whose data, based on five core samples from Globe-Progress, range between 3300 ms^{-1} and 4700 ms^{-1}. For comparison, the mudstone sample had comparatively low sonic P wave velocities ($v_{p\,(sat)}$ = 1677 ms^{-1} and $v_{p\,(dry)}$ = 1519 ms^{-1}).

The general trends that may be observed are:

- $v_{p\,(sat)}$ values (mean = 4357 ms^{-1}) are higher than $v_{p\,(dry)}$ (mean = 3911 ms^{-1}), which is to be expected as the velocity of water (1500 ms^{-1}) filling the voids in the saturated state is considerably greater than the velocity of air (330 ms^{-1}) filling the voids when the sample is oven dried.
- Values of $v_{s\,(sat)}$ (mean = 1792 ms^{-1}), are lower than $v_{s\,(dry)}$ (mean = 2411 ms^{-1}) because shear waves cannot pass through liquids, therefore slowing down the S wave velocity through a saturated sample.

Table 4.6: Sonic velocity and Dynamic Moduli of Elasticity summary statistics.

All samples (19 samples)

Core Sample	L (mm)	ρ_{sat} (kgm^{-3})	ρ_{dry} (kgm^{-3})	P_{sat} (μs)	S_{sat} (μs)	$v_{P\,(sat)}$ (ms^{-1})	$v_{S\,(sat)}$ (ms^{-1})	$\frac{v_{P\,(sat)}}{v_{S\,(sat)}}$	$E_{dyn\,(sat)}$ (GPa)	$\nu_{dyn\,(sat)}$ -	P_{dry} (μs)	S_{dry} (μs)	$v_{P\,(dry)}$ (ms^{-1})	$v_{S\,(dry)}$ (ms^{-1})	$\frac{v_{S\,(sat)}}{v_{S\,(dry)}}$	$E_{dyn\,(dry)}$ (GPa)	$\nu_{dyn\,(dry)}$ -
Mean	164.01	2713	2724	39.7	72.3	4357	2377	1.87	39.9	0.27	44.5	62.8	3911	2782	1.42	38.0	0.18
sd	17.25	32	31	15.0	18.4	728	544	0.29	14.8	0.10	16.8	23.7	721	566	0.16	14.0	0.21
Median	172.95	2707	2715	37.1	70.8	4537	2406	1.88	41.4	0.30	41.4	57.9	4131	2933	1.39	42.6	0.10
Range	59.65	130	134	70.1	79.9	3207	2113	0.93	56.8	0.35	77.8	108.1	3005	2593	0.67	48.5	0.85
Maximum	178.47	2785	2806	100.5	131.8	4884	3391	2.24	64.2	0.38	110.9	155.1	4524	3680	1.84	54.9	0.86
Minimum	118.82	2656	2672	30.4	51.9	1677	1278	1.31	7.4	0.03	33.1	47.0	1519	1086	1.17	6.4	0.01

Brecciated and highly fractured samples (4 samples)

Core Sample	L (mm)	ρ_{sat} (kgm^{-3})	ρ_{dry} (kgm^{-3})	P_{sat} (μs)	S_{sat} (μs)	$v_{P\,(sat)}$ (ms^{-1})	$v_{S\,(sat)}$ (ms^{-1})	$\frac{v_{P\,(sat)}}{v_{S\,(sat)}}$	$E_{dyn\,(sat)}$ (GPa)	$\nu_{dyn\,(sat)}$ -	P_{dry} (μs)	S_{dry} (μs)	$v_{P\,(dry)}$ (ms^{-1})	$v_{S\,(dry)}$ (ms^{-1})	$\frac{v_{S\,(sat)}}{v_{S\,(dry)}}$	$E_{dyn\,(dry)}$ (GPa)	$\nu_{dyn\,(dry)}$ -
Mean	146.83	2694	2676	37.1	81.8	3961	1792	2.21	23.8	0.37	43.8	61.2	3393	2411	1.40	30.3	0.13
sd	23.05	18	16	5.5	11.3	199	105	0.03	2.7	0.00	8.0	10.2	475	191	0.10	9.4	0.13
Median	147.36	2699	2679	35.8	78.9	3992	1803	2.21	23.9	0.37	44.5	63.0	3532	2474	1.43	33.1	0.08
Range	54.95	37	34	12.7	26.1	433	249	0.07	6.4	0.01	17.8	23.8	1088	429	0.21	21.6	0.28
Maximum	173.77	2709	2690	44.7	97.8	4146	1906	2.24	26.9	0.38	52.0	71.2	3798	2564	1.48	38.2	0.32
Minimum	118.82	2672	2656	32.0	71.7	3713	1657	2.18	20.5	0.37	34.2	47.4	2710	2135	1.27	16.6	0.04

Very well indurated samples (14 samples)

Core Sample	L (mm)	ρ_{sat} (kgm^{-3})	ρ_{dry} (kgm^{-3})	P_{sat} (μs)	S_{sat} (μs)	$v_{P\,(sat)}$ (ms^{-1})	$v_{S\,(sat)}$ (ms^{-1})	$\frac{v_{P\,(sat)}}{v_{S\,(sat)}}$	$E_{dyn\,(sat)}$ (GPa)	$\nu_{dyn\,(sat)}$ -	P_{dry} (μs)	S_{dry} (μs)	$v_{P\,(dry)}$ (ms^{-1})	$v_{S\,(dry)}$ (ms^{-1})	$\frac{v_{S\,(sat)}}{v_{S\,(dry)}}$	$E_{dyn\,(dry)}$ (GPa)	$\nu_{dyn\,(dry)}$ -
Mean	168.60	2726	2718	36.2	65.3	4661	2623	1.81	46.8	0.25	39.9	56.7	4230	3009	1.42	42.5	0.21
sd	13.21	22	23	2.5	9.3	155	380	0.22	9.4	0.10	3.5	7.5	190	341	0.18	11.5	0.23
Median	174.95	2719	2714	37.2	64.1	4727	2665	1.83	47.4	0.29	41.4	57.6	4247	3082	1.36	45.3	0.10
Range	38.45	84	82	7.6	30.6	483	1278	0.75	30.9	0.34	11.2	28.9	641	1315	0.67	44.8	0.85
Maximum	178.47	2780	2770	38.5	82.5	4884	3391	2.19	64.2	0.37	43.2	73.7	4524	3680	1.84	54.9	0.86
Minimum	140.03	2697	2688	30.9	51.9	4401	2113	1.43	33.3	0.03	32.0	44.8	3884	2365	1.17	10.1	0.01

Figure 4.9: Correlation plots between:

(a) saturated P and S wave sonic velocity ($v_{p\,(sat)}$, $v_{s\,(sat)}$)

(b) dry P and S wave sonic velocity ($v_{p\,(dry)}$, $v_{s\,(dry)}$)

(c) saturated density (ρ_{sat}) and saturated P wave velocity ($v_{p\,(sat)}$)

(d) dry density (ρ_{dry}) and dry P wave velocity ($v_{p\,(dry)}$)

(e) porosity (n) and saturated P wave velocity ($v_{p\,(sat)}$)

(f) porosity (n) and dry P wave velocity ($v_{p\,(dry)}$)

r = correlation coefficent
sandstone samples are diamond shaped
mudstone sample is square shaped

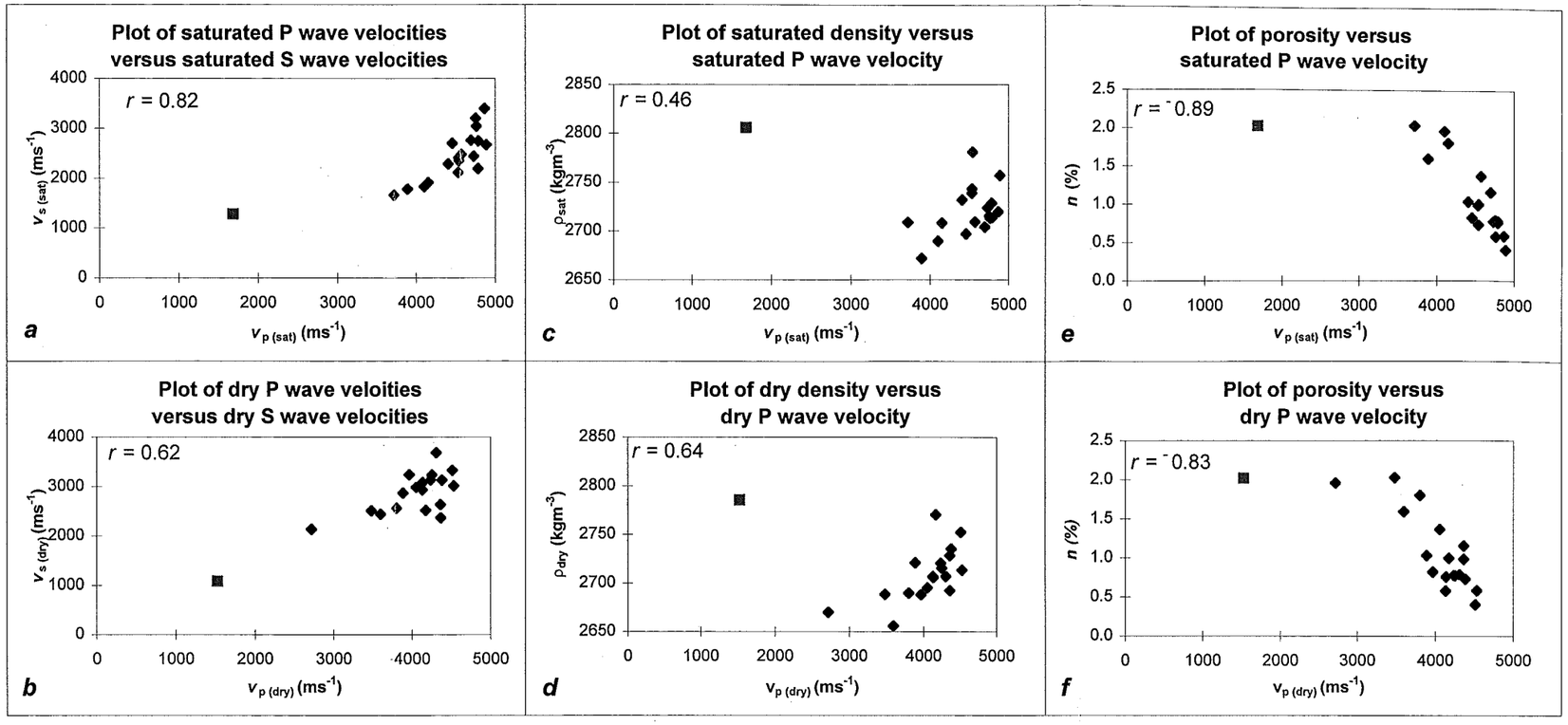

Figure 4.10: Correlation plots between:

(a) saturated dynamic Young's Modulus ($E_{dyn\,(dry)}$) and saturated dynamic Poisson's Ratio ($\nu_{dyn\,(sat)}$)

(b) dry dynamic Young's Modulus and dry dynamic Poisson's Ratio ($\nu_{dyn\,(dry)}$)

(c) saturated density (ρ_{sat}) and saturated dynamic Young's Modulus ($E_{dyn\,(sat)}$)

(d) dry density (ρ_{dry}) and dry dynamic Young's Modulus ($E_{dyn\,(dry)}$)

(e) porosity (n) and saturated dynamic Young's Modulus ($E_{dyn\,(sat)}$)

(f) porosity (n) and dry dynamic Young's Modulus ($E_{dyn\,(dry)}$)

r = correlation coefficent
sandstone samples are diamond shaped
mudstone sample is square shaped

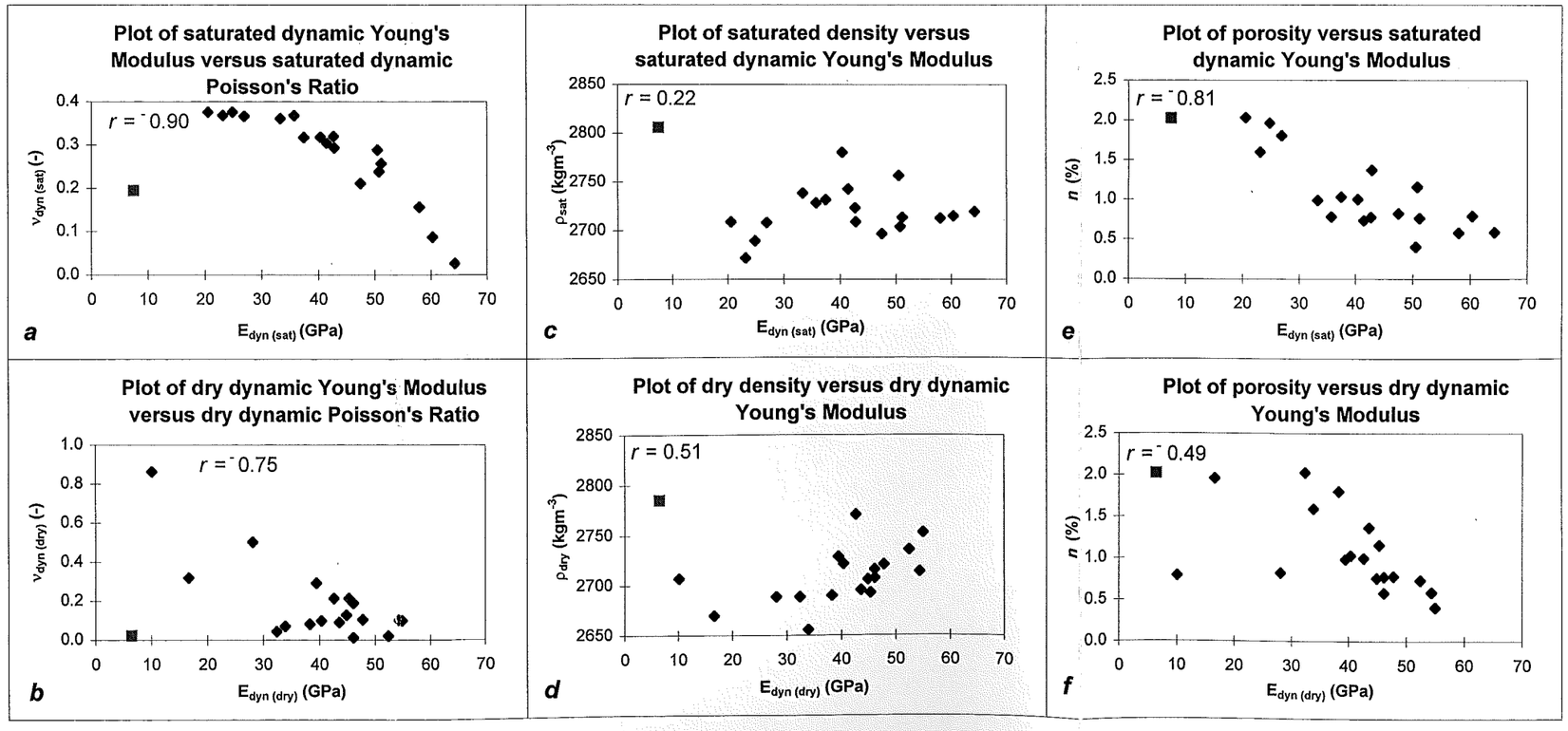

- Brecciated and highly fractured samples have lower mean velocities and modulii of elasticity than very well indurated samples.

The ratio of P wave sonic velocities to S wave velocities found are $v_{p\ (dry)}$: $v_{s\ (dry)}$ = 1.42:1 and $v_{p\ (sat)}$: $v_{s\ (sat)}$ = 1.87:1 (Figure 4.9a and 4.9b), which may be compared to the ratio of 1.5:1 that is normally assumed (Johnson and DeGraff, 1988). The reason why the saturated velocities ratio is significantly higher than 1.5:1 is because $v_{p\ (sat)}$ values are greater than $v_{p\ (dry)}$ and $v_{s\ (sat)}$ values are less than $v_{s\ (dry)}$ values. The ratio of P:S velocities may be used to estimate the S wave velocity of the rock mass from the P wave velocity of the rock mass found in Section 4.2.1, so that an approximation of the dynamic modulii of elasticity of the rock mass may be made.

Figures 4.9c and 4.9d shows plots of saturated and dry density against the saturated and dry P wave velocity. Both graphs show considerable scatter in the results (r = 0.46 and 0.64), but there is a general trend whereby P wave velocity increases with increasing density. Figures 4.9e and 4.9f plot porosity versus saturated and dry P wave velocity, and show very good negative correlations (r = ¯0.89 and ¯0.83) for porosity decreasing as P wave velocity increases. S wave velocities were not correlated with any other variable as S wave velocity data contains more scatter than the P wave velocities. This scatter is amplified in S wave velocities because the samples are not purely homogeneous or isotropic and any inhomogenity or anisotropy, such as fractures and veins, affect the propagation of shear waves more than the propagation of P waves, and this effect is more noticeable when the samples are saturated. The P wave velocity is also the seismic velocity used in the rippability classification systems, as detailed in Section 3.5.

Figures 4.10a and 4.10b plot the saturated and dry dynamic Young's Modulus versus the saturated and dry dynamic Poisson's Ratio. The correlation between the saturated data is very good (r = ¯0.90) but the correlation between the dry data is not as good (r = ¯0.75). Both plots show Young's Modulus increasing as Poisson's Ratio decreases. Figures 4.10c and 4.10d plot saturated and dry density against the saturated and dry Young's Modulii. Both graphs show very scattered data with very poor correlations (r = 0.22 and r = 0.51). The plots between porosity and saturated dynamic Young's Modulus (Figures 4.10e and

4.10f) shows a very good correlation (r = ¯0.81), but the correlation between porosity and dry dynamic Young's Modulus is poor (r = ¯ 0.49). Poisson's Ratio was not plotted against other data sets, as Poisson's Ratio does not tend to be as accurate when determined by dynamic methods rather than by static methods because small errors in sonic velocities can lead to large errors in Poisson's Ratio due to the nature of the formula (Jaeger and Cook, 1976; Siggins, 1993).

In general, the graphs show that porosity correlates better with sonic velocity and Young's Modulus than does density. This may be because density is affected by the inhomogeneity of veins and fractures that may alter the density of the rock sample.

4.3.5 UCS and stress-strain determination

4.3.5.1 Introduction

Strength is generally regarded as the fundamental quantitative engineering property of rock material, and of the three different types of strength (compressive, tensile and shear), uniaxial compressive strength (UCS) is the most commonly used as the values and ranges provide insight into possible site investigation and rock testing methods (Johnson and DeGraff, 1988). UCS values were determined on the same core samples used in Section 4.3.3 and 4.3.4 to find the ultimate strength of Greenland Group rock material and to compare logged values with measured values. The relationship between stress and strain was also determined so that the static Young's Modulus could be calculated and compared to the dynamic Young's Modulus.

4.3.5.2 Methodology

Testing methodology followed the suggested methods outlined by ISRM (1981), whereby the sample's L/D ratio must be 2.5-3/1 and loading must be 0.5 - 1.0 MPa/sec such that failure occurs within 5 - 10 minutes. The ultimate or failing stress (σ_c) is determined by dividing the maximum load (P) by the original cross sectional area of a sample (A_0). As

samples were the required length, samples were not standardised to a L:D ratio of 1/1 as suggested by Obert and Duvall (1967) and because the *in situ* moisture content was not known, samples were tested saturated as recommended by Pettifer and Fookes (1994) in their study on the excavatability of rock masses. The failure mechanism for each sample was also noted.

The strain rate for each sample was determined by measuring the change in length between two markers glued to the core sample 101.6 mm apart by using extensometers. The strain is calculated from the following formula:

$$\varepsilon = \frac{\Delta L}{L_0} \quad (\%)$$

where ΔL is the change in length and L_0 is the original sample length. The extensometers were calibrated to read strain directly, so the above formula was only used on the mudstone sample (GB92.19) that swelled when saturated such that L_0 became 102.4 mm. Strain was plotted against the loading stress to give the stress-strain plots included in Appendix D3.3, and which may be compared to typical stress-strain relationships (Figure 4.11). From these plots, Young's Static Modulus of Elasticity can be determined by three methods (Figure 4.12). $E_{s\ (50)}$ is Young's Modulus at 50% ultimate strength using the secant method, $E_{t\ (50)}$ is determined using the tangential method and E_{ave} determined using the averaged method. The Modulus most commonly used and quoted is $E_{t\ (50)}$ (Hawke and Mellor, 1970; Johnson and DeGraff, 1988).

4.3.5.3 Results

Stress-strain relationships are tabulated and graphed in Appendix D3.3 and an example is included as Figure 4.13. A summary of the failing strength results is tabulated in Table 4.7 and a complete list of data is included as Appendix D3.4.

General trends show that:

- The stress-strain plots in Appendix D3.3 (Figures D3.1-D3.18) are mainly linear, indicating that axial strain was almost purely elastic until failure.
- Brecciated, highly fractured or laminated samples failed at lower strengths (mean = 25.0 MPa) than very well indurated samples (mean = 103.9 MPa).

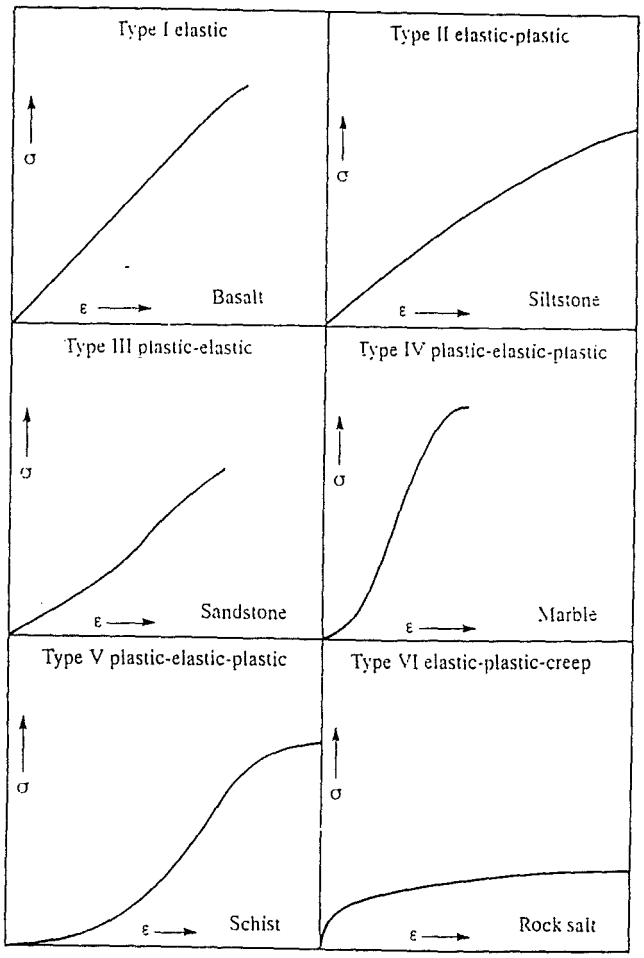

Figure 4.11: Typical stress-strain relationship curves for rocks in uniaxial compression loaded to failure (from FG Bell, 1993).

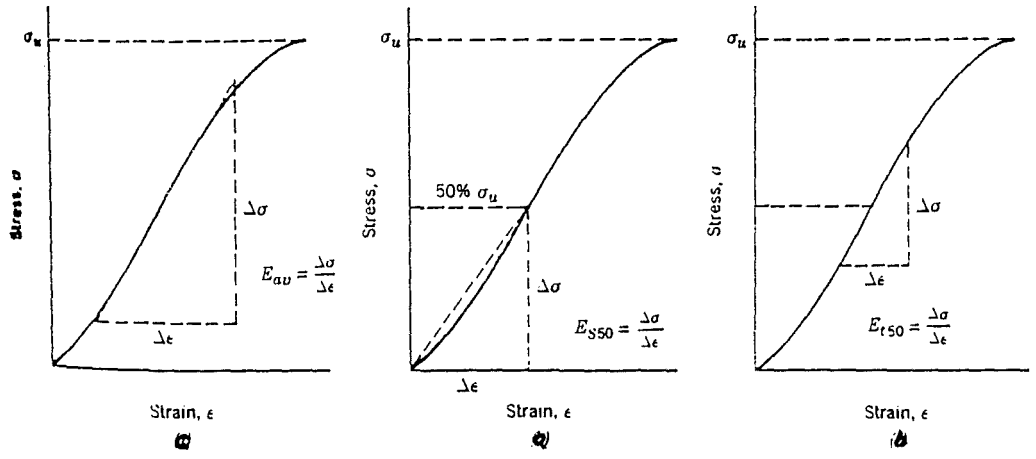

Figure 4.12: Determination of the static Young's Modulus by *(a)* the secant method, *(b)* the tangential method and *(c)* the averaged method (from Johnson and DeGraff, 1988).

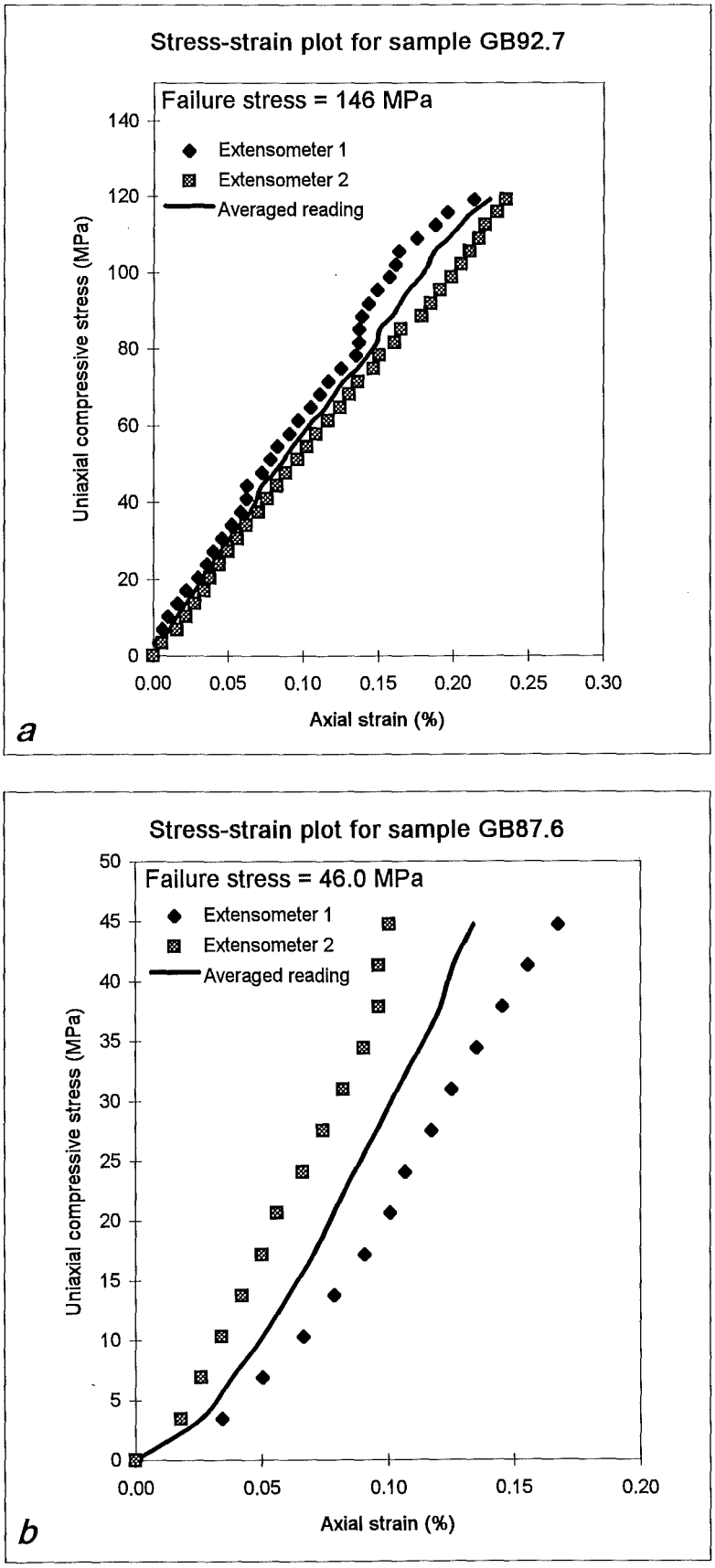

Figure 4.13: Typical stress-strain relationship for elastic (*a*) and plastic-elastic samples (*b*).

Table 4.7: Uniaxial compressive strength and Young's Modulus summary statistics

All samples

	ρ_{sat} (kgm^{-3})	L (mm)	D (mm)	A (mm^2)	P (kN)	σ_c (MPa)	$E_{s\,(50)}$ (GPa)	$E_{t\,(50)}$ (GPa)	E_{ave} (GPa)	$E_{dyn\,(sat)}$ (GPa)	$\frac{E_{dyn\,(sat)}}{E_{s\,(50)}}$	$\frac{E_{dyn\,(sat)}}{E_{t\,(50)}}$
Average	2724	164.01	61.02	2922	231.3	79.0	32.7	33.9	33.9	39.9	1.54	1.38
sd	31	17.25	0.19	19	146.2	49.7	15.7	15.1	15.1	14.8	0.87	0.54
Median	2715	172.95	61.07	2926	218.0	74.5	36.9	38.3	38.3	41.4	1.28	1.22
Range	134	59.65	0.63	60	453.5	153.6	50.5	50.5	50.5	56.8	3.53	1.98
Maximum	2806	178.47	61.31	2949	488.5	165.7	55.6	55.6	55.6	64.2	4.44	2.88
Minimum	2672	118.82	60.68	2888	35.0	12.1	5.1	5.1	5.1	7.4	0.91	0.91

Brecciated, highly fractured or laminated samples (6 samples)

	ρ_{sat} (kgm^{-3})	L (mm)	D (mm)	A (mm^2)	P (kN)	σ_c (MPa)	$E_{s\,(50)}$ (GPa)	$E_{t\,(50)}$ (GPa)	E_{ave} (GPa)	$E_{dyn\,(sat)}$ (GPa)	$\frac{E_{dyn\,(sat)}}{E_{s\,(50)}}$	$\frac{E_{dyn\,(sat)}}{E_{t\,(50)}}$
Average	2727	148.96	60.84	2904	72.8	25.0	12.2	15.8	15.8	23.8	2.42	1.88
sd	53	20.57	0.17	16	36.7	12.6	9.3	13.7	13.7	10.6	1.27	0.76
Median	2708	147.36	60.82	2903	61.8	21.3	8.6	10.2	10.2	23.9	1.85	1.61
Range	134	54.95	0.48	45	100.0	34.4	22.3	33.9	33.9	32.9	2.99	1.85
Maximum	2806	173.77	61.15	2934	135.0	46.5	27.4	39.0	39.0	40.3	4.44	2.88
Minimum	2672	118.82	60.68	2888	35.0	12.1	5.1	5.1	5.1	7.4	1.45	1.03

Very well indurated samples (13 samples)

	ρ_{sat} (kgm^{-3})	L (mm)	D (mm)	A (mm^2)	P (kN)	σ_c (MPa)	$E_{s\,(50)}$ (GPa)	$E_{t\,(50)}$ (GPa)	E_{ave} (GPa)	$E_{dyn\,(sat)}$ (GPa)	$\frac{E_{dyn\,(sat)}}{E_{s\,(50)}}$	$\frac{E_{dyn\,(sat)}}{E_{t\,(50)}}$
Average	2722	170.96	61.11	2930	304.5	103.9	40.6	40.9	40.9	47.3	1.20	1.19
sd	16	10.22	0.14	13	114.6	38.9	8.6	8.6	8.6	9.6	0.28	0.28
Median	2719	174.95	61.16	2935	287.5	98.9	39.8	40.0	40.0	47.4	1.14	1.14
Range	60	38.45	0.45	44	328.0	111.2	34.8	34.8	34.8	30.9	1.08	1.08
Maximum	2757	178.47	61.31	2949	488.5	165.7	55.6	55.6	55.6	64.2	1.99	1.99
Minimum	2697	140.03	60.85	2905	160.5	54.5	20.8	20.8	20.8	33.3	0.91	0.91

- Very well indurated samples had higher Young's Modulii (mean = 40.9 GPa) than brecciated, highly fractured and laminated samples (mean = 15.8 GPa).
- The mudstone sample had a higher strength than the brecciated, highly fractured and laminated sandstones (32.0 MPa) but Young's Modulus was lower (5.1 GPa).

Figure 4.14 shows the failure mechanism of some of the samples. All three failure mechanisms described by Hawke and Mellor (1970) occurred and some samples failed by a combination of the mechanisms. Other samples simply fractured or rock chips exploded from the samples.

Correlations between UCS and saturated density, porosity and saturated P wave velocity are given in Figure 4.15. Figure 4.16 plots the static Young's Modulus against saturated density, porosity and saturated P wave velocity and Figure 4.17 plots UCS, static and dynamic Young's Modulii. The correlation coefficient (r) for the sandstone samples is also included on each graph.

4.3.5.4 Discussion

Brecciated and highly fractured sandstone samples failed at low UCS values (< 25 MPa), very well indurated sandstone samples failed in two groupings: one > 100 MPa and the other at about 50 - 70 MPa. The low failure stress of the second group is most likely a result of end effects whereby stress is concentrated at the sample's ends. This might occur if samples are too short; the sample ends may not be exactly parallel to each other, perpendicular to the sides or ground smooth; and any problems with the testing machine. Despite the samples having a shaving that altered the symmetrical geometry to one of asymmetry, this did not appear to affect the failure mechanism in any way.

Analysis of the stress-strain graphs show that most samples failed in an elastic fashion (Figure 4.13a). The samples that did not were mainly brecciated or highly fractured, with a higher porosity (Figure 4.13b), and initial strain was plastic as the voids closed. Samples with an elastic stress-strain graph all have $E_{s\,(50)} = E_{t\,(50)} = E_{ave}$. Samples with plastic-elastic strain graphs all had higher $E_{t\,(50)}$ than $E_{s\,(50)}$, which is to be expected as $E_{s\,(50)}$ is a more conservative estimate of Young's Modulus (Johnson and DeGraff, 1988).

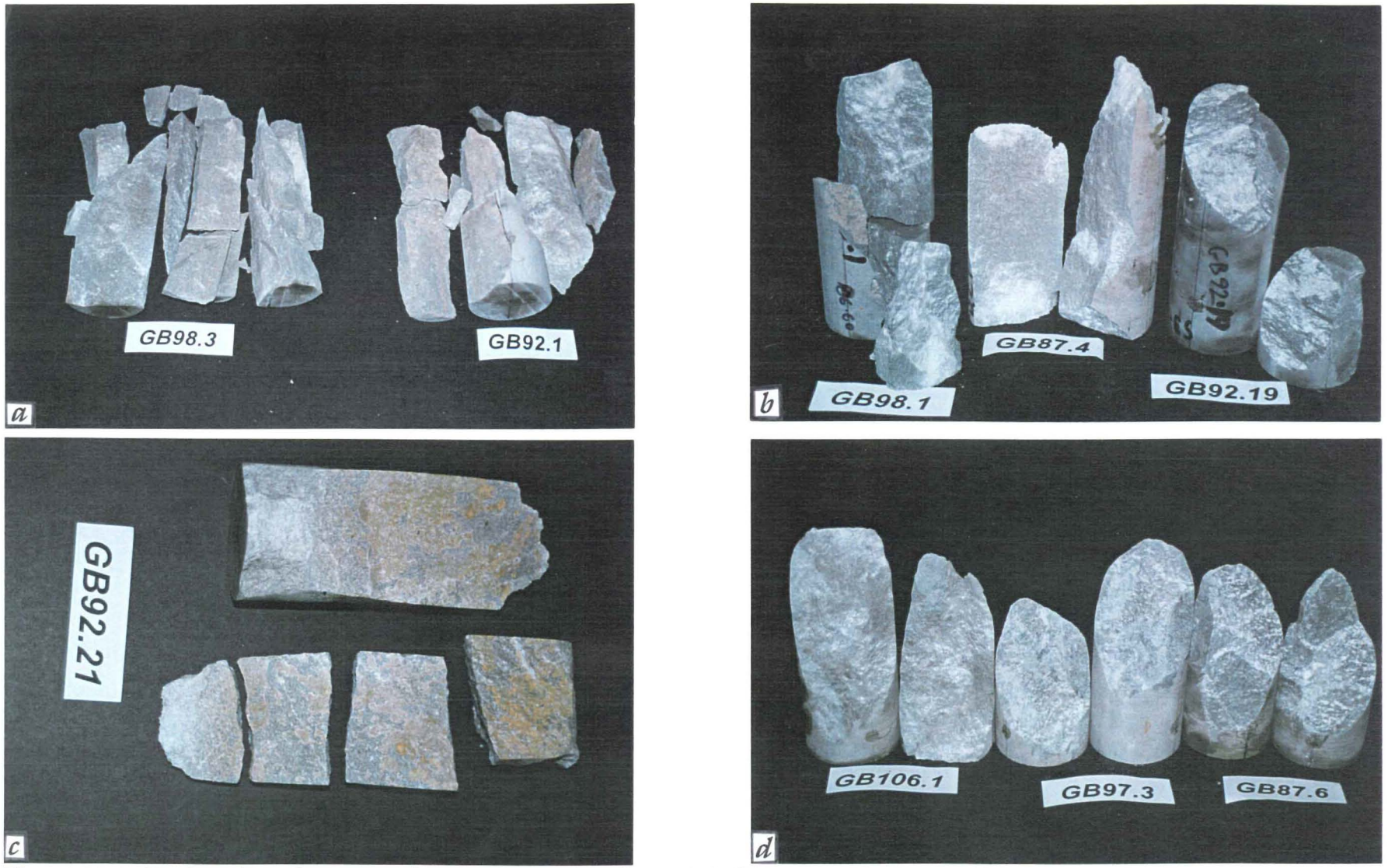

Figure 4.14: UCS testing of core samples. (*a*) Examples of cataclasis failure. (*b*) Examples of shear failure (GB92.19), axial cleavage failure (GB87.4) and combination of shear and cataclasis (GB98.1). (*c*) failure along a longitudinal quartz vein. (*d*) Examples of shear failure in brecciated sandstone.

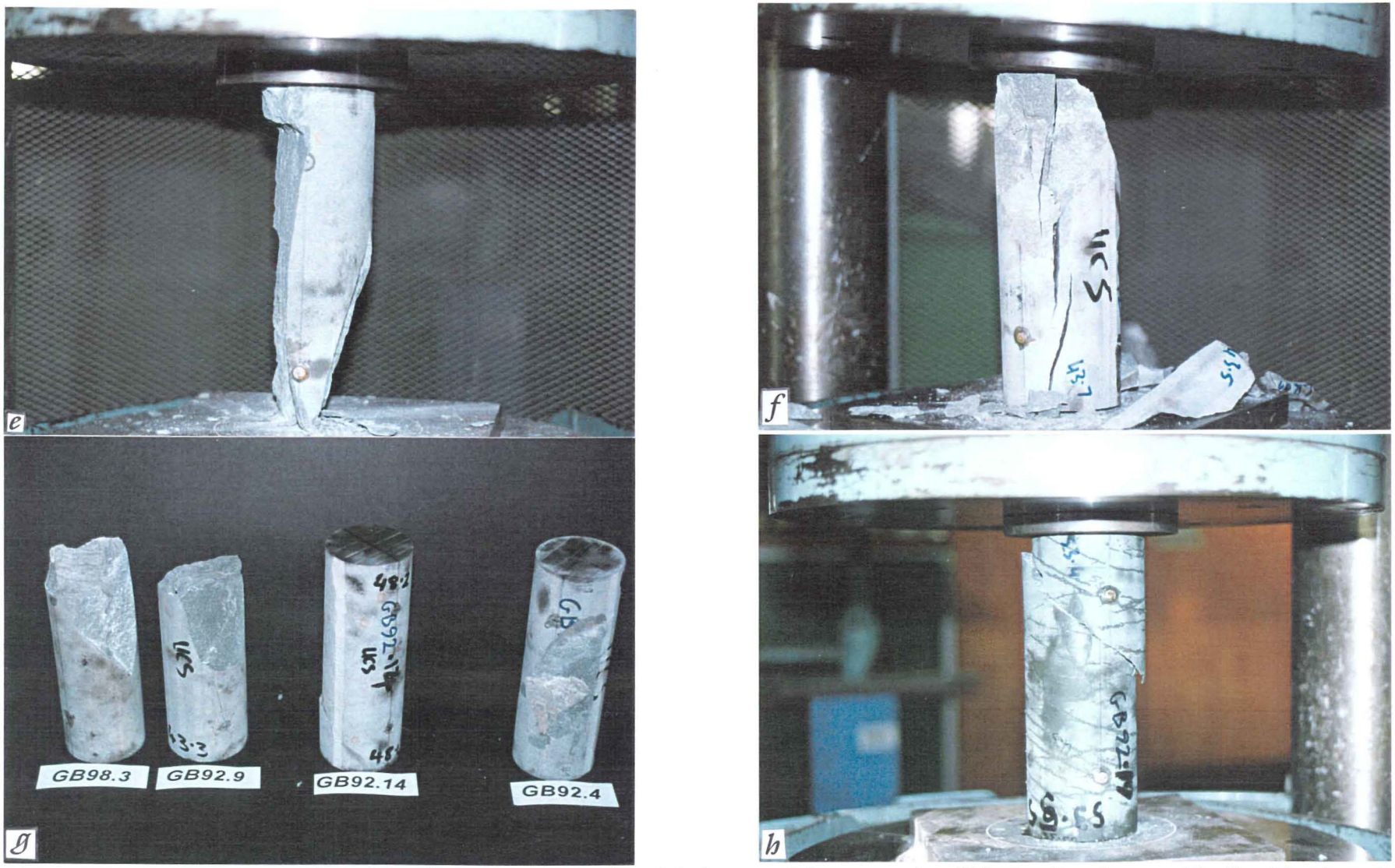

Figure 4.14 (continued): UCS testing of core samples. (*e*) axial cleavage failure, sample still in loading frame. (*f*) Combination of cataclasis and axial cleavage failure, sample still in loading frame. (*g*) Samples GB92.9 and GB98.3 contain internal crushing of sample and the development of a wedge. (*h*) Shearing failure of GB92.19 (mudstone sample). Note the water oozing out of microcracks and laminations.

Figure 4.15: Correlation plots between:
- *(a)* uniaxial compressive strength ($\sigma_{c\,(sat)}$) and saturated density (ρ_{sat})
- *(b)* uniaxial compressive strength ($\sigma_{c\,(sat)}$) and porosity (n)
- *(c)* uniaxial compressive strength ($\sigma_{c\,(sat)}$) and saturated P wave velocity ($v_{p\,(sat)}$)

r = correlation coefficent
sandstone samples are diamond shaped
mudstone sample is square shaped

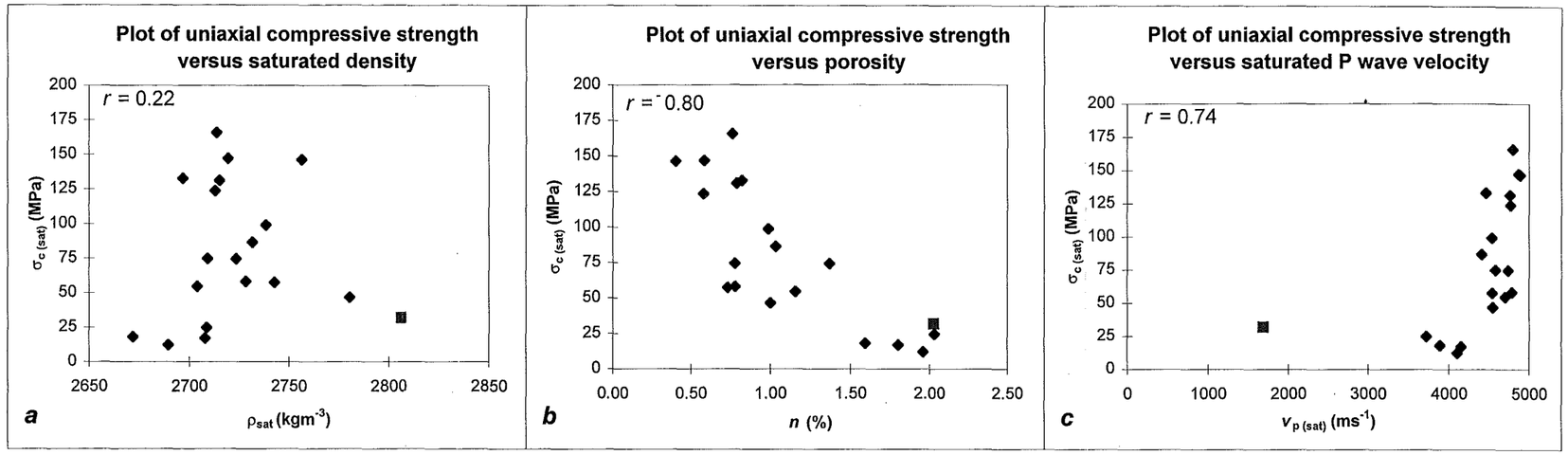

Figure 4.16: Correlation plots between:
- *(a)* static Young's Modulus ($E_{t\,(50)}$) and saturated density (ρ_{sat})
- *(b)* static Young's Modulus ($E_{t\,(50)}$) and porosity (n)
- *(c)* static Young's Modulus ($E_{t\,(50)}$) and saturated P wave velocity ($v_{p\,(sat)}$)

r = correlation coefficent
sandstone samples are diamond shaped
mudstone sample is square shaped

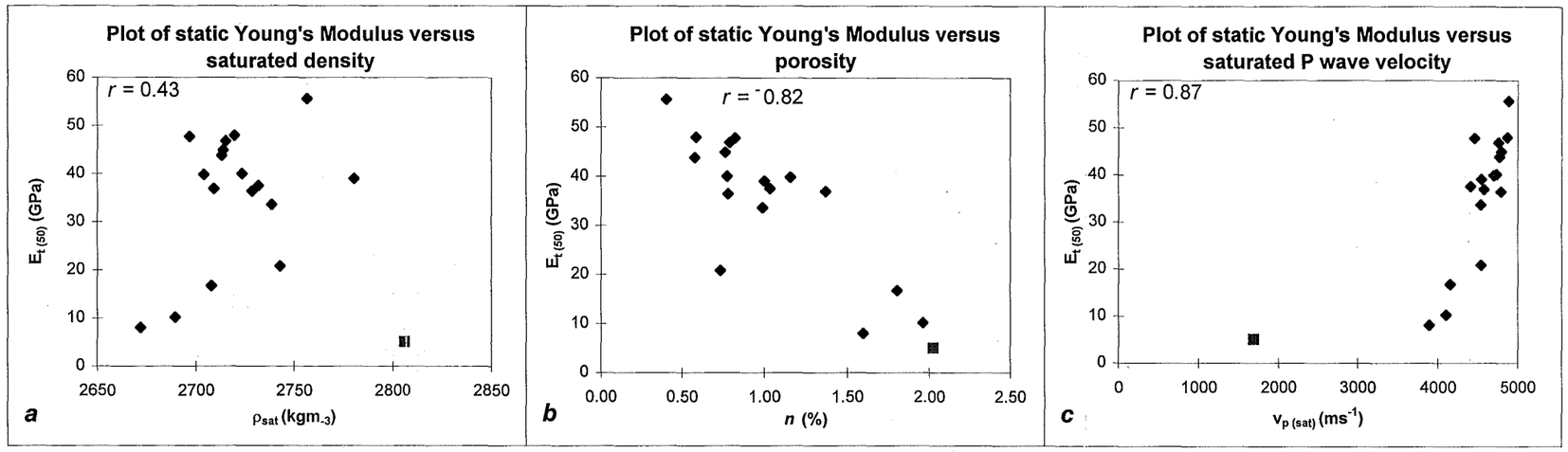

Figure 4.17: Correlation plots between:
- *(a)* uniaxial compressive strength ($\sigma_{c\,(sat)}$) static Young's Modulus ($E_{t\,(50)}$)
- *(b)* uniaxial compressive strength ($\sigma_{c\,(sat)}$) and saturated dynamic Young's Modulus ($E_{dyn\,(sat)}$)
- *(c)* static Young's Modulus ($E_{t\,(50)}$) and saturated dynamic Young's Modulus ($E_{dyn\,(sat)}$)

r = correlation coefficent
sandstone samples are diamond shaped
mudstone sample is square shaped

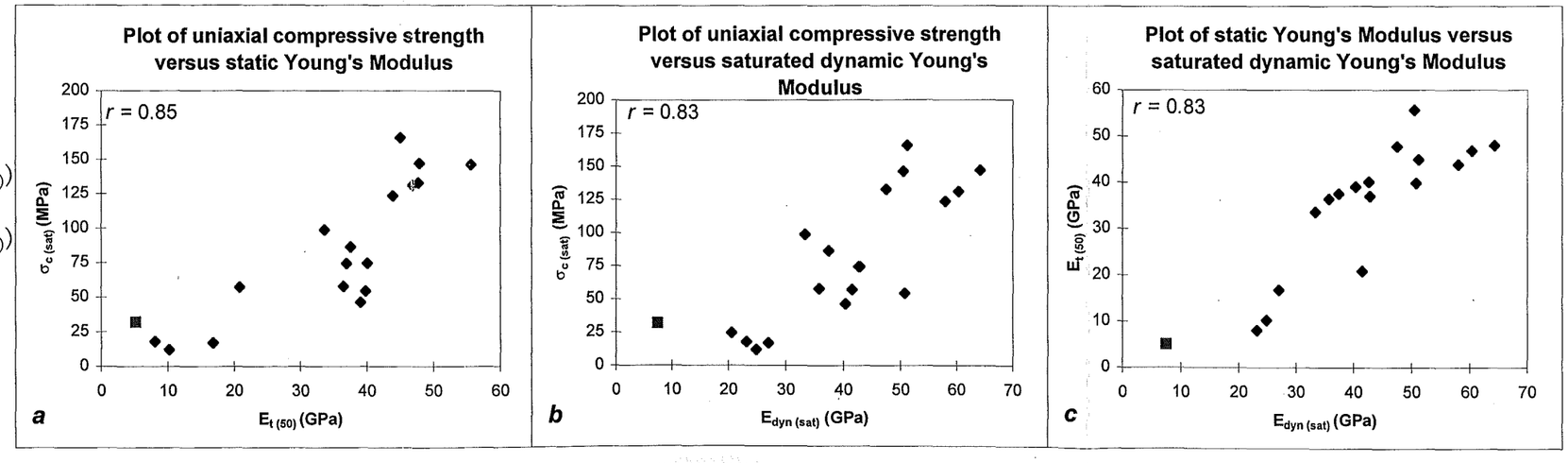

All three failure mechanisms described by Hawke and Mellor (1970) occur in the samples. Cataclasis failure is described as internal crushing and collapse of the sample, resulting in conical end fragments and long slivers of rock (Hawke and Mellor, 1970; Figure 4.14a). Shear failure is fracturing along one or two shear planes. Failure by shearing only occurs along pre-existing shear planes, which prove that the samples that failed by shearing are not purely homogeneous (Hawke and Mellor, 1970; Figures 4.14b, c, d). Axial cleavage is described as longitudinal splitting or cracking of the sample parallel to the loading direction (Hawke and Mellor, 1970; Figure 4.14b, d, g). Combinations of failure mechanisms also occurred, for example sample GB98.1 (Figure 4.14b), which has failed by a combination of shearing and cataclasis. Sample GB92.21 (Figure 4.14c) failed at a higher stress than the other samples because of a longitudinal quartz vein that effectively strengthened the sample (Figure 4.14c). The mudstone sample (GB92.19) failed along laminations (Figure 4.14b) and water oozed out of the sample as it was compressed (Figure 4.14h). Evidence of internal crushing of samples may be seen in Figure 4.14 as a whitish powder that occurs on the sheared surfaces and end cones.

Correlations between UCS and Young's Static Modulus with saturated density (Figure 4.15a and 4.16a) show poor correlation (r = 0.22 and r = 0.43 respectively), but the correlations between UCS and porosity (Figure 4.15b), and Young's Static Modulus and porosity (Figure 4.16b), are good (r = ¯0.80 and r = ¯0.82 respectively). These trends are similar to those shown in Figures 4.9a and 4.9b between density and porosity with P wave velocities. Hawke and Mellor and other workers (listed in Hawke and Mellor, 1970) have all found that porosity correlates well with UCS and Young's Modulus. P wave velocities (Figures 4.15c and 4.16c) also have very good correlation with UCS and Young's Static Modulus (r = 0.74 and r = 0.87 respectively). Figures 4.17a and 4.17b correlate UCS with Young's Static Modulus and Young's Dynamic Modulus, and again both plots have very good correlations (r = 0.85 and r = 0.83 respectively). These two correlations are very similar because Young's Static Modulus and Young's Dynamic Modulus (Figure 4.17c) are also closely related (r = 0.83), where the dynamic modulus is 1.4 times larger than the static modulus.

Young's Static Modulus may be compared with Young's Dynamic Modulus whereby the dynamic modulus is normally greater than the static modulus. This is because in

calculating the dynamic modulus the sample is induced with very low, purely elastic stresses that generally do not alter sample, whereas in determining the static modulus the sample undergoes stress that may alter the sample (Jaeger and Cook, 1976; Siggons, 1993). In very well indurated samples axial strain is almost purely elastic, therefore the static and dynamic modulii are almost identical. This may imply that the dynamic modulus determined on a rock mass, might also provide an accurate estimation of the *in situ* static modulus of a rock mass, which may be useful for determining the deformability of the open pit rock mass as excavation proceeds and the deformability of the rock mass beneath the waste rock stack and tailings dam. Likewise, the dynamic Poisson's Ratio may be used to estimate the static Poisson's Ratio, which is often assumed to be 0.25 for sandstones.

Samples with the lowest values of Young's Modulus show the greatest differences between E_{stat} and E_{dyn} (compare the ratios between E_{stat} and E_{dyn} in Table 4.7 for brecciated, highly fractured or laminated samples, and very well indurated samples) because of the more porous nature of the samples (Jaeger and Cook, 1976).

4.3.6 Point Load Index determination

4.3.6.1 Introduction

The Point Load Index ($I_{s\ (50)}$) is a measure of strength that is easily determined in a laboratory or field environment, and has been converted to a standard 50 mm diameter core sample. Samples to be tested do not need to be prepared as rigorously as samples required for UCS tests, yet the strength index is easily correlated to UCS by multiplying the Point Load Index by 20 (Hawkins, 1986; Pells, 1985; Pettifer and Fookes, 1994), although various other multipliers ranging from 8 - 43 have been used in the past (Pettifer and Fookes, 1994) and the most widely used multiplier is 24, first proposed by Broch and Franklin (1972). It is, therefore, important to find a correlation multiple that is site specific, that is, a multiple only suitable for rocks found on Globe Hill.

The point load test was also performed to determine strength values on unweathered, slightly weathered and moderately weathered yet very well indurated rocks to test the effect of weathering on the strength of samples, and also to provide additional data to compare strength values with logged strength values included in Macraes' core logging sheets. A site-specific strength correlation between the Point Load Index and UCS is also found, and where possible the anisotropy index is determined.

4.3.6.2 Methodology

Core samples adjacent to, and lithologically similar to samples tested for UCS were tested to find their Point Load Index. Where possible, the mean value from two or more tests was used for each comparison. The samples were prepared and tested following the suggested methods by ISRM (1985) and were tested at saturation either diametrically or axially depending on the sample's dimensions (Figure 4.18a).

Irregular lumps of slightly and moderately weathered, very well indurated sandstone were collected from outcrops and tested at their *in situ* moisture condition. Unweathered core samples were tested saturated as this is their expected *in situ* moisture condition, although this may not be the case if groundwater drains into adits or shafts, or along discontinuities. No highly weathered rock samples were collected, as highly weathered samples can behave similar to soils (ISRM, 1981), and therefore should not be a problem to excavate.

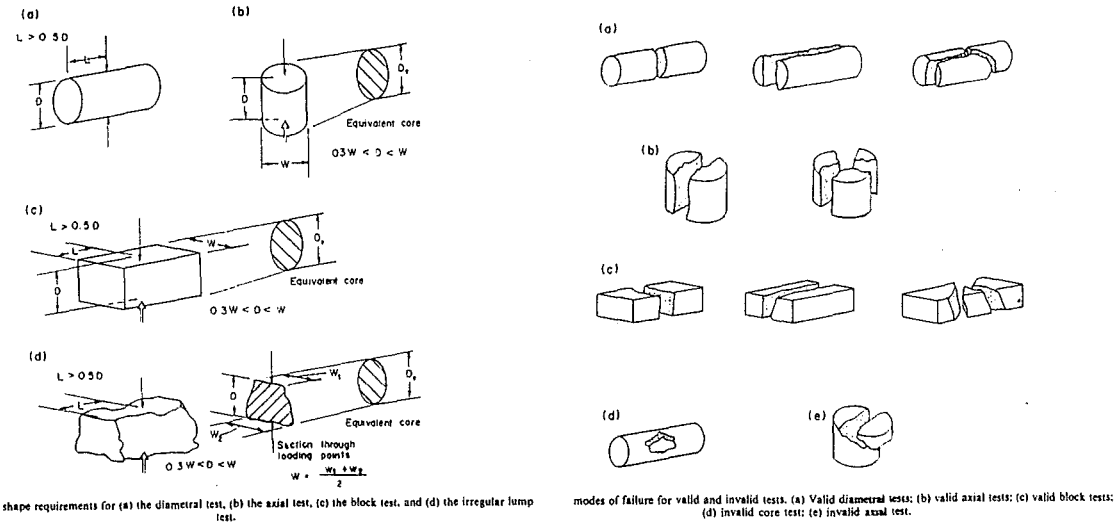

cimen shape requirements for (a) the diametral test, (b) the axial test, (c) the block test, and (d) the irregular lump test.

modes of failure for valid and invalid tests. (a) Valid diametral tests; (b) valid axial tests; (c) valid block tests; (d) invalid core test; (e) invalid axial test.

Figure 4.18: (*a*) Sample shape requirements for diametral, axial, block and irregular lump point load strength tests and (*b*) valid and invalid modes of point load failure (from ISRM, 1985).

4.3.6.3 Results

A summary of the results is tabulated in Table 4.8, and the full results are included as Appendix D3.5. Figure 4.19 shows valid failures for very well indurated and brecciated core samples. Unweathered, brecciated core samples failed at a very weak $I_{s\,(50)}$ (mean = 1.11 MPa) whereas unweathered, very well indurated core samples failed at high $I_{s\,(50)}$ values (mean = 6.49 MPa). Slightly weathered, very well indurated irregular lumps failed at a mean value of $I_{s\,(50)}$ = 5.06 MPa whereas moderately weathered, very well indurated irregular lumps failed at $I_{s\,(50)}$ = 2.68 MPa. A plot of $I_{s\,(50)}$ versus weathering grade is include in Section 4.3.7 along with data from the slake-durability test. Mudstone is the only strongly anisotropic lithology, however the degree of anisotropy could not be determined as there were no valid failures (see Figure 4.18b) for mudstone samples, although it was observed that the mudstone failed along laminations for the diametral test and was considerably stronger in the axial test (roughly perpendicular to laminations).

The Point Load Index ($I_{s\,(50)}$) was correlated with UCS values for 18 out of the 19 samples (the mudstone samples did not have any valid point load test result because they failed along pre-existing shears or laminations). The data is plotted as Figure 4.20a and has a correlation coefficient (r) equal to 0.76 and a regression multiple of 17. Figure 4.20a has also been replotted as Figure 4.20b, where five very well indurated sandstone samples that failed at weaker UCS values than expected, due to sample end effects, have been removed. The correlation coefficient (r) improves to 0.89 and the regression multiple increases to 20.

4.3.6.4 Discussion

Figure 4.18a shows that there appears to be two clusters of data, five UCS samples failed weaker than expected as a result of end effects. If these samples are removed from the correlation then r improves from 0.76 to 0.89 and the regression coefficient increases from 17 to 20 (Figure 4.18b). UCS values of Greenland Group rocks may now be calculated from $I_{s\,(50)}$ values using the following empirical formula:

$$\sigma_c = 20\ (I_{s(50)}) \quad \text{(MPa)}$$

which is the same empirical formula suggested by Pells (1985) for use with sandstones around Sydney, and also by Hawkins (1986) and Pettifer and Fookes (1994).

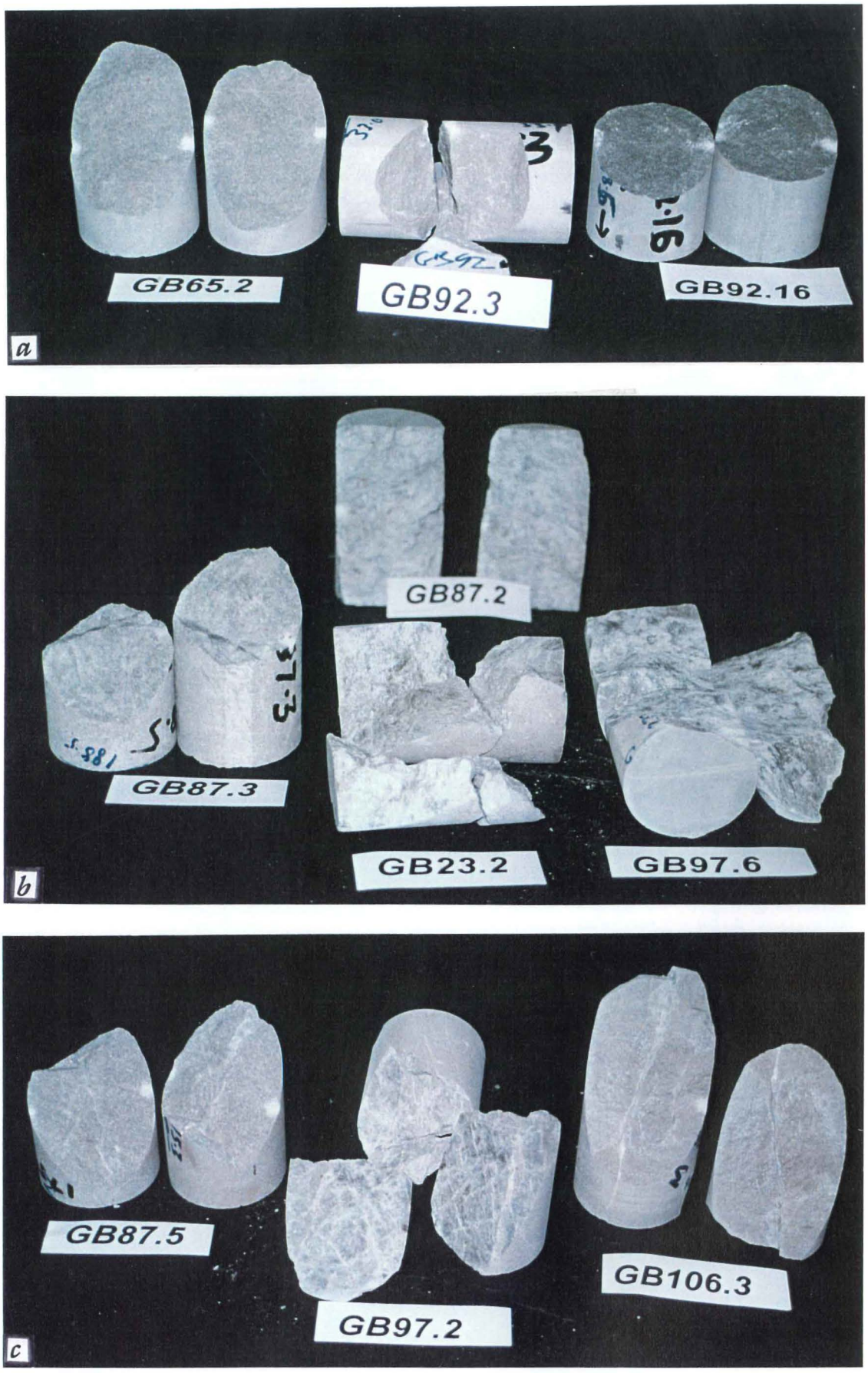

Figure 4.19: (*a* and *b*) Photos showing valid failures of point load tests. Samples in (*a*) are very well indurated and samples in (*b*) are brecciated. (*c*) shows invalid failures, where failure was on pre-existing shears.

Table 4.8: Point load test summary data for brecciated, highly fractured and laminated sandstone samples; unweathered, very well indurated samples; slightly weathered, very well indurated sandstone samples; and moderately weathered, very well indurated sandstone samples. There were no valid failures for mudstone samples.

All core sandstone samples

Summary statistic	Mean	sd	Median	Range	Maximum	Minimum
$I_{s\,(50)}$ (MPa)	4.47	3.12	5.00	9.26	9.70	0.44
Predicted UCS (MPa)	89	62	100	185	194	9

Brecciated, highly fractured and laminated core sandstone samples

Summary statistic	Mean	sd	Median	Range	Maximum	Minimum
$I_{s\,(50)}$ (MPa)	1.11	0.88	0.59	2.50	2.94	0.44
Predicted UCS (MPa)	22	18	12	50	59	9

Unweathered, very well indurated core sandstone samples

Summary statistic	Mean	sd	Median	Range	Maximum	Minimum
$I_{s\,(50)}$ (MPa)	6.49	1.98	6.61	7.73	9.70	1.97
Predicted UCS (MPa)	130	40	132	155	194	39

Slightly weathered irregular sandstone lumps

Summary statistic	Mean	sd	Median	Range	Maximum	Minimum
$I_{s\,(50)}$ (MPa)	5.06	1.91	5.03	7.47	8.36	0.89
Predicted UCS (MPa)	101	38	101	149	167	18

Moderately weathered irregular sandstone lumps

Summary statistic	Mean	sd	Median	Range	Maximum	Minimum
$I_{s\,(50)}$ (MPa)	2.68	1.77	2.78	5.59	5.90	0.31
Predicted UCS (MPa)	54	35	56	112	118	6

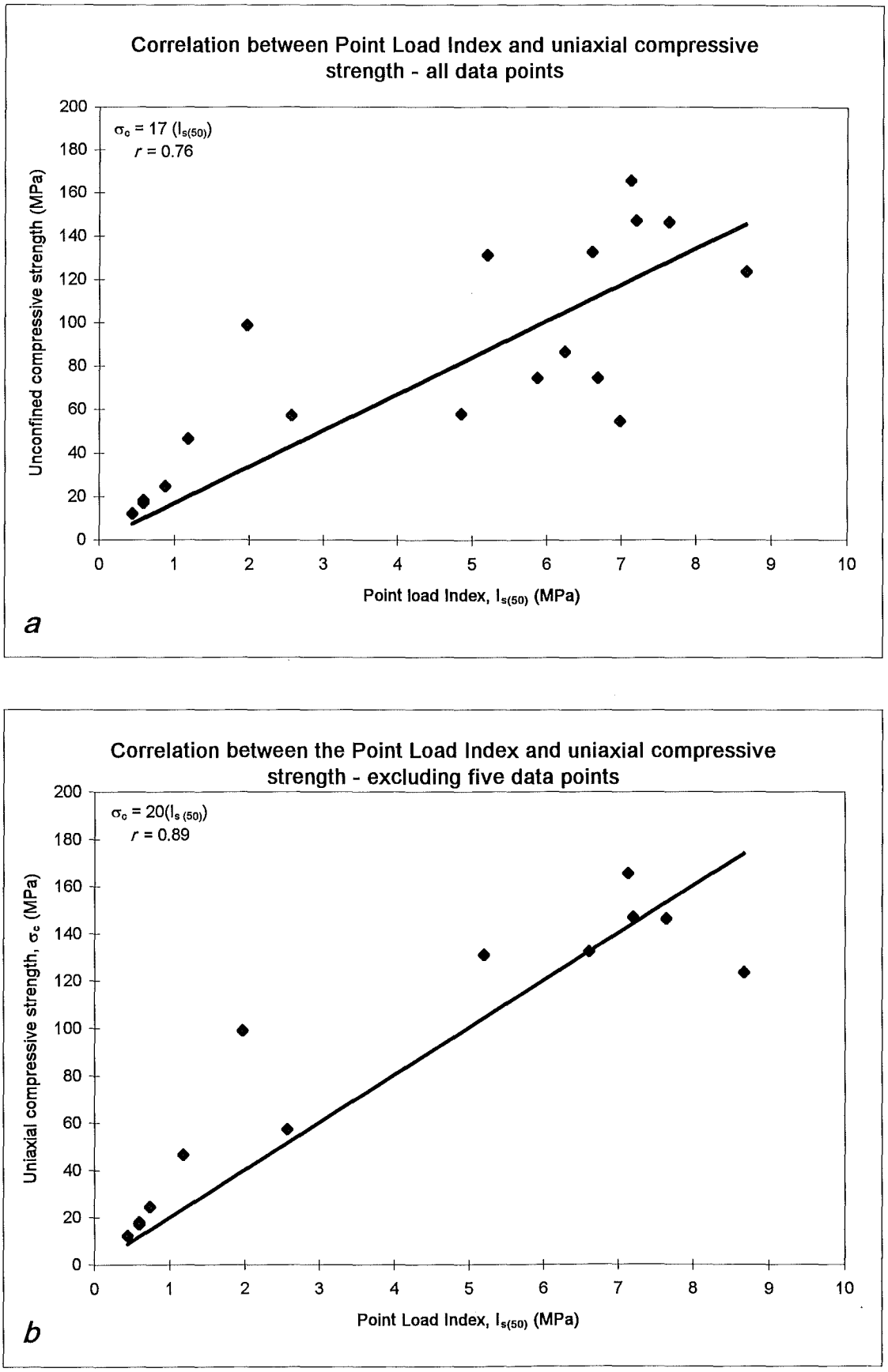

Figure 4.20: Site specific correlation between uniaxial compressive strength and Point Load Index. (*a*) includes all data points and (*b*) excludes five data points that failed that failed becasue of sample end effects.

$I_{s\,(50)}$ for unweathered, very well indurated core samples is greater than $I_{s\,(50)}$ for slightly weathered, very well indurated samples, which is greater than $I_{s\,(50)}$ for moderately weathered, very well indurated samples (Figure 4.20). This trend should be expected, and has also been found by Irfan and Dearman (1978), Hodder and Hetherington (1991) and Beetham and Coote (1994), because the strength of the rock is affected by the weathering grade of the samples. Beetham and Coote (1994) found the effects of weathering at Globe-Progress to approximately 30 m depth, but along discontinuities, weathering effects exist deeper depending upon the size and nature of the discontinuity. The change in strength of rock material due to weathering has implications on the type of site investigations performed. Site investigations cannot solely be performed on surface outcrops and it may be difficult to extrapolate surface data with subsurface data.

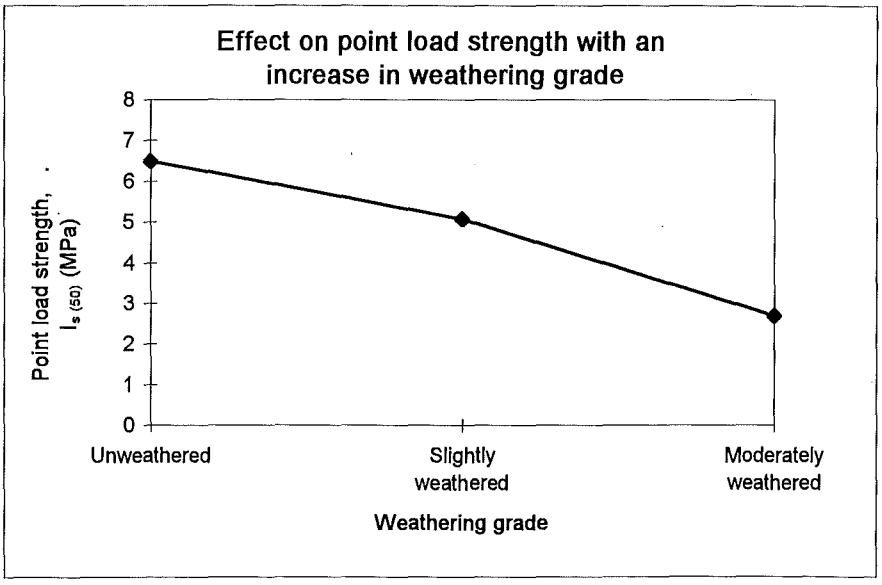

Figure 4.21: Plot of point load strength versus weathering grade. As weathering increases there is a corresponding drop in strength.

4.3.7 Slake-durability test

4.3.7.1 Introduction

The slake-durability test is designed to simulate natural wetting and drying weathering cycles by determining how durable, or resistant to weathering the rock sample is. This test was performed on unweathered, slightly weathered and moderately weathered samples from Globe-Progress to find the effect of weathering on the durability of the rock samples. The test is normally performed on weak rocks but it may be used on harder rocks to determine the state of weathering (Johnson and DeGraff, 1988) and was done at Globe Hill to determine whether or not weathering had a significant effect on the rock durability.

4.3.7.2 Methodology

Testing followed the suggested methodology recommended by ISRM (1981) whereby ten roughly spherical samples weighing between 40 and 60 grams each are placed in drums that are rotated at a rate of 20 rpm for 10 minutes, then oven dried. The simulated weathering cycle is repeated once more. The slake durability index, I_{d2}, is determined by comparing the samples mass initial mass with the mass after the second cycle. The test was performed twice so that results could be checked for consistency.

4.3.7.3 Results

The results are summarised in Table 4.9 and a complete set of results are given in Appendix D3.6. The Slake-durability Index is plotted against the weathering grades in Figure 4.22 and Figure 4.23 shows the samples after two slaking cycles.

Table 4.9: Slake durability results for unweathered, slightly weathered and moderately weathered samples.

Sample	I_{d2} (first test)	I_{d2} (second test)	I_{d2} (average)
Unweathered	99.5	99.3	99.4
Slightly weathered	98.9	98.7	98.8
Moderately weathered	98.1	98.1	98.1

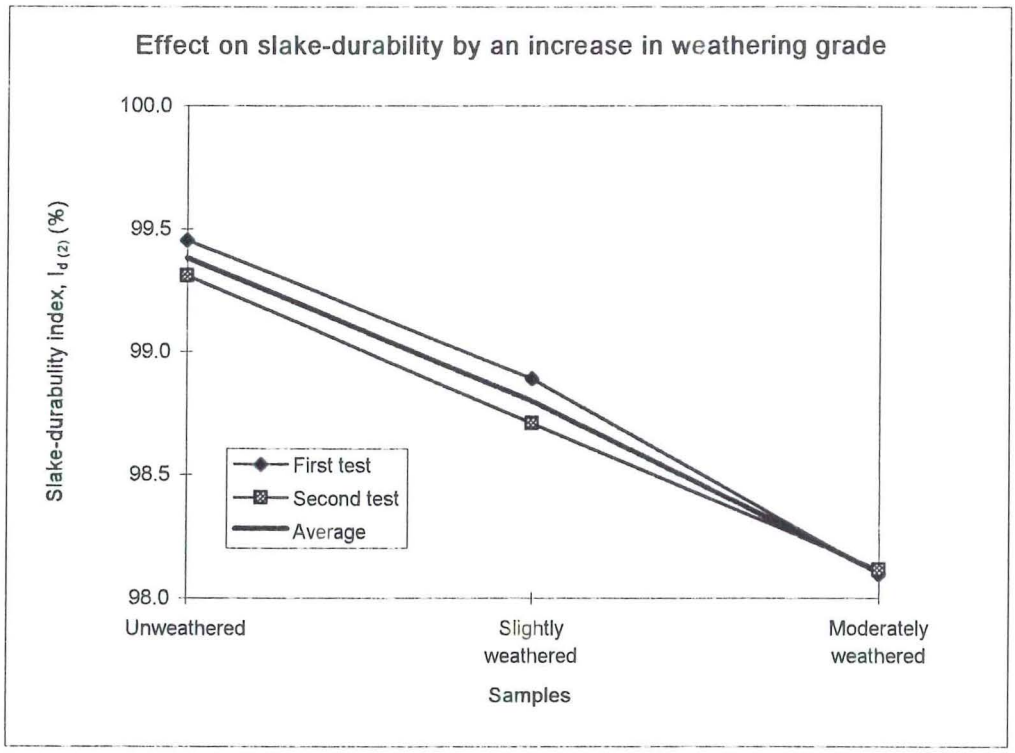

Figure 4.22: Plot of Slake-durability Index versus weathering grades. As weathering increases, the sample's durability decreases, although not by very much.

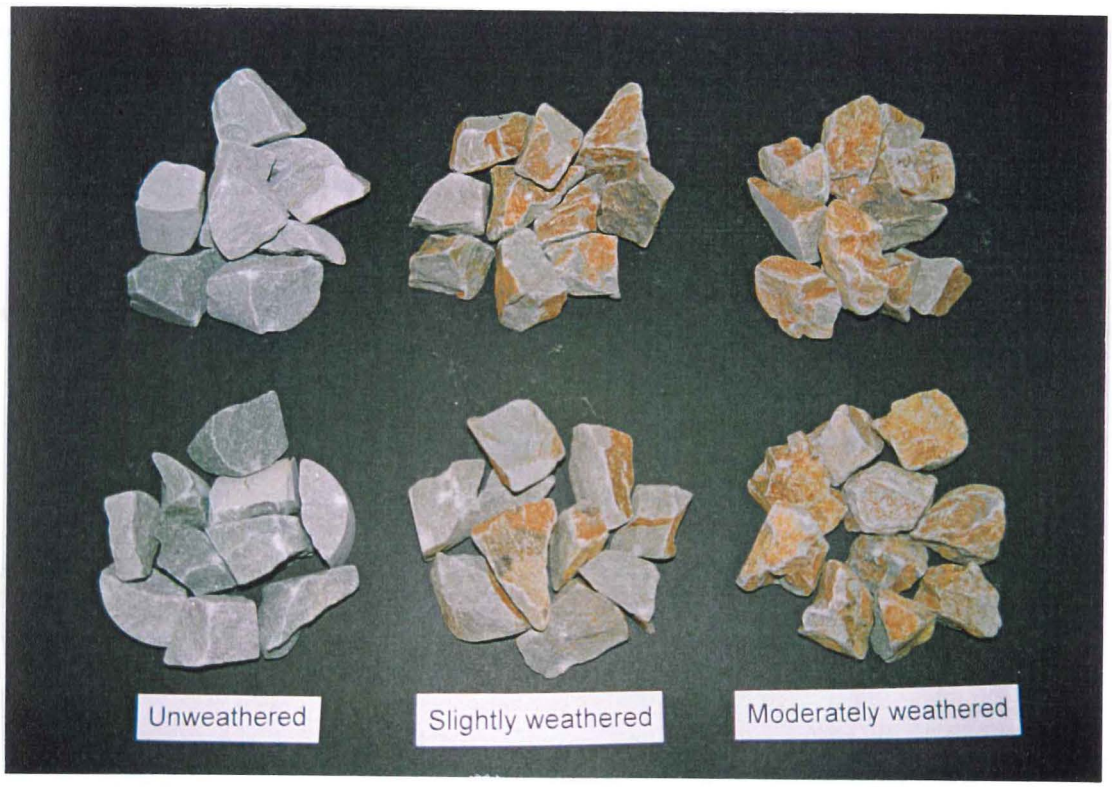

Figure 4.23: Photo showing the differences in slake-durability between differing weathering grades.

4.3.7.4 Discussion and interpretations

Table 4.10 shows the ISRM (1981) two cycle slake durability classification. All three weathering types may be classified as having very high durability with very little difference between weathering grades (Figure 4.22) indicating that weathering does not have much effect on the durability of the rock, although Figure 4.21 indicates that strength is affected by weathering. Material that passed through the drums in all three weathering types was mainly very finely ground mud sized particles with occasional small flakes and sand (increasing amounts with a increase in weathering). The tested samples are resistent because of their induration and well cemented matrix (Figure 4.23).

Table 4.10: Two cycle Slake-durability Index classification (after ISRM, 1981).

Slake-durability, I_{d2} (%)	Classification
0 - 30	Very low
30 - 60	Low
60 - 85	Medium
85 - 95	Medium high
95 - 98	High
98 - 100	Very high

4.4 Comparison between rock masses and rock materials

Seismic velocities found by the seismic refraction method can be compared with the sonic velocities determined on rock materials because both measure the velocity of an elastic wave propagating through a material or mass. Generally sonic velocities are significantly higher than seismic velocities because of the presence of discontinuities in the rock mass that may be filled with air, water, rock fragments or gouge. Deere *et al* (1967) proposed the seismic velocity index, which is the ratio of the rock mass velocity to the rock material velocity, squared:

$$I_v = \left(\frac{v_{field}}{v_{lab}}\right)^2$$

where I_v is the Seismic Velocity Index (dimensionless), v_{field} is the seismic velocity found in the field (ms^{-1}), v_{lab} is the sonic or seismic velocity found by laboratory testing. Deere also found that the Seismic Velocity Index can be correlated to RQD (Table 4.11).

Table 4.11: Seismic Velocity Index and RQD correlation.

I_v (-)	RQD (%)
0 - 0.2	0 - 20
0.2 - 0.4	20 - 40
0.4 - 0.6	40 - 60
0.6 - 0.8	60 - 80
0.8 - 1.0	80 - 100

I_v found at Globe Hill is about 0.25 ($2100^2/4350^2$), which is comparable to the average RQD of about 30% (determined in Section 4.5.3, Figure 4.26), but there is a minor discrepancy that is explained by the fact that fracturing is not the only parameter that influences v_{field}. Field velocities are seen as a measure of the effect of weathering, porosity, density, rock elasticity, water saturation, cementation, compaction, anisotropy, mineralogy and fracturing (Weaver, 1975; Palmer, 1980; Braybrooke, 1988), but by far the most important is fracturing.

Values of v_{field} range between 508 and 6667 ms^{-1} whereas values of v_{lab} range between 3900 and 4900 ms^{-1}. Field velocities may be greater than laboratory velocities of similar material if the rock material has very little or no discontinuities, or if the rock mass is very well confined (Johnson and DeGraff, 1988). This may explain values of v_{field} that range between 5000 to 6000 ms^{-1} (along SR2 and SR9), however the field velocities equalling 6667 ms^{-1} (along SR3 and SR16) appear to correlate with sulphide rich zones where sandstone has been altered to a sulphide rich sandstone, thus increasing the density and consequently, the field velocity of the rock (Figure 4.24).

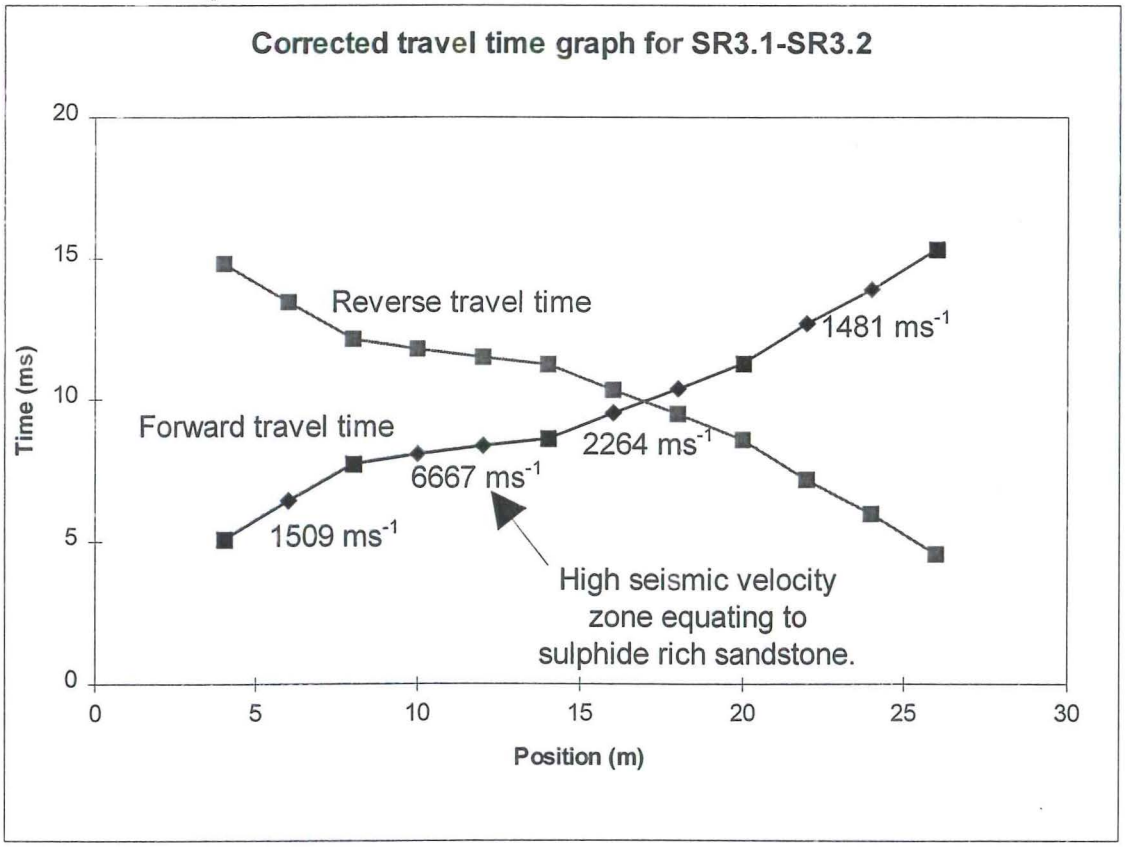

Figure 4.24: Corrected travel time graph along SR3.1 - SR3.2 and a photo of the outcrop adjacent to the survey line. The grey folded rock on the left hand side of the photo corresponds to the high velocity zone on the travel time graph.

The elastic properties of rock material may be used to estimate elastic properties of the rock mass. This assumes the rock mass will behave in an elastic fashion like the rock material, but that will probably not be the case as wide discontinuities and shears will be able to absorb some of the elastic energy if they are air or water filled. It also assumes that the ratio of P wave velocities to S wave velocities for rock material is the same for rock masses, which may not be the case if discontinuities contain significant quantities of water (as S waves cannot propagate through liquids). Aside from these two assumptions, using the formulae in Section 4.3.4.2 for the dynamic modulii of elasticity, and using v_p = 2100 ms^{-1} and v_s = 1300 ms^{-1} and ρ = 2300 kgm^{-3}, then $E_{dyn\ (rock\ mass)}$ = 9.2 GPa and $\nu_{dyn\ (rock\ mass)}$ = 0.19, where $v_{s\ (field)}$ and ρ_{RM} are estimated from:

$$v_{s\,(field)} \approx k \times v_{p\,(field)} \qquad \text{where: } k = \frac{1}{\left(v_{p\,(sat)}/v_{s\,(sat)} + v_{p\,(dry)}/v_{s\,(dry)} \right)/2}$$

$$\rho_{RM} \approx n(\rho_{infill}) + (1 - n)\rho_{lab} \qquad \text{where: } n \approx \frac{v_{infill} v_{lab}}{v_{field}(v_{lab} - v_{infill})} - \frac{v_{infill}}{v_{lab} - v_{infill}}$$

and where $v_{s(field)}$ is the field S wave velocity; $v_{p\ (field)}$ is the average field P wave velocity; k is the ratio of P:S waves determined from rock material samples; ρ_{RM} is the average density of rock material determined from the estimated porosity (n) of the rock mass; ρ_{infill} is an approximate density of infilling material (estimated to be 1500 kgm^3); ρ_{grain} is the grain density of sandstone (about 2700 kgm^3); v_{infill} is the velocity of discontinuity infilling (average is about 1000 ms^{-1}); v_{lab} is the sonic laboratory velocity (4750 ms^{-1}); and v_{field} is the field seismic velocity (2100 ms^{-1}; density and porosity formulae adapted from Nobes, 1989). Estimation of the dynamic Modulii of Elasticity of the rock mass uses average rock material and rock mass seismic velocity data, thereby giving average dynamic Modulii of Elasticity for the open pit area, and therefore, this data should be used a guideline only. More detailed tests, such as plate bearing tests or jack tests would need to be performed to accurately determine the Modulii of Elasticity of the rock mass.

This data may be useful for prediction of the rock mass as the pit is excavated (unloaded), behaviour of the pit under the influence of seismic shaking, behaviour of the rock mass below the tailings dam and rock waste stack, and if the open pit is to be excavated by drill and blast methods, the effect of blasting on the surrounding rock mass.

4.5 Drillcore log analysis

4.5.1 Introduction

Analyses and checks of the drillcore logs were performed to confirm the accuracy of logged data before applying ratings to them for rock mass and rippability classifications. Comparisons were made between logged strength values, and point load strength and UCS values tested by Beetham and Coote (1994) and this study. Two RQD data sets exist, which were compared, and the discontinuity spacing was compared to discontinuity spacing distribution models postulated by Priest and Hudson (1976). Other parameters such as rock type, grain size and weathering are all assumed to have been correctly logged as they are simple to describe and do not require any estimation of the parameter.

4.5.2 Strength comparisons

A comparison of the logged strength values and point load test and UCS tested samples show that strength has been consistently logged incorrectly. The majority of sandstone has been logged as R3 (equivalent UCS values equal 25 - 50 MPa), yet point load strength data from Beetham and Coote and this study, as well as UCS values from this study, range between 8 MPa and 260 MPa (Figure 4.25a; point load strength data converted to UCS by multiplying by 20). Therefore, some of the sandstone strengths have been over-estimated, but the majority have been under-estimated. From data collected from point load strength and UCS tests, a revised strength estimate was made for each logged rock mass unit (RMU) based on the logged lithology and strength (Figure 4.24b). The revised strength estimate includes a large group of data in the extremely weak to weak strength class (< 25 MPa) that is not present in the actual strength data set. This discrepancy arises because samples tested for strength by Beetham and Coote (1994) and in this study are biased towards selecting stronger samples. The assumptions made in determining the revised strength are included as Appendix E1.1.

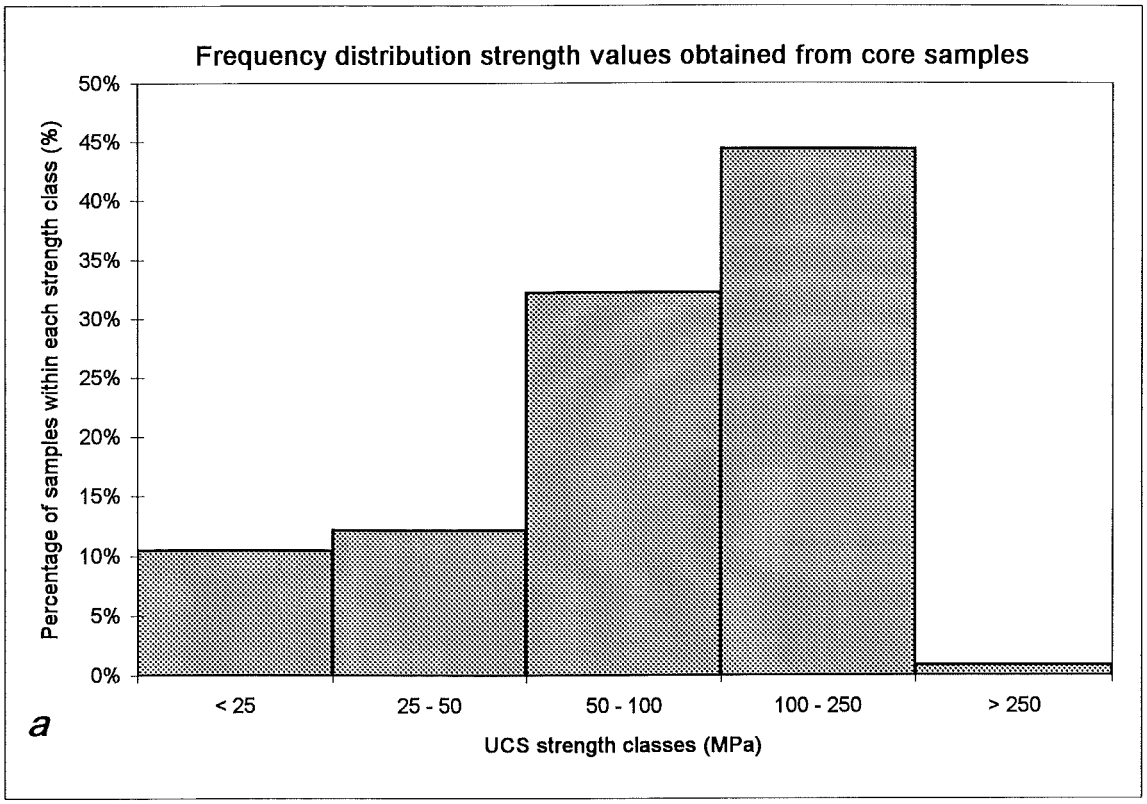

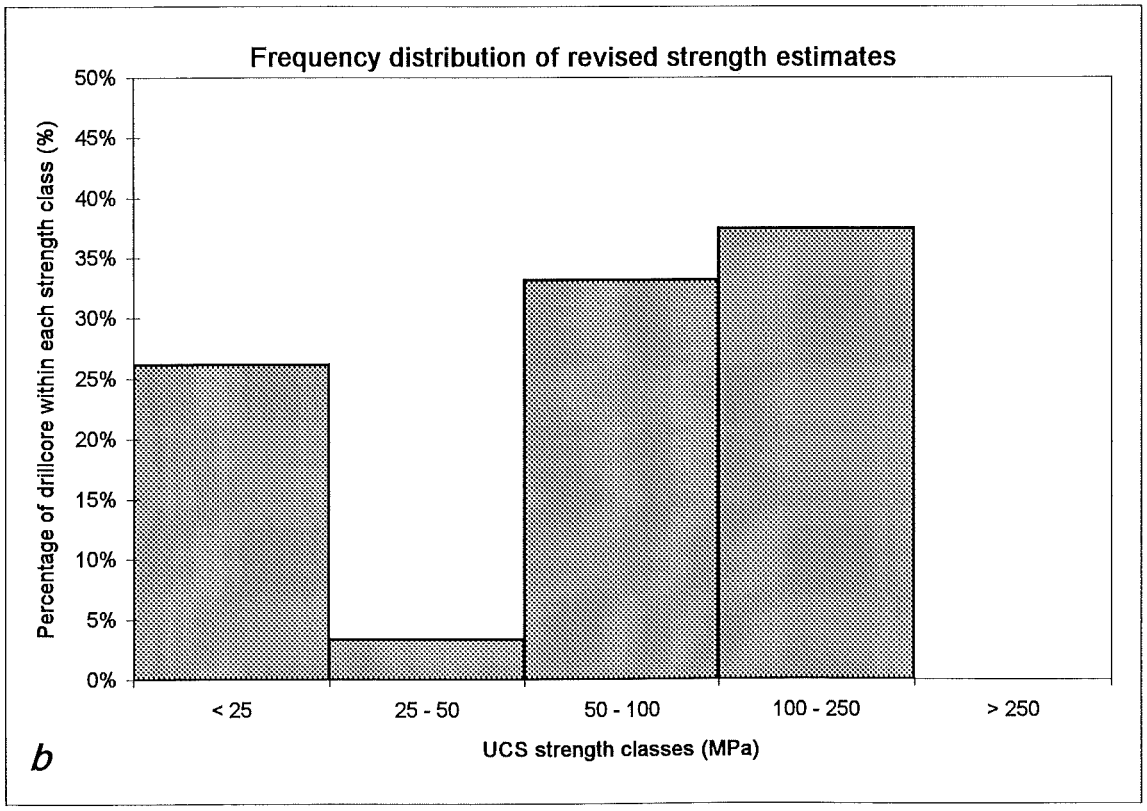

Figure 4.25: Frequency distribution of strength values from: (*a*) point load test (expressed as UCS values) and UCS test and (*b*) revised drill log strength estimates. Data are grouped into the strength classes suggested by Bienawski (1979) for use in the RMR System. Data in (*a*) reinterpreted from Beetham and Coote (1994; 72 point load samples), and from this work (24 point load samples, 19 UCS samples) and 10360m of drillcore was used determining (*b*).

4.5.3 RQD data sets comparison

RQD is included on the drillcore logs and was also recalculated in 1995 at different intervals to the drillcore logs. The first RQD data set was determined for every RMU, whereas the second RQD data set was determined for the core run. The spread of data between the two is virtually identical (Figure 4.26) and the mean RQD is the same for both data sets (30%), therefore it is assumed that the RQD has been correctly calculated.

4.5.4 Discontinuity spacing analysis

The discontinuity spacing parameter is similar to RQD, as both are measures of the fractured nature of the rock mass, and therefore Priest and Hudson (1976) found that RQD could be theoretically calculated from the discontinuity spacing using the following formula:

$$RQD_{Theoretical} = 100e^{-0.1I_f}(0.1I_f + 1) \quad (\%)$$

where the I_f is the discontinuity spacing index in metres and the theoretical RQD is a percentage. This formula is based on the assumption that discontinuities are random in nature, although this may not be the case at every site. Priest and Hudson (1980) found four different types of discontinuity spacing distribution patterns (Figure 4.23): evenly spaced distribution; clustered distribution; random distribution; and a combination of distribution patterns.

The evenly spaced distribution patterns occur in sedimentary rocks with consistent beds thickness and foliated metamorphic rocks. The clustered distribution occurs where a high frequency of low discontinuity spacings occur in clusters, and a low frequency of high discontinuity spacings occur between the clusters. This clustering effect normally occurs in alternating layers of sandstone and siltstone, or in sheared rock, as is the case at Globe-Progress. Random distributions occur in homogeneous rocks where no joint sets are present. The most common distribution pattern is the combination of distributions, which occur in geologically complex rock masses.

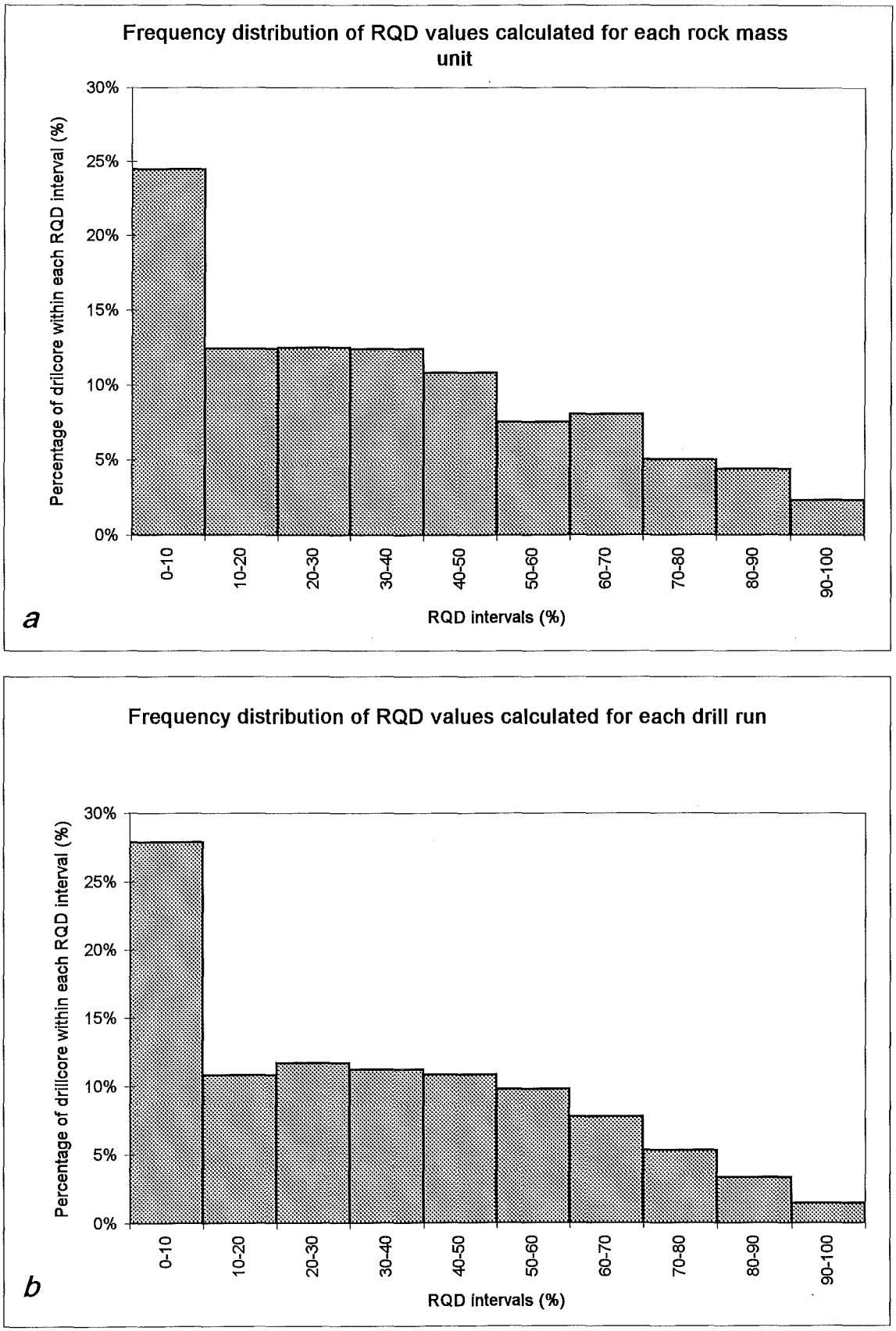

Figure 4.26: Comparison between: (*a*) RQD calculated for each rock mass unit; and (*b*) RQD calculated from the core run.

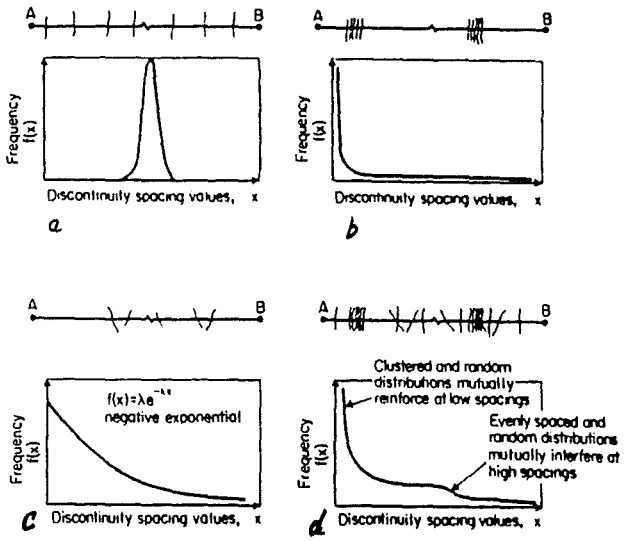

Figure 4.27: Theoretical discontinuity spacing distributions (From Priest and Hudson, 1980). (*a*) is an evenly spaced distribution, (*b*) is a clustered distribution, (*c*) is the random distribution and (*d*) is a combination of evenly spaced, clustered and random distributions.

Figure 4.27 shows the distribution of discontinuity spacings found at Globe-Progress. It is very similar to the clustered distribution, and therefore shows that discontinuities at Globe-Progress are not randomly distributed. A further check to this can be done by comparing the actual RQD (Figure 4.25) with the theoretically derived RQD (Figure 4.29), which show dissimilar patterns, proving that discontinuities are not randomly distributed and that they follow a clustered pattern.

It is thought that the logged fractures per metre parameter is over-estimated (M McKenzie *pers com*), hence, under-estimating the discontinuity spacing. Under-estimation of the discontinuity spacing is thought to be because drilling induced fractures may have been logged as natural fractures, and this will partly result in the clustered distribution pattern. The other reasons why the clustered distribution pattern occurs is because of the high percentage of sheared rock intersected by drilling, as most drillholes were targeted to intersect the Globe-Progress Shear Zone, and because interbedded siltstone-sandstone sequences, where most siltstone beds are thin (closely spaced) are very common at Globe-Progress.

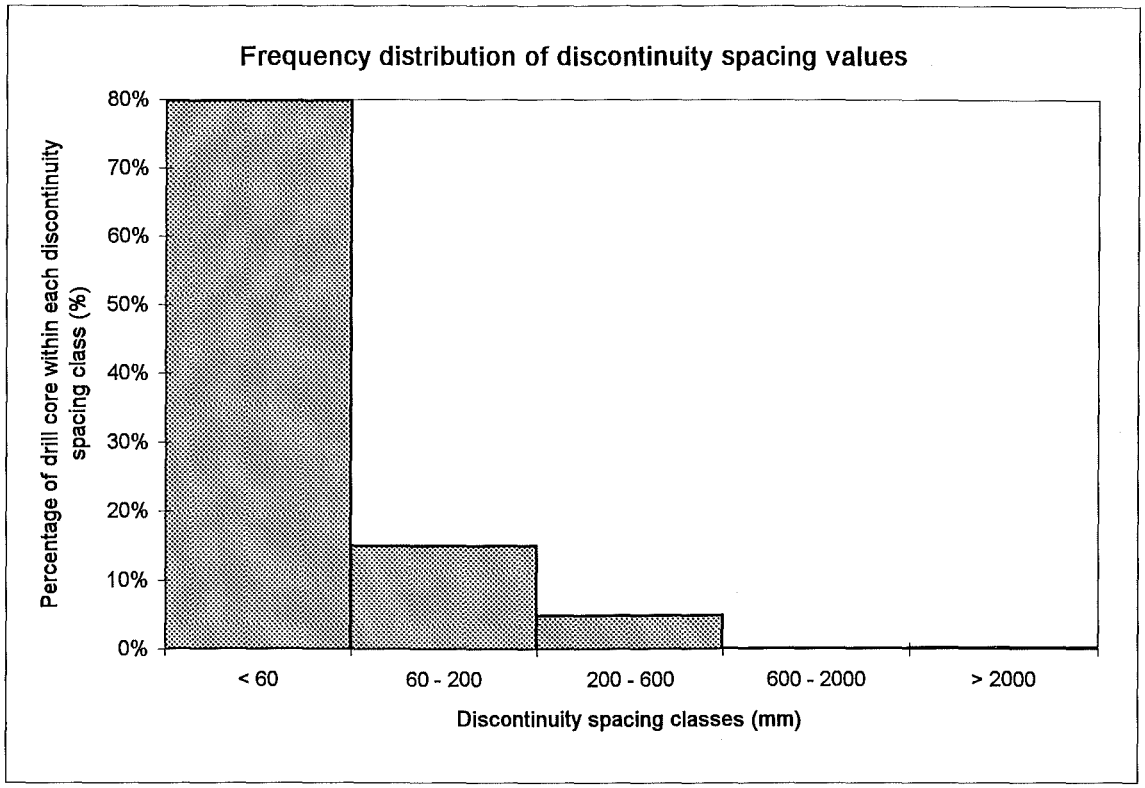

Figure 4.28: Frequency distribution of discontinuity spacing values from the fractures per metre count in drillcore logs, grouped into classes suggested by Bienawski (1979). The total length of drillcore from which data was obtained is 10360 m.

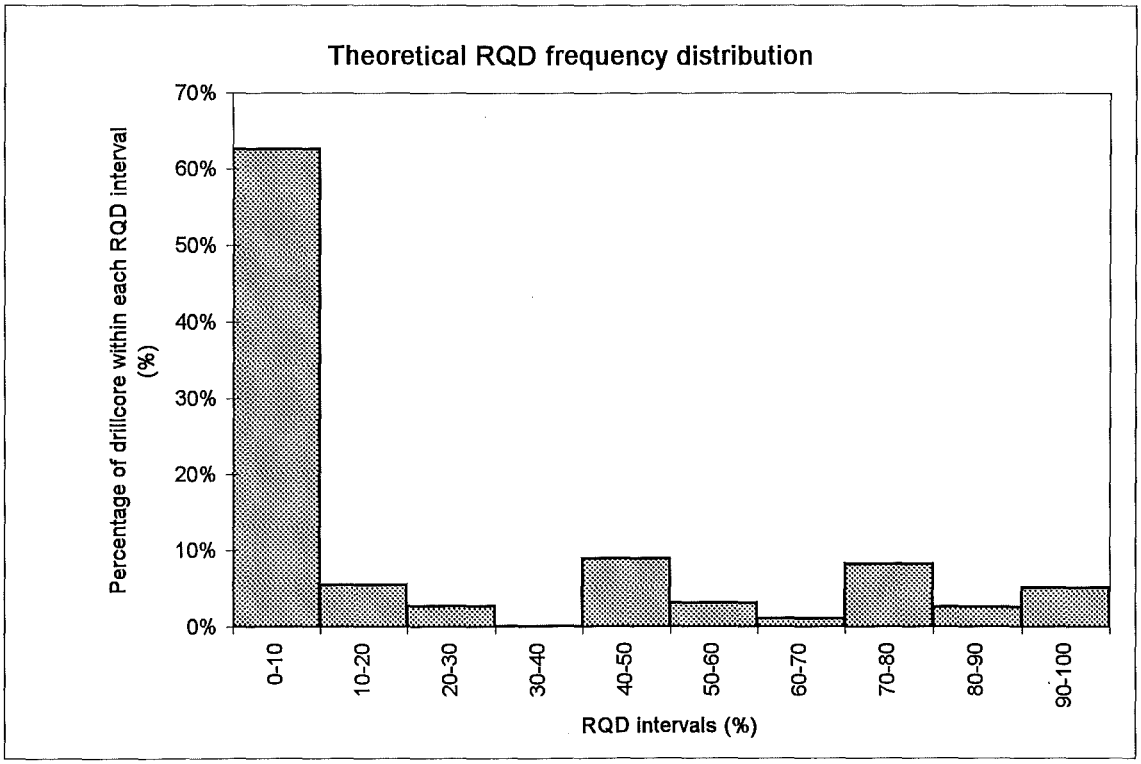

Figure 4.29: Theoretical RQD determined from Discontinuity Spacing Index.

4.5.5 Other logged data

Logged parameters such as rock type, colour, grain size, weathering and alteration, and discontinuity descriptions such as type, habit, roughness, infilling and infilling width are all easily described as they are based on visual descriptions rather than estimations (like the rock material strength and discontinuity spacing parameters). Therefore, it is assumed that logged data such as rock type, colour, grain size, weathering, alteration, discontinuity type, habit, roughness, infilling and infilling width have been logged correctly.

4.6 Synthesis

4.6.1 Field testing

Globe-Progress has been studied in detail by many workers, including Barrell (1992; geotechnical line mapping), Rattenbury (1994; structural mapping) and Jowett *et al* (1996; bench zero geotechnical mapping). The abundance of field investigations meant very little additional field work was required. Seismic refraction line traverses were surveyed to collect rock mass seismic velocity data, which could be used as a preliminary rippability assessment (see Section 5.2.2) and also for comparisons with sonic velocities determined from core samples of rock material. Fifteen seismic refraction surveys were performed at Globe-Progress and five seismic refraction survey lines were performed at General Gordon, site of the waste rock stack. Frequency distribution diagrams of seismic velocities grouped into 500 ms^{-1} were plotted and the mean seismic velocity at each site was calculated to be 2100 ms^{-1} at Globe-Progress, 1950 ms^{-1} at General Gordon, and in total, a mean seismic velocity of 2100 ms^{-1} was found.

4.6.2 Laboratory testing

The following laboratory tests were performed on drillcore to acquire quantitative geotechnical information of rock materials found at Globe-Progress:

- Porosity-density determination
- Sonic velocity determination
- Stress-strain relationship
- UCS and point load strength comparison
- Slake durability determination

In addition to the above tests, the point load strength and slake-durability of moderately weathered and slightly weathered irregular lumps were compared to point load strength and slake-durability of unweathered core samples.

There were three broad groups of rock material tested:

- Very well indurated sandstone
- Brecciated or highly fractured sandstone
- Mudstone

The mean values from the tests listed above for each type of rock material are given in Table 4.12. In addition to the above tests, the point load strength and slake-durability of unweathered, slightly weathered and moderately weathered samples were tested to find the effect of weathering on strength and durability of the rock material (Table 4.13).

4.6.3 Drill core analysis

An analysis of drillcore log data was performed to assess the reliability of drillcore data. It was found that:

- logged strength values had been under-estimated.
- RQD was logged correctly.
- Distribution of discontinuity spacing data follows a clustered distribution whereby closely spaced discontinuities are more common than widely spaced discontinuities.

Table 4.12: A summary of mean results of geotechnical properties for very well indurated sandstone, brecciated and highly fractured sandstone and mudstone.

Geotechnical test variable	Very well indurated sandstone	Brecciated and highly fractured sandstone	Mudstone	Combined data
Dry Density (kgm^{-3})	2718	2676	2785	2713
Saturated density (kgm^{-3})	2726	2694	2806	2724
Porosity (%)	0.84	1.84	2.02	1.11
Saturation moisture content (%)	0.31	0.68	0.72	0.41
Saturated P wave velocity (ms^{-1})	4661	3961	1677	4357
Saturated S wave velocity (ms^{-1})	2623	1792	1278	2377
Dry P wave velocity (ms^{-1})	4230	3393	1519	3911
Dry S wave velocity (ms^{-1})	3009	2411	1086	2782
Saturated E_{dyn} (GPa)	46.8	23.8	7.4	39.9
Saturated v_{dyn} (-)	0.25	0.37	0.19	0.27
Dry E_{dyn} (GPa)	42.5	30.3	6.4	38.0
Dry v_{dyn} (-)	0.21	0.13	0.02	0.18
Saturated UCS (MPa)	103.9	25.0	32.0	79.0
Saturated $E_{t\,(50)}$	40.9	15.8	5.1	33.9
Saturated $I_{s\,(50)}$ (MPa)	6.49	1.11	-	4.47

Table 4.13: Summary point load strength and slake-durability data for unweathered, slightly weathered and moderately weathered core and irregular lump samples.

Geotechnical test variable	Unweathered core	Slightly weathered irregular lumps	Moderately weathered irregular lumps
Point load strength (MPa)	6.49	5.06	2.68
Slake-durability (%)	99.4	98.8	98.1

Other parameters such as rock type; grain size; weathering; alteration; and defect type, habit, roughness and infilling are assumed to have been correctly logged as they are easily assessed whilst logging, and do not require any estimation of properties (unlike strength).

Chapter 5

Rippability evaluation of the proposed open pit mine at Globe-Progress

5.1 Introduction

Chapters 2 and 3 briefly discussed various rock mass and rippability classification methods and detailed the techniques most suited for classifying the open pit rock mass at Globe-Progress. Chapter 4 provided additional data and analysed the drillcore log data that was used in the rock mass classifications. In this chapter the rock mass and rippability methods detailed in Chapters 2 and 3, using data discussed in Chapter 4, are applied to the rock mass at Globe-Progress.

The first stage in classifying the rock mass was to apply two simple methods that may be performed at the feasibility and early investigation stage of a project (Section 5.2), followed by a more detailed investigation that fully characterises the rock mass using a suite of geological and geotechnical properties (Sections 5.3 and 5.4). This type of rock mass assessment may be performed during the investigation and design stages of a project. The classification systems used should not be used as stand-alone site investigation studies. They should be compared with other forms of geotechnical investigations, but they can be used as guides to the location of areas that will be easy or difficult to excavate.

5.2 Preliminary rippability evaluation

5.2.1 Introduction

An initial or preliminary rippability assessment was performed to test whether or not a more detailed rippability evaluation was required. If the preliminary analyses showed that the excavatability of the pit to be marginal to non-rippable (very hard ripping to blasting), then blasting would most likely be used and the excavatability of the pit would not be required. If the preliminary analyses show that the pit is rippable (easy to hard ripping), then a more detailed rippability investigation would be required to identify the diggable, easy ripping, moderate ripping and hard ripping zones. The preliminary rippability assessments performed are both simply achieved with minimal effort and interpretation, and therefore can be used in the feasibility and early site investigation stages of a project.

The approach undertaken was to use two different methods: one involving determination of seismic velocities, similar to the approach undertaken by bulldozer manufacturers and contractors, such as Caterpillar and Komatsu, who wish to sell their ripping machinery to the buyer; and the other method involves comparing the spacing of discontinuities in a rock mass and the corresponding rock material strength, the two parameters most influential on the excavatability of a rock mass. This approach is commonly known as the Size-Strength Method and plots the strength of a rock material against its block size or discontinuity spacing. The method was originally designed by Franklin *et al* (1971) and was recently updated by Pettifer and Fookes (1994).

5.2.2 Seismic velocity determination

5.2.2.1 Komatsu's site visit report

A study to determine seismic velocities at Globe-Progress was undertaken by John (1994) for Komatsu, and involved limited seismic velocity determination at four sites (see Figure 4.1 for locations). Site 1A and 1B and 3 were within the defined pit limits, although no data was obtained at site 3 because of the heavily fractured nature of the rock at this

location (John, 1994). Site 2 was just outside the pit limits but at a lower ground level, possibly indicative of the structure within the open pit. Site 4 was on a back road leading into the proposed mine site, where the rock mass is expected to be typical of that found in the open pit.

Tests were performed with geophone spacings at 3 m, 7 m, and 12.3 m at site 1A, 3 m, 7 m, and 12 m at site 1B, 3 m, 8 m and 12 m at site 2 and 3 m, 7 m, 13 m, at site 4. All tests were performed three times to check the consistency in results. All tests were found to be consistent, with the tests performed at 3m spacing yielding higher velocities (range between 968 ms^{-1} and 2200 ms^{-1}) the tests performed at wider spacing (ranging between 609 ms^{-1} and 2000 ms^{-1}).

The report is lacking in details but it appears that no attempt has been made to process the results following a standard method of data interpretation such as the Generalised Reciprocal Method, therefore the velocities are apparent velocities, which are always less than true velocities (see Appendix D2.1.2 for the definitions of apparent and true seismic velocities), and are therefore not indicative of the rock mass quality.

John's (1994) recommendations based on field tests and observations on drillcore were:

- at least 60% of the rock mass is likely to be rippable using a Komatsu D475A-2 bulldozer at a productivity rate of 450 m^3/hr
- at least 80% of the rock mass is likely to be rippable using the Komatsu D575A-2 bulldozer at a productivity rate of 850 m^3/hr

The productivity figures quotes are at 80% efficiency, meaning the bulldozer is ripping 80% of the time. MacGregor et al (1994) stated that bulldozers normally rip 54% (range between 30% and 90%) of the time if the bulldozer is just ripping and turning, or 21% (range between 1% and 60%) of the time if the bulldozer is required to push scrapers and/or doze loose material, therefore the productivity figures quoted by Komatsu are likely to be higher than the actual productivity.

5.2.2.2 Rippability assessment based on seismic velocities determined in this study

Twenty seismic refraction survey lines performed at Globe-Progress and General Gordon (Figure 4.1, in map and table box) were used to assess the rippability at both locations and the data was combined to provide an assessment of the rippability of the mine site. The methodology, results and discussion of the seismic refraction surveys are included in Section 4.2 and Appendix D2, therefore this section involves reinterpreting the data for a rippability assessment.

Reinterpretation of Figures 4.4 to 4.6 involved adding the rippable, marginal and non-rippable zones of sandstone, siltstone and claystone for Komatsu's D575A-2 bulldozer (bulldozer recommended by John, 1994; Figure 3.1 and 3.2), as shown in Figures 5.1-5.3. These lithologies are all likely to be found in the open pit area and all have the same rippable, marginal and non-rippable zones according to Komatsu's D575A-2 ripper performance charts (Figure 3.4; John, 1994). The cumulative frequency line was also plotted on the graphs and where this line intersects a rippability zone boundary, then the cumulative frequency shows the quantity of the open pit area that fits into the rippability zone.

At Globe-Progress 80% of the pit area is rippable and 90% is rippable and marginal, thus only 10% of the pit area is unrippable (Figure 5.1). This 10% is where seismic velocities are greater than 3700 ms^{-1}, and the location of these are in sulphide-rich sandstone (for example SR3; Figure 4.24) or parallel to the strike of bedding planes, therefore not intersecting as many discontinuities as at other sites (For example SR2 and SR5). The data from General Gordon (Figure 5.2) is not as detailed as that from Globe-Progress but is still indicative of the area to be ripped. The results are the same as at Globe-Progress where 80% of the area is rippable and 10% of the area is unrippable. Therefore the combined data (Figure 5.3) for the mine site suggests that 80% of the rock mass is rippable, 90% is rippable to marginal, and 10% of the mine site is expected to be non-rippable.

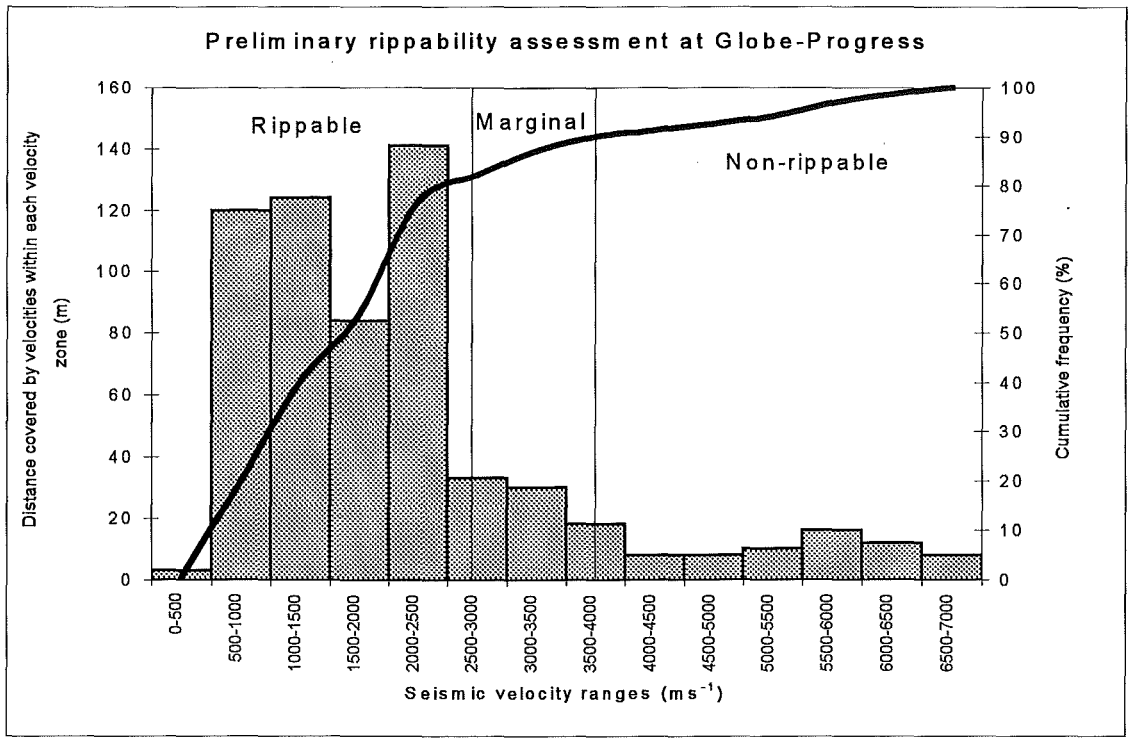

Figure 5.1: Preliminary rippability assessment for Globe-Progress based on seismic velocity data and rippable, marginal and non-rippable zones for Komatsu's D575A-2 Bulldozer (bulldozer data from John, 1994).

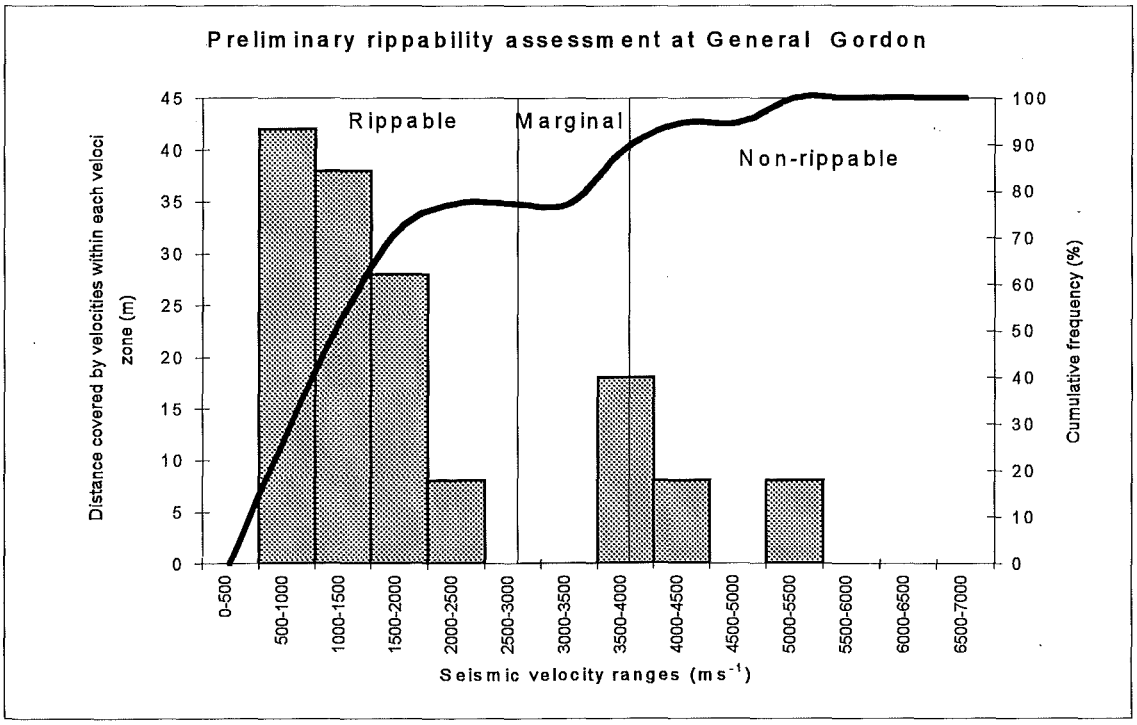

Figure 5.2: Preliminary rippability assessment for General Gordon based on seismic velocity data and rippable, marginal and non-rippable zones for Komatsu's D575A-2 Bulldozer (bulldozer data from John, 1994).

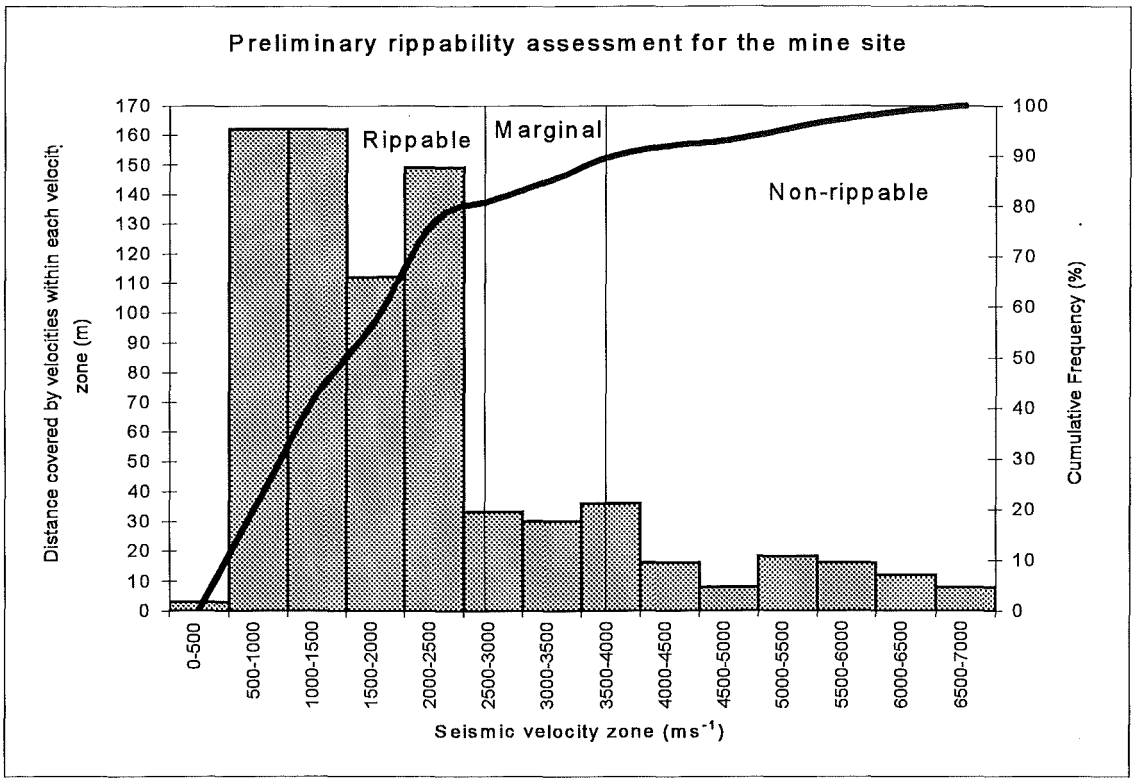

Figure 5.3: Preliminary rippability assessment for the mine site based on seismic velocity data and rippable, marginal and non-rippable zones for Komatsu's D575A-2 Bulldozer (bulldozer data from John, 1994).

The rippable, marginal and non-rippable zones are from Komatsu's bulldozer performance charts and are likely to be highly optimistic (MacGregor *et al*, 1994; Beetham and Richards, 1995), therefore it is probable that greater than 10% of the mine site will be unrippable, although the actual percentage cannot be determined from the available data but a comparison can be made with the size-strength assessment in Section 5.2.3.2.

5.2.2.3 Comparison between Komatsu's data and data from this study

Seismic refraction surveys performed in this study were performed at Komatsu site 1B (SR6.1 - SR6.2), site 2 (SR19.1 - SR19.2) and site 3 (SR18.1 - SR18.2) so that data from both studies could be compared. Seismic velocities found by both studies are compared in Table 5.1.

Resolution of data from this study is equal to two metres, that is the variation in seismic velocities along a seismic refraction line can be determined to within two metres, whereas John's (1994) velocities were determined by placing two geophones spaced 3m, 7 m or 12 to 13 m apart and recording the time taken to travel between them, thus not revealing any variations in the seismic velocity of the rock mass. For example, along SR6.1-SR6.2 (Komatsu site 1B), data from this study records an alternating sequence of sandstone and siltstone layers (Figure 4.7) that John's data cannot differentiate.

Table 5.1: Comparison between seismic velocities determined by Komatsu (John, 1994) and seismic velocities from this study. Komatsu's data is the average of three readings taken over the same distance whereas data from this study is the seismic velocity at the position along the seismic refraction line.

Komatsu site 1B		SR6.1-SR6.2 (this study)		Komatsu site 2		SR19.1 - SR19.2 (this study)		Komatsu site 3	SR18.1 - SR18.2 (this study)	
Length (m)	Velocity (ms^{-1})	Length (m)	Velocity (ms^{-1})	Length (m)	Velocity (ms^{-1})	Length (m)	Velocity (ms^{-1})		Length (m)	Velocity (ms^{-1})
3	2181	4 - 8	1633	3	989	4 - 8	772	No data	4 - 10	839
7	1981	8 - 14	1034	8	990	8 - 30	2146	could be	10 -12	2352
12	1496	14 - 16	3636			30 - 36	4444	determined	12 - 20	629
		16 - 18	1053					at this site	20 - 28	1000
		18 - 20	3333							
		20 - 22	870							
		22 - 24	3636							
		24 - 26	1639							
Weighted mean values										
	1744		1867		990		2405	-		949

Mean velocities found at site 1B and SR6 are comparable, but Komatsu's data is determined over a shorter distance and provides an average velocity that does not delineate any variations in the rock mass, unlike the survey performed in this study, which records an alternating sequence of sandstone and siltstone. Mean velocities found at Komatsu's site 2 and SR19 are completely different, however the velocities found at site 2 are comparable with the velocities found along the start of the SR19 (4 - 8 m). If John (1994) had extended his survey at this location or started at the other end of the outcrop, he would have expected higher seismic velocities that are more representative of the location. John (1994) could not record any data at site 3, yet this study was able to, although the seismic velocity is low due to the fractured nature of the rock mass at this location (Figure 5.4).

Figure 5.4: Photo taken along SR18.1 - SR18.2 from the start of the survey line to approximately 12 m (the stake is on the 10 m mark and is 1 m high) showing the highly fractured rock mass with corresponding low seismic velocities (839 ms^{-1}).

Overall, John (1994) predicts the same result as this study for a Komatsu D575A-2 bulldozer (80% of the pit is rippable), although it is unclear how he derived the 80% rippable figure as all his seismic velocity data fit into the rippable zone for the bulldozer.

5.2.3 Size-strength preliminary assessment

5.2.3.1 Introduction

This assessment uses the two most important variables that affect a rock mass, namely rock material strength and rock mass discontinuity spacing. A complete discussion on this method of assessment is included in Section 3.5.2 and this approach follows the revised

Size-Strength Method of Pettifer and Fookes (1994), who plot the block size (or discontinuity spacing) versus the point load strength of the rock material. UCS can be used by converting UCS values to point load strength values by dividing by twenty (Pettifer and Fookes, 1994), but Pettifer and Fookes recommend the use of the point load strength data as it is easy to obtain in both a field and laboratory setting.

5.2.3.2 Methodology

Two sets of data from Globe-Progress were plotted. Data set 1 plots the discontinuity spacing and strength data from the drillhole logs and is shown as Figure 5.5. The second data set plots point load strength data determined in this study and by Beetham and Coote (1994) versus logged discontinuity spacing values for the rock mass unit (RMU) the point load strength sample originally came from (Figure 5.6).

5.2.3.3 Results

The size strength graphs shown in Figures 5.5 and 5.6 are plotted on the same scales as used by Pettiifer and Fookes, however this truncates a sizeable amount of data with discontinuity spacings less than 0.02 m, which would fit in the easy and hard digging zones. Most of the rock classed as diggable is brecciated rock from the Globe-Progress Shear Zone, which is likely to be dug by an excavator (M McKenzie, *pers com*).

Figure 5.5 shows that the majority of data points fit into the diggable and easily rippable zones, with a few samples in the hard, very hard and extremely hard ripping rippable zones. No data falls into the blasting zone, therefore suggesting that blasting will not be required to excavate the open pit.

Figure 5.6 shows most data points fitting into the hard digging and easy to hard ripping zones. One sample fits into the blasting zone, indicating that some blasting of the rock mass may be required. The strength values on Figure 5.6 are higher than the strength values on Figure 5.5. This is because samples selected for point load strength testing were biased toward samples that were likely to be strong, as weak samples should not be used for point load testing (Bieniawski, 1979; Hawkins, 1986; Pettifer and Fookes, 1994), and

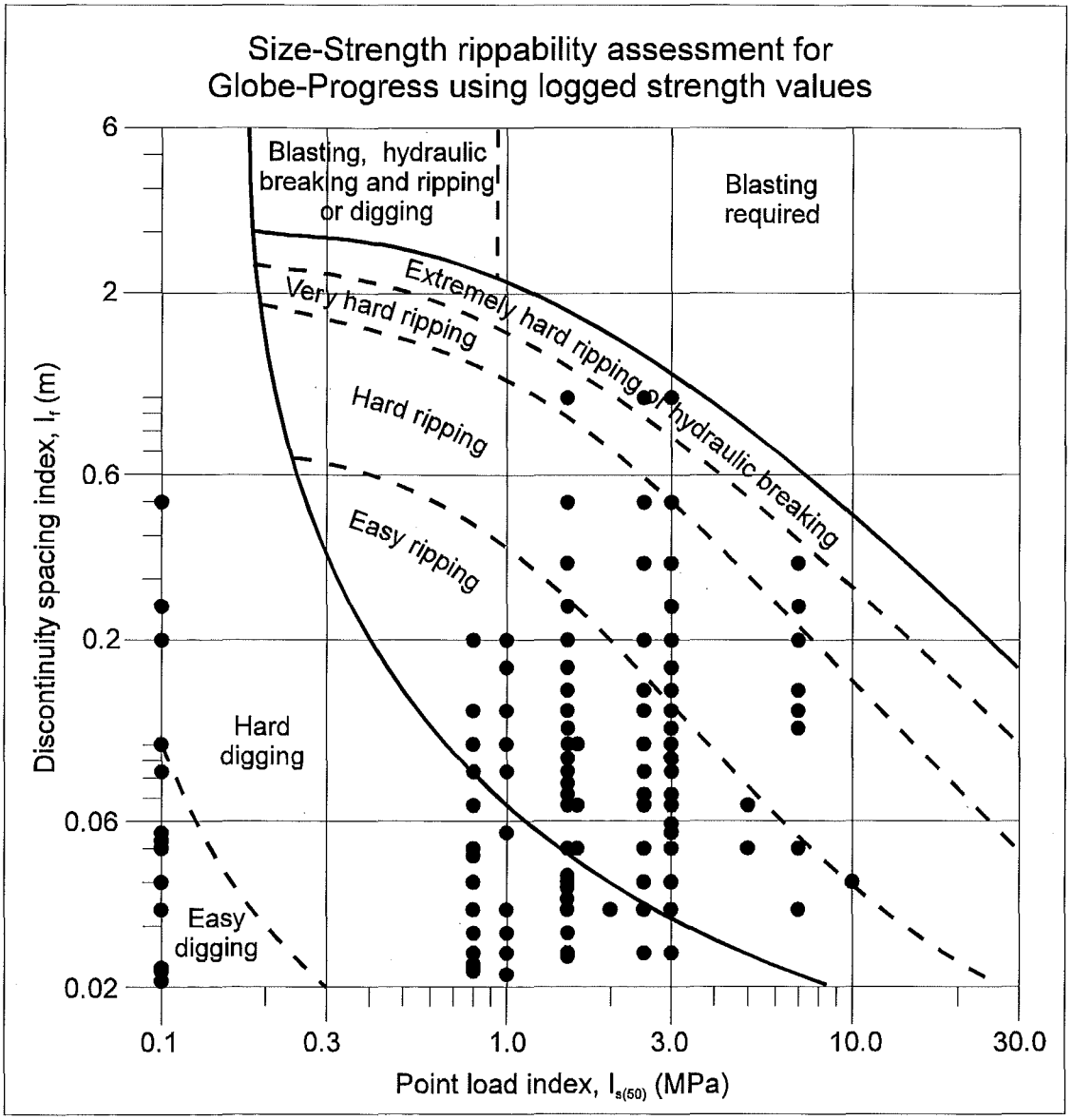

Figure 5.5: Size-Strength rippability assessment for drillcore strength and discontinuity spacing data from every RMU. A total of 2643 data point are used, most of which duplicate themselves and others plot off the scales in the easy and hard digging zones.

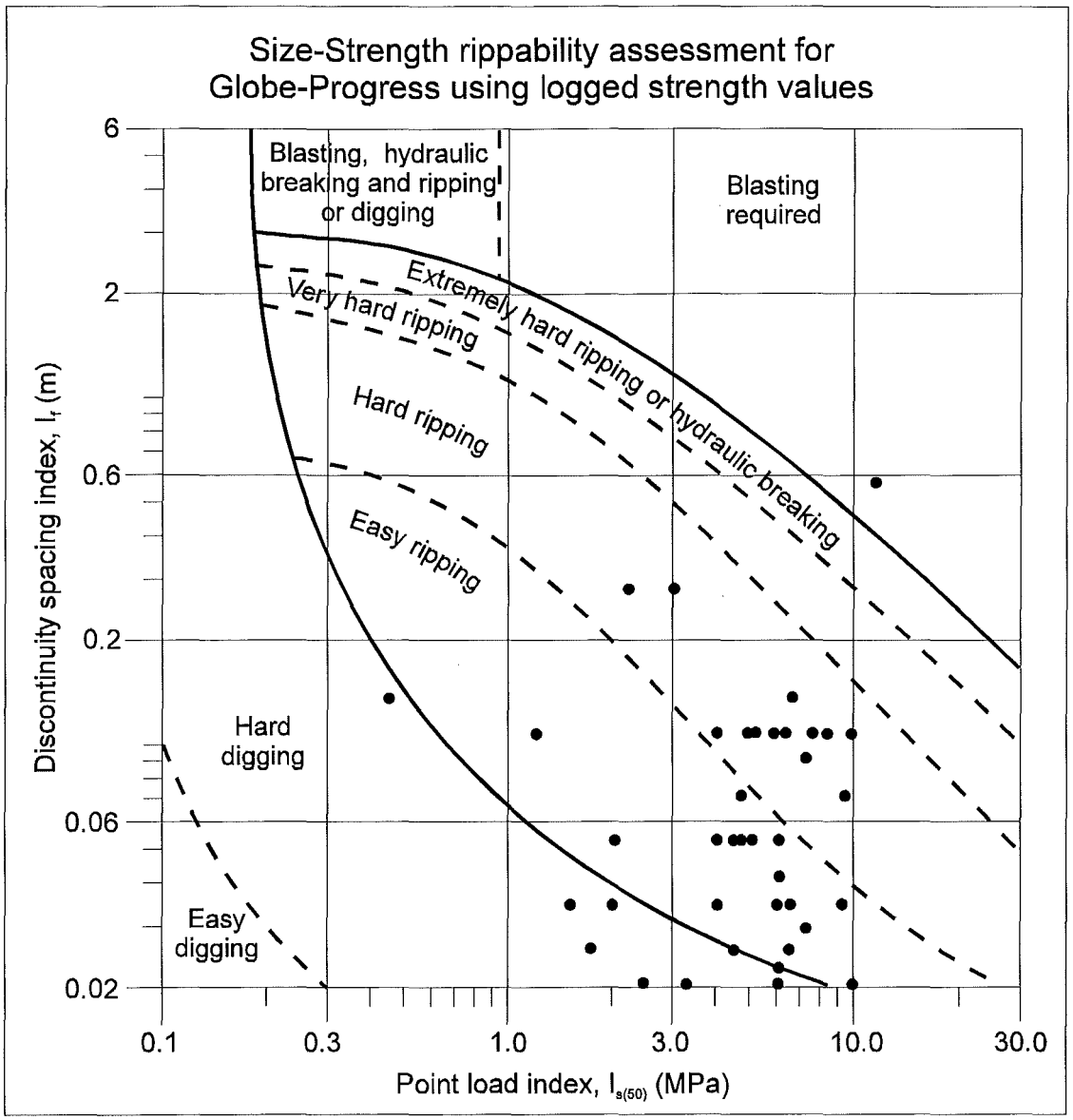

Figure 5.6: Size-Strength rippability assessment for point load strength data from Beetham and Coote (1994) and this study, and their corresponding discontinuity spacing values from drillcore logs. Some data plots off the scales, but not as much as in Figure 5.4 because samples point load tested have generally come from relatively strong core where discontinuity spacings are generally larger than those found in relatively weak or brecciated core.

also because the logged strength values have been under-estimated. Despite the bias toward sampling stronger specimens, Figure 5.6 should be used as the correct size-strength rippability prediction chart as the sampling bias creates a more conservative excavatability estimation, which is better than an over-estimation of the excavatability during a feasibility study, because an over-estimation of the excavatability of a site may lead to under-design during the project design stage.

5.3 RMR assessment

5.3.1 Introduction

The rock mass rating system was chosen to classify the rock mass because of its ease of use, standardisation with ISRM rock mass descriptions, and also because of its suitability to the characterisation of relatively shallow rock structures. It may also be calculated from Macraes drillcore data logs.

A database of 106 diamond drilled core exists for the rock mass at Globe-Progress, totalling in excess of 17 000 metres of core. However, only 10 360 metres contained sufficient information to calculate its RMR. The other 6 640 metres of drill core is either logged as precollar, stopes, fill or lost core, or has not been logged in sufficient detail (for example, drillcore logged by CRAE).

5.3.2 Methodology

Calculation of the RMR follows Table 2.7 and 2.8 and Figures 2.3, 2.4 and 2.5. A complete discussion on generalisations and assumptions made for each parameter is included as Appendix E1 and a brief discussion on each variable is included below.

A comparison between logged strength values and point load test with UCS tested samples shows that strength has been logged incorrectly (see Section 4.5). Some of the sandstone strengths have been over-estimated, but the majority have been under-estimated. Therefore a revised strength estimate was used for each logged RMU, and this was devised from the logged lithology and strength for each RMU. The assumptions made in determining the revised strength are included in Appendix E1.1.

RQD for the drillcore has twice been calculated. A comparison between the two is included in Section 4.5 and shows the spread of data between the two to be virtually identical, therefore it is assumed that the RQD has been correctly calculated and no adjustments were required for this variable.

The Discontinuity Spacing Index follows a clustered distribution pattern. It was also thought that it may have been under-estimated (see Section 4.6), but because the discontinuity spacing parameter follows a logarithmic scale, any error is minimised, and therefore no adjustment or correction was applied to this data set.

The condition of discontinuities parameter is only determined for the main discontinuity in each RMU. As all the parameters used to calculate the discontinuity condition parameter are easily determined, it is assumed that they have been logged correctly and no corrections or adjustments have been made.

The groundwater variable is the only variable that could not be determined from the drillcore data and no information could be found on the in situ groundwater condition, but, as most of the drillcore is below the water table, it is likely that the rock mass will be saturated. However, during mining the open pit is expected to be drained such that the pit should be completely dry, although this may be a problem at Globe-Progress where rainfall is high (see Table 1.1), and therefore the rock mass in the open pit is expected to be damp (J Taylor *pers com*). Three groundwater scenarios (dry, damp and saturated) have been determined for the RMR, thus calculating three possible values of RMR.

The RMR includes a discontinuity orientation correction factor that adjusts the basic RMR depending on the application of the RMR; for example, if the RMR is to be determined for slope stability, then different corrections are applied than if the RMR was applied to a tunnel or other underground excavation (see Table 2.7C). For both of these applications, a discontinuity orientation favourable to the stability of the excavation will be unfavourable to its excavatability. For this reason, the inverse of Bieniawski's (1979) discontinuity orientation descriptions were used; that is, if a discontinuity is favourable for a stability analysis, then it will be unfavourable for excavatability. Rattenbury (1994) found the most persistent discontinuity to be bedding and therefore the orientation of bedding surfaces is used for this parameter. To correctly calculate the orientation of bedding surfaces from drillcore, the drillcore needs to be orientated, which it is not at Globe-Progress. Rattenbury (1994) reorientated some core samples to obtain discontinuity orientations at depth. He found that bedding planes appeared to be consistent with depth, therefore surface bedding orientations could be used as an approximation of the discontinuity orientation at depth.

This thesis is concerned with assessing the rippability or excavatability of the open pit, and therefore discontinuity orientation corrections are adjusted according to the favourability or unfavourability of a discontinuity to excavatability rather than stability. If, in the future, the RMR is required for a stability application, then only a simple reversal of the ratings is required, for example, a favourable discontinuity in an excavatability application has a rating of ¯10, which can easily be adjusted to unfavourable, with a rating of ¯2, for a stability application.

5.3.3 Results

The RMR for every logged RMU is shown in Tables 5.2 to 5.12 (ten drillholes per table; included in map and table box), along with essential data from drillcore logs. Strength, RQD, discontinuity spacing, discontinuity condition and discontinuity orientation have been plotted in Figures 5.7 to 5.11 using data ranges used in the RMR System to show the distribution of data for each parameter. As the data set is very large, the frequency distribution for each parameter should be indicative of the rock mass within the open pit,

for example, 80% of the discontinuities are rated favourable or very favourable to excavating, therefore 80% of the discontinuities in the open pit area should be favourable or very favourable to excavating. Frequency distribution plots of the three RMR scenarios are shown in Figure 5.12 and contoured plans of the RMR assuming damp groundwater conditions is given in Figures 5.13-5.22 (in map and table box).

5.3.4 Discussion

The strength distribution (Figure 5.7b) is trimodal, where the weakest strengths represent brecciated or shear zone rock mass and the highest strength are represented by very well indurated sandstone. The intermediate mode represents strength estimates of siltstone and mudstone and interbedded sandstone-siltstone sequences. The revised strength data were based on point load strength (converted to UCS) and UCS, and on lithological drillcore data. The distribution of quantitatively determined strength is given in Figure 5.7a, and the discrepancy between the distribution patterns of the revised strength estimate and actual strength data is explained by the fact that strength tests were biased toward testing strong samples rather than weak samples (although limited testing was done on weak samples), because the weaker rock is mainly breccia or clay pug, in which strength values cannot readily be quantified.

Figure 5.8 and 5.9 plot the distribution of RQD and discontinuity spacing classes used in the RMR System and show that most of the drillcore quality is weak, with a cluster of very closely spaced discontinuities. This may be an effect of the drilling, whereby holes were targeted to intersect the shear zone, therefore intersecting relatively more sheared rock.

Figure 5.10 shows the distribution of the condition of discontinuities parameter from the RMR System. The maximum rating possible is 30 for unweathered, very rough discontinuities with no separation, infilling or continuity, and the minimum rating possible is 0 for extremely weathered, slickensided or polished discontinuities with separation and infilling greater than 5 mm and continuity of greater than 20 m (see Table 2.7b). The spread of discontinuity condition ratings found from drillcore is 5 to 30, with a mean of 19, which indicates most of the discontinuities are of moderate quality.

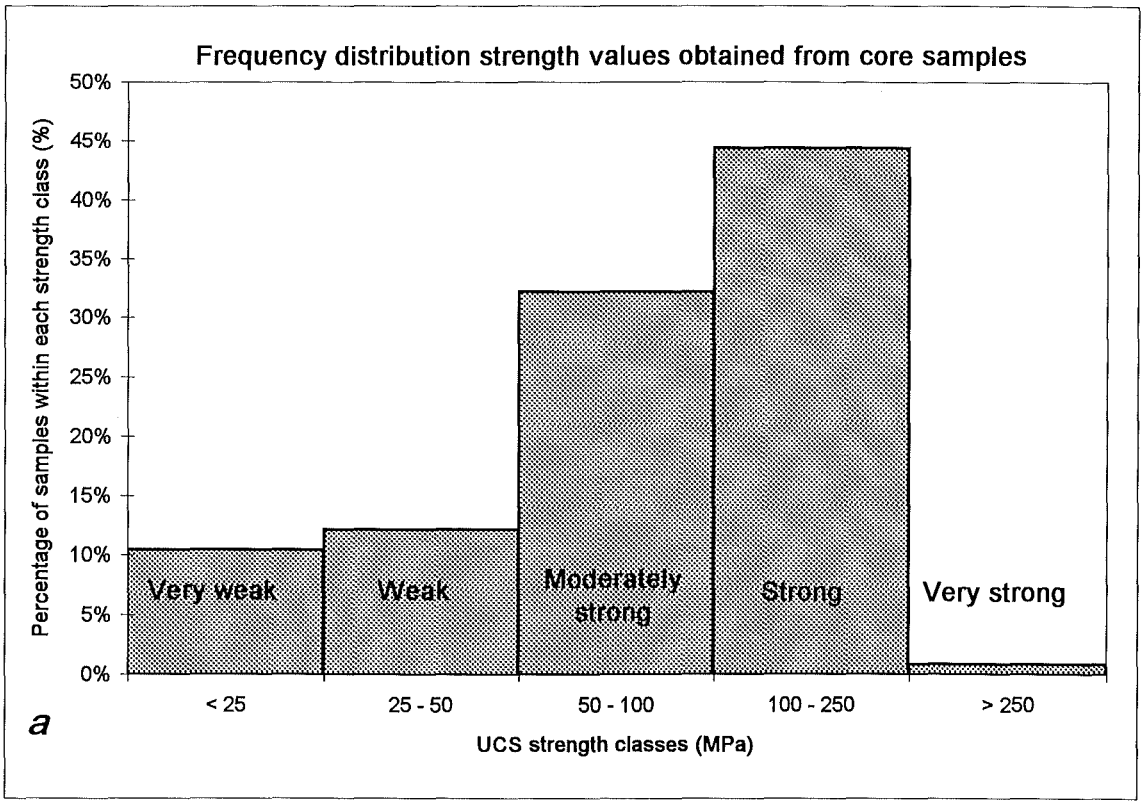

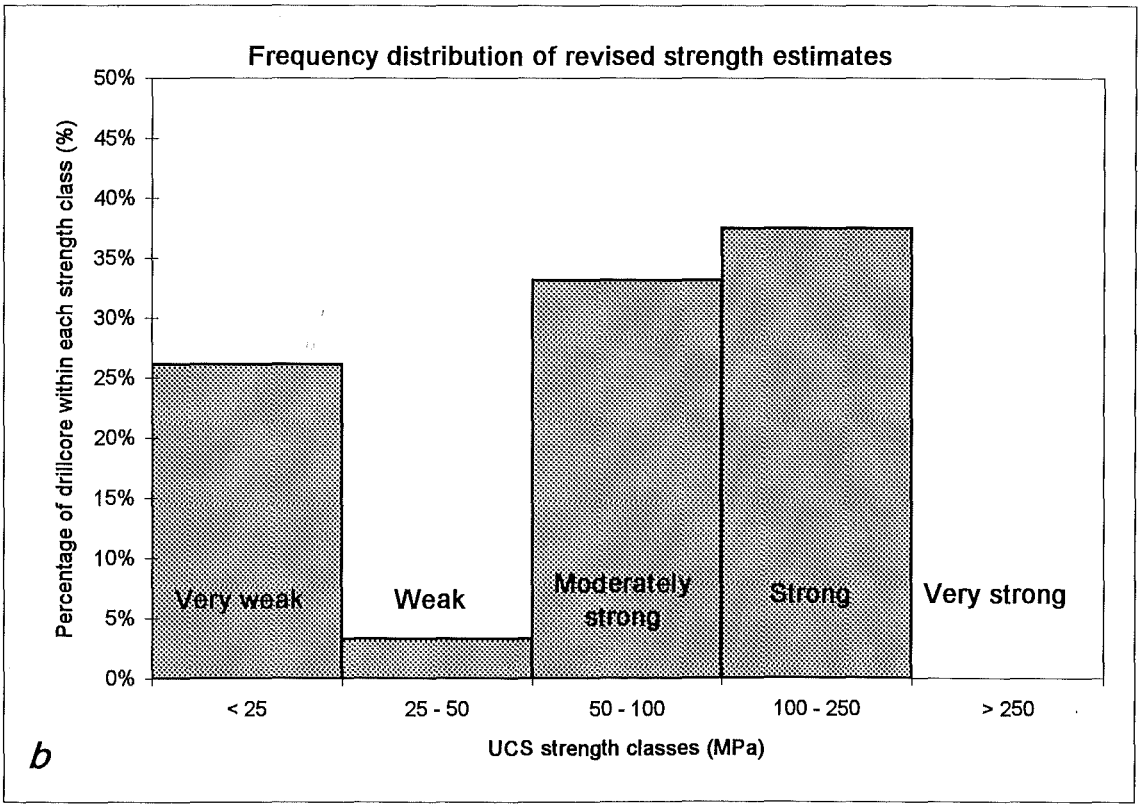

Figure 5.7: Frequency distribution of strength values from: (*a*) point load test (expressed as UCS values) and UCS test and (*b*) revised drill log strength estimates. Data are grouped into the strength classes suggested by Bienawski (1979) for use in the RMR System. Data in (*a*) reinterpreted from Beetham and Coote (1994; 72 point load samples), and from this work (24 point load samples, 19 UCS samples) and 10360m of drillcore was used determining (*b*).

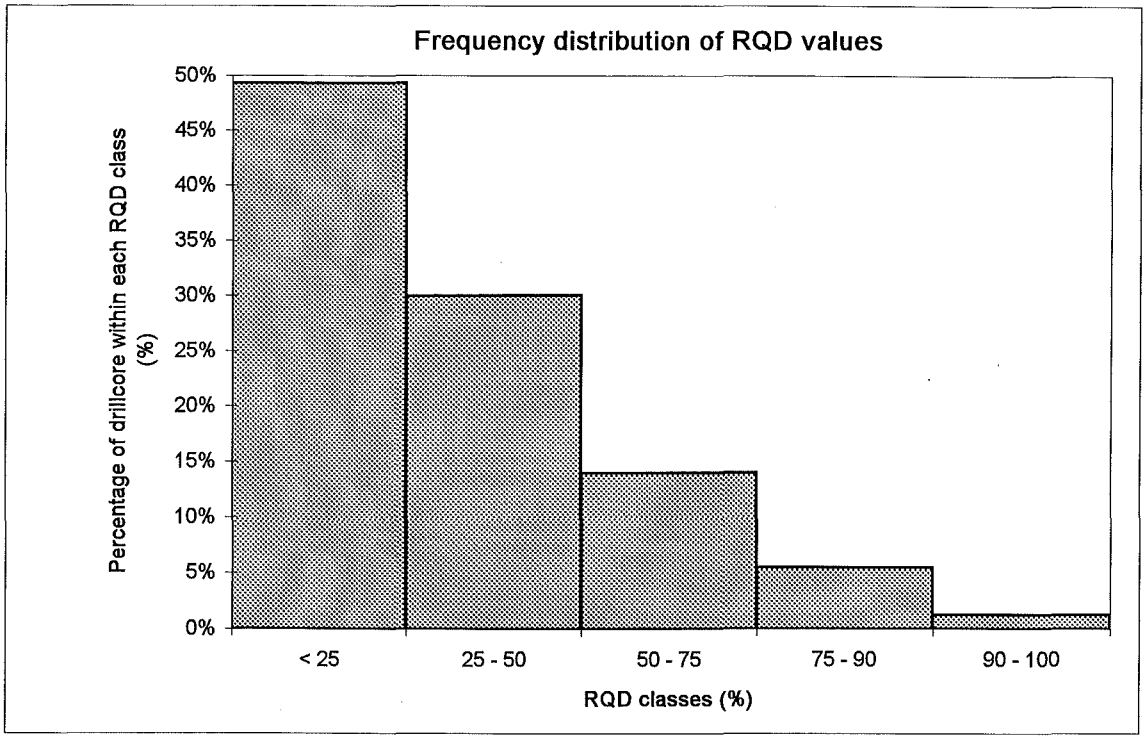

Figure 5.8: Frequency distribution of RQD values from drillcore logs grouped into classes suggested by Bienawski (1979). The total length of drillcore from which drillcore data was obtained equals 10360 m.

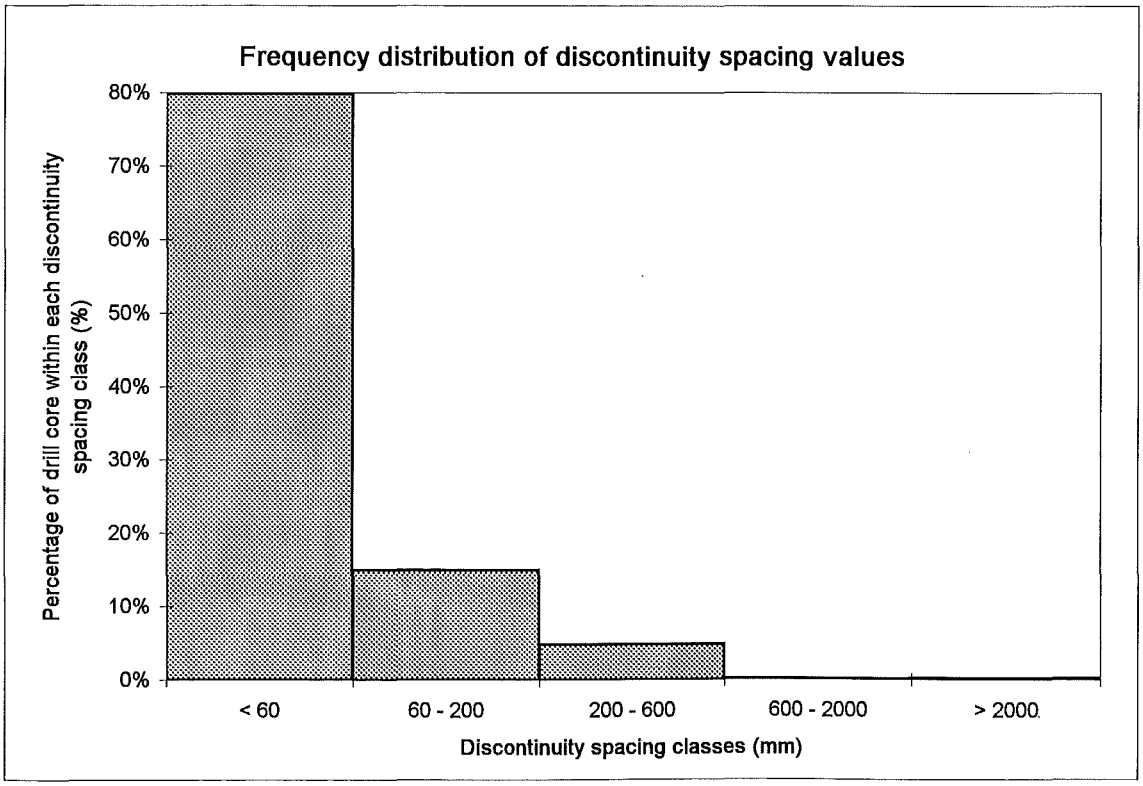

Figure 5.9: Frequency distribution of discontinuity spacing values from the fractures per metre count in drillcore logs, grouped into classes suggested by Bienawski (1979). The total length of drillcore from which data was obtained is 10360m.

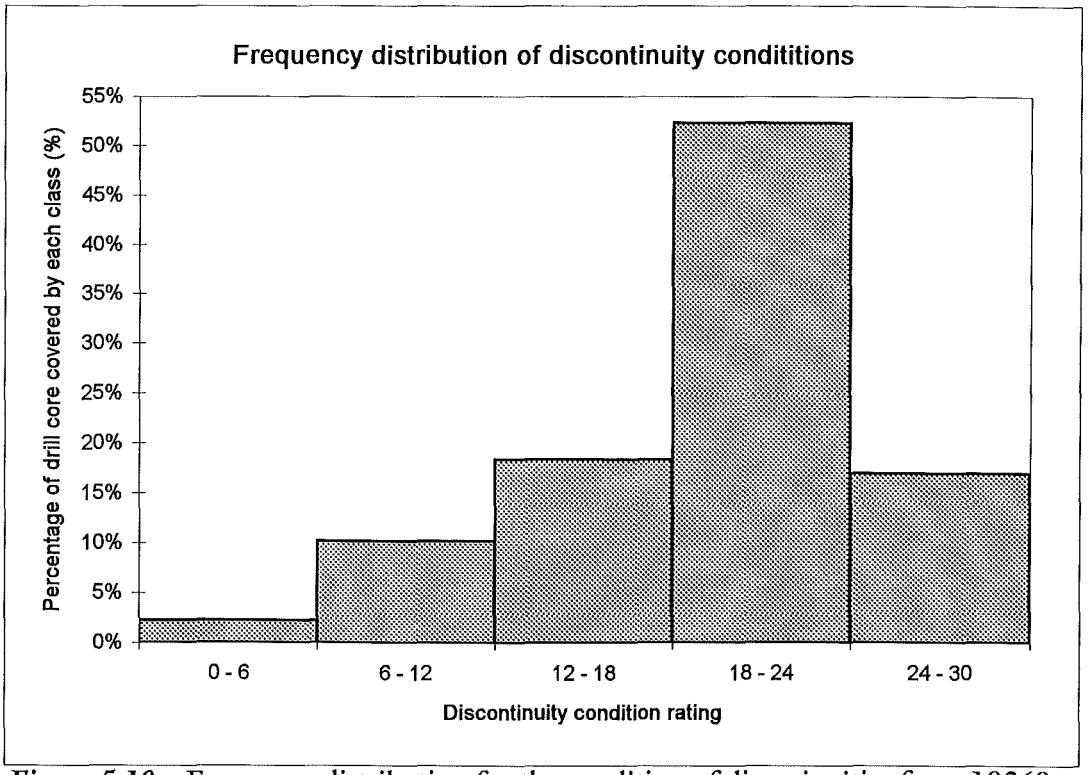

Figure 5.10: Frequency distribution for the condition of disontinuities from 10360m of drillcore data. Data is groups into the ratings suggested by Bienawski (1979) for descibing discontinuity conditions.

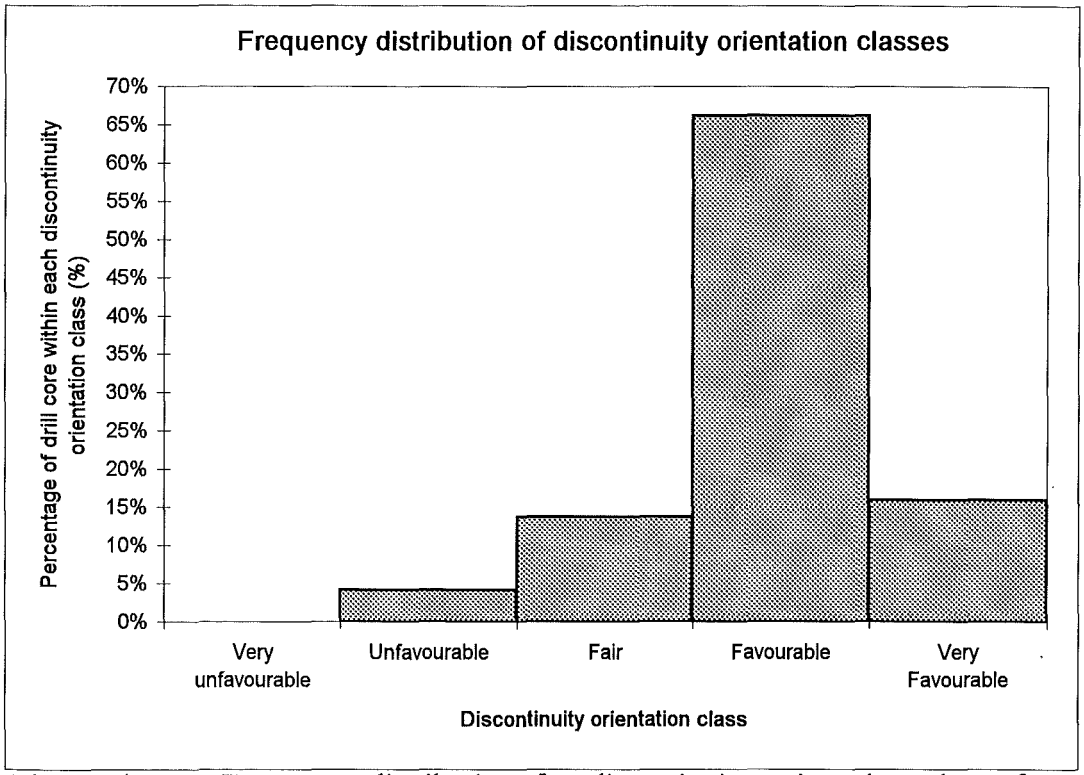

Figure 5.11: Frequency distribution for discontinuity orientation classes from 10360m of drillcore data. The classes suggested for excavating are from Minty and Kearns (1983).

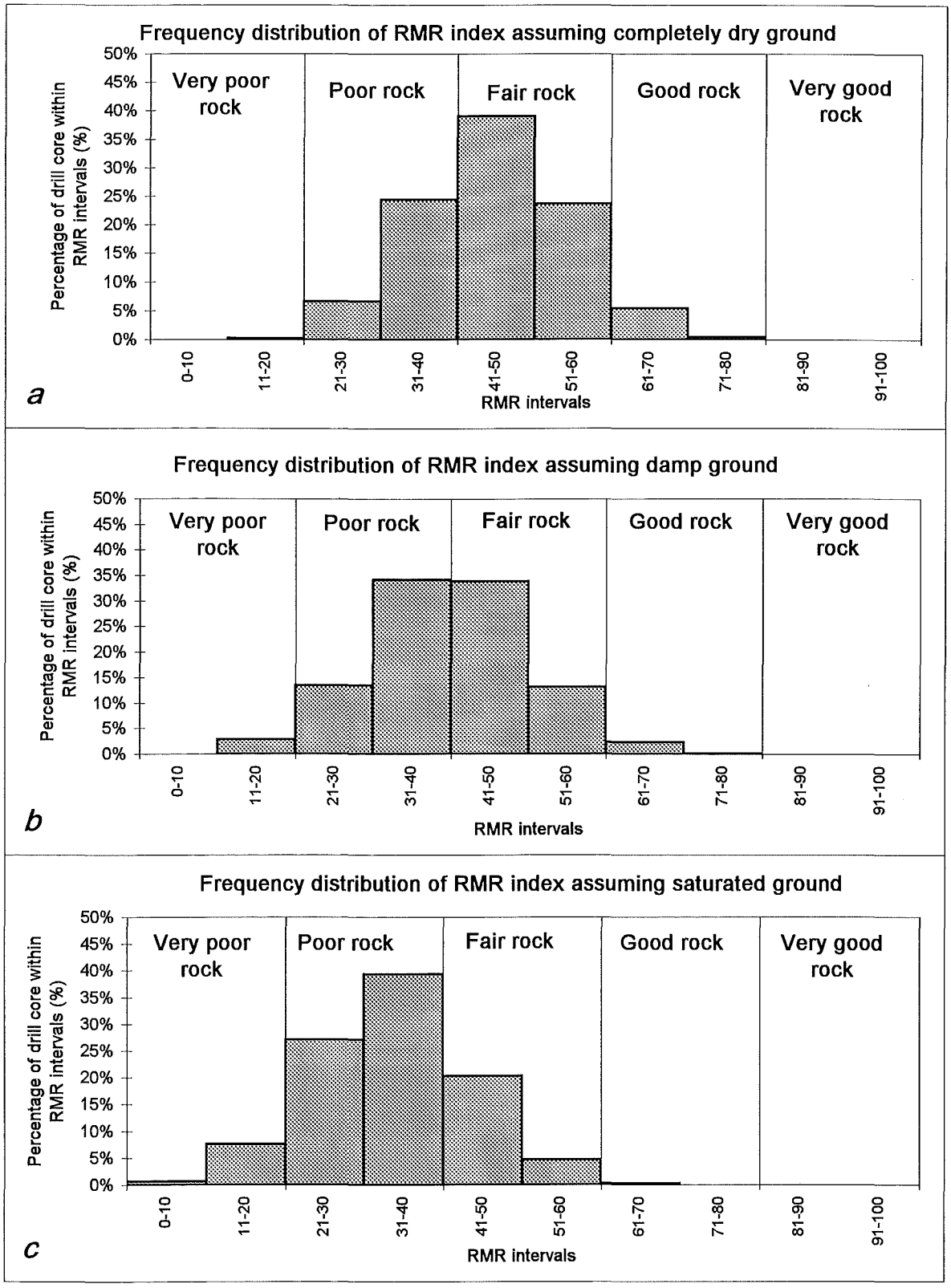

Figure 5.12: Frequency distribution of the Rock Mass Rating Index for three groundwater scenarios. The distribution has been weighted for the length covered in a drillhole, such that the RMR intervals represent the percentage of the open pit.

The frequency distribution plot of discontinuity orientation (Figure 5.11), where the discontinuity orientation is the orientation of bedding surfaces, shows that greater than 80% of the bedding surfaces are favourable or very favourable for excavation in a east to west direction.

Figure 5.12 shows the calculated RMR assuming the open pit will be dry, damp and saturated. The RMR Index is greater for a dry pit (mean = 45 with a range between 18 and 89) and the mean and data ranges decrease with increasing water content (the damp RMR Index mean = 40 with a range between 13 and 84; and the saturated RMR Index mean = 34 with a range between 7 and 78). Most of the rock mass in the three scenarios is either poor or fair (RMR index between 20 and 60) and very little very good rock (RMR Index greater than 80) exists.

Figures 5.13 to 5.22 show contoured plans of the damp RMR (groundwater scenario most likely to occur in the pit) values at 20 m bench heights through the pit. These plans have been produced using Medsystem, a mine modelling computer package, and modelled using a weighted inverse distance^3 modelling technique (see Appendix E5) using a block dimension of 5 m × 5 m. Only rock mass data within the pit boundary are plotted and data is further constrained by using a two domain pit model, where any RMR value intersecting the Globe-Progress Shear Zone domain is only extrapolated within that domain and any RMR value intersecting the overburden domain will only be extrapolated within that domain. This effectively constrains data such that weak rock will not be predicted outside of the shear zone domain and good quality rock in the overburden domain will not be extrapolated into the shear zone domain. The maximum distance data is extrapolated is 80 m where drillhole data are sparse but most drillholes are less than 50 m apart (see Figure 4.1), therefore giving a relatively accurate model.

The plans show two zones of poor to very poor rock, one following the Globe-Progress Shear Zone (see Figure 4.1 for location of the shear zone in relation to the pit outline) curving around the northern and eastern pit walls, while the other zone is along the western wall of the open pit (see Figures 5.15 to 5.17 through the centre of the pit). The majority of overburden is classed as fair to poor rock, but there are areas of good rock (see Figures 5.15 to 5.17). No very good rock is estimated in the bench plans, although there

may be small areas between the bench levels. The plans also show relatively poor rock in the fold axis of the Globe-Progress Shear Zone (see Figures 5.14, 5.17, 5.19 and 5.20), which should be expected as fold axes are often zones of greater deformation. The same trends are shown on plans of overburden leachability, where high sulphide zones (more likely to leach) are located in the fold axis of the Globe-Progress Shear Zone, along the western wall and the shear zone itself (J Taylor, *pers com*) and inert zones (not expected to leach) are located where there are zones of good rock. There does not appear to be any significant decrease in rock mass quality associated with the weathered rock mass near pit surface (compare Figures 5.13 and 5.14, near the pit surface, with Figures 5.20 and Figure 5.19, near the pit base), which was proven for rock material in Chapter 4.

5.4 Final rippability evaluation

5.4.1 Introduction

The final rippability evaluation involved determining the rippability of the proposed open pit area using a suite of geological and geotechnical parameters. Two rippability prediction methods were chosen, one method was based on the RMR System, classifying the rock mass, and the other method attempts to predict the productivity of a chosen bulldozer. The first method used was the Weaver Rippability Prediction Method (Weaver, 1975). This is an outdated system based on the first RMR system by Bieniawski (1973), so was modified to follow the current RMR system of Bieniawski (1989). The second method used was devised by MacGregor *et al* (1994). It is a statistical based method that finds the best correlation between various geological and geotechnical parameters and the productivity of a chosen bulldozer.

5.4.2 Weaver's Rippability Method (1975)

5.4.2.1 Introduction

This method is based on Bieniawski's 1973 RMR System, therefore it is outdated as the RMR System has been modified three times (see Bieniawski, 1976, 1979, 1989). The system also predicts the size of ripping bulldozer suitable, but the largest bulldozer in 1975 was Caterpillar's D9 (about 42 tonnes, compared to the largest bulldozer today, Komatsu's D575A-2 at 134 tonnes), therefore Weaver's 1975 method is expected to be very conservative.

5.4.2.2 Methodology

Calculation of Weaver's Rippability Rating Method follows Tables 3.2 and 2.8. Assumptions and generalisations made for each parameter are outlined in Appendix E2 and a short discussion follows below. Weaver's Rippability Rating System is based on Bieniawski's 1973 RMR System, substituting groundwater and RQD for the seismic velocity of the rock mass, therefore, the same assumptions made for the RMR are made for this rating system, although the class intervals and ratings are slightly different.

Seismic velocities were determined on the surface, where the rock mass has undergone weathering and joint relaxation. For this reason it was decided not to attempt correlating seismic velocities with drillcore data, instead, the mean seismic velocity (2100 ms^{-1}) was used as an estimate of the seismic velocity of the rock mass, although the seismic velocity may be higher at depth where the rock mass is unweathered and joints less open.

5.4.2.3 Results

Weaver's Rippability Rating for every RMU is included on Tables 5.2 to 5.12 along with the essential data from the drillcore logs. Frequency distribution graphs of the rock material hardness, and discontinuity spacing (using different classes to those in the RMR System) are given as Figures 5.23 and 5.24. Weathering was not plotted up as most of the rock mass is unweathered. The discontinuity orientation frequency distribution is the same as in Figure 5.10. The frequency distribution of the rippability classes are shown in

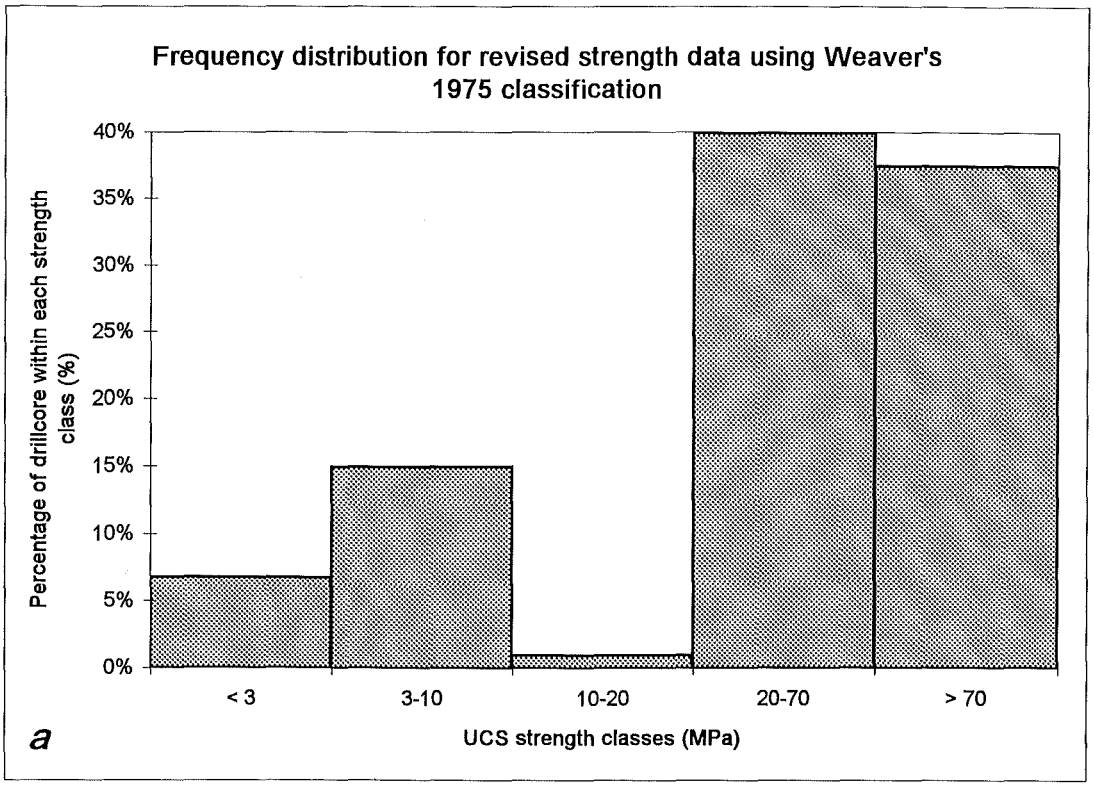

Figure 5.23: Frequency distribution of revised strength data using strength classes suggested by Weaver (1975) for use in his rippability classification system.

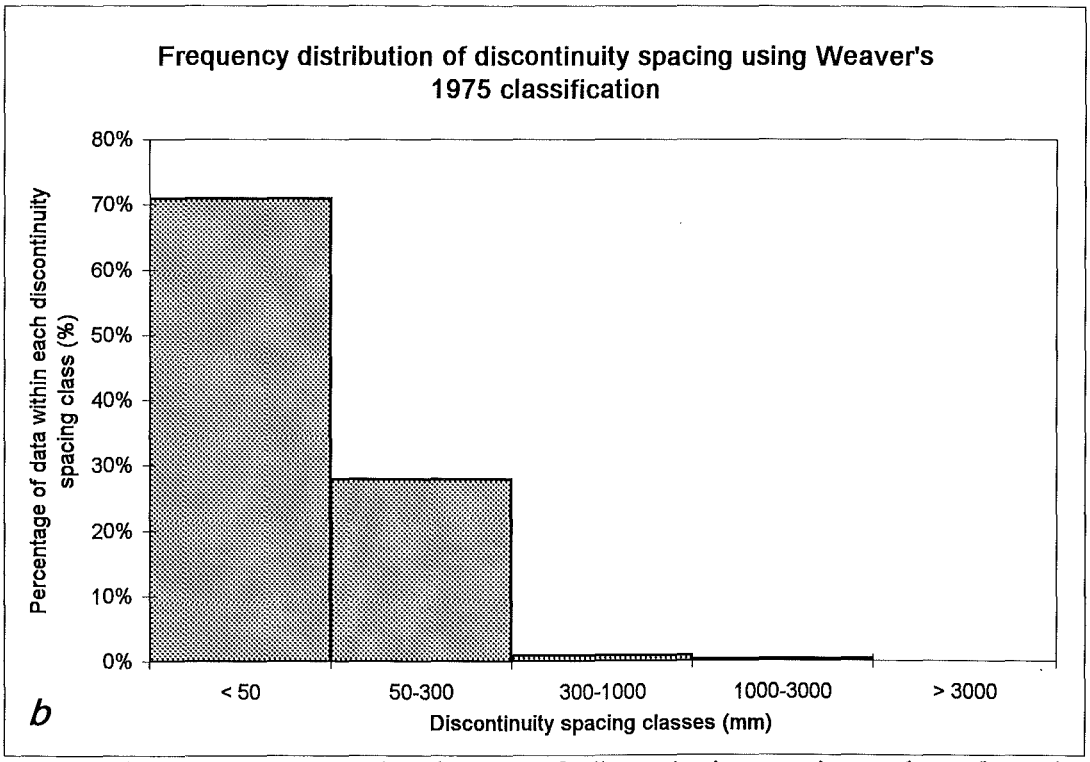

Figure 5.24: Frequency distribution of discontinuity spacing values from the fractures per metre count in drillcore logs, grouped into classes suggested by Weaver (1975) for use in his rippability classification system.

Figure 5.25. Weaver's Rippability Rating Index ranges between 38 and 87 and has a mean of 57. No plans have been plotted showing the distribution of rippability classes because of the outdated and conservative nature of the method, instead rippability plans using the Modified Weaver Rippability Rating Method are plotted (see Section 5.4.3). however this method provides a useful comparison with the other methods used (Section 5.5).

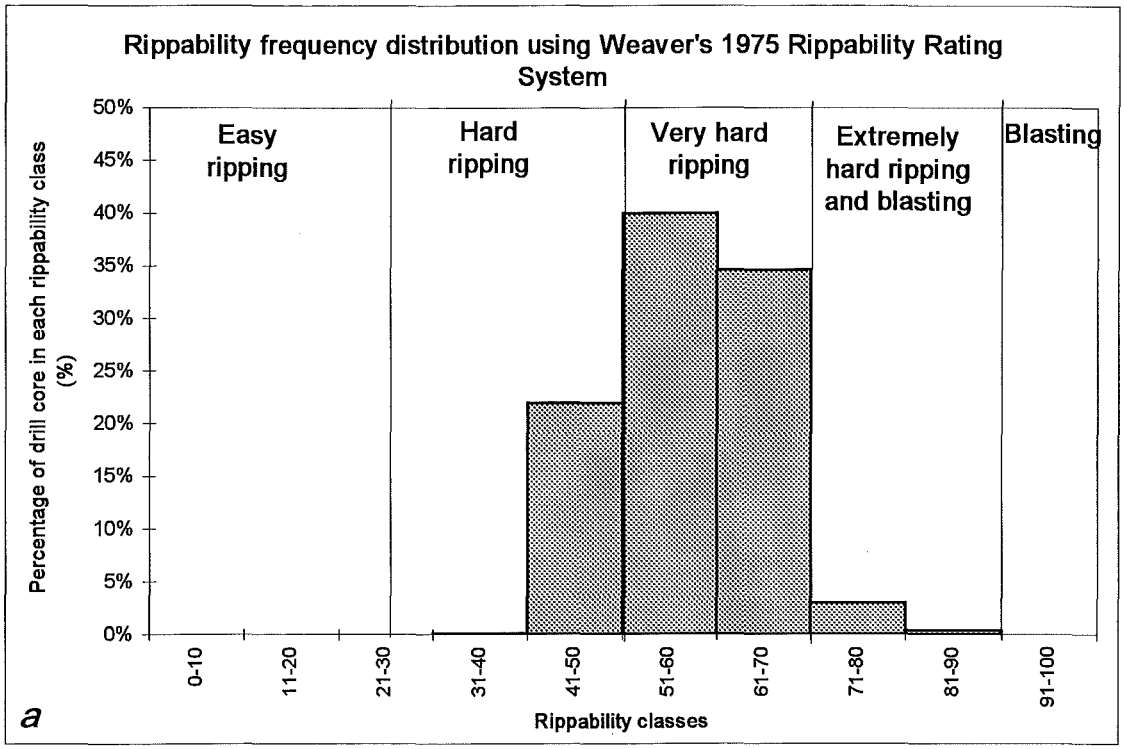

Figure 5.25: Frequency distribution for Weaver's 1975 Rippability Rating.

5.4.2.4 Discussion

Figure 5.25 shows that most of the pit is expected to be hard to very hard ripping, with some areas of extremely hard ripping (fair to very good rock quality), which is more or less one class of rock quality better than predicted by the RMR System in Section 5.3, and therefore, this system is conservative as it over-estimates the rock mass quality and its excavatability by predicting blasting as the most suitable excavation technique where in fact ripping with a large bulldozer should be possible.

5.4.3 The Modified Weaver Rippability Rating

5.4.3.1 Introduction

Weaver's 1975 method has been updated in Table 3.3 to follow Bieniawski's 1989 RMR System. This updates the rippability system so that parameters and their ranges now follow ISRM terminology. The seismic velocity ranges have also increased to account for the increase in bulldozer sizes and capabilities, but the ranges are lower than those used by Komatsu and Caterpillar as their seismic velocities ranges are considered to over-estimate the rippability of a rock mass (Braybrooke, 1988; MacGregor *et al*, 1994).

5.4.3.2 Methodology

Calculation of the Modified Weaver Rippability Ratings follow Tables 3.3 and 2.8 and Figures 2.3, 2.4 and 2.5. The generalisations and assumptions used to calculate this rating are the same as for the RMR, except that there is no groundwater or RQD variable, both of which have been replaced with the average seismic velocity of the pit area (2100 ms^{-1}).

5.4.3.2 Results

The Modified Weaver Rippability Rating for each RMU is shown in Tables 5.2-5.12 (in map and table box). The frequency distribution for each parameter (except for seismic velocity), is the same as for the RMR (Figures 5.7 to 5.11) and the frequency distribution for the rippability ratings are shown as Figure 5.26. The Modified Rippability Rating Index ranges between 27 and 81, with a mean of 50. The rippability ratings have also been plotted on Figures 5.27 to 5.36 (in map and table box) using the same modelling technique used to plot the RMR distribution (Section 5.3).

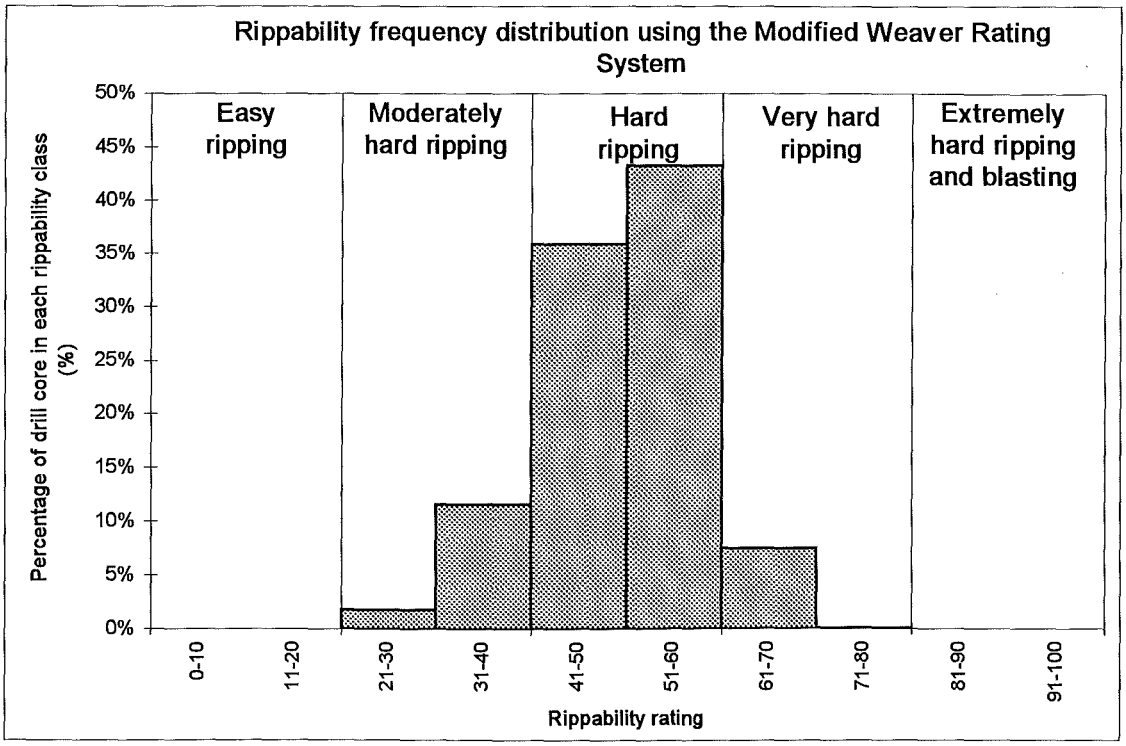

Figure 5.26: Frequency distribution ratings using the Modified Weaver Rippability Rating System.

5.4.3.4 Discussion

The distribution of the rippability index (Figure 5.26) shows that almost 80% of the pit is expected to be hard to rip, moderately hard ripping is expected in almost 15% of the pit and 5% is expected to be very hard to rip. The distribution also shows that none of the pit is expected to be easy to rip and almost none of the pit is expected to require blasting. The distribution pattern formed is a result of the seismic velocity parameter being averaged for the whole pit area, therefore giving a minimum possible rating of 24 for the whole pit (without correcting for the discontinuity orientation). As stated earlier, the seismic velocity parameter replaces RQD and groundwater condition used in the RMR System, and, therefore, areas where RQD = 0 (very poor rock mass quality) are assigned a rating of 24, thus over-estimating the rock mass quality. The averaged seismic velocity was used because it is not realistically possible to extrapolate seismic velocities determined on the surface with a rock mass at depth, and therefore, this method should not be used unless ripping very shallow excavations, such as road cuts or realignments, or unless there is downhole seismic refraction or reflection data available.

The rippability plans (Figures 5.27 to 5.36; in map and table box) show that most of the pit is expected to be hard to rip. The plans do not delineate the shear zone along the northern and eastern pit walls, or the Chemist Shop Fault along the western pit wall. Therefore these plans should not be relied upon for any planning.

5.4.4 Prediction of Productivity.

5.4.4.1 Introduction

MacGregor *et al's* (1994) method of predicting the productivity of a selected bulldozer was used on drillcore data. The method does not rate the rock mass like the RMR System or Weaver's Rippability Rating System, rather it selects parameters that influence the excavatability of a rock mass the most, and predicts the productivity from a correlation formula between the expected productivity and the influencing parameters. As it does not rate the rock mass on a set scale (although some of the parameters are rated) and because it uses parameters easily determined during site investigations or from drillcore data, it may serve as a useful comparison with results from the RMR System.

MacGregor recommends using two equations to relate the productivity back to the rock mass. Equation 4 is based on 354 case studies of ripping in all rock types and Equation 8 is based on case studies of ripping only in sedimentary rock masses (the number of case studies is unknown).

5.4.4.2 Methodology

Calculation of the expected productivity uses the formulae in Table 3.8 and the description of each variable is given in Table 3.9 and Appendix B3. Generalisations and assumptions made are included in Appendix E4 and a brief description of each variable is included below.

The revised UCS estimate was used and the distribution of this is the same as in Figure 5.7c. The generalisations and assumptions made in estimating the revised strength are discussed in Appendix E1.1.

Ratings from Table 3.9 are assigned to the logged weathering parameter. Fresh or unweathered rock is assigned a rating of 1 and extremely weathered, a rating of 10. The weathering applies to rock material, not weathering on discontinuities surfaces. The distribution of weathering data was not plotted as most of the drillcore is unweathered. The grain size ratings follow those listed in Table 3.9. Boulders and cobbles are assigned a rating of 7 and silt and clay, a rating of 1. The grain size ratings were derived from drillcore log data.

The seismic velocity parameter uses the average seismic velocity of 2100 ms^{-1} for the pit area. This may over-estimate the velocity in shear zones where clay, pug and breccia are common and under-estimate the seismic velocity in massive overburden but the surface seismic refraction data cannot realistically be correlated down drillcore, where the rock mass structure may change significantly.

A roughness rating (Table 3.9) is applied to the logged roughness description. Smooth or polished discontinuity surfaces are assigned a rating of 1 and very rough discontinuity surfaces are assigned a rating of 4. The distribution is plotted in Figure 5.37.

It is assumed that there are three defect sets in the pit area. Bedding and cleavage are the two most common defect sets and the third set is comprised of clustered joints (see Appendix E4.6). The discontinuity spacing frequency distribution plot (Figure 4.28) and the theoretically derived RQD (Figure 4.29) suggest that there is a large clustering of small discontinuity spacing values, which represent brecciated rock masses, as well as a small random distribution of joints, therefore three defect sets have been assumed instead of two (bedding and cleavage).

The discontinuity spacing parameter is the inverse of the logged fractures per metres parameter and is measured in millimetres. The distribution is the same as that plotted in Figure 4.28.

The structure rating applies a rating to the overall structural appearance of a rock mass. It is based on bedding and joint spacing, where a rock mass with massively spaced beds and widely spaced discontinuities are assigned a rating of 1 and soils are assigned a rating of 19. The frequency distribution of the ratings is given in Figure 5.38.

Two equations may be used to predict the productivity in sedimentary rocks. The first equation (Equation 4, Table 3.8) is based on ripping case studies from all rock types and the other equation (Equation 8, Table 3.8) is based on ripping data from sedimentary rocks only. Equation 4 uses UCS, weathering, grain size, seismic velocity, roughness, the number of discontinuity sets and the structure rating to provide a correlation with productivity, and Equation 8 uses UCS, seismic velocity, roughness and discontinuity spacing only. Equation 4 has a correlation coefficient, R^2, of 0.58 and Equation 8 has a correlation coefficient, R^2, of 0.52. Both coefficients are relatively low, but they are the best correlations possible from combinations of the 26 parameters listed in Appendix B3, and will provide relatively accurate estimates of the productivity (MacGregor *et al*, 1994).

5.4.4.3 Results

The productivity estimates using Equation 4 and Equation 8 and the mass of Komatsu's D475A-2 and D575A-2 and Caterpillar's D10 bulldozer for every logged RMU are listed in Tables 5.2 to 5.12 (in map and table box) and the frequency distribution of the estimated productivity for each bulldozer size using both equations are plotted in Figure 5.39 and 5.40. The estimated productivity for the D575A-2 using Equation 8 and productivity classes suggested by MacGregor *et al* (1994), are plotted as bench level plans, and which are given as Figures 5.41 to 5.50 (in map and table box). Equation 8 is recommended by MacGregor *et al* (1994) for use in sedimentary rocks and the D575A-2 bulldozer was recommended by John (1994). A summary of the estimated productivity using Equations 4 and 8 and the D10, D475A-2 and D575A-2 bulldozers is given in Table 5.13.

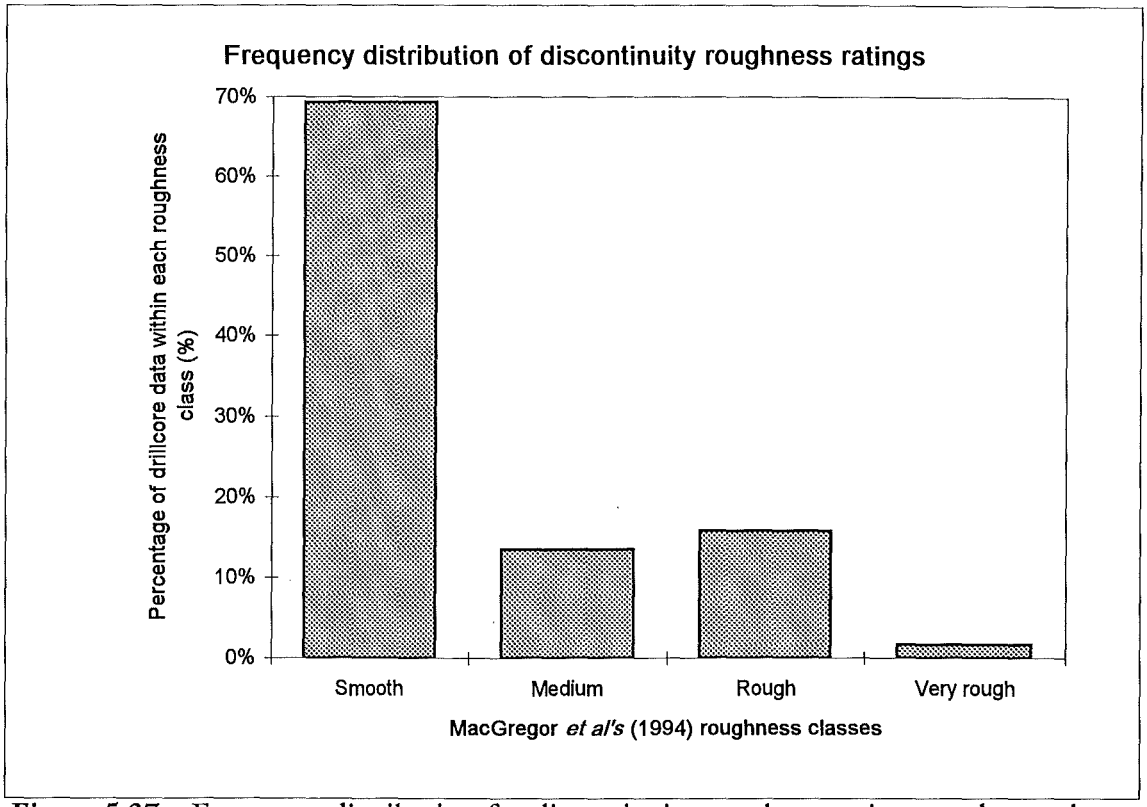

Figure 5.37: Frequency distribution for discontinuity roughness using roughness classes described by MacGregor *et al* (1994).

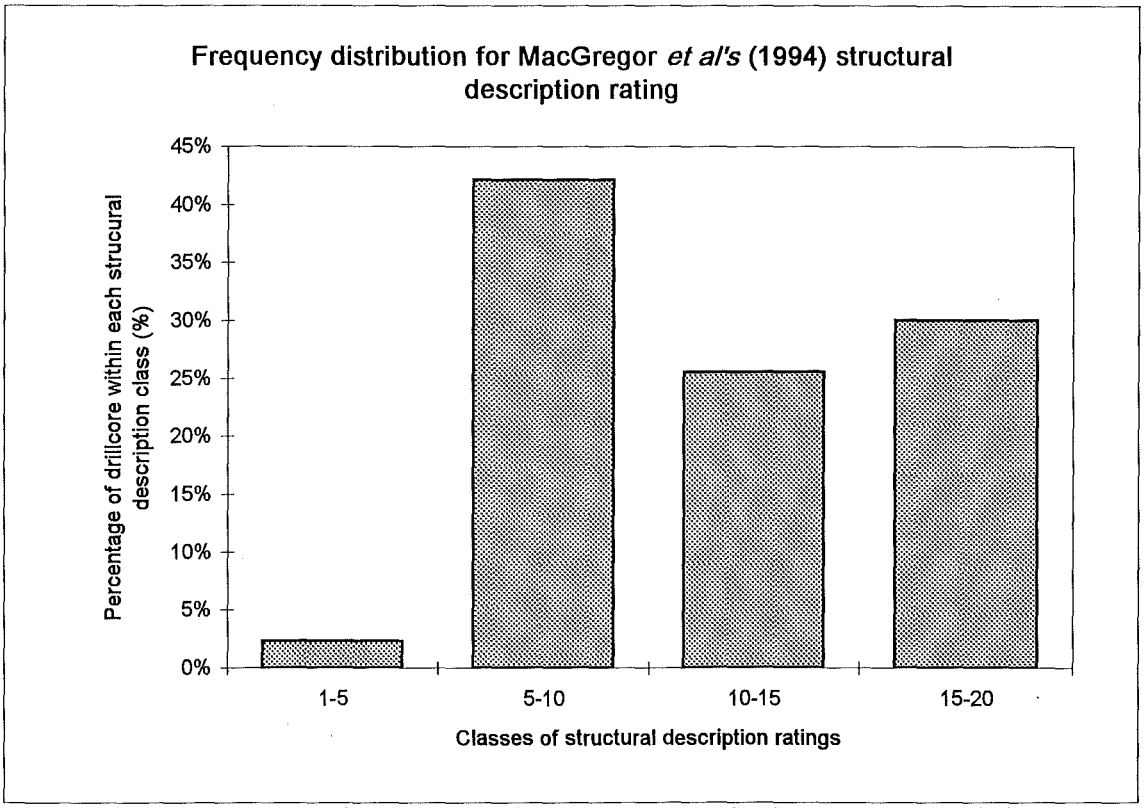

Figure 5.38: Frequency distribution of MacGregor *et al's* (1994) structural description ratings grouped into classes of 5 rating values each.

Table 5.13: Summary of estimated productivity for D10, D475A-2 and D575A-2 bulldozers.

Bulldozer model	Productivity (m^3/hr) Mean	Range	Expected ripping conditions
Equation 4			
D10	1050	0 - 4800	• 46% difficult and very difficult ripping • 52% easy and medium ripping
D475A-2	1500	0 - 6900	• 39% difficult and very difficult ripping • 62% very easy to medium ripping
D575A-2	3000	0 - 13750	• 46% medium to very difficult ripping • 54% Easy and very easy ripping
Equation 8			
D10	850	70 - 4150	• 74% difficult and very difficult ripping • 25% easy and medium ripping
D475A-2	1250	100 - 5600	• 63% difficult ripping • 30% very easy to medium ripping
D575A-2	2450	200 - 11900	• 72% moderate and difficult ripping • 26% very easy ripping

5.4.4.4 Discussion

The distribution of expected productivity values (Figures 5.39 and 5.40; Table 5.13) shows that the Equation 4 produces a wider range and a higher mean than Equation 8. This trend was also found by MacGregor *et al* (1994) who suggested that Equation 8 should be used to estimate bulldozer productivity and also to be compared with Equation 4 data. The wider range in Equation 4 data makes estimation of the rippability of the site harder to predict as the data ranges suggest two or more different sized bulldozers should be used whereas with Equation 8 data, most data fits into one or two productivity classes, therefore requiring only one sized bulldozer to excavate the overburden. For instance, using Equation 8 data, 74% of the open pit is expected to be difficult to very difficult to rip using a D10, 63% is expected to be difficult to rip with a D475A-2 and 72 % is expected to be medium to difficult to rip with a D575A-2 bulldozer.

As the D575A-2 provides the most productive ripping capabilities, bench level plans plotting the estimated productivity have been produced as Figures 5.41 to 5.50 (in map and table box). These plans have been modelled using inverse distance[3] modelling (see

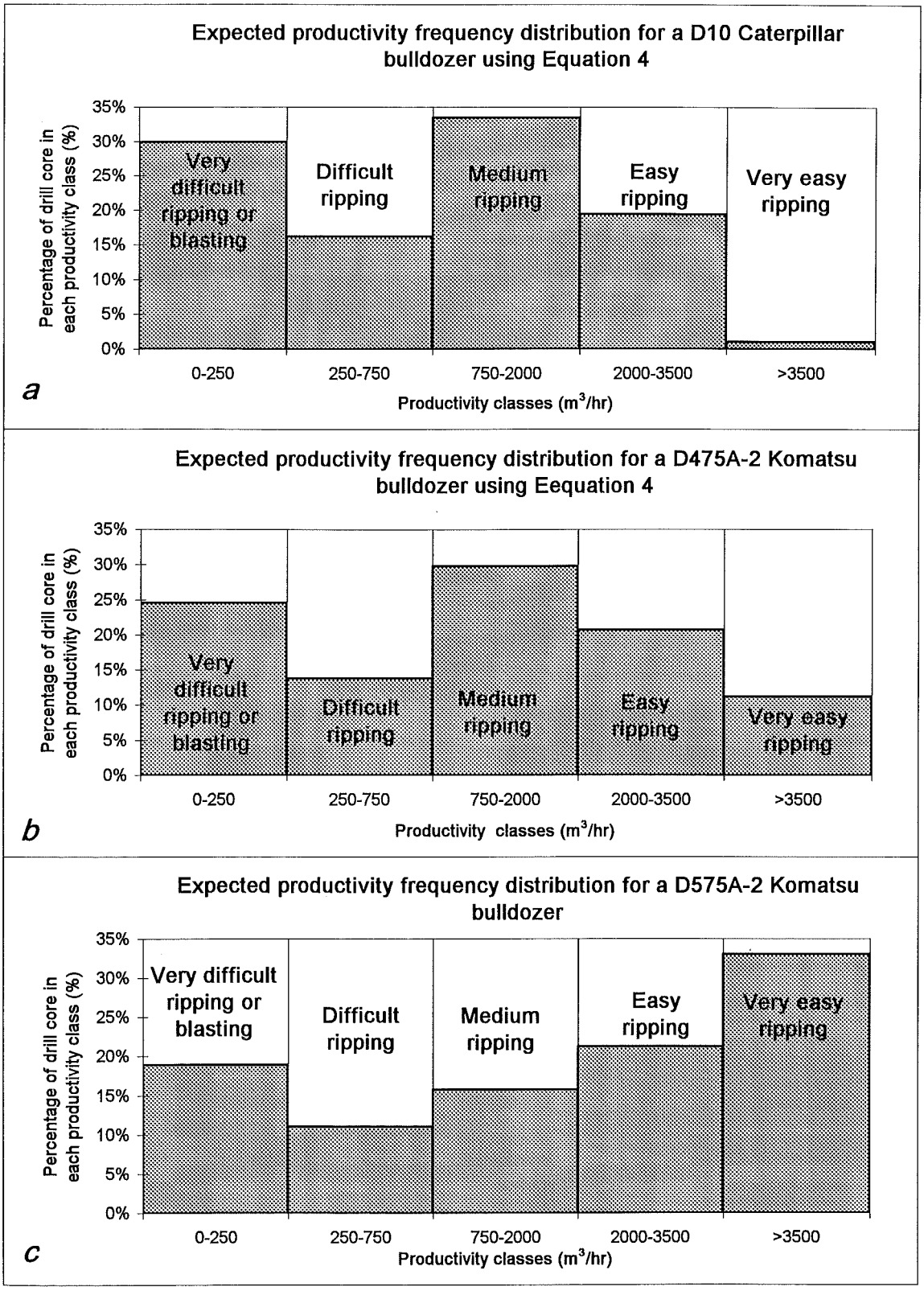

Figure 5.39: Frequency distribution of MacGregor *et al's* (1994) Productivity Prediction estimated for three large bulldozers using equation 4. The percentage may be used to estimate the percentage of open pit fitting to each class.

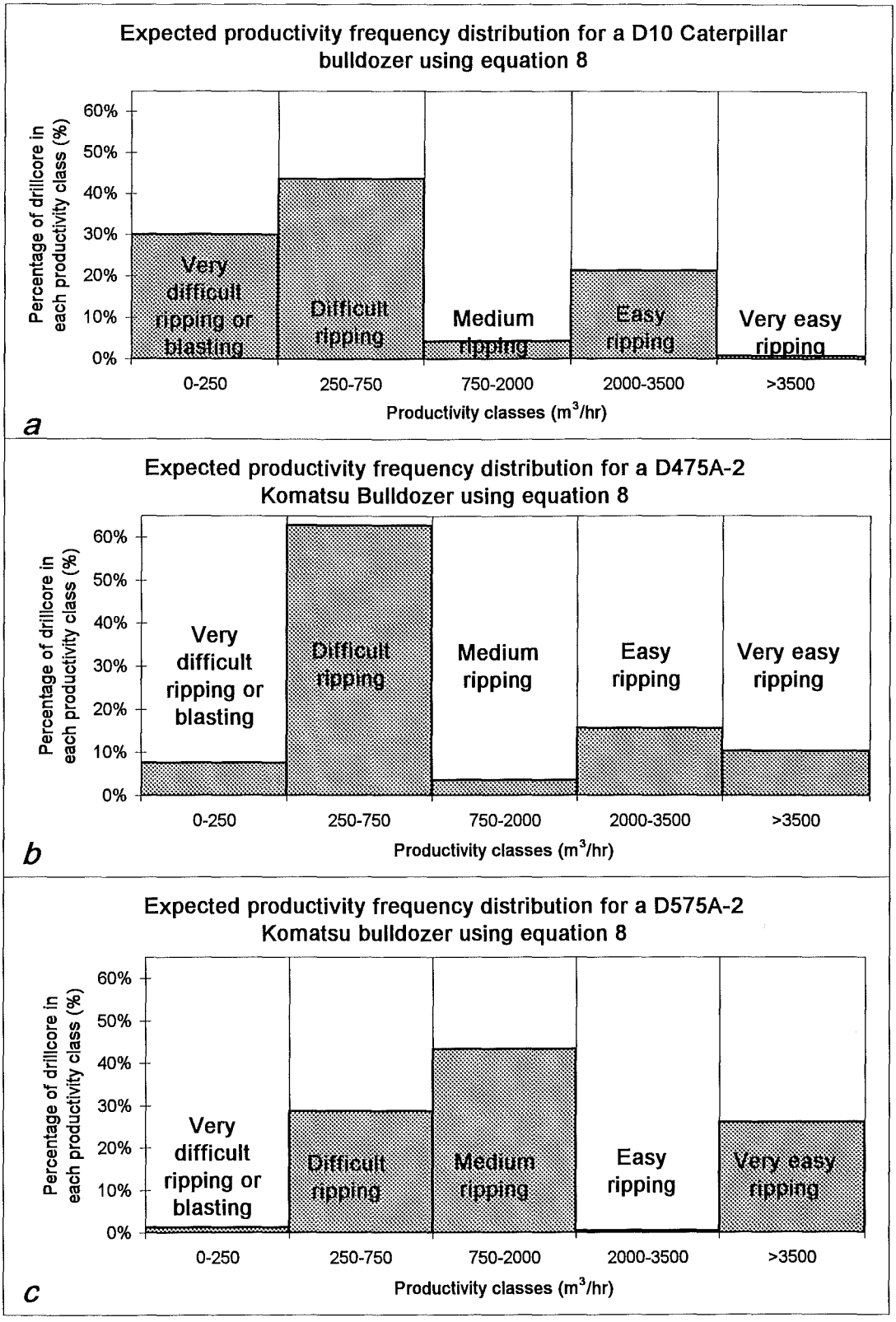

Figure 5.40: Frequency distribution of MacGregor *et al's* (1994) Productivity Prediction estimated for three large bulldozers using equation 8. The percentage may be used to estimate the percentage of open pit fitting to each class.

Appendix E5) into $5m^2$ blocks, and where productivity data are constrained to either the ore zone domain or the overburden domain. The maximum extrapolation of data is 80m, although most drillholes are less than 50m apart (Figure 4.1), therefore the plans should be reasonably accurate. It should be noted, however, that the drillhole data plotted in Figure 5.40 predicts no easy ripping for the open pit area, yet the plans (Figures 5.41 to 5.50) show that easy ripping should be expected. This is an effect of the block modelling where values are extrapolated within each domain such that difficult ripping grades into very easy ripping.

The productivity plans show similar trends to their corresponding RMR plan (Figures 5.13 to 5.22; in map and table box). The Globe-Progress Shear Zone is clearly delineated as zone of very easy rippability following the northern and eastern pit walls (see Figures 5.43 to 5.47) whereas most of the overburden is expected to be medium and difficult ripping (Figures 5.43 to 5.47). The western wall (location of the Chemist Shop Fault) is also outlined as a zone of very easy ripping (Figures 5.44 to 5.46). The base of the pit is expected to be easy to very easy to rip (Figure 5.49 and 5.50) as the ore zone flattens out with depth. There is also a zone of easy to very easy ripping that follows the axial fold hinge of the Globe-Progress Shear Zone (Figures 5.43 to 5.48). The axial fold hinge is associated with greater deformation of the rock mass than the fold limbs, where moderate to difficult ripping is expected (for example, Figures 5.41, 5.42, 5.44 to 5.47). The same trend is observed in the RMR plots (Figure 5.13 to 5.22).

The distribution of data (Figures 5.39 and 5.40) and the bench plans (Figures 5.41 to 5.50) show that this method is comparable to the excavatability predicted by the RMR System, and therefore, the RMR System and the productivity prediction method can be used in conjunction to identify the areas of easy ripping, such as the Globe-Progress Shear Zone and western wall (both of which could most likely be dug) and areas of difficult and very difficult ripping, where blasting may be more beneficial.

5.5 Comparison between methods

5.5.1 Comparison between preliminary rippability prediction methods

The preliminary rippability estimation using seismic velocity determination predicts that 90% of the pit area is rippable or marginal, and 10% of the pit will be unrippable. This estimate is based on surface data only, and therefore, it should not used as a prediction of the whole pit. Size-strength determination uses drillcore data, and thus, can be used to provide a three dimensional preliminary rippability assessment of the open pit rather than a two dimensional assessment using seismic refraction techniques. This method predicted that almost all of the pit will be rippable.

The seismic refraction rippability assessment should be a better estimator of the rippability of a rock mass because seismic velocities are dependant upon the strength, density, weathering, compaction and fracturing of a rock mass (Weaver, 1975; Palmer, 1980; Braybrooke, 1988) whereas the size-strength method is only dependant upon the strength and fracturing of a rock mass. Therefore, in open pit or quarry design, downhole seismic refraction or reflection surveys should be performed to provide a three-dimensional rippability model. However, surface seismic refraction surveys such as those performed in this study are useful for determining the excavatability of shallow excavations such as road cuts or alignments.

5.5.2 Comparison between rock mass and rippability evaluations

The three methods chosen to evaluate the rippability of the open pit were all easily determined from drillcore data and limited field investigations to provide three-dimensional rippability models of the open pit.

The first method used was the RMR System, which predicts the quality of the rock mass. This may be compared to the rock mass quality of Hoek and Brown (1980) who correlate their rock mass quality with the RMR, but as the rock mass quality is relatively old and the RMR System has been updated since 1980, the correlation between the two may not be very accurate. This is illustrated in Figure 5.51, which plots Beetham and Coote (1994)

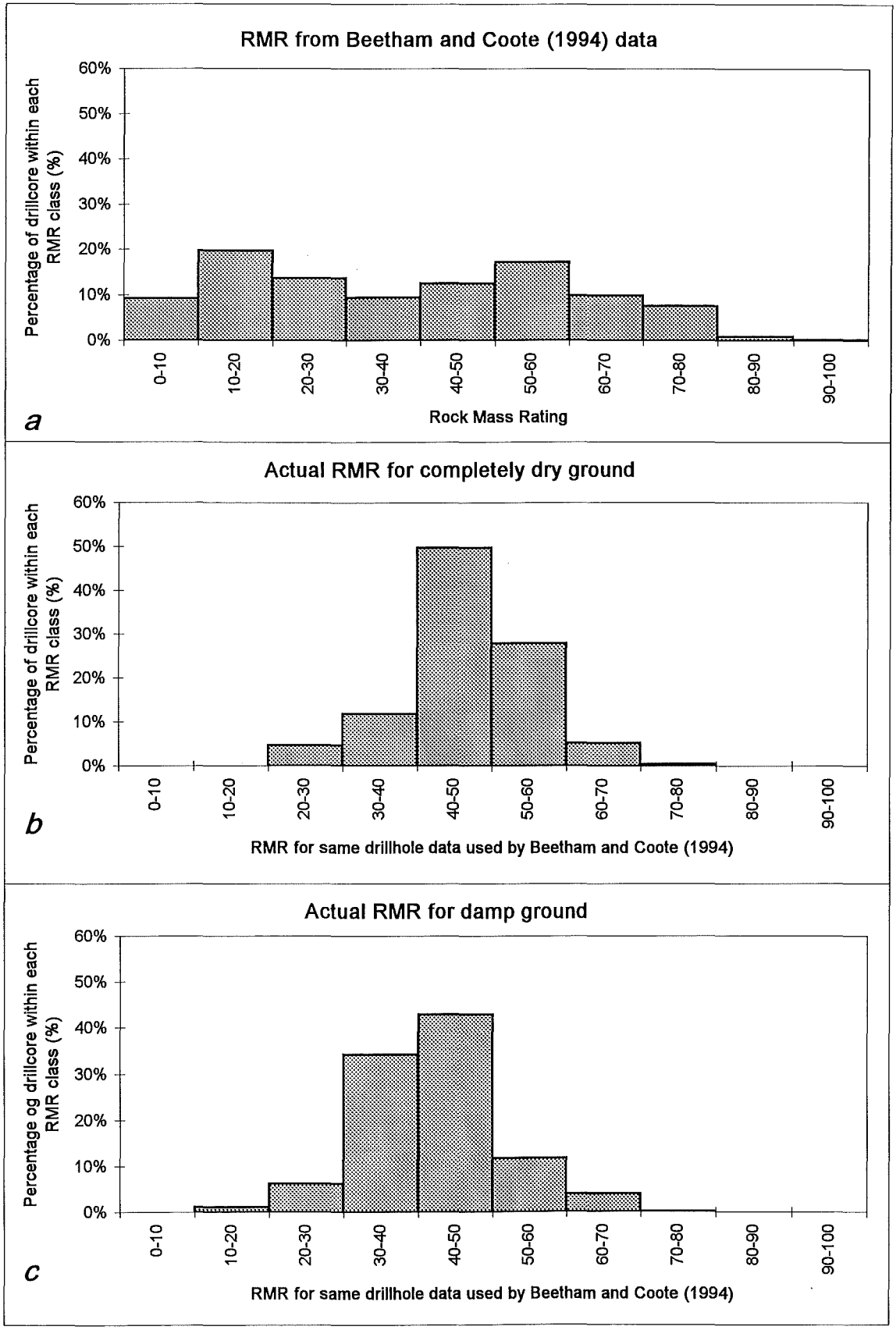

Figure 5.51: Comparison between RMR determined by Beetham and Coote (1994; *a*) and this study on the same drillcore data (*b* and *c*). Beetham and Coote (1994) logged the rock mass quality of Hoek and Brown (1980), which may be correlated with the RMR, whereas this study calculates the actual RMR for an excavation.

qualitatively logged, rock mass quality (converted to RMR) with the quantitatively determined RMR (assuming a completely dry and a damp rock mass) using the same drillcore data. The differences between the two are because of the outdated correlation between rock mass quality and RMR used and because Beetham and Coote (1994) qualitatively logged the drillcore, which may not be as accurate as a quantitative assessment, but it still provides a relatively accurate assessment considering the speed a qualitative assessment takes compared to the time taken to quantitatively log a rock mass.

Weaver's 1975 Rippability Rating Method estimates the quality of the rock mass to be approximately one category of rock greater than that predicted by the RMR System, and therefore over-estimates the quality of the rock mass and the type of excavation equipment that could be used. The Modified Weaver Rippability Rating System updates the 1975 version, but also over-estimates the quality of the rock mass. This over-estimation is due to the use of seismic velocities as a parameter, but as the aim of this thesis was to produce a three-dimensional rock mass and rippability model and because seismic velocities were only determined at the surface, then this method should not be used to estimate the rippability of an excavation such as an open pit or quarry, however it can be used to determine the rippability of shallow excavations, such as road cuttings. Furthermore, because seismic velocities are seen as a measure of other parameters affecting the rippability of a site, they should only be used as a preliminary assessment, similar to the approach undertaken in Section 5.2.2 as other methods such as the RMR System fully describe the rock mass using parameters that influence the rock mass, not parameters, such as seismic velocity, that are influenced by other parameters.

MacGregor *et al's* (1994) Productivity Prediction Method classes the rock mass into ranges of productivity based on a selected bulldozer. The method uses parameters that were statistically found to influence rippability of a rock mass. Some parameters such as the bulldozer operator and wear and tear of the ripper influence the rippability of a site to some degree but these parameters cannot be determined during a site investigation. Two equations may be used to predict the productivity of a site, one related to all rock types and the other related to sedimentary rocks only. Equation 4, related to all rock types, estimates a wider range of productivity values and a greater mean value that Equation 8 (used for sedimentary rocks only), and therefore, data using Equation 8 are plotted for bench levels.

RMR, Modified Weaver Rippability Rating and Productivity bench level plans have been produced (in map box) and may be compared. The rippability rating method predicts most of the open pit to be hard ripping and does not delineate zones that should be easily rippable, such as the western wall (location of the Chemist Shop Fault) and the Globe-Progress Shear Zone. For this reason, the rippability plans should not be used to model the excavatability of the pit, instead, the RMR or Productivity Prediction Method or a combination of the two could be used to model the excavatability of the open pit. Note, however, that the productivity prediction should only be used for Komatsu's D575A-2 bulldozer (or another similar sized bulldozer), as the productivity is dependant upon the mass of the bulldozer and the method of ripping, that is, the method assumes excavation is by bulldozer ripping, not digging or a combination of blasting and ripping. However, MacGregor, *et al* (1994) recommend using their method to identify zones that will be easy or difficult to excavate whatever the excavation technique used.

Both the RMR and Productivity Prediction methods appear to accurately assess the excavatability of the rock mass. Both methods identify the Globe-Progress Shear Zone and western wall as being very easy and easy to excavate (or very poor to poor rock mass quality) and both methods predict weaker rock in the axial hinge of the Globe-Progress Shear Zone and better rock mass quality (or more difficult excavatability) on the limbs of the shear zone. Therefore both methods can be used with some confidence to model the excavatability of the open pit.

5.6 Synthesis

The rippability assessment undertaken for this thesis was to first perform a preliminary assessment that could be performed at the feasibility or early site investigation stages of a project, then, if ripping appears to be feasible, apply a more comprehensive rippability assessment.

The first preliminary assessment performed was seismic velocity determination at Globe-Progress and General Gordon. The seismic refraction surveys were performed along roads and drill pads, adjacent to outcrops. This method was used because the seismic velocity of a rock mass is dependant upon the strength, weathering, density and fracturing of the rock mass (Weaver, 1975; Palmer, 1980; Braybrooke, 1988). Results show that 90% of the pit area is rippable and marginal, and 10% of the open pit area is unrippable.

The other preliminary assessment method used was the Revised Size-Strength Chart, which plots the strength of a rock material against the discontinuity spacing (or block size) of the rock mass. This method had the advantage over seismic velocity determination in that the data could be used from the drill log data, thereby giving a three-dimensional assessment. Results show that almost none of the open pit area would require blasting and that most of the data actually fits into easy and hard digging classes.

Both preliminary assessments confirmed that it would be possible to rip the overburden in the open pit and dig the shear zone, however a more detailed rippability assessment should be performed to fully characterise the rock material and rock mass in the open pit.

The complete rock mass characterisation and rippability assessment should not be performed on its own, rather, it should be compared to at least one other method (preferably more if possible) to aid interpretation and identification of diggable, easy ripping, difficult ripping and blasting zones. The methods chosen to assess the excavatability of the rock mass in the open pit were the RMR System, Weaver's 1975 Rippability Rating System and MacGregor *et al's* (1994) Productivity Prediction Method. The RMR System and MacGregor *et al's* (1994) Productivity Prediction Method both delineate the Globe-Progress Shear Zone and western wall as being of poor quality, and hence, easily rippable and the rest of the pit to be moderate to difficult ripping, with very rare locations that may require blasting, whereas a modified version of Weaver's Rippability Rating System predicts greater than 80% of the open pit to be hard ripping and does not delineate weaker or stronger rippability zones.

Chapter six

Summary, conclusions and further work

6.1 Summary

6.1.1 General

The Globe-Progress proposed open pit mine is located within Greenland Group sediments that are highly deformed. Because of this, ripping is seen as a feasible excavating alternative to drill and blast techniques. In suitable ground ripping has many benefits over drill and blast methods including:

- economically advantageous
- improved safety
- ease of automation
- accuracy of finished excavation dimensions
- excavation walls remain undamaged
- product size usually handled by conveyors
- suitable where there are limitations on the level of vibrations
- bulldozers are multipurpose machines that may also be used for dozing, scraping, stockpiling and moving equipment.

The aims of this thesis were to evaluate the rippability of the open pit, with the aim of producing a three dimensional block model of the rock mass and rippability of the open pit. To achieve this primary aim suitable rock mass and rippability classification systems were required along with drillcore data and data from supplementary geotechnical investigations.

6.1.2 Rock mass and rippability classifications

There are many rock mass classifications in use, most of which are too specific, or too general for use at Globe-Progress. The two most commonly used rippability classification methods in use today are the RMR System (Bieniawski 1973, 1976, 1979, 1989), which was originally designed to estimate the support requirements in shallow tunnel excavations, and the Q System (Barton *et al*, 1974), which was originally designed for use in deep excavations. Both systems have been modified from stability orientated classifications to excavatability orientated classifications by Weaver, 1975 (1973 RMR System) and Kirsten, (Q System), where excavatability is the inverse of stability. As the RMR System was originally designed for use in shallow excavations, because of its ease of use and interpretation, it was decided to classify the rock mass using the RMR System and rippability using Weaver's 1975 Rippability Rating Method. Weaver's (1975) method was also updated to follow the most recent RMR System by Bieniawski (1989). As a comparison, the expected productivity was also estimated following the approach undertaken by MacGregor *et al* (1994).

6.1.3 Geotechnical investigations

A combination of field and laboratory work was undertaken to provide additional data and to quantify drillcore data for use in the rock mass and rippability classifications.

Field work undertaken involved visually inspecting most outcrops to determine what defects noticed in drillcore were doing on the outcrop scale. This work helped form some of the generalisations and assumptions used in calculating the rock mass and rippability evaluations. Seismic refraction surveys were also performed to provide a preliminary rippability assessment, for use as an additional parameter in rippability evaluations and for comparison with sonic velocities determined of rock material. Twenty seismic refraction lines were performed, fifteen at Globe-Progress and five at General Gordon (site of waste rock stack and tailings dam, but also containing significant quantities of ore that may be extracted). Summarised results are given in Table 6.1.

Table 6.1: Summary of seismic velocity results

Location	Total length of survey lines (m)	Mean (ms^{-1})	Range (ms^{-1})
Globe-Progress	615	2100	620 - 6667
General Gordon	150	1950	508 - 5000
Combined	765	2100	508 - 6667

Laboratory tests were performed on drillcore samples and irregular lump samples. Due to the highly fractured nature of the drillcore (both natural and drilling induced), it was hard to select suitable samples for testing. Three distinctly different rock types were identified for testing, brecciated or highly fractured, very well indurated sandstone and mudstone. Due to the fragile nature of the mudstone samples only one sample was tested for porosity-density, sonic velocity and UCS tests.

The following laboratory tests were performed:

- Porosity-density
- Sonic velocity and dynamic Modulii of Elasticity
- Stress-strain relationship
- UCS
- Point load strength
- Effect of weathering on samples.

Porosity-density data are not required for any of the rock mass classifications used but ISRM (1981) recommend reporting the data as it is one of the fundamental physical properties of rock material. Table 6.2 includes summarised porosity-density data.

Sonic velocity tests were performed to determine the sonic velocity of the rock material so it can be compared to the seismic velocity of a rock mass. The dynamic Modulii of Elasticity can also be calculated from P and S Waves and the density of the sample. A summary of results is included in Table 6.2.

Stress-strain tests performed to determine the relationship between stress and strain and to find the static Young's Modulus, which can be compared with the dynamic Young's Modulus. Summarised results are included in Table 6.2. As well as finding the stress-strain relationship of samples, samples were loaded until failure to determine their uniaxial compressive strength (UCS). The mean values for each rock type is shown in Table 6.2.

Samples of drillcore adjacent to and lithologically similar to UCS samples were tested to find their point load strength so that a site specific correlation between UCS and point load strength could be determined. It was found that UCS = $20(I_{s\ (50)})$, a relationship also suggested by Pells (1985), Hawkins (1986) and Pettifer and Fookes (1994). Point load strength and slake-durability tests were also performed on slightly weathered and moderately weathered irregular lumps and unweathered core samples to test the effect of weathering on the rock material quality. Summarised results are included in Table 6.2.

Table 6.2: Summary data from all geotechnical laboratory tests.

Geotechnical test variable	Very well indurated sandstone	Brecciated and highly fractured sandstone	Mudstone	Combined data
Dry Density (kgm^{-3})	2718	2676	2785	2713
Saturated density (kgm^{-3})	2726	2694	2806	2724
Porosity (%)	0.84	1.84	2.02	1.11
Saturation moisture content (%)	0.31	0.68	0.72	0.41
Saturated P wave velocity (ms^{-1})	4661	3961	1677	4357
Saturated S wave velocity (ms^{-1})	2623	1792	1278	2377
Dry P wave velocity (ms^{-1})	4230	3393	1519	3911
Dry S wave velocity (ms^{-1})	3009	2411	1086	2782
Saturated E_{dyn} (GPa)	46.8	23.8	7.4	39.9
Saturated ν_{dyn} (-)	0.25	0.37	0.19	0.27
Dry E_{dyn} (GPa)	42.5	30.3	6.4	38.0
Dry ν_{dyn} (-)	0.21	0.13	0.02	0.18
Saturated UCS (MPa)	103.9	25.0	32.0	79.0
Saturated $E_{t\ (50)}$	40.9	15.8	5.1	33.9
Saturated $I_{s\ (50)}$ (MPa)	6.49	1.11	-	4.47

Geotechnical test variable	Unweathered core samples	Slightly weathered irregular lumps	Moderately weathered irregular lumps
Point load strength (MPa)	6.49	5.06	2.68
Slake-durability (%)	99.4	98.8	98.1

The above tests were all performed to assist in the quantitative analysis of drillcore data. It was found that strength was mostly under-estimated, and it was occasionally over-estimated. Therefore, using the point load strength from this study and Beetham and Coote's (1994) data, the logged strengths were revised to give a better approximation of the strength of the rock material. RQD was logged twice using different intervals. Both distributions are similar, therefore it is assumed that RQD has been correctly calculated. Discontinuity spacing data follows a clustered distribution, where there is a concentration of very close discontinuities. Other drillcore parameters such as grain size and weathering are assumed to have been logged correctly.

6.1.4 Preliminary rippability evaluations

Two preliminary tests were performed to ascertain whether or not it was feasible to rip the open pit. The first method involved determining variations in seismic velocities around the open pit and comparing those with rippable, marginal and non-rippable zones for the Bulldozer recommended by John (1994) for use in ripping the open pit. The second method plots the strength of rock material versus its corresponding discontinuity spacing on a revised size-strength graph (Pettifer and Fookes, 1994).

Seismic velocity determination results show that 90% of the pit area is rippable or marginal and 10% of the open pit area is unrippable. The size-strength method suggests that almost all of the pit area is rippable.

Both methods suggest that is feasible to rip the pit and therefore, it was decided to perform a more detailed investigation that would identify zones of easy ripping (or poor rock), moderately hard ripping (fair rock) and difficult ripping (good rock).

6.1.5 Complete rock mass and rippability evaluation

The RMR System was designed for use in tunnel stability but is easily adapted for use in excavations, using the methodology outlined in Section 2.3.2. A summary of the results found assuming a completely dry rock mass, damp rock mass and saturated rock mass is included in Table 6.3.

Weaver's 1975 Rippability Rating Method was based on the original 1973 RMR System, therefore is outdated as has been modified to follow the most recent RMR System (Bieniawski, 1989). The results are summarised in Table 6.3. It should be noted that the original rippability rating and the modified version both predict a class of rock one better than that estimated by the RMR System because the seismic velocity has been averaged over the whole open pit.

MacGregor *et al* (1994) attempt to predict the productivity of a chosen bulldozer by statistically analysing all parameters that affect the productivity of a bulldozer. Only parameters that may be quantified during a site investigation are used. Parameters such as bulldozer operator and wear and tear on machinery are not quantifiable during a site investigation stage, but they should be recorded during actual ripping or during ripping trials to further refine the ripping model. The expected productivity results for a D575A-2 bulldozer and included in Table 6.3.

Table 6.3: Summary of rock mass and rippability classification predictions.

Rock mass Classification	Mean	Range	Rock mass quality	Rippability prediction
RMR (completely dry)	45	18 - 89	Fair	Moderate
RMR (damp)	40	13 - 84	Poor to fair	Easy to moderate
RMR (saturated)	34	7 - 78	Poor	Easy
Weaver's 1975 method	57	38 - 87	Good	Very hard
Modified Weaver method	50	27 - 81	Good	Hard
Productivity for D575A-2 using Equation 8	3350	200 - 11900	Good to poor	Very easy to hard

Bench level plans have been plotted up for the RMR, Modified Weaver Rippability Rating and MacGregor *et al's* (1994) expected productivity and are included in the map and table box. Zones easy to excavate are the Globe-Progress Shear Zone, which follows the northern and eastern pit walls, and the western pit wall, where the Chemist Shop Fault is located. There is also a weak zone in the axial hinge of the Globe-Progress Shear Zone that has undergone more deformation than the shear limbs (adjacent to the axial hinge. The shear limbs are generally fair to good rock, which equates to moderate to hard (difficult) ripping using a D575A-2 bulldozer.

6.2 Conclusions

- Seismic refraction surveys are an excellent site investigation technique that can be performed at the feasibility and early investigation stages of a project because the seismic velocity of a rock mass is dependent upon its weathering, strength, density, porosity, compaction and fracturing, and therefore provides an overall assessment of the rock mass quality.

- Seismic velocity determination on the mine site rock mass found that 90% of the open pit area is of rippable to marginal rippability and that 10% of the pit area is expected to be unrippable using Komatsu's D575A-2 bulldozer.

- The Size-Strength Excavatability Method is another excellent site investigation method that can be performed early in a projects planning stages, as it plots the two properties of a rock mass most influential to excavatability.

- Size-strength determination found that almost all of the pit area should be easy digging through to very hard ripping, with a very small proportion of the pit area requiring blasting.

- The preliminary rippability assessment undertaken estimates that most of the pit will be diggable to rippable, and therefore a more accurate site investigation utilising a suite of geological and geotechnical parameters was performed to identify locations of diggable, rippable and blastable zones.

- Analyses of the drillcore data found that strength values were logged incorrectly, some values were over-estimated but most values were under-estimated. Therefore a revised strength estimate was determined based on quantitative strength measurements and the logged lithology.

- The RMR System is the best rock mass classification method to use in classifying the rock mass in the open pit as it uses a thorough rock material and discontinuity description, whereas the other major rock mass classification system (the Q System) is more applicable to characterising rock masses in deep tunnels and underground excavations.

- The RMR System was designed for use in predicting the stability of tunnels but is easily modified to predict the excavatability of a rock mass by reversing the discontinuity orientation parameter such that a favourable orientation in a stability analysis will be unfavourable for an excavation.

- Most of the rock mass in the open pit is rated poor to fair and the weaker rock masses are located in the western pit wall (where the Chemist Shop Fault is located), following the Globe-Progress Shear Zone along the northern and eastern pit walls and in the fold axis of the Globe-Progress Shear.

- Weaver's 1975 Rippability Rating Method was originally adapted from Bieniawski's 1973 RMR System, and therefore should be updated to follow Bieniawski's 1989 RMR System. This modification has been performed by replacing the RQD and groundwater parameters in the RMR System with a seismic velocity parameter in the rippability rating method and reversing the discontinuity orientation ratings. However, seismic velocities of rock masses are also functions of degree of weathering, density and

strength, and it is therefore, probably better to use a modified version of the RMR System to assess the excavatability of a rock mass.

- There is less of a data spread in the rippability rating as it requires a seismic velocity parameter, which was averaged for the pit area because seismic velocities determined on the ground surface will be less than seismic velocities determined on unweathered, less fractured (or relaxed) rock masses at depth. This has the effect of over-estimating the rock mass quality and prediction of the most appropriate form of excavation.

- MacGregor *et al's* (1994) Productivity Prediction Method was determined by correlating parameters influential to rippability with the productivity of a bulldozer. However the correlation is not very good ($R^2 = 0.58$), and therefore, there must have been considerable scatter original data set. MacGregor *et al* (1994) noted this problem and recommended locating areas that should be difficult to rip.

- There are similar trends between the RMR Index and estimated productivity of a Komatsu D575A-2 bulldozer, whereby locations of poor rock mass equate to high productivity and zones of easy ripping. However most of the easy ripping zones are located in brecciated and sheared rock that contain significant quantities of pug, and thus acts in a plastic manner such that a heavy bulldozer should not attempt ripping the shear zone.

- Areas identified to be hard to excavate could be saturated to weaken the rock mass and assist with excavation, however this may lead to other problems associated with groundwater.

- The contoured plans of RMR Index, Rippability Rating and estimated productivity give a visual representation of the excavatability of a rock mass, but these plans should not be used on their own. If excavation of the pit proceeds, orientated geotechnical drillholes should be drilled to provide additional data for use in determining the excavatability of the rock mass.

- Modelling techniques such as inverse distance and Kriging are normally applied to estimate ore reserves and the ratio of waste rock to ore, but this study has shown that these modelling techniques can easily be applied to rock mass classification methods to characterise the rock mass.

6.3 Further work

- It is possible to apply the methodology used here to assess the excavatability of rock mass at other sites in the Reefton Goldfield, and if underground mining is contemplated then the rock mass can be classified using the Q system or one of the RMR extensions designed for use in hard rock undergound mining.

- This study has provided a preliminary excavatability assessment, based on seismic refraction data, at General Gordon. A complete excavatability assessment, following procedures used in the study, could be performed once computer drillcore logs are completed.

- Pit wall stability can be determined using Romana's (1985) Slope Mass Rating, which is a modification of the RMR System, and the results can be compared to kinematic slope stability assessments.

- It may be advantageous to quantitatively test rock material parameters at other exploration sites so that the information can be used in core logging.

- As excavation proceeds, comparisons should be made between actual bench level data and predicted bench level data. If ripping is to be used then the estimated productivity for the chosen bulldozer should be compared to the actual ripping and other factors such as the length of ripping runs and wear and tear of ripper tips and bulldozer tracks should be carefully monitored to further refine the estimated productivity of a bulldozer.

Acknowledgements

The following people all deserve my gratitude and appreciation for their help and assistance during the course of this study.

Firstly, thanks to Macraes, Reefton for encouraging their head office as to the value of this project and to Macraes, Head Office, for their "enthusiasm" shown in student research.

Secondly thanks to my supervisor David Bell for all the encouragement and guidance (and red wine), and for providing helpful comments on all chapter drafts plus for staying up past the witching hour reading my final thesis draft.

Thirdly thanks to the staff at Macraes Reefton, especially Mark McKenzie (Project Geologist) for experience in the field of rock mass classification and to John Taylor (Senior Mine Planning Engineer) for his advice on various mining matters and plotting up of computer plans. I am also indebted to Colin Legge of Medsystems, Australia for generating the plans in the map box (delaying his trip down south by half a day) and designing a printing routine so that I didn't have to crash the big very expensive computer. A big slap on the back must also go to Jimmy and Ron who slaved away banging a sledgehammer against a metal plate in very hot sun (very rarely) and pouring rain (most commonly) and probably wondering what they were doing?? Thanks also to Des MacKenzie for the photos of Komatsu's "super dozer" and Lisa for photocopying, binding various reports and ordering pizzas etc etc. Thanks also to everyone else I met at Reefton including the chef at Cee Cee's (but not the chef at the hospital).

Fourthly, thanks to the Mason Trust for financial assistance with travel and thesis preparation costs and to Macraes, Reefton for the accommodation, food, field assistance and printing of plans and tables.

Thanks also to Joc Campbell, David Nobes, Jarg Pettinga and Steve Weaver of the academic staff at University of Canterbury and Laurie Richards from Lincoln University for providing helpful comments on various parts of this thesis.

Thanks also to the technical staff in the Geological Sciences Department, especially Mike Finnemore for his computer literacy; Cathy Knight for the organising of gear, setting up of lab equipment, useful advice and help with fieldwork during the early stages of this project etc etc etc; Arthur Nicholas for workshop advice and slides; Rob Spiers for putting up with me as I cut samples, Kerry Swanson for photos and slides and Michelle Wright for money.

Thanks again to Dave Bell, Cathy Knight and Jonny McNee for their assistance in smashing core samples in the civil engineering materials lab and to George Clark from the civil engineering materials lab for allowing us to do so.

More thanks to my classmates, Al, Anna, Carl, Chris, Jonny, Nick, Rachel, Sarah and Sonia and other friends who have kept me sane away from varsity.

Still more thanks to my Parents and sisters for putting up with me over the last few months and especially thanks for all the microwaveable meals.

Lastly, thanks to Macraes for the use of the four wheel drive (PTO)....

Oops!

NB: There were no dents or scratches - just a little bit of mud on the other side.

And if you were wondering what effect the writing up of an engineering geological thesis and using excel can do to the body then PTO.

Tailpiece

Arrrrrgh!!!!!

References

Abad, J; B Celada; E Chacon; V Gutierrez; and E Hidalgo; 1983: Application of geomechanical classification to predict the convergence of coal mine galleries and to design their supports, *Proceedings of the 5th International Congress on Rock Mechanics*, ISRM, Melbourne, volume 2, pages E15-E19.

Abdullatif, OM and DM Cruden; 1983: The relationship between rock mass quality and ease of excavation, *Bulletin of the International Association of Engineering Geology*, volume 28, pages 183-187.

Adams, CJD; CT Harper; and MG Laird; 1975: K-Ar ages of low grade metasediments of the Greenland and Waiuta Groups in Westland and Buller, New Zealand, *New Zealand Journal of Geology and Geophysics*, volume 18, pages 39-48.

Allaby, A and M Allaby; 1991: *The Concise Oxford Dictionary of Earth Sciences*, Oxford University Press, Oxford, 410 pages.

Anon; 1994: Report to Mark McKenzie, *Report by Works Consultancy Services*, 2 pages.

Atkinson, T; 1970: Ground preparation by ripping in open pit mining, *Mining Magazine*, volume 122, pages 458-469.

Australian Geomechanics Society; 1975: Engineering classification of sedimentary rocks in the Sydney area, *Australian Geomechanical Journal*, volume G5, number 1.

Barrell, D; 1992: Geotechnical line mapping, Globe-Progress Prospect, Reefton, *Unpublished Report for Macraes Mining Company Limited, Reefton*, 58 pages.

Barry, JM; 1993: *The History and Mineral Resources of the Reefton Goldfield*, Resource Information Report 15, Energy and Resources Division, Ministry of Commerce, 59 pages.

Barry, JM; 1994: "Deeps" drilling programme 1993/1994 and geology of the Globe-Progress Deposit, *Unpublished Report for Macraes Mining Company Limited, Reefton.*

Barton, N; R Lein; and J Lunde; 1974: Engineering classification of rock masses for the design of tunnel support, *Rock Mechanics*, volume 6, pages 189-236.

Beetham RD; and L Richards; 1995: Globe-Progress Mining Project. Assessment of open pit geometry, *Unpublished Report for Macraes Mining Company Limited, Reefton*, 26 pages.

Beetham, RD and TP Coote; 1994: Geotechnical relogging and systematic point load testing of selected drill cores from the proposed Globe-Progress open pit mine, *Unpublished Report for Macraes Mining Company Limited, Reefton.*

Bell DH; and JR Pettinga; 1983: Presentation of geological data *Engineering for Dams and Canals: Proceedings of Technical Groups, The Institute of Professional Engineers, New Zealand*, volume 9: 4(G), pages 4.1-4.35.

Bell, DH and NA Crampton; 1986: Panel report: Engineering geological evaluation of tunnelling conditions, Lyttelton-Woolston LPG Project, Christchurch, New Zealand, *Proceedings of the 5th International Association Engineering Geology Congress*, Buenos Aires, pages 2485-2501.

Bell, FG; 1992: *Engineering in Rock Masses*, Butterworth-Heinemann Ltd, Oxford, 580 pages.

Bieniawski, ZT; 1973: Engineering classifications of jointed rock masses, *Transactions of the South African Institute of Civil Engineers,* volume 15, pages 335-344.

Bieniawski, ZT; 1976: Rock mass classifications in rock engineering, *Proceedings of the Symposium of Exploration for Rock Engineering*, AA Balkema, Johannesburg, volume 1, pages 97-106.

Bieniawski, ZT; 1978: Determining rock mass deformability: Experience from case histories, *International Journal of Rock Mechanics and Mining Sciences*, volume 15, pages 237-247.

Bieniawski, ZT; 1979: The Geomechanics Classification in rock engineering applications, *Proceedings of the Fourth International Congress on Rock Mechanics,* ISRM, Montreux, volume 2, pages 41-48.

Bieniawski, ZT; 1984: *Rock Mechanics Design in Mining and Tunnelling*, AA Balkema, Rotterdam, 272 pages.

Bieniawski, ZT; 1989: *Engineering Rock Mass Classifications: A Complete Manual For Engineers and Geologists in Mining, Civil, and Petroleum Engineering*, John Wiley and Sons, New York, 251 pages.

Bieniawski, ZT; 1993: Classification of rock masses for engineering: The RMR System and future trends, *Comprehensive Rock Engineering, Principles, Practice and Projects: Volume 3 Rock Testing and Site Characterisation*, edited by JA Hudson, Pergamon Press, Oxford, volume 3, pages 553-573.

Bieniawski, ZT and CM Orr; 1986: Rapid site appraisal for dam foundations by the Geomechanics Classification, *Proceedings of the 12th Congress on Large Dams,* ICOLD, Mexico City, pages 483-501.

Bowen, FE; 1964: *Geological Map of New Zealand, Sheet 15: Buller*, scale 1:250 000.

Bradshaw, MA; and BD Hegan; 1983: Stratigraphy and structure of the Devonian rocks of Inangahua Outlier, Reefton, New Zealand, *New Zealand Journal of Geology and Geophysics*, volume 11, pages 92-122.

Braybrooke, JC; 1988: The state of the art of rock cuttability and rippability prediction, *Proceedings of the Fifth Australia New Zealand Conference on Geomechanics*, pages 13-42.

Brekke, TL; 1968: Blocky and seamy rock in tunnelling, *Bulletin of the Association of Engineering Geology*, volume 5, pages 1-12.

Brewster, PJ; 1984: Ripping techniques, *Australian Geomechanics Society - Excavation Characteristics Seminar*, November 1984.

Broch, E; and JA Franklin; 1972: The point load strength test, *The International Journal of Rock Mechanics and Mining Science*, volume 9, pages 669-697.

Bullock, SJ; 1978: The case for using multichannel seismic refraction equipment and techniques for site investigation, *Bulletin of the Association of Engineering Geologists*, volume 15, pages 19-35.

Church, HK; 1981: *Excavation Handbook*, McGraw-Hill, New York, 1024 pages.

Coffey and Partners; 1989: Preliminary geotechnical study, Globe-Progress Mine, Reefton, *Unpublished Report for CRA Exploration Limited, Reefton*, 93 pages.

Cooper, AF and D Craw; 1992: Petrographic analysis and report on core samples from the Globe-Progress Project area, Reefton, *Unpublished Report for Macraes Mining Company Limited, Reefton*, 44 pages.

Cooper, RA; 1974: Age of the Greenland and Waiuta Groups, *New Zealand Journal of Geology and Geophysics*, volume 17, pages 955-962.

Cooper, RA; 1989: Early Palaeozoic Terranes of New Zealand, *Journal of the Royal Society of New Zealand*, volume 19, pages 73-112.

Deere, DU; 1967: Geological considerations, *Rock Mechanics in Engineering Practice*, edited by KG Stagg and O Zienkiewicz, John Wiley and Sons, London, pages 1-20.

Deere, DU; AJ Hendron; FA Patton; and EJ Cording; 1968: Design of surface and near surface construction in rock, *Proceedings of the 8th US Symposium on Rock Mechanics*, AIME, New York, pages 237-302.

Deere, DU; RB Peck; H Parker; JE Monsees; and B Schmidt; 1970: Design of tunnel support systems, *Highway Research Record*, volume 339, pages 26-33.

Dight, PM and JK Cadman; 1992: Geotechnical study for the Globe-Progress gold deposit, Reefton, New Zealand, *Unpublished Report for Macraes Mining Company Limited, Reefton*, 60 pages.

Edge, AB and TH Laby; 1931: *The Principles and Practice of Geophysical Prospecting*, Cambridge University Press.

Einstein, HH; DE Thompson; AS Azzouz; KP O'Reilly; MS Schultz; and S Ordun; 1983: Comparison of five empirical tunnel classification methods - accuracy, effect of subjectivity and available information, *Proceedings of the 5th International Congress on Rock Mechanics*, ISRM, Melbourne, volume 1, pages C303-C313.

Farmer, IW; 1983: *Engineering Behaviour of Rocks*, Second edition, Chapman and Hall, London, 208 pages.

Fookes, PG; WR Dearman; and JA Franklin; 1971: Some engineering aspects of rock weathering with field examples from Dartmoor and elsewhere, *Quarterly Journal of Engineering Geology*, volume 4, pages 139-185.

Fowell, RJ; 1993: The mechanics of rock cutting, *Comprehensive Rock Engineering, Principles, Practice and Projects: Volume 4, Excavation, Support and Monitoring*, edited by JA Hudson, Pergamon Press, Oxford, pages 155-176.

Franklin, JA; E Broch; and G Walton; 1971: Logging the mechanical character of rock, *Transactions of the Institution of Mining and Metallurgy*, volume 80A, pages 1-9.

Gage, M; 1948: The geology of the Reefton quartz lodes, *New Zealand Geological Bulletin 45*, 72 pages.

Gage, M and FA McNeill; 1940: Geophysical investigations in the area between Waiuta and Merrijigs, *New Zealand Journal of Science and Technology*, volume 22, pages 155-165.

Ghose, AK and NM Raju; 1981: Characterisation of rock mass vis-à-vis application of rock bolting in Indian coal measures, *Proceedings of the 22nd US Symposium on Rock Mechanics*, MIT, Cambridge, pages 422-427.

Hancox, GT and S Beanland; 1994: Evaluation of fault displacement hazard at the Globe-Progress mine site area, Reefton, *Unpublished Report for Macraes Mining Company Limited, Reefton.*

Hatherly, PJ and MJ Neville; 1986: Experience with the Generalised Reciprocal Method of seismic refraction interpretation for shallow engineering site investigation, *Geophysics*, volume 51, pages 255-265.

Hawkes, I and M Mellor; 1970: Uniaxial testing in rock mechanics laboratories, *Engineering Geology*, volume 4, pages 177-285.

Hawkins, AB; 1986: Rock descriptions, *Site Investigation Practice: Assessing BS5930*, edited by AB Hawkins, Geological Society, Engineering Geology Special Publication 2, pages 59-66.

Hawkins, LV; 1961: The Reciprocal Method of routine shallow seismic refraction investigations, *Geophysics*, volume 26, pages 806-819.

Henderson, J; 1917: The geology and mineral resources of the Reefton Subdivision, *New Zealand Geological Bulletin 18*, 232 pages.

Henderson, J; 1921: Reefton Coalfield, *New Zealand Journal of Science and Technology*, volume 4, pages 18-24.

Hodder, APW; and Hetherington, JR; 1991: A quantitative study of the weathering of Greywacke, *Engineering Geology*, volume 31, pages 353-368.

Hoek, E and ET Brown; 1980: *Underground Excavations in Rock*, Institution of Mining and Metallurgy, London, 527 pages.

Hughes, S; 1992: The geology of the Globe-Progress gold-antimony-arsenic deposit, Reefton, Westland, *Unpublished Report for Macraes Mining Company Limited, Reefton*, 32 pages.

Irfan, TY; and WR Dearman; 1978: Engineering classification and index properties of a weathered granite, *Bulletin of the International Association of Engineering Geology*, volume 17, pages 79 - 90.

ISRM; 1981: *Rock Characterisation, Testing and Monitoring. International Society for Rock Mechanics Suggested Methods,* ET Brown (editor), Pergamon Press, Oxford, 211 pages.

ISRM; 1985: Suggested method for determining point load strength, *International Journal of Rock Mechanics, Mining Sciences and Geomechanics Abstracts*, volume 22, pages 51-60.

Jaeger, JC; and NGW Cook; 1976: *Fundamentals of Rock Mechanics*, Second edition, Chapman and Hall, London, 585 pages.

John, I; 1994: Site visit report, Globe-Progress development, near Reefton, New Zealand, *Unpublished Report for Macraes Mining Company Limited, Reefton*, 13 pages.

Johnson, RB; and JV DeGraff; 1988: *Principles of Engineering Geology*, John Wiley and Sons, New York, 497 pages.

Jowett, T; H McLauchlan; and P Lundy; 1996: Bench-zero mapping, *Unpublished Report for Macraes Mining Company Limited, Reefton.*

Kendorski, F; R Cummings, ZT Bieniawski; and E Skinner; 1983: Rock mass classification for block caving mine drift support, *Proceedings of the 5th International Congress on Rock Mechanics*, ISRM, Melbourne, volume 1, pages B51-B63.

Kirsten, HAD; 1982: A classification system for excavation in natural materials, *Transactions of the South African Institute of Civil Engineers*, volume 24, pages 293-308.

Koczanowski, M; GR Mostyn; and F MacGregor; 1991: An expert system for rock rippability assessment, *Proceedings of the Seventh International Congress on Rock Mechanics,* ISRM, Montreux, volume 3, pages 275-279.

Laird, MG; 1972: Sedimentology of the Greenland Group in the Paparoa Range, West Coast, South Island, New Zealand, *New Zealand Journal of Geology and Geophysics*, volume 15, pages 372-393.

Laird, MG and D Shelley; 1974: Sedimentation and early tectonic history of the Greenland Group, Reefton, New Zealand, *New Zealand Journal of Geology and Geophysics*, volume 17, pages 839-854.

Laubscher, DH; 1977: Design aspects and effectiveness of support systems in different mining situations, *Transactions of the Institute of Mining and Metallurgy*, volume 86, pages A1-A7.

MacGregor, F; R Fell; GR Mostyn; G Hocking; and G McNally; 1994: The estimation of rock rippability, *Quarterly Journal of Engineering Geology*, volume 27, pages 123-144.

Martin, JM; 1986: Predicting the rippability of sandstone in Southeast Queensland, *Proceedings of the 13th Australian Road Research Board Conference*, pages 119-132.

McGovern-Wilson, R; 1992: Globe Hill Archaeological Survey, *Unpublished Report for Macraes Mining Company Limited, Reefton*, 205 pages.

Minty, EJ and GK Kearns; 1983: Rock mass workability, *Collected Case Studies in Engineering Geology, Hydrogeology and Environmental Geology*, edited by MJ Knight, EJ Minty, RB Smith, Geological Society of Australia Special Publication 11, pages 59-81.

MMCL; 1996: *Annual Report 1995*, 64 pages.

Modriniak, N and E Marsden; 1938: Experiments in Geophysical Survey in New Zealand, *New Zealand Department of Science and Industrial Research Geological Memoirs*, volume 4, 90 pages.

Motor Holdings Komatsu Limited; 1996: Komatsu's big dozers for heavy metal fans everywhere, *On track, the Bulletin for Construction, Forestry, Mining and Quarrying*, April-May 1996, pages 4-5.

Muir, RJ; SD Weaver; JD Bradshaw; GN Eby; JA Evans; and TR Ireland; In press: Geochemistry of the Karamea Batholith, New Zealand, and comparisons with the Lachlan Fold Belt granites of Southeast Australia, *Lithos*.

Nakao, K; S Iihoshi; and S Koyama; 1983: Statistical reconsiderations on the parameters for geomechanics classification, *Proceedings of the 5th International Congress on Rock Mechanics*, ISRM, Melbourne, volume 1, pages B13-B16.

Nathan, S; 1976: Geochemistry of the Greenland Group (Early Ordovician), New Zealand, *New Zealand Journal of Geology and Geophysics*, volume 19, pages 683-706.

Nobes, DC; 1989: A test of a simple model of the acoustic vlocity in marine sediments, *Journal of the Acoustic Society of America*, volume 86, pages 290-294.

NZGS; 1988: *Guidelines for the field description of soils and rocks in engineering use*, 42 pages.

Obert, L; and Duvall, WI; 1967: *Rock Mechanics and the Design of Structures in Rock*, John Wiley and Sons, New York, 650 pages.

Olivier, HJ; 1979: A new engineering geological rock durability classification, *Engineering Geology*, volume 14, pages 255-279.

Orr, CM; 1992: Assessment of rock slope stability using the Rock Mass Rating (RMR) System, *Proceedings of the Australian Institute of Mining and Metallurgy*, number 2, pages 25-29.

Palmer, D; 1980: *The Generalised Reciprocal Method of Seismic Refraction Interpretation*, Society of Exploration Geophysicists, 104 pages.

Parry, C; 1993: The Globe-Progress Project, Reefton, *New Zealand Mining*, volume 10, June 1993, pages 8-11.

Pells, PJN; 1985: Engineering properties of the Hawkesbury Sandstone, *Engineering Geology of the Sydney Region*, edited by PJN Pells, Balkema, Rotterdam, pages 179-197.

Pettifer, GS; and PG Fookes; 1994: A revision of the graphical method for assessing the excavatability of rock, *Quarterly Journal of Engineering Geology*, volume 27, pages 145-164.

Priest, SD and JA Hudson; 1976: Discontinuity Spacings in Rock, *International Journal of Rock Mechanics, Mining Sciences and Geomechanics Abstracts*, volume 13, pages 135-148.

Raine, JI; 1980: Palynology of the Triassic Topfer Formation, Reefton, South Island, New Zealand, *Abstracts of the Fifth Gondwana Symposium, Wellington, New Zealand, 1980.*

Raine, JI; 1984: Outline of a palynological zonation of Cretaceous to Paleogene terrestrial sediments in the West Coast region, South Island, New Zealand, *New Zealand Geological Survey Report 109*, 82 pages.

Rattenbury, MS; 1994: Structural geology of the Globe Hill area, Reefton, *Unpublished Report for Macraes Mining Company Limited, Reefton.* 34 pages.

Romana, M; 1985: New adjustment ratings for application of Bieniawski Classification to slopes, *Proceedings of the International Symposium of Rock Mechanics in Excavations, Mining and Civil Works*, ISRM, Mexico City, page 59-68.

Rose, D; 1982: Revising Terzaghi's tunnel rock load coefficients, *Proceedings of the 23rd US Symposium on Rock Mechanics*, AIME, New York, pages 953-960.

Rutledge, JC and RL Preston; 1978: New Zealand experience with engineering classifications of rock for the prediction of tunnel support, *Proceedings of the International Tunnelling Symposium*, Tokyo, pages 23-29.

Sandbak, LA; 1985: Roadheader drift excavation and geomechanics rock classification, *Proceedings of Rapid excavations and Tunnelling Conference*, AIME, New York, volume 2, page 902-916.

Serafim, JL and JP Pereira; 1983: Considerations of the geomechanics classification of Bieniawski, *Proceedings of the International Symposium of Engineering Geological Underground Construction*, LNEC, Lisbon, volume 1, pages II.33-II.42.

Siggons, AF; 1993: Dynamic elastic tests for rock engineering, *Comprehensive Rock Engineering, Principles, Practice and Projects: Volume 3 Rock Testing and Site Characterisation*, edited by JA Hudson, Pergamon Press, Oxford, volume 3, pages 601-634.

Sinha, RS; 1988: Discussion of the RSR Model, *Proceedings of the Symposium on Rock Classification for Engineering Purposes*, ASTM Special Technical Publication 984, Philadelphia, pages 35-49.

Smith, HJ; 1987: Estimating the mechanical dredgeability of rock, *Proceedings of the 28th US Symposium on Rock Mechanics*, AA Balkema, Boston, pages 943-935.

Smith, WD and KR Berryman; 1983: Revised estimates of earthquake hazard in New Zealand, *Bulletin of the New Zealand National Society for Earthquake Engineering*, volume 16.

Sokal, RR; 1974: Classification: purposes, principles, progress and prospects, *Science*, volume 185, pages 1115-1123.

Suggate, RP; 1957: The geology of the Reefton Subdivision, *New Zealand Geological Bulletin 56*, 146 pages.

Swan, ARH and M Sandilands; 1995: *Introduction to Geological Data Analysis*, Blackwell Science Limited, Oxford, 446 pages.

Terzaghi, K; 1946: Rock defects and loads on tunnel support, *Rock Tunnelling With Steel Supports*, edited by RV Proctor and T White, Commercial Shearing Company, Youngstown, USA, pages 15-99.

Tsiambaos, G and D Telli; 1992: Application of rock mass classification systems on stability of limestone slopes, *Proceedings of the 6th International Symposium on Landslides*, Christchurch, New Zealand, AA Balkema, Rotterdam, volume 2, pages 1065-1069.

Udd, JE and H Wang; 1985: A comparison of some approaches to the classification of rock masses for geotechnical purposes, *Proceedings of the 26th US Symposium on Rock Mechanics*, Rapid City, South Dakota, volume 1, pages 69-78.

Unal, E; 1983: *Design Guidelines and Roof Control Standards for Coal Mine Roofs*, PhD thesis, Pennsylvania State University, Pennsylvania, 355 pages.

Urquhart, DF; 1956: The investigation of deep leads by the seismic refraction method, *Bulletin, Bureau of Mineral Resources, Australia,* Volume 35.

Venkateswarlu, V; 1986: *Geomechanics Classification of Coal Measure Rocks vis-à-vis Roof Supports*, PhD thesis, Indian School of Mines, Dhanbad, 251 pages.

Von Haast, J; 1861: *Report of a topographical and geological exploration of the western districts of the Nelson Province, New Zealand.*

Weaver, JM; 1975: Geological factors significant in the assessment of rippability, *Transactions of the South African Institute of Civil Engineers,* volume 17, pages 313-316.

Wickham, GE; HR Tiedemann; and EH Skinner; 1972: Support determination based on geologic predictions, *Proceedings of the Rapid Excavation and Tunnelling Conference*, AIME, New York, volume 1, pages 43-64.

Wickham, GE; HR Tiedemann; and EH Skinner; 1974: Ground Support Prediction Model - RSR Concept, *Proceedings of the Rapid Excavation and Tunnelling Conference*, AIME, New York, pages 691-707.

Williams, GJ; 1930: Report on the Reefton Coalfield, *Applied Journal for the House of Representatives, New Zealand*, volume C-2B, 2.

Woodward Clyde; 1994: Surface water hydrology, Globe-Progress Project, Reefton, *Unpublished Report for Macraes Mining Company Limited, Reefton*, 63 pages.

Appendix A

Historical Overview

A1 Previous work

Geological investigations in the Reefton area have occurred in three main phases: the discovery and mining of gold and coal in the Reefton area (1880-1920); the revival of mining in the 1930s and closure of the last hard rock mine in the area in 1951, leading to renewed exploration of the Reefton Coalfields (1930-1965); and renewed exploration in the 1980s and 1990s by CRA and Macraes Mining Company Limited (Macraes).

The first geological investigation in the Reefton area was by Sir Julius Von Haast (1861), who performed a brief exploratory survey. It was not until 1917, that a detailed geological report was made on the Reefton Subdivision (Henderson, 1917). Henderson also gives a detailed account of early exploration in the Reefton area. Goldmining in the Reefton Goldfield started to decline in the 1920s with the closure of the Globe-Progress mine. Many reports published of the Reefton area in the 1920s were of the Reefton Coalfield (for example, Henderson, 1921; Williams, 1930).

During the depression of the 1930s, interest in gold mining was revived and geological and geophysical surveys were performed in 1935 to assist in gold exploration. The results were published by Modriniak and Marsden (1938) and Gage and McNeil (1940). Gage (1948) wrote a comprehensive evaluation of the Reefton Goldfield, describing the geology of the Reefton Goldfield and history of each gold mine in the goldfield. After the closure in 1951 of the last hard rock gold mine in the Reefton area, Suggate (1957) reevaluated the geology, first mapped by Henderson in 1917, emphasising the coal resources found in the district. The 1:250 000 geological map of Buller was produced by Bowen (1964), but it does not discuss the Reefton goldfield in any detail.

When the price of gold increased in the early 1980s CRA reexplored and reevaluated the resources of the Reefton goldfield, producing many unpublished reports on various prospects. The most likely mining prospect was found to be Globe-Progress and preliminary geological and geotechnical investigations were performed (for example, Coffey and Partners, 1989; Lew and Corner, 1988). After CRA sold the exploration licences to Macraes Mining Company Limited in 1991, Macraes commissioned many detailed geological, geotechnical and environmental reports on the Globe-Progress prospect (for example Barrell, 1992; Dight and Cadman, 1992; Hughes, 1992, Woodward Clyde, 1994). Macraes also assisted in helping Barry (1993) publish a detailed account of the history and resources of the Reefton Goldfield.

A2 Mining history

The gold rush on the West Coast started in 1865 when placer deposits were discovered all over the West Coast but the first placer deposits in the Reefton Goldfield were not discoverd until early 1866. Many other discoveries followed, with gold being found in almost all creeks in the Reefton area, however they were not as rich as other placer deposits on the West Coast.

By 1869 the major gold rush on the West Coast was over and the population began to decline everywhere except Reefton, where, in 1870, gold bearing quartz lodes were discovered in Murray Creek. Within a year, crushing plants were crushing the ore and by early 1873, six batteries were working in the Murray Creek and Crushington area. Further discoveries were made north of Reefton in Larry, Boatman and Caples Creeks.

In 1976, quartz lodes were discovered south of Reefton, the most important of which were on Globe Hill. Two companies, Union Company and Oriental Company, originally worked on Globe Hill. Union Company established a battery in Devils Creek in 1878, but the ore crushed was not profitable so the battery was sold to the Oriental Company, who also found their claim to be unpayable. In 1882, the Union Company restructured to form the Globe Company and developed a new orebody. They erected a battery on the

Inangahua River. In 1886, after two years of unprofitable mining, with the company on the verge of liquidation, another quartz lode was discovered on the western boundary of their claim. An adit was driven and defined an ore shoot over 200 metres long and four metres wide. The A Shaft was sunk to help develop the ore body and eventually went down to the sixth level before the ore became unprofitable.

Meanwhile, The Oriental Company was working several low grade orebodies without any success and went into liquidation just before the Globe Company found the Globe orebody. The new owner formed the Progress Company and discovered that one of the orebodies the Oriental Company decided was unpayable was actually the westward continuation of the Globe orebody. So the Progress Company drove two adits as well as an underground shaft.

During the 1880s and early 1890s, as ore reserves exhausted, many companies went into receivership because they paid out excessively high dividends and did not have any funds for future exploration and development. In 1895, David Ziman, an investor with mining experience in South Africa, visited the Reefton Goldfield, bought many of the mines and formed Consolidated Goldfields of New Zealand.

The Globe Company and the Progress Company were amalgamated to form the subsidiary Progress Mines of New Zealand. Development was increased by the sinking of the B Shaft, establishment of an aerial ropeway to transport ore and building of a new treatment plant on the Inangahua River. In 1907 the B shaft had reached the eleventh level where the orebody was seen to terminate against the Chemist Shop Fault. Further exploration could not locate the orebody anywhere else. Ore reserves eventually ran out in 1920 and the tailings were treated until 1928. After geological and geophysical experiments in the 1930s, two boreholes were sunk west of the fault zone, but no ore was found before one of the holes entered the fault zone. The Globe-Progress Mine was the second largest mine in the Reefton Goldfield with over 13 000 kg of gold extracted from ore at an average grade of 12.2 g/t.

The largest mine in the Reefton Goldfield was the Blackwater Mine at Waiuta. In 1906 Consolidated Goldfields formed Blackwater Mines Limited to mine at Waiuta. The

orebody eventually accounted for 35% of the total gold mined in the Reefton Goldfield. The mine eventually closed in 1951 after the Prohibition Shaft collapsed after reaching the seventeenth level. Over 22 000 kg of gold was produced at an average grade of 14.2 g/t. Macraes is currently evaluating reopening Blackwater Mine, as well as reexploring other prospects in the Reefton Goldfield such as Alexander Creek, Auld Creek and Merrijigs.

A complete account of the history of mining in the Reefton Goldfield may be found in Henderson (1917) and updated by Gage (1948). Latham (1984) and Barry (1993) also provide detailed historical accounts of mining in the area.

A3 Archeological value of Globe Hill

Globe-Progress was the second largest producer of gold in the Reefton Goldfield, but, because of the ease of access to the mine site, most buildings and equipment were removed after the mine closed. Therefore, the old mine site is not as large a tourist centre as other sites in the Reefton Goldfield such as Murrays Creek. There are, however, still a large number of sites on Globe Hill that are protected by the Historic Places Act, 1980.

Remnants of shafts (Figure A.1) and building sites are present on Globe Hill, but the only building left standing is a vault that was most likely used to store mine plans and papers (McGovern-Wilson, 1992). Small dams continue to dam creeks in the area and most of the entrances to adits are still standing, having not collapsed in over 100 years (Figure A.2).

Macraes presently collect and catalogue any discarded mining equipment found, and while the open pit is being excavated, any other mining equipment left in adits and other underground workings will also be saved. Macraes also propose to develop an information centre for visitors and tourists to the mine site.

Figure A1.1: Remnants of the B shaft.

Figure A1.2: The Union Adit.

Appendix B

Terminology

B1 Macraes' geotechnical and geological log descriptions

Rock mass descriptions

Code	Description
PRE	Precollar
RMU	Lengths of core with similar lithology, weathering, alteration, strength, RQD and defect type.
CRA	Information transcribed from CRA logs
SD	Specific defects that are of engineering significance
GD	General defects described in order of importance

Orientated core

Code	Description
FO	Forward orientation (down hole from mark)
BO	Back orientation (up hole from mark)
OR	Orientated
NO	Not orientated

Note: Angle measured from the orientation line. Distances to the defect are positive if measured in a clockwise sense looking down the hole and negative if measured in an anticlockwise sense facing down the hole.

Colour

Code	Colour	Code	Colour
FA	Fawn	BL	Blue
GN	Green	BLK	Black
GY	Grey	BR	Brown
OR	Orange	KH	Khaki
YE	Yellow	TN	Tan
WH	White	BU	Buff
CR	Cream	LIME	Lime green

Note: Prefix code with Lt (light), Dk (dark), Me (medium). With colour combinations, the dominant hue is the first code. Some drill logs contain colour codes classified according to a standardised rock colour chart.

Lithology

Code	Description
SS	Sandstone
ST	Siltstone
IB	Interbedded silts and sands
IS	Interbedded silts and muds
FLY	Flysch, upward fining graded bed sequence
MaSS	Distinctive sandstone unit
CLAY	Undifferentiated clays
PUG	soft blue/black clay
QT	Quartz lode
SCRE	Scree or colluvium
RUBB	Undifferentiated rubble
GRAV	Undifferentiated gravels

Code	Description
SOIL	Surface organic material
Bx	Mixed parent breccia
HBx	Host rock breccia
QBx	Quartz breccia
PBx	Pug breccia
DRVE	Mine development
STPE	Stope
FILL	Stope fill
CAVE	Caved rubble in open stope
WOOD	Woody material in stopes
LC	Lost core
NX	No exposure

Grain size

<125μ	125-250μ	250-500μ	500-1000μ	1-2mm	2-4mm	4-64mm	>64mm
VFS	FS	MS	CS	VCS	GRAN	PEBB	COBB

Note: After Folk et al, 1970.

Weathering

Code	Description
FR	Fresh
SW	Partial staining with iron oxides
MW	Pervasive staining with iron oxides
HW	Onset of chemical decomposition
EW	Reduced to clay

Note: Prefix with He (haematite), Li (limonite), Si (silica)

Alteration

Code	Description
FR	Fresh
SA	Partial bleaching or discolouration
MA	Pervasive bleaching
HA	Onset of chemical decomposition
EA	Altered to clay

Note: Prefix with Bk (black sulphide), Chl (chlorite), Se (sericite), Si (silica), Cb (carbonate).

Rock strength

Code	Aproximate UCS (MPa)	Description
S1 or EW	< 0.025	Easily moulded to a thread
S2 or EW	0.025 - 0.05	Crumbled easily
R1 or VW	1 - 5	Crumbled as a hammer
R2 or W	5 - 20	Indents with a hammer
R3 or MS	20 - 50	Fractures with a hammer
R4 or S	50 - 100	Fractures with a hard hammer blow
R5 or VS	100 - 250	Very hard to break
R6 or ES	> 250	Can only be chipped with a hammer

Rock quality designation (RQD)

$$RQD = \frac{\text{total length of pieces} < 100\text{ mm}}{\text{total length of RMU}} \ (\%)$$

Defect type

Code	Description
BD	Bedding
tCT	top contact
bCT	bottom contact
CV	Cleavage
JN	Joint
GJ	Group of joints
FT	Fault
SH	Sheared (slickensided)
VN	Vein
STZ	Shattered zone
CZ	Crushed zone (no internal fabric)

Code	Description
PT	Parting (bedding)
BX	Breccia
LI	Lineation
BK	Irregular breaks
DC	Decomposed zone
PG	Pug
SC	Schistocity
ST	Stringers
DI	Drilling induced
SZ	Sheared zone
Qvn	Quartz vein

Defect habit

Code	Description
PL	Planar
CU	Curved
UN	Undulating or wavy
ST	Stepped

Code	Description
IR	Irregular
AN	Anastomosing
BO	Boudinaged

Roughness

Code	Description
SM	Smooth
PO	Polished
RO	Rough

Code	Description
SE	Serrated
SS	Slickensided
SEGM	Segmented

Defect infilling

Code	Description
QT	Quartz
PG	Pug
CL	Clean
Su	Sulphides
Li	Limonite
He	Haematite
Cb	Carbonate
Ma	Magnesite
Sb	Antimony
Sd	Siderite
Py	Pyrite

Code	Description
RF	Rock fragments
g	Gravelly
s	Sandy
z	Silty
c	Clayey
G	Gravel
S	Sand
Z	Silt
C	Clay
mn	Minor
hp	High plasticity

Note: Fillings are listed 1, 2, 3 in order of the greatest percentage by volume.

Infilling width

Code	Description
CL	Clean
ST	Stained

Code	Description
VN	Vein
VNL	Veinlet

Note: If the width is greater than 2 mm, then record the thickness.

Defect termination (line traverses only)

Code	Description
NO	Not observed
JN	Joint
SZ	Sheared zone
BSZ	Bedding sheared zone

Code	Description
CZ	Crushed zone
BD	Bedding
DI	Dies out

Note: Where termination is of same type in both directions, a single abbreviation is used. Where two tpyes of termination are observed, the first term is the left strike termination (as viewed in the plane of traverse) or the up-dip termination.

Moisture content (line traverses only)

Description	Dry	Wet	Moist
Code	D	W	M

B2 ISRM geotechnical descriptions (ISRM, 1981)

Discontinuity orientation

- The orientation of a discontinuity in space is described by the dip of the line of steepest declination measured from the horizontal, and by the dip direction measured clockwise from true north.

Discontinuity spacing

Spacing	Description
< 20 mm	Extremely close spacing
20 - 60 mm	Very close spacing
60 - 200 mm	Close spacing
200 - 600 mm	Moderate spacing
600 - 2000 mm	Wide spacing
2000 - 6000 mm	Very wide spacing
> 6000 mm	Extremely wide spacing

Discontinuity persistence

Spacing	Description
< 1 m	Very low persistence
1 - 3 m	Low persistence
3 - 10 m	Medium persistence
10 -20 m	High persistence
> 20 m	Very high persistence

Discontinuity roughness

Class	Description		
I	Stepped	Rough (or irregular)	
II		Smooth	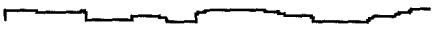
III		Slickensided	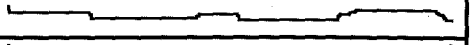
IV	Undulating	Rough	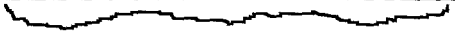
V		Smooth	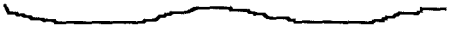
VI		Slickensided	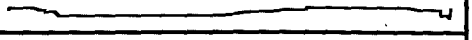
VII	Planar	Rough	
VIII		Smooth	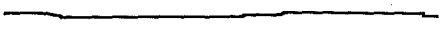
IX		Slickensided	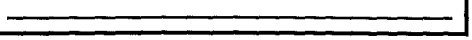

Wall strength

When describing the wall strength of a discontinuity, both the strength and weathering should be described.

Weathering grades of a rock mass

Term	Description	Grade
Fresh	No visible sign of rock material weathering: prehaps slight discolouration on major discontinuity surfaces.	I
Slightly weathered	Discolouration indicates weathering of rock material and discontinuity surfaces. All the rock material may be discoloured by weathering and be somewhat weaker externally than in its fresh condition.	II
Moderately weathered	Less thanhalf of the rock material is decomposed and/or disintergrated soil. Fresh or discoloured rock is present either as a continous framework or as corestones.	III
Highly weathered	More than half of the rock material is decomposed and/or disintergrated to a soil. Fresh or discoloured rock is present either as a discontinuous framework or as corestones.	IV
Completely weathered	All rock material is decomposed and/or disintergrated to soil. The original mass structure is still largely intact.	V
Residual soil	All rock material is converted to soil. The mass structure and material fabric are destroyed. There is a large change in volume, but the soil has not been significantly transported.	VI

Weathering grades(or alteration) of rock material

Term	Description
Fresh	No visible sign of weathering of the rock material.
Discoloured	The colour of the original fresh rock material is changed. The degree of change from the origninal colour should be indicated. If the colour change is confined to particular mineral constituents this should be mentioned.
Decomposed	The rock is weathered to the condition of a soil in which the original material fabric is still intact, but some or all of the mineral grains are decomposed.
Disintegrated	The rock is weathered to the condition of a soil in which the original fabric is still intact. The rock is friable, but the mineral grains are not decomposed.

Note: The stages of weathering may be subdivided using qualifying terms, for example "slightly discoloured", "moderately discoloured", "highly discoloured".

Strength of discontinuity walls

Grade	Description	Field identification	Approximate range of UCS values (MPa)
S1	Very soft clay	Easily penetrated several inches by fist.	< 0.025
S2	Soft clay	Easily penetrated several inches by thumb.	0.025 - 0.05
S3	Firm clay	Can be penetrated several inches by thumb with moderate effort.	0.05 - 0.10
S4	Stiff clay	Readily indented by thumb but penetrated only with great effort.	0.10 - 0.25
S5	Very stiff clay	Readily indented by thumbnail.	0.25 - 0.50
S6	Hard clay	Indented with difficulty by thumbnail.	> 0.50

Strength of discontinuity walls (continued)

Grade	Description	Field identification	Approximate range of UCS values (MPa)
R0	Extremely weak rock	Indented by thumbnail.	0.25 - 1.0
R1	Very weak rock	Crumbles under firm blows with point of geological hammer, can be peeled by a pocketknife.	1 - 5
R2	Weak rock	Can be peeled by a pocketknife with difficulty, shallow indentations made by firm blow with point of geological hammer.	5 - 25
R3	Medium strong rock	Cannot be scraped or peeled with a pocketknife, specimen can be fractured with single firm blow of a geological hammer.	25 - 50
R4	Strong rock	Specimen requires more than one blow of a geological hammer to fracture it.	50 - 100
R5	Very strong rock	Specimen requires many blows of a geological hammer to fracture it.	100 - 250
R6	Extremely strong rock	Specimen can only be chipped with geological hammer.	> 250

Note Grades S1 - S6 apply to cohesive soils, for example clays, silty clays and combinations of silts and clays with sand generally slow draining. Discontinuity wall strength will generally be characterised be grades R0 - R6 (rock) while S1 - S6 (clay) will generally apply to filled discontinuities (see Filling).
Some rounding of strength values have been made when converting to SI units.

Discontinuity aperture

Aperture	Description	
< 0.1 mm	Very tight	
0.1 - 0.25 mm	Tight	Closed fractures
0.25 - 0.5 mm	Partly open	
0.5 - 2.5 mm	Open	
2.5 - 10 mm	Moderately wide	Gapped features
> 10 mm	Wide	
1 - 10 cm	Very wide	
10 - 100 cm	Extremely wide	Open fractures
> 100 cm	Cavernous	

Discontinuity filling

The following should be described:

- width
- weathering grades
- mineralogy
- particle size
- filling strength
- previous displacement
- water content and permeability

Seepage

Unfilled discontinuities	
Seepage rate	**Description**
I	The discontinuity is very tight and dry, water flow along it does not appear possible.
II	The discontinuity is dry with no evidence of water flow.
III	The discontinuity is dry but shows evidenceof water flow such as rust, staining etc.
IV	The discontinuity is damp but no free water is present.
V	The discontinuity shows seepage, occassional drops of water, but no continuous flow.
VI	The discontinuity shows a continuous flow of water. Estimate the flow in l/min, and describe the pressure, for example, low, medium, high.

Filled discontinuities	
Seepage rate	**Description**
I	The filling materials are heavily consolidated and dry, significant flow appears unlikely due to very low permeability.
II	The filling materials are damp, but no free water is present.
III	The filling materials are wet, have occassional drops of water.
IV	The filling materials show signs of outwash, continuous flow of water. Estimate the flow in l/min.
V	The filling materials are washed out locally, considerable water flow along outwash channels. Estimate the flow in l/min and describe the pressure, foe example, low, medium, high.
VI	The filling materials are washed out completely, very high water pressures experienced, especially on first exposure. Estimate the flow in l/min and describe the pressure, foe example, low, medium, high.

Rock mass (for example tunnel wall)	
Seepage rate	**Description**
I	Dry walls and roof, no detectable seepage.
II	Minor seepage, specify dripping discontinuities.
III	Medium inflow, specify discontinuities with continous flow. Estimate the flow in l/min per 10m length of excavation.
IV	Major inflow, specify discontinuities with strong flows. Estimate the flow in l/min per 10m length of excavation.
V	Exceptionally high inflow, specify source of exceptional flows. Estimate the flow in l/min per 10m length of excavation.

Number of discontinuity sets

Class	Description
I	Massive, occasional random joints
II	One joint set
III	One joint sets plus random joints
IV	Two joint sets
V	Two joint sets plus random joints
VI	Three joint sets
VII	Three joint sets plus random joints
VIII	Four or more joint sets
IX	Crushed rock, earthlike

Block size and shape

Size

Description	J_v (joints/m^3)
Very large blocks	< 1
Large blocks	1 - 3
Medium sized blocks	3 - 10
Small blocks	10 - 30
Very small blocks	> 30

Note: values of $J_v > 60$ would represent crushed rock, typical of a clay free crushed zone.

Shape

Shape	Description
Massive	Few joints or very wide spacing.
Blocky	Approximately equidimensional.
Tabular	One dimension considerably smaller than the other two.
Columnar	One dimension considerably larger than the other two.
Irregular	Wide variations of block size and shape.
Crushed	Heavily jointed to "sugar cube".

B3 MacGregor *et al's* (1994) rippability parameter descriptions

1. Rock type

Rating	Description
1	Claystone
2	Mudstone
3	Shaly mudstone
4	Siltstone
5	Shale
6	Interbedded sandstone/mudstone
7	Interbedded sandstone/siltstone
8	Interbedded sandstone/shale
9	Silty sandstone
10	Sandstone
11	Pebbly sandstone
12	Metasiltstone
13	Phyllite
14	Metasandstone
15	Gneiss
16	Porphyry
17	Microsyenite
18	Dacite
19	Granite

2. Grain size

2.1: Sedimentary

Description	Grain diameter	Rating
Boulders	200 - 600 mm	7
Cobbles	60 - 200 mm	7
Coarse gravel	20 - 60 mm	7
Medium gravel	6 - 20 mm	6
Fine gravel	2 - 6 mm	5
Coarse sand	0.6 - 2 mm	4
Medium sand	0.2 - 0.6 mm	3
Fine sand	0.06 - 0.2 mm	2
Silt, clay	< 0.06 mm	1

2.2: Igneous

Description	Grain diameter	Rating
Very coarse	> 30 mm	7
Coarse	5 - 30 mm	5
Medium	1 - 5 mm	3
Fine	< 1 mm	1
Glassy	0 mm	1

3. Rock weathering

3.1: Sedimentary (based on Australian Geomechanics Society, 1975)

Term	Symbol	Description
Extremely weathered	EW	Rock substance affected by weathering to the extent that the rock exhibits soil properties, that is, it can be remoulded and can be classified according to the Unified Classification System, but the texture of the original rock is still evident.
Highly weathered	HW	Rock substance affected by weathering to the extent that limonite staining or bleaching affects the whole of the rock substance and other signs of chemical of physical decomposition are evident. Porosity and strength may be increased or decreased compared to the fresh rock usually as a result of iron leaching or deposition. The colour and strength of the original fresh rock substance is no longer recognisable.
Moderately weathered	MW	Rock substance affected by weathering to the extent that staining extends throughout the rock substance and the original colour of the fresh rock is no longer recognisable.
Slightly weathered	SW	Rock substance affected by weathering to the extent that partial staining and discolouration of the rock substance usually by limonite has taken place. The colour and texture of the fresh rock are recognisable.
Fresh	FR	Rock substance unaffected by weathering.

3.2: Igneous and metamorphic (based on Moye, 1955)

Term	Symbol	Description
Extremely weathered rock	EW	Rock that retains most of the original rock texture (fabric) but the bond between its mineral constituents is weakened by chemical weathering to the extent that the rock will disintergrate when immersed and gently shaken in water. In engineering usage this is a soil.
Highly weathered rock	HW	Rock that is weakened by chemical weathering to the extent that dry pieces about the size of a 50 mm diameter drill core can be broken by hand across the rock fabric. Highly weathered rock does not readily disintergrate when immersed in water.
Moderately weathered rock	MW	Rock that exhibits considerable evidence of chemical weathering, such as discolouration and loss of strength but that has sufficent remaining strength to prevent dry pieces about the size of 50 mm diameter drill core (of inherently hard rock) being broken by hand across the rock fabric. Moderately weathered rock does not ring when struck with a hammer.
Slightly weathered rock	SW	Rock that exhibits some evidence of chemical weathering, such as discolouration, but has suffered little reduction in strength. Except for some inherently soft rocks, slighly weathered rock rings when struck with a hammer.
Fresh with limonite stained joints	FRSt	Joint faces coated or stained with limonite but the blocks between joints are unweathered.
Fresh	FR	Rock that exhibits no evidence of chemical weathering. Joint faces may be clean or coated with clay, calcite, chlorite or other minerals.

Note: The degrees of rock weathering may be gradational. Intermediate stages are described by dual symbols with the predominant degree of weathering first, for example, EWHW.

3.3: Substance weathering rating

Rating	Description
1	Fresh
3	Fresh with stained joints
3	Slightly weathered to fresh
4	Slightly weathered
5	Moderate to/and slightly weathered
6	Moderately weathered
7	Highly to moderately weathered
8	Highly weathered
9	Highly to extremely weathered
10	Extremely weathered

Note: The rating only applies to the rock substance, not the joints or weathering adjacent to joints.

4. Unconfined compressive strength

The best estimate of the unconfined compresive strength of the rock mass in a ripped area taken primarily from UCS tests on ripped material, but also from estimates of UCS from other tests like the point load test, and also in some cases from information given in the geotechnical investigation reports for the each area. The UCS value given is the in situ moisture condition result rather than the result of tests on saturated samples (in MPa).

5. Structural description

Rating	Rocks with bedding		Rocks without bedding		
	Bedding	Defects	Joint set 1	Joint set 2	Joint set 3
1	Massive	Very wide	Very wide	Very wide	Very wide
2	Massive	Wide-very wide			
3	Massive-thick	Wide-very wide	Wide	Very wide	Very wide
4	Thick	Wide-very wide	Wide	Wide	Very wide
6	Thick	Wide	Wide	Wide	Wide
7	Thick, but weakness parallel to bedding	Wide-very wide			
8	Medium-thick	Wide-very wide	Medium	Wide	Wide
9	Medium-thick	Medium-wide	Medium	Medium	Wide
11	Medium	Medium-wide	Medium	Medium	Medium
12	Medium A	Medium-wide			
13	Medium B	Medium-wide			
14	Medium C	Medium-wide	Close	Medium	Medium
15	Thin-Medium	Close-wide			
16	Thin	Close-wide	Close	Close	Medium
17	Laminated	Close-wide			
18	Thin	Close	Close	Close	Close
19	Soil		Soil		

Bedding		Joints	
Massive	> 2 m	Very wide	> 2 m
Thick	0.6 m - 2 m	Wide	0.6 m - 2 m
Medium	200 mm - 0.6 m	Medium	200 mm - 0.6 m
Medium A (interbedded sst and cong)	200 mm - 0.6 m	Close	60 mm - 200 mm
Medium B (interbedded sst and shale	200 mm - 0.6 m	Very close	< 60 mm
Medium C (interbedded sst)	200 mm - 0.6 m		
Thin	60 mm - 200 mm		
Laminated or very thin	< 60 mm		

6. Number of defect sets

The number of defect sets including bedding.

7. Defect dip angle

Maximum angle of dip of the defect plane from horizontal (in degrees).

8. Defect dip direction

Direction of maximum angle of dip of the defect plane, perpendicular to the direction of strike (in degrees).

9. Defect persistence length

Observed length of defect across exposure (in metres).

10. Defect spacing

Spacing of the dominant defect set (in millimetres).

11. Defect wall strength

Rating	Description	UCS (MPa)
1	Very strong	< 240
2	Strong to very strong	
3	Strong	< 70
4	Medium strong to strong	
5	Medium strong	< 24
6	Weak to medium strong	
7	Weak	< 7
8	Very weak to weak	
9	Very weak	<2.4
10	Extremely weak to very weak	
11	Extremely weak	< 0.7

12. Initial block volume

Product of the mean dimensions of the intial blocks (in cubic metres).

13. Defect roughness

Rating	Description	
1	Smooth	A/L = < 0.05
2	Medium	A/L = 0.05 - 0.10
3	Rough	A/L = 0.10 - 0.15
4	Very rough	A/L = > 0.15

Note: A/L is the ratio of amplitude to length.

14. Defect aperture width

Average width of defect apertures (in mm).

15. Field seismic velocity

Seismic refraction velocity obtained before excavation at the site begins (in ms^{-1}).

16. Relative orientation of ripping

The smallest angle between the direction of the ripping runs and the direction of the dip of the dominent defect in the area (in degrees).

17. Cover thickness

Average thickness of loose material over the undisturbed rock to be ripped in an area (in metres).

18. Ease of ripping

Ease of ripping is a subjective assessment by the observer.

Rating	Description
1	Very easy
2	Easy
3	Easy to medium
4	Medium
5	Medium to difficult
6	Difficult
7	Very difficult

19. Bulldozer mass

Mass of operating bulldozer, including tine and full fuel tank (tonnes).

20. Ripper boot condition

Rating	Description
1	Good
2	Acceptable
3	Worn to acceptable
4	Worn
5	Broken

21. Bulldozer tracks condition

Rating	Description
1	Good
2	Acceptable
3	Worn to acceptable
4	Worn

22. Bulldozer movement restrictions

Rating	Description
1	No restrictions
2	Width < 50 m
3	Width < 20 m
4	Width < 10 m
5	Length < 50 m, width < 20 m
6	Length < 50 m, width < 10 m
7	Length < 20 m, width < 20 m
8	Length < 20 m, width < 10 m

23. Operator

Identification of bulldozer operator

24. Number of runs

Number of ripping runs recorded for each calculation of productivity in an area.

25. Minimum run productivity

The lowest value of the intact run productivities calculated for an area, calculated by assessing productivity for individual runs in an area.

26. Area intact productivity

The sum of all the products of the intact run area and run length, divided by the sum of all the run times in the area.

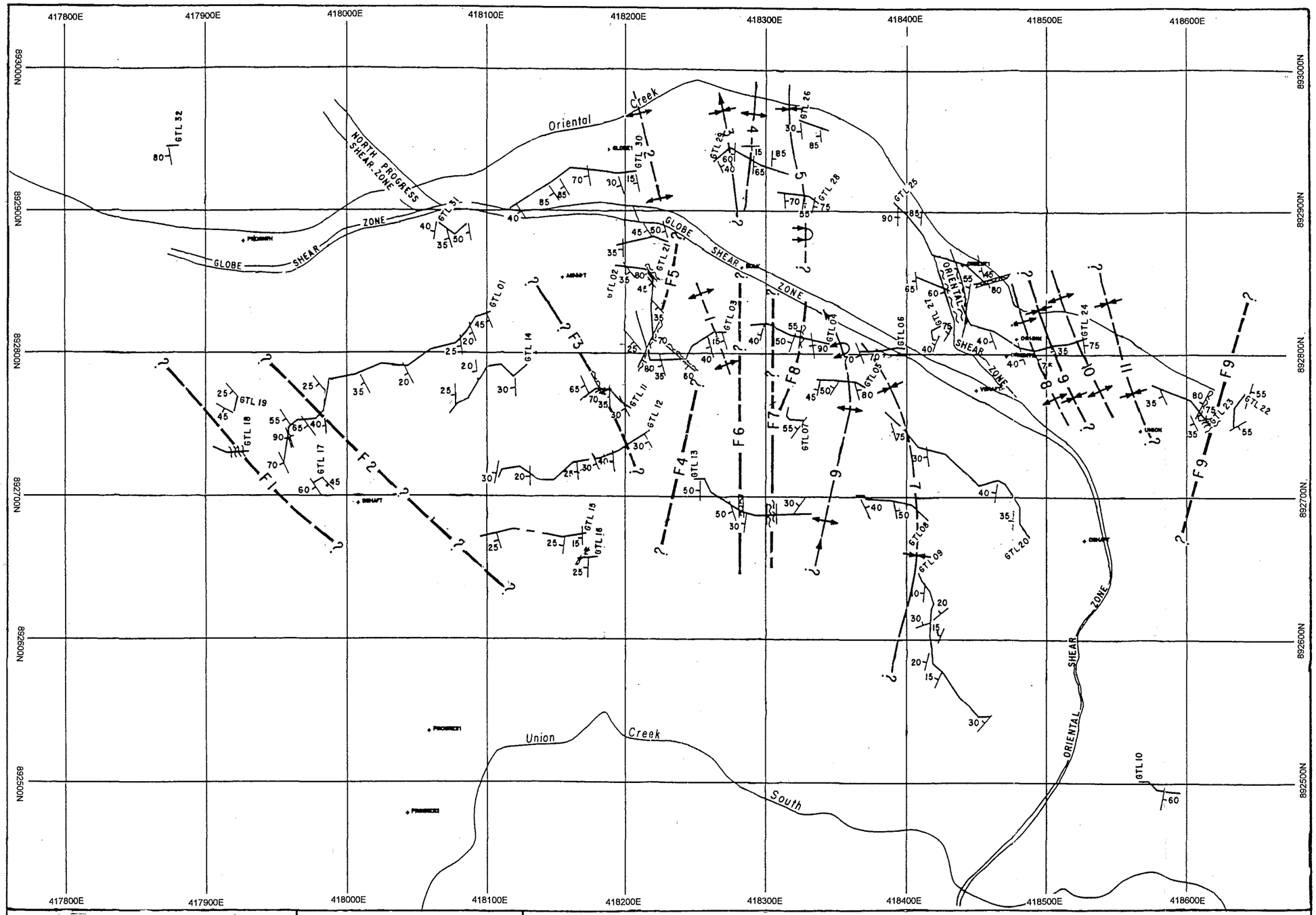

Figure C1

Barrell's structural geology map

(modified from Barrell, 1992)

N
W E
S

0 50 100 m

Scale: 1:3000

KEY

- Bedding Attitude
- Sheared Zone Attitude
- Sheared Rock, Attitude Unknown
- Faults (Identified Numerically): known / inferred
- Fold Axes (Identified Numerically): known / inferred
- Syncline
- Anticline
- Upright
- I Limb Overturned

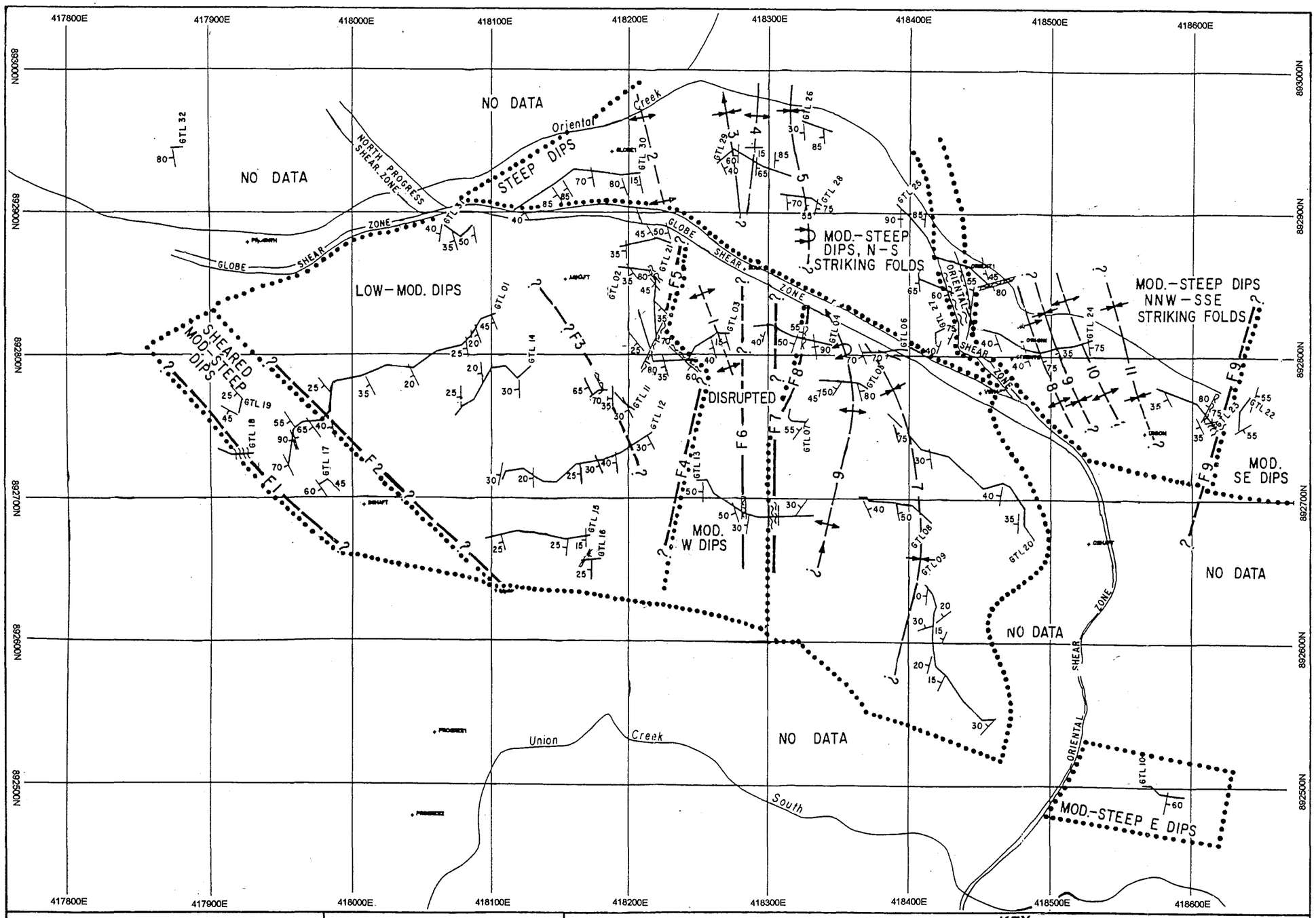

Figure C2

Barrell's structural domain map

(modified from Barrell, 1992)

Appendix D

Field and laboratory testing results

D1 List of symbols and abbreviations

D1.1 Generalised Reciprocal Method terminology

Symbol	Description	Unit
T_f	Forward travel time	ms
T_r	Reverse travel time	ms
T_d	Time-depth function	ms
T_{cf}	Corrected forward travel time	ms
T_{cr}	Corrected reverse travel time	ms
V_1	Velocity of refracted seismic wave	ms^{-1}
DCF	Depth correction factor	ms^{-1}
D_r	Radial depth	m
GRL	Ground reduced level	m

D1.2 Laboratory testing terminology

Symbol	Description	Unit
L	Averaged core sample length	mm
D	Averaged core sample diameter	mm
A	Area of core sample end	mm^2
V	Volume of core sample	mm^3
V_v	Void volume of core sample	mm^3
M_{sat}	Saturated mass of core sample	kg
M_{dry}	Dry mass of core sample	kg
ρ_{sat}	Saturated density of core sample	kgm^{-3}
ρ_{dry}	Dry density of core sample	kgm^{-3}
n	Porosity of core sample	%
P_{sat}	Saturated P wave time	μs
P_{dry}	Dry P wave time	μs
S_{sat}	Saturated S wave time	μs
S_{dry}	Dry S wave time	μs
$v_{P\,(sat)}$	Saturated P wave velocity	ms^{-1}
$v_{P\,(dry)}$	Dry P wave velocity	ms^{-1}
$v_{S\,(sat)}$	Saturated S wave velocity	ms^{-1}
$v_{S\,(dry)}$	Dry S wave velocity	ms^{-1}
$E_{dyn\,(sat)}$	Saturated dynamic Young's Modulus	GPa
$E_{dyn\,(dry)}$	Dry dynamic Young's Modulus	GPa
$\nu_{dyn\,(sat)}$	Saturated dynamic Poisson's Ratio	-
$\nu_{dyn\,(dry)}$	Dry dynamic Poisson's Ratio	-
P	Compressive load	kN
σ_c	Uniaxial compressive strength	MPa
$E_{s\,(50)}$	Young's Modulus (secant method)	GPa
$E_{t\,(50)}$	Young's Modulus (tangential method)	GPa
E_{ave}	Young's Modulus (average method)	GPa

D2 Seismic refraction survey data

D2.1 The Generalised Reciprocal Method

D2.1.1 Introduction

The Generalised reciprocal method (GRM) is the interpretation method most commonly used on seismic refraction data. It is a variation of the reciprocal method developed from Hawkins (1961) after earlier work by Edge and Laby (1931) and Urquhart (1956). The reciprocal method uses the reciprocal time (travel time) between two geophones to find the seismic velocity of the rock mass below the geophones. The GRM involves combining the reciprocal time with forward and reverse travel times to more accurately define the time to the refractor.

The reciprocal method assumes a planar refractor between the forward and reverse seismic waves, therefore refractor irregularities are smoothed out (Palmer, 1980), whereas the GRM uses an XY distance (distance between two shot points) that may be adjusted to produce a more detailed refractor (Hatherly and Neville, 1986). Both methods are insensitive to dip angles up to 20° (Palmer, 1980) unlike other methods such as the delay time method and the intercept time method that require planar refractors with dips less than 5° (Palmer 1980).

For the seismic line traverses surveyed, the optimum XY distance was not calculated as it is not always possible to calculate it when the refractor is less than 20m deep because of factors such as irregular topography, variable near-surface layers and inhomogeneous rock mass (Hatherly and Neville, 1986). Instead, a zero XY spacing has been used and makes the GRM similar to the Reciprocal Method of Hawkins (1961), which Palmer (1980) shows to be a special case of the GRM.

D2.1.2 Data processing

Forward and reverse travel times are plotted against the shot points as time-distance curves. These plots give the apparent seismic velocities of the refractor and are shown in Figures D2.1 - D2.24 as uncorrected travel time graphs. From these plots, the initial velocity (V_0) is calculated from the first few travel times recorded, which are direct arrivals and represent the velocity of the upper layer. Using the total forward and reverse times, an average reciprocal time maybe calculated by the expression:

$$T_R = \frac{(T_{f\,total} + T_{r\,total})}{2} \qquad (s)$$

where T_R is the reciprocal time, $T_{f\,total}$ is the total forward time and $T_{r\,total}$ is the total reverse time. Using the reciprocal time and forward and reverse times at each shot point, the depth to the refractor in units of time is calculated by:

$$T_d = \frac{(T_f + T_r - T_R)}{2} \qquad (s)$$

where T_f is the forward travel time, T_r is the reverse travel time and T_d is the time-depth. The time-depth is subtracted from the forward and reverse travel times at each shot point to give the corrected forward and reverse travel times:

$$\begin{aligned} T_f - T_d &= T_{cf} \\ T_r - T_d &= T_{cr} \end{aligned} \qquad (s)$$

where T_{cf} is the corrected forward travel time and T_{cr} is the corrected reverse travel time. The corrected travel times represent the travel time to a point on the refractor below each shot position. The corrected forward and reverse travel times are plotted with respect to the shot position so that true seismic velocities may be calculated. These plots are shown in Appendix D2.2. Using the initial seismic velocity and seismic velocity of the refractor, a depth conversion factor (DCF) is calculated from the expression:

$$DCF = \frac{V_0 V_1}{(V_1^2 - V_0^2)^{1/2}} \qquad (ms^{-1})$$

The DCF is multiplied by the time-depth to give a radial depth (D_r) to the refractor. The GRL (ground reduced level) and radial depths for each shot point may be plotted to show a cross section of the survey line.

D2.2 Processed Data

Definition of terms used in the data tables:

Position	Location of hammer site from geophone 1 (m)
T_f	Forward travel time (ms)
T_r	Reverse travel time (ms)
T_d	Time-depth (ms)
T_{cf}	Corrected forward travel time (ms)
T_{cr}	Corrected reverse travel time (ms)
V_1	Velocity of refracted wave (ms^{-1})
DCF	Depth correction factor (ms^{-1})
D_r	Radial depth (m)
GRL	Ground reduced level (m)

Table D2.1: Seismic Refraction Line 1.1-1.2

Position (m)	T_f (ms)	T_r (ms)	T_d (ms)	T_{cf} (ms)	T_{cr} (ms)	V_1 (ms^{-1})	DCF (ms^{-1})	D_r (m)	GRL (m)
0	0.56	22.80				820			450.79
0.5	1.24					820			450.76
1	1.92					820			450.73
1.5	2.60					820			450.69
2	3.80	22.00				820			450.65
2.5	4.20					820			450.60
3	4.60					820			450.56
4	5.44	20.60	1.77	3.67	18.83	1923	907	1.60	450.46
6	7.80	19.60	2.45	5.35	17.15	1923	907	2.22	450.25
8	9.00	19.20	2.85	6.15	16.35	1923	907	2.58	450.10
10	12.30	19.60	4.70	7.60	14.90	1923	907	4.26	449.84
12	14.90	20.20	6.30	8.60	13.90	1923	907	5.71	449.52
14	17.30	22.00	8.40	8.90	13.60	1923	907	7.62	449.19
16	19.20	21.00	8.85	10.35	12.15	1923	597	5.28	448.89
18	19.80	20.40	8.85	10.95	11.55	1923	597	5.28	448.63
20	20.80	16.00	7.15	13.65	8.85	740	894	6.39	448.40
22	21.20	15.40	7.05	14.15	8.35	4000	576	4.06	448.20
24	22.40	11.60	5.75	16.65	5.85	800	812	4.67	448.03
26	20.60	7.20	2.65	17.95	4.55	1538	614	1.63	447.85
27		5.80				588			447.76
27.5		4.96				588			447.71
28	21.00	3.58				588			447.66
28.5		2.80				588			447.61
29		1.92				588			447.53
29.5		1.12				588			447.49
30	22.20	0.40				588			447.44

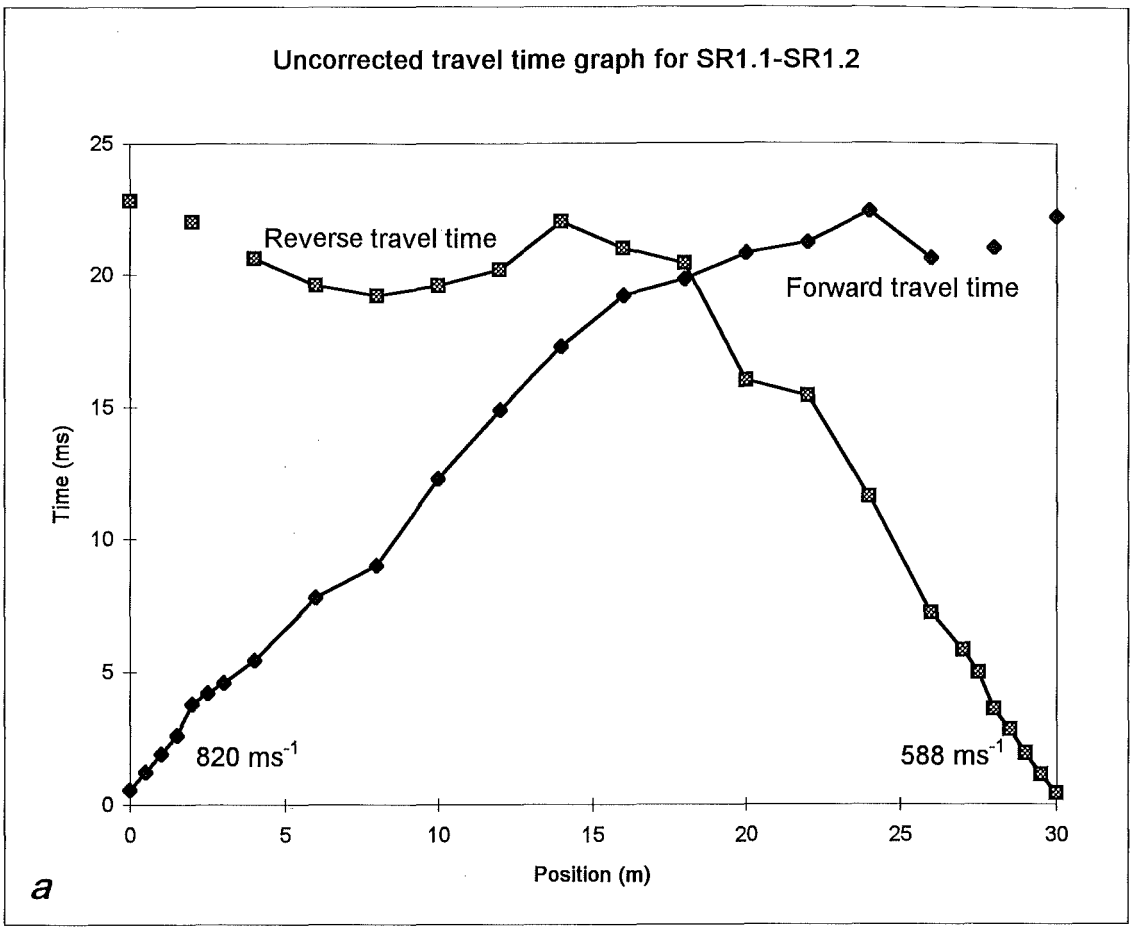

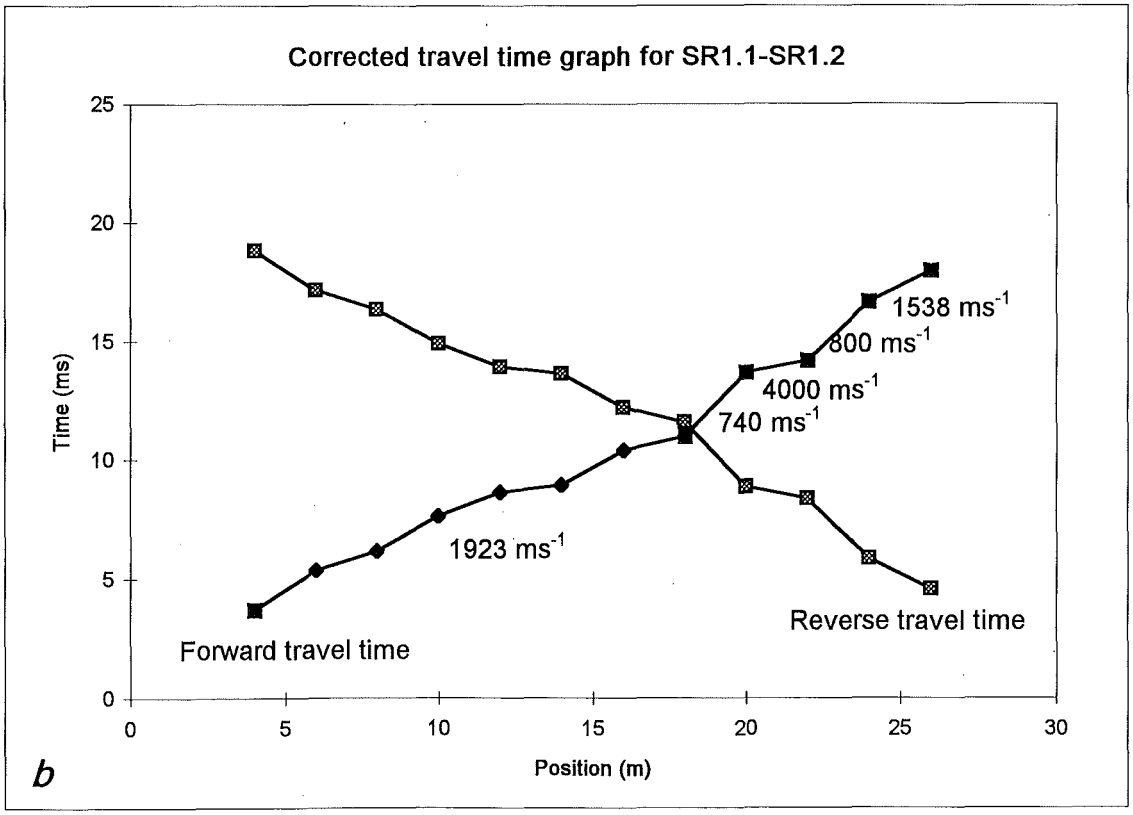

Figure D2.1: Uncorrected (*a*) and corrected (*b*) travel time graphs.

Table D2.2: Seismic Refraction Line 1.2-1.3

Position (m)	T_f (ms)	T_r (ms)	T_d (ms)	T_{cf} (ms)	T_{cr} (ms)	V_1 (ms^{-1})	DCF (ms^{-1})	D_r (m)	GRL (m)
0	0.20	73.20				634			447.44
0.5	1.20					634			447.40
1	1.88					634			447.36
1.5	2.84					634			447.29
2	3.52					634			447.24
2.5	3.88					634			447.21
3	5.24	70.80				634			447.17
4	6.50					634			447.08
6	10.10	69.20	1.75	8.35	67.45	769	849	1.49	446.92
9	15.40	68.40	4.00	11.40	64.40	769	849	3.40	446.68
12	18.90	62.40	2.75	16.15	59.65	769	849	2.34	446.37
15	20.40	59.60	2.10	18.30	57.50	1519	615	1.29	446.00
18	20.80	56.40	0.70	20.10	55.70	1519	615	0.43	445.67
21	21.20	55.60	0.50	20.70	55.10	2704	583	0.29	445.37
24	22.80	55.60	1.30	21.50	54.30	2704	583	0.76	445.06
27	24.40	54.80	1.70	22.70	53.10	2704	583	0.99	444.84
30	26.80	54.40	2.70	24.10	51.70	2704	583	1.57	444.67
33	28.00	54.00	3.10	24.90	50.90	2704	583	1.81	444.45
36	29.80	53.20	3.60	26.20	49.60	2704	583	2.10	444.09
39	31.00	52.40	3.80	27.20	48.60	2704	583	2.22	443.84
42	33.20	52.00	4.70	28.50	47.30	2704	583	2.74	443.55
45	36.40	50.40	5.50	30.90	44.90	2704	583	3.21	443.26
48	36.80	48.80	4.90	31.90	43.90	2704	583	2.86	443.07
51	35.20	46.40	2.90	32.30	43.50	2704	583	1.69	442.83
54	55.20	24.00	1.70	53.50	22.30	142			442.57
57	56.00	23.60	1.90	54.10	21.70	2069	593	1.13	442.40
60	56.40	21.20	0.90	55.50	20.30	2069	593	0.53	442.15
63	57.60	20.80	1.30	56.30	19.50	2069	593	0.77	441.79
66	62.40	20.40	3.50	58.90	16.90	2069	593	2.08	441.41
69	64.00	19.80	4.00	60.00	15.80	2069	593	2.37	441.08
72	65.60	18.60	4.20	61.40	14.40	2069	593	2.49	440.73
75	69.20	16.50	4.95	64.25	11.55	2069	593	2.94	440.35
77		11.60				490			440.22
78	72.80	9.80				490			440.14
78.5		8.30				490			440.10
79		7.72				490			440.07
79.5		6.36				490			440.03
80		2.80				490			440.00
80.5		1.44				490			439.96
81	78.40	0.76				490			439.94

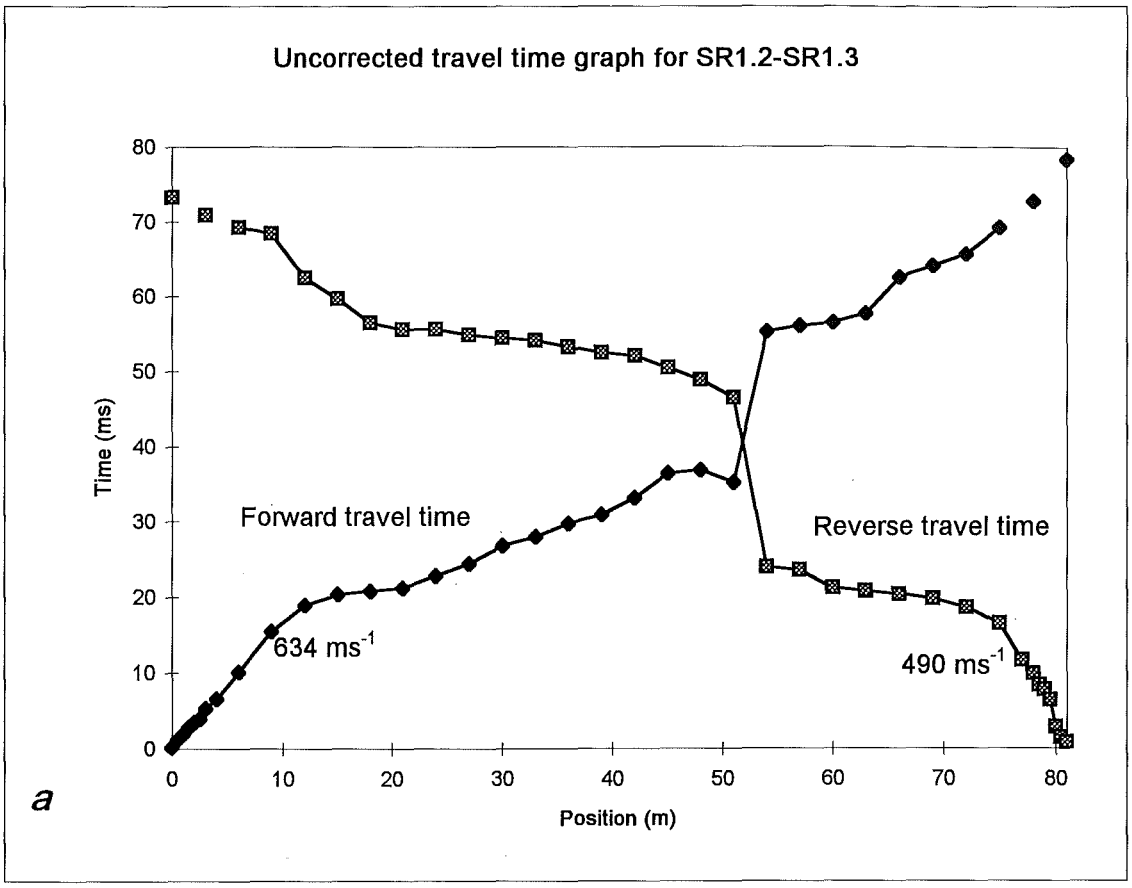

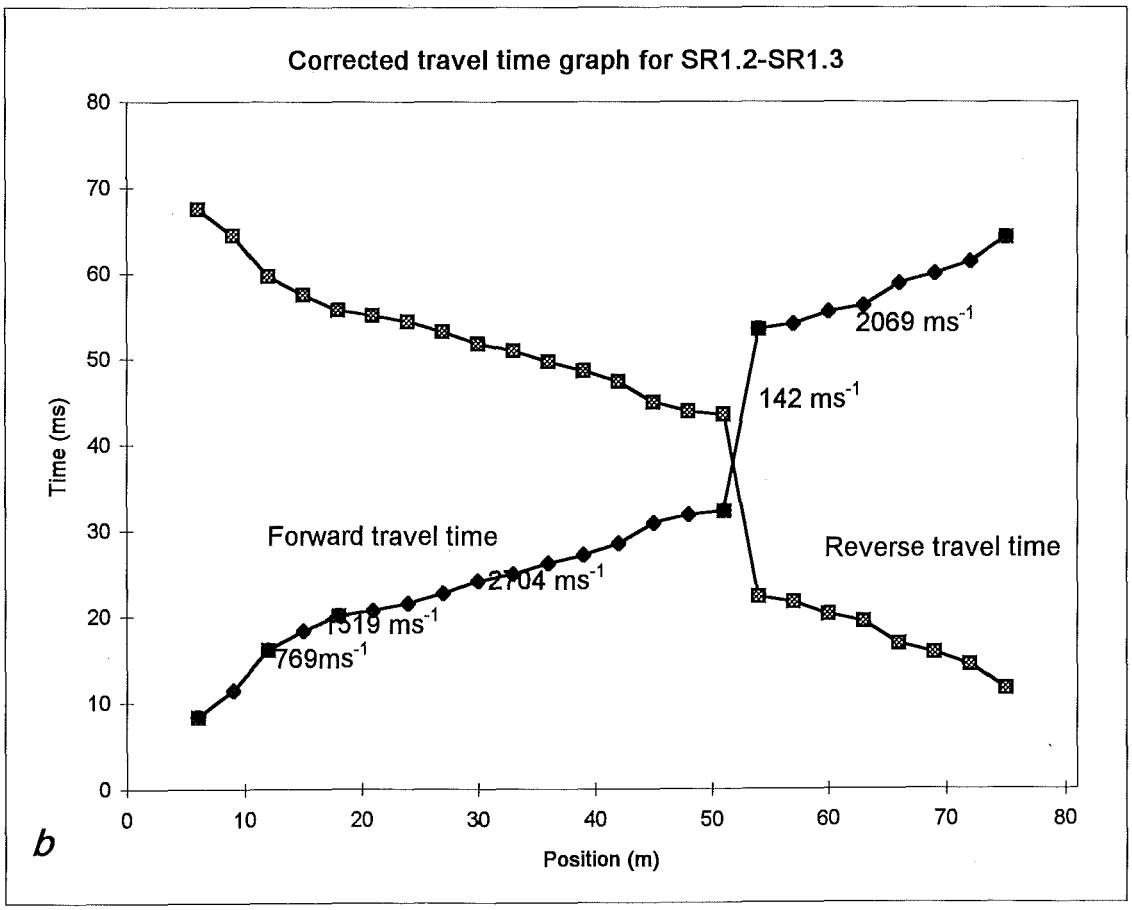

Figure D2.2: Uncorrected (*a*) and corrected (*b*) travel time graphs.

Table D2.3: Seismic Refraction Line 2.1-2.2

Position (m)	T_f (ms)	T_r (ms)	T_d (ms)	T_{cf} (ms)	T_{cr} (ms)	V_1 (ms^{-1})	DCF (ms^{-1})	D_r (m)	GRL (m)
0	0.76	14.00				1071			443.78
0.5	1.16					1071			443.77
1	1.68					1071			443.77
1.5	2.04					1071			443.76
2	2.16	13.20				1071			443.76
2.5	2.82					1071			443.72
3	3.56					1071			443.70
4	4.00	11.80	0.83	3.18	10.98	2462	1223	1.01	443.69
6	4.80	11.20	0.93	3.88	10.28	2462	1223	1.13	443.58
8	5.80	9.40	0.52	5.28	8.88	2462	1223	0.64	443.52
10	6.90	8.80	0.78	6.13	8.03	2462	1223	0.95	443.38
12	7.60	8.20	0.82	6.78	7.38	2462	1223	1.01	443.26
14	9.20	8.10	1.58	7.63	6.53	2462	1223	1.93	443.18
16	9.90	8.00	1.88	8.03	6.13	2462	1223	2.29	443.18
18	11.10	8.00	2.48	8.63	5.53	2462	1223	3.03	443.21
20	13.20	8.00	3.53	9.68	4.48	2462	1223	4.31	443.14
22	13.20	7.80	3.43	9.78	4.38	5536	1117	3.83	443.06
24	13.40	7.50	3.38	10.03	4.13	5536	1117	3.77	442.98
26	13.30	6.60	2.88	10.43	3.73	5536	1117	3.21	442.89
28	12.90	5.50	2.13	10.78	3.38	5536	1117	2.37	442.74
30	12.80	4.80	1.73	11.08	3.08	5536	1117	1.93	442.60
32	13.40	3.90	1.58	11.83	2.33	5536	1117	1.76	442.54
34	13.80	3.52	1.59	12.22	1.94	5536	1117	1.77	442.51
36	14.30	3.32	1.74	12.57	1.59	5536	1117	1.94	442.46
37		2.96				1119			442.47
37.5		2.68				1119			442.45
38	14.70	2.48				1119			442.44
38.5		1.90				1119			442.43
39		1.42				1119			442.42
39.5		0.78				1119			442.41
40	14.30	0.28				1119			442.35

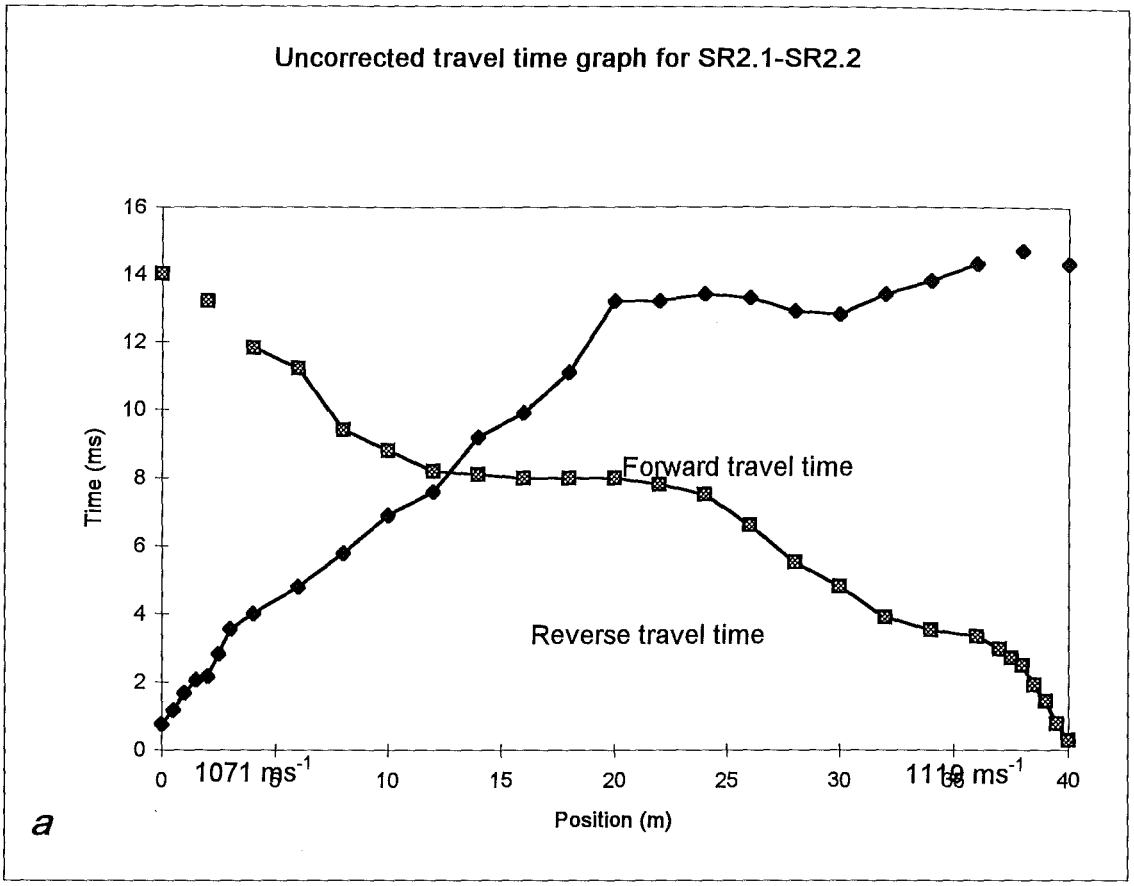

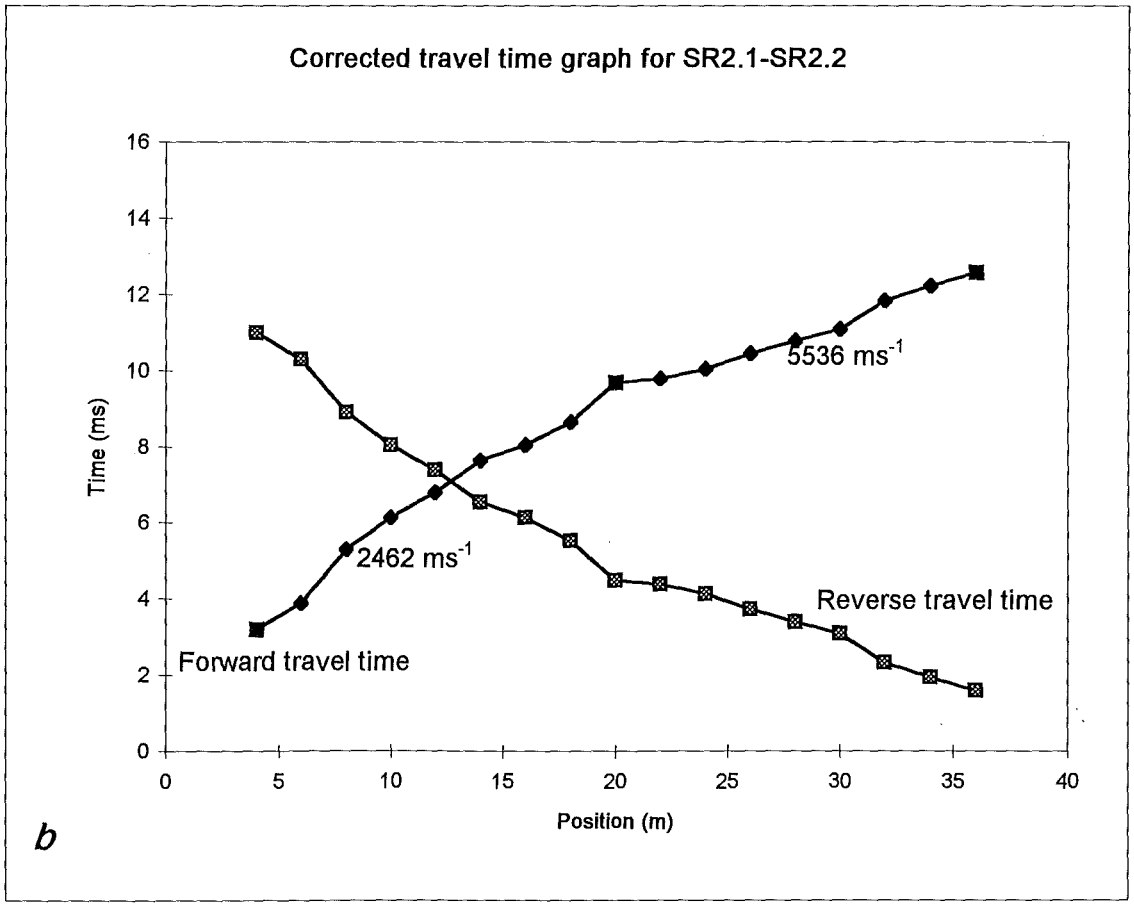

Figure D2.3: Uncorrected (*a*) and corrected (*b*) travel time graphs.

Table D2.4: Seismic Refraction Line 2.2-2.3

Position (m)	T_f (ms)	T_r (ms)	T_d (ms)	T_{cf} (ms)	T_{cr} (ms)	V_1 (ms^{-1})	DCF (ms^{-1})	D_r (m)	GRL (m)
0	0.40	9.40				1315			442.35
0.5	0.80					1315			442.35
1	1.18	8.60				1315			442.34
1.5	1.52					1315			442.34
2	1.88					1315			442.33
2.5	1.88					1315			442.30
3	2.68	8.00	0.39	2.29	7.61	5051	1630	0.64	442.29
5	2.72	7.90	0.36	2.49	7.54	5051	1630	0.59	442.29
7	3.88	7.50	0.74	3.14	6.76	5051	1630	1.21	442.37
9	4.00	6.70	0.40	3.60	6.30	5051	1630	0.65	442.46
11	4.84	6.52	0.73	4.11	5.79	5051	1630	1.19	442.58
13	6.52	7.88	2.25	4.27	5.63	5051	1630	3.67	442.71
15	9.20	7.00	3.15	6.05	3.85	1124	544	1.72	442.92
17	9.30	6.00	2.70	6.60	3.30	3636	495	1.34	443.15
17.5		5.30				490			443.24
18		5.24				490			443.30
18.5		3.20				490			443.35
19	10.50	1.72				490			443.40
19.5		0.76				490			443.45
20	10.40	0.20				490			443.49

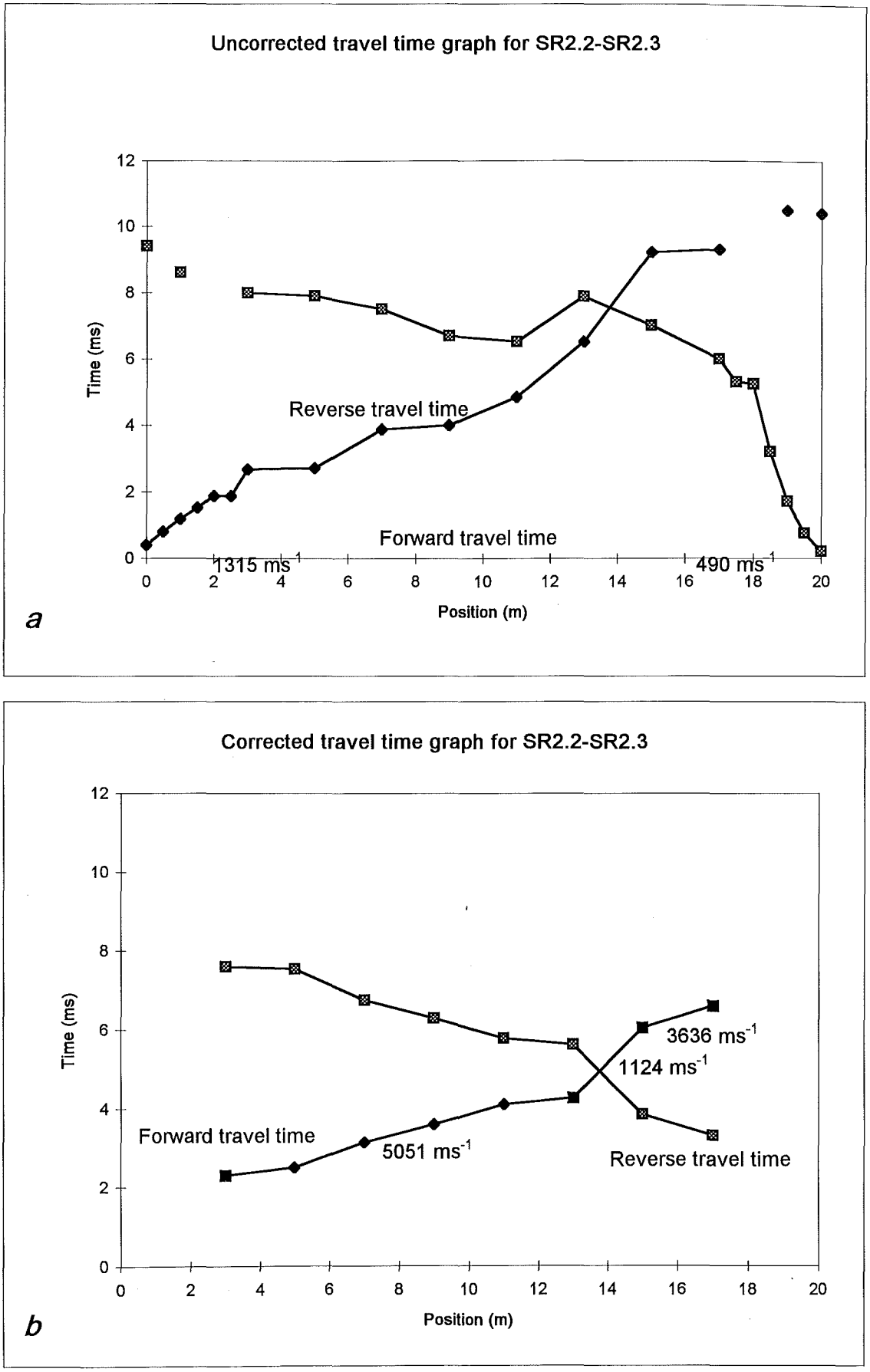

Figure D2.4: Uncorrected (*a*) and corrected (*b*) travel time graphs.

Table D2.5: Seismic Refraction Line 3.1-3.2

Position (m)	T_f (ms)	T_r (ms)	T_d (ms)	T_{cf} (ms)	T_{cr} (ms)	V_1 (ms^{-1})	DCF (ms^{-1})	D_r (m)	GRL (m)
0	0.36	20.00				769			531.00
0.5	3.56					769			530.99
1	5.60					769			530.99
1.5	6.90					769			530.98
2	7.50	19.80				769			530.97
2.5	7.80					769			530.97
3	8.20					769			530.95
4	8.40	18.10	3.33	5.08	14.78	1509	786	2.61	530.93
6	9.40	16.40	2.98	6.43	13.43	1509	786	2.34	530.80
8	9.80	14.20	2.08	7.73	12.13	1509	786	1.63	530.61
10	10.10	13.80	2.03	8.08	11.78	6667	701	1.42	530.55
12	10.50	13.60	2.13	8.38	11.48	6667	701	1.49	530.54
14	10.80	13.40	2.18	8.63	11.23	6667	701	1.52	530.53
16	11.70	12.50	2.18	9.53	10.33	2264	733	1.59	530.53
18	13.10	12.20	2.73	10.38	9.48	2264	733	2.00	530.63
20	14.20	11.50	2.93	11.28	8.58	2264	733	2.14	530.70
22	15.50	10.00	2.83	12.68	7.18	1481	790	2.23	530.81
24	16.80	8.90	2.93	13.88	5.98	1481	790	2.31	530.99
26	17.80	7.00	2.48	15.33	4.53	1481	790	1.96	531.18
27		5.32				625			531.28
27.5		4.72				625			531.34
28	18.70	3.44				625			531.41
28.5		2.90				625			531.48
29		2.40				625			531.53
29.5		1.68				625			531.58
30	19.70	0.60				625			531.66

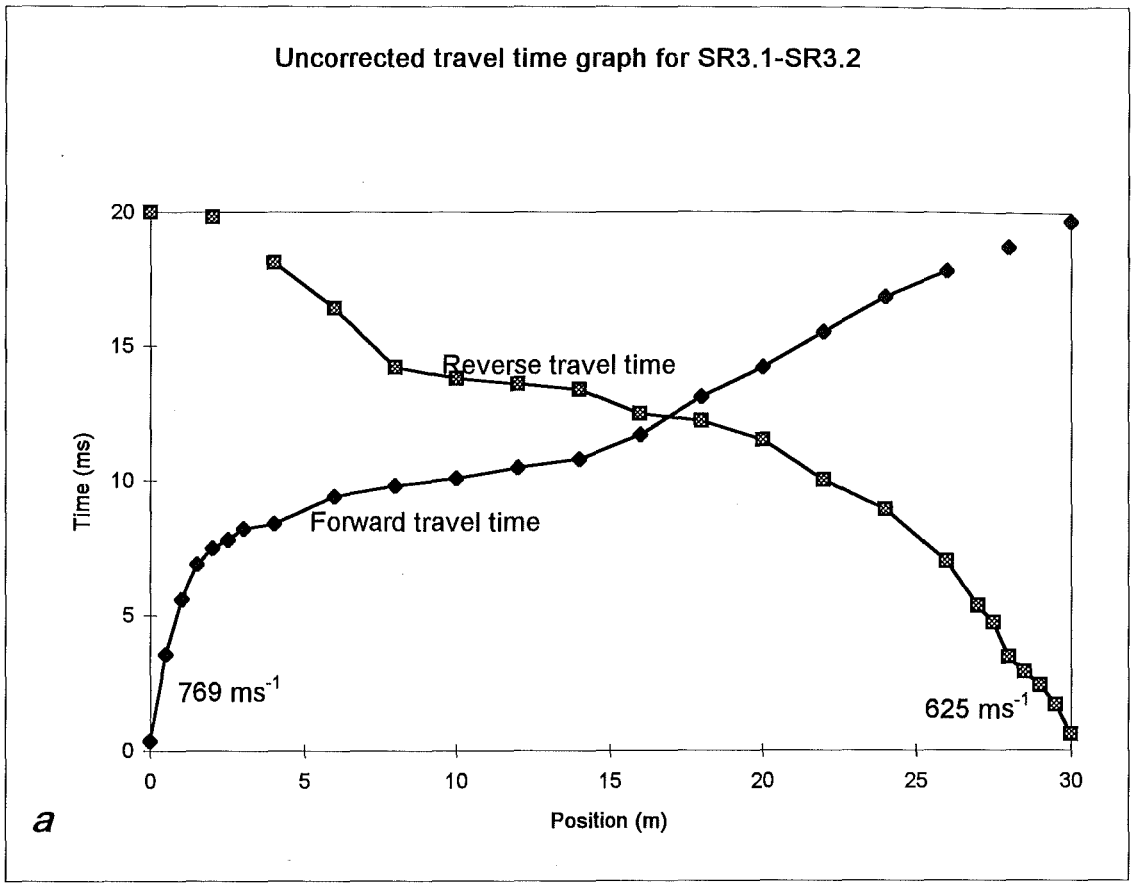

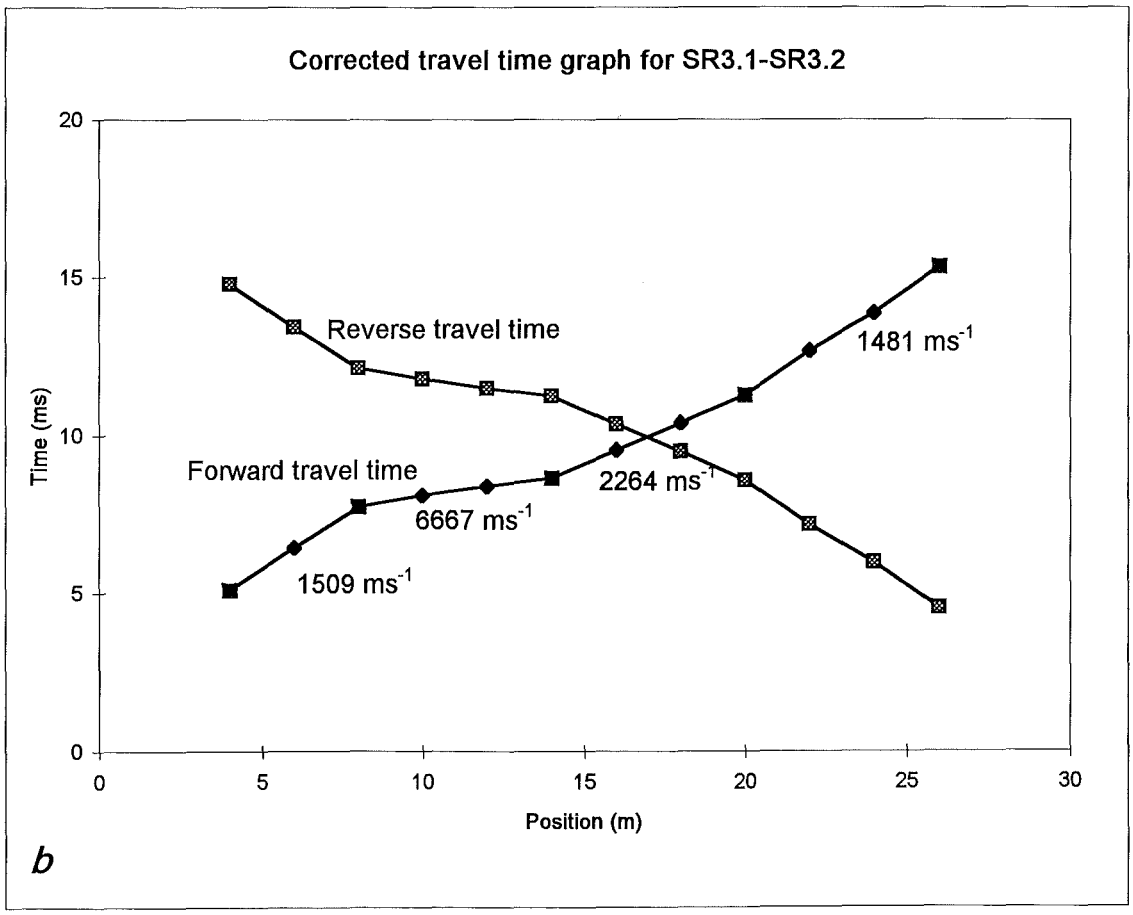

Figure D2.5: Uncorrected (a) and corrected (b) travel time graphs for SR3.1-SR3.2.

Table D2.6: Seismic Refraction Line 4.1-4.2

Position (m)	T_f (ms)	T_r (ms)	T_d (ms)	T_{cf} (ms)	T_{cr} (ms)	V_1 (ms^{-1})	DCF (ms^{-1})	D_r (m)	GRL (m)
0	0.44	23.40				901			502.01
0.5	0.68					901			501.99
1	1.16					901			501.96
1.5	2.32					901			501.93
2	3.00	22.20				901			501.90
2.5	3.16					901			501.88
3	3.92					901			501.87
4	4.88	22.20	1.29	3.59	20.91	1163	1425	1.84	501.86
6	7.76	21.20	2.23	5.53	18.97	1163	1425	3.18	501.85
8	10.10	21.80	3.70	6.40	18.10	1163	479	1.77	501.85
10	14.00	21.00	5.25	8.75	15.75	1163	479	2.52	501.88
12	15.20	20.00	5.35	9.85	14.65	1391	467	2.50	501.87
14	17.20	19.20	5.95	11.25	13.25	1391	467	2.78	501.85
16	19.70	18.10	6.65	13.05	11.45	1391	467	3.11	501.85
18	20.00	15.50	5.50	14.50	10.00	1391	467	2.57	501.85
20	19.80	13.90	4.60	15.20	9.30	2222	452	2.08	501.89
22	19.40	12.30	3.60	15.80	8.70	2222	452	1.63	501.95
24	21.50	12.20	4.60	16.90	7.60	2222	452	2.08	502.00
26	21.80	10.10	3.70	18.10	6.40	2222	452	1.67	502.02
27		8.00				443			501.99
27.5		6.60				443			501.98
28	23.20	5.32				443			501.97
28.5		3.92				443			501.96
29		2.88				443			501.96
29.5		1.68				443			501.96
30	25.60	1.08				443			501.96

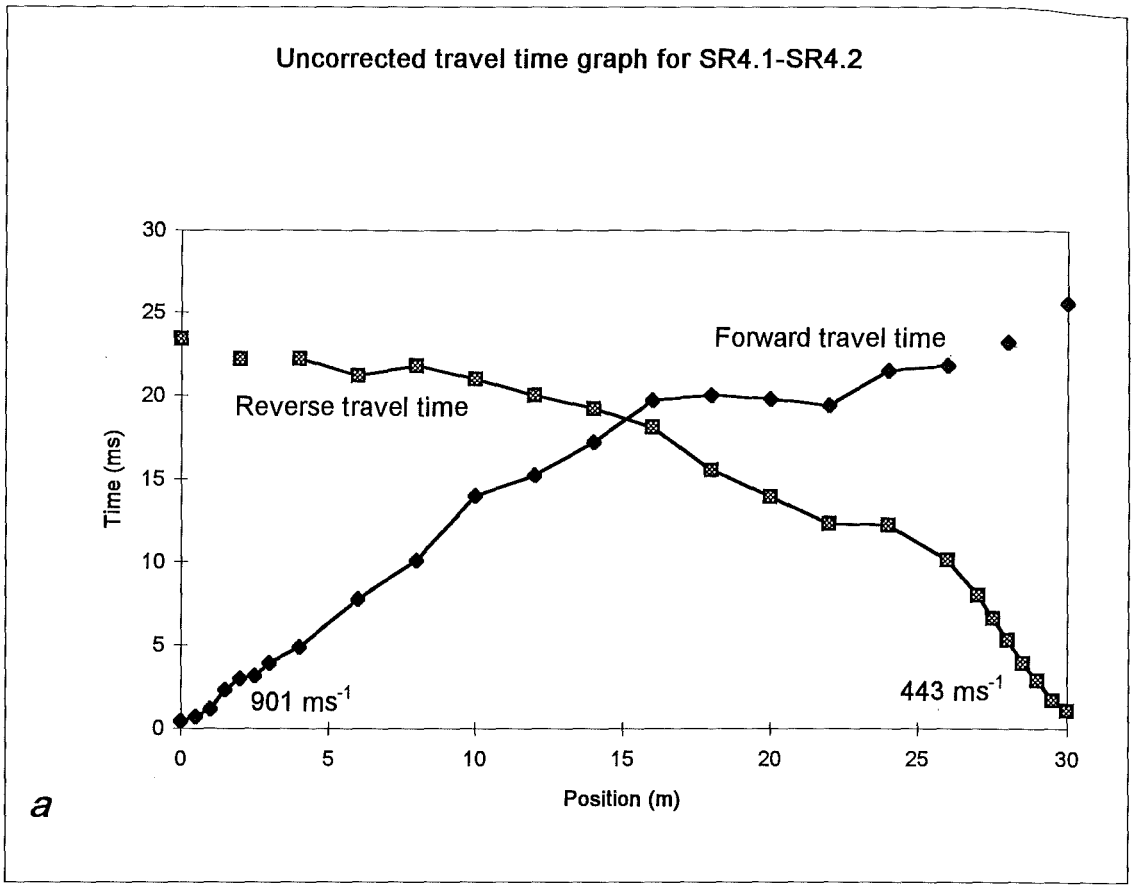

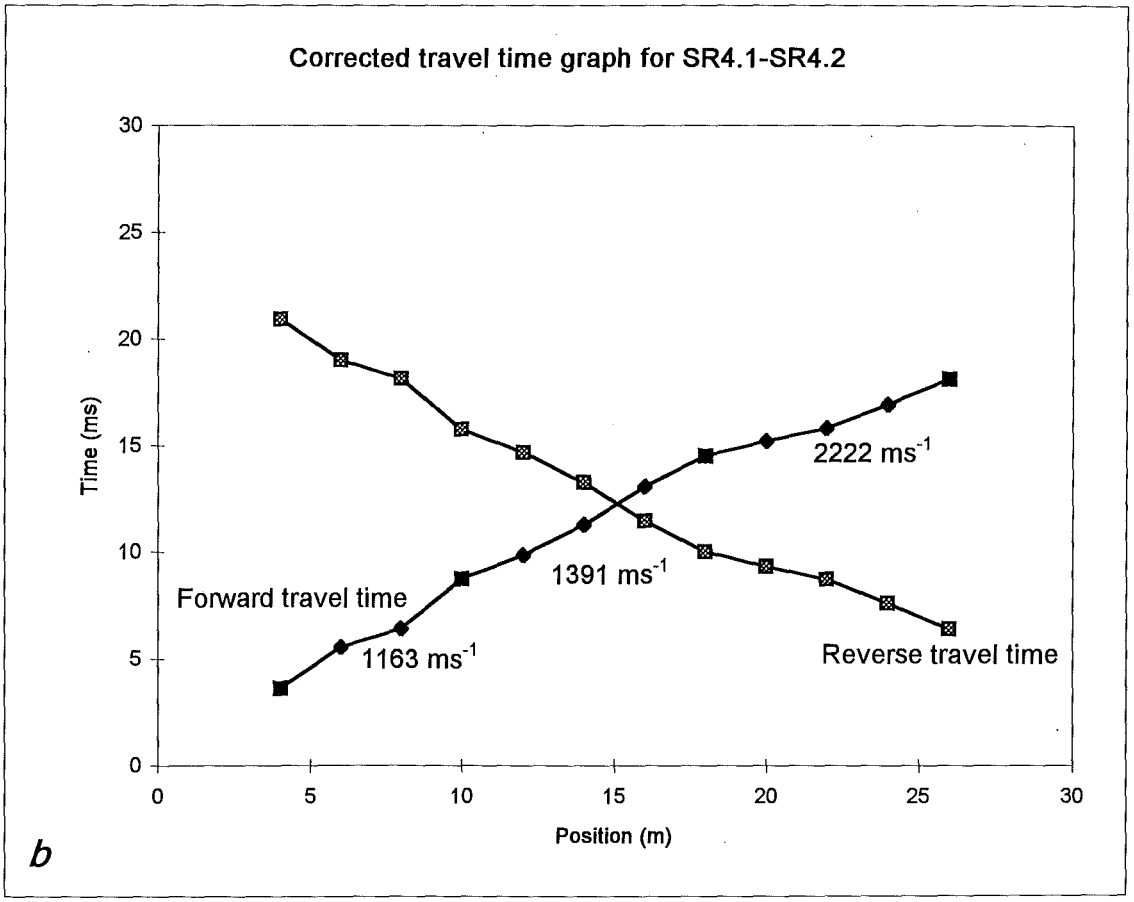

Figure D2.6: Uncorrected (*a*) and corrected (*b*) travel time graphs.

Table D2.7: Seismic Refraction Line SR5.1-SR5.2

Position (m)	T_f (ms)	T_r (ms)	T_d (ms)	T_{cf} (ms)	T_{cr} (ms)	V_1 (ms^{-1})	DCF (ms^{-1})	D_r (m)	GRL (m)
0	0.16	32.80				709			515.67
0.5	0.88					709			515.67
1	2.36					709			515.69
1.5	3.08					709			515.72
2	3.96	30.80				709			515.76
2.5	4.60					709			515.79
3	5.00					709			515.82
4	5.80	31.00	1.50	4.30	29.50	1556	778	1.17	515.88
6	8.40	29.40	2.00	6.40	27.40	1556	778	1.56	515.97
8	10.00	28.00	2.10	7.90	25.90	1556	778	1.63	515.89
10	11.40	27.00	2.30	9.10	24.70	1556	778	1.79	516.00
12	12.40	26.60	2.60	9.80	24.00	1556	778	2.02	516.21
14	15.00	27.00	4.10	10.90	22.90	1556	778	3.19	516.45
16	17.60	26.80	5.30	12.30	21.50	1556	778	4.12	516.76
18	18.60	25.80	5.30	13.30	20.50	1556	778	4.12	517.02
20	21.40	24.80	6.20	15.20	18.60	1154	873	5.41	517.19
22	23.00	22.60	5.90	17.10	16.70	1154	873	5.15	517.39
24	23.80	20.60	5.30	18.50	15.30	1154	873	4.62	517.43
26	24.40	20.20	5.40	19.00	14.80	3636	709	3.83	517.46
28	24.00	18.80	4.50	19.50	14.30	3636	709	3.19	517.49
30	23.40	17.80	3.70	19.70	14.10	3636	709	2.62	517.51
32	23.80	16.50	3.25	20.55	13.25	3636	709	2.30	517.56
34	24.00	15.30	2.75	21.25	12.55	3636	709	1.95	517.58
36	24.60	12.30	1.55	23.05	10.75	1083	908	1.41	517.52
38	26.20	9.50	0.95	25.25	8.55	1083	908	0.86	517.51
40	27.80	6.96	0.48	27.32	6.48	1083	908	0.44	517.50
42	28.80	5.32	0.16	28.64	5.16	1083	908	0.15	517.54
43		5.00				682			517.56
43.5		4.68				682			517.58
44	30.60	3.88				682			517.62
44.5		3.12				682			517.69
45		2.68				682			517.76
45.5		1.44				682			517.83
46	34.80	0.60				682			517.83

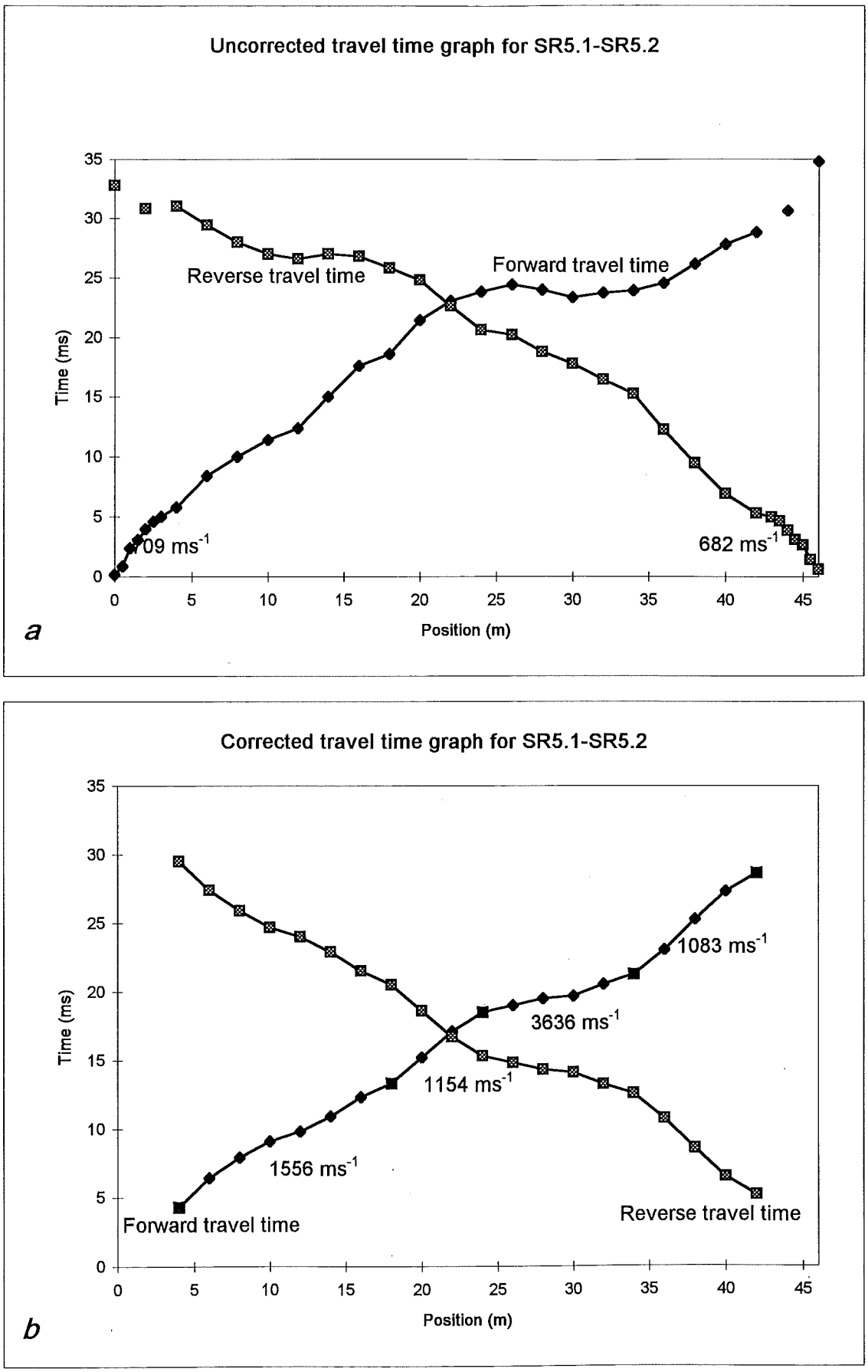

Figure D2.7: Uncorrected (**a**) and corrected (**b**) travel time graphs.

Table D2.8: Seismic Refraction Line SR5.2-SR5.3

Position (m)	T_f (ms)	T_r (ms)	T_d (ms)	T_{cf} (ms)	T_{cr} (ms)	V_1 (ms^{-1})	DCF (ms^{-1})	D_r (m)	GRL (m)
0	1.04	34.80				858			517.83
1	2.68					858			517.98
2	3.88	33.40				858			517.97
3	4.80					858			518.09
4	5.70	32.80	1.95	3.75	30.85	2182	933	1.82	518.19
6	7.70	32.60	2.85	4.85	29.75	2182	933	2.66	518.39
8	9.20	31.60	3.10	6.10	28.50	2182	933	2.89	518.65
10	12.10	32.40	4.95	7.15	27.45	2182	933	4.62	518.91
12	13.60	32.60	5.80	7.80	26.80	2182	933	5.41	519.11
14	14.70	33.00	6.55	8.15	26.45	2182	933	6.11	519.28
16	15.60	31.20	6.10	9.50	25.10	2182	933	5.69	519.44
18	15.00	29.40	4.90	10.10	24.50	2182	933	4.57	519.56
20	15.20	28.80	4.70	10.50	24.10	2182	933	4.39	519.65
22	17.00	27.60	5.00	12.00	22.60	2182	933	4.67	519.74
24	17.40	27.40	5.10	12.30	22.30	6000	867	4.42	519.83
26	17.60	27.40	5.20	12.40	22.20	6000	867	4.51	519.78
28	18.20	26.80	5.20	13.00	21.60	6000	867	4.51	519.71
30	18.40	24.60	4.20	14.20	20.40	1875	965	4.05	519.67
32	20.20	24.00	4.80	15.40	19.20	1875	965	4.63	519.66
34	22.00	24.20	5.80	16.20	18.40	1875	965	5.60	519.72
36	22.00	23.60	5.50	16.50	18.10	6000	867	4.77	519.76
38	21.80	22.60	4.90	16.90	17.70	6000	867	4.25	519.76
40	21.60	21.80	4.40	17.20	17.40	6000	867	3.81	519.88
42	24.00	22.20	5.80	18.20	16.40	2105	411	2.38	520.00
44	23.60	19.40	4.20	19.40	15.20	2105	411	1.72	520.07
46	23.60	17.40	3.20	20.40	14.20	2105	411	1.31	520.15
48	25.40	17.80	4.30	21.10	13.50	2105	411	1.77	520.23
50	26.60	17.20	4.60	22.00	12.60	2105	411	1.89	520.31
52	26.40	16.30	4.05	22.35	12.25	2105	411	1.66	520.41
54	27.40	15.50	4.15	23.25	11.35	2105	411	1.70	520.60
56	28.20	15.30	4.45	23.75	10.85	2105	411	1.83	520.84
58	29.20	13.80	4.20	25.00	9.60	2105	411	1.72	521.06
60	30.00	12.50	3.95	26.05	8.55	2105	411	1.62	521.21
62	31.20	11.30	3.95	27.25	7.35	2105	411	1.62	521.37
64	32.40	10.70	4.25	28.15	6.45	2105	411	1.75	521.50
66	33.80	9.50	4.35	29.45	5.15	2105	411	1.79	521.57
68	34.80	8.60	4.40	30.40	4.20	2105	411	1.81	521.72
70	34.80	6.50	3.35	31.45	3.15	2105	411	1.38	521.75
71		5.90				403			521.79
72	34.40	5.00				403			521.85
73		3.00				403			521.90
74	34.40	0.04				403			521.93

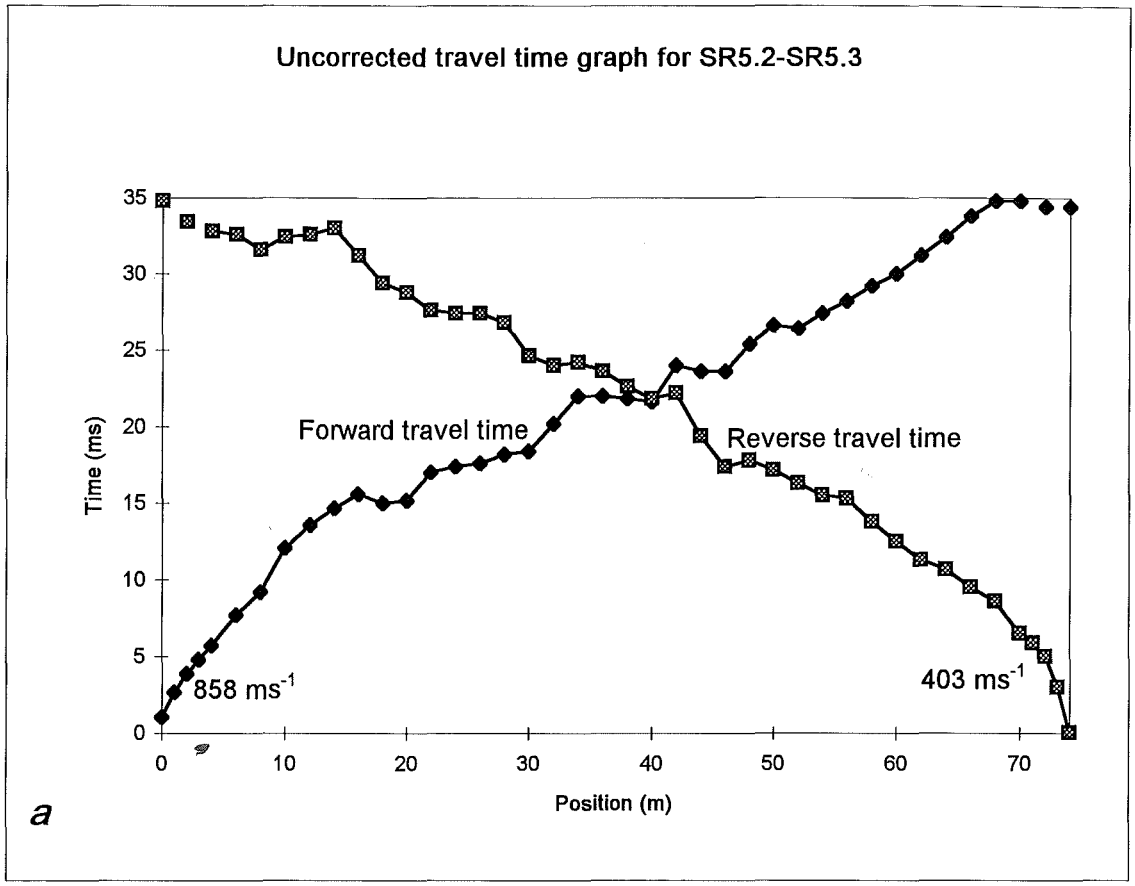

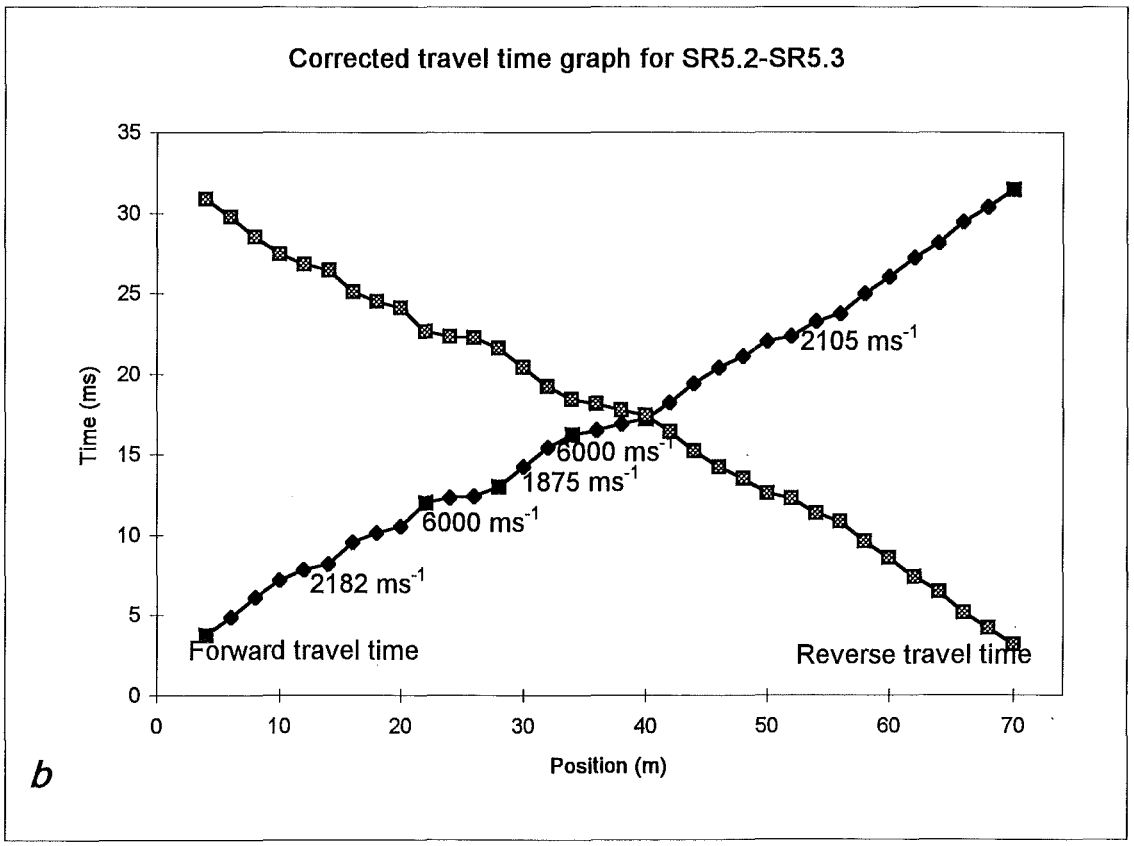

Figure D2.8: Uncorrected (a) and corrected (b) travel time graphs for SR5.2-SR5.3.

Table D2.9: Seismic Refraction Line SR6.1-SR6.2

Position (m)	T_f (ms)	T_r (ms)	T_d (ms)	T_{cf} (ms)	T_{cr} (ms)	V_1 (ms^{-1})	DCF (ms^{-1})	D_r (m)	GRL (m)
0	0.44	24.80				442			506.34
0.5	1.52					442			506.28
1	2.92					442			506.21
1.5	3.96					442			506.15
2	4.96	23.60				442			506.08
2.5	6.32					442			506.02
3	8.30					442			505.97
4	9.50	21.00	2.45	7.05	18.55	1633	618	1.51	505.86
6	11.20	20.00	2.80	8.40	17.20	1633	618	1.73	505.74
8	13.10	19.70	3.60	9.50	16.10	1633	618	2.22	505.71
10	15.40	17.60	3.70	11.70	13.90	1034	697	2.58	505.52
12	18.00	16.70	4.55	13.45	12.15	1034	697	3.17	505.34
14	19.60	14.60	4.30	15.30	10.30	1034	697	3.00	505.18
16	20.00	13.90	4.15	15.85	9.75	3636	585	2.43	505.01
18	22.00	12.10	4.25	17.75	7.85	1053	691	2.94	504.78
20	22.40	11.30	4.05	18.35	7.25	3333	587	2.38	504.61
22	24.80	9.10	4.15	20.65	4.95	870	773	3.21	504.43
24	25.00	8.20	3.80	21.20	4.40	3636	585	2.22	504.28
26	25.20	5.96	2.78	22.42	3.18	1639	618	1.72	504.12
27		4.88				714			504.03
27.5		4.16				714			503.99
28	25.80	3.16				714			503.96
28.5		3.10				714			503.94
29		2.20				714			503.91
29.5		1.80				714			503.84
30	26.40	0.36				714			503.81

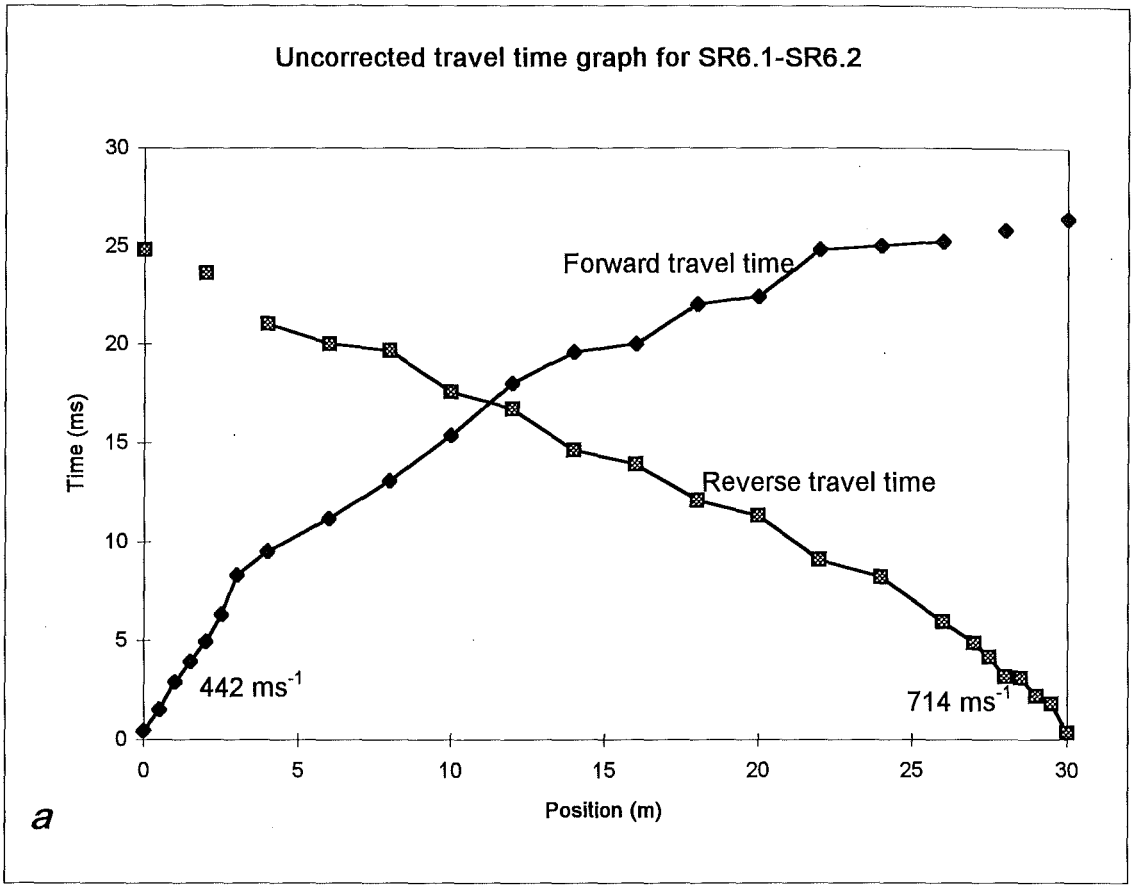

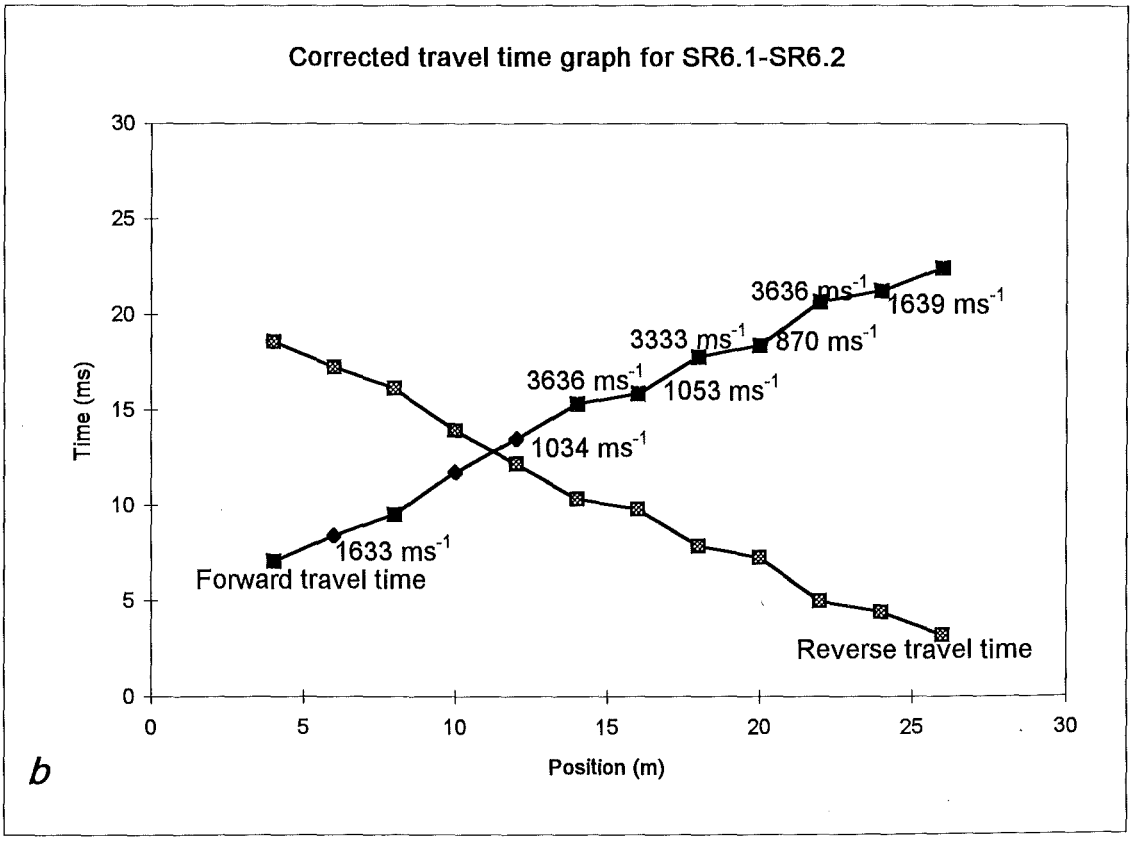

Figure D2.9: Uncorrected (a) and corrected (b) travel time graphs.

Table D2.10: Seismic Refraction Line SR7.1-SR7.2

Position (m)	T_f (ms)	T_r (ms)	T_d (ms)	T_{cf} (ms)	T_{cr} (ms)	V_1 (ms^{-1})	DCF (ms^{-1})	D_r (m)	GRL (m)
0	0.48	26.80				374			546.25
0.5	1.48					374			546.23
1	2.36					374			546.22
1.5	3.80					374			546.21
2	5.20	24.20				374			546.21
2.5	6.60					374			546.28
3	8.50					374			546.28
4	10.60	24.60	4.30	6.30	20.30	1000	403	1.73	546.29
6	13.50	24.20	5.55	7.95	18.65	1000	403	2.24	546.37
8	17.40	23.80	7.30	10.10	16.50	1000	790	5.77	546.29
10	16.40	18.40	4.10	12.30	14.30	1000	790	3.24	545.99
12	15.00	16.20	2.30	12.70	13.90	4444	626	1.44	545.66
14	15.60	15.80	2.40	13.20	13.40	4444	626	1.50	545.26
16	17.80	15.60	3.40	14.40	12.20	1875	657	2.23	545.08
18	18.80	14.10	3.15	15.65	10.95	1875	657	2.07	544.84
20	20.20	14.00	3.80	16.40	10.20	1875	657	2.50	544.83
22	20.20	9.80	1.70	18.50	8.10	1200	724	1.23	544.93
24	21.20	6.80	0.70	20.50	6.10	1200	724	0.51	545.1
26	21.80	5.60	0.40	21.40	5.20	1200	724	0.29	545.2
27		5.20				620			545.23
27.5		4.30				620			545.26
28	23.40	3.50				620			545.29
28.5		2.44				620			545.33
29		1.84				620			545.39
29.5		1.16				620			545.44
30	26.40	0.36				620			545.52

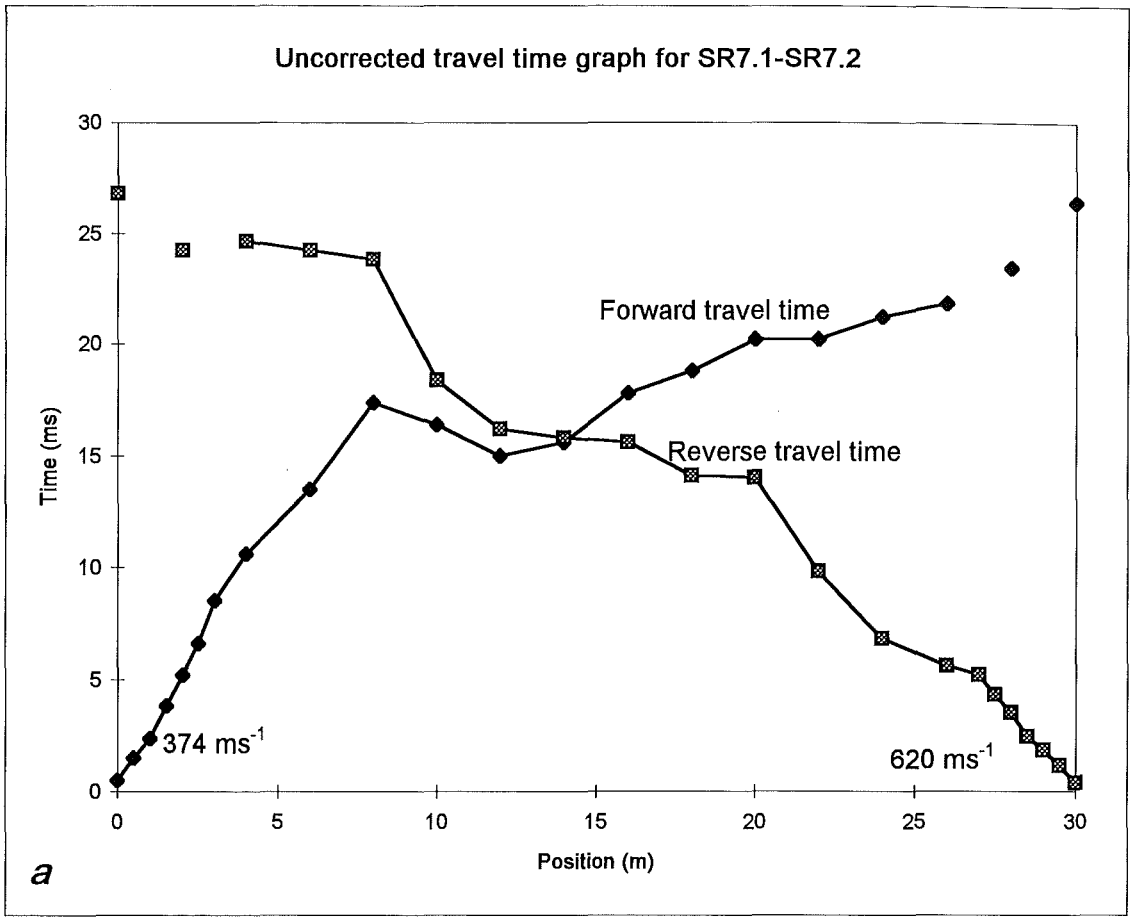

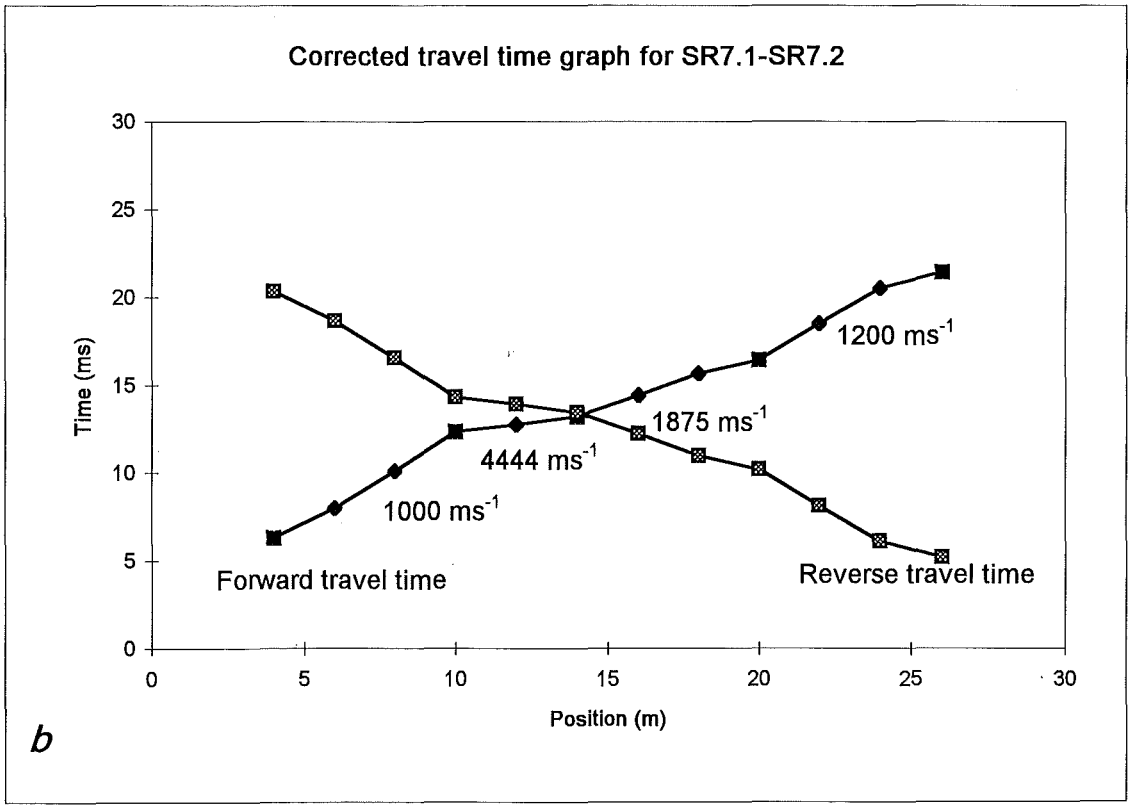

Figure D2.10: Uncorrected (*a*) and corrected (*b*) travel time graphs.

Table D2.11: Seismic Refraction Line SR8.1-SR8.2

Position (m)	T_f (ms)	T_r (ms)	T_d (ms)	T_{cf} (ms)	T_{cr} (ms)	V_1 (ms^{-1})	DCF (ms^{-1})	D_r (m)	GRL (m)
0	0.00	16.40				1205			503.44
0.5	0.52					1205			503.50
1	1.32					1205			503.54
1.5	1.50					1205			503.59
2	1.80	16.40				1205			503.65
2.5	2.20					1205			503.70
3	2.80					1205			503.76
4	3.32	15.60	1.04	2.29	14.57	3838	1269	1.31	503.81
6	4.30	15.40	1.43	2.88	13.98	3838	1269	1.81	503.93
8	4.60	14.60	1.18	3.43	13.43	3838	1269	1.49	503.97
10	4.50	13.80	0.73	3.78	13.08	3838	1269	0.92	504.05
12	4.90	13.20	0.63	4.28	12.58	3838	1269	0.79	504.08
14	5.60	12.80	0.77	4.83	12.03	3838	1269	0.98	504.29
16	6.60	12.60	1.18	5.43	11.43	3838	1269	1.49	504.50
18	7.10	12.70	1.48	5.63	11.23	3838	1269	1.87	504.73
20	9.90	14.40	3.73	6.18	10.68	3838	1269	4.73	504.88
22	12.10	15.00	5.13	6.98	9.88	3838	1269	6.50	504.97
24	13.80	13.40	5.18	8.63	8.23	1460	838	4.34	505.10
26	14.60	11.40	4.58	10.03	6.83	1460	838	3.84	505.29
28	15.00	9.40	3.78	11.23	5.63	1460	838	3.16	505.49
30	16.40	7.70	3.63	12.78	4.08	1460	838	3.04	505.83
32	16.40	5.60	2.58	13.83	3.03	1460	838	2.16	506.11
33		4.88				714			506.26
33.5		4.50				714			506.34
34	17.00	3.90				714			506.37
34.5		3.60				714			506.43
35		2.80				714			506.49
35.5		1.80				714			506.54
36	17.30	0.36				714			506.61

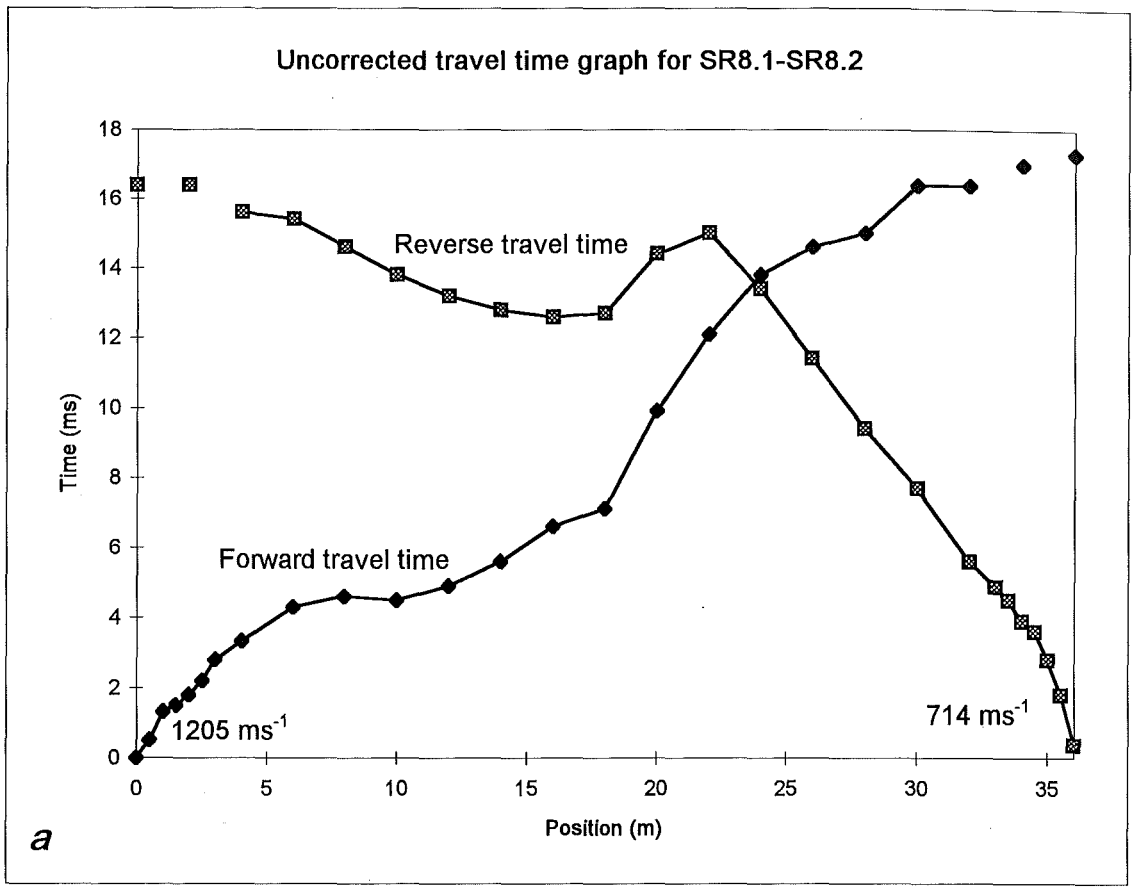

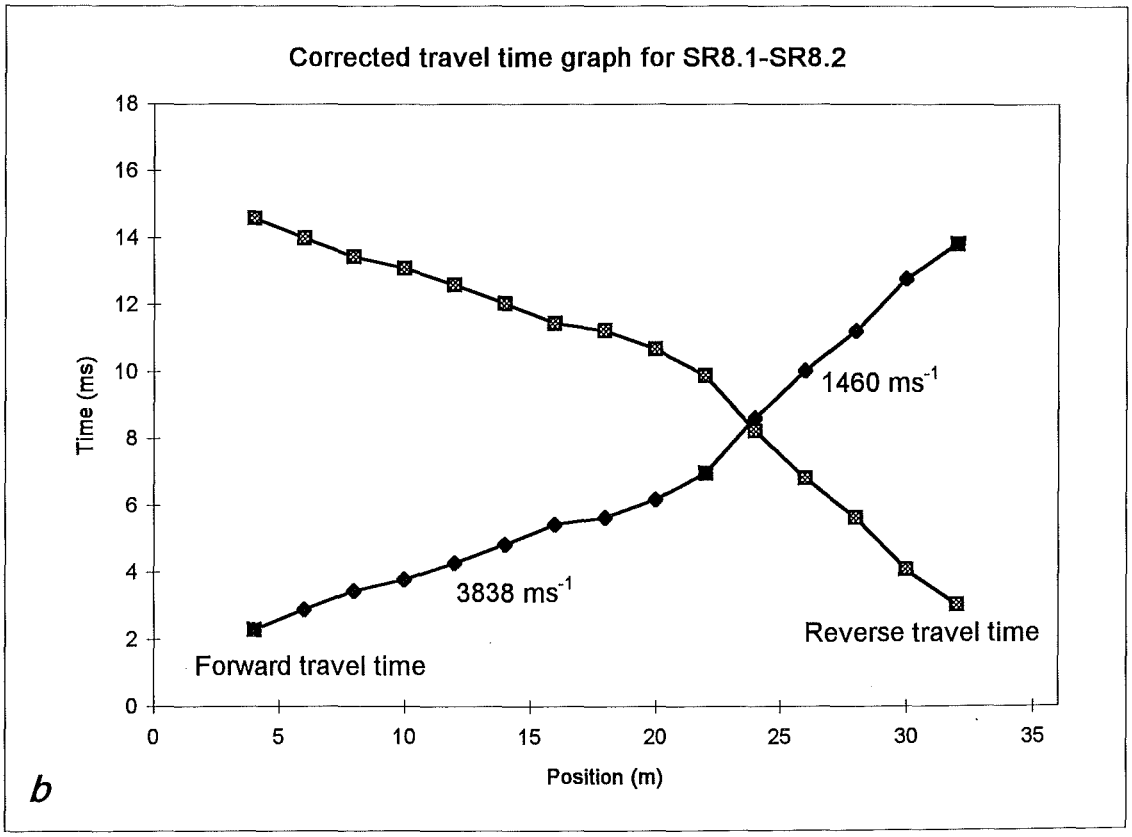

Figure D2.11: Uncorrected (a) and corrected (b) travel time graphs.

Table D2.12: Seismic Refraction Line SR9.1-SR9.2

Position (m)	T_f (ms)	T_r (ms)	T_d (ms)	T_{cf} (ms)	T_{cr} (ms)	V_1 (ms^{-1})	DCF (ms^{-1})	D_r (m)	GRL (m)
0	0.76	29.60				538			580.28
0.5	1.32					538			580.28
1	2.68					538			580.29
1.5	3.68					538			580.30
2	5.04	28.80				538			580.31
2.5	5.90					538			580.30
3	7.20					538			580.29
4	8.20	27.40	3.10	5.10	24.30	1081	620	1.92	580.28
6	11.20	26.20	4.00	7.20	22.20	1081	620	2.48	580.24
8	13.20	25.00	4.40	8.80	20.60	1081	620	2.73	580.23
10	14.00	23.60	4.10	9.90	19.50	1915	561	2.30	580.03
12	14.00	22.00	3.30	10.70	18.70	1915	561	1.85	579.96
14	14.20	20.40	2.60	11.60	17.80	1915	561	1.46	579.91
16	15.20	20.00	2.90	12.30	17.10	1915	561	1.63	579.92
18	15.60	18.80	2.50	13.10	16.30	1915	561	1.40	579.93
20	17.60	18.40	3.30	14.30	15.10	1915	561	1.85	579.86
22	19.20	17.20	3.50	15.70	13.70	1915	561	1.96	579.63
24	20.60	16.20	3.70	16.90	12.50	1915	561	2.07	579.81
26	21.80	14.80	3.60	18.20	11.20	1915	561	2.02	579.91
28	22.00	13.80	3.20	18.80	10.60	5000	541	1.73	579.94
30	22.00	13.40	3.00	19.00	10.40	5000	541	1.62	579.94
32	23.00	12.80	3.20	19.80	9.60	2254	554	1.77	579.92
34	24.00	12.00	3.30	20.70	8.70	2254	554	1.83	579.82
36	25.00	11.30	3.45	21.55	7.85	2254	554	1.91	579.73
38	25.40	9.70	2.85	22.55	6.85	2254	554	1.58	579.67
40	25.00	8.60	2.10	22.90	6.50	5000	875	1.84	579.61
42	25.60	8.30	2.25	23.35	6.05	5000	875	1.97	579.56
44	26.80	7.00	2.20	24.60	4.80	1990	956	2.10	579.32
46	27.00	5.68	1.64	25.36	4.04	1990	956	1.57	579.28
47		4.88				862			579.14
47.5		3.96				862			579.08
48	28.20	3.32				862			579.03
48.5		3.08				862			578.98
49		2.52				862			578.93
49.5		2.04				862			578.89
50	29.20	1.04				862			578.83

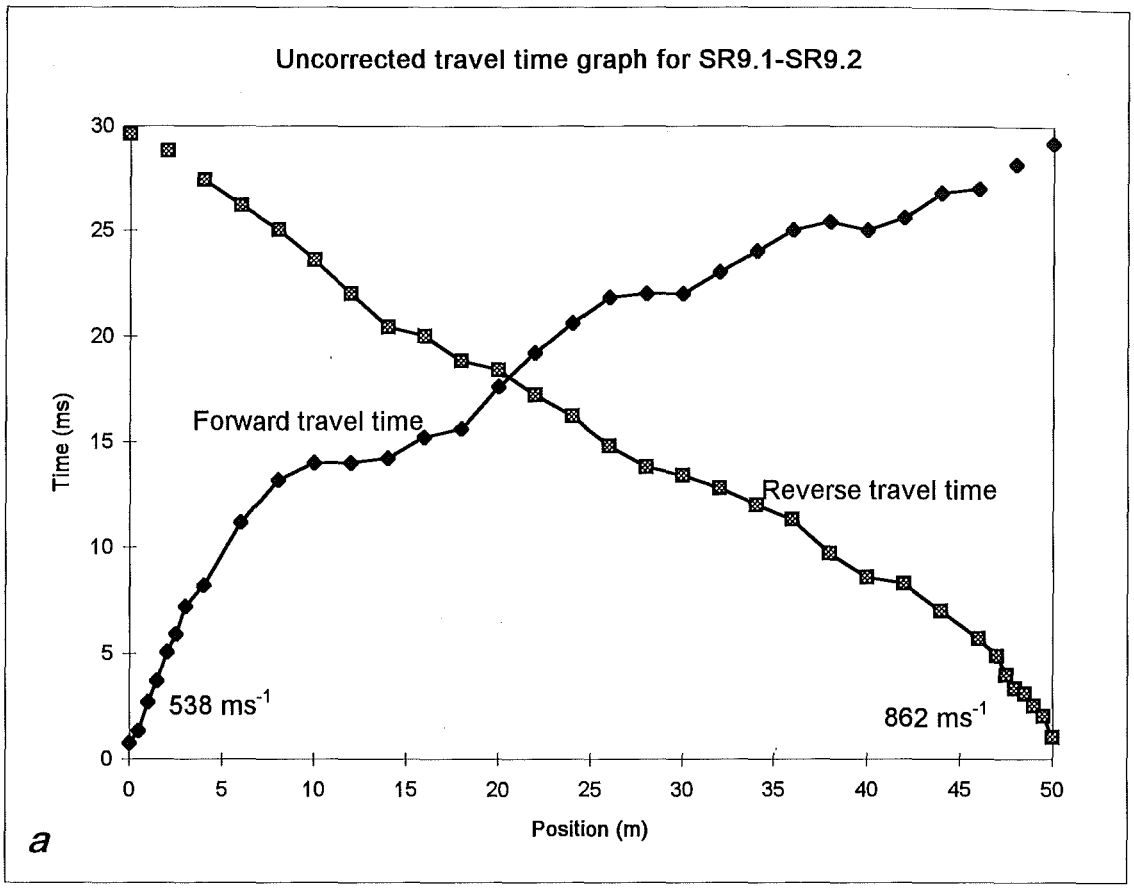

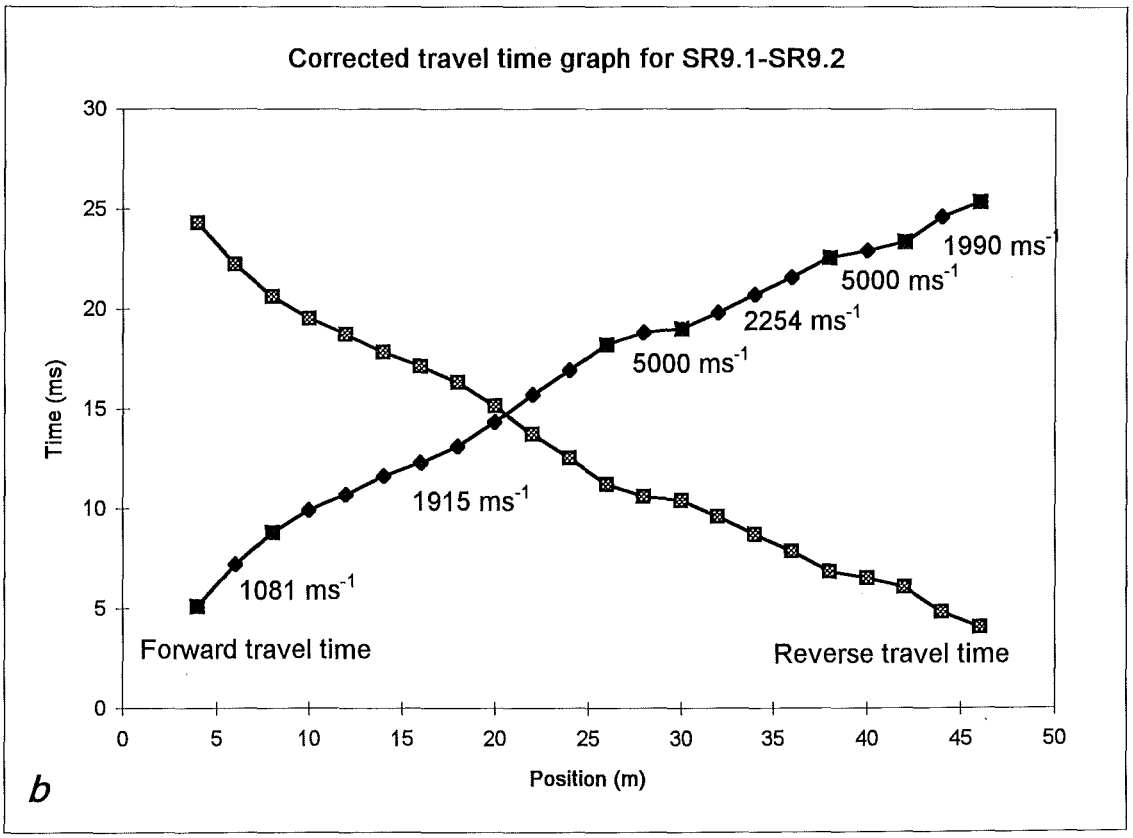

Figure D2.12: Uncorrected (a) and corrected (b) travel time graphs.

Table D2.13: Seismic Refraction Line SR10.1-SR10.2

Position (m)	T_f (ms)	T_r (ms)	T_d (ms)	T_{cf} (ms)	T_{cr} (ms)	V_1 (ms^{-1})	DCF (ms^{-1})	D_r (m)	GRL (m)
0	0.04	38.40				194			556.31
0.5	3.60					194			556.35
1	6.00					194			556.38
1.5	9.10					194			556.39
2	12.20	34.00				194			556.43
2.5	13.70					194			556.46
3	15.50					194			556.48
4	11.60	39.00	6.20	5.40	32.80	741	201	1.25	556.60
6	12.40	33.90	4.05	8.35	29.85	741	201	0.81	556.92
8	16.00	34.00	5.90	10.10	28.10	741	201	1.19	557.22
10	16.40	29.20	3.70	12.70	25.50	741	201	0.74	557.27
12	24.40	31.40	8.80	15.60	22.60	741	201	1.77	557.53
14	29.40	29.80	10.50	18.90	19.30	741	201	2.11	557.76
16	26.80	26.60	7.60	19.20	19.00	4000	359	2.73	558.17
18	28.40	26.80	8.50	19.90	18.30	4000	359	3.06	558.75
20	29.80	24.00	7.80	22.00	16.20	1154	377	2.94	559.16
22	29.60	21.40	6.40	23.20	15.00	1154	377	2.41	559.62
24	30.60	17.40	4.90	25.70	12.50	1154	377	1.85	560.15
26	31.00	14.80	3.80	27.20	11.00	1154	377	1.43	560.66
28	30.80	12.00	2.30	28.50	9.70	1154	377	0.87	561.00
30	33.60	11.20	3.30	30.30	7.90	1154	377	1.24	561.23
31		8.60				358			561.37
31.5		7.70				358			561.46
32	36.20	5.50				358			561.55
32.5		3.90				358			561.61
33		3.24				358			561.66
33.5		1.04				358			561.70
34	38.00	0.04				358			561.73

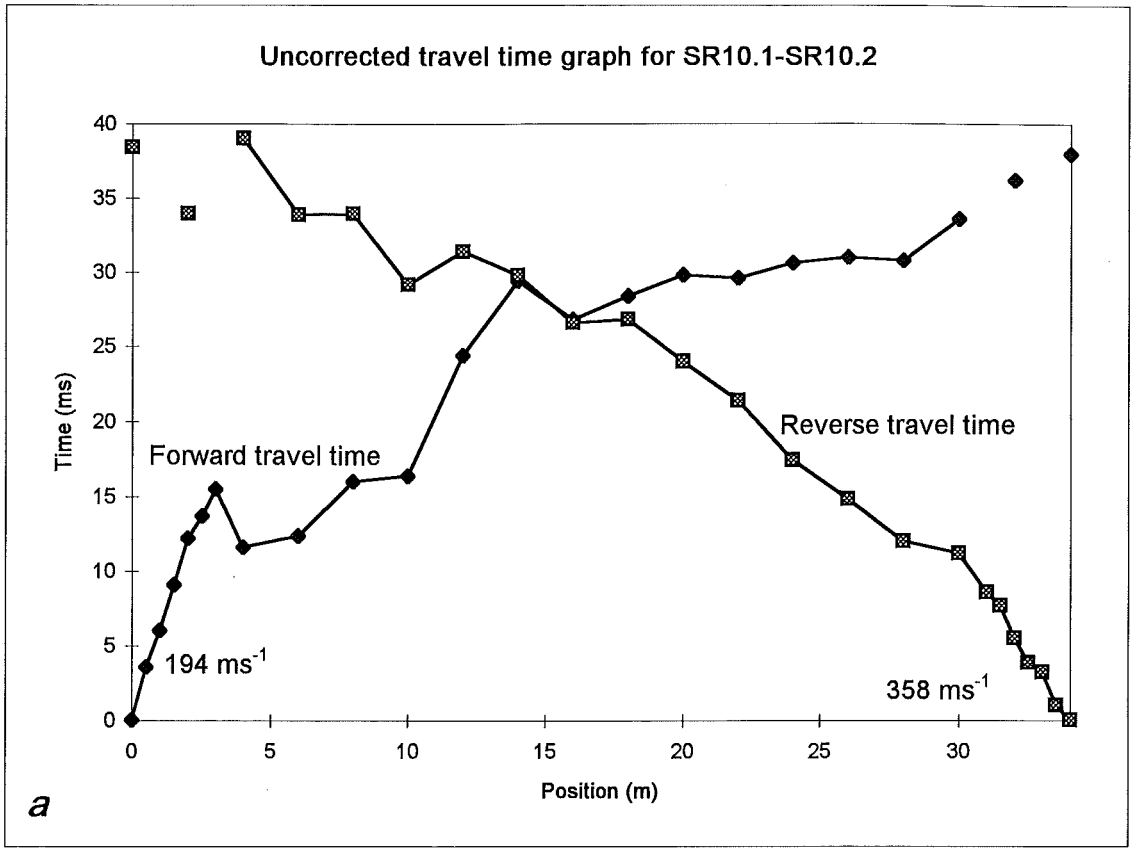

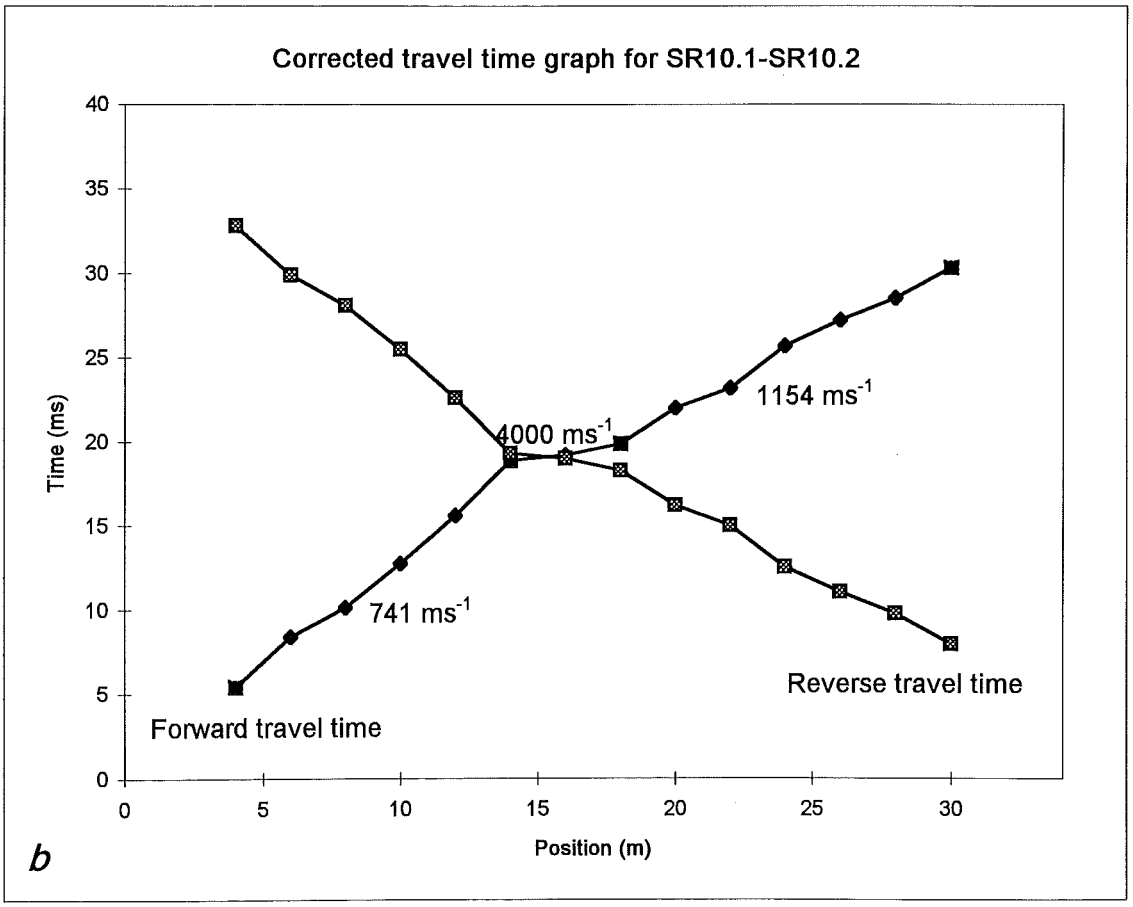

Figure D2.13: Uncorrected (a) and corrected (b) travel time graphs.

Table D2.14: Seismic Refraction Line SR11.1-SR11.2

Position (m)	T_f (ms)	T_r (ms)	T_d (ms)	T_{cf} (ms)	T_{cr} (ms)	V_1 (ms^{-1})	DCF (ms^{-1})	D_r (m)	GRL (m)
0	0.60	57.00				360			509.50
0.5	1.68					360			509.49
1	2.72					360			509.48
1.5	4.12					360			509.47
2	5.60	57.20				360			509.47
2.5	7.40					360			509.44
3	8.50					360			509.43
4	11.70	56.80	5.95	5.75	50.85	897	381	2.27	509.38
6	16.60	54.80	7.40	9.20	47.40	897	381	2.82	509.36
8	19.80	55.20	9.20	10.60	46.00	897	381	3.51	509.42
10	23.80	54.00	10.60	13.20	43.40	897	381	4.04	509.45
12	27.20	52.80	11.70	15.50	41.10	897	381	4.46	509.55
14	28.40	51.20	11.50	16.90	39.70	897	381	4.39	509.60
16	32.00	46.80	11.10	20.90	35.70	508	486	5.39	509.64
18	34.00	42.00	9.70	24.30	32.30	508	486	4.71	509.68
20	38.80	38.00	10.10	28.70	27.90	508	486	4.90	509.72
22	39.60	36.80	9.90	29.70	26.90	804	390	3.86	509.81
24	40.80	34.40	9.30	31.50	25.10	804	390	3.63	509.94
26	41.20	32.40	8.50	32.70	23.90	804	390	3.32	510.08
28	40.80	28.00	6.10	34.70	21.90	804	390	2.38	510.32
30	43.60	25.80	6.40	37.20	19.40	804	390	2.50	510.58
32	45.60	21.80	5.40	40.20	16.40	804	390	2.11	510.77
34	49.60	17.10	5.05	44.55	12.05	804	390	1.97	510.96
36	52.40	11.80	3.80	48.60	8.00	804	390	1.48	511.03
37		9.30				341			511.03
37.5		7.70				341			511.05
38	54.00	6.16				341			511.10
38.5		4.64				341			511.13
39		3.16				341			511.15
39.5		1.12				341			511.15
40	56.20	0.08				341			511.09

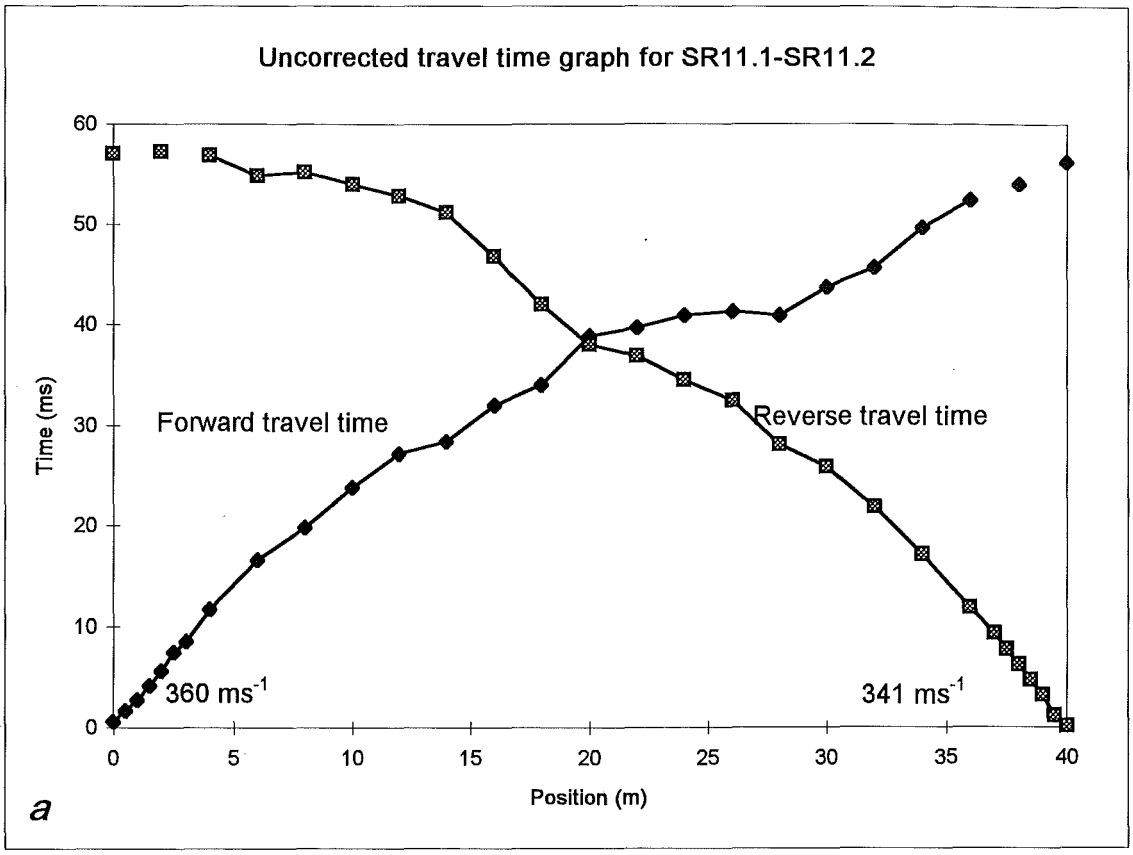

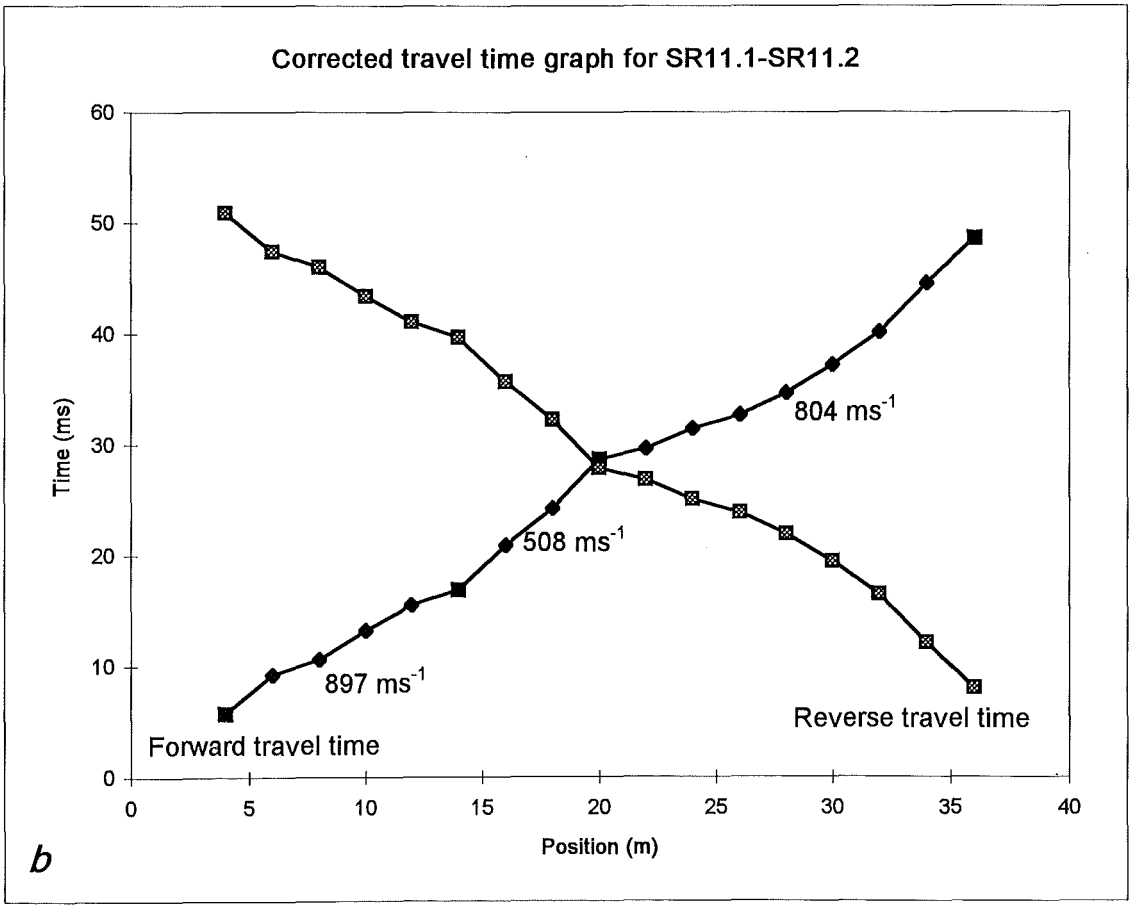

Figure D2.14: Uncorrected (a) and corrected (b) travel time graphs.

Table D2.15: Seismic Refraction Line SR12.1-SR12.2

Position (m)	T_f (ms)	T_r (ms)	T_d (ms)	T_{cf} (ms)	T_{cr} (ms)	V_1 (ms^{-1})	DCF (ms^{-1})	D_r (m)	GRL (m)
0	0.80	25.40				743			535.00
0.5	1.12					743			535.04
1	1.68					743			535.07
1.5	2.36					743			535.10
2	3.32	25.00				743			535.13
2.5	3.88					743			535.20
3	4.84					743			535.24
4	5.64	24.40	2.37	3.27	22.03	1461	863	2.05	535.32
6	6.80	23.60	2.55	4.25	21.05	1461	863	2.20	535.42
8	8.60	23.00	3.15	5.45	19.85	1461	863	2.72	535.42
10	9.90	21.60	3.10	6.80	18.50	1461	863	2.68	535.29
12	11.50	20.80	3.50	8.00	17.30	1461	863	3.02	535.11
14	13.00	18.40	3.05	9.95	15.35	1461	863	2.63	535.08
16	14.00	16.00	2.35	11.65	13.65	1461	863	2.03	534.91
18	14.40	14.00	1.55	12.85	12.45	1461	863	1.34	534.59
20	19.80	13.20	3.85	15.95	9.35	645	617	2.38	534.14
22	19.80	11.20	2.85	16.95	8.35	1622	464	1.32	533.95
24	20.20	8.20	1.55	18.65	6.65	1622	464	0.72	533.90
26	21.00	7.00	1.35	19.65	5.65	1622	464	0.63	533.81
27		6.80				446			533.74
27.5		5.70				446			533.74
28	22.20	4.90				446			533.72
28.5		3.64				446			533.70
29		2.64				446			533.66
29.5		1.00				446			533.69
30	25.20	0.08				446			533.72

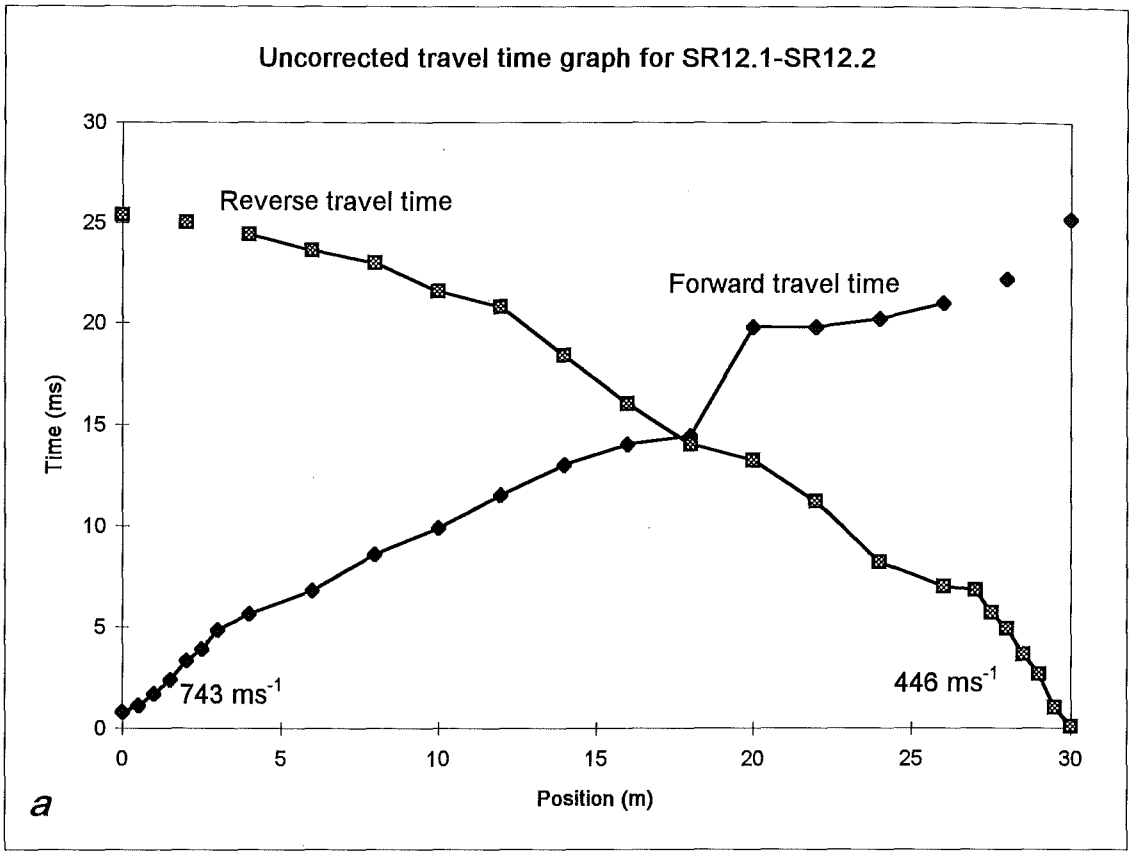

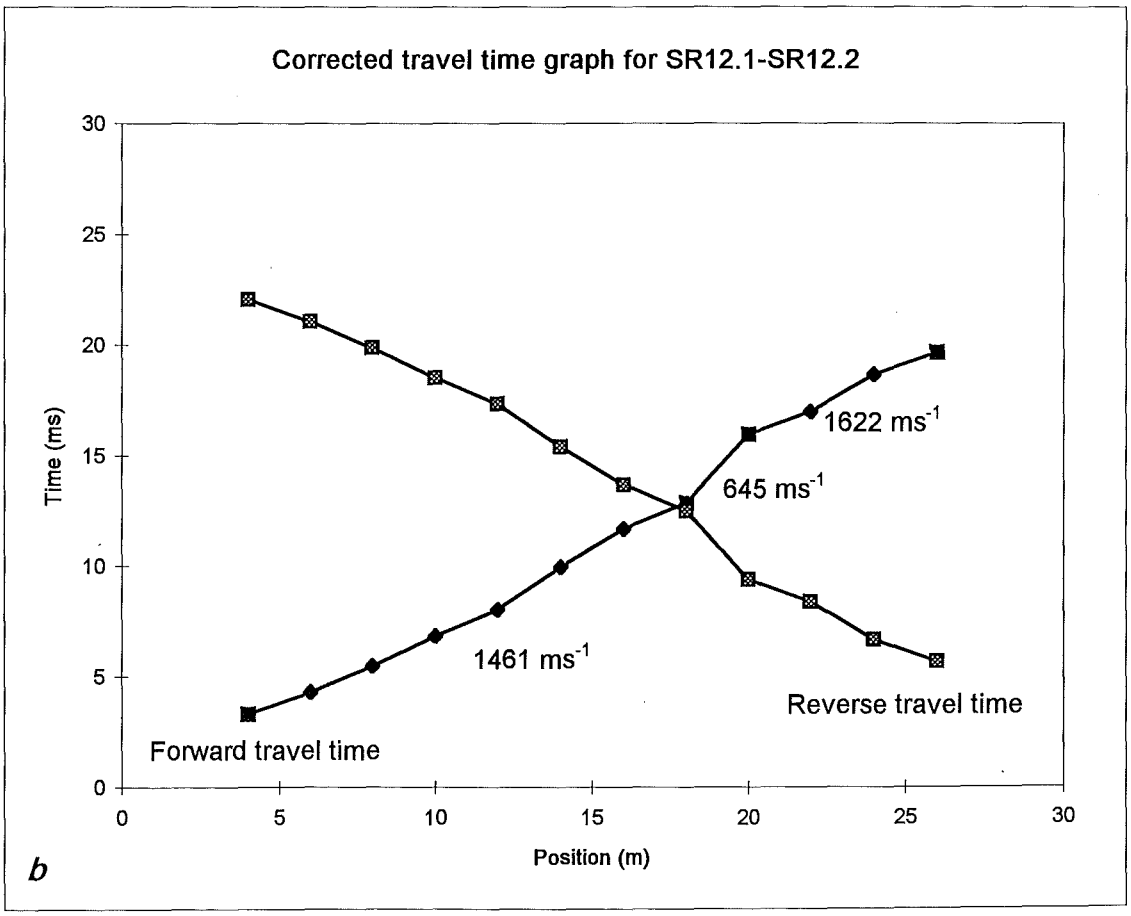

Figure D2.15: Uncorrected (*a*) and corrected (*b*) travel time graphs.

Table D2.16: Seismic Refraction Line SR13.1-SR13.2

Position (m)	T_f (ms)	T_r (ms)	T_d (ms)	T_{cf} (ms)	T_{cr} (ms)	V_1 (ms^{-1})	DCF (ms^{-1})	D_r (m)	GRL (m)
0	0.04	25.80				690			544.52
0.5	1.12					690			544.52
1	1.52					690			544.53
1.5	2.48					690			544.53
2	3.76	25.00				690			544.54
2.5	4.68					690			544.56
3	4.96					690			544.58
4	5.84	24.40	2.02	3.82	22.38	1355	802	1.62	544.58
6	8.76	23.00	2.78	5.98	20.22	1355	802	2.23	544.54
8	13.00	24.00	5.40	7.60	18.60	1355	802	4.33	544.52
10	15.50	25.20	7.25	8.25	17.95	1355	802	5.81	544.49
12	17.60	24.40	7.90	9.70	16.50	1355	802	6.33	544.38
14	20.20	24.00	9.00	11.20	15.00	1355	802	7.22	544.28
16	21.00	24.40	9.60	11.40	14.80	3275	706	6.78	544.17
18	21.60	24.20	9.80	11.80	14.40	3275	706	6.92	544.01
20	21.80	24.00	9.80	12.00	14.20	3275	706	6.92	543.88
22	21.40	22.20	8.70	12.70	13.50	3275	706	6.14	543.71
24	22.40	21.60	8.90	13.50	12.70	3275	706	6.28	543.51
26	23.00	21.20	9.00	14.00	12.20	3275	706	6.35	543.39
28	21.80	18.00	6.80	15.00	11.20	3275	706	4.80	543.28
30	21.20	15.40	5.20	16.00	10.20	3275	706	3.67	543.07
32	20.00	13.60	3.70	16.30	9.90	3275	706	2.61	542.87
34	21.20	12.60	3.80	17.40	8.80	3275	553	2.10	542.63
36	21.60	11.30	3.35	18.25	7.95	3275	553	1.85	542.39
38	21.80	10.50	3.05	18.75	7.45	3275	553	1.69	542.22
40	23.40	11.00	4.10	19.30	6.90	3275	553	2.27	542.07
42	23.60	10.30	3.85	19.75	6.45	3275	553	2.13	541.91
44	25.20	9.50	4.25	20.95	5.25	1600	580	2.46	541.74
46	25.80	7.50	3.55	22.25	3.95	1600	580	2.06	541.58
47		5.90				545			541.47
47.5		5.10				545			541.40
48	25.20	4.16				545			541.36
48.5		4.00				545			541.32
49		2.72				545			541.28
49.5		1.20				545			541.25
50	26.60	0.16				545			541.22

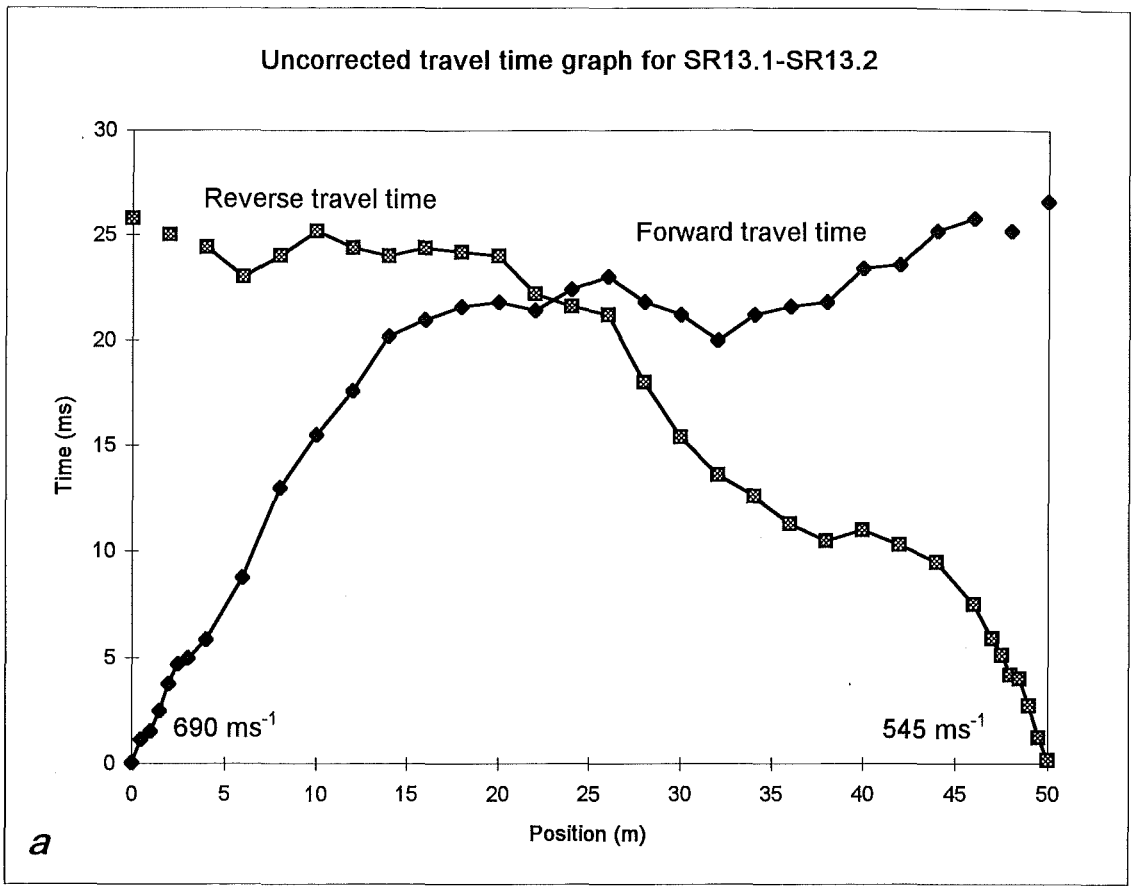

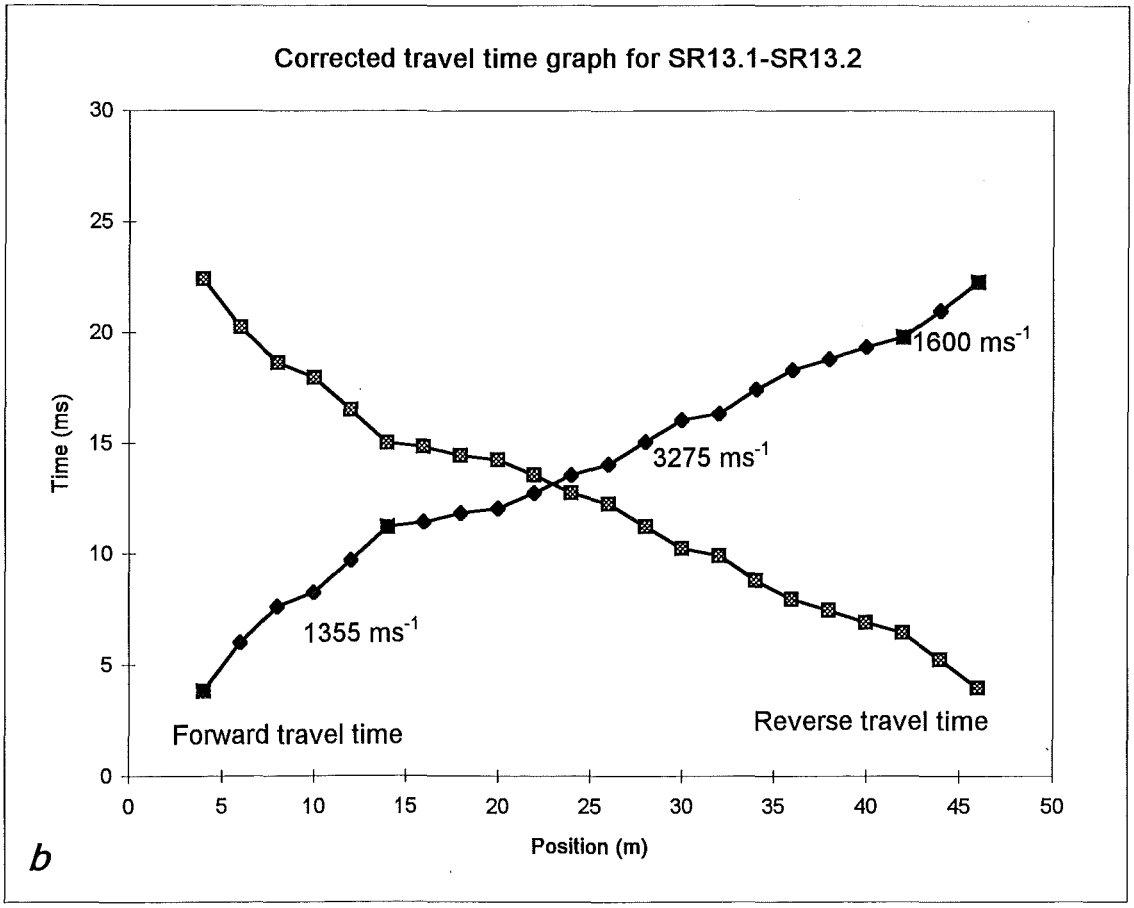

Figure D2.16: Uncorrected (*a*) and corrected (*b*) travel time graphs.

Table D2.17: Seismic Refraction Line SR14.1-SR14.2

Position (m)	T_f (ms)	T_r (ms)	T_d (ms)	T_{cf} (ms)	T_{cr} (ms)	V_1 (ms^{-1})	DCF (ms^{-1})	D_r (m)	GRL (m)
0	1.12	32.80				501			520.01
0.5	1.68					501			519.94
1	2.48					501			519.85
1.5	4.04					501			519.83
2	4.88	32.60				501			519.80
2.5	6.20					501			519.78
3	7.30					501			519.70
4	9.10	33.40	5.35	3.75	28.05	1519	531	2.84	519.57
6	11.40	33.20	6.40	5.00	26.80	1519	531	3.40	519.31
8	12.50	31.60	6.15	6.35	25.45	1519	531	3.26	518.95
10	12.80	29.20	5.10	7.70	24.10	1519	531	2.71	518.72
12	13.40	28.80	5.20	8.20	23.60	2173	515	2.68	518.40
14	16.10	30.40	7.35	8.75	23.05	2173	515	3.78	518.06
16	15.90	27.00	5.55	10.35	21.45	2173	191	1.06	517.67
18	18.70	28.40	7.65	11.05	20.75	2173	191	1.46	517.36
20	19.40	26.60	7.10	12.30	19.50	2173	191	1.35	516.99
22	22.00	24.60	7.40	14.60	17.20	750	196	1.45	516.69
24	23.60	20.80	6.30	17.30	14.50	750	196	1.24	516.63
26	25.60	16.80	5.30	20.30	11.50	750	196	1.04	516.45
28	26.60	15.40	5.10	21.50	10.30	2286	191	0.97	516.21
30	27.00	14.70	4.95	22.05	9.75	2286	191	0.94	515.95
31		13.60				190			515.83
31.5		12.30				190			515.73
32	29.40	11.70				190			515.63
32.5		8.90				190			515.59
33		5.70				190			515.52
33.5		4.20				190			515.44
34	30.80	1.20				190			515.35

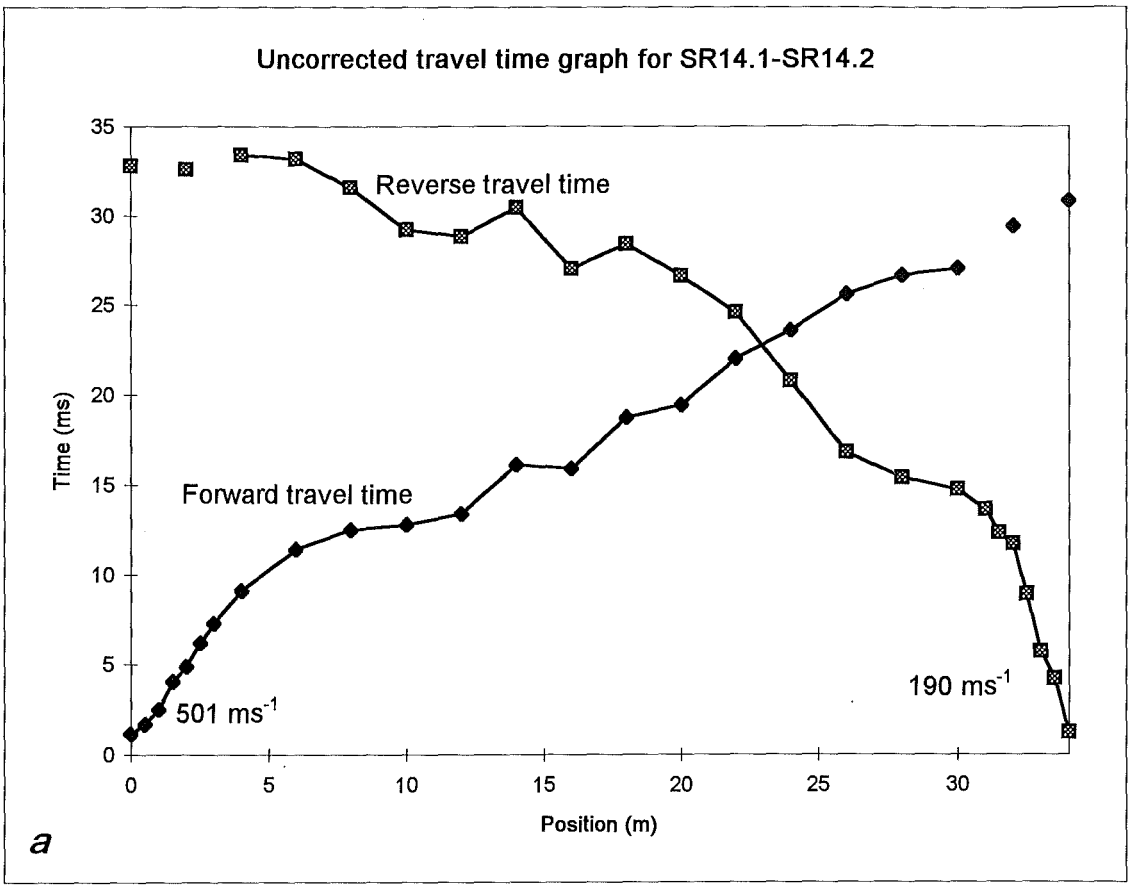

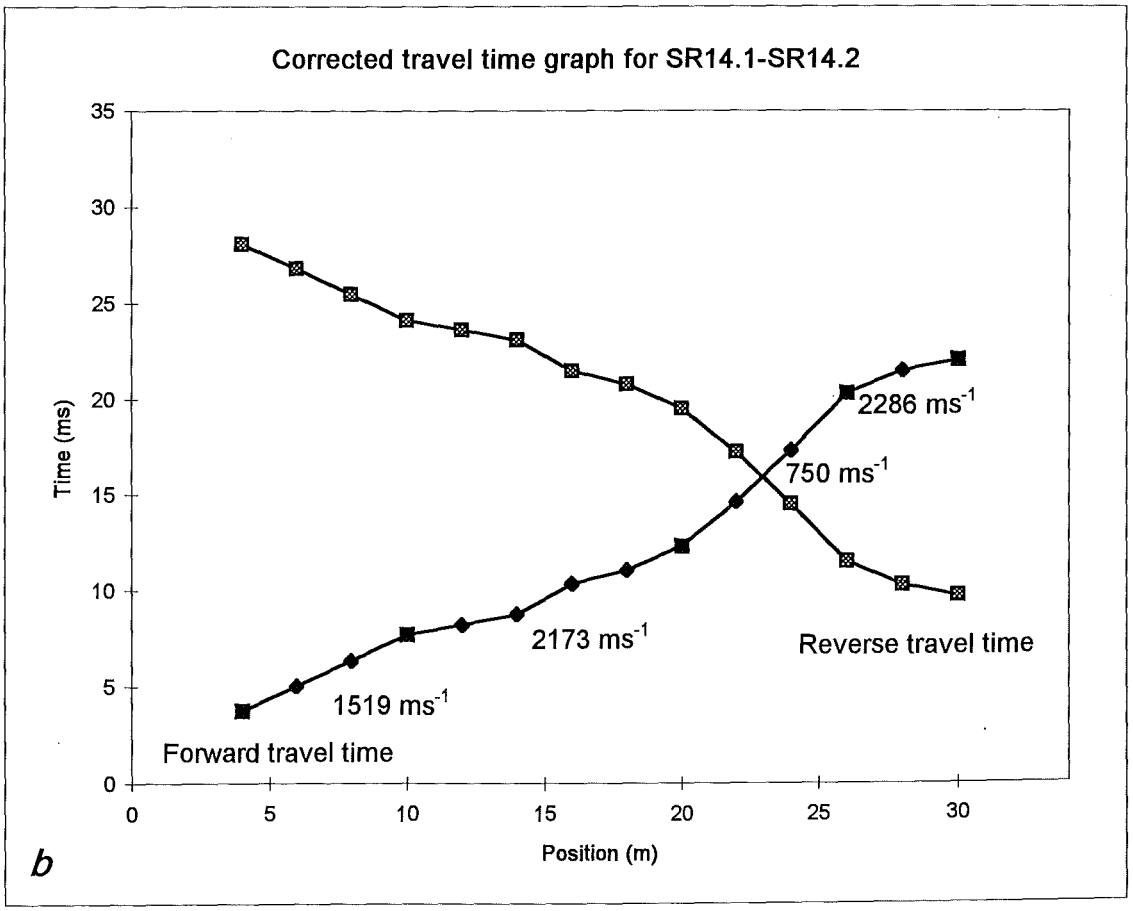

Figure D2.17: Uncorrected (*a*) and corrected (*b*) travel time graphs.

Table D2.18: Seismic Refraction Line SR15.1-SR15.2

Position (m)	T_f (ms)	T_r (ms)	T_d (ms)	T_{cf} (ms)	T_{cr} (ms)	V_1 (ms^{-1})	DCF (ms^{-1})	D_r (m)	GRL (m)
0	0.56	50.00				366			542.53
0.5	1.72					366			542.49
1	2.92					366			542.46
1.5	4.36					366			542.44
2	5.84	47.60				366			542.42
2.5	6.96					366			542.40
3	8.30					366			542.34
4	11.50	47.60	3.85	7.65	43.75	899	401	1.54	542.25
6	14.00	45.20	3.90	10.10	41.30	899	401	1.56	542.08
8	17.80	44.40	5.40	12.40	39.00	899	401	2.16	541.83
10	21.00	44.00	6.80	14.20	37.20	899	401	2.72	541.61
12	24.40	42.80	7.90	16.50	34.90	899	401	3.17	541.40
14	29.40	40.40	9.20	20.20	31.20	899	401	3.69	541.20
16	33.40	38.80	10.40	23.00	28.40	899	401	4.17	540.95
18	36.00	37.20	10.90	25.10	26.30	899	401	4.37	540.69
20	37.60	36.00	11.10	26.50	24.90	899	401	4.45	540.47
22	38.00	34.00	10.30	27.70	23.70	899	401	4.13	540.23
24	40.40	32.00	10.50	29.90	21.50	899	401	4.21	540.00
26	42.80	29.20	10.30	32.50	18.90	899	401	4.13	539.76
28	44.00	26.20	9.40	34.60	16.80	899	401	3.77	539.48
30	45.60	23.80	9.00	36.60	14.80	899	401	3.61	539.13
32	48.80	22.60	10.00	38.80	12.60	899	401	4.01	538.94
34	47.20	19.20	7.50	39.70	11.70	1463	584	4.38	538.81
36	50.00	17.80	8.20	41.80	9.60	1463	584	4.78	538.68
38	50.40	16.00	7.50	42.90	8.50	1463	584	4.38	538.56
40	53.60	11.20	6.70	46.90	4.50	661	947	6.34	538.47
42	54.40	7.90	5.45	48.95	2.45	661	947	5.16	538.30
43		6.48				542			538.19
43.5		5.64				542			538.16
44	53.60	4.72				542			538.09
44.5		3.96				542			538.03
45		2.84				542			537.99
45.5		1.52				542			537.93
46	52.80	0.52				542			537.85

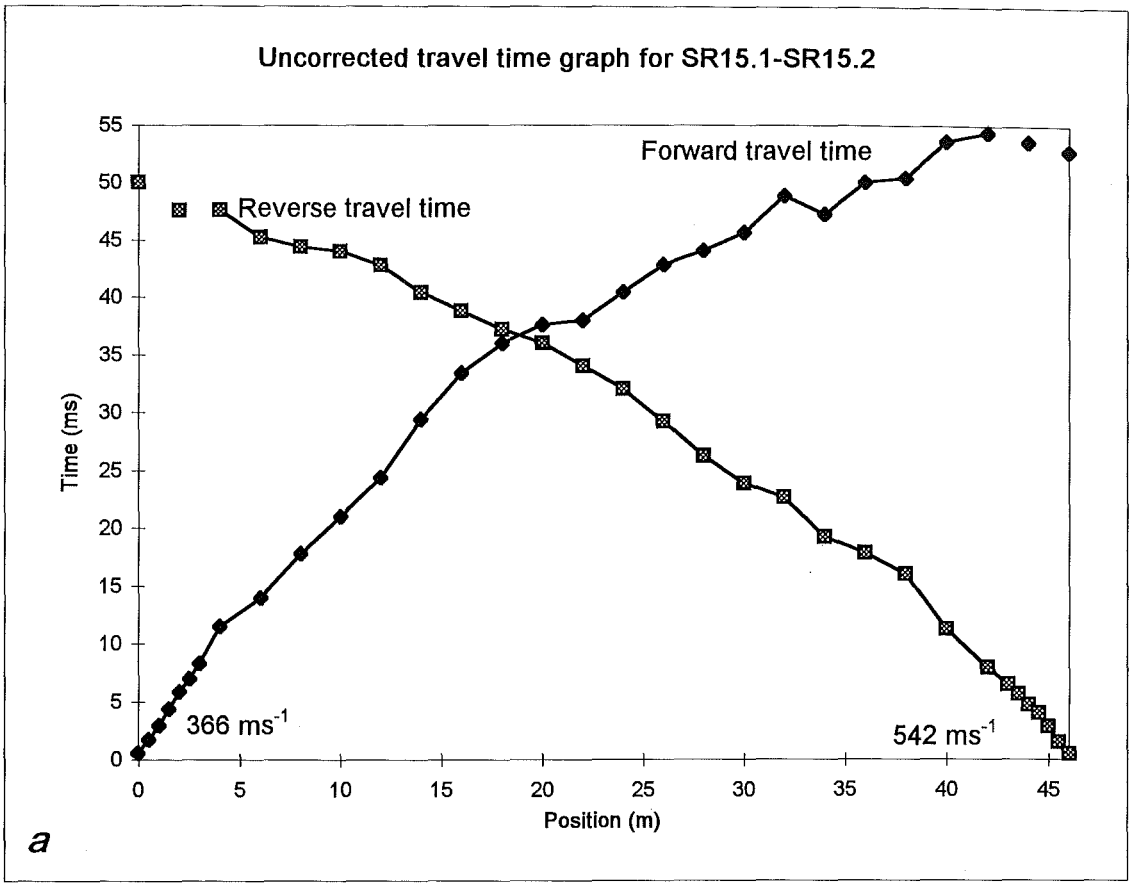

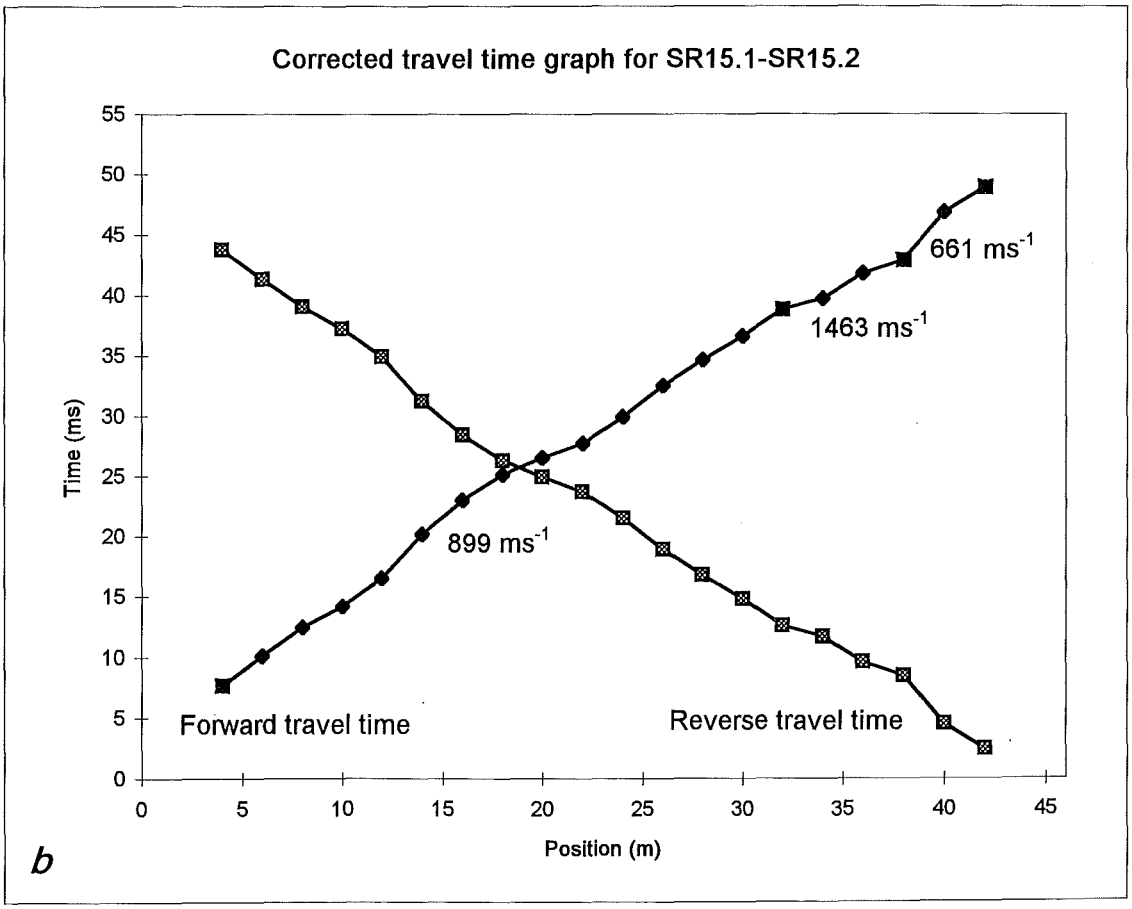

Figure D2.18: Uncorrected (*a*) and corrected (*b*) travel time graphs.

Table D2.19: Seismic Refraction Line SR16.1-SR16.2

Position (m)	T_f (ms)	T_r (ms)	T_d (ms)	T_{cf} (ms)	T_{cr} (ms)	V_1 (ms^{-1})	DCF (ms^{-1})	D_r (m)	GRL (m)
0	0.04	40.60				402			537.01
0.5	1.34					402			537.17
1	2.50					402			537.24
1.5	4.36					402			537.36
2	5.20	40.80				402			537.43
2.5	6.70					402			537.49
3	7.50					402			537.55
4	8.50	38.80	3.80	4.70	35.00	620	528	2.01	537.68
6	12.10	34.40	3.40	8.70	31.00	620	528	1.80	537.86
8	15.40	32.80	4.25	11.15	28.55	1429	419	1.78	538.06
10	16.00	31.20	3.75	12.25	27.45	1429	419	1.57	538.06
12	17.80	29.40	3.75	14.05	25.65	1429	419	1.57	538.03
14	19.40	28.40	4.05	15.35	24.35	1429	419	1.70	537.94
16	22.40	25.40	4.05	18.35	21.35	667	901	3.65	537.91
18	21.80	23.40	2.75	19.05	20.65	2222	552	1.52	537.78
20	22.00	21.40	1.85	20.15	19.55	2222	552	1.02	537.60
22	24.60	19.00	1.95	22.65	17.05	860	685	1.34	537.39
24	27.20	16.20	1.85	25.35	14.35	860	685	1.27	537.53
26	29.40	14.00	1.85	27.55	12.15	860	685	1.27	537.74
28	30.60	11.00	0.95	29.65	10.05	860	685	0.65	537.84
30	31.80	8.90	0.50	31.30	8.40	860	685	0.34	537.83
32	36.00	7.50	1.90	34.10	5.60	860	685	1.30	537.86
33		5.50				536			537.88
33.5		4.60				536			537.95
34	37.80	3.48				536			537.90
34.5		2.80				536			537.92
35		1.52				536			537.95
35.5		0.80				536			538.01
36	38.80	0.04				536			538.09

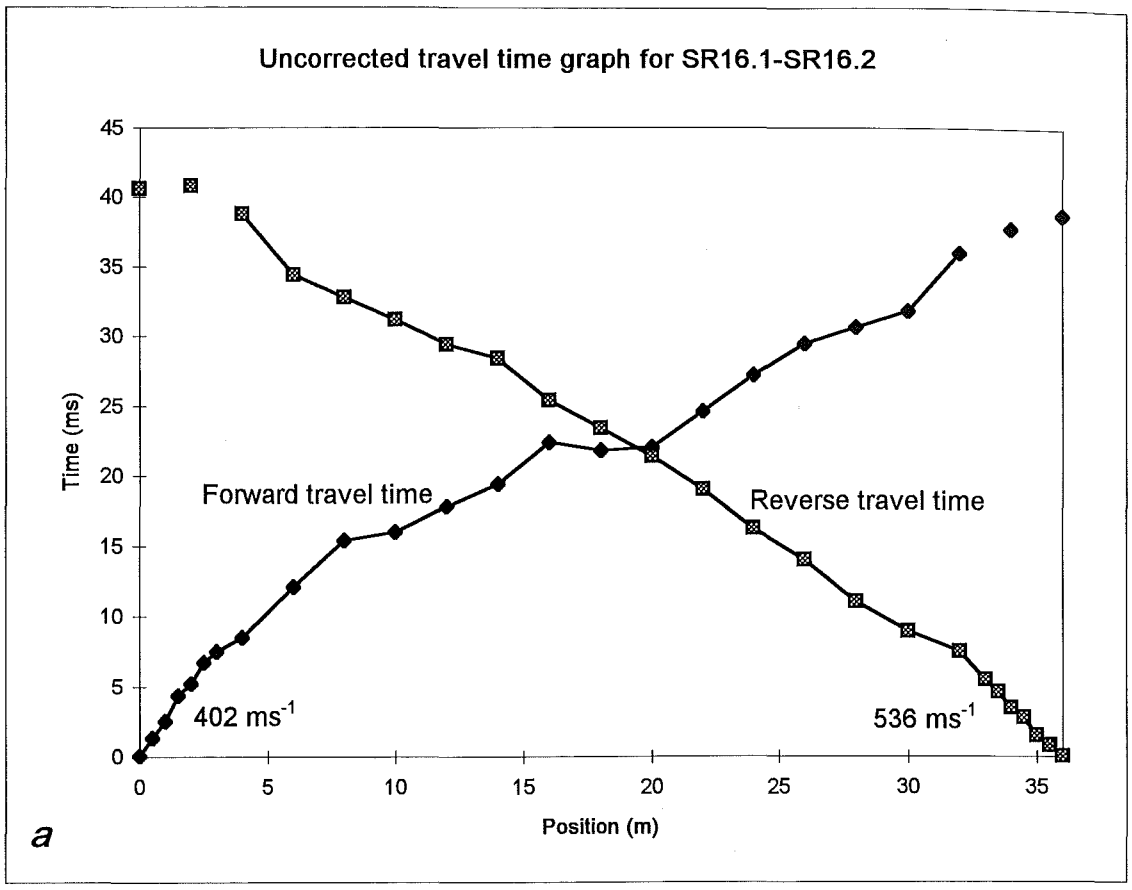

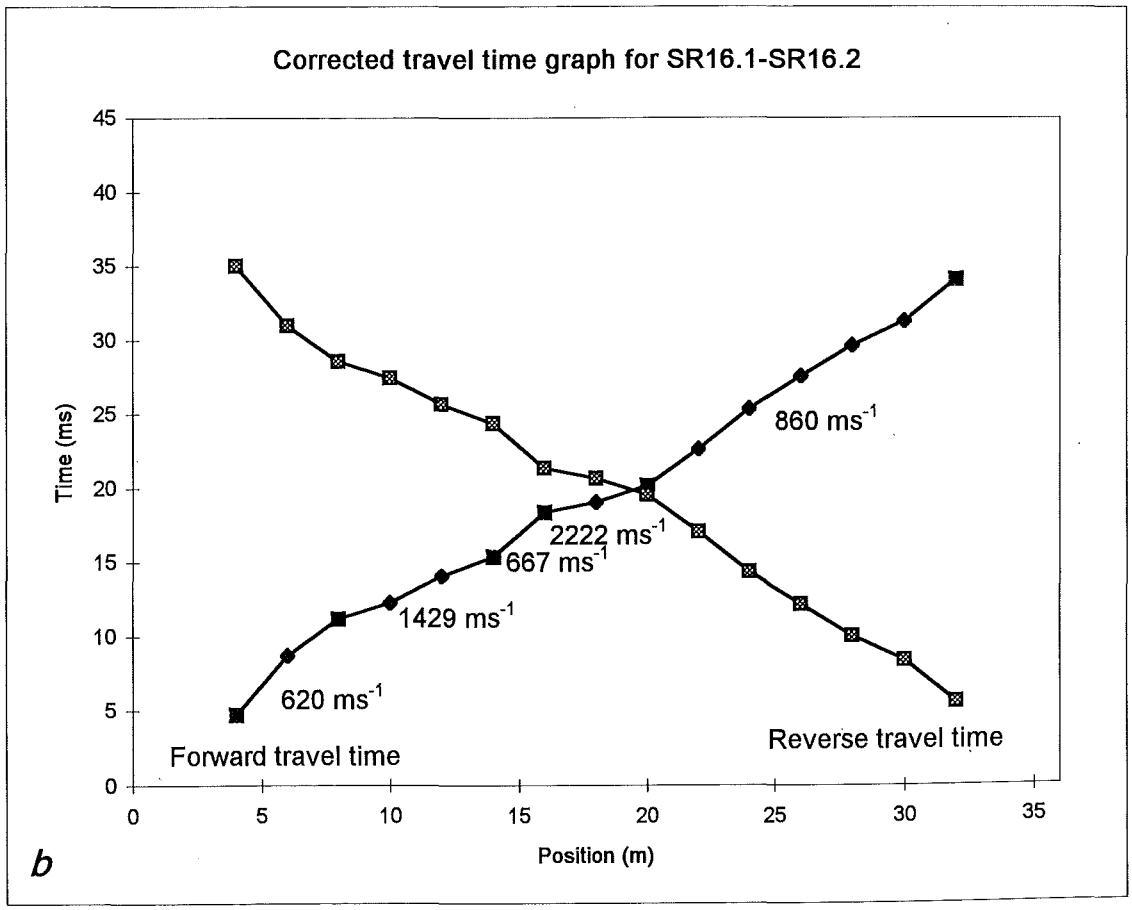

Figure D2.19: Uncorrected (*a*) and corrected (*b*) travel time graphs.

Table D2.20: Seismic Refraction Line SR16.2-SR16.3

Position (m)	T_f (ms)	T_r (ms)	T_d (ms)	T_{cf} (ms)	T_{cr} (ms)	V_1 (ms^{-1})	DCF (ms^{-1})	D_r (m)	GRL (m)
0	0.04	20.00				509			538.09
0.5	1.04					509			538.11
1	2.72					509			538.15
1.5	4.24					509			538.16
2	5.12	20.70				509			538.19
2.5	5.96					509			538.22
3	6.52					509			538.25
4	7.90	18.00	2.60	5.30	15.40	625	877	2.28	538.26
6	12.60	17.70	4.80	7.80	12.90	625	877	4.21	538.33
8	18.70	16.00	7.00	11.70	9.00	625	877	6.14	538.34
10	20.00	14.50	6.90	13.10	7.60	1569	538	3.71	538.42
12	20.60	12.80	6.35	14.25	6.45	1569	538	3.42	538.41
14	21.00	12.60	6.45	14.55	6.15	6667	510	3.29	538.42
16	20.80	9.70	4.90	15.90	4.80	1515	997	4.89	538.43
18	20.20	5.90	2.70	17.50	3.20	1515	997	2.69	538.43
20	21.20	4.88	2.69	18.51	2.19	1515	997	2.68	538.35
21		3.72				833			538.32
21.5		2.88				833			538.28
22	22.20	2.24				833			538.24
22.5		1.44				833			538.19
23		1.24				833			538.17
23.5		0.64				833			538.18
24	21.40	0.08				833			538.10

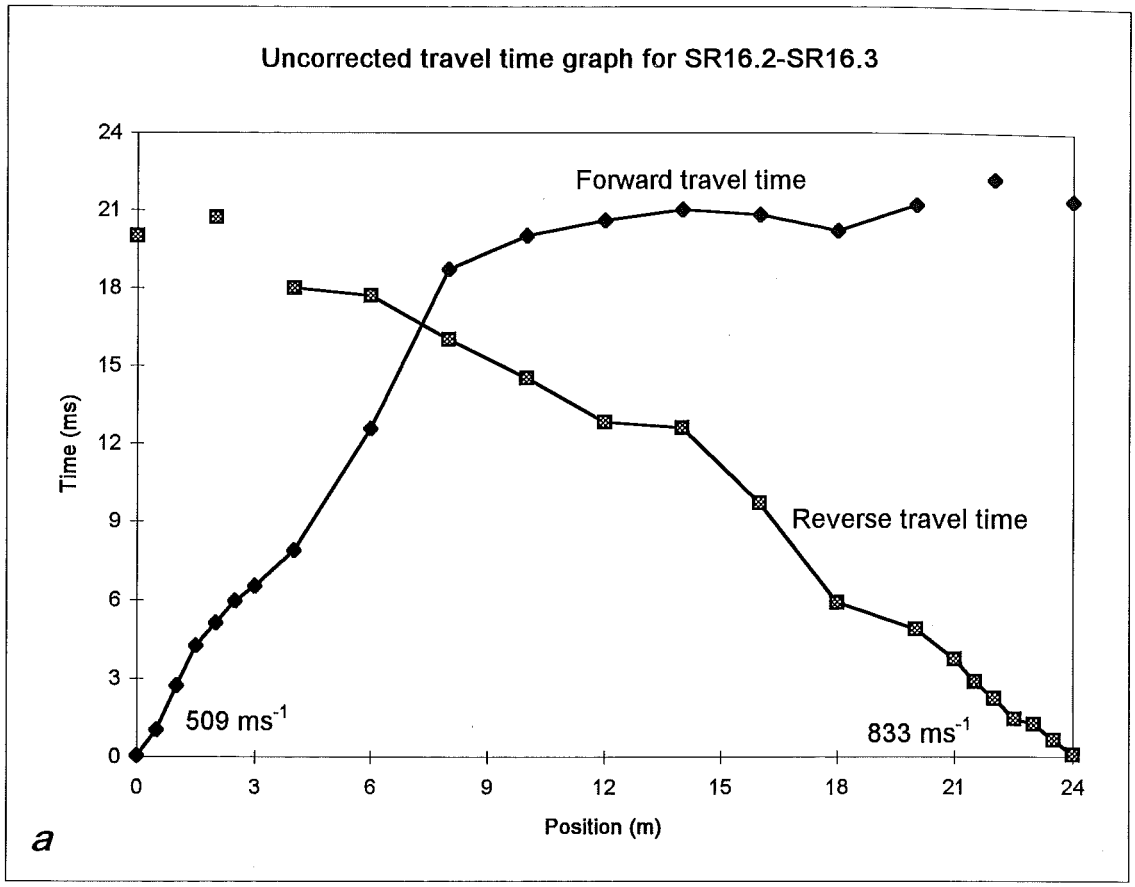

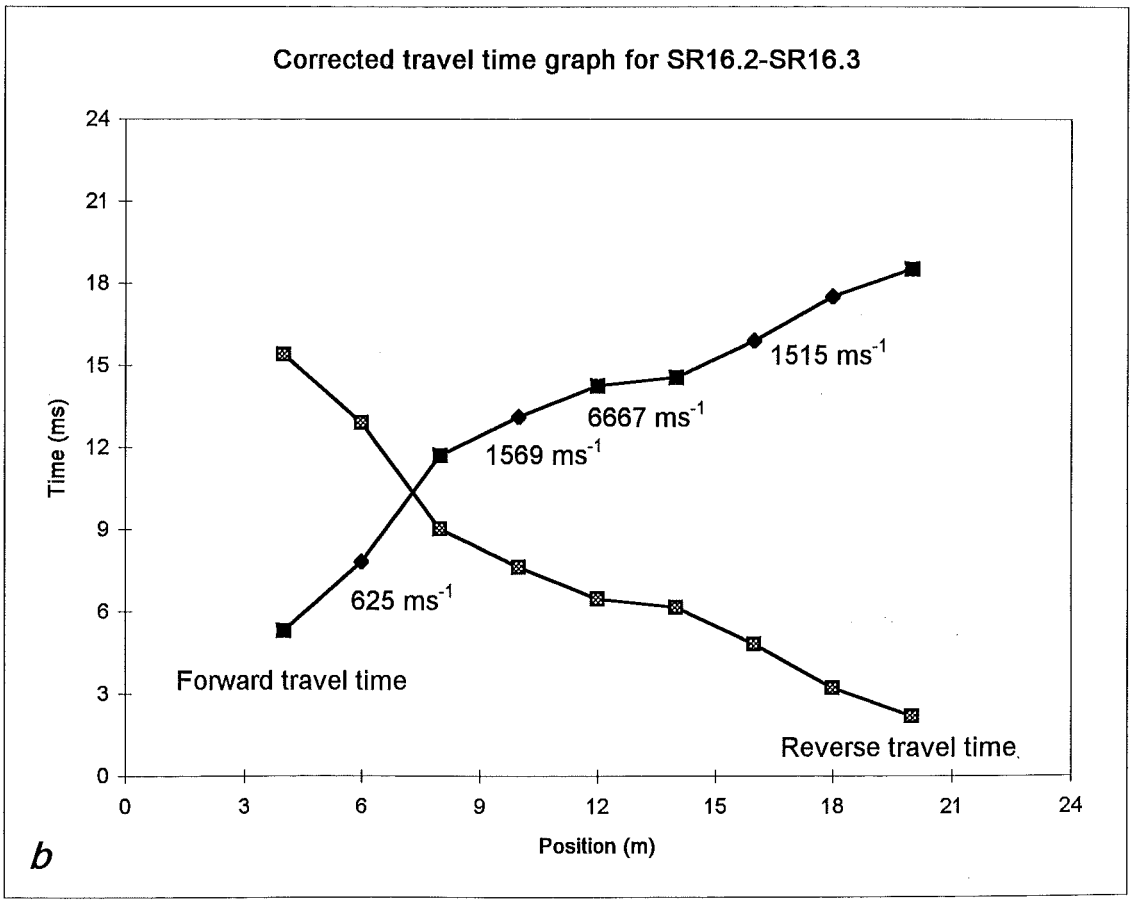

Figure D2.20: Uncorrected (*a*) and corrected (*b*) travel time graphs.

Table D2.21: Seismic Refraction Line SR17.1-SR17.2

Position (m)	T_f (ms)	T_r (ms)	T_d (ms)	T_{cf} (ms)	T_{cr} (ms)	V_1 (ms^{-1})	DCF (ms^{-1})	D_r (m)	GRL (m)
0	0.56	26.40				524			525.49
0.5	1.00					524			525.50
1	2.60					524			525.56
1.5	4.08					524			525.54
2	5.64	24.40				524			525.48
2.5	6.20					524			525.50
3	6.50					524			525.53
4	8.20	24.20	3.10	5.10	21.10	1379	566	1.76	525.63
6	10.50	23.60	3.95	6.55	19.65	4571	527	2.08	525.81
8	11.50	24.00	4.65	6.85	19.35	4571	527	2.45	526.04
10	12.60	24.60	5.50	7.10	19.10	4571	527	2.90	526.38
12	13.80	24.40	6.00	7.80	18.40	4571	527	3.16	526.81
14	15.40	25.00	7.10	8.30	17.90	4571	527	3.75	527.38
16	16.40	23.20	6.70	9.70	16.50	1579	555	3.72	527.89
18	17.40	21.80	6.50	10.90	15.30	1579	555	3.61	528.43
20	20.00	22.00	7.90	12.10	14.10	1579	555	4.39	528.77
22	20.50	21.40	7.85	12.65	13.55	3636	530	4.16	529.18
24	21.40	17.00	6.10	15.30	10.90	734	371	2.26	529.57
26	22.60	12.60	4.50	18.10	8.10	734	371	1.67	530.03
27		10.10				331			530.28
27.5		8.50				331			530.42
28	24.20	6.90				331			530.56
28.5		5.64				331			530.68
29		3.00				331			530.83
29.5		1.44				331			530.96
30	26.00	0.52				331			531.01

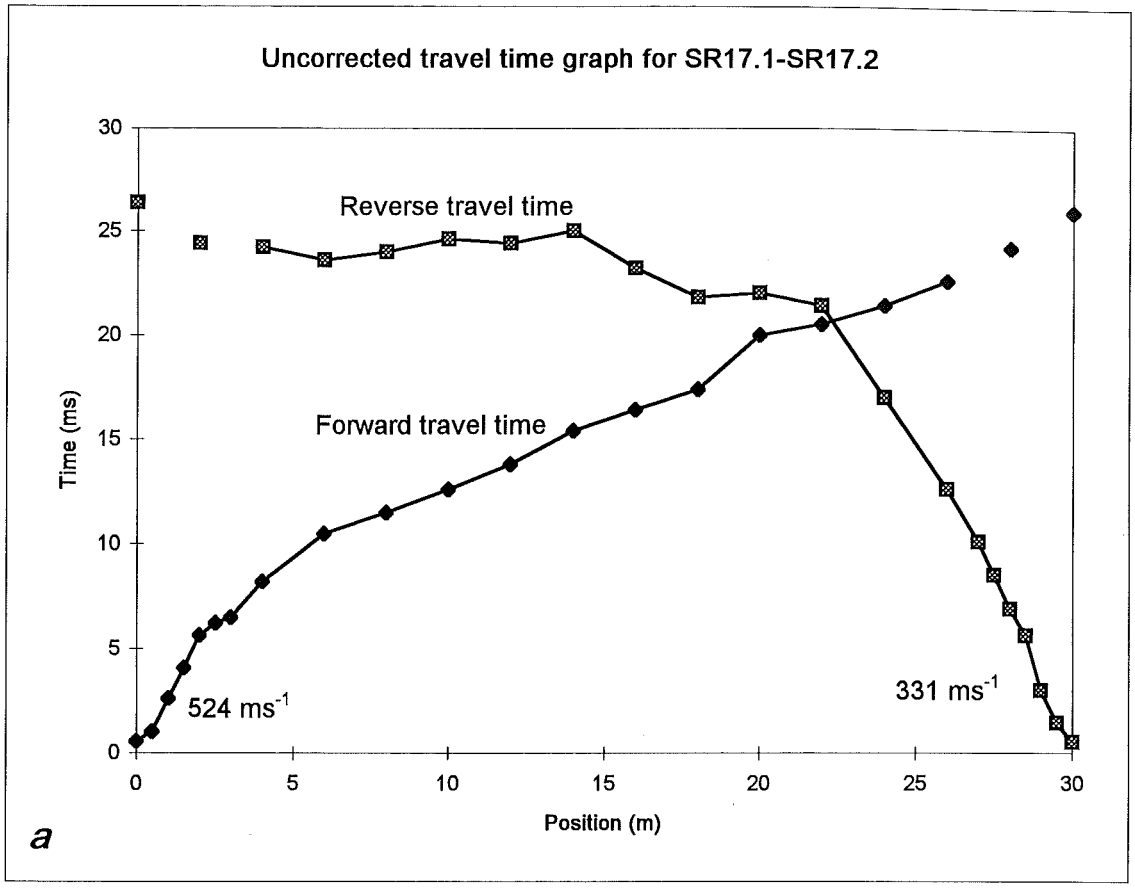

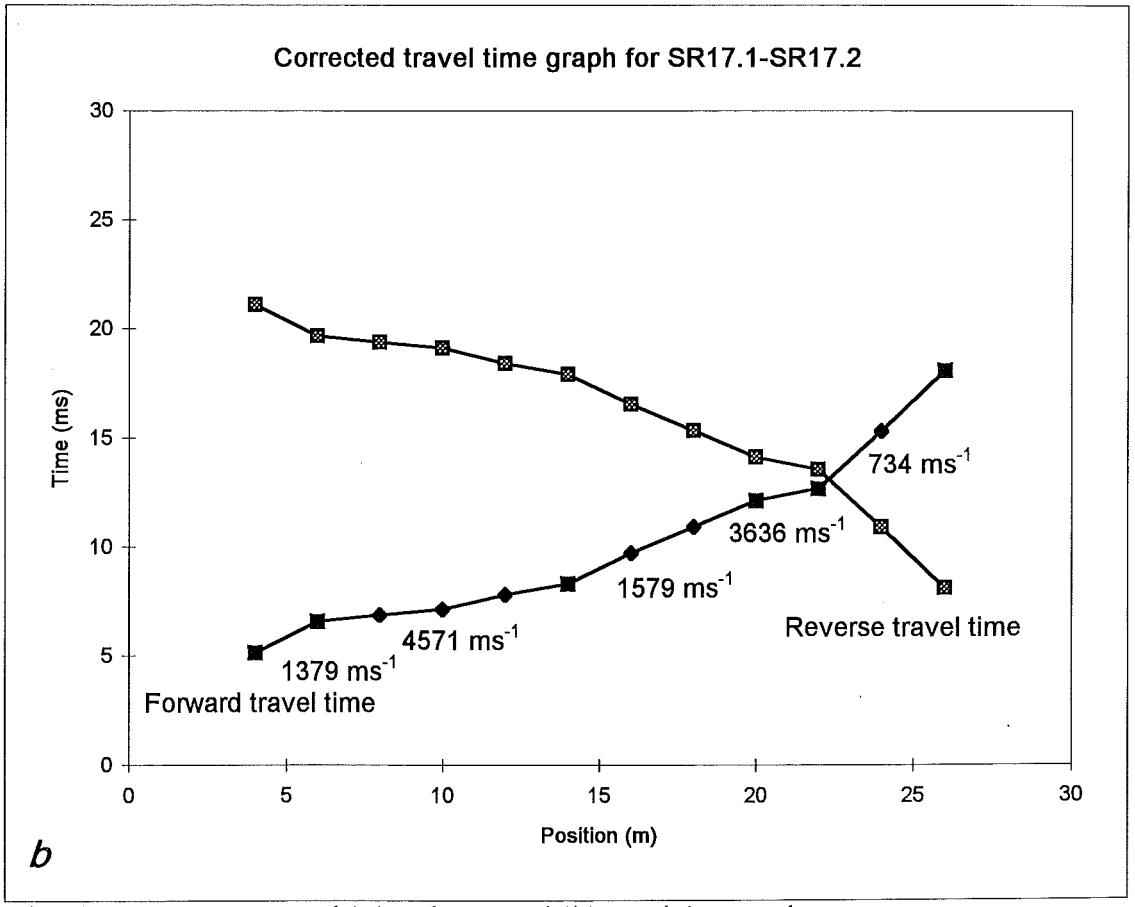

Figure D2.21: Uncorrected (*a*) and corrected (*b*) travel time graphs.

Table D2.22: Seismic Refraction Line SR18.1-SR18.2

Position (m)	T_f (ms)	T_r (ms)	T_d (ms)	T_{cf} (ms)	T_{cr} (ms)	V_1 (ms^{-1})	DCF (ms^{-1})	D_r (m)	GRL (m)
0	0.08	39.60				595			563.69
0.5	1.16					595			563.66
1	2.12					595			563.61
1.5	3.44					595			563.59
2	4.00	38.60				595			563.57
2.5	4.52					595			563.54
3	5.16					595			563.51
4	6.80	37.40	1.80	5.00	35.60	839	844	1.52	563.41
6	9.80	35.40	2.30	7.50	33.10	839	844	1.94	563.23
8	13.20	34.40	3.50	9.70	30.90	839	844	2.95	562.96
10	16.90	33.20	4.75	12.15	28.45	839	844	4.01	562.81
12	18.60	33.20	5.60	13.00	27.60	2352	615	3.44	562.73
14	22.00	31.40	6.40	15.60	25.00	629	1835	11.74	562.41
16	25.20	28.00	6.30	18.90	21.70	629	1835	11.56	562.16
18	30.00	25.20	7.30	22.70	17.90	629	1835	13.39	561.74
20	33.40	22.60	7.70	25.70	14.90	629	1835	14.13	561.40
22	34.00	19.80	6.60	27.40	13.20	1000	398	2.63	561.05
24	35.60	17.30	6.15	29.45	11.15	1000	398	2.45	560.74
26	35.80	13.30	4.25	31.55	9.05	1000	398	1.69	560.41
28	38.20	11.40	4.50	33.70	6.90	1000	398	1.79	560.08
29		9.50				370			559.91
29.5		7.52				370			559.87
30	40.40	5.76				370			559.74
30.5		3.72				370			559.64
31		2.24				370			559.58
31.5		1.08				370			559.57
32	41.60	0.60				370			559.56

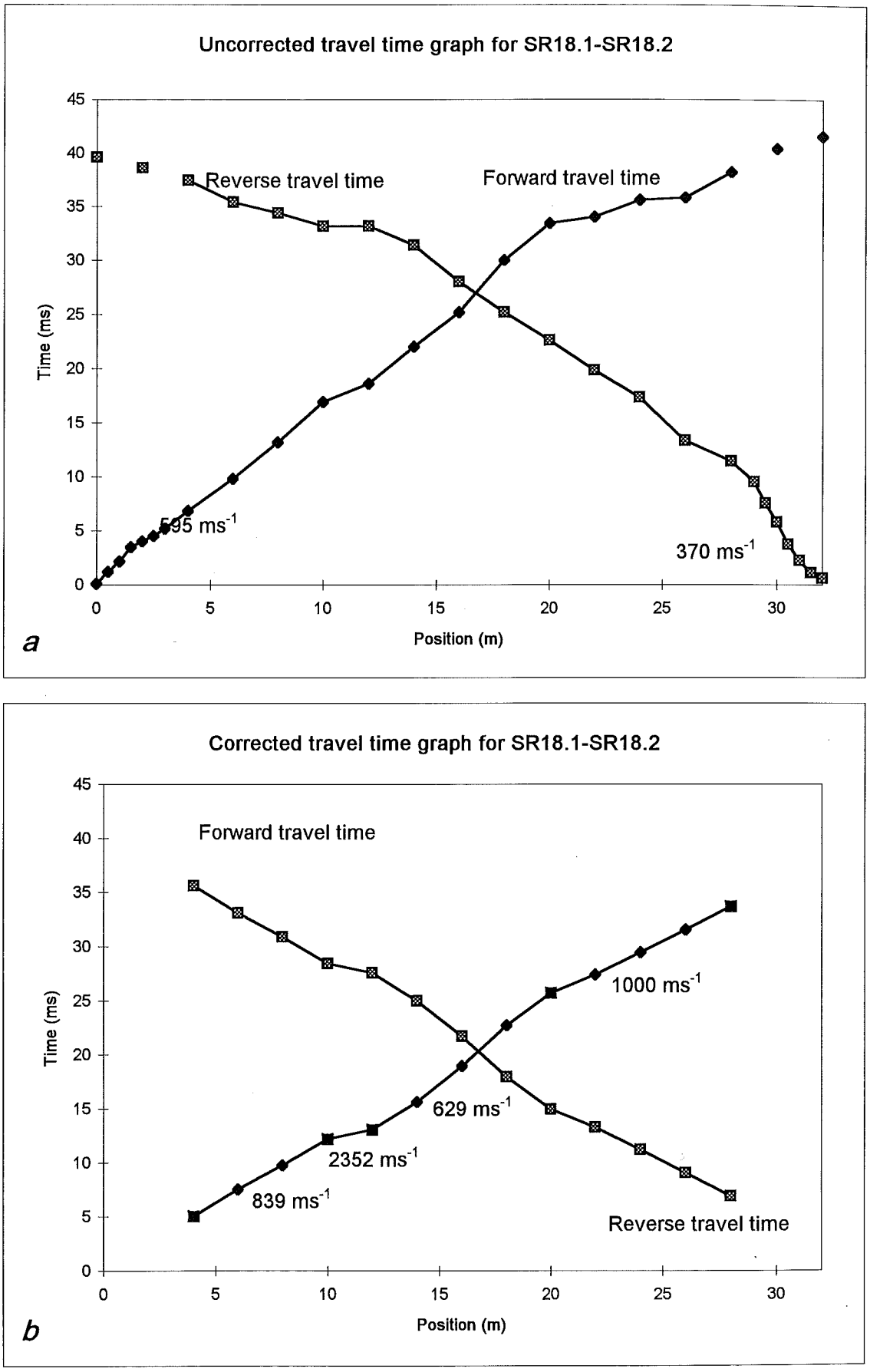

Figure D2.22: Uncorrected (*a*) and corrected (*b*) travel time graphs.

Table D2.23 : Seismic Refraction Line SR19.1-SR19.2

Position (m)	T_f (ms)	T_r (ms)	T_d (ms)	T_{cf} (ms)	T_{cr} (ms)	V_1 (ms^{-1})	DCF (ms^{-1})	D_r (m)	GRL (m)
0	0.08	23.20				592			444.59
0.5	0.80					592			444.64
1	1.40					592			444.50
1.5	2.80					592			444.46
2	3.52	23.60				592			444.41
2.5	4.68					592			444.34
3	5.20					592			444.28
4	6.84	23.20	3.27	3.57	19.93	772	922	3.02	444.18
6	10.80	22.40	4.85	5.95	17.55	772	922	4.47	443.96
8	15.60	21.60	6.85	8.75	14.75	772	922	6.32	443.78
10	18.90	23.60	9.50	9.40	14.10	2146	1430	13.58	443.63
12	20.20	22.20	9.45	10.75	12.75	2146	1430	13.51	443.49
14	20.60	20.60	8.85	11.75	11.75	2146	1430	12.66	443.39
16	18.20	15.80	5.25	12.95	10.55	2146	1430	7.51	443.51
18	18.50	14.60	4.80	13.70	9.80	2146	1430	6.86	443.65
20	18.80	13.70	4.50	14.30	9.20	2146	1430	6.43	443.44
22	16.50	10.10	1.55	14.95	8.55	2146	1430	2.22	443.15
24	17.90	8.90	1.65	16.25	7.25	2146	1430	2.36	443.12
26	19.60	8.60	2.35	17.25	6.25	2146	1430	3.36	443.35
28	20.00	7.50	2.00	18.00	5.50	2146	1430	2.86	443.64
30	21.40	6.90	2.40	19.00	4.50	2146	1430	3.43	443.68
32	22.20	6.80	2.75	19.45	4.05	4444	1235	3.40	443.85
34	20.40	4.32	0.61	19.79	3.71	4444	1235	0.75	443.73
36	20.80	3.60	0.45	20.35	3.15	4444	1235	0.56	443.73
37		3.04				1190			443.77
37.5		2.80				1190			443.72
38	24.40	2.64				1190			443.74
38.5		1.72				1190			443.75
39		1.48				1190			443.67
39.5		0.56				1190			443.64
40	23.80	0.24				1190			443.63

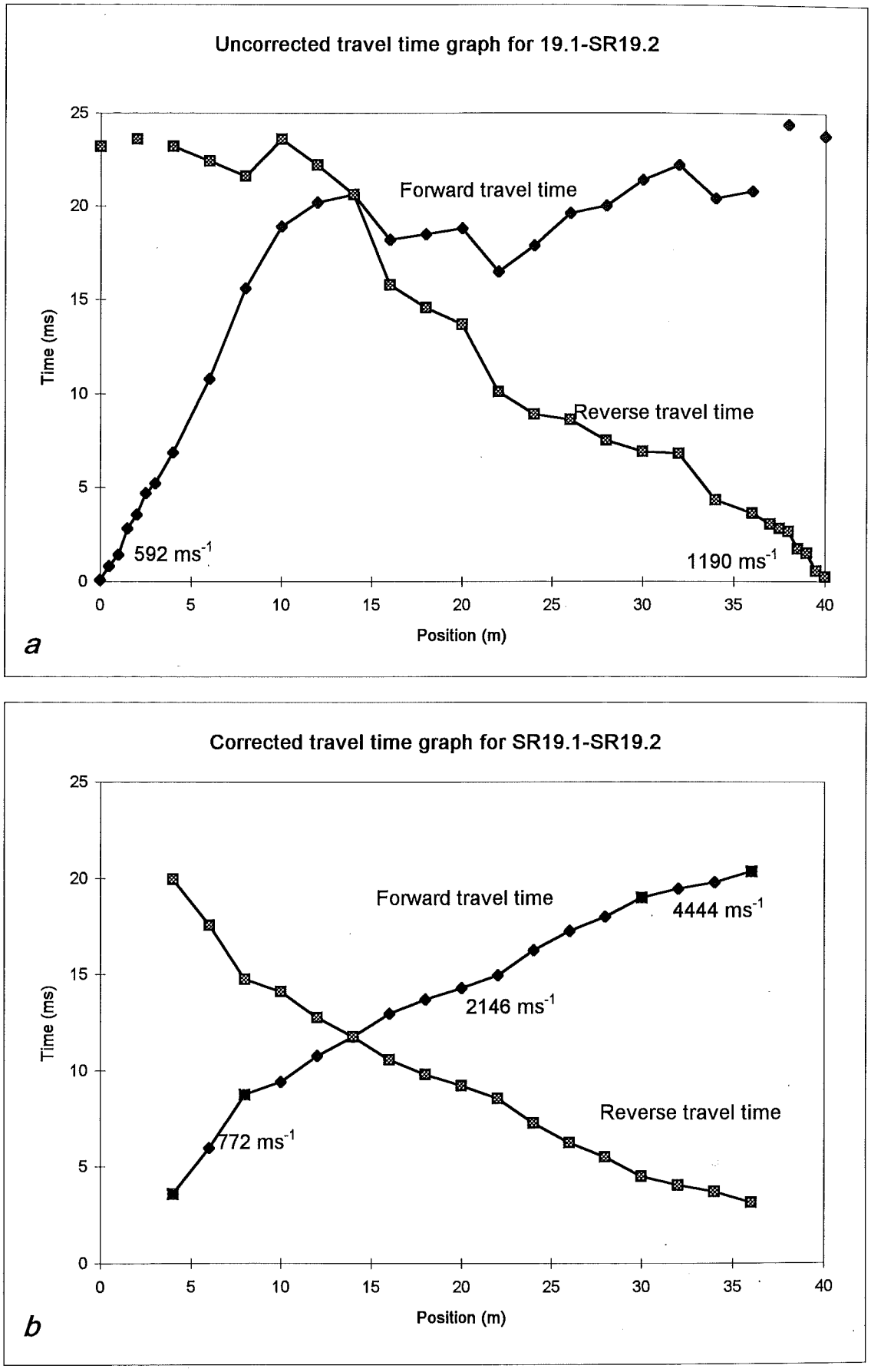

Figure D2.23: Uncorrected (*a*) and corrected (*b*) travel time graphs.

Table D2.24: Seismic Refraction Line SR20.1-SR20.2

Position (m)	T_f (ms)	T_r (ms)	T_d (ms)	T_{cf} (ms)	T_{cr} (ms)	V_1 (ms^{-1})	DCF (ms^{-1})	D_r (m)	GRL (m)
0	0.08	73.60				469			532.60
0.5	1.84					469			532.58
1	2.60					469			532.59
1.5	3.44					469			532.56
2	5.00	72.90				469			532.54
2.5	6.68					469			532.55
3	7.76					469			532.54
4	8.60	70.50	3.70	4.90	66.80	632	784	2.90	532.51
6	9.80	67.60	2.85	6.95	64.75	632	784	2.23	532.47
8	13.60	62.10	2.00	11.60	60.10	632	784	1.57	532.41
10	16.10	60.40	2.40	13.70	58.00	632	784	1.88	532.28
12	21.00	56.20	2.75	18.25	53.45	632	784	2.16	532.15
14	25.00	52.00	2.65	22.35	49.35	632	784	2.08	532.16
16	27.60	50.80	3.35	24.25	47.45	632	784	2.63	532.02
18	31.60	49.20	4.55	27.05	44.65	632	784	3.57	531.95
20	30.20	45.20	1.85	28.35	43.35	1290	532	0.98	531.91
22	31.40	45.60	2.65	28.75	42.95	1290	532	1.41	531.93
24	34.20	45.60	4.05	30.15	41.55	1290	532	2.16	531.88
26	35.00	43.60	3.45	31.55	40.15	1290	532	1.84	531.86
28	36.20	42.00	3.25	32.95	38.75	1290	532	1.73	531.86
30	38.00	40.40	3.35	34.65	37.05	1290	532	1.78	531.83
32	41.20	39.40	4.45	36.75	34.95	1290	532	2.37	531.75
34	44.80	39.00	6.05	38.75	32.95	1290	532	3.22	531.59
36	46.80	38.00	6.55	40.25	31.45	1290	532	3.49	531.45
38	47.20	33.80	4.65	42.55	29.15	1290	532	2.47	531.29
40	46.00	31.00	2.65	43.35	28.35	1475	522	1.38	531.34
42	45.60	29.60	1.75	43.85	27.85	1475	522	0.91	531.57
44	47.60	29.00	2.45	45.15	26.55	1475	522	1.28	531.73
46	50.00	29.40	3.85	46.15	25.55	1475	522	2.01	531.92
48	51.20	28.20	3.85	47.35	24.35	1475	522	2.01	532.18
50	53.00	26.40	3.85	49.15	22.55	1475	522	2.01	532.48
52	54.60	24.90	3.90	50.70	21.00	1475	522	2.04	532.79
54	55.80	20.70	2.40	53.40	18.30	755	649	1.56	533.16
56	58.80	16.50	1.80	57.00	14.70	755	649	1.17	533.64
58	60.60	13.80	1.35	59.25	12.45	755	649	0.88	533.96
60	62.40	10.00	0.35	62.05	9.65	755	649	0.23	534.29
62	64.20	7.90	0.20	64.00	7.70	755	649	0.13	534.62
63		6.88				514			534.73
63.5		5.64				514			534.82
64	66.80	4.40				514			534.84
64.5		2.96				514			534.86
65		1.84				514			534.87
65.5		1.04				514			534.88
66	69.80	0.12				514			534.89

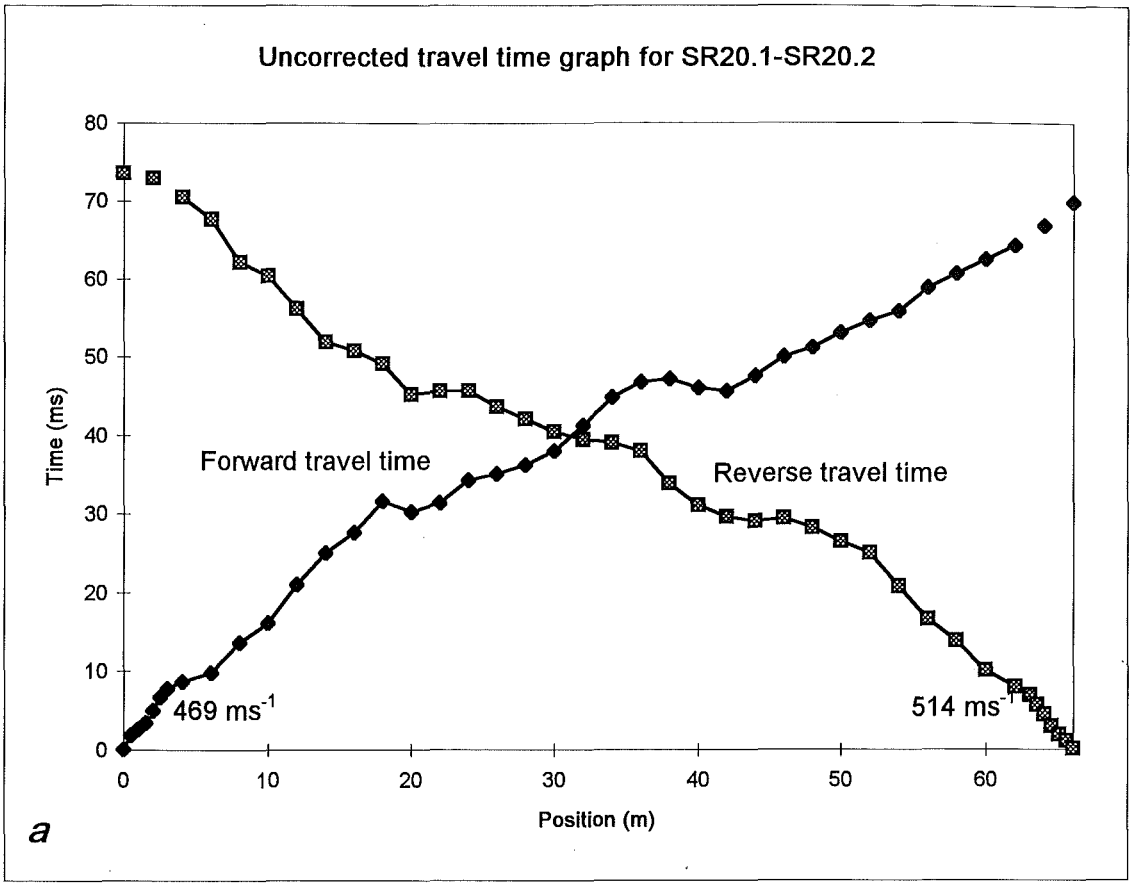

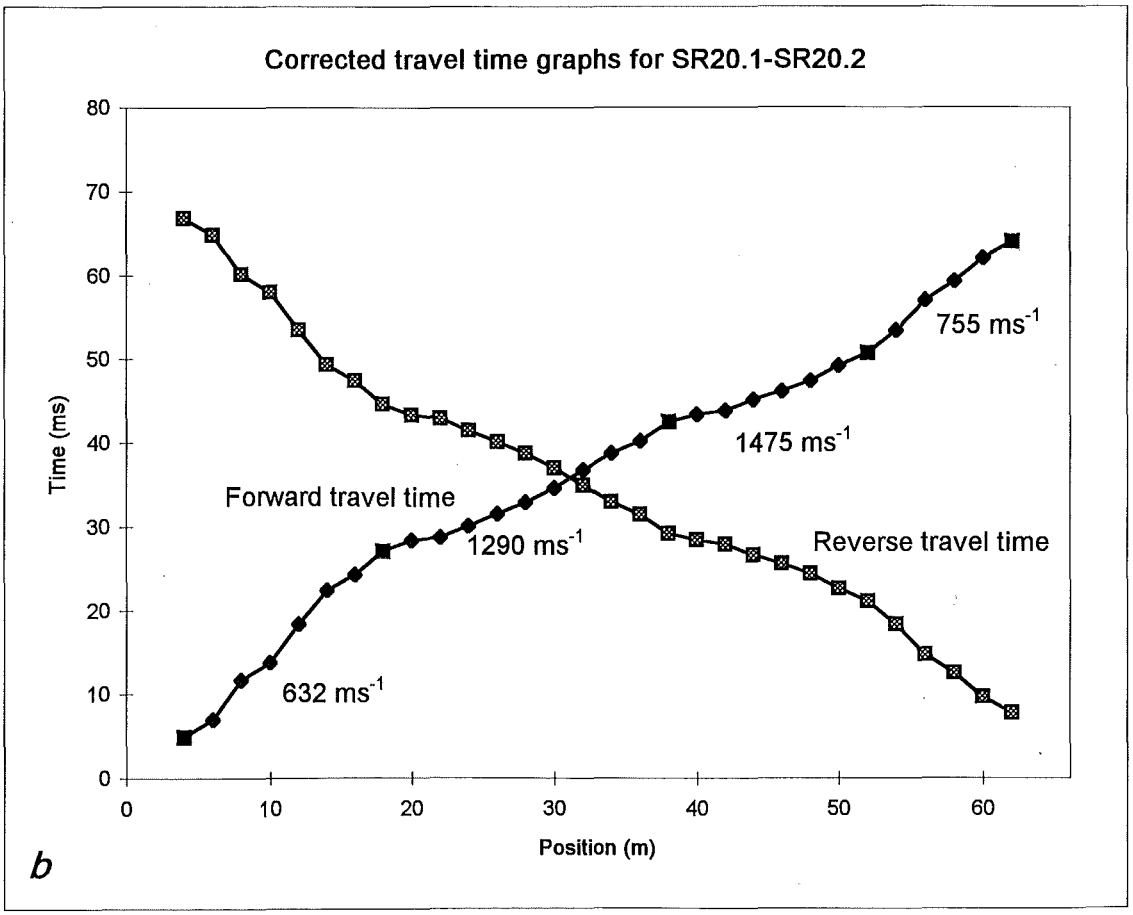

Figure D2.24: Uncorrected (*a*) and corrected (*b*) travel time graphs.

D2.3: Seismic refraction data repeatability results

Table D2.25: Seismic Refraction Line 2.1-2.2 (repeated data only)

Position (m)	T_f (ms)	T_r (ms)	T_d (ms)	T_{cf} (ms)	T_{cr} (ms)	V_1 (ms^{-1})	DCF (ms^{-1})	D_r (m)	GRL (m)
0	0.64	14.20				1010			443.78
0.5	1.08					1010			443.77
1	1.60					1010			443.77
1.5	2.04					1010			443.76
2	2.12	12.80				1010			443.76
2.5	2.76					1010			443.72
3	3.50					1010			443.70
4	4.04	11.60	0.67	3.37	10.93	2568	1260	0.84	443.69
6	4.84	10.80	0.67	4.17	10.13	2568	1260	0.84	443.58
8	5.80	9.80	0.65	5.15	9.15	2568	1260	0.82	443.52
10	6.74	8.60	0.52	6.22	8.08	2568	1260	0.66	443.38
12	7.60	8.50	0.90	6.70	7.60	2568	1260	1.13	443.26
14	9.10	8.30	1.55	7.55	6.75	2568	1260	1.95	443.18
16	9.80	8.00	1.75	8.05	6.25	2568	1260	2.20	443.18
18	11.00	8.00	2.35	8.65	5.65	2568	1260	2.96	443.21
20	13.00	8.10	3.40	9.60	4.70	2568	1260	4.28	443.14
22	13.20	7.90	3.40	9.80	4.50	5245	1157	3.93	443.06
24	13.30	7.40	3.20	10.10	4.20	5245	1157	3.70	442.98
26	13.40	6.40	2.75	10.65	3.65	5245	1157	3.18	442.89
28	13.20	5.60	2.25	10.95	3.35	5245	1157	2.60	442.74
30	13.20	4.80	1.85	11.35	2.95	5245	1157	2.14	442.60
32	13.40	4.20	1.65	11.75	2.55	5245	1157	1.91	442.54
34	13.60	3.48	1.39	12.21	2.09	5245	1157	1.61	442.51
36	14.20	3.20	1.55	12.65	1.65	5245	1157	1.79	442.46
37		2.96				1250			442.47
37.5		2.68				1250			442.45
38	14.50	2.40				1250			442.44
38.5		1.96				1250			442.43
39		1.60				1250			442.42
39.5		0.70				1250			442.41
40	14.40	0.20				1250			442.35

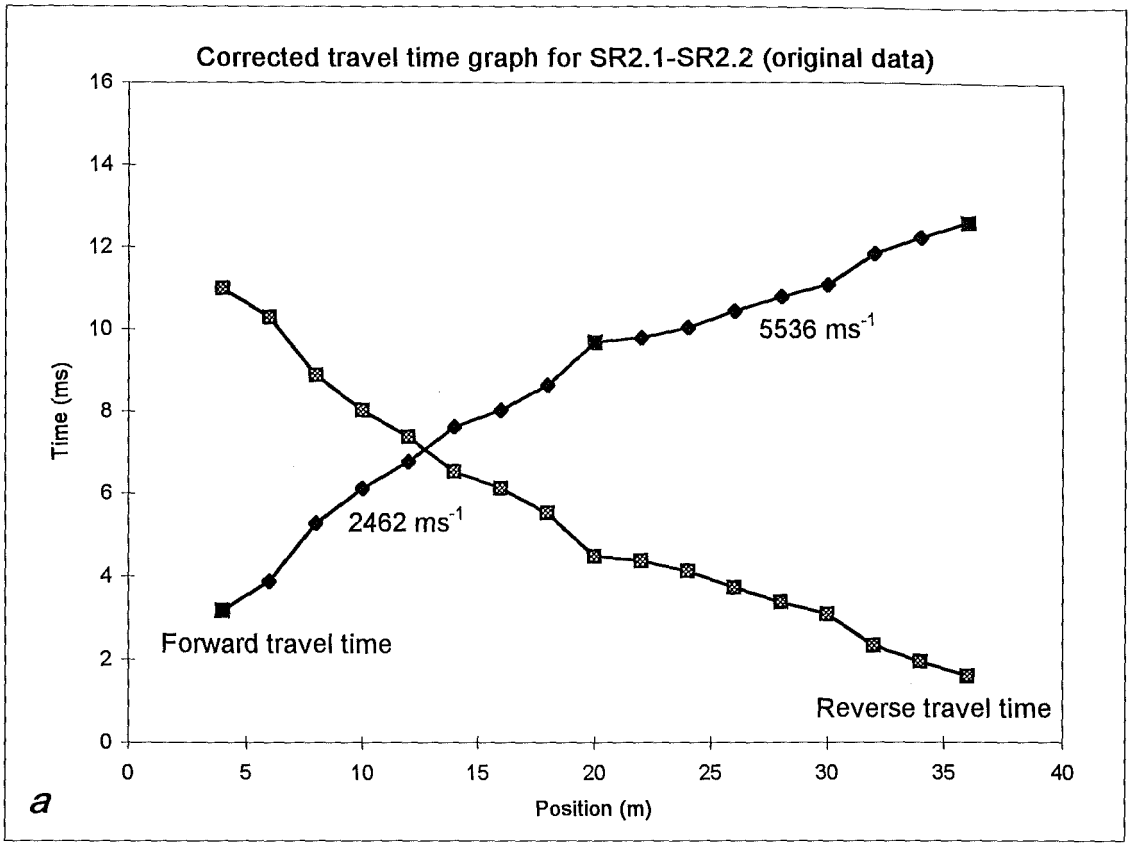

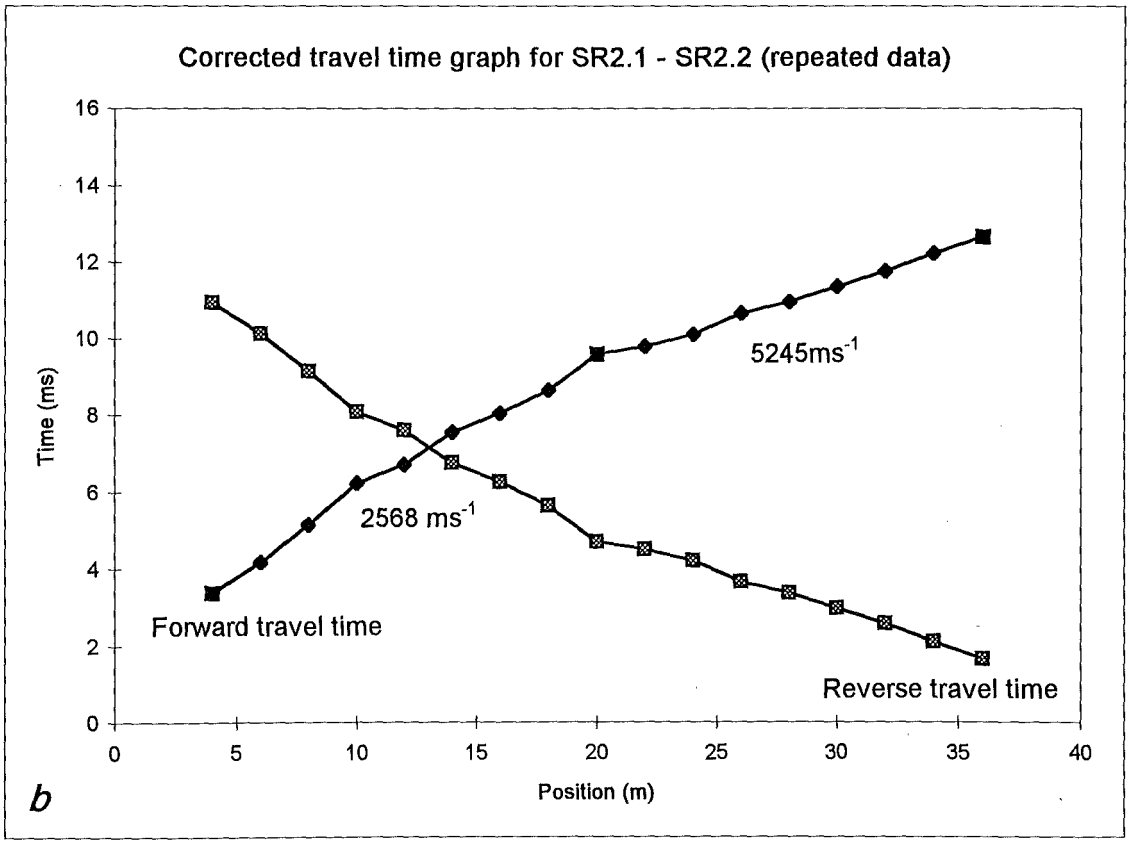

Figure D2.25: Corrected travel time graphs for original (*a*) and repeated data (*b*) for SR2.1 - SR2.2. Both graphs show remarkably similar travel time curves, indicating that the seismic refraction survey results are accurate.

Table D2.26: Seismic Refraction Line 3.1-3.2 (repeated data only)

Position (m)	T_f (ms)	T_r (ms)	T_d (ms)	T_{cf} (ms)	T_{cr} (ms)	V_1 (ms^{-1})	DCF (ms^{-1})	D_r (m)	GRL (m)
0	0.24	19.60				476			531.00
0.5	1.65					476			530.99
1	4.85					476			530.99
1.5	6.50					476			530.98
2	7.40	18.80				476			530.97
2.5	7.30					476			530.97
3	7.50					476			530.95
4	8.40	18.30	3.58	4.83	14.73	1403	529	1.89	530.93
6	8.90	16.40	2.88	6.03	13.53	1403	529	1.52	530.80
8	9.80	14.00	2.13	7.68	11.88	1403	529	1.63	530.61
10	10.20	13.70	2.18	8.03	11.53	6000	497	1.42	530.55
12	10.50	13.10	2.03	8.48	11.08	6000	497	1.49	530.54
14	10.70	12.90	2.03	8.68	10.88	6000	497	1.52	530.53
16	11.60	12.50	2.28	9.33	10.23	2553	505	1.59	530.53
18	13.20	12.20	2.93	10.28	9.28	2553	505	2.00	530.63
20	14.00	11.50	2.98	11.03	8.53	2553	505	2.14	530.70
22	15.80	10.30	3.28	12.53	7.03	1452	527	2.23	530.81
24	16.80	8.80	3.03	13.78	5.78	1452	527	2.31	530.99
26	17.50	7.80	2.88	14.63	4.93	1452	527	1.96	531.18
27		5.38				513			531.28
27.5		4.26				513			531.34
28	18.60	3.56				513			531.41
28.5		2.80				513			531.48
29		2.20				513			531.53
29.5		1.48				513			531.58
30	19.50	0.48				513			531.66

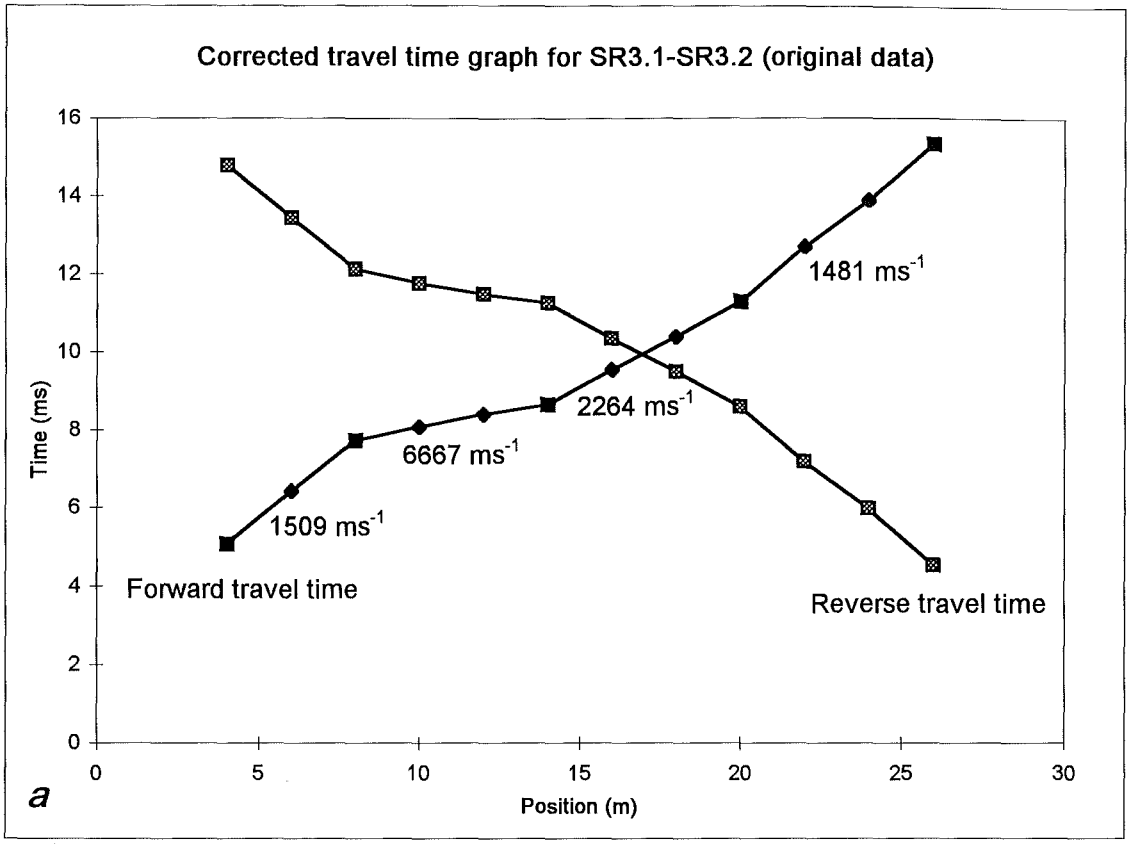

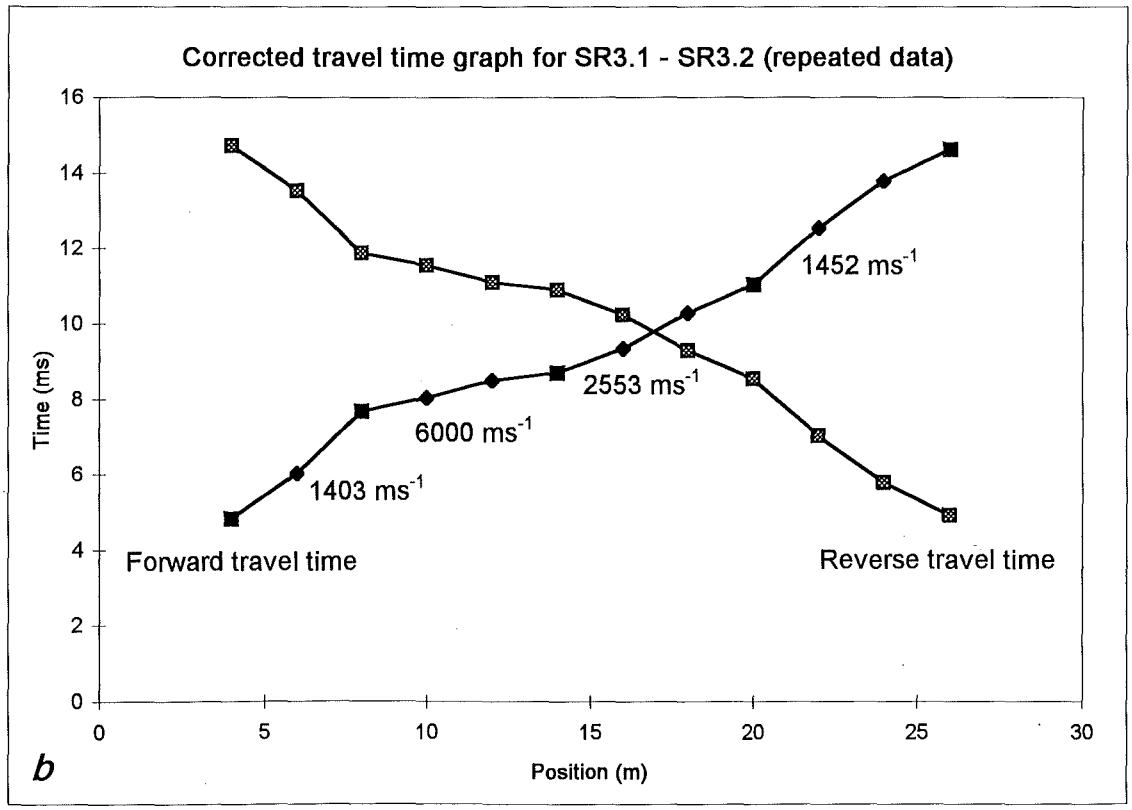

Figure D2.26: Corrected travel time graphs for original (*a*) and repeated data (*b*) for SR3.1 - SR3.2. Both graphs show remarkably similar travel time curves, indicating that the seismic refraction survey results are accurate.

D3 Laboratory test results

D3.1 Porosity-density data

Table D3.1 : Porosity-density data

Core sample	L (mm)	D (mm)	V (mm^3)	M_{sat} (kg)	M_{dry} (kg)	V_v (mm^3)	ρ_{sat} (kgm^{-3})	ρ_{dry} (kgm^{-3})	n (%)	I_{sat} (%)
GB23.3	118.82	60.85	0.345	0.928	0.935	0.007	2709	2688	2.03	0.75
GB65.3	166.03	61.13	0.487	1.310	1.314	0.004	2697	2688	0.82	0.30
GB87.1	173.77	60.70	0.502	1.334	1.342	0.008	2672	2656	1.59	0.60
GB87.4	174.95	61.07	0.512	1.381	1.388	0.007	2709	2695	1.37	0.50
GB87.6	137.93	60.85	0.401	1.110	1.114	0.004	2780	2770	1.00	0.36
GB92.1	176.45	61.27	0.520	1.399	1.405	0.006	2704	2692	1.15	0.43
GB92.4	172.95	61.16	0.508	1.374	1.378	0.004	2715	2707	0.79	0.29
GB92.7	168.99	61.18	0.496	1.366	1.368	0.002	2757	2752	0.40	0.15
GB92.9	165.05	61.18	0.485	1.319	1.324	0.005	2732	2721	1.03	0.38
GB92.12	176.89	60.85	0.514	1.398	1.402	0.004	2728	2721	0.78	0.29
GB92.14	175.84	61.20	0.517	1.403	1.407	0.004	2723	2716	0.77	0.28
GB92.17	176.59	61.19	0.519	1.404	1.407	0.003	2713	2707	0.58	0.21
GB92.19	168.51	61.15	0.494	1.377	1.387	0.010	2806	2785	2.02	0.72
GB92.21	178.47	61.31	0.526	1.424	1.428	0.004	2713	2706	0.76	0.28
GB97.1	153.82	60.68	0.444	1.195	1.203	0.008	2708	2690	1.80	0.67
GB97.3	140.90	60.80	0.409	1.091	1.099	0.008	2689	2670	1.96	0.73
GB98.1	174.31	60.88	0.507	1.383	1.388	0.005	2738	2728	0.99	0.36
GB98.3	176.00	61.00	0.514	1.394	1.397	0.003	2719	2714	0.58	0.21
GB106.1	140.03	61.05	0.410	1.121	1.124	0.003	2743	2735	0.73	0.27

Table D3.2: Sonic velocity and Dynamic Moduli of Elasticity data

Core Sample	L (mm)	ρ_{sat} (kgm^{-3})	ρ_{dry} (kgm^{-3})	P_{sat} (μs)	S_{sat} (μs)	$v_{P\,(sat)}$ (ms^{-1})	$v_{S\,(sat)}$ (ms^{-1})	$\frac{v_{P\,(sat)}}{v_{S\,(sat)}}$	$E_{dyn\,(sat)}$ (GPa)	$\nu_{dyn\,(sat)}$ -	P_{dry} (μs)	S_{dry} (μs)	$v_{p\,(dry)}$ (ms^{-1})	$v_{S\,(dry)}$ (ms^{-1})	$\frac{v_{S\,(sat)}}{v_{S\,(dry)}}$	$E_{dyn\,(dry)}$ (GPa)	$\nu_{dyn\,(dry)}$ -
GB23.3	118.82	2709	2688	32.0	71.7	3713	1657	2.24	20.5	0.38	34.2	47.4	3474	2507	1.39	32.3	0.04
GB65.3	166.03	2697	2688	37.3	61.6	4451	2695	1.65	47.4	0.21	41.9	51.3	3963	3236	1.22	28.0	0.50
GB87.1	173.77	2672	2656	44.7	97.8	3888	1777	2.19	23.1	0.37	48.4	71.2	3590	2441	1.47	33.9	0.07
GB87.4	174.95	2709	2695	38.3	70.8	4568	2471	1.85	42.8	0.29	43.2	58.7	4050	2980	1.36	43.5	0.09
GB87.6	137.93	2780	2770	30.4	58.8	4537	2346	1.93	40.3	0.32	33.1	54.8	4167	2517	1.66	42.6	0.21
GB92.1	176.45	2704	2692	37.6	64.1	4693	2753	1.70	50.7	0.24	40.5	67.0	4357	2634	1.65	45.3	0.21
GB92.4	172.95	2715	2707	36.4	54.1	4751	3197	1.49	60.3	0.09	40.2	47.0	4302	3680	1.17	10.1	0.86
GB92.7	168.99	2757	2752	34.6	63.4	4884	2665	1.83	50.4	0.29	37.5	50.8	4506	3327	1.35	54.9	0.10
GB92.9	165.05	2732	2721	37.5	72.4	4401	2280	1.93	37.4	0.32	42.5	57.6	3884	2865	1.36	40.3	0.10
GB92.12	176.89	2728	2721	37.0	80.9	4781	2186	2.19	35.7	0.37	41.8	56.5	4232	3131	1.35	47.8	0.10
GB92.14	175.84	2723	2716	37.2	72.2	4727	2435	1.94	42.6	0.32	41.4	54.4	4247	3232	1.31	46.1	0.19
GB92.17	176.59	2713	2707	37.1	58.1	4760	3039	1.57	57.9	0.16	42.8	60.2	4126	2933	1.41	46.1	0.01
GB92.19	168.51	2806	2785	100.5	131.8	1677	1278	1.31	7.4	0.19	110.9	155.1	1519	1086	1.40	6.4	0.02
GB92.21	178.47	2713	2706	37.3	65.2	4785	2737	1.75	51.1	0.26	43.2	57.9	4131	3082	1.34	44.8	0.13
GB97.1	153.82	2708	2690	37.1	80.7	4146	1906	2.18	26.9	0.37	40.5	60.0	3798	2564	1.48	38.2	0.08
GB97.3	140.90	2689	2670	34.4	77.0	4096	1830	2.24	24.8	0.38	52.0	66.0	2710	2135	1.27	16.6	0.32
GB98.1	174.31	2738	2728	38.5	82.5	4527	2113	2.14	33.3	0.36	40.0	73.7	4358	2365	1.84	39.4	0.29
GB98.3	176.00	2719	2714	36.2	51.9	4862	3391	1.43	64.2	0.03	38.9	58.4	4524	3014	1.50	54.3	0.10
GB106.1	140.03	2743	2735	30.9	58.2	4532	2406	1.88	41.4	0.30	32.0	44.8	4376	3126	1.40	52.3	0.02

D3.3 Stress-strain data and plots

Table D3.3: Stress-strain data for sample GB65.3.

Axial load (kN)	Axial stress (MPa)	Demec 1	Relative change	Axial strain (%)	Demec 2	Relative change	Axial strain (%)	Average strain (%)
0	0.0	862	0	0	738	0	0	0
10	3.4	860	2	0.0040	733	5	0.0101	0.0070
20	6.8	857	5	0.0101	728	10	0.0201	0.0151
30	10.2	853	9	0.0182	724	14	0.0281	0.0232
40	13.6	849	13	0.0263	720	18	0.0362	0.0312
50	17.1	849	13	0.0263	719	19	0.0382	0.0322
60	20.5	848	14	0.0283	714	24	0.0482	0.0383
70	23.9	840	22	0.0444	710	28	0.0563	0.0504
80	27.3	837	25	0.0505	707	31	0.0623	0.0564
90	30.7	833	29	0.0586	704	34	0.0683	0.0635
100	34.1	830	32	0.0646	700	38	0.0764	0.0705
110	37.5	827	35	0.0707	696	42	0.0844	0.0776
120	40.9	824	38	0.0768	692	46	0.0925	0.0846
130	44.3	821	41	0.0828	688	50	0.1005	0.0917
140	47.7	816	46	0.0929	685	53	0.1065	0.0997
150	51.2	812	50	0.1010	682	56	0.1126	0.1068
160	54.6	809	53	0.1071	679	59	0.1186	0.1128
170	58.0	806	56	0.1131	675	63	0.1266	0.1199
180	61.4	803	59	0.1192	670	68	0.1367	0.1279
190	64.8	800	62	0.1252	666	72	0.1447	0.1350
200	68.2	796	66	0.1333	662	76	0.1528	0.1430
210	71.6	793	69	0.1394	659	79	0.1588	0.1491
220	75.0	790	72	0.1454	656	82	0.1648	0.1551
230	78.4	786	76	0.1535	652	86	0.1729	0.1632
240	81.9	783	79	0.1596	648	90	0.1809	0.1702
250	85.3	779	83	0.1677	643	95	0.1910	0.1793
260	88.7	775	87	0.1757	639	99	0.1990	0.1874
270	92.1	772	90	0.1818	635	103	0.2070	0.1944
280	95.5	769	93	0.1879	632	106	0.2131	0.2005
290	98.9	767	95	0.1919	628	110	0.2211	0.2065
300	102.3	762	100	0.2020	624	114	0.2291	0.2156
310	105.7	758	104	0.2101	619	119	0.2392	0.2246
320	109.1	754	108	0.2182	614	124	0.2492	0.2337
330	112.6	751	111	0.2242	610	128	0.2573	0.2408
340	116.0	748	114	0.2303	607	131	0.2633	0.2468
350	119.4	744	118	0.2384	601	137	0.2754	0.2569
Failure stress:								
389	132.7							
50% failure stress and strain:								
194.5	66.4		64	0.1293		74	0.1487	0.1390
E_{s50} (GPa)	47.7							
E_{t50} (GPa)	47.7							
E_{ave} (GPa)	47.7							

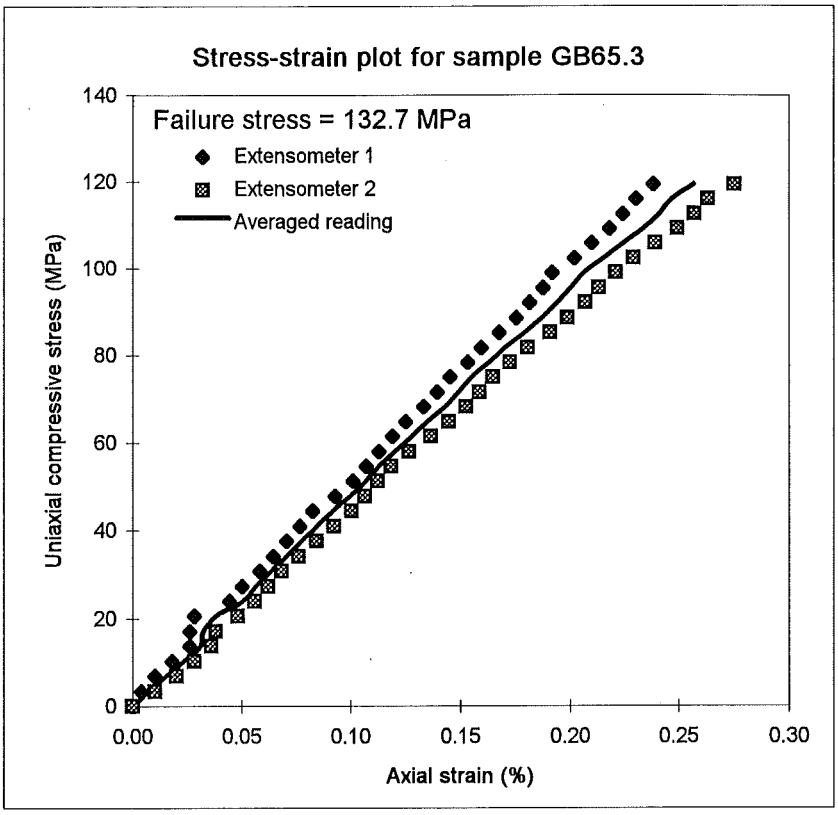

Figure D3.1: Stress-strain relationship for sample GB65.3.

Table D3.4: Stress-strain data for sample GB87.1

Axial load (kN)	Axial stress (MPa)	Demec 1	Relative change	Axial strain (%)	Demec 2	Relative change	Axial strain (%)	Average strain (%)
0	0.0	857	0	0	736	0	0	0
10	3.5	780	75	0.1515	724	12	0.0241	0.0878
20	6.9	735	120	0.2424	712	24	0.0482	0.1453
30	10.4	706	149	0.3010	697	39	0.0784	0.1897
40	13.8	677	178	0.3596	680	56	0.1126	0.2361
50	17.3	595	260	0.5252	635	101	0.2030	0.3641
Failure stress:								
52	18.0							
50% failure stress and strain:								
26	9.0		137.5	0.2778		33	0.0663	0.1720
E_{s50} (GPa)	5.2							
E_{t50} (GPa)	8.0							
E_{ave} (GPa)	8.0							

Table D3.5: Stress-strain data for sample GB87.4

Axial load (kN)	Axial stress (MPa)	Demec 1	Relative change	Axial strain (%)	Demec 2	Relative change	Axial strain (%)	Average strain (%)
0	0.0	873	0	0	741	0	0	0
10	3.4	863	10	0.0202	739	2	0.0040	0.0121
20	6.8	853	20	0.0404	734	7	0.0141	0.0272
30	10.2	847	26	0.0525	731	10	0.0201	0.0363
40	13.7	840	33	0.0667	729	12	0.0241	0.0454
50	17.1	832	41	0.0828	725	16	0.0322	0.0575
60	20.5	826	47	0.0949	723	18	0.0362	0.0656
70	23.9	821	52	0.1050	721	20	0.0402	0.0726
80	27.3	816	57	0.1151	721	20	0.0402	0.0777
90	30.7	811	62	0.1252	720	21	0.0422	0.0837
100	34.1	807	66	0.1333	715	26	0.0523	0.0928
110	37.6	802	71	0.1434	710	31	0.0623	0.1029
120	41.0	798	75	0.1515	704	37	0.0744	0.1129
Failure stress:								
218	74.4							
50% failure stress and strain:								
109	37.2		70	0.1414		30	0.0603	0.1009
E_{s50} (GPa)	36.9							
E_{t50} (GPa)	36.9							
E_{ave} (GPa)	36.9							

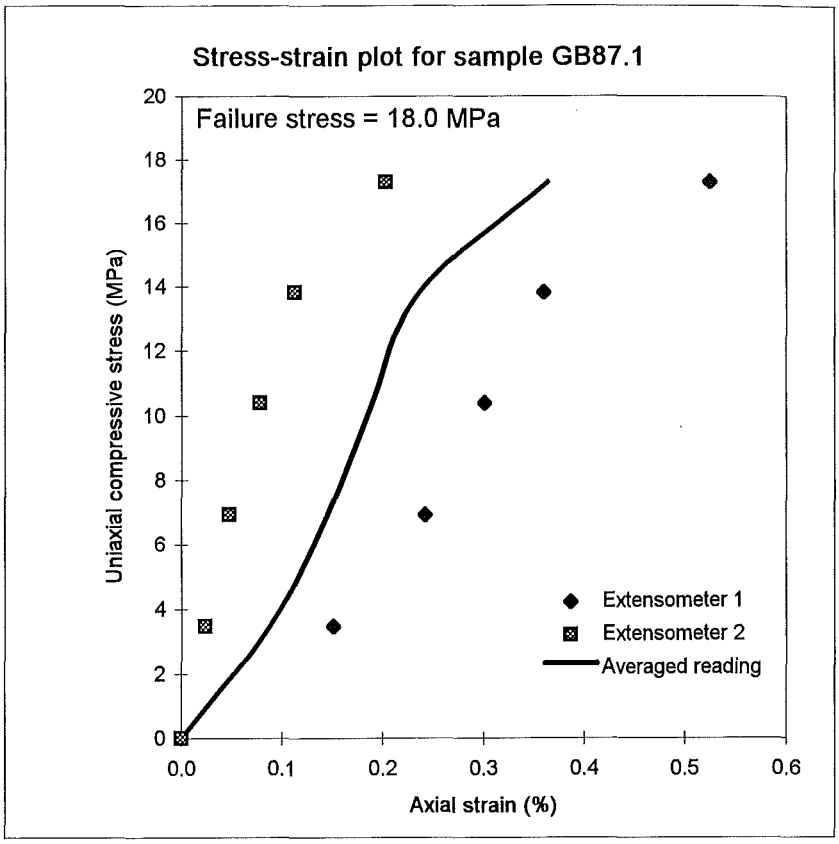

Figure D3.2: Stress-strain relationship for sample GB87.1.

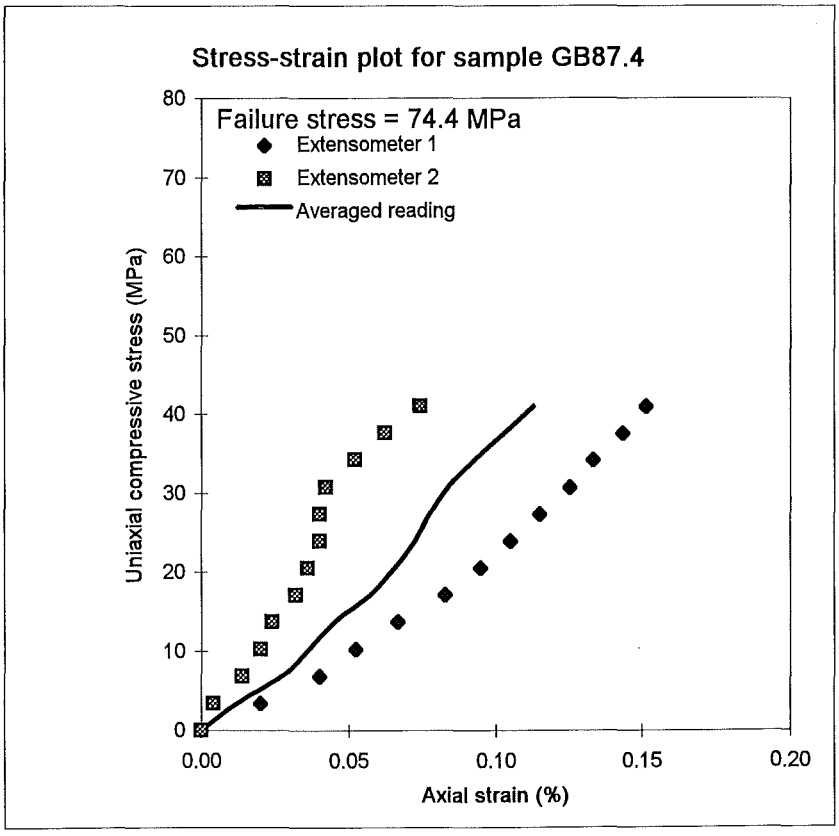

Figure D3.3: Stress-strain relationship for sample GB87.4.

Table D3.6: Stress-strain data for sample GB87.6

Axial load (kN)	Axial stress (MPa)	Demec 1	Relative change	Axial strain (%)	Demec 2	Relative change	Axial strain (%)	Average strain (%)
0	0.0	877	0	0	754	0	0	0
10	3.4	860	17	0.0343	745	9	0.0181	0.0262
20	6.9	852	25	0.0505	741	13	0.0261	0.0383
30	10.3	844	33	0.0667	737	17	0.0342	0.0504
40	13.8	838	39	0.0788	733	21	0.0422	0.0605
50	17.2	832	45	0.0909	729	25	0.0503	0.0706
60	20.7	827	50	0.1010	726	28	0.0563	0.0786
70	24.1	824	53	0.1071	721	33	0.0663	0.0867
80	27.5	819	58	0.1172	717	37	0.0744	0.0958
90	31.0	815	62	0.1252	713	41	0.0824	0.1038
100	34.4	810	67	0.1353	709	45	0.0905	0.1129
110	37.9	805	72	0.1454	706	48	0.0965	0.1210
120	41.3	800	77	0.1555	706	48	0.0965	0.1260
130	44.8	794	83	0.1677	704	50	0.1005	0.1341
Failure stress:								
135	46.5							
50% failure stress and strain:								
67.5	23.2		52	0.1050		32	0.0643	0.0847
E_{s50} (GPa)	27.4							
E_{t50} (GPa)	39.0							
E_{ave} (GPa)	39.0							

Table D3.7: Stress-strain data for sample GB92.1

Axial load (kN)	Axial stress (MPa)	Demec 1	Relative change	Axial strain (%)	Demec 2	Relative change	Axial strain (%)	Average strain (%)
0	0.0	868	0	0	735	0	0	0
10	3.4	866	2	0.0040	731	4	0.0080	0.0060
20	6.8	860	8	0.0162	726	9	0.0181	0.0171
30	10.2	855	13	0.0263	723	12	0.0241	0.0252
40	13.6	852	16	0.0323	718	17	0.0342	0.0332
50	17.0	847	21	0.0424	712	23	0.0462	0.0443
60	20.4	844	24	0.0485	707	28	0.0563	0.0524
70	23.8	841	27	0.0545	703	32	0.0643	0.0594
80	27.2	837	31	0.0626	698	37	0.0744	0.0685
90	30.6	834	34	0.0687	693	42	0.0844	0.0766
100	34.0	831	37	0.0747	688	47	0.0945	0.0846
110	37.4	828	40	0.0808	686	49	0.0985	0.0896
120	40.7	825	43	0.0869	684	51	0.1025	0.0947
130	44.1	822	46	0.0929	680	55	0.1106	0.1017
140	47.5	818	50	0.1010	675	60	0.1206	0.1108
150	50.9	815	53	0.1071	670	65	0.1307	0.1189
160	54.3	809	59	0.1192	665	70	0.1407	0.1299
Failure stress:								
160.5	54.5							
50% failure stress and strain:								
80.25	27.2		31	0.0626		37	0.0744	0.0685
E_{s50} (GPa)	39.8							
E_{t50} (GPa)	39.8							
E_{ave} (GPa)	39.8							

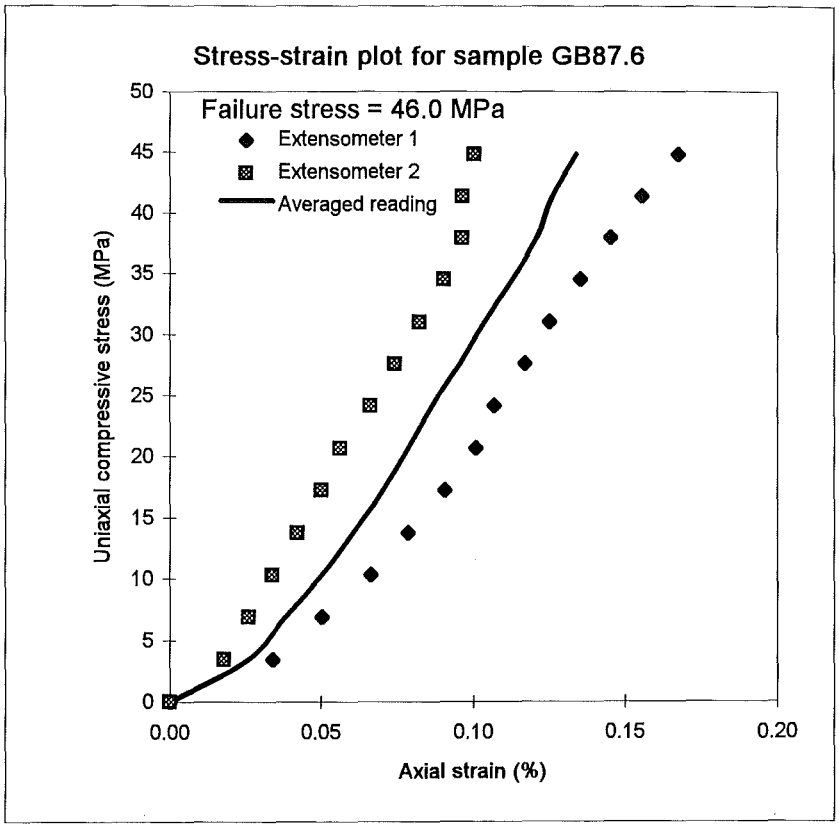

Figure D3.4: Stress-strain relationship for sample GB87.6.

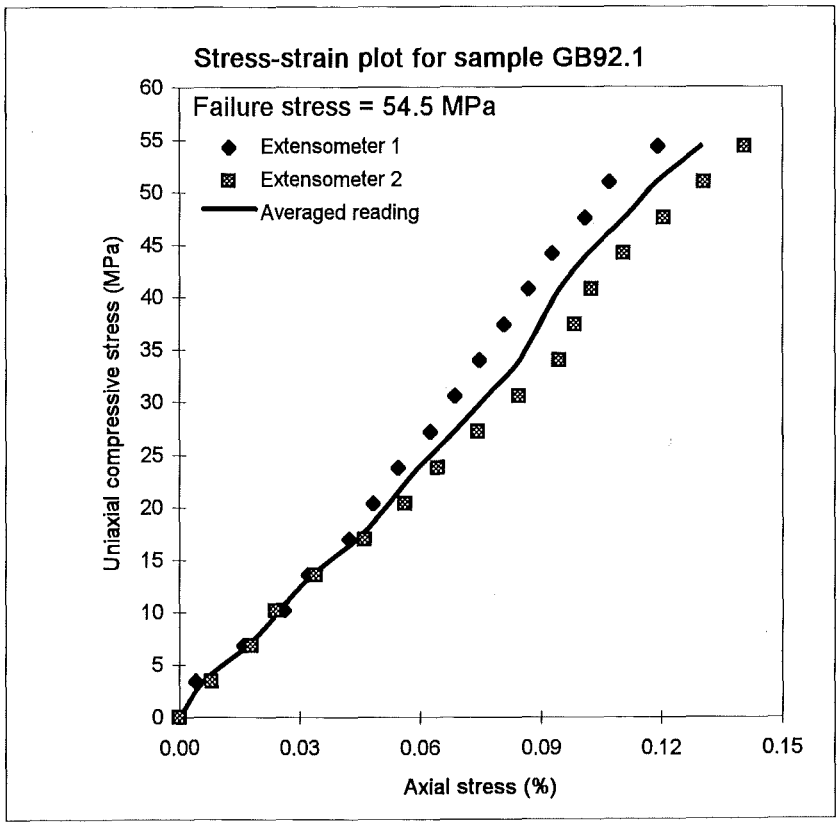

Figure D3.5: Stress-strain relationship for sample GB92.1.

Table D3.8: Stress-strain data for sample GB92.4

Axial load (kN)	Axial stress (MPa)	Demec 1	Relative change	Axial strain (%)	Demec 2	Relative change	Axial strain (%)	Average strain (%)
0	0.0	866	0	0	728	0	0	0
10	3.4	862	4	0.0081	724	4	0.0080	0.0081
20	6.8	856	10	0.0202	723	5	0.0101	0.0151
30	10.2	851	15	0.0303	721	7	0.0141	0.0222
40	13.6	847	19	0.0384	719	9	0.0181	0.0282
50	17.0	843	23	0.0465	717	11	0.0221	0.0343
60	20.4	840	26	0.0525	713	15	0.0302	0.0413
70	23.9	836	30	0.0606	710	18	0.0362	0.0484
80	27.3	833	33	0.0667	701	27	0.0543	0.0605
90	30.7	829	37	0.0747	697	31	0.0623	0.0685
100	34.1	825	41	0.0828	694	34	0.0683	0.0756
110	37.5	822	44	0.0889	691	37	0.0744	0.0816
120	40.9	819	47	0.0949	686	42	0.0844	0.0897
130	44.3	815	51	0.1030	681	47	0.0945	0.0987
140	47.7	812	54	0.1091	679	49	0.0985	0.1038
150	51.1	809	57	0.1151	676	52	0.1045	0.1098
160	54.5	805	61	0.1232	672	56	0.1126	0.1179
170	57.9	802	64	0.1293	669	59	0.1186	0.1239
180	61.3	799	67	0.1353	667	61	0.1226	0.1290
190	64.7	795	71	0.1434	662	66	0.1327	0.1380
200	68.1	792	74	0.1495	659	69	0.1387	0.1441
210	71.6	789	77	0.1555	657	71	0.1427	0.1491
220	75.0	786	80	0.1616	654	74	0.1487	0.1552
230	78.4	783	83	0.1677	652	76	0.1528	0.1602
240	81.8	779	87	0.1757	649	79	0.1588	0.1673
250	85.2	774	92	0.1858	645	83	0.1668	0.1763
260	88.6	770	96	0.1939	642	86	0.1729	0.1834
Failure stress:								
384.5	131.0							
50% failure stress and strain:								
192.25	65.5		72	0.1454		67	0.1347	0.1401
E_{s50} (GPa)	46.8							
E_{t50} (GPa)	46.8							
E_{ave} (GPa)	46.8							

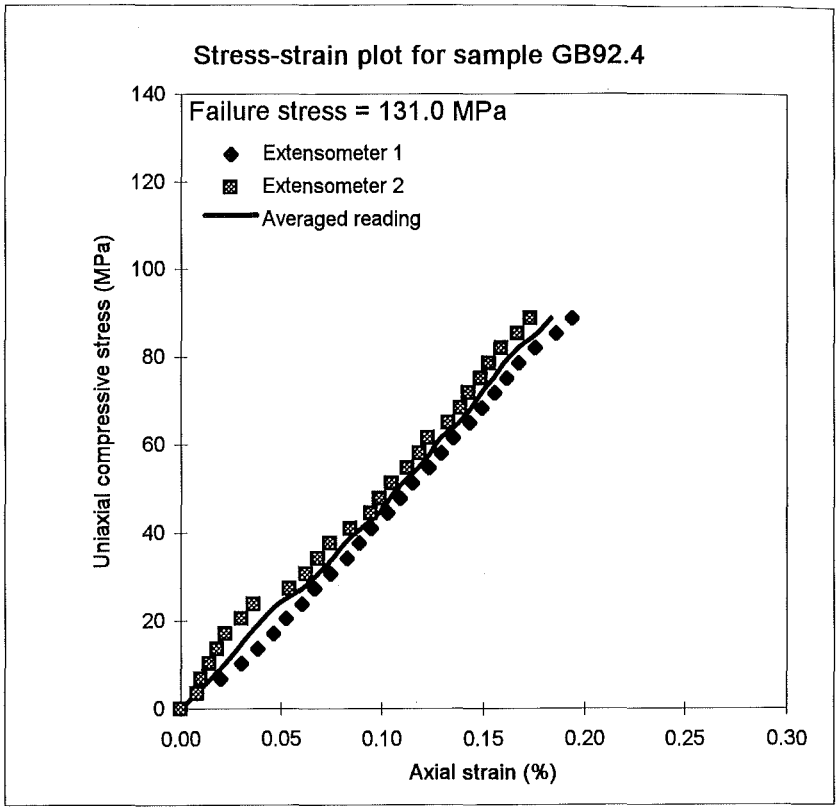

Figure D3.6: Stress-strain relationship for sample GB92.4.

Table D3.9: Stress-strain data for sample GB92.7

Axial load (kN)	Axial stress (MPa)	Demec 1	Relative change	Axial strain (%)	Demec 2	Relative change	Axial strain (%)	Average strain (%)
0	0.0	855	0	0	733	0	0	0
10	3.4	853	2	0.0040	730	3	0.0060	0.0050
20	6.8	852	3	0.0061	725	8	0.0161	0.0111
30	10.2	850	5	0.0101	722	11	0.0221	0.0161
40	13.6	847	8	0.0162	719	14	0.0281	0.0222
50	17.0	844	11	0.0222	716	17	0.0342	0.0282
60	20.4	840	15	0.0303	714	19	0.0382	0.0342
70	23.8	837	18	0.0364	711	22	0.0442	0.0403
80	27.2	835	20	0.0404	708	25	0.0503	0.0453
90	30.6	832	23	0.0465	705	28	0.0563	0.0514
100	34.0	829	26	0.0525	702	31	0.0623	0.0574
110	37.5	826	29	0.0586	698	35	0.0704	0.0645
120	40.9	824	31	0.0626	695	38	0.0764	0.0695
130	44.3	824	31	0.0626	692	41	0.0824	0.0725
140	47.7	819	36	0.0727	689	44	0.0884	0.0806
150	51.1	816	39	0.0788	685	48	0.0965	0.0876
160	54.5	814	41	0.0828	682	51	0.1025	0.0927
170	57.9	810	45	0.0909	679	54	0.1085	0.0997
180	61.3	807	48	0.0970	675	58	0.1166	0.1068
190	64.7	803	52	0.1050	671	62	0.1246	0.1148
200	68.1	800	55	0.1111	668	65	0.1307	0.1209
210	71.5	797	58	0.1172	665	68	0.1367	0.1269
220	74.9	793	62	0.1252	660	73	0.1467	0.1360
230	78.3	788	67	0.1353	658	75	0.1508	0.1430
240	81.7	787	68	0.1374	653	80	0.1608	0.1491
250	85.1	787	68	0.1374	651	82	0.1648	0.1511
260	88.5	786	69	0.1394	644	89	0.1789	0.1591
270	91.9	784	71	0.1434	641	92	0.1849	0.1642
280	95.3	781	74	0.1495	638	95	0.1910	0.1702
290	98.7	777	78	0.1576	634	99	0.1990	0.1783
300	102.1	775	80	0.1616	631	102	0.2050	0.1833
310	105.5	774	81	0.1636	628	105	0.2111	0.1873
320	109.0	768	87	0.1757	625	108	0.2171	0.1964
330	112.4	762	93	0.1879	623	110	0.2211	0.2045
340	115.8	758	97	0.1959	619	114	0.2291	0.2125
350	119.2	749	106	0.2141	616	117	0.2352	0.2246
Failure stress:								
429.5	146.2							
50% failure stress and strain:								
214.75	73.1		60	0.1212		70.5	0.1417	0.1315
E_{s50} (GPa)	55.6							
E_{t50} (GPa)	55.6							
E_{ave} (GPa)	55.6							

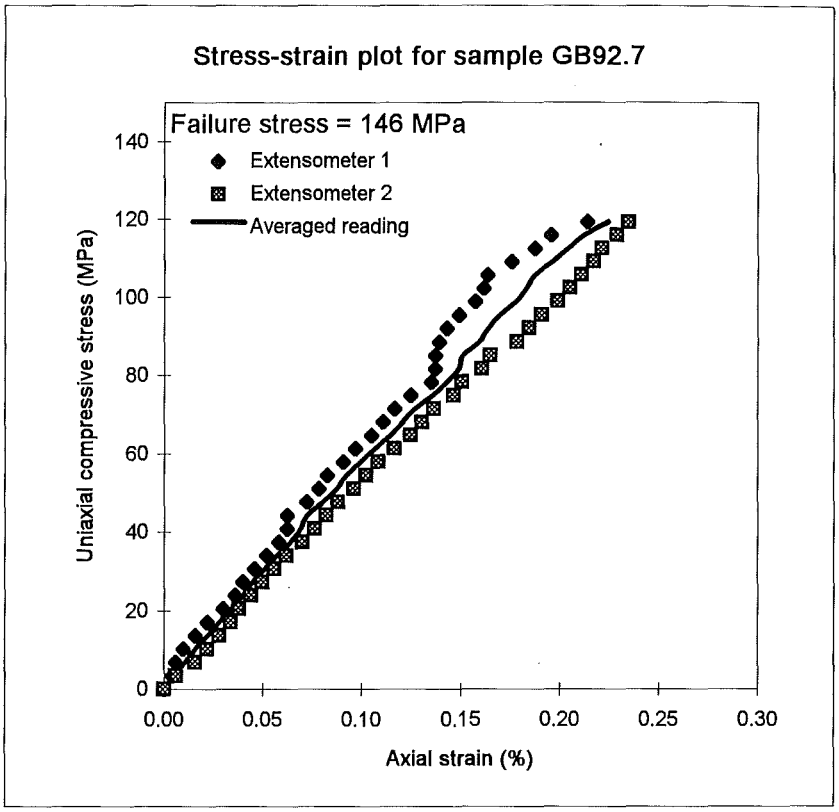

Figure D3.7: Stress-strain relationship for sample GB92.7.

Table D3.10: Stress-strain data for sample GB92.9

Axial load (kN)	Axial stress (MPa)	Demec 1	Relative change	Axial strain (%)	Demec 2	Relative change	Axial strain (%)	Average strain (%)
0	0.0	866	0	0	748	0	0	0
10	3.4	854	12	0.0242	743	5	0.0101	0.0171
20	6.8	846	20	0.0404	741	7	0.0141	0.0272
30	10.2	842	24	0.0485	737	11	0.0221	0.0353
40	13.6	837	29	0.0586	734	14	0.0281	0.0434
50	17.0	833	33	0.0667	731	17	0.0342	0.0504
60	20.4	827	39	0.0788	726	22	0.0442	0.0615
70	23.8	823	43	0.0869	721	27	0.0543	0.0706
80	27.2	819	47	0.0949	718	30	0.0603	0.0776
90	30.6	814	52	0.1050	716	32	0.0643	0.0847
100	34.0	809	57	0.1151	711	37	0.0744	0.0948
110	37.5	805	61	0.1232	707	41	0.0824	0.1028
120	40.9	801	65	0.1313	703	45	0.0905	0.1109
130	44.3	796	70	0.1414	699	49	0.0985	0.1199
140	47.7	792	74	0.1495	693	55	0.1106	0.1300
150	51.1	788	78	0.1576	689	59	0.1186	0.1381
160	54.5	782	84	0.1697	684	64	0.1286	0.1492
170	57.9	777	89	0.1798	678	70	0.1407	0.1602
180	61.3	774	92	0.1858	675	73	0.1467	0.1663
190	64.7	769	97	0.1959	671	77	0.1548	0.1754
200	68.1	765	101	0.2040	666	82	0.1648	0.1844
210	71.5	762	104	0.2101	663	85	0.1709	0.1905
220	74.9	752	114	0.2303	659	89	0.1789	0.2046
230	78.3	745	121	0.2444	653	95	0.1910	0.2177
240	81.7	740	126	0.2545	649	99	0.1990	0.2268
Failure stress:								
254	86.5							
50% failure stress and strain:								
127	43.2		68.5	0.1384		48	0.0965	0.1174
E_{s50} (GPa)	36.8							
E_{t50} (GPa)	37.5							
E_{ave} (GPa)	37.5							

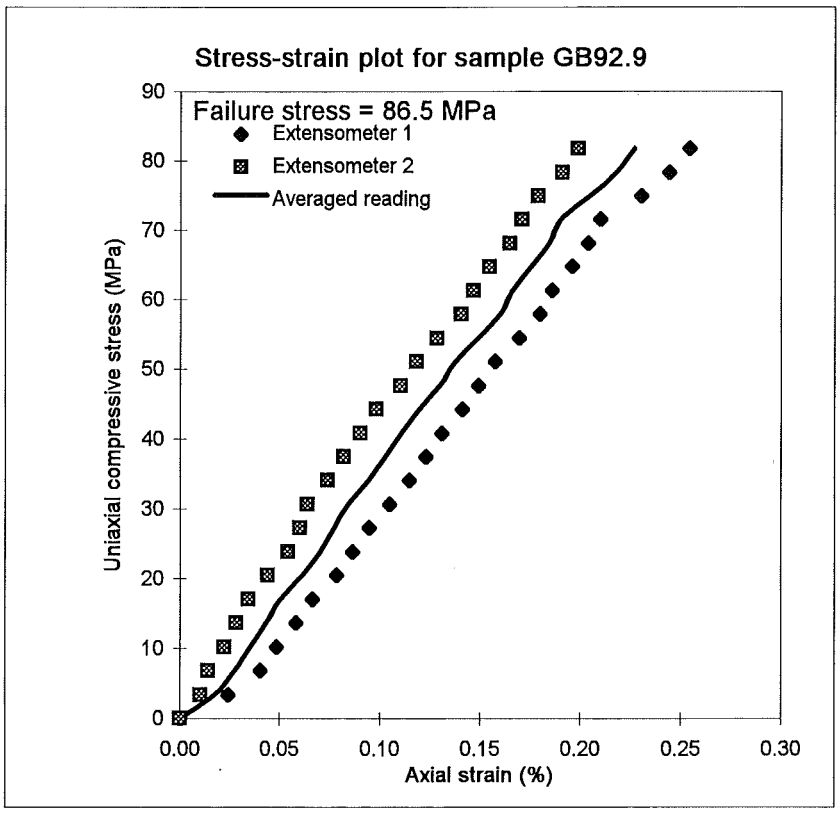

Figure D3.8: Stress-strain relationship for sample GB92.9.

Table D3.11: Stress-strain data for sample GB92.12

Axial load (kN)	Axial stress (MPa)	Demec 1	Relative change	Axial strain (%)	Demec 2	Relative change	Axial strain (%)	Average strain (%)
0	0.0	865	0	0	760	0	0	0
10	3.4	862	3	0.0061	757	3	0.0060	0.0060
20	6.9	861	4	0.0081	752	8	0.0161	0.0121
30	10.3	858	7	0.0141	748	12	0.0241	0.0191
40	13.8	855	10	0.0202	743	17	0.0342	0.0272
50	17.2	850	15	0.0303	737	23	0.0462	0.0383
60	20.7	845	20	0.0404	726	34	0.0683	0.0544
70	24.1	838	27	0.0545	723	37	0.0744	0.0645
80	27.5	833	32	0.0646	719	41	0.0824	0.0735
90	31.0	827	38	0.0768	712	48	0.0965	0.0866
100	34.4	822	43	0.0869	708	52	0.1045	0.0957
110	37.9	817	48	0.0970	703	57	0.1146	0.1058
120	41.3	813	52	0.1050	697	63	0.1266	0.1158
130	44.8	808	57	0.1151	688	72	0.1447	0.1299
140	48.2	804	61	0.1232	679	81	0.1628	0.1430
150	51.6	800	65	0.1313	672	88	0.1769	0.1541
160	55.1	784	81	0.1636	655	105	0.2111	0.1873
Failure stress:								
168.5	58.0							
50% failure stress and strain:								
84.25	29.0		35	0.0707		44	0.0884	0.0796
E_{s50} (GPa)	36.4							
E_{t50} (GPa)	36.4							
E_{ave} (GPa)	36.4							

Table D3.12: Stress-strain data for sample GB92.14

Axial load (kN)	Axial stress (MPa)	Demec 1	Relative change	Axial strain (%)	Demec 2	Relative change	Axial strain (%)	Average strain (%)
0	0.0	869	0	0	739	0	0	0
10	3.4	858	11	0.0222	738	1	0.0020	0.0121
20	6.8	851	18	0.0364	732	7	0.0141	0.0252
30	10.2	845	24	0.0485	728	11	0.0221	0.0353
40	13.6	839	30	0.0606	725	14	0.0281	0.0444
50	17.0	835	34	0.0687	722	17	0.0342	0.0514
60	20.4	830	39	0.0788	718	21	0.0422	0.0605
70	23.8	826	43	0.0869	714	25	0.0503	0.0686
80	27.2	822	47	0.0949	710	29	0.0583	0.0766
90	30.6	818	51	0.1030	705	34	0.0683	0.0857
100	34.0	814	55	0.1111	700	39	0.0784	0.0947
110	37.4	811	58	0.1172	698	41	0.0824	0.0998
120	40.8	807	62	0.1252	697	42	0.0844	0.1048
130	44.2	804	65	0.1313	693	46	0.0925	0.1119
140	47.7	800	69	0.1394	689	50	0.1005	0.1199
Failure stress:								
219	74.5							
50% failure stress and strain:								
109.5	37.3		58	0.1172		41	0.0824	0.0998
E_{s50} (GPa)	37.4							
E_{t50} (GPa)	40.0							
E_{ave} (GPa)	40.0							

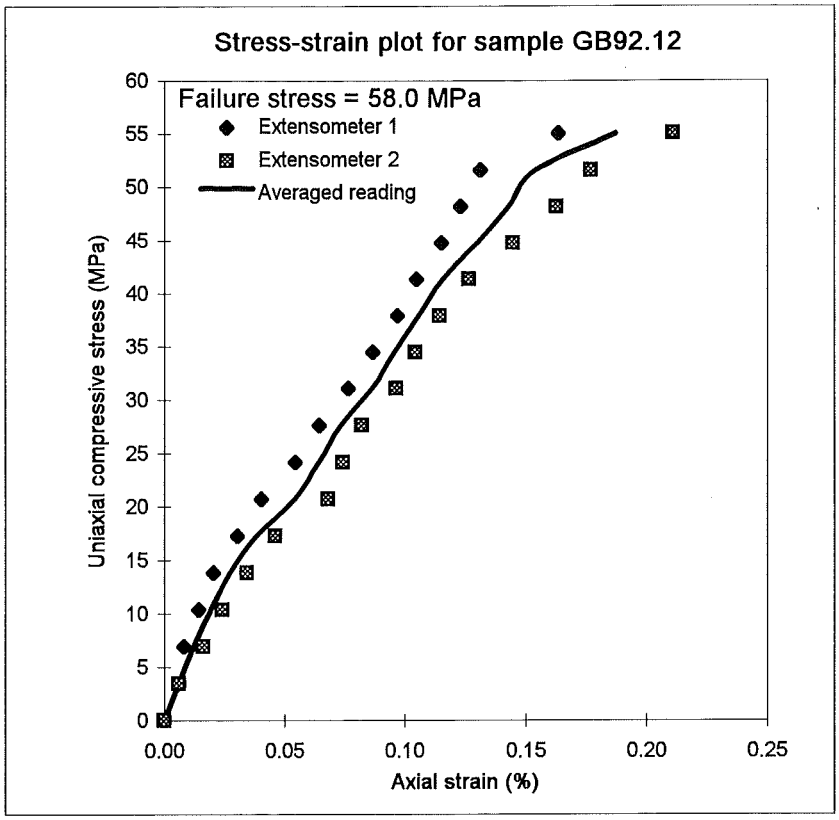

Figure D3.9: Stress-strain relationship for sample GB92.12.

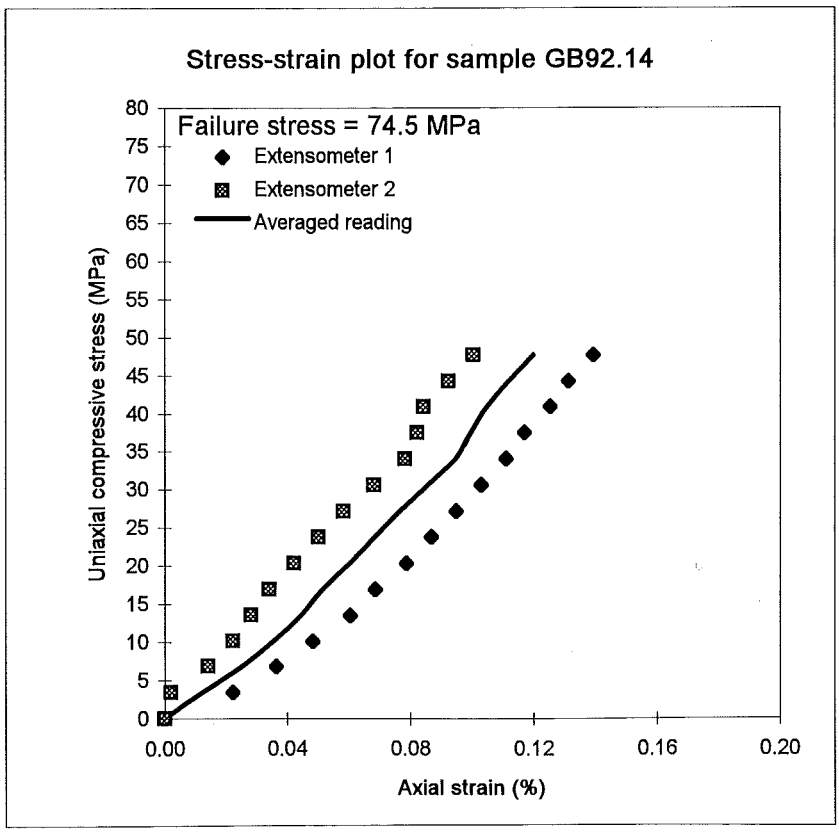

Figure D3.10: Stress-strain relationship for sample GB92.14.

Table D3.13: Stress-strain data for sample GB92.17

Axial load (kN)	Axial stress (MPa)	Demec 1	Relative change	Axial strain (%)	Demec 2	Relative change	Axial strain (%)	Average strain (%)
0	0.0	810	0	0	744	0	0	0
10	3.4	804	6	0.0121	743	1	0.0020	0.0071
20	6.8	799	11	0.0222	740	4	0.0080	0.0151
30	10.2	795	15	0.0303	736	8	0.0161	0.0232
40	13.6	789	21	0.0424	732	12	0.0241	0.0333
50	17.0	786	24	0.0485	729	15	0.0302	0.0393
60	20.4	782	28	0.0566	722	22	0.0442	0.0504
70	23.8	777	33	0.0667	718	26	0.0523	0.0595
80	27.2	774	36	0.0727	714	30	0.0603	0.0665
90	30.6	770	40	0.0808	713	31	0.0623	0.0716
100	34.0	767	43	0.0869	710	34	0.0683	0.0776
110	37.5	763	47	0.0949	706	38	0.0764	0.0857
120	40.9	759	51	0.1030	703	41	0.0824	0.0927
130	44.3	756	54	0.1091	700	44	0.0884	0.0988
140	47.7	752	58	0.1172	739	5	0.0101	0.0636
150	51.1	792	18	0.0364	710	34	0.0683	0.0524
Failure stress:								
363	123.6							
50% failure stress and strain:								
181.5	61.8	Not determinable from data						
E_{s50} (GPa)	43.8	(Estimate based on E_{ave})						
E_{t50} (GPa)	43.8	(Estimate based on E_{ave})						
E_{ave} (GPa)	43.8							

Table D3.14: Stress-strain data for sample GB92.19

Axial load (kN)	Axial stress (MPa)	Demec 1	Relative change	Axial strain (%)	Demec 2	Relative change	Axial strain (%)	Average strain (%)
0	0.0	990	0	0	1058	0	0	0
10	3.4	918	72	0.1788	1018	40	0.0991	0.1390
20	6.8				998	60	0.1486	0.1486
30	10.2	Demec gauge			972	86	0.2131	0.2131
40	13.6	broke from			948	110	0.2725	0.2725
50	17.0	sample			924	134	0.3320	0.3320
60	20.4				899	159	0.3939	0.3939
70	23.9				872	186	0.4608	0.4608
80	27.3				848	210	0.5203	0.5203
90	30.7				826	232	0.5748	0.5748
Failure stress:								
94	32.0							
50% failure stress and strain:								
47	16.0					127	0.3146	0.3146
E_{s50} (GPa)	5.1							
E_{t50} (GPa)	5.1							
E_{ave} (GPa)	5.1							

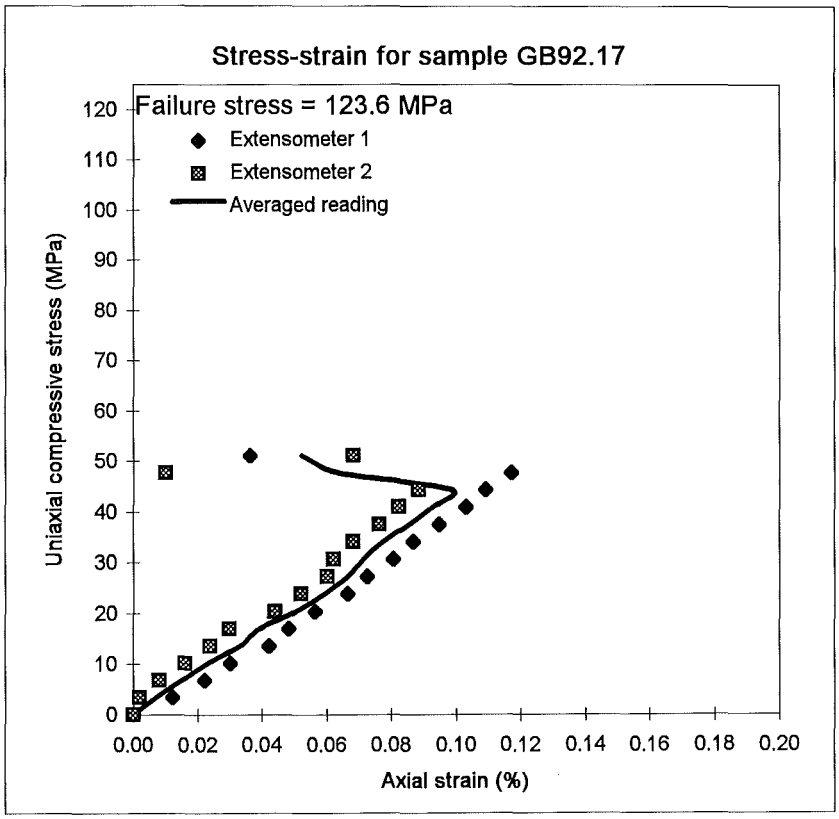

Figure D3.11 : Stress-strain relationship for sample GB92.17.

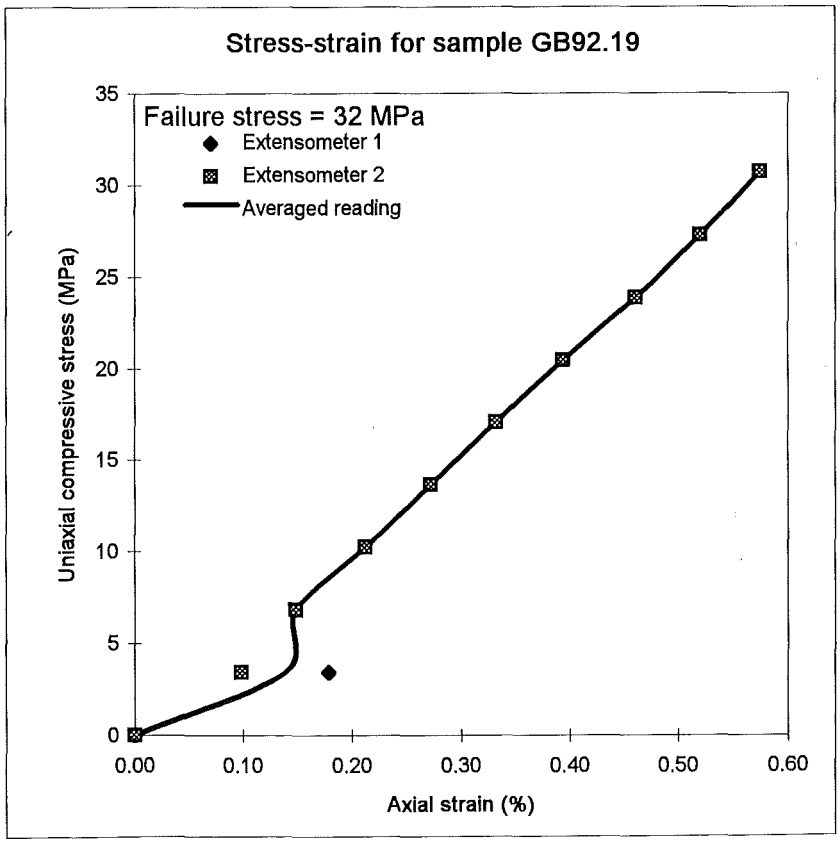

Figure D3.12: Stress-strain relationship for sample GB92.19.

Table D3.15: Stress-strain data for sample GB92.21

Axial load (kN)	Axial stress (MPa)	Demec 1	Relative change	Axial strain (%)	Demec 2	Relative change	Axial strain (%)	Average strain (%)
0	0.0	868	0	0	736	0	0	0
10	3.4	865	3	0.0061	730	6	0.0121	0.0091
20	6.8	858	10	0.0202	722	14	0.0281	0.0242
30	10.2	852	16	0.0323	718	18	0.0362	0.0343
40	13.6	849	19	0.0384	714	22	0.0442	0.0413
50	17.0	844	24	0.0485	710	26	0.0523	0.0504
60	20.3	839	29	0.0586	705	31	0.0623	0.0604
70	23.7	835	33	0.0667	701	35	0.0704	0.0685
80	27.1	832	36	0.0727	701	35	0.0704	0.0715
90	30.5	828	40	0.0808	700	36	0.0724	0.0766
100	33.9	826	42	0.0848	685	51	0.1025	0.0937
110	37.3	824	44	0.0889	682	54	0.1085	0.0987
120	40.7	822	46	0.0929	677	59	0.1186	0.1058
130	44.1	819	49	0.0990	675	61	0.1226	0.1108
140	47.5	816	52	0.1050	670	66	0.1327	0.1189
150	50.9	815	53	0.1071	665	71	0.1427	0.1249
160	54.3	814	54	0.1091	662	74	0.1487	0.1289
170	57.6	810	58	0.1172	657	79	0.1588	0.1380
180	61.0	807	61	0.1232	657	79	0.1588	0.1410
190	64.4	804	64	0.1293	656	80	0.1608	0.1450
200	67.8	801	67	0.1353	651	85	0.1709	0.1531
210	71.2	797	71	0.1434	649	87	0.1749	0.1591
220	74.6	795	73	0.1475	644	92	0.1849	0.1662
230	78.0	791	77	0.1555	638	98	0.1970	0.1763
240	81.4	787	81	0.1636	636	100	0.2010	0.1823
250	84.8	784	84	0.1697	635	101	0.2030	0.1863
260	88.2	780	88	0.1778	632	104	0.2090	0.1934
270	91.6	776	92	0.1858	629	107	0.2151	0.2005
280	94.9	775	93	0.1879	629	107	0.2151	0.2015
290	98.3	772	96	0.1939	624	112	0.2251	0.2095
300	101.7	768	100	0.2020	617	119	0.2392	0.2206
310	105.1	765	103	0.2081	614	122	0.2452	0.2266
320	108.5	762	106	0.2141	609	127	0.2553	0.2347
330	111.9	756	112	0.2262	605	131	0.2633	0.2448
340	115.3	754	114	0.2303	602	134	0.2693	0.2498
350	118.7	750	118	0.2384	599	137	0.2754	0.2569
360	122.1	746	122	0.2464	598	138	0.2774	0.2619
Failure stress:								
488.5	165.6							
50% failure stress and strain:								
244.25	82.8		82.5	0.1667		100.5	0.2020	0.1843
E_{s50} (GPa)	44.9							
E_{t50} (GPa)	44.9							
E_{ave} (GPa)	44.9							

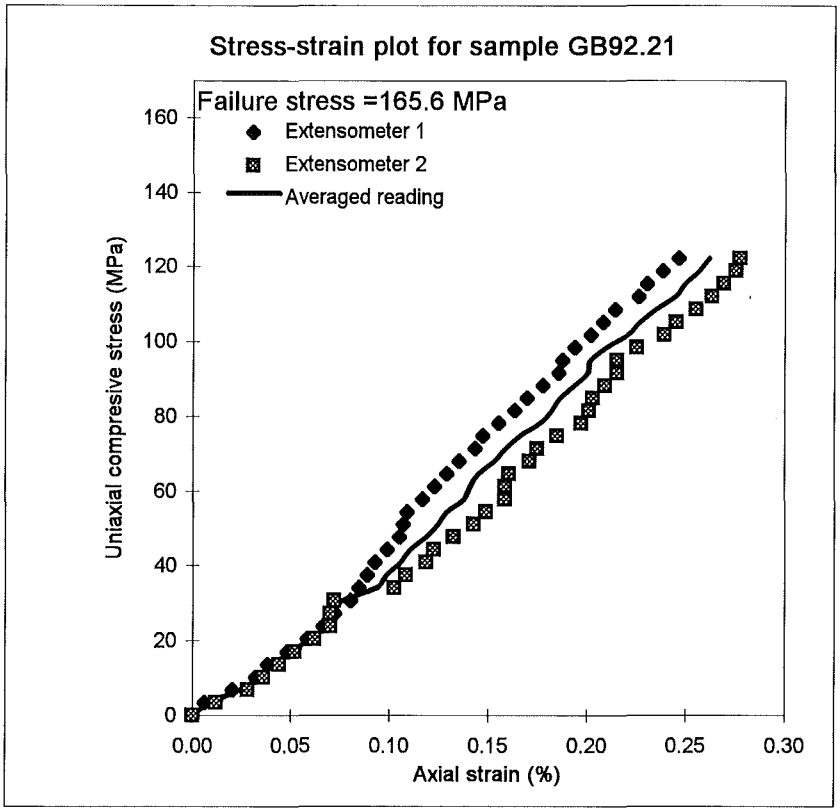

Figure D3.13: Stress-strain relationship for sample GB92.21.

Table D3.16: Stress-strain data for sample GB97.1

Axial load (kN)	Axial stress (MPa)	Demec 1	Relative change	Axial strain (%)	Demec 2	Relative change	Axial strain (%)	Average strain (%)
0	0.0	868	0	0	744	0	0	0
10	3.5	857	11	0.0222	728	16	0.0322	0.0272
20	6.9	847	21	0.0424	716	28	0.0563	0.0494
30	10.4	839	29	0.0586	704	40	0.0804	0.0695
40	13.9	832	36	0.0727	693	51	0.1025	0.0876
Failure stress:								
49	17.0							
50% failure stress and strain:								
24.5	8.5		24.5	0.0495		33.5	0.0673	0.0584
E_{s50} (GPa)	14.5							
E_{t50} (GPa)	16.7							
E_{ave} (GPa)	16.7							

Table D3.17: Stress-strain data for sample GB97.3

Axial load (kN)	Axial stress (MPa)	Demec 1	Relative change	Axial strain (%)	Demec 2	Relative change	Axial strain (%)	Average strain (%)
0	0.0	874	0	0	722	0	0	0
10	3.4	850	24	0.0485	700	22	0.0442	0.0464
20	6.9	834	40	0.0808	681	41	0.0824	0.0816
30	10.3	821	53	0.1071	662	60	0.1206	0.1138
Failure stress:								
35	12.1							
50% failure stress and strain:								
17.5	6.0		34.5	0.0697		35	0.0704	0.0700
E_{s50} (GPa)	8.6							
E_{t50} (GPa)	10.2							
E_{ave} (GPa)	10.2							

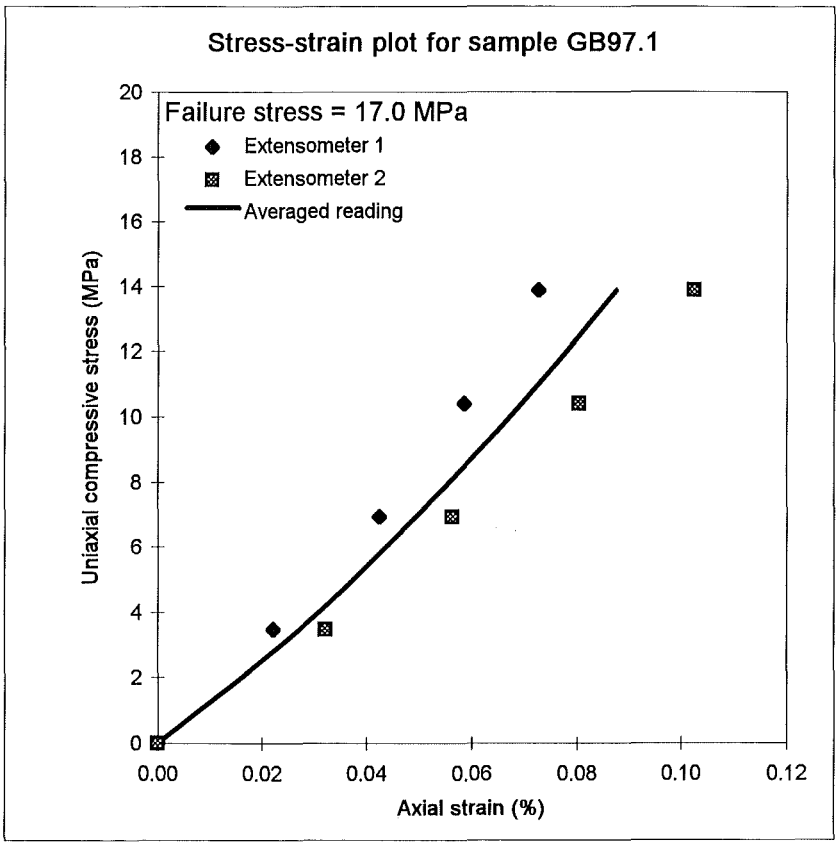

Figure D3.14: Stress-strain relationship for sample GB97.1.

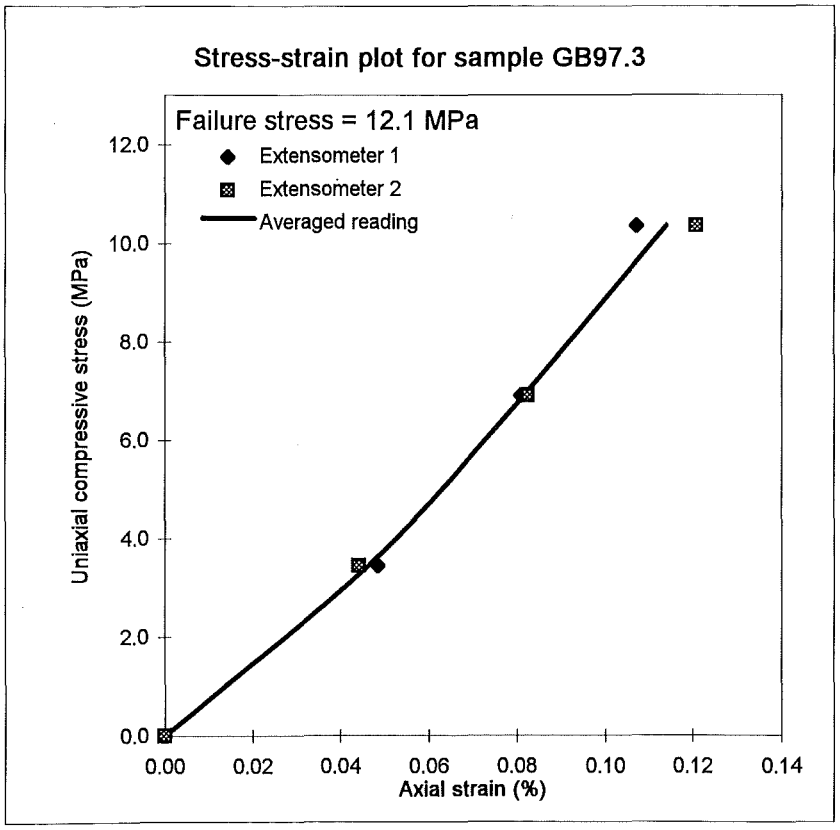

Figure D3.15: Stress-strain relationship for sample GB97.3.

Table D3.18: Stress-strain data for sample GB98.1

Axial load (kN)	Axial stress (MPa)	Demec 1	Relative change	Axial strain (%)	Demec 2	Relative change	Axial strain (%)	Average strain (%)
0	0.0	870	0	0	747	0	0	0
10	3.4	870	0	0.0000	736	11	0.0221	0.0111
20	6.9	867	3	0.0061	728	19	0.0382	0.0221
30	10.3	865	5	0.0101	721	26	0.0523	0.0312
40	13.8	861	9	0.0182	716	31	0.0623	0.0402
50	17.2	853	17	0.0343	711	36	0.0724	0.0534
60	20.6	849	21	0.0424	704	43	0.0864	0.0644
70	24.1	846	24	0.0485	697	50	0.1005	0.0745
80	27.5	843	27	0.0545	691	56	0.1126	0.0836
90	30.9	838	32	0.0646	683	64	0.1286	0.0966
100	34.4	834	36	0.0727	676	71	0.1427	0.1077
110	37.8	831	39	0.0788	670	77	0.1548	0.1168
120	41.3	827	43	0.0869	666	81	0.1628	0.1248
130	44.7	824	46	0.0929	661	86	0.1729	0.1329
140	48.1	821	49	0.0990	654	93	0.1869	0.1430
150	51.6	818	52	0.1050	645	102	0.2050	0.1550
160	55.0	816	54	0.1091	642	105	0.2111	0.1601
170	58.5	807	63	0.1273	636	111	0.2231	0.1752
180	61.9	804	66	0.1333	629	118	0.2372	0.1853
190	65.3	801	69	0.1394	621	126	0.2533	0.1963
200	68.8	797	73	0.1475	613	134	0.2693	0.2084
210	72.2	793	77	0.1555	608	139	0.2794	0.2175
220	75.7	789	81	0.1636	602	145	0.2915	0.2275
230	79.1	785	85	0.1717	598	149	0.2995	0.2356
240	82.5	781	89	0.1798	593	154	0.3095	0.2447
250	86.0	777	93	0.1879	586	161	0.3236	0.2557
260	89.4	772	98	0.1980	581	166	0.3337	0.2658
270	92.8	767	103	0.2081	574	173	0.3477	0.2779
Failure stress:								
287.5	98.9							
50% failure stress and strain:								
143.75	49.4		50	0.1010		96	0.1930	0.1470
E_{s50} (GPa)	33.6							
E_{t50} (GPa)	33.6							
E_{ave} (GPa)	33.6							

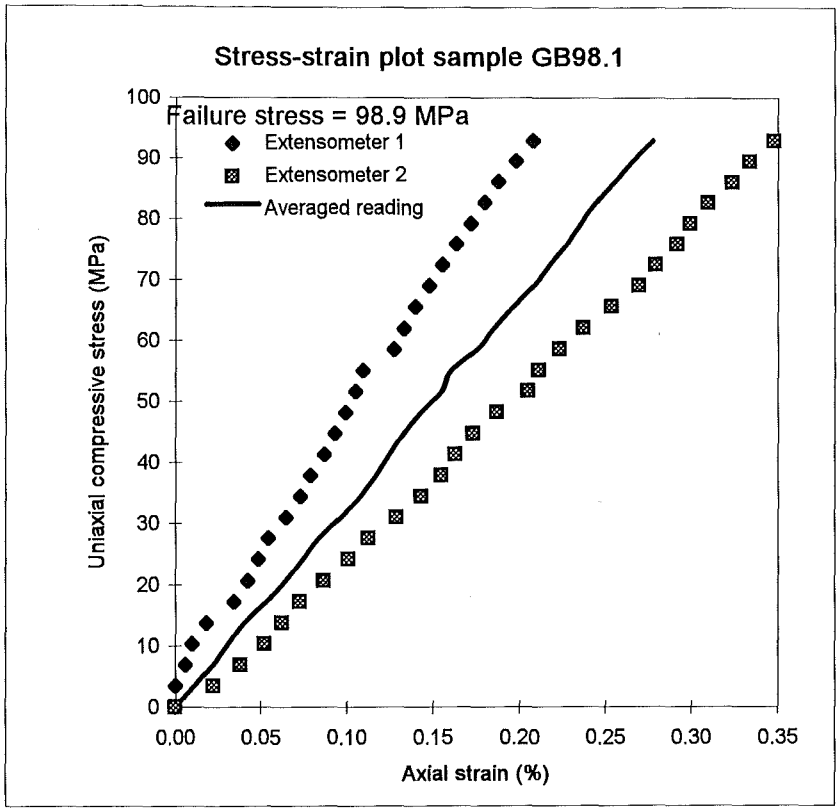

Figure D3.16: Stress-strain relationship for sample GB98.1.

Table D3.19: Stress-strain data for sample GB98.3

Axial load (kN)	Axial stress (MPa)	Demec 1	Relative change	Axial strain (%)	Demec 2	Relative change	Axial strain (%)	Average strain (%)
0	0.0	867	0	0	737	0	0	0
10	3.4	866	1	0.0020	729	8	0.0161	0.0091
20	6.9	865	2	0.0040	726	11	0.0221	0.0131
30	10.3	858	9	0.0182	721	16	0.0322	0.0252
40	13.7	855	12	0.0242	715	22	0.0442	0.0342
50	17.1	854	13	0.0263	705	32	0.0643	0.0453
60	20.6	853	14	0.0283	700	37	0.0744	0.0513
70	24.0	852	15	0.0303	695	42	0.0844	0.0574
80	27.4	849	18	0.0364	689	48	0.0965	0.0664
90	30.8	846	21	0.0424	684	53	0.1065	0.0745
100	34.3	844	23	0.0465	680	57	0.1146	0.0805
110	37.7	842	25	0.0505	676	61	0.1226	0.0866
120	41.1	840	27	0.0545	673	64	0.1286	0.0916
130	44.5	839	28	0.0566	670	67	0.1347	0.0956
140	48.0	837	30	0.0606	664	73	0.1467	0.1037
150	51.4	835	32	0.0646	659	78	0.1568	0.1107
160	54.8	828	39	0.0788	656	81	0.1628	0.1208
170	58.2	824	43	0.0869	655	82	0.1648	0.1258
180	61.7	821	46	0.0929	650	87	0.1749	0.1339
190	65.1	819	48	0.0970	646	91	0.1829	0.1399
200	68.5	816	51	0.1030	642	95	0.1910	0.1470
210	71.9	814	53	0.1071	639	98	0.1970	0.1520
220	75.4	814	53	0.1071	636	101	0.2030	0.1550
230	78.8	811	56	0.1131	633	104	0.2090	0.1611
240	82.2	806	61	0.1232	630	107	0.2151	0.1691
250	85.6	803	64	0.1293	627	110	0.2211	0.1752
260	89.1	800	67	0.1353	622	115	0.2312	0.1832
270	92.5	796	71	0.1434	618	119	0.2392	0.1913
280	95.9	793	74	0.1495	614	123	0.2472	0.1984
290	99.3	790	77	0.1555	610	127	0.2553	0.2054
300	102.8	787	80	0.1616	606	131	0.2633	0.2125
310	106.2	783	84	0.1697	604	133	0.2673	0.2185
320	109.6	780	87	0.1757	600	137	0.2754	0.2256
330	113.1	778	89	0.1798	595	142	0.2854	0.2326
340	116.5	774	93	0.1879	590	147	0.2955	0.2417
350	119.9	769	98	0.1980	586	151	0.3035	0.2507
360	123.3	765	102	0.2060	583	154	0.3095	0.2578
370	126.8	761	106	0.2141	579	158	0.3176	0.2659
Failure stress:								
429	147.0							
50% failure stress and strain:								
214.5	73.5		53	0.1071		99.5	0.2000	0.1535
E_{s50} (GPa)	47.9							
E_{t50} (GPa)	47.9							
E_{ave} (GPa)	47.9							

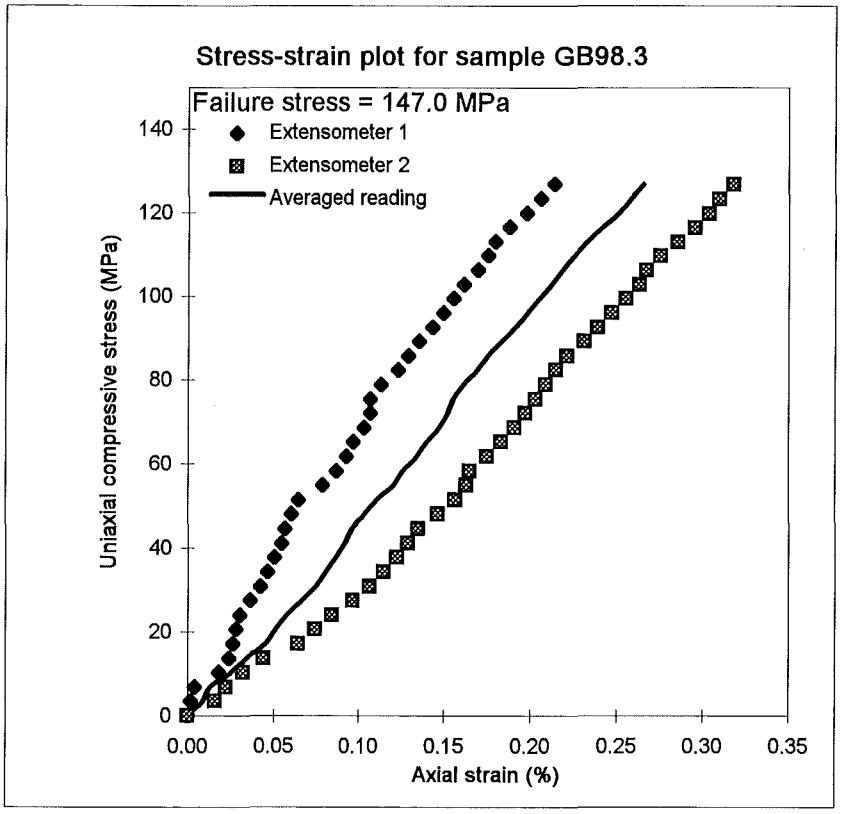

Figure D3.17: Stress-strain relationship for sample GB98.3.

Table D3.20: Stress-strain data for sample GB106.1

Axial load (kN)	Axial stress (MPa)	Demec 1	Relative change	Axial strain (%)	Demec 2	Relative change	Axial strain (%)	Average strain (%)
0	0.0	875	0	0	732	0	0	0
10	3.4	875	0	0.0000	720	12	0.0241	0.0121
20	6.8	871	4	0.0081	713	19	0.0382	0.0231
30	10.3	867	8	0.0162	706	26	0.0523	0.0342
40	13.7	864	11	0.0222	702	30	0.0603	0.0413
50	17.1	860	15	0.0303	700	32	0.0643	0.0473
60	20.5	857	18	0.0364	613	119	0.2392	0.1378
70	23.9	855	20	0.0404	614	118	0.2372	0.1388
80	27.4	851	24	0.0485	618	114	0.2291	0.1388
90	30.8	848	27	0.0545	624	108	0.2171	0.1358
100	34.2	844	31	0.0626	598	134	0.2693	0.1660
110	37.6	841	34	0.0687	573	159	0.3196	0.1941
120	41.0	837	38	0.0768	541	191	0.3839	0.2303
130	44.5	834	41	0.0828	543	189	0.3799	0.2314
140	47.9	831	44	0.0889	548	184	0.3698	0.2294
150	51.3	828	47	0.0949	552	180	0.3618	0.2284
160	54.7	829	46	0.0929	559	173	0.3477	0.2203
Failure stress:								
167.5	57.3							
50% failure stress and strain:								
83.75	28.6		25	0.0505		112	0.2251	0.1378

E_{s50} (GPa)	20.8	
E_{t50} (GPa)	20.8	(Estimate based on E_{s50})
E_{ave} (GPa)	20.8	(Estimate based on E_{s50})

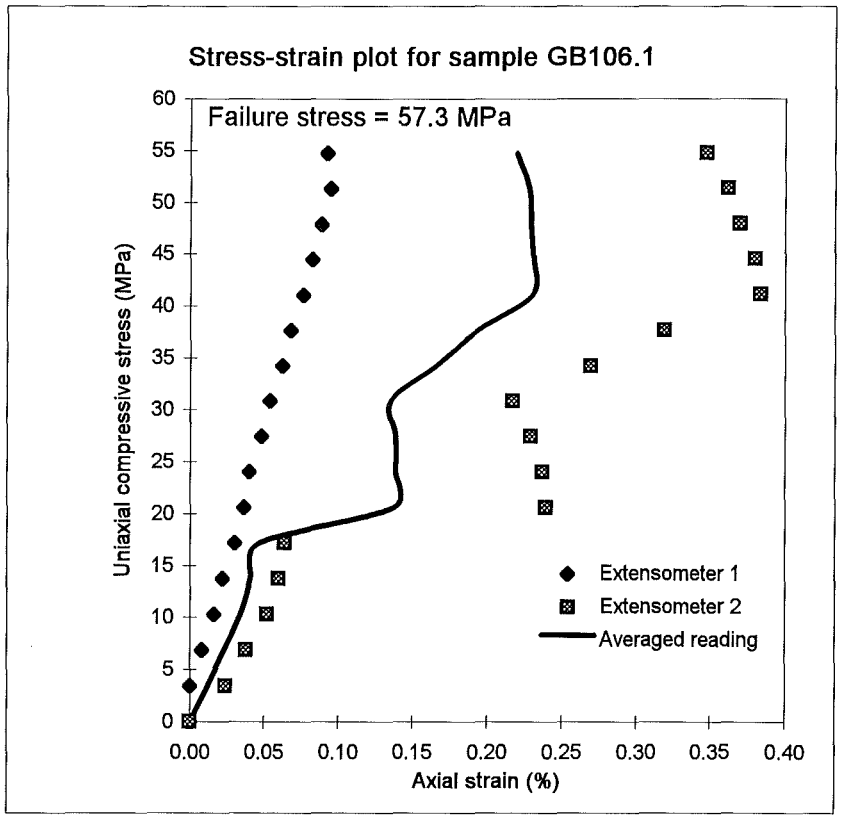

Figure D3.18: Stress-strain relationship for sample GB106.1.

Table D3.21: Uniaxial compressive strength and Young's Modulus data

Core sample	Time to failure (min)	Failure mechanism	ρ_{sat} (kgm^{-3})	L (mm)	D (mm)	A (mm^2)	P (kN)	σ_c (MPa)	$E_{s\,(50)}$ (GPa)	$E_{t\,(50)}$ (GPa)	E_{ave} (GPa)	$E_{dyn\,(sat)}$ (GPa)	$\frac{E_{dyn\,(sat)}}{E_{s\,(50)}}$	$\frac{E_{dyn\,(sat)}}{E_{t\,(50)}}$
GB23.3	3:00	Shear	2709	118.82	60.85	2905	71.5	24.6	-	-	-	20.5	-	-
GB65.3	12:30	Combination	2697	166.03	61.13	2932	389.0	132.7	47.7	47.7	47.7	47.4	0.99	0.99
GB87.1	2:30	Shear	2672	173.77	60.70	2891	52.0	18.0	5.2	8.0	8.0	23.1	4.44	2.88
GB87.4	7:20	Axial cleavage	2709	174.95	61.07	2926	218.0	74.5	36.9	36.9	36.9	42.8	1.16	1.16
GB87.6	4:30	Shear	2780	137.93	60.85	2905	135.0	46.5	27.4	39.0	39.0	40.3	1.47	1.03
GB92.1	6:20	Cataclasis	2704	176.45	61.27	2945	160.5	54.5	39.8	39.8	39.8	50.7	1.27	1.27
GB92.4	12:10	Fracturing	2715	172.95	61.16	2935	384.5	131.0	46.8	46.8	46.8	60.3	1.29	1.29
GB92.7	12:50	Combination	2757	168.99	61.18	2937	429.5	146.3	55.6	55.6	55.6	50.4	0.91	0.91
GB92.9	8:20	Combination	2732	165.05	61.18	2937	254.0	86.5	36.8	37.5	37.5	37.4	1.02	1.00
GB92.12	4:30	Axial cleavage	2728	176.89	60.85	2905	168.5	58.0	36.4	36.4	36.4	35.7	0.98	0.98
GB92.14	7:40	Shear	2723	175.84	61.20	2938	219.0	74.5	37.4	40.0	40.0	42.6	1.14	1.07
GB92.17	11:00	Fracturing	2713	176.59	61.19	2937	363.0	123.6	43.8	43.8	43.8	57.9	1.32	1.32
GB92.19	3:00	Shear	2806	168.51	61.15	2934	94.0	32.0	5.1	5.1	5.1	7.4	1.45	1.45
GB92.21	16:00	Shear	2713	178.47	61.31	2949	488.5	165.7	44.9	44.9	44.9	51.1	1.14	1.14
GB97.1	1:40	Shear	2708	153.82	60.68	2888	49.0	17.0	14.5	16.7	16.7	26.9	1.85	1.61
GB97.3	1:40	Shear	2689	140.90	60.80	2900	35.0	12.1	8.6	10.2	10.2	24.8	2.88	2.43
GB98.1	8:50	Combination	2738	174.31	60.88	2908	287.5	98.9	33.6	33.6	33.6	33.3	0.99	0.99
GB98.3	13:00	Cataclasis	2719	176.00	61.00	2919	429.0	147.0	47.9	47.9	47.9	64.2	1.34	1.34
GB106.1	4:30	Shear	2740	140.03	61.05	2924	167.5	57.3	20.8	20.8	20.8	41.4	1.99	1.99

D3.5 Point load test data

Table D3.22: Point load test data for unweathered core samples

Sample	W (mm)	D (mm)	L (mm)	P (kN)	De^2 (mm^2)	De (mm)	I_s MPa	F	$I_{s(50)}$ (MPa)	UCS (MPa)
GB23.1		61	104	2	3721	61	0.54	1.09	0.59	12
GB23.2		61	103	3	3721	61	0.81	1.09	0.88	18
GB65.2		61	103	22.5	3721	61	6.05	1.09	6.61	132
GB87.2		61	100	2	3721	61	0.54	1.09	0.59	12
GB87.3		61	113	2	3721	61	0.54	1.09	0.59	12
GB87.5		61	98	20	3721	61	5.37	1.09	5.88	118
GB87.7		61	125	4	3721	61	1.07	1.09	1.18	24
GB92.2		61	94	16	3721	61	4.30	1.09	4.70	94
GB92.3		61	104	31.5	3721	61	8.47	1.09	9.26	185
GB92.6	61	58		20.5	4502	67	4.55	1.14	5.20	104
GB92.8		61	74	26	3721	61	6.99	1.09	7.64	153
GB92.11	61	59		25	4593	68	5.44	1.15	6.24	125
GB92.13		61	92	16.5	3721	61	4.43	1.09	4.85	97
GB92.15		61	94	28	3721	61	7.52	1.09	8.23	165
GB92.16		61	119	17.5	3721	61	4.70	1.09	5.14	103
GB92.18a		61	62	33	3721	61	8.87	1.09	9.70	194
GB92.18b		61	61	26	3721	61	6.99	1.09	7.64	153
GB92.22	61	41		21.5	3184	56	6.75	1.06	7.13	143
GB97.2		61	123	2	3721	61	0.54	1.09	0.59	12
GB97.4		61	63	1.5	3721	61	0.40	1.09	0.44	9
GB98.2	61	60		8	4682	68	1.71	1.15	1.97	39
GB98.4		61	102	24.5	3721	61	6.58	1.09	7.20	144
GB106.2		61	122	10	3721	61	2.69	1.09	2.94	59
GB106.3		61	121	7.5	3721	61	2.02	1.09	2.20	44

Table D3.23: Point load test data for slightly weathered irregular lumps.

Sample	W (mm)	D (mm)	L (mm)	P (kN)	De^2 (mm^2)	De (mm)	I_s MPa	F	$I_{s(50)}$ (MPa)	UCS (MPa)
1	63	50	45	11.5	4011	63	2.87	1.11	3.19	64
2	75	32	40	11.5	3056	55	3.76	1.05	3.94	79
3	95	55	120	25	6653	82	3.76	1.25	4.68	94
4	66	48	93	26.5	4034	64	6.57	1.11	7.32	146
5	75	69	137	11	6589	81	1.67	1.24	2.08	42
6	73	53	91	12	4926	70	2.44	1.16	2.84	57
7	59	38	111	17.5	2855	53	6.13	1.03	6.32	126
8	84	47	140	26	5027	71	5.17	1.17	6.05	121
9	70	63	113	24	5615	75	4.27	1.20	5.13	103
10	61	43	107	18	3340	58	5.39	1.07	5.75	115
11	59	38	84	13	2855	53	4.55	1.03	4.69	94
12	68	64	103	26.5	5541	74	4.78	1.20	5.72	114
13	64	53	103	28	4319	66	6.48	1.13	7.33	147
14	63	62	100	18	4973	71	3.62	1.17	4.23	85
15	70	59	108	20	5258	73	3.80	1.18	4.50	90
16	54	35	106	13	2406	49	5.40	0.99	5.36	107
17	53	40	58	11	2674	52	4.11	1.02	4.18	84
18	48	38	113	5	2298	48	2.18	0.98	2.13	43
19	94	54	120	22	6463	80	3.40	1.24	4.22	84
20	65	60	111	30.5	4966	70	6.14	1.17	7.17	143
21	54	30	54	18	2063	45	8.73	0.96	8.36	167
22	55	54	71	18	3782	61	4.76	1.10	5.22	104
23	53	39	55	15	2632	51	5.70	1.01	5.77	115
24	62	33	82	16.5	2605	51	6.33	1.01	6.39	128
25	77	46	118	3.5	4510	67	0.78	1.14	0.89	18
26	43	35	58	5	1889	43	2.65	0.94	2.49	50
27	55	40	93	13	2801	53	4.64	1.03	4.76	95
28	65	39	93	3	3228	57	0.93	1.06	0.98	20
29	45	27	79	3	1547	39	1.94	0.90	1.74	35
30	59	33	83	12.5	2479	50	5.04	1.00	5.03	101
31	39	30	56	12	1490	39	8.06	0.89	7.17	143
32	100	85	135	27	10823	104	2.49	1.39	3.47	69
33	100	79	135	36	10059	100	3.58	1.37	4.90	98
34	93	50	137	16.5	5921	77	2.79	1.21	3.38	68
35	54	46	90	25	3163	56	7.90	1.05	8.33	167
36	48	33	90	12.5	2017	45	6.20	0.95	5.91	118
37	80	31	106	14	3158	56	4.43	1.05	4.67	93
38	60	38	102	20	2903	54	6.89	1.03	7.13	143
39	47	27	63	10	1616	40	6.19	0.91	5.61	112
40	61	28	70	15.5	2175	47	7.13	0.97	6.91	138

Table D3.23 (cont.): Point load test data for slightly weathered irregular lumps.

Sample	W (mm)	D (mm)	L (mm)	P (kN)	De^2 (mm^2)	De (mm)	I_s MPa	F	$I_{s(50)}$ (MPa)	UCS (MPa)
41	51	27	60	5	1753	42	2.85	0.92	2.63	53
42	63	29	80	12.5	2326	48	5.37	0.98	5.29	106
43	47	27	70	8	1616	40	4.95	0.91	4.49	90
44	36	27	69	12	1238	35	9.70	0.85	8.28	166
45	60	46	79	27	3514	59	7.68	1.08	8.30	166
46	56	40	75	22.5	2852	53	7.89	1.03	8.13	163
47	40	20	63	8	1019	32	7.85	0.82	6.42	128
48	41	34	71	16	1775	42	9.01	0.93	8.35	167
49	57	34	60	11	2468	50	4.46	1.00	4.44	89
50	52	31	79	7	2052	45	3.41	0.96	3.26	65
51	53	40	68	14	2699	52	5.19	1.02	5.28	106
52	46	35	63	7	2050	45	3.41	0.96	3.27	65
53	54	33	72	12	2269	48	5.29	0.98	5.17	103
54	46	30	71	12.5	1757	42	7.11	0.92	6.57	131
55	61	52	58	15	4039	64	3.71	1.11	4.14	83
56	58	54	77	14	3988	63	3.51	1.11	3.90	78
57	53	41	65	12.5	2767	53	4.52	1.02	4.62	92

Table D3.24: Point load test data for moderately weathered irregular lumps.

Sample	W (mm)	D (mm)	L (mm)	P (kN)	De^2 (mm^2)	De (mm)	I_s MPa	F	$I_{s(50)}$ (MPa)	UCS (MPa)
1	70	39	103	2	3476	59	0.58	1.08	0.62	12
2	43	35	76	3	1916	44	1.57	0.94	1.47	29
3	60	28	65	1	2139	46	0.47	0.97	0.45	9
4	52	32	112	5.5	2119	46	2.60	0.96	2.50	50
5	52	28	64	6.5	1854	43	3.51	0.93	3.28	66
6	45	30	78	10.5	1719	41	6.11	0.92	5.61	112
7	47	31	72	1	1855	43	0.54	0.94	0.50	10
8	56	47	96	15	3351	58	4.48	1.07	4.78	96
9	58	29	82	3.5	2142	46	1.63	0.97	1.58	32
10	35	35	98	1	1560	39	0.64	0.90	0.58	12
11	52	42	91	14.5	2781	53	5.21	1.02	5.34	107
12	71	38	75	1	3435	59	0.29	1.07	0.31	6
13	43	41	74	4.5	2245	47	2.00	0.98	1.96	39
14	39	39	83	7.5	1937	44	3.87	0.94	3.66	73
15	58	42	96	10.5	3102	56	3.39	1.05	3.55	71
16	67	41	86	10	3498	59	2.86	1.08	3.08	62
17	64	40	71	12	3259	57	3.68	1.06	3.91	78
18	47	32	64	12	1915	44	6.27	0.94	5.90	118
19	31	26	71	3.5	1026	32	3.41	0.82	2.79	56
20	63	34	71	4.5	2727	52	1.65	1.02	1.68	34
21	73	43	83	10	3997	63	2.50	1.11	2.78	56

D3.6 Slake-durability test data

Table D3.25: Slake durability test data.

Sample	Mass 1 (kg)	Mass 2 (kg)	Mass 3 (kg)	Drum mass (kg)	I_{d1} (%)	I_{d2} (%)
UW 1	2.810	2.808	2.807	2.260	99.6	99.5
UW 2	2.838	2.835	2.834	2.260	99.5	99.3
SW 1	2.801	2.798	2.795	2.260	99.4	98.9
SW 2	2.725	2.722	2.719	2.260	99.4	98.7
MW 1	2.721	2.715	2.711	2.196	98.9	98.1
MW 2	2.673	2.667	2.664	2.196	98.7	98.1

Appendix E

Determination of parameters used in rock mass and rippability evaluation methods

E1 The RMR System

E1.1 Strength

The rating for strength was found by multiplying the revised strength by the formula in Figure 2.3:

$$\text{Rating} = -0.0002(\text{UCS})^2 + 0.106(\text{UCS}) + 1$$

where UCS is the unconfined compressive strength in MPa.

The revised strength was determined by analysing the logged strength and logged rock unit. The distribution of strength data found by Beetham and Cootes (1994) and this study, shows three modes at about 125 MPa, 50 MPa and 20 MPa. Competent sandstone units logged as R3, R4 or R5 were assigned a strength of 125 MPa (or a rating of 11). Siltstone units were assigned a strength of 50 MPa (or a rating of 6), brecciated sandstone and rock logged as HBX and QBX (with a logged strength of R1-R3) were assigned a strength of 10 MPa (or a rating of 2), and any other brecciated rock, clay and pug with a logged strength of S1-S6, assigned a strength of 0 MPa (or a rating of 1). If the logged strength is, for example, S1R3 or R1R4 and the rock unit is interbedded sandstone-siltstone or flysch sequence (IB, IS or FLY), then the strength assigned to the more competent units was halved as the weakness of the less competent lithology will weaken the overall strength of the rock mass. For example, rocks logged as S1R3 were assigned a strength of 65 MPa (halve of 125 MPa).

E1.2 RQD

The ratings for RQD were determined by multiplying the logged RQD value by the formula in Figure 2.4:

$$\text{Rating} = 0.0006(\text{RQD})^2 + 0.11(\text{RQD})^2 + 3$$

where RQD is a percentage.

E1.3 Discontinuity spacing

This parameter has been logged by Macraes as fractures per metre, which is the inverse of discontinuity spacing, therefore the reciprocal of the logged fractures per metre value was calculated to find the average discontinuity spacing for every rock mass unit. Using the formulae in Figure 2.5, if the spacing is less than 400 mm, then the following formula is used:

$$\text{Rating} = -1 \times 10^{-5}(\text{Spacing})^2 + 0.017(\text{Spacing}) + 5$$

or where the spacing is greater than 400 mm:

$$\text{Rating} = -1 \times 10^{-6}(\text{Spacing})^2 + 0.00865(\text{Spacing}) + 6.7$$

where the spacing is in millimetres.

E1.4 Discontinuity conditions

E1.4.1 Length, persistence or continuity

This parameter cannot be determined exactly for drillcore data (unless the discontinuity occurs longitudinally down the drillcore - which is very rare), therefore the main defect type in each rock mass unit is assigned a rating based on its general characteristics. The termination and persistence of discontinuities mapped on line traverses were logged by Barrell (1992). This data coupled with observations made of outcrops led to the following generalisations (logged descriptions in brackets):

- Breaks (BK), cleavage (CV), schistocity (SC), lineations (LI), veinlets (VNL) and drilling induced fractures (DI) are all generally less than one metre in length and are assigned a rating of 6.
- Partings (PT), stringers (ST) and veins (VN) are generally more continuous, therefore are assigned a rating of 4.

- Joints (JN) generally range between one and 10 metres, therefore are assigned a rating of 3.5 (mean of ratings 3 and 4).
- Bedding planes (BD, tCT, bCT) generally range between three and twenty metres so are assigned a rating of 2 (mean of 1 and 3).
- Shears (SH), shear zones (SZ), crush zones (CZ), shattered zones (STZ), decomposed zones (DC), faults (FT), pug (PG) and breccia (BX) are generally persistent if the rock unit is brecciated, so are assigned a rating of 0, but if the rock unit is a sandstone or similar, then the discontinuity persistence is not as great, and the parameter is assigned a rating of 3.

E1.4.2 Separation

The separation, spacing or infilling width of a discontinuity is described by Macraes as being clean (CL), stained (ST), a vein (VN) or a veinlet (VNL) and if the spacing is greater than 2 mm, then the thickness is recorded. If no data is recorded then it is assumed that the separation is zero and is given a rating of 6. If the discontinuities are clean or stained, or vein or veinlet are recorded, then a rating of 5 is assigned, based on an average of the ratings assigned to spacings between 0 and 1 mm. If the separation is between 1 - 5 mm, the rating is 1 and if the separation is greater than 5 mm, then the rating is 0.

E1.4.3 Roughness

Discontinuities have been logged as rough (RO), smooth (SM), rough-smooth (ROSM), polished (PO), slickensided (SS), serrated (SE) or segmented (SEGM). The following ratings are applied:

- Serrated and segmented discontinuities are given a rating of 6
- Rough discontinuities given a rating of 5
- Smooth-rough discontinuities are given a rating of 3
- Smooth discontinuities are assigned a rating of 1
- Polished and slickensided discontinuities are assigned a rating of 0.

If the separation is wide enough, or if the discontinuity is infilled with clay or pug, the influence of roughness will be negligible (Bieniawski, 1989), therefore in rock mass units with sufficiently wide infilling, the roughness is assigned a rating of 0.

E1.4.4 Infilling

If the discontinuities in a rock mass unit are infilled, then the three most prominent types of infilling are recorded, although only the most common infilling type is used to assign a rating. Infilling materials were sorted into hard and soft, for example, pug and clay are soft, and quartz mineralisation is hard. The infilling width was also used to assign ratings:

- If no data is recorded then the rating is 6.
- If the main filling type is hard, and the infilling width is greater than 5 mm, then the rating is 4.
- If the main filling type is hard and the infilling width is less than 5 mm, then the rating is 2.
- If the main filling type is soft and the infilling width is greater than 5 mm, then the rating is 2.
- If the main filling type is soft and the infilling width is less than 5 mm, then the rating is 0.

E1.4.5 Weathering

No information on the weathering of discontinuity surfaces was included on the drill logs, but the weathering of the rock mass unit was instead. The rock mass unit weathering was used and assumed to be the same as the weathering on discontinuity surfaces based on observations made on drillcore. Most of the drillcore material and discontinuity surfaces are unweathered, except near the surface, where rock mass units may be slightly weathered, moderately weathered or highly weathered and the discontinuity surfaces may be a weathering grade lower, therefore introducing a small error into the weathering parameter of the RMR.

E1.5 Groundwater

The rock mass below the watertable is expected to be saturated unless groundwater is able to drain along adits, shafts or discontinuities. The open pit is expected to be drained so that the open pit should be completely dry, although this may be a problem at Globe-Progress because of high rainfall (see Section 1.3.5). Therefore three scenarios are used in calculating the RMR. The rock mass is assumed to be saturated, damp, and completely dry.

E1.6 Discontinuity orientation

To excavate the open pit, it is advantageous to use the favourability of the discontinuity orientations to assist excavation. The most common discontinuity, or the discontinuity most beneficial to excavatability and rippability are bedding planes. Rattenbury (1994) structurally mapped the open pit area, mapping bedding plane orientations from outcrops, and reorientating core to check bedding plane orientations at depth. Core reorientation involved orientating the core according the recorded hole azimuth and inclination, then rotating the core until the cleavage orientation or cleavage-bedding intersection lineation matches that of the regional mean. The reorientation of core assumes that (from Rattenbury, 1994):

- The core length has not been inverted during handling,
- The regional mean cleavage/intersection lineation reflects the local cleavage/intersection lineation orientation where the core was drilled,
- The bedding orientation in the core is representative of the region around the core.

He found that bedding planes appeared to be consistent with depth. Therefore to determine the favourability of a discontinuity orientation, it was first assumed that excavation will proceed in a east to west direction, parallel to the main dip direction (perpendicular to the strike), then the favourability was assessed following Minty and Kearns' (1983) guidelines (Table 2.8).

E2 Weaver's 1975 Rippability Rating System

E2.1 Seismic velocity

Twenty seismic refraction surveys were performed over the mine site (see Figure 4.1 for locations) to obtain the seismic velocity of the rock mass. Only velocities for the surficial rock mass was determined as the depth of penetration was never more than 15 metres (see Tables D2.1 - D2.24). Seismic velocity data cannot be extrapolated far because of the variable nature of the rock mass and it is most likely that the seismic velocities of the rock mass at depth will be greater than those found on the surface (Beetham and Richards, 1995). For this reason the average seismic velocity found in Section 4.2.1.4 of 2100 ms^{-1} was used in the classification. Using Weaver's 1975 Classification, this seismic velocity classifies the rock mass as good rock and assigns a rating of 24 to the rock mass. An attempt was made at assigning sheared and brecciated rock masses a lower seismic velocity but the seismic refraction surveys were not able to differentiate sheared and brecciated rock masses as opposed to highly fractured or openly fractured rock masses (as shown in Figure 5.4), and therefore an average seismic velocity was used for the whole site.

E2.2 Hardness

Weaver (1975) uses the term hardness as opposed to strength and categorises rock's hardness according to the terminology and strength values in Table E2.1.

Table E2.1: Weaver's (1975) rock hardness definition

Rock hardness	Strength correlation (MPa)	Rating
Extremely hard rock	> 70	10
Very hard rock	20 - 70	5
Hard rock	10 - 20	2
Soft rock	3 - 10	1
Very soft rock	1.7 - 3	0

To assign the rating for this parameter, the revised strength (determination of the revised strength is explained in Section E1.1) was assigned a rating according to Table E2.1.

E2.3 Weathering

Weaver (1975) uses weathering of the rock mass as opposed to weathering of discontinuity surfaces like Bieniawski (1989). Weathering of the rock mass was logged by Macraes and is assigned a rating according to Table 3.3.

E2.4 Joint spacing

This parameter was logged by Macraes as fractures per metre, which is the inverse of joint spacing, and therefore the inverse of the fractures per metre parameter was calculated to find the average joint spacing for every rock mass unit. The average joint spacing was then assigned a rating using Table 3.3.

E2.5 Joint continuity

This parameter cannot be determined exactly for drillcore data (unless the discontinuity occurs longitudinally down the drillcore - which is very rare), therefore the main defect type in each rock mass unit is assigned a rating based on its general characteristics. The termination and persistence of discontinuities mapped on line traverses were logged by Barrell (1992). This data coupled with observations made of outcrops led to the following generalisations (logged descriptions in brackets):

- Breaks (BK), cleavage (CV), schistocity (SC), lineations (LI), veinlets (VNL) and drilling induced fractures (DI) are all generally non-continuous to slightly continuous and are assigned a rating of 5.
- Partings (PT), bedding (BD), bedding contacts(tCT, bCT), joints (JT), joint sets (GJ), stringers (ST) and veins (VN) are continuous and do not normally contain any infilling gouge, and therefore are assigned a rating of 3.
- Shears (SH), shear zones (SZ), crush zones (CZ), shattered zones (STZ), decomposed zones (DZ), faults (FT), pug (PG) and breccia (BX) are generally continuous and contain gouge, and therefore are given a rating of 0.

E2.6 Joint gouge

This parameter requires both joint separation (or infilling width) and the predominant type of infilling to determine the rating for every rock mass unit. The infilling width is described as either, clean (CL), stained (ST), a vein (VN) or a veinlet (VNL) and if the width is greater than 2 mm, then the thickness is also recorded. If no data is logged, then it is assumed that there is no joint separation. Ratings are assigned using Table 3.3 as follows:

- Veins, stained or clean surfaces or no separation are assigned a rating of 5.
- If the infilling width is greater than 2 mm and there is no infilling, then they are assigned a rating of 4.
- If the main infilling type is clay or pug and the infilling width is less than 5 mm, then they are given a rating of 3.
- If the predominant infilling type is clay or pug and the infilling width is greater than 5 mm, then the rock mass unit is assigned a rating of 1.

E2.7 Discontinuity orientation

Weaver (1975) did not quantify what a favourable or unfavourable strike and dip orientation was, and therefore Minty and Kearns (1983) strike and dip orientation guidelines (Table 2.8) were used to determine the favourability of an orientation. Ratings were assigned using Table 3.3 and the assumptions outlined in Section E1.6.

E3 The Modified Weaver Rippability Rating System

As this system is based on the latest RMR System, the same assumptions made in determining the RMR System (Appendix E1) are used in calculating the Modified Weaver Rippability Rating System, except that groundwater and RQD parameters are replaced by a seismic velocity parameter, which was averaged for the whole pit (as discussed in Section E2.1).

E4 MacGregor, *et al's* (1994) productivity estimation equations

E4.1 UCS

MacGregor *et al's* (1994) productivity estimation equations require the actual unconfined compressive strength as opposed to a rating value. The revised strength estimate has been used for this parameter and the assumptions and generalisations made in determining the revised strength are outlined in Section E1.1.

E4.2 Weathering

MacGregor *et al* (1994) use weathering of the rock mass in their equations as opposed to weathering of discontinuity surfaces. Weathering of the rock mass was logged by Macraes and is assigned a rating according to the descriptions in Table 3.9.

E4.3 Grain size

MacGregor *et al* (1994) found the grain size to be a major influence on the productivity of a bulldozer. Macraes logged the grain size of the sediments, and therefore, the grain size is assigned ratings according to Table 3.9. If the grain size varies, for example fine sand and course sand are present in the drillcore, then MacGregor *et al's* (1994) ratings are averaged such that, for example, FSCS (fine sand - coarse sand) is assigned a rating of 2.75 (mean of 2 and 3.5).

E4.4 Seismic velocity

MacGregor *et al* (1994) require the actual seismic velocity in their productivity estimation equations. The average seismic velocity was used for this parameter (as explained in Section E2.1). The seismic velocity parameter does not influence the final productivity as much as strength and the structural rating, therefore any lack of variation in the seismic velocity parameter is not very important.

E4.5 Defect roughness

Macraes logged defect or discontinuity roughness and this parameter is assigned a rating according to the description given in Table 3.9.

E4.6 Number of defect sets

This parameter requires only the number of defect sets and not their orientation with respect to the ripping direction. The two most penetrative defect sets are bedding and cleavage. The clustered joint set pattern found in Section 4.5.4 roughly equate to one defect set because of its distribution pattern (see Figure 4.27b). Therefore it is assumed that there are three defect sets in open pit area.

E4.7 Defect spacing

MacGregor *et al* (1994) use the actual defect spacing in their productivity equations. Macraes logged fractures per metre, which is the inverse of defect spacing, and therefore, the inverse of fractures per metre was used for this parameter.

E4.8 Structure rating

MacGregor *et al's* (1994) structural rating is the relationship between bedding and defect spacing. This parameter is assigned ratings according to Table 3.9. The logged rock unit parameter was used for this parameter using the following assumptions (logged descriptions in brackets) based on field observations:

- Breccia (Bx), host rock breccia (HBx), pug breccia (PBx), quartz breccia (QBx), gravel (GRAV), clay (CLAY), pug (PUG), scree material (SCRE), rubble (RUBB) and soil (SOIL) were all assigned a rating of 19.
- Interbedded silts and muds (IS) and interbedded silts, muds and breccia (ISBx) were assigned a rating of 17.
- Quartz lodes (QT) were assigned a rating of 16.
- Interbedded silts, sands and muds (IBIS) were assigned a rating of 15.

- Interbedded silts and sand (IB) were assigned a rating of 13.
- Flysch sequences (FLY) were assigned a rating of 7.
- Sandstone beds (SS) were assigned a rating of 6.
- Massive sandstone units were assigned a rating of 2.

E5 Inverse distance weighted average data modelling method

This method was used to assign rock mass and rippability ratings, and productivity estimations to the rock mass within the open pit. The open pit has been block modelled into two domains, one containing waste rock, and the other containing the Globe-Progress Shear Zone, and where block sizes are 5 m x 5 m by 2.5 m depth. Each block was assigned a weighted average according to the control blocks of known ratings determined from drillhole data, in other words, if a drillhole intersects a block, then the drillhole rating at that point is assigned to the block. If greater than one rock mass unit intersects the control block (which is common as most rock mass units are less than 2.5 m thick) then the values are averaged. This then allows the ratings to be contoured. Popular contouring methods include triangulation, weighted inverse distance or Kreiging.

The contouring method used on the ratings data was modelled using the weighted inverse distance method whereby blocks are estimated by weighted control blocks (Swan and Sandilands, 1995). For example, if three control blocks R_1, R_2, and R_3 at distances d_1, d_2, and d_3 are used to estimate another block rating (R'), then the estimated block rating is equal to:

$$R' = \frac{\left(R_1/d_1\right) + \left(R_2/d_2\right) + \left(R_3/d_3\right)}{\left(1/d_1\right) + \left(1/d_2\right) + \left(1/d_3\right)}$$

This is a weighted average of R_1, R_2, and R_3, where R is multiplied by the weighting (distance). If all distances were the same, then R' would simply be the average of R_1, R_2, and R_3.

The common notation of the above equation is written as:

$$R' = \frac{\sum_{i=1}^{n}\left(R_i / d_i\right)}{\sum_{i=1}^{n}\left(1 / d_i\right)}$$

If large distances are used, then the distance weighting may be varied by squaring or cubing the distance weighting, that is, $(1/d^2)$ or $(1/d^3)$, making the data more reliable.

Block modelling the data assumed a maximum distance of 80 m, and therefore the distance weighting was cubed. The estimates produced for every block is within the range of the contributing control blocks, and which is adequate for these purposes as ranges are plotted rather than actual values.